PERFORMANCE AND EFFECTIVENESS OF OMNI-DIRECTIONAL STERN DRIVE TUGS

by

Paul Anthony Brandner, BE(Hons)

Submitted in Fulfilment of the
Requirements for the Degree of
Doctor of Philosophy

Civil + Mechanical Engineering

University of Tasmania

November, 1995

graduating 1997

DECLARATION

This Thesis contains no material which has been accepted for a degree or diploma by the University or any other institution, except by way of background information and duly acknowledged in the Thesis, and to the best of the Candidate's knowledge and belief no material previously published or written by another person except where due acknowledgment is made in the text of the Thesis.

Paul Brandner

November, 1995

AUTHORITY OF ACCESS

This Thesis may be made available for loan and limited copying in accordance with the *Copyright Act of 1968.*

Paul Brandner

November, 1995

ABSTRACT

Shiphandling tugs are a critical aspect of ship manoeuvring in confined waters. Knowledge of their performance and effective use in various situations provide necessary guidance for the marine pilot and tug master to improve shiphandling techniques. Shiphandling simulators are a well accepted tool for training of marine pilots, development of port operational procedures and port development studies. Realistic simulation of shiphandling manoeuvres requires not only a reliable hydrodynamic model of the ship, but also precise representation of the forces available from the assisting tugs.

In the past, the limited capabilities of tugs meant that force prediction and evaluation of operating procedures was a relatively simple matter. However, the push for expanding and more efficient port operations has led to a new generation of shiphandling tugs being introduced into major Australian ports during the 1980's. These tugs are of greater displacement, power and manoeuvrability compared with their twin screw predecessors and represent a significant technological step. Increased manoeuvrability of the so called *omni-directional stern drive tug* has been achieved through the fitting of azimuthing thrusters, which are capable of producing thrust in any direction. The enhanced manoeuvrability of the omni-directional stern drive tug and increased power has enabled significant increases to be made in the efficiency of shiphandling operations, particularly in the ability to assist at speed. However, to fully realise the potential of these complex vessels a more thorough understanding of their hydrodynamic aspects is required. Further, with increased speed greater consideration needs to be given to the interaction of tug forces with those produced by the ship's rudder, propeller and hull.

To investigate the performance and effectiveness of omni-directional stern drive tugs, a series of physical model tests has been performed. Hydrodynamic forces acting on the hull and thrusters have been measured, with particular attention being paid to hydrodynamic interactions between thrusters and the thrusters and hull. Measurements were initially made of forces acting on a bare tug hull and a single thruster in open water. Thruster-thruster interaction was determined from measurement of forces acting on twin thrusters in open water and thruster-hull interaction was determined from measurement of total forces and those acting on the thrusters of a self-propelled free-running model.

Data derived from the model tests has been used to construct a mathematical model which may be solved using equilibrium or, in the time domain, as may be desired for real time simulation. Quasi-steady predictions of tug forces have been used to identify general performance, optimum operating techniques and the influence of tug forces on ship motions in confined waters. In cooperation with Australian towage operators, practical findings from this investigation have been detailed in a manual to assist tug masters and marine pilots.

In addition to harbour tugs, this work may also provide insight into the manoeuvring of escort tugs and other vessels with omni-directional propulsion.

ACKNOWLEDGMENT

This work is taken from investigations carried out by the author at the Australian Maritime College as part of ongoing research into ship manoeuvring and simulation. This work has been supported by the Australian Maritime College, The Adelaide Steam Ship Company Ltd., Howard Smith Industries Ltd.-Towage and Salvage Division and the Australian Maritime Engineering CRC Ltd.

The author is indebted to many people within these organisations for their valuable assistance and dedication. In particular, to Captain Robert Tasker for initiating this project and developing industry support, and for his continuing interest and to Dr. Martin Renilson, who as associate supervisor provided ongoing guidance and productive comment. Part of this work was made possible from industry grants and use of full scale vessels for which the author gratefully acknowledges the efforts of Captain David Mailler, Captain Ken Ross and Captain Graeme Levy.

The author is also indebted to Professor Mike Davis, who as supervisor provided valuable comments and guidance in compiling the thesis.

Special thanks are extended to the many colleagues, indeed too many to mention, at the AMC for their assistance in performing the numerous model and simulation investigations and to Mr. Neil Fleck for freely providing design information on the tugs considered in this work.

Finally, the author wishes to thank friends and family for their never ending encouragement.

NOMENCLATURE

A Area

B moulded beam

c propeller blade chord @ 0.7 radius

C_B block coefficient,

$$C_B = \frac{\nabla}{LBT}$$

C'_N thruster moment coefficient,

$$C'_N = \frac{N}{\frac{1}{2}\rho A_O D_O \left[V_A^2 + (0.7\pi n D_O)^2\right]}$$

C'_Q thruster torque coefficient,

$$C'_Q = \frac{Q}{\frac{1}{2}\rho A_O D_O \left[V_A^2 + (0.7\pi n D_O)^2\right]}$$

C'_T thruster total force coefficient,

$$C'_T = \frac{T}{\frac{1}{2}\rho A_O \left[V_A^2 + (0.7\pi n D_O)^2\right]}$$

C'_X thruster longitudinal force coefficient,

$$C'_X = \frac{X}{\frac{1}{2}\rho A_O \left[V_A^2 + (0.7\pi n D_O)^2\right]}$$

C'_Y thruster transverse force coefficient,

$$C'_Y = \frac{Y}{\frac{1}{2}\rho A_O \left[V_A^2 + (0.7\pi n D_O)^2\right]}$$

C_N normal drag coefficient of propeller race

C_∇ volumetric coefficient,

$$C_\nabla = \frac{\nabla}{L^3}$$

D diameter

e'_Y hull sway force centre of pressure

$$e'_Y = \frac{e_Y}{L} = \frac{N'_H}{Y'_H}$$

E_N normal entrainment coefficient

F_H^* coefficient for contribution of hull force to tug force,

$$F_H^* = \frac{F_H}{\frac{1}{2}\rho A_O (0.7\pi D_O)^2 \left(n_p^2 + n_s^2\right) C'_{X,\beta_P=0}}$$

F_{TUG}^* tug force coefficient,

$$F_{TUG}^* = \frac{F_{TUG}}{\frac{1}{2}\rho A_O (0.7\pi D_O)^2 \left(n_p^2 + n_s^2\right) C'_{X,\beta_P=0}}$$

F_n Hull Froude Number,

$$F_n = \frac{V}{\sqrt{gL}}$$

GM initial metacentric height

k propeller race coefficient

k_{HR} hull flow rectification factor

K roll moment in tug fixed coordinate system

K_Q propeller torque coefficient,

$$K_Q = \frac{Q}{\rho n^2 D_O^5}$$

K_T propeller thrust coefficient,

$$K_T = \frac{T}{\rho n^2 D_O^4}$$

l'_{TUG} location of tug force in ship fixed coordinate system

$$l'_{TUG} = \frac{N'_{TUG}}{Y'_{TUG}}$$

l'_r ship yaw stability lever in ship fixed coordinate system

$$l'_r = \frac{N'_r}{Y'_r - \Delta'}$$

l'_v ship sway stability lever in ship fixed coordinate system

$$l'_v = \frac{N'_v}{Y'_v}$$

L reference length (length between perpendiculars)

L_{CLD} distance from thruster centre of rotation to leading edge of duct

L_{CTD} distance from thruster centre of rotation to trailing edge of duct

n propeller revolutions per second

N yaw moment in tug fixed coordinate system

$\frac{\partial N'}{\partial \beta'_H}$ non-dimensional derivative of $N - \beta_H$ curve at equilibrium,

$$\frac{\partial N'}{\partial \beta'_H} = \frac{\partial N}{\partial \beta_H} \frac{1}{½ \rho V^2 T L^2}$$

N'_H hull yaw moment coefficient,

$$N'_H = \frac{N_H}{½ \rho V^2 T L^2}$$

N^*_H hull yaw moment coefficient,

$$N^*_H = \frac{N_H}{½ \rho A_O L (0.7\pi D_O)^2 \left(n_p^2 + n_s^2\right) C'_{X,\beta_P=0}}$$

N^*_{HT} coefficient for hull yaw moment due to thruster-hull interaction,

$$N^*_{HT} = \frac{N_{HT}}{½ \rho A_O L (0.7\pi D_O)^2 \left(n_p^2 + n_s^2\right) C'_{X,\beta_P=0}}$$

N'_r derivative of yaw moment with respect to yaw velocity for ship

$$N'_r = \frac{N_r}{½ \rho V^2 L^3}$$

N'_v derivative of yaw moment with respect to sway velocity for ship

$$N'_v = \frac{N_v}{½ \rho V^2 L^3}$$

$N^*_{\beta\delta}$ yaw moment coefficient for thruster-hull interaction as a function of apparent advance angle and thruster angle

N^*_δ yaw moment coefficient for thruster-hull interaction as a function of thruster angle

P propeller pitch

r' non-dimensional yaw velocity

$$r' = \frac{rL}{V} = \frac{L}{R}$$

R radius of turn

R_V velocity ratio,

$$\beta_P = \frac{V}{V_R} = \frac{\tan \beta_{PV}}{\tan \beta_{PR}}$$

R_{nH} Tug Hull Reynolds Number,

$$R_{nH} = \frac{VL}{\nu}$$

R_{nP} Propeller Blade Reynolds Number,

$$R_{nP} = \frac{c}{\nu}\sqrt{V_A^2 + (0.7\pi n D_O)^2}$$

s thruster spacing

t thrust deduction fraction

T draft to baseline

u' non-dimensional surge velocity,

$$u' = \frac{u}{V}$$

u_A component of thruster advance velocity along tug's x-axis

v' non-dimensional sway velocity,

$$v' = \frac{v}{V}$$

v_A component of thruster advance velocity along tug's y-axis

V velocity of tug/ship

V_A thruster advance velocity

V_a propeller induced axial velocity

V_E entrainment velocity

V_t propeller induced tangential velocity

w wake fraction

x ordinate

x_e semi-major axis of assumed bow fender profile

x_f distance along the tug's x-axis to the bow fender

X surge force in tug fixed coordinate system

X'_H hull surge force coefficient,

$$X'_H = \frac{X_H}{\frac{1}{2}\rho V^2 BT}$$

X^*_H hull surge force coefficient,

$$X^*_H = \frac{X_H}{\frac{1}{2}\rho A_O (0.7\pi D_O)^2 (n_p^2 + n_s^2) C'_{X,\beta_P=0}}$$

X^*_{HT} coefficient for hull surge force due to thruster-hull interaction,

$$X^*_{HT} = \frac{X_{HT}}{\frac{1}{2}\rho A_O (0.7\pi D_O)^2 (n_p^2 + n_s^2) C'_{X,\beta_P=0}}$$

$X^*_{\beta\delta}$ surge force coefficient for thruster-hull interaction as a function of apparent advance angle and thruster angle

X^*_δ surge force coefficient for thruster-hull interaction as a function of thruster angle

y ordinate

y_e minor axis of assumed bow fender profile

Y sway force in tug fixed coordinate system

Y'_H hull sway force coefficient,

$$Y'_H = \frac{Y_H}{\frac{1}{2}\rho V^2 TL}$$

Y^*_H hull sway force coefficient,

$$Y^*_H = \frac{Y_H}{\frac{1}{2}\rho A_O (0.7\pi D_O)^2 \left(n_p^2 + n_s^2\right) C'_{X,\beta_P=0}}$$

Y^*_{HT} coefficient for hull sway force due to thruster-hull interaction,

$$Y^*_{HT} = \frac{Y_{HT}}{\frac{1}{2}\rho A_O (0.7\pi D_O)^2 \left(n_p^2 + n_s^2\right) C'_{X,\beta_P=0}}$$

Y'_r derivative of sway force with respect to yaw velocity for ship

$$Y'_r = \frac{Y_r}{\frac{1}{2}\rho V^2 L^3}$$

Y'_v derivative of sway force with respect to sway velocity for ship

$$Y'_v = \frac{Y_v}{\frac{1}{2}\rho V^2 L^3}$$

$Y^*_{\beta\delta}$ sway force coefficient for thruster-hull interaction as a function of apparent advance angle and thruster angle

Y^*_δ sway force coefficient for thruster-hull interaction as a function of thruster angle

z ordinate

Greek symbols

α phase angle between thruster advance velocity and thrust vector

β_H drift angle of tug hull,

$$\beta_H = \arctan\left(\frac{v}{u}\right)$$

β_P propeller advance angle,

$$\beta_P = \arctan\left(\frac{V_A}{0.7\pi n D_O}\right)$$

β_{PR} propeller race advance angle,

$$\beta_{PR} = \arctan\left(\frac{V_R}{0.7\pi n D_O}\right)$$

β_{PV} apparent propeller advance angle,

$$\beta_{PV} = \arctan\left(\frac{V}{0.7\pi n D_O}\right)$$

γ yaw rate angle

$$\gamma = \arctan\left(\frac{rL}{u}\right)$$

δ thruster angle of rotation

Δ mass displacement

Δ' non-dimensional mass displacement

$$\Delta' = \frac{\Delta}{\frac{1}{2}\rho L^3}$$

∇ volume displacement

ζ slope of propeller race trajectory relative to freestream

η_u' coefficient for surge velocity at thruster locations due to hull-thruster interaction

η_v' coefficient for sway velocity at thruster locations due to hull-thruster interaction

θ thruster angle of attack

ν kinematic viscosity

ξ proportion of thruster affected by anothers race

ρ density

ϕ roll angle

χ azimuth of tug/ship force relative to freestream

Subscripts

A thruster advance velocity

H hull

T thruster

P propeller

R propeller race

O propeller disk

S reaction to tug force or force from ship

p port thruster

s starboard thruster

l leading thruster

t trailing thruster

i,j thruster

Abbreviations

AMC	Australian Maritime College
CAORF	Computer Aided Operations Research Facility
ITTC	International Towing Tank Conference
MARIN	Maritime Research Institute Netherlands
NSFI	Ship Research Institute of Norway
RINA	Royal Institution of Naval Architects
SNAME	Society of Naval Architects and Marine Engineers
SSPA	Swedish State Shipbuilding Experimental Tank
VBD	Duisburg Experimental Institute for Lake and River Ship Construction

CONTENTS

Appendices

1.2 Recent Ship, Tug and Harbour Developments

Many smaller ships are now fitted with manoeuvring devices such as bow/stern thrusters and high lift rudders, making them less dependent on tug assistance for harbour manoeuvring. However, at the same time, economic considerations have lead to changes in port admittance policy and ship design which have made other ships more dependent on tug assistance. Increasing export trade has introduced the requirement for ports to increase both the size of vessels admitted and the frequency of movements which, in many cases, involves expansion of the port environmental operating window.

The ships which have become most dependent on tug assistance are large bulk carriers and tankers, which in addition to large inertia forces are also affected by large aerodynamic forces when handled in the ballast condition and large hydrodynamic forces in the deep laden condition, particularly with diminishing under keel clearance. The controllability of these ships varies dramatically due to large variations in the power-to-displacement ratio and, in recent years, there has been a trend toward its reduction. Clearly, significant savings in machinery and running costs can be achieved by reducing the installed power, with only minor reduction in seagoing speed. Controllability, to some extent, has been further reduced by the introduction of control systems prolonging the life of propulsion machinery by limiting the rate at which propeller revolutions may be varied.

In response, during the 1980's, requirements for increased towage capacity/quality and economic considerations relating to a number of factors led to tug design undergoing significant change. These changes generally involved the use of fewer tugs with considerably greater displacement, power and manoeuvrability to perform existing and expanding shiphandling tasks, as described by Webb, 1985, Ross, 1988 and Ross, 1992. Increased manoeuvrability has been achieved with the introduction of omni-directional drive tugs, i.e. tugs with propulsion or thrusters capable of producing thrust in any direction. Tugs of this type may be categorised on the basis of the hull configuration and the type of thrusters employed. There are two preferred hull configurations, the *tractor* hull and *stern drive* (*pusher*) hull and two preferred thruster types, the *cycloidal* thruster and *azimuthing* thruster which may be combined to give four omni-directional (drive) tug types, as shown in Figure 1.1.

Azimuthing thrusters as used on tugs consist of a ducted propeller driven through two pairs of 90 bevel gears, supported on bearings such that the duct, impeller and lower gear case assembly may be rotated to any azimuth. A typical azimuthing thruster is shown in Figure 1.2(a). A ducted propeller is invariably used since generally propellers operate at loadings where charateristics are significantly enhanced with the addition of a duct. The propeller may be fixed or controllable pitch. Due to its simplicity the fixed pitch alternative is generally used for shiphandling tugs. The cycloidal thruster or propeller consists of a rotating disc mounted flush with the hull, a number of vertical blades are distributed around its periphery with the capability that their pitch or angle of attack may be controlled such that the net thrust produced may be in any direction. By its nature the propeller is controllable pitch, hence thrusters of this type are conventionally designed with this capability. The locus traced by the centre of each blade as the propeller advances is that of a cycloid, which is why such propellers are known as cycloidal propellers. Of this type of propeller the most well known and that used solely as tug propulsion is the *Voith Schneider Propeller*, as shown in Figure 1.2(b).

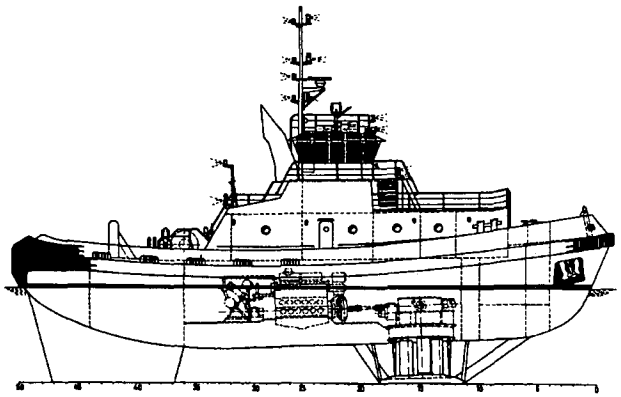

a) Tractor with Cycloidal Thrusters (Voith Water Tractor)

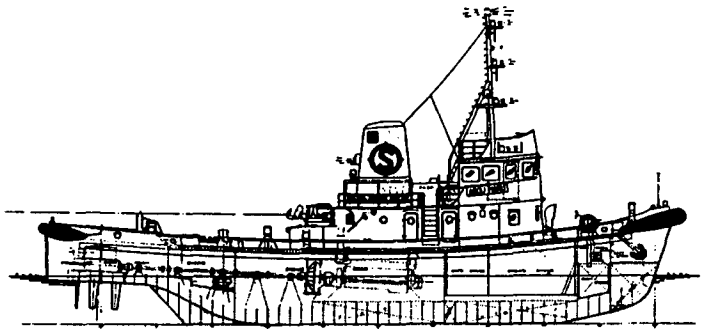

(b) Stern Drive with Cycloidal Thrusters

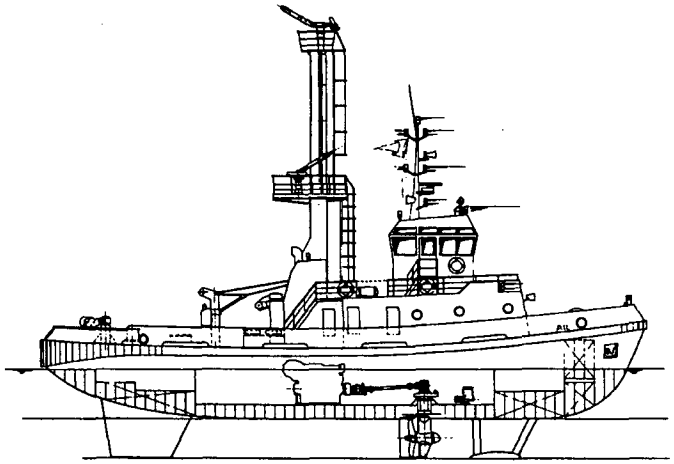

(c) Tractor with Azimuthing Thrusters

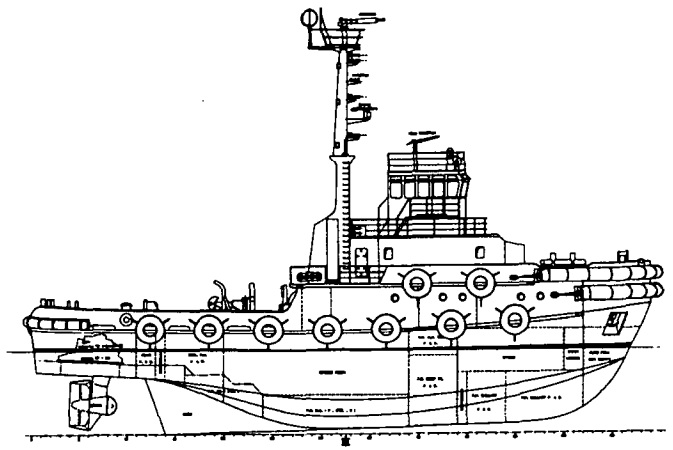

(d) Stern Drive with Azimuthing Thrusters

Figure 1.1 Types of Omni-directional (Drive) Tugs

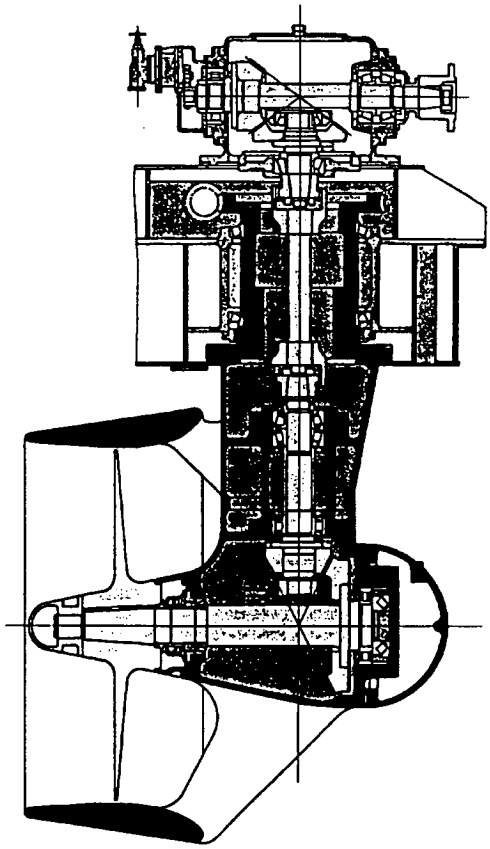

(a) Azimuthing Thruster

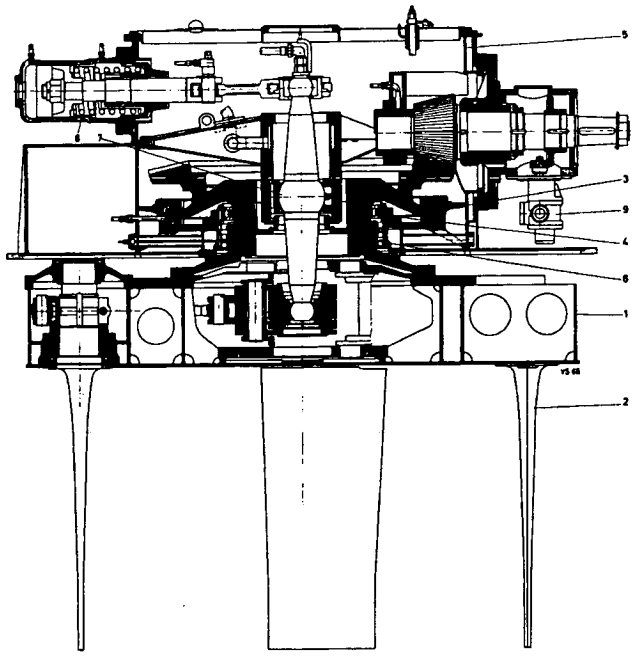

(b) Cycloidal Thruster (Voith Schneider Propeller)

Figure 1.2 Types of Omni-directional Propulsion or Thrusters

The concept of the omni-directional drive tug is not new, being first introduced by Baer, 1953, of the Voith company, Germany. This tug was of the tractor configuration with twin Voith Schneider propellers located underneath the forebody. The so named *Voith Water Tractor* quickly became popular in Europe and parts of America and New Zealand. A modern Voith Water Tractor is shown in Figure 1.1(a). The Voith Water Tractor was introduced as a more efficient and safer towing concept, overcoming many of the problems associated with the poor manoeuvrability and unsafe configuration of the existing conventional tug, Baer, 1973. These problems, in particular, include the risk of so called *stemming* and *girting*, as shown in Figure 1.3. Stemming involves loss of control that may occur manoeuvring about the ship's forebody when underway, resulting in the tug being pinned against the forebody or stem and consequently capsized. The difficulty of manoeuvring in this area is due to the inflexion and acceleration of the flow field about the forebody leading to the tug experiencing rapidly varying sway forces and yaw moments, as shown by Dand, 1975 and Dand, 1977. Girting may occur at the forward or aft end of the ship being assisted and involves the ship overtaking the tug resulting in the line coming on to the tug's beam introducing the possibility of capsize. The Voith Water Tractor with increased manoeuvrability and being designed to operate with the line over the stern only, essentially eliminates the risk of stemming and girting. Voith Schneider propellers have also been fitted to tugs in the stern drive configuration, as shown in Figure 1.1(b), however, this arrangement never achieved popularity and is long since out of use.

More recently, tugs of both the tractor and stern drive configuration have been fitted with azimuthing thrusters, as shown in Figure 1.1(c) and (d). In the past, high cost and lack of thrusters in the size range required have prevented universal acceptance of the omni-directional concept. The choice of tug configuration has been the subject of considerable debate and depends, among other factors, on the nature of the port, the shiphandling techniques employed and, to some extent, on a port's history of development. In Australia the stern drive configuration with azimuthing thrusters or *omni-directional stern drive tug* is predominant.

The manoeuvrability of omni-directional stern drive tugs and increased power has enabled significant increases to be made in the efficiency of shiphandling operations. However, to fully realise the potential of these complex vessels, more performance information is required. Capabilities of the Voith Water Tractor have been extensively investigated by Voith, Baer, 1971, including development of the so called *indirect* towing method, as shown in Figure 1.4(a). This method is intended for use at higher speeds where direct towing is less effective and involves making use of hull-skeg lifting effects to impart force to the line. Methods of shiphandling using the tractor tug are well defined as a development of the so called *Line Towage* or *European* Method, as described by Spaulding, 1982 and Hensen, 1990. This method of ship assist involves transmission of tug forces predominantly through the line. With the advent of the omni-directional stern drive tug being later than that of the tractor, less is known about its capabilities, although methods of shiphandling developed with conventional tugs were quickly found compatible, i.e. the *Push-Pull* or *American* Method, also described by the above mentioned authors. In this case, tugs are made fast on short lines, at least one over the tug bow allowing the tug to easily push or pull. The indirect method of towing has also been suggested for the omni-directional stern drive tug also, as shown in Figure 1.4(b)

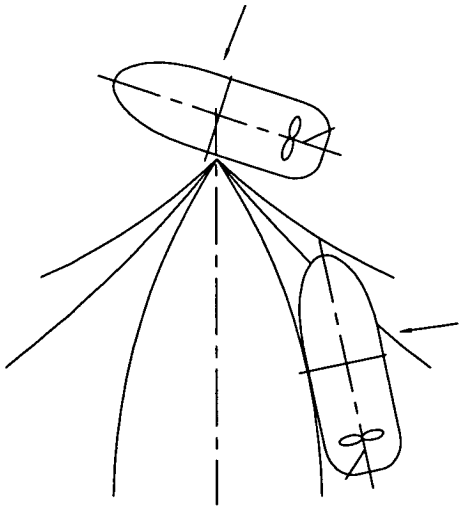

(a) Stemming

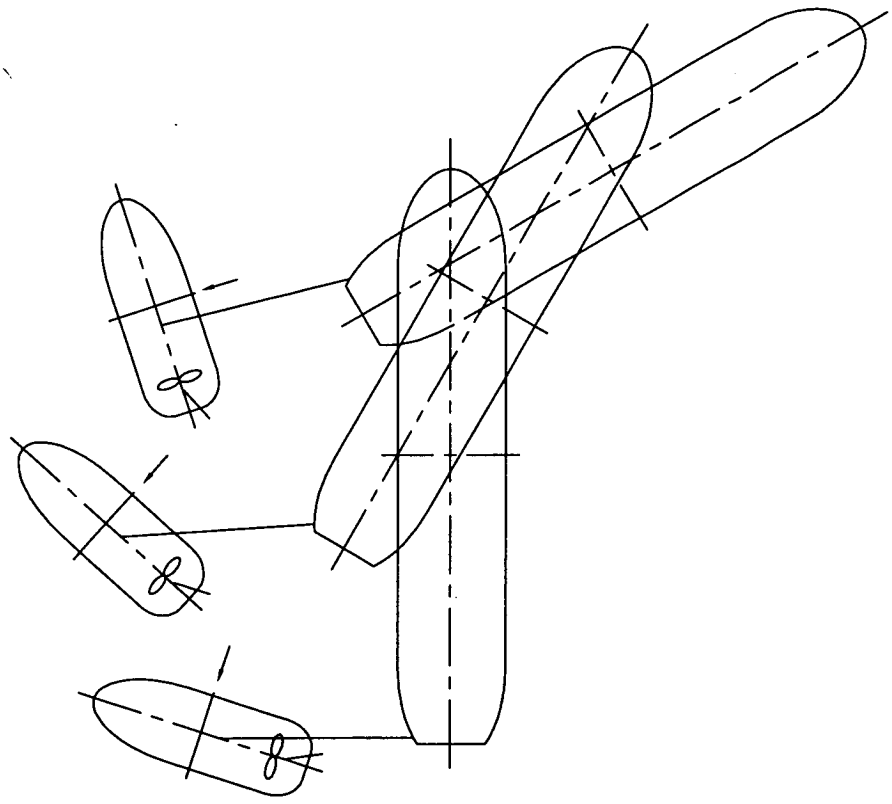

(b) Girting

Figure 1.3 Risk of Capsize with the Conventional Tug

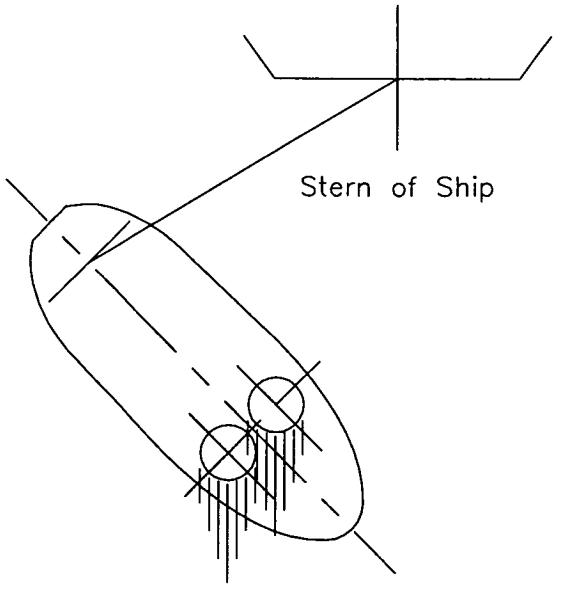

(a) Voith Water Tractor

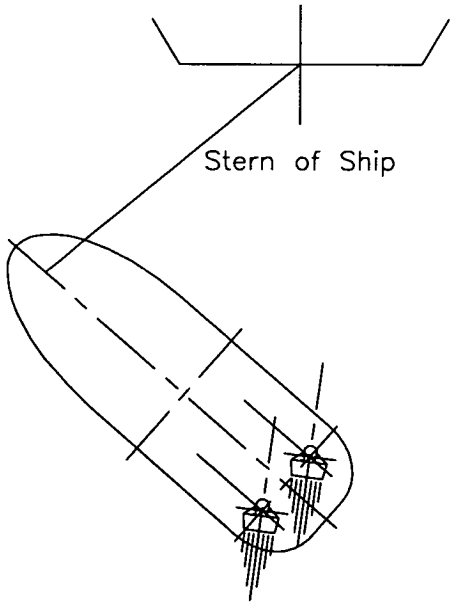

(b) Omni-directional Stern Drive Tug

Figure 1.4 The Indirect Towing Method

Tasker, 1988, through the course of simulation studies and industry consultation, identified the need for a more thorough understanding of the forces that tugs apply to a ship when underway, particularly omni-directional stern drive tugs. Tasker also discussed, in the context of the Port of Newcastle, the role of tugs in difficult pilotages. Further insight into this can be gained from simulated pilotages and the comparison of estimated tug forces with others acting on the ship. Figure 1.6 shows a simulated entry to Port Kembla which was carried out on the shiphandling simulator at the AMC. This pilotage consists of the approach to the harbour entrance, a 420m radius 90° turn in the outer harbour followed by entry to the inner harbour through a narrow cut where the ship is finally swung and berthed. At the harbour entrance, in addition to the low underkeel clearance, there may be wind, swell and current to contend with, further complicating the approach and turn. The speed of the ship at the entry and exit of the turn are important to both maintain control and at the same time reduce the ship's momentum to an acceptable value once inside the inner harbour. For this particular example no seastate or wind have been simulated, nor the current either inside or outside the harbour. The ship model used for the simulation is of a 180,000 tonne DWT post cape size bulk carrier in full load condition. The ship is 300m long, 50m beam and 15m draft which for this port gives a depth/draft ratio of 1.1. To initiate the turn at the harbour entrance, as shown in Figure 1.6(a), all tugs are operated at full power in addition to use of the rudder and the engine to increase the rudder's effectiveness. Three tugs are deployed, as shown in Figure 1.5, the starboard quarter tug providing steering forces, the starboard shoulder tug providing braking forces to reduce the way and maintain propeller race over the rudder and the tug on the centre lead aft providing a combination of these. The rudder is deflected to the full 35° and the engine order moved from dead slow ahead to half ahead as can be seen from Figure 1.6(b). Tug forces applied to the ship have been taken from estimates from Brandner and Renilson, 1994. To compare the effectiveness of the rudder and tugs, plots of sway forces and yaw moments due to each are shown in Figures 1.6(c) and (d) respectively. The magnitude of the forces and moments from the rudder and tugs are similar, as can be seen from Figures 1.6(c) and (d). It should be mentioned that the braking forces applied by the shoulder tug and aft tug contribute nothing to steering forces and enhance the steering force from the rudder. From Figure 1.6(b), it can be seen that following the ahead engine order there is an astern order to reduce speed which renders the rudder ineffective and therefore, the tugs must be relied upon for steering forces. From Figures 1.6(c) and (d), it can be seen that in terms of area under the curves, or sway and yaw momentum imparted, the tugs have indeed played a greater role than the rudder. Clearly, manoeuvring studies of this kind require not only a reliable hydrodynamic model of the ship, but also precise representation of the forces available from the assisting tugs.

Tasker, 1988, furthermore, detailed the need for a rigorous tug mathematical model to be included in the shiphandling simulator at the AMC. Mathematical models, as used in shiphandling simulators for determining ship motions and performance, are based on a modular structure, i.e., forces acting on the hull, propulsion, and appendages are evaluated separately. Interactions between these elements are likewise determined by separate algorithms. The success of the modular manoeuvring model is well documented, e.g. Dand, 1987 and Ankudinov et al., 1993 and, hence, is an appropriate concept for the development of a model for tug manoeuvring. As with ship manoeuvring, the flow field about the hull and thrusters

is considered largely beyond theoretical prediction methods and the majority of model inputs need to be determined from experimental data.

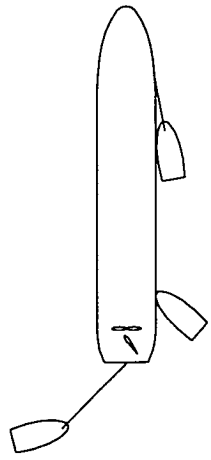

Figure 1.5 Tug Deployment for Simulated Entry to Port Kembla

In view of the preceding discussion the objectives of the present investigation may be defined as follows:

- perform model tests to identify relevant hydrodynamic phenomena and provide a basis for development of a physically motivated mathematical model;
- assemble the data required for the development of a mathematical model which may be solved using equilibrium and which may be extended to solution in the time domain, as may be desired for real time simulation;
- identify general performance of omni-directional stern drive tugs;
- identify optimum operating techniques; and
- identify the influence tugs have on ship motions in confined waters.

(a) Ship Trajectory

Figure 1.6 Simulated Entry of Post Cape Size Bulk Carrier to Port Kembla

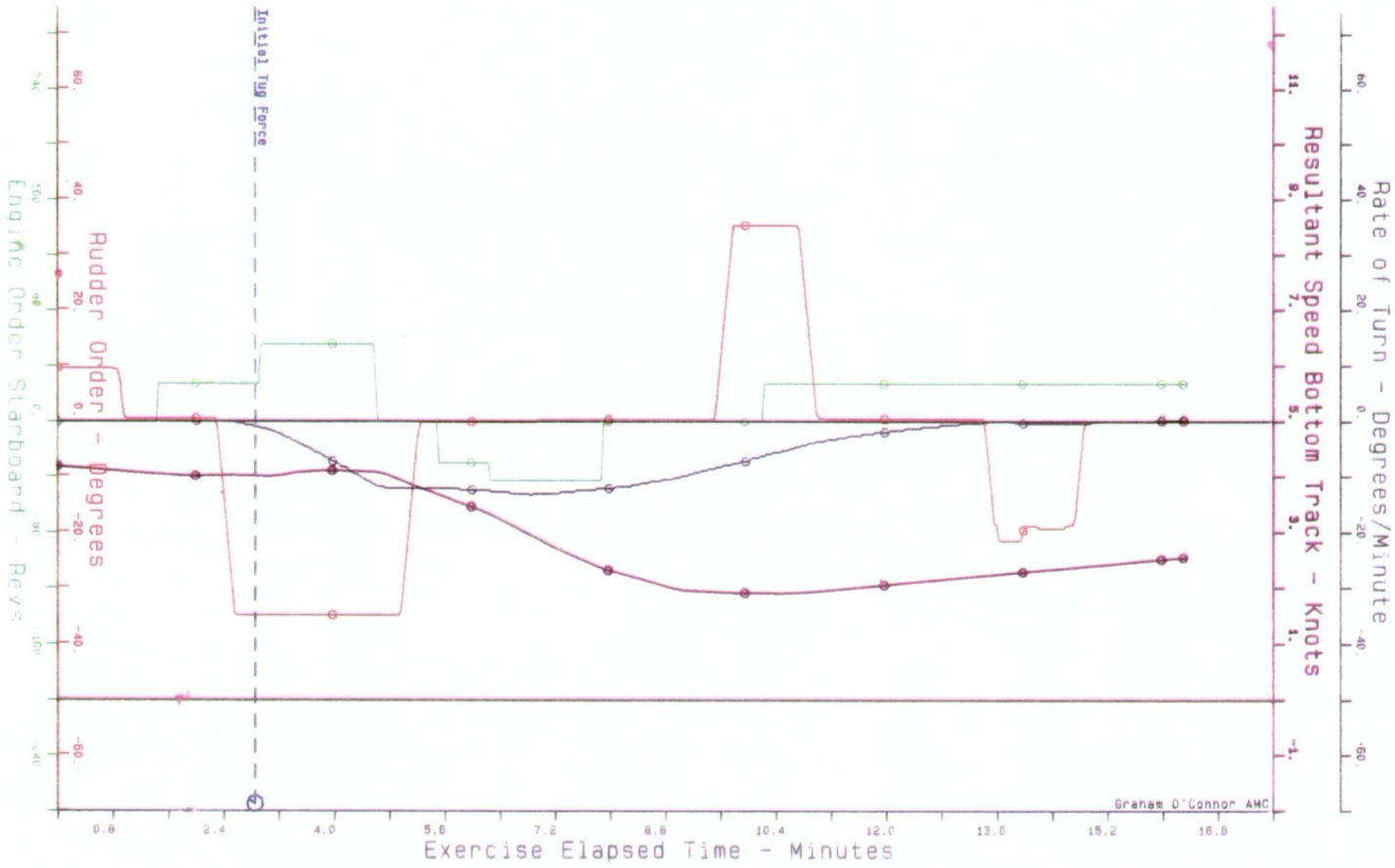

(b) Engine Order, Rudder Order, Speed and Rate of Turn

Figure 1.6 Simulated Entry of Post Cape Size Bulk Carrier to Port Kembla

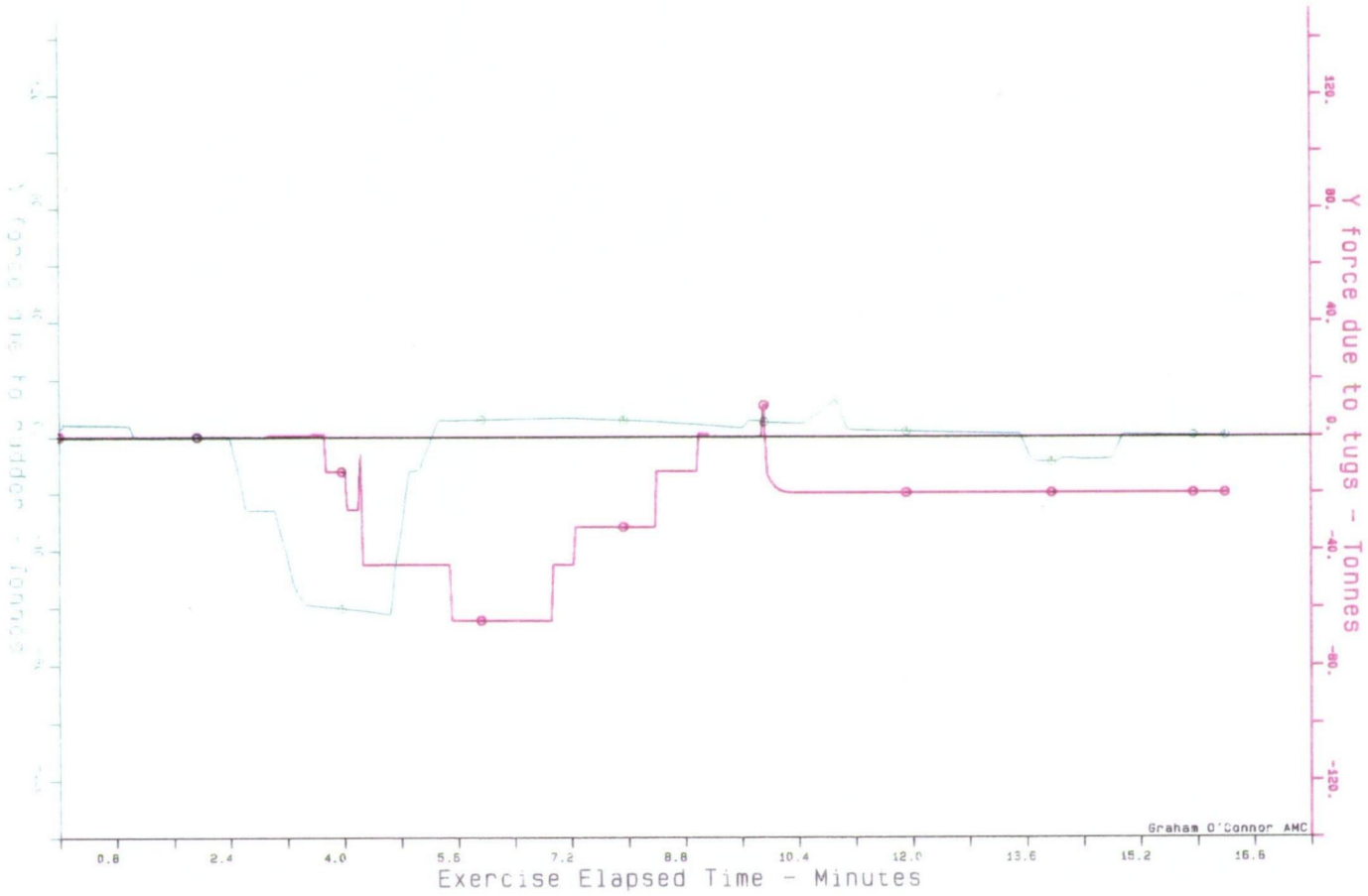

(c) Comparison of Sway Forces from Rudder and Tugs

Figure 1.6 Simulated Entry of Post Cape Size Bulk Carrier to Port Kembla

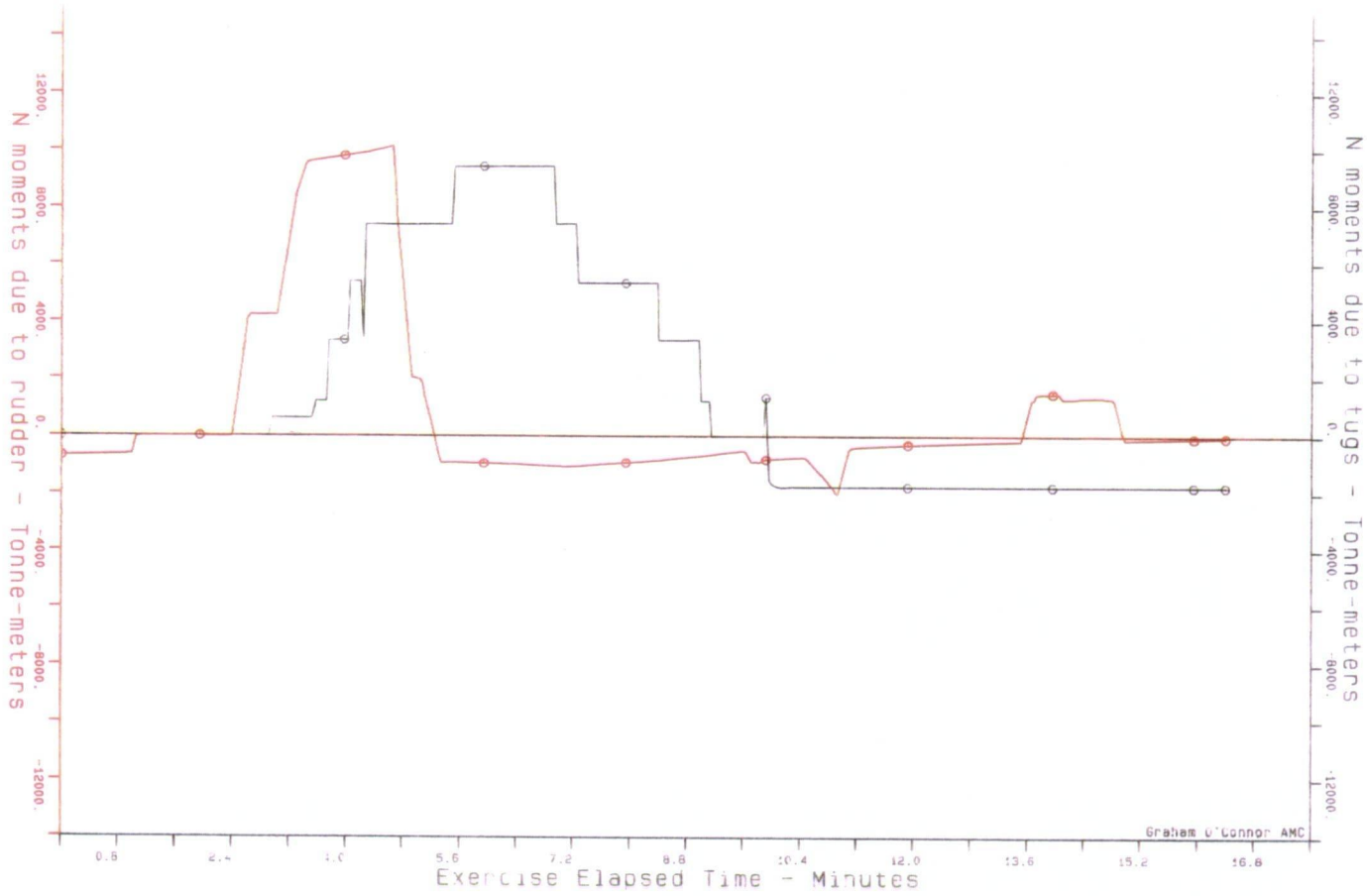

(d) Comparison of Yaw moments from Rudder and Tugs

Figure 1.6 Simulated Entry of Post Cape Size Bulk Carrier to Port Kembla

1.3 Tug Manoeuvring Model

Until recently, few formal mathematical models for simulation of tug forces have been developed. Tregardh, 1975, detailed the mathematical model used on the SSPA simulator for the effects of conventional tugs and Voith Water Tractors. Using basic tug parameters, simple representations for hull and propulsive forces are calculated from which the equations of motion for the tug are solved simultaneously with those of the ship. Also included are time delays and limits on operation. McIlroy et al 1981, describe the model used on the CAORF simulator, which has the capability to simulate conventional and all forms of omni-directional drive tugs. However, this model possesses some limitations, e.g. only one propulsive device can be modelled and the thrust must be in line with the tug's axis when pulling or pushing. Kose et al., 1987, using experimental data for forces acting on the hull and azimuthing thrusters of an omni-directional stern drive tug, presented static force predictions for operation in the pushing mode. Khattab, 1989, presented a four degree of freedom mathematical model similar to a traditional ship manoeuvring model for conventional twin screw tugs, intended for tug design and training. Static force predictions for omni-directional stern drive tugs have been presented by Renilson et al., 1992 and Brandner, 1992; the model developed uses general experimental data for hull and thruster forces and includes consideration of optimum combinations of thruster forces. However, experimental and theoretical investigations have since shown optimum thruster combinations are not of practical concern. More general predictions for omni-directional stern drive tugs with simple thruster combinations have been presented by Brandner and Renilson, 1994 and Brandner and Tasker, 1994. Ottoson, 1994, detailed the mathematical model for tug forces on the SSPA's PC based simulation package *PORTSIM* which can simulate the effects of conventional and all forms of omni-directional drive tugs. This model is similar to that presented by Tregardh, 1975, differing in that equilibrium is used to obtain tug forces rather than solution of the equations of motion.

In the wake of recent maritime disasters and an identified need for *escort tugs*, significant investigations into omni-directional drive tug performance at high speed have been carried out. These investigations employ a similar modular approach using experimental data for thrusters and hull as used by Kose et al., 1987 and Renilson et al., 1992. Detailed investigations have been carried out by Hutchison et al., 1993, into the capabilities of the Voith Water Tractor. This study centred around development of an enhanced Voith Water Tractor for escort duty. Investigations into stern drive and tractor tug capabilities for escort duty have been presented by Hendy and Freathy, 1993, where a dynamic model was used to examine the behaviour of the tug in extreme situations such as tug capsize. Predictions of stern drive tug performance have also been presented by Sas et al., 1993. Most recently, Gale et al., 1994, have presented some simple analyses and results from model tests for a modified omni-directional stern drive tug with bulbous bow to improve performance as an escort tug operating in the indirect mode.

Formulation of a quasi-steady mathematical model and methods of solution are considered in Chapter 2 and representation of hull and thruster forces and interactions are considered in the following chapters. As mentioned above, a number of models have been developed; however, few details of measured hull and thruster forces have actually been published and there has been little mention of interactions between the tug hull and thrusters. Results of investigations into interactions between ship hull and tug hull have been presented by e.g. Dand, 1975, Dand, 1977 and Kose et al.,

1 INTRODUCTION

1.1 Simulation of Ship/Tug Interaction

For some time, shiphandling simulators have been accepted as a tool for port design and development, training of marine pilots and development of port operational procedures. Tugs are frequently involved in such studies and exert forces on the ship of the same order as those from the environment and produced by the rudder and propeller. Hence, the precision with which the tug forces can be predicted will, to a large extent, control the precision of the simulation. Much work has been done to improve the prediction of forces from the environment and produced by the ship's rudder and propeller, Lewis, 1988. Less is known about the performance of tugs and what influence they have on ship manoeuvres.

A number of significant studies have been carried out where particular attention has been paid to the role of tugs and the critical nature of this aspect has been demonstrated. Ashburner and Norrbin, 1980, as part of the study into the widening and deepening of the Suez Canal, describe full scale trials and extensive real-time/fast-time simulations investigating the tug assisted stopping and handling of ships in the canal. This study considered various deployments of both *Voith Tractor* and stern drive omni-directional drive tugs (refer Figure 1.1) from which recommendations were made for safe handling techniques. The model used for simulation of tug effects was derived specially for this study and, although drawing on a range of work, was relatively simple. Dand, 1984, performed model experiments and simulations to investigate handling of disabled ships in severe weather with tugs. In this case, as is realistic, tug forces were assumed to be constant. Elzinga and Stuurman, 1986, describe how the MARIN simulator was used to determine whether disabled ships could be safely towed into Rotterdam-Europoort, and to develop procedures for handling such incidents. Van Maanen et al. 1987, used the SSPA simulator to investigate the influence of a windscreen on ship manoeuvring with tug assistance in the Caland Canal (Rotterdam). The tugs simulated in this study were Voith Tractors, the forces used were based on recommendations from Voith which were varied in accordance with tug masters present during the simulation. Bogaerts et al., 1987, describe an extensive simulation study investigating lock entry manoeuvres at Terneuzen. The effects of conventional tugs were simulated using a mathematical model based on equilibrium and supplemented by advice from interviews with tug masters.

In general, the procedures investigated in the above mentioned studies involved relatively straight forward tug manoeuvres at slow speeds. In most cases it is generally accepted that the tugs under consideration did not possess the displacement, power or manoeuvrability to render significant assistance at high speeds. In situations where large ships were handled, then large numbers of tugs were required. The simplicity of tug usage in many cases meant that great complexity in mathematical models for tug forces were not necessary and, in some cases, the experience of tug masters and pilots alone were used to realistically simulate the influence of tugs. However, a number of significant changes have occurred over the last ten years in the types of ships, the tugs being used to assist them and, consequently, the methods employed. This is particularly so in the context of many Australian operations.

1987. As discussed above, interactions between the ship hull and tug hull seriously affect the ability of the conventional tug to safely manoeuvre alongside the ship, particularly around the forebody. These problems are however, largely overcome with omni-directional stern drive tugs. Clearly, a tug operating in the pushing mode may be affected by such interactions although Kose et al., 1987, showed that the hydrodynamic forces acting on a tug hull at various drift angles and positions along the ship's side were generally unaffected by interactions. However, Kose et al performed their experiments in deep water only. Results of an investigation into interactions between the tug propeller race and ship hull have been presented by Dand, 1982, which showed that significant losses occur in operations of pulling a ship off a berth in shallow water. These interactions are of interest only at low speed as methods of tug deployment when underway, generally do not involve the propeller race being directed toward the ship hull. The interactions described above generally have only isolated affects on tug performance which may be avoided by appropriate tug deployment. Of interest generally are interactions between the thrusters and the thrusters and hull. The following discussion considers the available information on these interactions and, in view of this, what model tests were carried out at the AMC.

Due to the extreme proportions of tug hull forms, hydrodynamic hull forces cannot be obtained from regression equations and other information available in the literature for conventional ships. Of most importance are the forces due to pure sway (particularly at high drift angles) since this is the predominant motion performed by the tug when actually assisting the ship. Forces due to pure yaw and combined yaw and sway motions are important for general manoeuvring such as moving around the ship and position keeping. Kose et al., 1987, measured forces acting on an omni-directional stern drive hull form, including oblique towing tests for drift angles up to 90° and pure yaw, pure sway and pure yaw and constant drift angle PMM tests. Although the coefficients presented by Kose et al., are valuable, particularly for a dynamic manoeuvring model, they do not cover all drift angles and presumably yaw rate angles and their combinations. Khattab, 1989, calculated forces due to the full range of drift and yaw rate angles for a conventional twin screw hull form, although no results for combined sway and yaw motions where given. However, these forces may be of limited use due to differences in hull form between conventional and omni-directional stern drive tugs, involving changes in the afterbody to accommodate the thrusters and consequent redistribution of buoyancy. Further, Khattab has provided no experimental data to validate the calculations.

To determine more information on the forces acting on typical omni-directional stern drive hull forms, a series of oblique tests have been carried out in the towing tank at the AMC. Although these tests do not provide all the information needed for complete modelling, they do provide the most important data for sway motions at high drift angles from which static predictions have been made. These experiments and methods of determining and representing forces due to sway and yaw are described in Chapter 3.

A number of investigations into the performance of azimuthing thrusters have been carried out, mainly due to extensive applications on ocean exploration vessels utilising dynamic positioning systems and other vessels where enhanced manoeuvrability and position keeping capability are required.

Experiments were performed at MARIN, by Oosterveld and van Oortmerssen, 1972 and Oosterveld, 1973, to investigate the characteristics of an azimuthing thruster for the complete range of angles of attack and advance angles. These measurements were of a thruster fitted with a MARIN 19A duct and Ka 4-70 propeller. The 19A duct (among others) and Ka series screws were developed as a result of comprehensive systematic experiments performed at MARIN, Van Manen, 1954, 1957, Van Manen et al., 1959, 1966 and Oosterveld, 1970, 1972. This duct has a simple shape with straight outer profile and axial cylindrical form at the propeller location. The Ka series screws are characterised by Kaplan type blades for improved cavitation properties and flat faces and uniform pitch for simpler construction. Details of the 19A duct and Ka series screws are given in Appendix C.

A series of experiments performed at NSFI investigating azimuthing thruster characteristics also considered the effect of a large range of angles of attack and advance angles, Minsaas and Lehn, 1978. Virtually identical experiments to those of Oosterveld and van Oortmerssen were made for both pusher and tractor configured thrusters. The thrusters tested were fitted with a MARIN 19A duct and NSFI P-927 propeller.

Experiments performed at VBD, by Müller,1981, investigated the influence of a large range of angles of attack on open and ducted propellers. However, the range of advance angles investigated was not as extensive as that in the above mentioned studies. The thruster was fitted with VBD Simplified Duct No.2 and modified Wageningen B4.55 screw.

Other experimental results at a limited range of angles of attack and advance angles include Bussemaker and Corlett, 1971, van Leest and Bussemaker, 1976, and van der Made and Bussemaker, 1976, of which the last two are more applicable to dynamic positioning due to the small range of advance angles considered.

The data of Oosterveld and van Oortmerssen and Minsaas and Lehn is particularly suited for use in developing a mathematical model, since the thrusters tested are close to those used on omni-directional stern drive tugs and the experiments cover the complete range of operating parameters. These results do, however, exhibit some anomalies which are discussed in Chapter 4. As part of the present investigation, measurements of thruster forces have also been made at the AMC as part of a series to determine interactions and are compared with the above mentioned results.

Thrusters operating in close vicinity interact due to the induced velocity that each produces, resulting in each thruster operating at effectively higher advance angles with consequent loss of thrust. Vessels utilising dynamic positioning systems are generally fitted with groups of thrusters which have led to interaction phenomena being investigated for the case of low speeds and relatively large thruster spacings. English, 1975, discussed the nature of interaction between thrusters and experimental investigations have been carried out by Wise and English, 1975, English and Wise, 1975, van der Made and Bussemaker, 1976, Lehn, 1980 and Moberg and Hellstrom, 1983. Further work has also been presented by Van den Boom and Nienhuis, 1983, Nienhuis, 1986(1), 1986(2), Davison et al., 1987 and Nienhuis, 1992. Nienhuis, 1986(1) proposed a semi-empirical method for prediction of thruster interaction based on the assumption that the propeller race at some distance from the thruster behaves as a turbulent jet. Nienhuis, 1992, confirmed this assumption with LDV

measurements of the propeller race from thrusters and correlation of this method with experimental data has been reported by Davison et al., 1987.

Shiphandling tugs are relatively compact vessels with large installed power requiring proportionately large thrusters and, due to practical considerations, both thrusters are located at one end, resulting in extremely close spacing. The enhanced performance of omni-directional drive tugs has led to shiphandling operations being performed at high speeds in contrast to the low speed limitation of previous generation tugs. Hence, the nature of interaction between thrusters in this situation is considerably different to that described above for low speed and large thruster spacings. In this case, interaction depends on the influence of angle of attack and advance angle on propeller race velocity and trajectory and the extended flow field for both thrusters. Insight into the nature of this interaction can be gained from the behaviour of turbulent jets in a cross flow. Comprehensive reviews of the relevant literature on this subject are provided in Rajaratnam, 1976 and Schetz, 1980.

In conventional ship manoeuvring models, hull-rudder-propulsion interactions are of significant concern. The factors: thrust deduction and wake fraction, as used in resistance and propulsion studies, are commonly extended to manoeuvring studies. The first factor accounts for the difference in resistance between bare hull and that in the presence of the propeller (more properly resistance augmentation), the second, the difference in propeller operating condition between open water and behind hull. Harvald, 1967, performed experiments to measure the wake fraction and thrust deduction factors in the four quadrants of revolutions and ship speed for a large range of advance coefficients. Significant variations were found in each factor depending on the propeller loading, although, these were attributed, in part, to the definitions of the wake fraction and thrust deduction factors. Harvald's results were limited to the cases of 0 and 180° drift angle and 0 rate of turn; to include the effects of transverse velocity, other factors need to be introduced. The straightening effect the hull has on the flow into the propeller and rudder is accounted for with a flow straightening or flow rectification factor. For normal manoeuvring motion the influence of drift angle and rate of turn on the above mentioned factors have been investigated by Yumuro, 1975, Inoue et al., 1981 and Kose, 1982. Numerous other factors and coefficients are also defined for interactions, including the propeller operating in oblique flow, interaction between propeller and rudder and interaction between hull and rudder, etc. A number of these interactions have been investigated by Ogawa and Kasai, 1978, in addition to the above mentioned references.

When thrusters are used for combined steering and propulsion, somewhat different interactions between the hull and thruster can be expected, due to the greater complexity of the thruster induced flow and hull motions from the enhanced manoeuvrability. Vessels utilising dynamic positioning systems are generally fitted with groups of thrusters which has led to investigations into thruster-hull interaction as well as thruster-thruster interaction, as described above. Wise and English, 1975, and English and Wise, 1975, present results of an experimental investigation into thruster-hull interaction for a drill ship at zero and low speed. Significant interactions were found, however, since thruster forces where not measured, their precise magnitude could not be established. Similar investigations have been carried out by Norrby and Ridley, 1980 and Lehn, 1981. Moberg and Hellstrom, 1983, investigated thruster hull-interactions for a semi-submersible rig, finding significant interactions due to direct impingement of the race on the pontoons. Further

experiments into thruster-hull interaction have been carried out by Nienhuis, 1992, including single and twin hull-floaters and the influence of bilge shape.

To quantify interaction effects, an extensive series of model tests have been performed at the AMC. Initially, thruster forces were measured in the open water condition for one, then two thrusters, which enabled the effects of pure thruster-thruster interaction to be determined. The results from these experiments and a simple mathematical model for thruster-thruster interaction are presented in Chapter 5. One of the models used for the bare hull tests was then fitted with the thrusters used for the open water measurements and free running tests were performed, from which interaction between thrusters in the behind condition and the hull and thrusters could be determined. The effects of various interactions have been determined from these experiments and a simple mathematical model for interactions between the hull and thrusters is presented in Chapter 6.

Static force predictions for the complete range of practical modes of operation of an omni-directional stern drive tug have been presented in Chapter 7. Finally, this work has had a number of practical outcomes with regard to optimum tug operation and the influence tug forces have on ship motions, a summary of these results is presented in Chapter 8.

2 FORMULATION OF MATHEMATICAL MODEL

2.1 Introduction

To investigate fully the interaction of tugs with an assisted ship requires simultaneous solution of the equations of motion for both the tug(s) and the ship. Using this approach, dynamic effects such as time to move about the vessel, time to apply power and the possibility of line failure are accounted for precisely. This method requires not only the ship, but also the tug(s) to be controlled by a human (or controller) which is an advantage in that the human element is involved in the simulation. On the other hand, it can be argued that such human involvement is subjective in the absence of realistic perceptions and is costly in terms of manpower (particularly where multiple tugs are used) where the objective of simulation, in part, may be to reduce this requirement. Numerical solution of ship motions as well as those of a number of tugs is also costly in terms of computer power. Furthermore, for fast time simulation this approach introduces greater complexity in attempting to incorporate some form of artificial control.

The above discussed points are, in part, an issue of simulation and are somewhat beyond the scope of the present investigation. Clearly, an interactive *time domain* solution is the preferred method of modelling where extreme precision is required. However, differences between the dynamic response of the ship and tug are sufficiently large that, with respect to the tug, the ship may be regarded as an inertial frame. Therefore, while actually assisting the ship, tug perfomance may be derived from consideration of equilibrium. For the majority of simulation studies, *quasi-steady* forces derived for various speeds and modes of operation implemented with suitable delay or response times would be satisfactory. In view of this, only quasi-steady predictions of tug forces are considered as they are satisfactory for identifying general capabilities and fundamental interactions with other forces acting on the ship. As outlined in the objectives in Chapter 1, the representations developed in the present investigation are also intended to provide a basis for extension to a dynamic model.

2.2 Tug Equilibrium

In considering equilibrium of the tug, forces are assumed to be a result of the following contributions:

- reaction force from the ship;
- hydrodynamic forces acting on the tug hull;
- hydrodynamic forces acting on the thrusters; and
- hydrodynamic forces acting on hull and thrusters resulting from their interaction.

A number of studies investigating the effects of interactions between the ship hull and tug hull and the tug propeller race and ship hull have been carried out, as discussed in Chapter 1. As it was shown that generally these interactions have only isolated effects on tug performance hence, they are not considered in the present investigation.

The coordinate system and force representations for the tug are shown in Figure 2.1. The force imparted to the ship, either by pushing or pulling is represented in polar coordinates (F_{TUG}, χ) with respect to the free stream direction.

The angle of the tug with respect to the free stream direction or drift angle is defined in the usual way, as follows:

$$\beta_H = -\arctan\left(\frac{v}{u}\right) \tag{2.1}$$

where u and v are the surge and sway velocities respectively.

To establish equilibrium of the tug, forces in surge and sway and moments in yaw and roll are considered, hence, respectively, the following equations must be satisfied:

$$X_H + X_S + X_T = 0 \tag{2.1}$$
$$Y_H + Y_S + Y_T = 0 \tag{2.2}$$
$$N_H + N_S + N_T = 0 \tag{2.3}$$
$$K_H + K_S + K_T = -\Delta g GM \sin\phi \tag{2.4}$$

where the subscripts H, S and T denote contributions from the hull, ship and thrusters respectively. The contributions due to interactions between the thrusters and between the thrusters and hull are included in the respective terms. Forces and moments in heave and pitch respectively are small and may be ignored.

Initial investigations into the solution of equations 2.1 to 2.4 concentrated on a method by which equilibrium could be determined such that combinations of thruster forces are optimum. The method developed is presented in Renilson et al., 1992 and Brandner, 1992, and involves calculation of required thruster forces, given other forces acting on the tug from which the required thruster operating conditions were found. A similar method was also used by Hutchison et al., 1993, to calculate forces available from a Voith Schneider tractor tug designed for escort. This method is, however, computationally intensive and it was found that improvements in combined thruster forces that could be achieved were generally not significant and not compatible with a practical control system. Therefore, a simpler solution technique was developed which is essentially the reverse of the previous method. For a given velocity, tug drift angle, thruster angle and throttle setting, the force and moment elements contained in equations 2.1 to 2.4 are calculated according to the overall scheme listed below.

- From the given parameters, the operating point for each thruster is calculated including the influence of hull-thruster interaction and thruster-thruster interaction. Assuming a diesel prime mover with constant maximum torque and governing based on revolutions, the propeller revolutions for each thruster are varied until either maximum torque is reached or revolutions corresponding to those of the throttle setting are reached. Given the operating point for each thruster the forces and moments, X_T, Y_T, N_T, K_T, due to the thruster forces may be calculated.

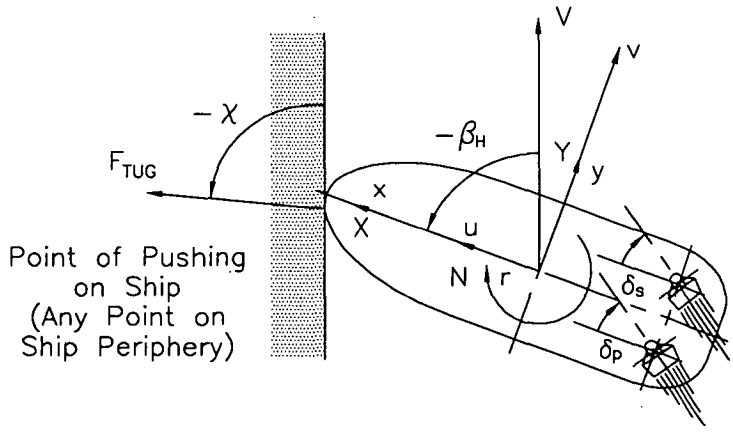

(a) Pushing

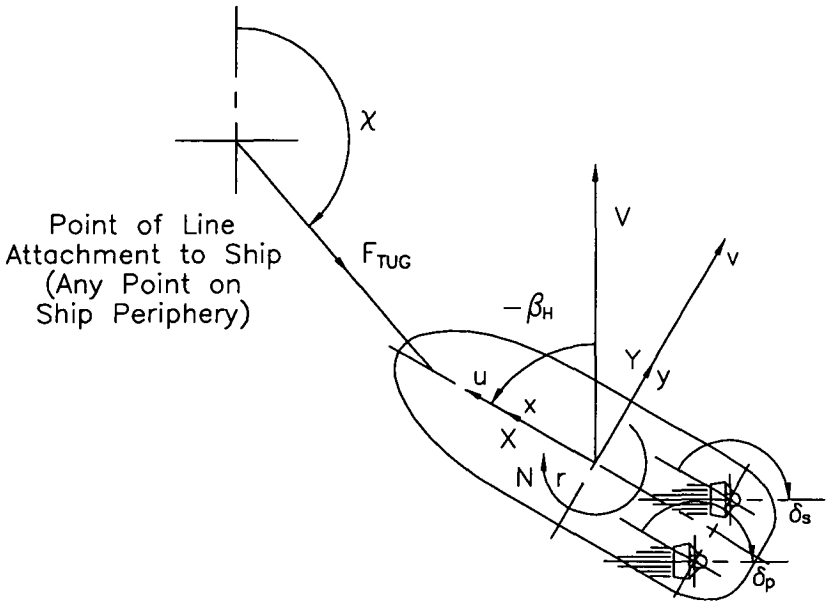

(b) Pulling

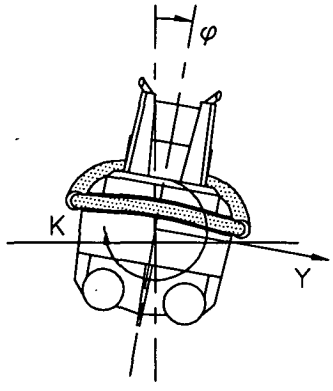

(c) View from Astern

Figure 2.1 Coordinate Systems and Force Representation

- From the given parameters and the thruster operating points, the forces and moments, X_H, Y_H, N_H, K_H, due to the hull forces, including the influence of the thrusters on the hull, may be calculated.

- from the above, the forces and moments, X_S, Y_S, N_S, K_S, due to the force at the tow point or point of contact may be calculated.

Equations 2.1 and 2.2 may be satisfied at any drift angle with the appropriate values of X_S, and Y_S, however, the resulting N_S which is a function of these forces may not satisfy equation 2.3. Hence, an iterative procedure is required to obtain the value of the drift angle, β_H, required to satisfy equation 2.3. Once equilibrium in the horizontal plane is established the roll angle ϕ required to satisfy equation 2.4 may be calculated. The validity of this position of equilibrium may then be determined against the following criteria:

- comparison of the angle of heel with predetermined limits; and

- if operating in the pulling mode, whether there is interference between the tug's line and superstructure.

To assist in determining how realistic a particular position of static equilibrium is, the mathematical model may be further used to assess the stability of a calculated position of equilibrium. That is, to determine whether given a small disturbance, such as might occur from swell, change in current or the ship's propeller race the tug will return to its previous or a new position of equilibrium or does it require continual control input from the tug operator. Figure 2.2 shows a tug in static equilibrium pulling off the port quarter. If given a disturbance then it may drift to non-equilibrium positions as shown. Also shown are the directions of the restoring moments required to return the tug to its original position with no movement of the thrusters or variation in engine revolutions needed. It can be seen for an increasing drift angle a negative moment is required and for a decreasing drift angle a positive moment is required. To determine the position of equilibrium a curve is constructed of the sum of the moments acting as a function of the drift angle, where this curve is zero is the drift angle corresponding to equilibrium. By considering the sign of the derivative, $\partial N/\partial \beta_H$, of the curve at the point of equilibrium it is possible to determine whether this position is stable or unstable. If the derivative is negative the equilibrium is stable, if it is zero it is neutral and if positive it is unstable. Further, the magnitude of the derivative indicates the magnitude of the stabilising/destabilising moment.

Using the method of equilibrium determination described above, any combination of thruster rotations and propeller revolutions may be used to determine equilibrium, as may be performed in reality. It has been found that equal angles of thruster rotation and propeller revolutions generally result in the combined thrust being close to optimum.

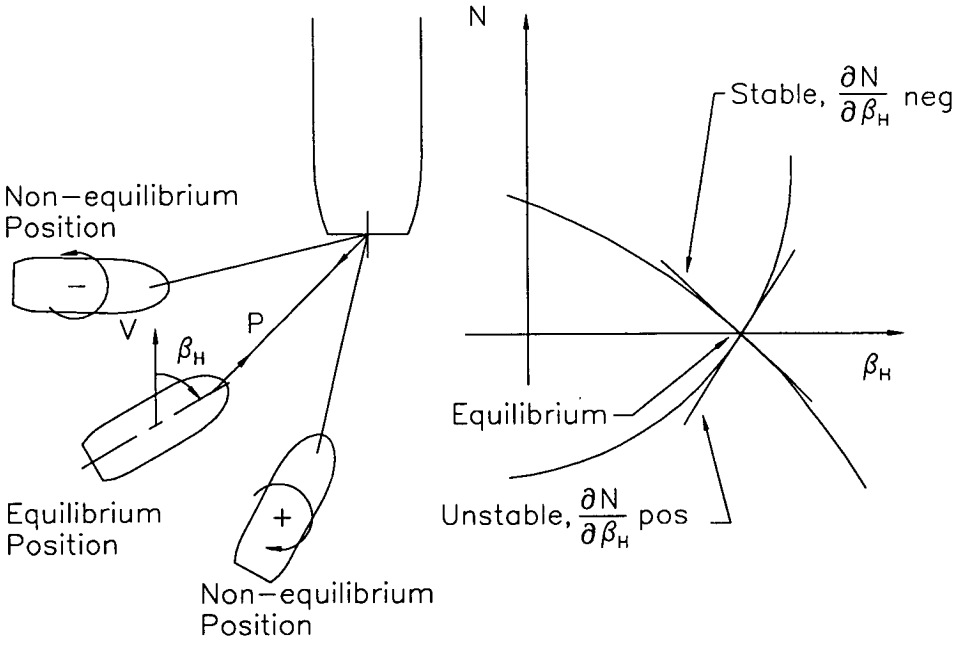

Figure 2.2 Stability of Equilibrium Position

Thruster forces and propeller torque are derived from open water thruster characteristics which are considered in detail in Chapter 4. The effective operating conditions for each thruster, due to interactions between thrusters and between hull and thrusters, are considered in Chapters 5 and 6 respectively.

Hull forces are calculated as the sum of two contributions, that is, forces that act on the bare hull for a particular operating condition and those that are the result of appended thrusters for the same operating condition. Forces acting on the bare tug hull are considered in Chapter 3 and those due to interactions between thrusters and hull are considered in Chapter 6.

The reaction force from the ship which balances that from the tug, may act at either a tow point position (if the tug is operating in the pulling mode) or at the point of contact on the bow fendering (for operation in the pushing mode) as shown in Figure 2.1. Omni-directional stern drive tugs generally operate using a tow point forward as mentioned in Chapter 1, although these tugs may also be operated conventionally using an aft tow point. Unlike the position of a tow point which remains fixed, the line of action of the reaction for pushing is not fixed but is a function of the angle between the tug and ship centre-lines. This also depends on the tug's bow fender profile. An elliptical bow fendering profile is assumed for this analysis. The influence of various methods of force transfer on tug performance is considered in detail in the following chapters.

The complete mathematical model is presented in Chapter 7 along with full scale force predictions for a typical Australian omni-directional stern drive tug. Force predictions are presented as polar diagrams of (F_{TUG}, χ) as shown in Figure 2.1 for various speeds and modes of tug operation.

3 HULL FORCES

3.1 Introduction

As discussed in Chapter 2, to investigate the capabilities of omni-directional stern drive tugs, surge and sway forces and yaw and roll moments need to be considered. The forces and moments resulting from pure sway are of most interest, since this is the predominant motion performed by the tug when actually assisting the ship. For quasi-steady predictions only damping forces and moments due to pure sway motions need to be considered. To cover all combinations of surge and sway velocities, forces may be considered a function of the drift angle, as defined by equation 2.1:

$$\beta_H = -\arctan\left(\frac{v}{u}\right) \tag{2.1}$$

where u and v are the surge and sway velocities respectively.

Limited data exists on forces acting on tug hulls for a range of drift angles. Results from oblique towing tests with an omni-directional stern drive hull form for drift angles up to 90° have been presented by Kose et al., 1987. The model used for these experiments was, however, only 0.5m in length (1:60 scale) introducing the possibility of significant errors due to scale effects. Calculated forces for a conventional twin screw hull form for the full range of drift angles have been presented by Kattab, 1989. There are considerable discrepancies between the data for each of these investigations and it is unclear to what degree these can be attributable to differences in hull form or the methods used to determine the forces. It is therefore uncertain whether the existing data could be applied to omni-directional stern drive hull forms typical of Australian tugs.

A series of oblique towing experiments have been performed at the AMC to examine in detail the forces acting on typical Australian tug hull forms. In these experiments the influence of a number of parameters were investigated as part of a program to measure hydrodynamic interactions between the tug hull and thrusters. General details of the experimental facilities and apparatus used at the AMC are given in Appendix B.

It should be mentioned that although the investigations of Kose et al., 1987, and Kattab, 1989, are limited for specific forces due to pure sway, they are of particular assistance in development of the range of forces that would be required for dynamic modelling. Kose et al., in addition to oblique towing tests, also performed extensive PMM tests with the tug model mentioned above. From these tests, added mass and damping coefficients for surge, sway and yaw were determined, however, the coefficients do not cover all regions of combined motion. Kattab, 1989, developed a dynamic model based on an earlier presented model, Kattab, 1987. This model adopted some of the concepts proposed by Oltman and Sharma, 1984, on *four quadrant* modelling of hull forces, which covers all possible combined sway and yaw motions. Oltman and Sharma proposed the representation of forces due to pure sway as a function of the drift angle, as defined by equation 2.1 and those due to pure yaw as a function of the yaw rate angle, defined as follows:

$$\gamma = \arctan\left(\frac{rL}{u}\right) \tag{3.1}$$

where r is the yaw rate and L is the length between perpendiculars. Oltman and Sharma also proposed an elegant method of determining the forces as the sum of contributions from ideal fluid effects, hull lifting effects and hull cross flow effects. Using a related approach, Kattab, 1989, presented forces not only for all drift angles, but also all yaw rate angles. However, the method proposed by Kattab, 1987, accounts for combined sway and yaw motions differently to that of Oltman and Sharma and no results were presented for such effects in Kattab, 1989. Finally, to include roll as a further degree of freedom, Kattab, 1989, used the method proposed by Hirano and Takashina, 1980, to account for the influence of combined sway, yaw and roll motions.

3.2 Oblique Towing Experiments

3.2.1 Experimental Matrix

Forces in surge and sway and moments in yaw and roll acting on a particular tug hull due to oblique motion, may be considered a function of the following parameters:

$$\left(X_H, Y_H, N_H, K_H\right) = f\left(\beta_H, F_n, \phi\right) \tag{3.2}$$

where, F_n is the hull Froude Number based on the length between perpendiculars and ϕ is the angle of heel. For omni-directional stern drive tugs, drift angles may vary between 0 and ±180° since the tug may operate running ahead $|\beta_H| \leq 90°$ or astern $|\beta_H| \geq 90°$. The latter, however, is considerably less common, for reasons of controllability discussed in Sections 6.2 and 7.2. Measurements were actually made at drift angles varying between 0 and ±180° at intervals of 10°. Positive and negative drift angles were tested to account for coupling effects between surge and sway force transducers and any hull asymmetries, from which, corrected results for $0° \leq \beta_H \leq 180°$ were derived. Omni-directional stern drive tugs may run at Froude Numbers approaching 0.4, however, when actually assisting a ship, this is reduced to around 0.25. Tests were performed at Froude Numbers covering the latter range to investigate the influence of wave-making on hull forces. For the present investigation, only small angles of heel consistent with practical operating limits are considered, up to 10°. Hence, forces and moments are assumed to be independent of the angle of heel.

The variation of hull forms of omni-directional stern drive tugs may be enough to significantly alter hull force characteristics. These changes are not, however, large enough to justify any systematic investigation. Armstrong, 1988, showed that for a collection of Australian tugs, the major hull form parameters, such as ratios of length, beam and draft and the block and prismatic coefficients varied within a relatively narrow band. To investigate the influence of hull form, two models have been tested. The first, of a 32m tug intended for combined harbour and offshore salvage work, and the second, of a more recent 30m tug intended for dedicated harbour work. Basic hull form parameters for each model in the condition tested are given in Table 3.1, where L, B and T are the length between perpendiculars, the moulded beam and draft

to the baseline respectively. The hull form coefficients C_B and C_∇ given in Table 3.1 are the block and volumetric coefficients respectively, defined as follows;

$$C_B = \frac{\nabla}{LBT} \tag{3.3}$$

$$C_\nabla = \frac{\nabla}{L^3} \tag{3.4}$$

The hull form parameters for these two models are sufficiently different for this class of vessel to provide an acceptable indication of the variation of hull forces with hull form.

Model	L/B	L/T	B/T	C_B	C_∇
32m	2.77	6.13	2.21	0.53	0.31
30m	2.61	6.37	2.44	0.43	0.29

Table 3.1 Hull Form Parameters for Tug Models

A further aspect of hull form is the draft or load condition at which the tugs operate. To investigate this, experiments have also been performed at displacements corresponding to possible operating extremes. These experiments were carried out on the 30m tug model only and were in even keel. Use of the 32m tug model is limited purely to assessing the influence of hull form on hull forces. The 30m tug model is also used for free running experiments with thrusters fitted and is the model referred to in Chapter 6. The experiments described in this chapter were carried out on bare hulls only. Details of the full scale vessels upon which the models are based and details of the hull forms for each model are given in Appendix A. The scale of both models is 1:25 which results in model sizes that can be practically tested for the full range of drift angles without incurring significant tank interference effects.

3.2.2 Experimental Results

Surge and sway forces and yaw moments were measured with the models free in pitch, heave and roll. It is assumed that the vertical centre of pressure of the sway force acts at the centroid of the underwater lateral profile area and is independent of the drift angle, thus, allowing calculation of the roll moment. To minimise roll, the models were ballasted to achieve the greatest possible metacentric height and the tow points were located as close as possible to the calculated vertical centre of pressure. The 32m tug model is of solid timber construction and consequently, it was not possible to achieve a large metacentric height and well located tow points constraining the tests that could be performed. However, as mentioned above, the purpose of these experiments is to assess the influence of hull form on hull forces and for this the 32m model is therefore satisfactory. The 30m tug model, being of composite construction, was easily ballasted and towed such that minimal heel resulted.

The coordinate system used to represent measured forces and moments is located at midships, as shown in Figure 2.1. The measured forces and moments have been non-dimensionalised using the following scheme for surge and sway forces and yaw moments respectively:

$$X'_H = \frac{X_H}{\frac{1}{2}\rho V^2 BT} \tag{3.5}$$

$$Y'_H = \frac{Y_H}{\frac{1}{2}\rho V^2 LT} \tag{3.6}$$

$$N'_H = \frac{N_H}{\frac{1}{2}\rho V^2 L^2 T} \tag{3.7}$$

and the non-dimensional longitudinal postion of the sway force may be approximated in the usual way;

$$e'_Y = \frac{e_Y}{L} = \frac{N'_H}{Y'_H} \tag{3.8}$$

The reference areas used in equations 3.6 to 3.8 are combinations of L, B and T corresponding to the relevant profile areas. The use of these reference areas provides assistance in assessing the influence of variations in the ratios of L, B and T on non-dimensional forces, although the difference in reference areas must be considered in comparing the magnitudes of X'_H and Y'_H.

The results are presented in Figures 3.1, 3.2 and 3.3, as a function of the drift angle with either the draft fixed and the Froude Number a parameter, or the Froude Number fixed and the draft a parameter. Results from tests on the 32m tug model are presented in Figure 3.1. As mentioned above, no experiments with different drafts were performed with this model. Results from tests on the 30m tug model are presented in Figures 3.2 and 3.3, for fixed draft and fixed Froude Number respectively.

The coefficients have been corrected for skin friction according to the ITTC standard method for resistance correction, assuming the skin friction vector is independent of the drift angle, that is, equal always to that for zero drift angle and acts always opposite to the direction of motion. This correction has a negligibly small effect on the sway coefficients, but a large effect on the surge coefficients at small drift angles and has been applied to ensure correct resistance values. Stimulation of turbulent flow over the models was created by cylindrical studs attached along stations both toward the stem and stern to ensure stimulation irrespective of whether the stem or stern is the leading edge. The stations where studs were attached are approximately 10% of the waterline length from the respective intersections of the stem and transom with the waterline. Studs were also attached toward the trailing edge of the skeg to maximise turbulence stimulation when the stern is the leading edge. The dimensions of the studs are 3mm diameter by 3mm length and where attached at 20mm centres. The drag of the studs has been ignored since this is negligible compared with the measured forces. This can be shown from consideration of the stud profile area and typical drag coefficients. The minimum Froude Number tested is approximately 0.11. Below this value the results become inconsistent which, most likely, can be attributed to scale effects due to low hull Reynolds Number. The Reynolds Number, based on the length between perpendiculars, corresponding to this Froude Number is approximately $R_{nH} = 4.3\times10^5$ below which such effects can be expected.

3.2.3 Discussion of Results

From Figure 3.1 it can be seen that for each Froude Number not all drift angles could be tested due to the limitation of heel for the 32m tug model mentioned above. However, in reality the majority of tugs may be somewhat limited in drift angles that can be maintained at the higher Froude Numbers due to heel angle limitations. A large range of Froude Numbers have been tested and, as can be seen from Figure 3.1, with only minimal influence on the measured coefficients. From this it can be concluded that the influence of the Froude Number can be ignored for the range of speeds appropriate to ship assist operations. On this basis the 30m tug model has been tested over a smaller range of Froude Numbers, as shown in Figure 3.2. Once again, it can be seen that the Froude Number has only minimal influence on the measured coefficients. As the results are essentially Froude Number independent, results for a typical Froude Number of 0.18 are chosen as the basis for calculation of hull forces used later in Chapters 6 and 7. The experimental data points are used directly in the mathematical model. Intermediate points are calculated using polynomial interpolation. The data could, of course, be represented using functions such as a Fourier series or a formal hydrodynamic model in four quadrants as suggested by Oltman and Sharma, 1984.

The influence of hull form on hull forces can be assessed by comparing the results from the tests on the 32 and 30m tug models. The surge force coefficient, X'_H, for both models varies considerably as a function of drift angle, demonstrating the effects of significant fore-aft asymmetry characteristic of omni-directional stern drive hull forms. There are clear differences between X'_H for each model, particularly in the range $40° < \beta_H < 140°$ which demonstrates the sensitivity of surge forces to changes in hull form at high drift angles where the flow is fully separated. From the results, it can be seen that generally the surge force coefficients are small compared with the sway force coefficients. The former is derived using a reference area of BT whereas the latter is derived using a reference area of LT which is greater by a factor of the L/B ratio, as listed in Table 3.1, indicating surge forces are significantly smaller than sway forces. Hence, surge forces may be considered important only for resistance and for the purposes of manoeuvring prediction, these differences may be ignored.

The sway force coefficients for each model are quite similar for the full range of drift angles. Unlike the smooth lifting characteristics of slender hull forms, two discontinuities are apparent, reflecting stall for when the stem is the leading edge and when the stern is the leading edge. The former occurs at approximately $\beta_H = 50°$ and $\beta_H = 60°$ for the 32 and 30m tug models respectively and the latter occurs at approximately $\beta_H = 120°$ for both models. The coefficients for the 32m tug model are greater than those for the 30m tug model throughout, particularly at high drift angles, although the differences may be regarded as small. The yaw moment coefficients for the 32m tug model are somewhat greater than those for the 30m tug model for the full range of drift angles. Given the similarity in sway force coefficients, this indicates that the non-dimensional centre of pressure for the 32m tug model is further away from midships than for the 30m tug model. This is apparent from Figures 3.1(b) and 3.2(b) particularly at small drift angles. From this quantity of data, it is not possible to establish any relationship between the variation of yaw moments and the hull form parameters. As the models tested represent significantly different hull forms for this type of vessel, it could be expected that yaw moments for typical hull forms would be within the range measured. Therefore,

satisfactory estimates of yaw moments for a typical hull form could be determined from mean coefficients interpolated from the data of both models.

Comparison of the results from each of the tug models demonstrates the influence of hull form on hull forces for normal operating drafts or load conditions. The influence of draft corresponding to extremes of loading condition on hull forces can be seen from Figure 3.3. The variations in all the coefficients are small, particularly when compared with those due to the different hull shapes. Therefore, the influence of loading condition for even keel can realistically be ignored. From the results, it can be concluded that, in general, variations in hull form typical of this type of vessel and those due to variation of load condition are not sufficient to introduce significant changes in the hull force coefficients used here. That is, non-dimensionalising the measured forces using combinations of L, B and T corresponding to the relevant profile areas is satisfactory in accounting for expected changes in the ratios of these parameters. Therefore, generic predictions of hull forces can be determined from the measured coefficients for hull forms with parameters similar to the models tested.

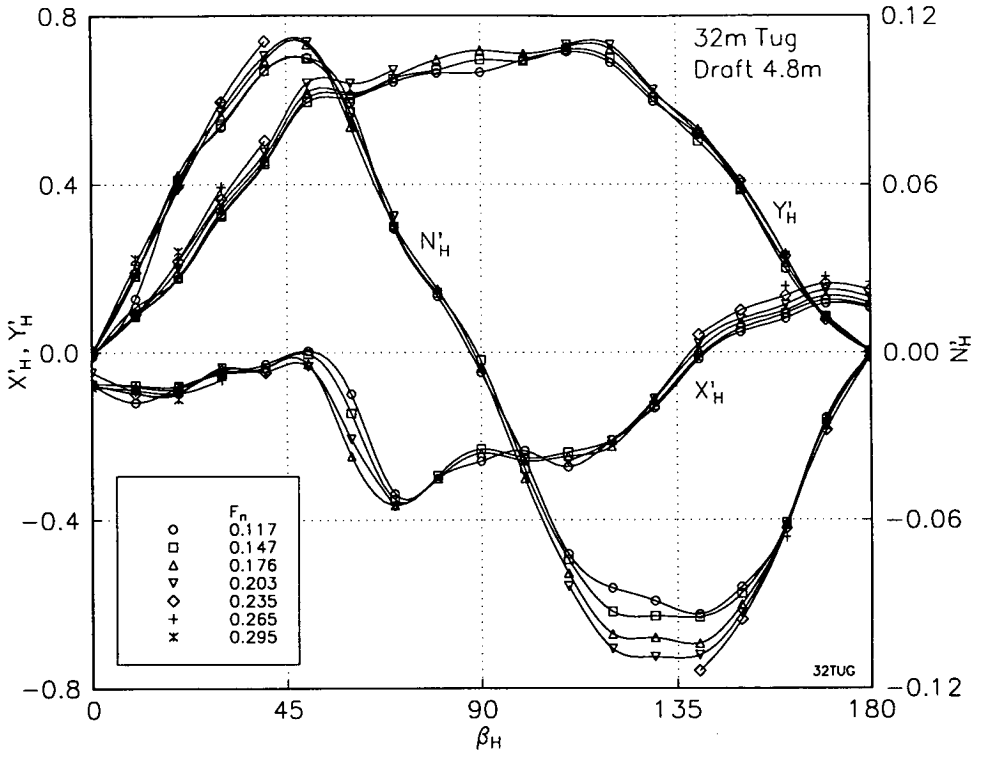

(a) Surge, Sway and Yaw Coefficients

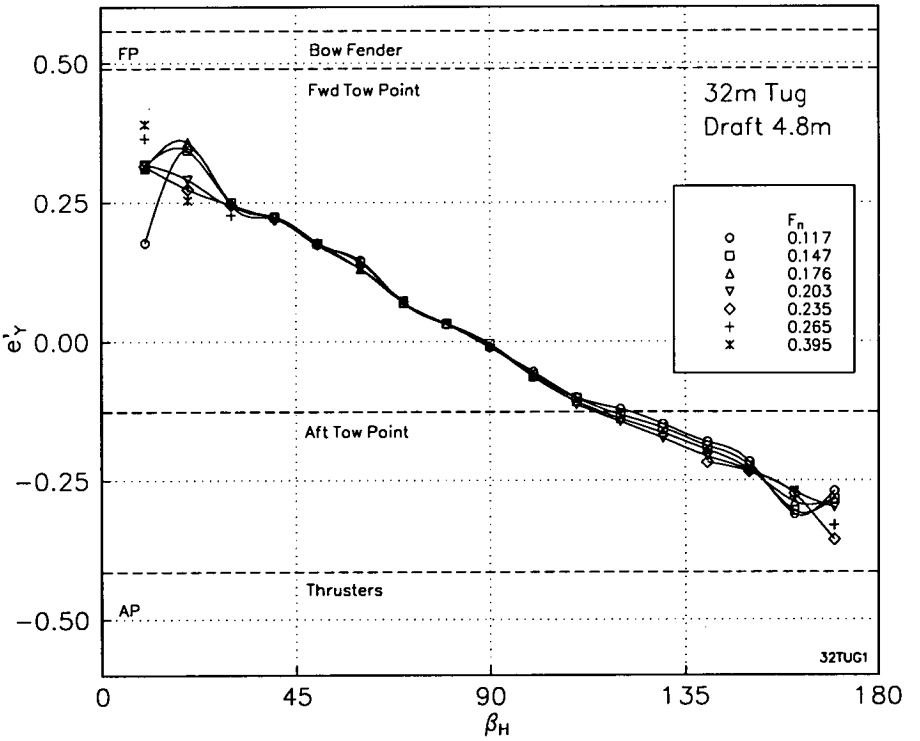

(b) Longitudinal Position of the Sway Force

Figure 3.1 Measured Hull Force Characteristics for 32m Tug Model as a Function of the Drift Angle with Froude Number a Parameter and Fixed Draft.

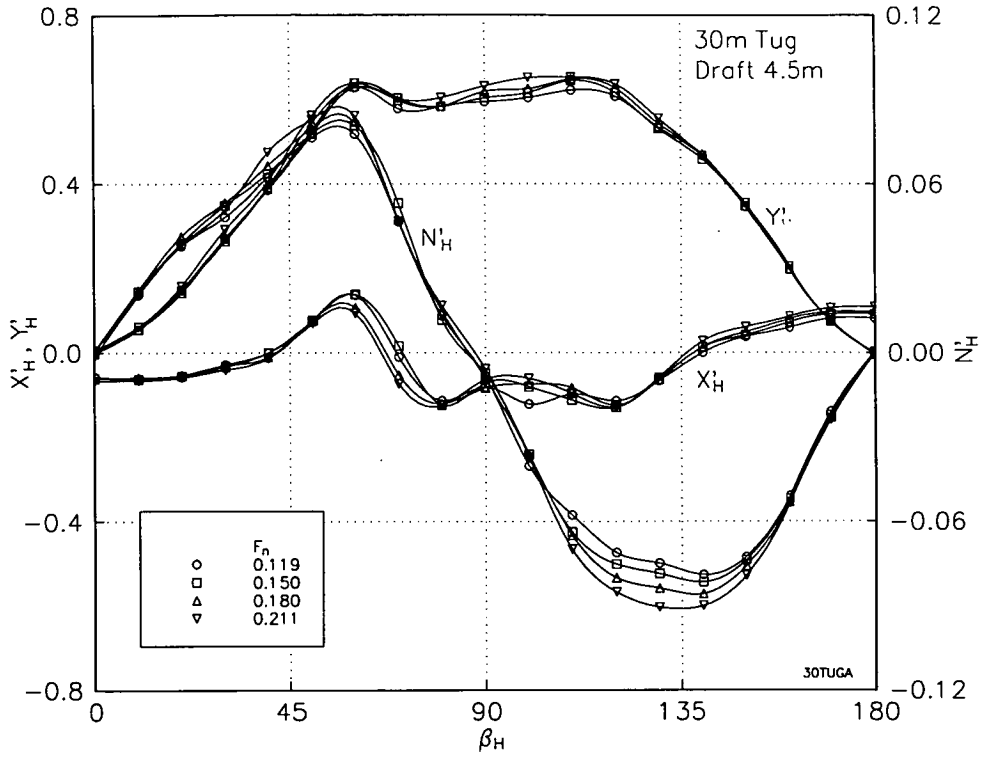

(a) Surge, Sway and Yaw Coefficients

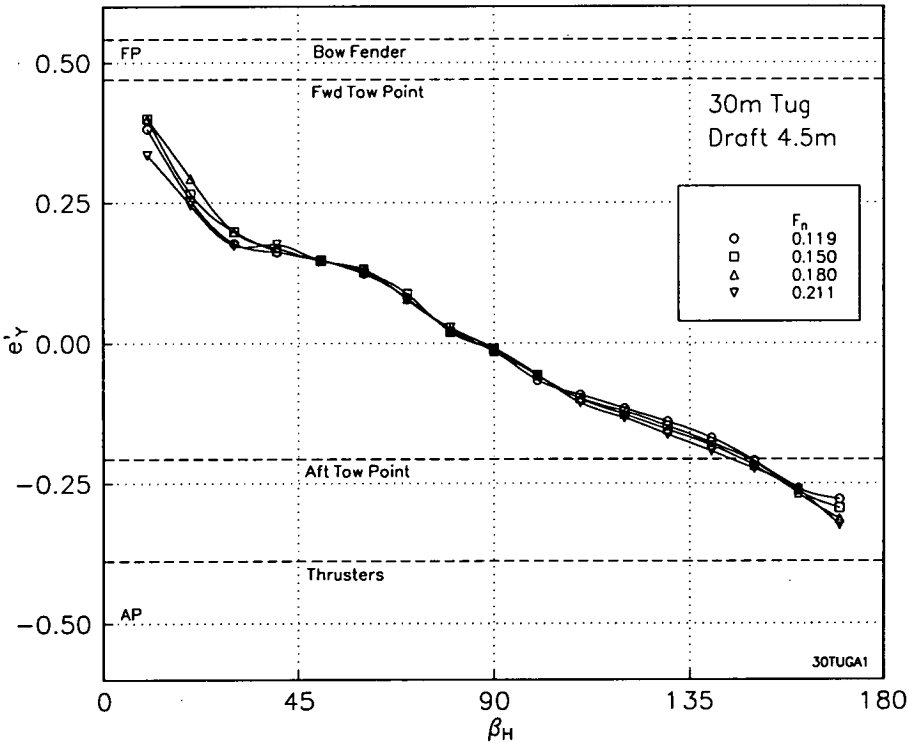

(b) Longitudinal Position of the Sway Force

Figure 3.2 Measured Hull Force Characteristics for 30m Tug Model as a Function of the Drift Angle with Froude Number a Parameter and Fixed Draft.

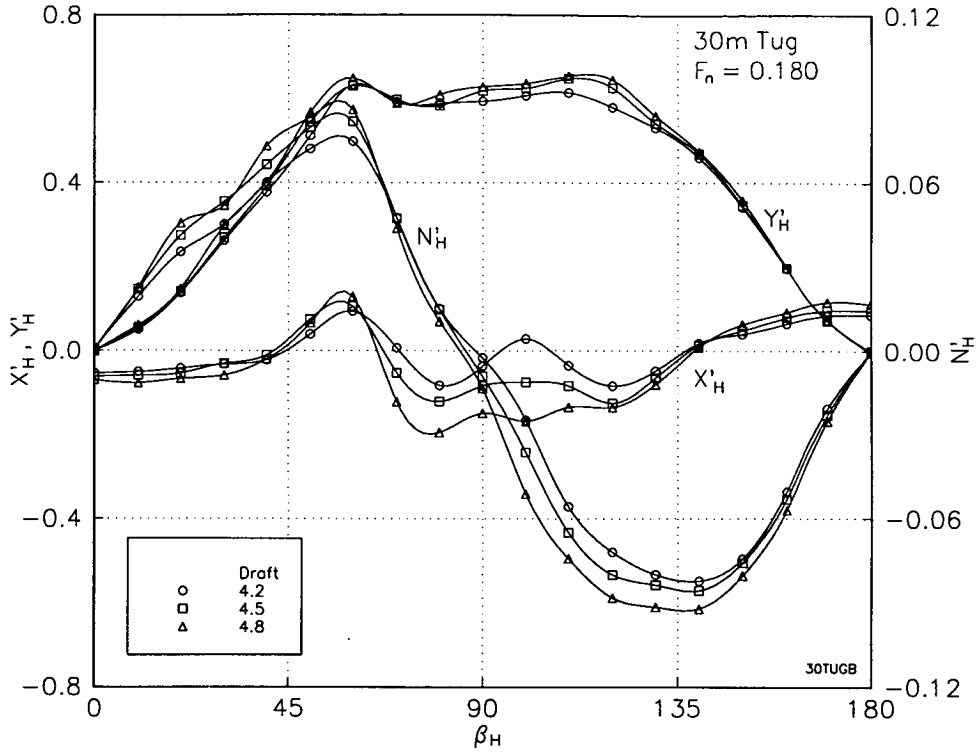

(a) Surge, Sway and Yaw Coefficients

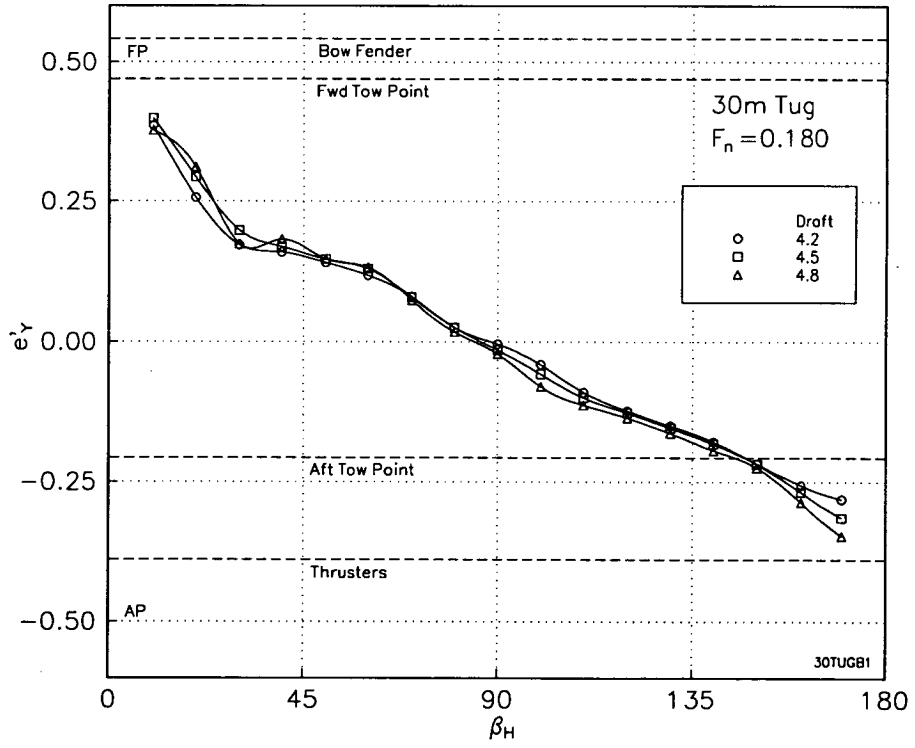

(b) Longitudinal Position of the Sway Force

Figure 3.3 Measured Hull Force Characteristics for 30m Tug Model as a Function of the Drift Angle with Draft a Parameter and Fixed Froude Number.

4 THRUSTER FORCES

4.1 Introduction

Two types of thrusters are employed as the major propulsion on omni-directional drive tugs, namely *azimuthing thrusters* and *vertical axis thrusters*. A general description of the mechanics and construction of each type is presented in Chapter 1. As mentioned in Chapter 1, the present investigation essentially concentrates on performance of azimuthing thrusters due to the proliferation of tugs fitted with this type of thruster in Australia. There is very little information available in the literature on the performance of vertical axis thrusters and they are fitted to very few tugs hence, a detailed study into their performance is considered beyond the scope of this investigation.

For a thruster operating in open water, forces and moments in the horizontal plane and propeller torque may be considered a function of the following parameters:

$$(X, Y, N, Q) = f(\beta_P, \theta, P) \tag{4.1}$$

The propeller pitch P is usually defined at 0.7 of the radius as shown in Figure 4.1. The propeller advance angle β_P is derived from the speed of advance V_A and the blade velocity at 0.7 of the radius as shown in Figure 4.1, i.e.:

$$\beta_P = \arctan\left(\frac{V_A}{0.7\pi n D_O}\right) \tag{4.2}$$

The thruster angle of attack θ is defined in the coordinate system as shown in Figure 4.2. In the case of zero angle of attack, forces, moments and propeller torque in non-dimensional form are essentially only dependent on the advance angle and pitch. For thrusters operating in oblique flow they are also a function of the angle of attack. Thruster characteristics may be considered a function of the advance angle with the angle of attack a parameter. However, at non-zero angles of attack the advance angle is intended only to represent the relative magnitudes of V_A and $0.7\pi n D_O$ and clearly loses any physical meaning with regard to flow/blade relative velocity that it has at zero angle of attack. Further simplifications may be made to Equation 4.1 and are discussed in the following sections.

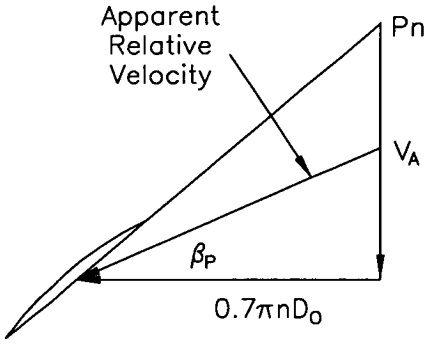

Figure 4.1 Propeller Pitch Ratio and Advance Angle for Zero Angle of Attack

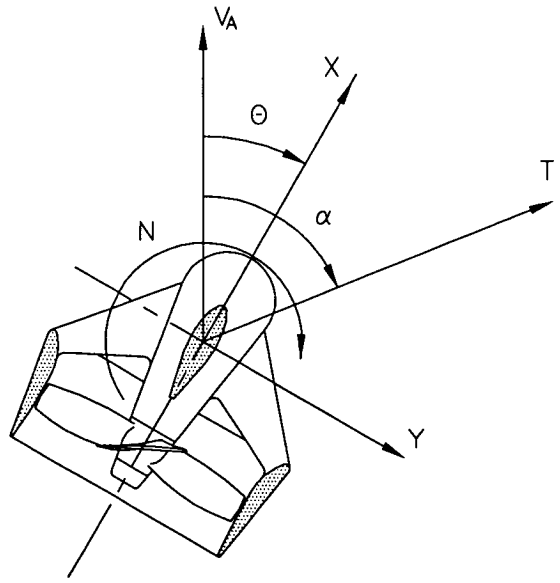

Figure 4.2 Rectangular and Polar Coordinate Systems

Due to the complex nature of the flow field about thrusters in oblique flow, theoretical methods of propeller analysis have, to date, generally not proven adequate in predicting characteristics. Dewhurst, 1972, developed an empirical model for azimuthing thruster forces by considering individual hydrodynamic forces from impeller, nozzle and gear-case, etc. This model, primarily intended for design of dynamic positioning systems, is limited in its application to a small range of advance angles. Dewhurst suggested values of the advance coefficient J of between 0 to 0.3, i.e. advance angles between 0 to 7.8°. Oosterveld and van Oortmerssen, 1972 and Oosterveld, 1973, attempted to represent the characteristics of a thruster by extrapolating a Fourier series representation of four quadrant measurements for the same duct and propeller. Using this approach, it is not possible to predict thruster side force and turning moment and is only intended for small angles of attack up to 30°. For the purposes of tug performance prediction, Hendy and Freathy, 1993, have developed a mathematical model for vertical axis thrusters applicable to the complete range of steering angles and advance angles. This model is an extension of the theoretical method for zero steering angle developed by Zhu, 1981. Hendy and Freathy have, however, only validated this approach with limited experimental data. In order to predict tug performance, particularly in the time domain, it is desirable that thruster characteristics be known for the complete range of angles of attack and advance angles, i.e. $0° \leq \theta < 360°$ and $0° \leq \beta_P \leq 90°$ respectively. For the present study, thruster characteristics have been developed directly from experimental results which are discussed in the following sections.

Experiments performed at MARIN, by Oosterveld and van Oortmerssen, 1972 and Oosterveld, 1973, investigated the characteristics of an azimuthing thruster for the complete range of angles of attack and advance angles. These measurements were of a thruster fitted with a MARIN 19A duct and Ka 4-70 propeller (details of the 19A duct, Ka series screws and the thruster tested are given in Appendix C).

A series of experiments performed at NSFI, by Minsaas and Lehn, 1978, investigating azimuthing thruster characteristics also considered the complete range of angles of attack and advance angles. Virtually identical experiments to those of

Oosterveld and van Oortmerssen where made for both pusher and tractor configured thrusters. The thrusters tested where fitted with a MARIN 19A duct and NSFI P-927 propeller (details of the P-927 screw and the thruster tested are given in Appendix C).

Most modern thrusters used on tugs and other vessels are fitted with MARIN 19A ducts (or very similar) and MARIN Ka series screws (or derivations of these) particularly in the Australasian region. This makes the results of Oosterveld and van Oortmerssen, and Minsaas and Lehn applicable in attempting to create a mathematical model for azimuthing thruster performance. A discussion of results from these experiments, and others performed at the AMC as part of the present study is given below. Experimental results are non-dimensionalised using the following coefficients:

Longitudinal force coefficient
$$C'_X = \frac{X}{\frac{1}{2}\rho A_0\left[V_A^2 + (0.7\pi n D_0)^2\right]} \tag{4.3}$$

Transverse force coefficient
$$C'_Y = \frac{Y}{\frac{1}{2}\rho A_0\left[V_A^2 + (0.7\pi n D_0)^2\right]} \tag{4.4}$$

Total force coefficient
$$C'_T = \frac{T}{\frac{1}{2}\rho A_0\left[V_A^2 + (0.7\pi n D_0)^2\right]} \tag{4.5}$$

Moment coefficient
$$C'_N = \frac{N}{\frac{1}{2}\rho A_0 D_0\left[V_A^2 + (0.7\pi n D_0)^2\right]} \tag{4.6}$$

Torque coefficient
$$C'_Q = \frac{Q}{\frac{1}{2}\rho A_0 D_0\left[V_A^2 + (0.7\pi n D_0)^2\right]} \tag{4.7}$$

These coefficients have the advantage that they are defined for all values of β_P, unlike the standard K_T, K_Q coefficients which use only the propeller revolutions n and hence are undefined when $n = 0$ ie, $\beta_P = 90°$.

4.2 MARIN Open Water Experiments

To fully define the characteristics of propellers operating in axial flow four combinations of advance velocity and revolutions need to be considered, i.e. four quadrants are usually defined, as follows:

- 1st quadrant V_A positive, n positive $0° \le \beta_P \le 90°$;
- 2nd quadrant V_A positive, n negative $90° \le \beta_P \le 180°$;
- 3rd quadrant V_A negative, n negative $180° \le \beta_P \le 270°$; and
- 4th quadrant V_A negative, n positive $270° \le \beta_P \le 360°$.

Oosterveld and van Oortmerssen, 1972, used this approach to represent measured thruster characteristics. In the case of a thruster, the propeller only rotates in one direction thus, only two quadrants need be considered, i.e. the advance angle was varied in the range $-90° \le \beta_P \le +90°$ corresponding to the first and fourth quadrants. This then requires the thruster to be rotated to angles of attack in the range $0° \le \theta \le \pm 90°$. Oosterveld and van Oortmerssen tested angles of attack in the range $0° \le \theta \le -90°$. In order to account for the influence of direction of propeller rotation, angles of attack in the range $0° \le \theta \le +90°$ would also need to be considered.

Measurements for a range of positive angles of attack were also made and it was concluded that the influence of the direction of propeller rotation was negligible. These results are presented in Figures 4.3 to 4.6. Measurements of longitudinal force, transverse force, turning moment and propeller torque are presented as functions of the advance angle with the angle of attack as a parameter. Longitudinal and transverse forces were corrected for the open water resistance of the surface piercing strut used to tow the thruster.

A propeller or thruster operating in the first quadrant ($0° \leq \beta_P \leq +90°$, $0° \leq \theta \leq \pm 90°$) is often termed to be operating in *positive* flow conditions and in the case of the fourth quadrant ($0° \leq \beta_P \leq -90°$, $0° \leq \theta \leq \pm 90°$), *negative* flow conditions. Positive flow conditions are characterised by small blade angles of attack and, hence, low torque. Conversely, negative flow conditions are characterised by large angles of attack and high torque, with the possibility of stall and unsteady flow. Figure 4.7 shows blade velocity diagrams for positive and negative flow conditions at zero thruster angle of attack, demonstrating the above mentioned points. The velocities V_a and V_t which are added to the advance and blade velocities, as shown in Figure 4.7, represent induced velocities in the axial and tangential directions respectively. Modern tug thrusters operate frequently in the negative flow condition for a range of angles of attack, making this of particular interest. In this condition there exists not only the possibility of blade stall, but also separation of flow from the duct, gear-case, strut and duct supporting fins. The unsteady nature of such a flow field can create further thrust and torque fluctuations in addition to those from the cyclic variation of blade angle of attack. Negative flow conditions also significantly influence interaction between propeller and prime mover which is considered in Chapters 2 and 7.

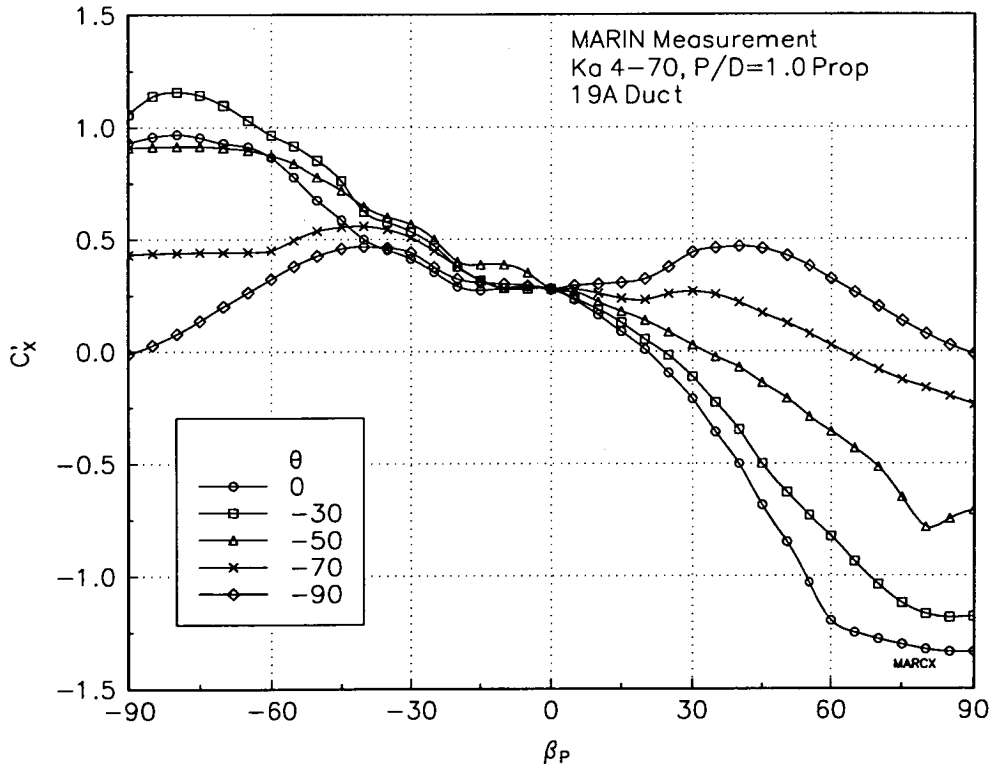

Figure 4.3 MARIN Experiments, Longitudinal Force,
from Oosterveld and van Oortmerssen, 1972

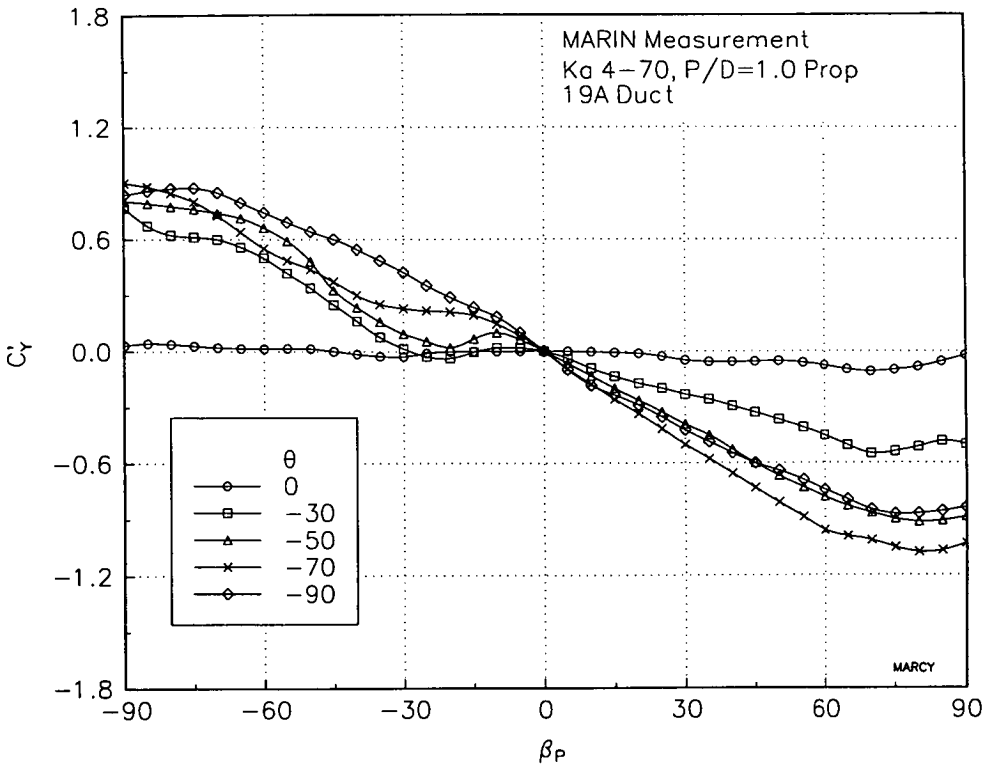

Figure 4.4 MARIN Experiments, Transverse Force,
from Oosterveld and van Oortmerssen, 1972

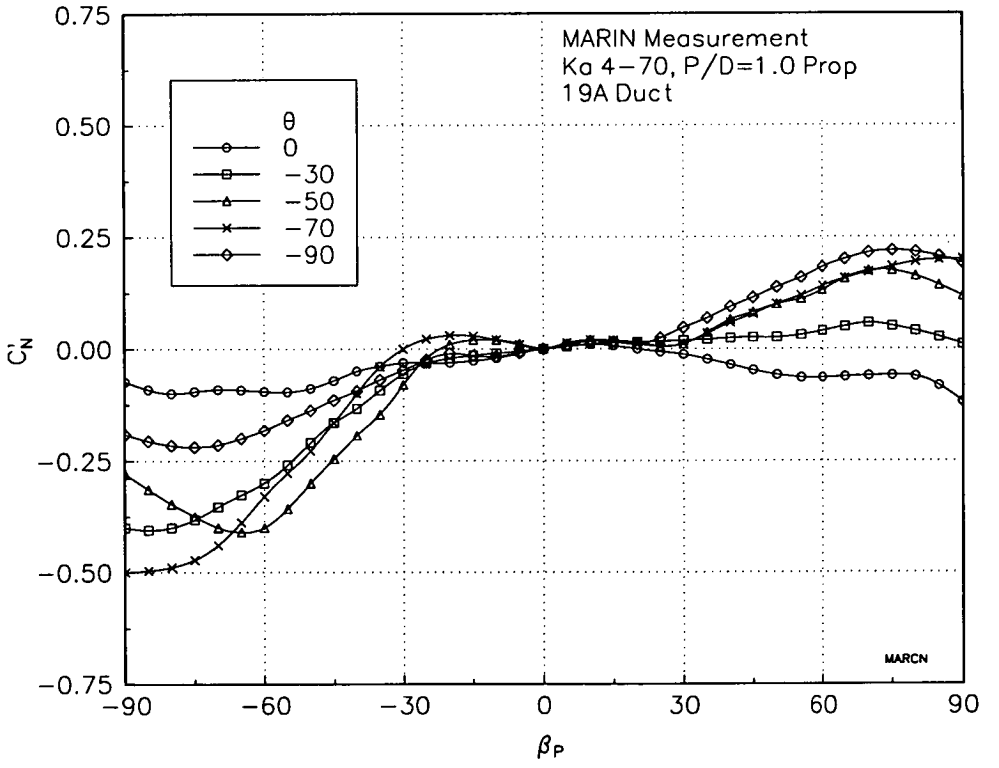

Figure 4.5 MARIN Experiments, Turning Moment,
from Oosterveld and van Oortmerssen, 1972

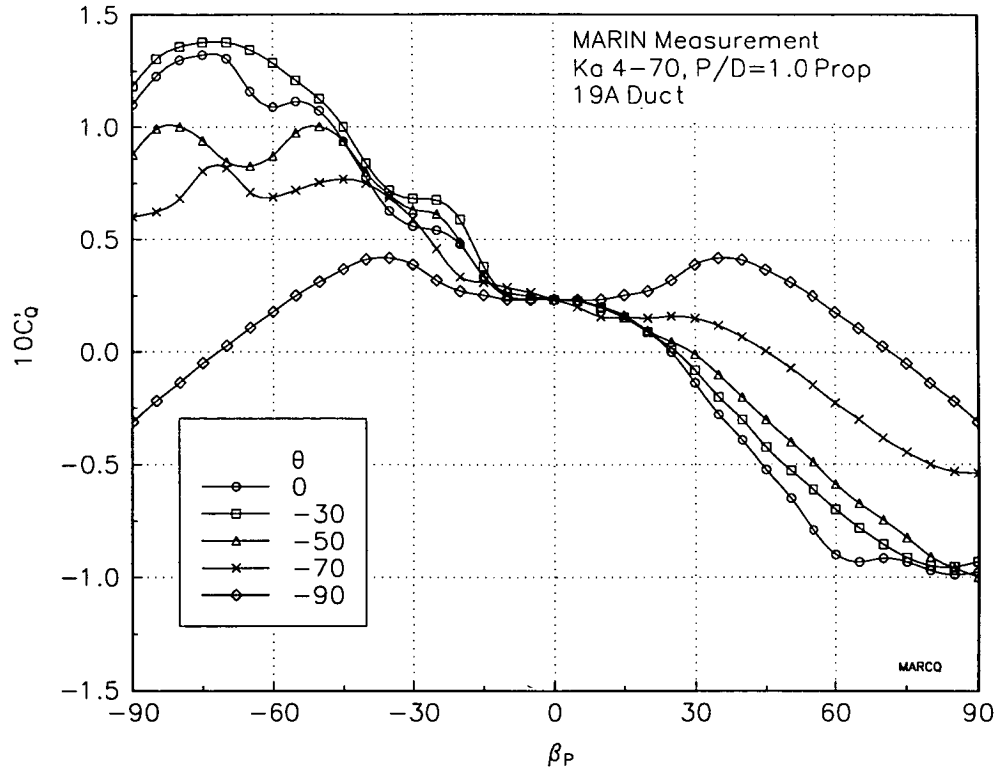

Figure 4.6 MARIN Experiments, Propeller Torque,
from Oosterveld and van Oortmerssen, 1972

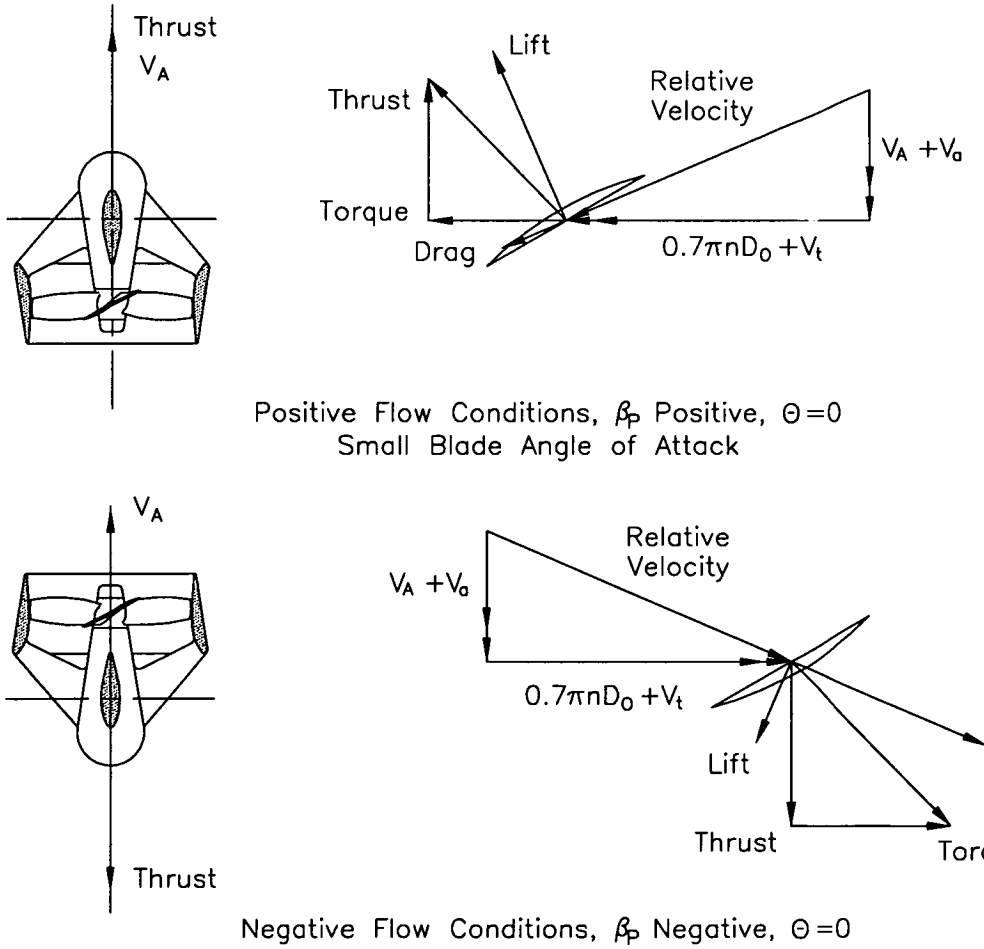

Figure 4.7 Blade Velocity Diagrams for Positive and Negative Flow Conditions

As the thruster turning moments generally equate to only 1 to 2% of the total moment created from the hull and thruster forces they may be neglected. Using the same reasoning it is possible to show that this simplification is also justified for cases of non-uniform inflow such as is expected due to thruster-thruster and thruster-hull interaction. The turning moments are of more concern with regard to the azimuthing dynamics of the thruster. For reasons of simplicity, most azimuthing thrusters fitted to tugs are fixed pitch. As a result of the above, Equation 4.1 may be simplified for a particular thruster as follows:

$$(X,Y,Q) = f(\beta_P,\theta) \tag{4.8}$$

As an alternative to the first and fourth quadrant representation used by Oosterveld and van Oortmerssen, the first quadrant only may be considered, i.e. the advance angle in the range $0° \leq \beta_P \leq +90°$. This then requires the angle of attack to be in the range $0° \leq \theta \leq \pm 180°$, ignoring the influence of the direction of rotation of the propeller. This representation is favoured in the present study as it is more compatible with other coordinate systems used which are described in Chapter 2. Using this representation, it is possible to consider not only rectangular coordinates *X, Y*, but also polar coordinates *T, α*, as shown in Figure 4.2. Further insight into the general performance of thrusters can be gained from polar thrust characteristics at a number of advance angles. Oosterveld and van Oortmerssen made measurements at angles of attack of 0, −30, −50, −70, and −90°, equivalent to 0, −30, −50, −70, −90, 110, 130, 150 and 180° in the representation described above. Polar plots have been generated by interpolating values of longitudinal and transverse forces every 10° using cubic splines. Transverse forces have been set to zero for angles of attack of 0 and 180°, the polar plots are presented in Figures 4.8 to 4.12.

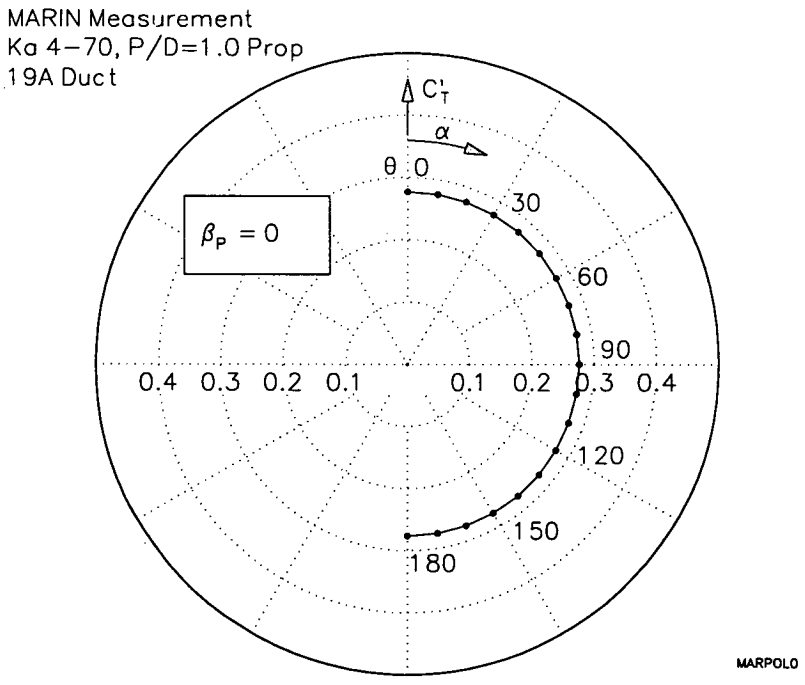

Figure 4.8 MARIN Experiments, Polar Thrust Characteristic, $\beta_P = 0°$, Adapted from Oosterveld and van Oortmerssen, 1972

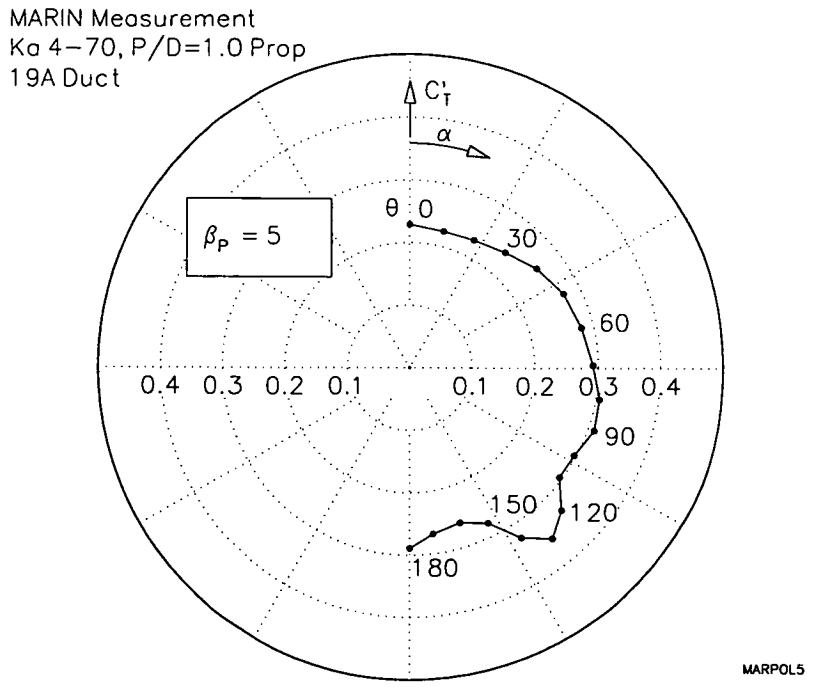

Figure 4.9 MARIN Experiments, Polar Thrust Characteristic, $\beta_P = 5°$, Adapted from Oosterveld and van Oortmerssen, 1972

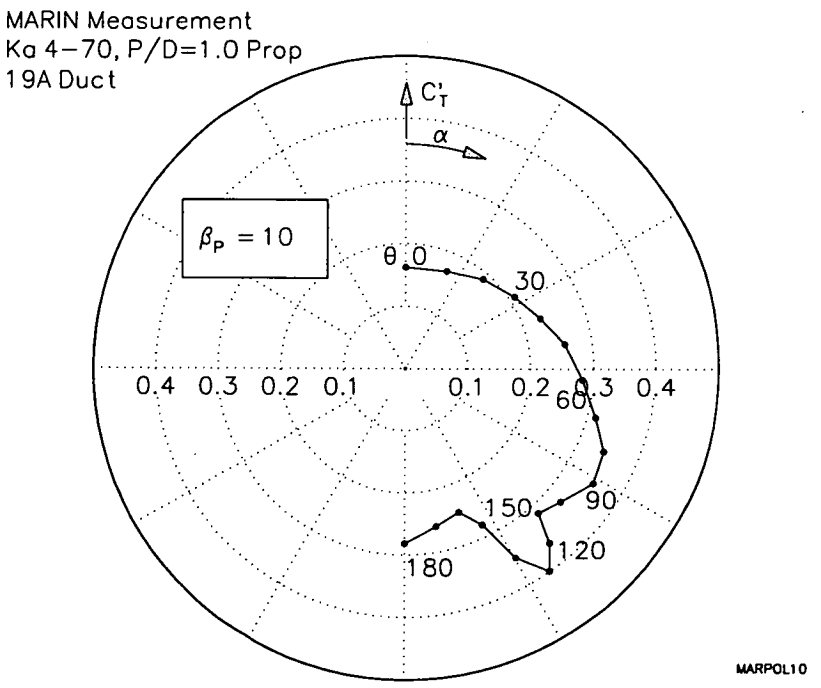

Figure 4.10 MARIN Experiments, Polar Thrust Characteristic, $\beta_P = 10°$, Adapted from Oosterveld and van Oortmerssen, 1972

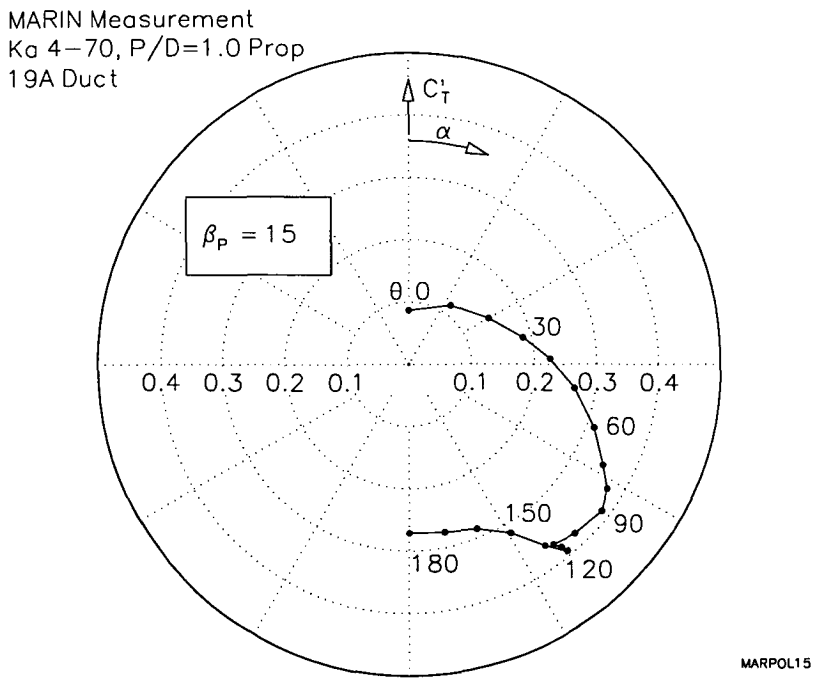

Figure 4.11 MARIN Experiments, Polar Thrust Characteristic, $\beta_P = 15°$, Adapted from Oosterveld and van Oortmerssen, 1972

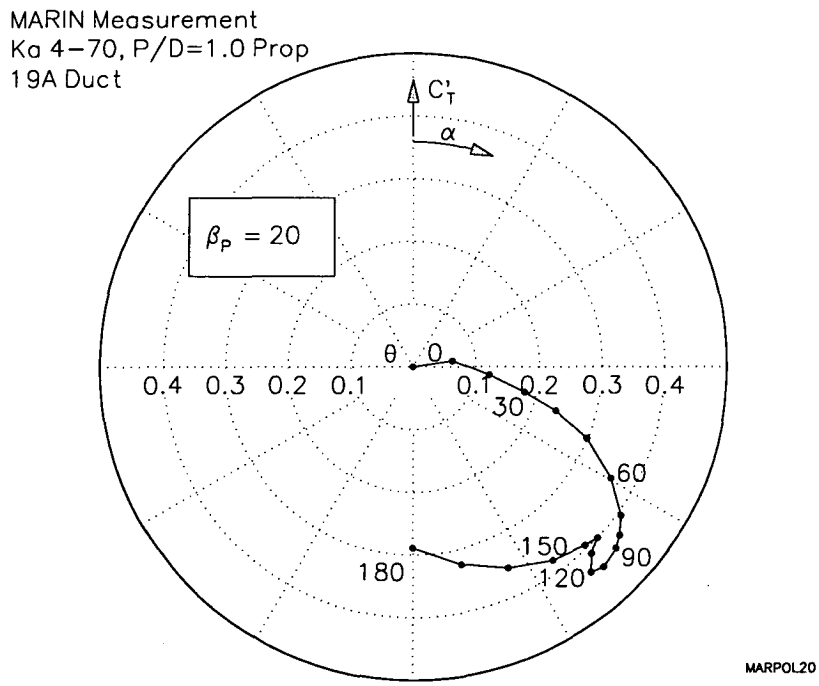

Figure 4.12 MARIN Experiments, Polar Thrust Characteristic, $\beta_P = 20°$, Adapted from Oosterveld and van Oortmerssen, 1972

The polar plots show specifically the increase in thrust with angle of attack due to increased propeller blade angle of attack and increased drag of the strut, gearcase and duct supporting fins. A notable feature of the polar plots is the fluctuations in thrust magnitude and direction at the angles of attack corresponding to negative flow conditions ($90° \leq \theta \leq 180°$). For favourable control it is preferable that the magnitude and direction of the thrust vector vary smoothly with increasing angle of attack. At advance angles of 5 and 10°, the angle of the thrust vector increases smoothly with the angle of attack but there are significant fluctuations in the magnitude. Whereas, at advance angles of 15 and 20° fluctuations in the magnitude of the thrust vector are reduced but it can be seen that at certain angles of attack the rate of change of direction with angle of attack actually reverses sign. Such features can most likely be attributed to flow separation effects expected in negative flow conditions, as mentioned above. Similar polar plots may also be developed for propeller torque where similar fluctuations are also present.

4.3 NSFI Open Water Experiments

Minsaas and Lehn, 1978, tested thrusters of both pusher and tractor configuration. For the present investigation only the pusher configuration is of interest. Unlike the experiments of Oosterveld and van Oortmerssen, where the thruster was tested using a surface piercing strut, Minsaas and Lehn tested the thruster below a ground board. Further, the strut, gear-case and duct supporting fins are somewhat different to those of the thruster tested by Oosterveld and van Oortmerssen. The results are presented in Figures 4.13 to 4.16, using the same two quadrant representation as that used by Oosterveld and van Oortmerssen.

Polar thrust diagrams have been developed from these results using the same procedure as that used for the MARIN data. The polar plots are presented in Figures 4.17 to 4.21, using the same coordinate system, as shown in Figure 4.2.

It can be seen that, overall, the NSFI results appear to compare quite favourably with the MARIN results in the two quadrant representation. However, in polar coordinates, where a smaller range of advance angles and thrust coefficients is considered, significant differences can be seen particularly in negative flow conditions. At 10° advance angle it can be seen that there is a significant discontinuity in the rate of change of magnitude and direction of the thrust vector with the angle of attack. A large fluctuation in the magnitude of the thrust vector is also present at 20° advance angle. As indicated with the MARIN results, such features can most likely be attributed to flow separation effects expected in negative flow conditions.

The fluctuations in thrust magnitude present in the NSFI results are greater than those present in the MARIN results. However, in both cases these represent significant changes at full scale, particularly at normal operating speeds where thruster characteristics largely determine a tug's general performance. The influence of these fluctuations on the forces imparted by the tug are discussed in Chapter 7.

It must be kept in mind that both the MARIN and NSFI experiments were performed to identify overall thruster characteristics and not precisely those in the range $0° < \beta_P < 25°$ where they have greatest effect on a tug's performance. This would imply that further more detailed data in this range of advance angles is required. In part, this has been achieved with experiments performed at the AMC.

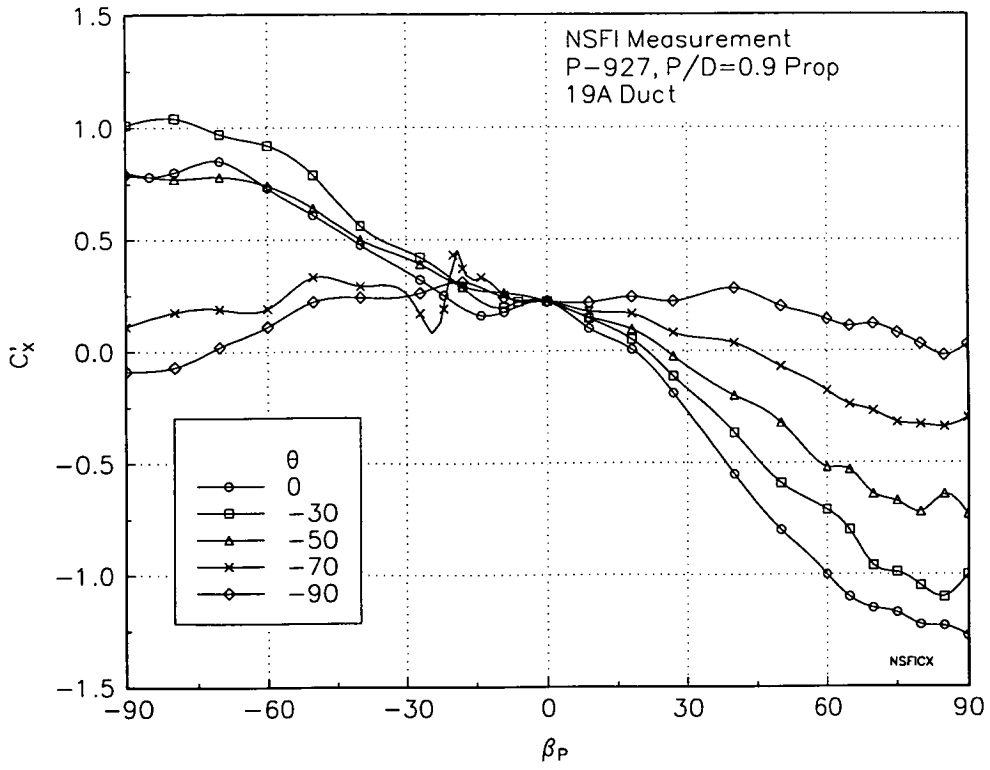

Figure 4.13 NSFI Experiments, Longitudinal Force,
from Minsaas and Lehn, 1978

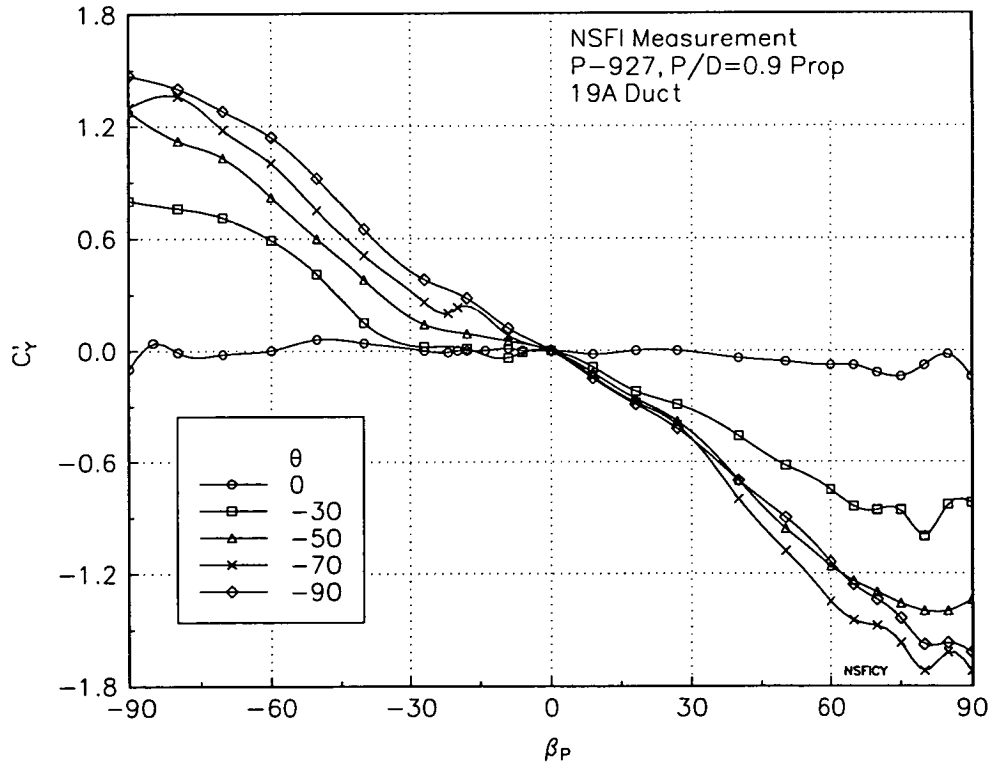

Figure 4.14 NSFI Experiments, Transverse Force,
from Minsaas and Lehn, 1978

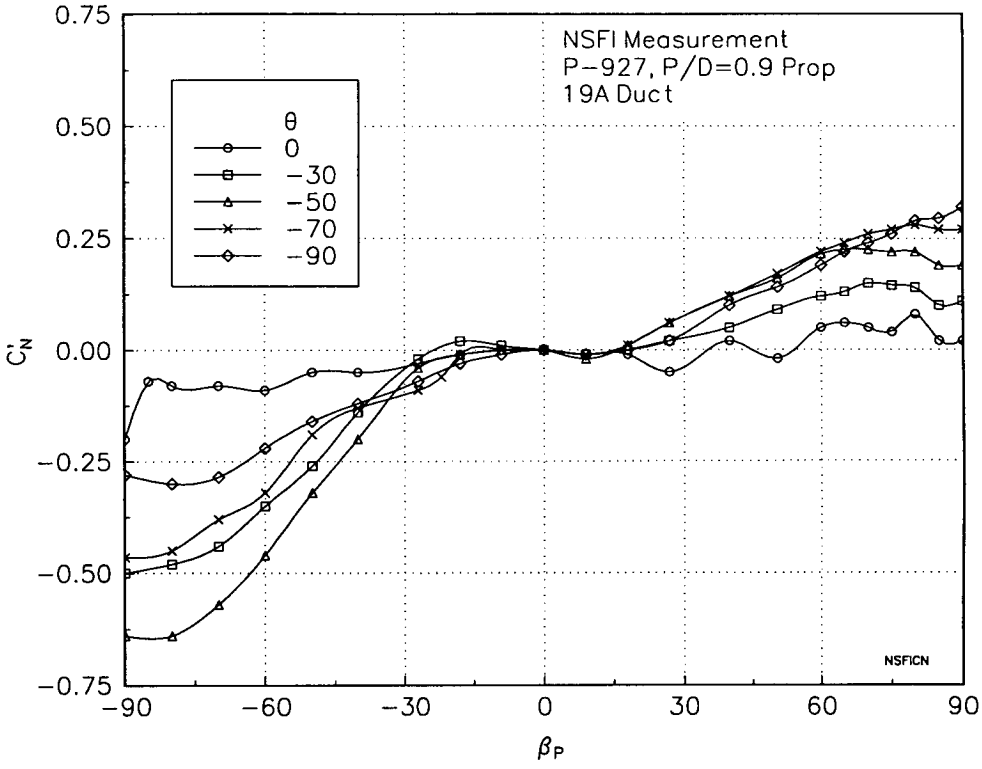

Figure 4.15 NSFI Experiments, Turning Moment,
from Minsaas and Lehn, 1978

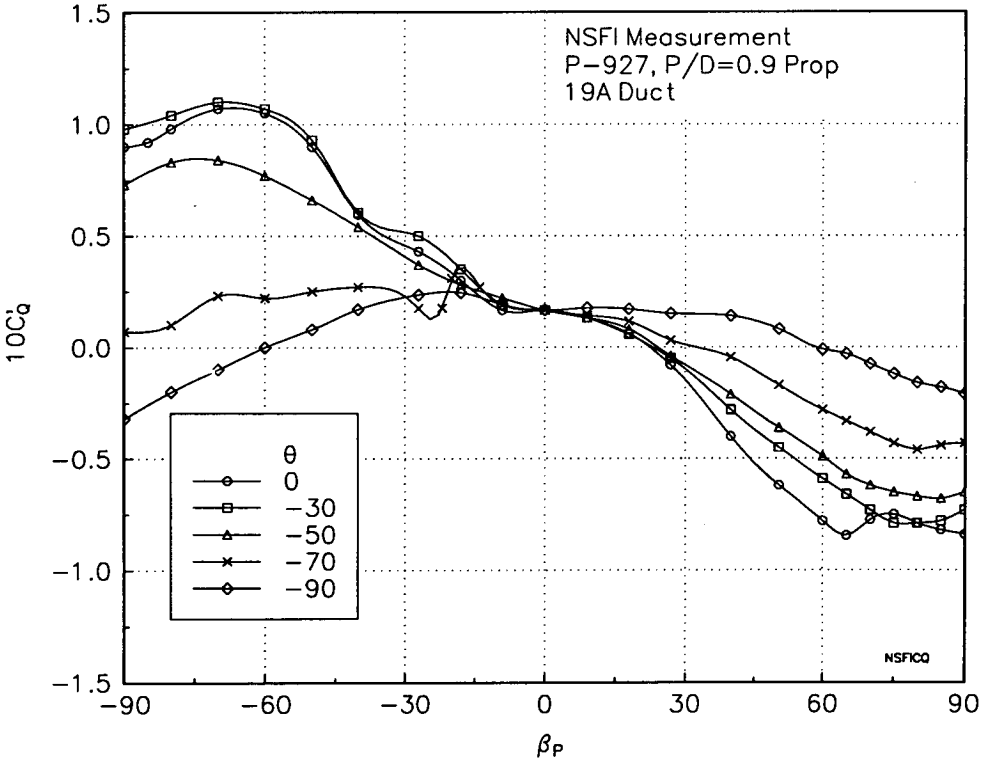

Figure 4.16 NSFI Experiments, Propeller Torque,
from Minsaas and Lehn, 1978

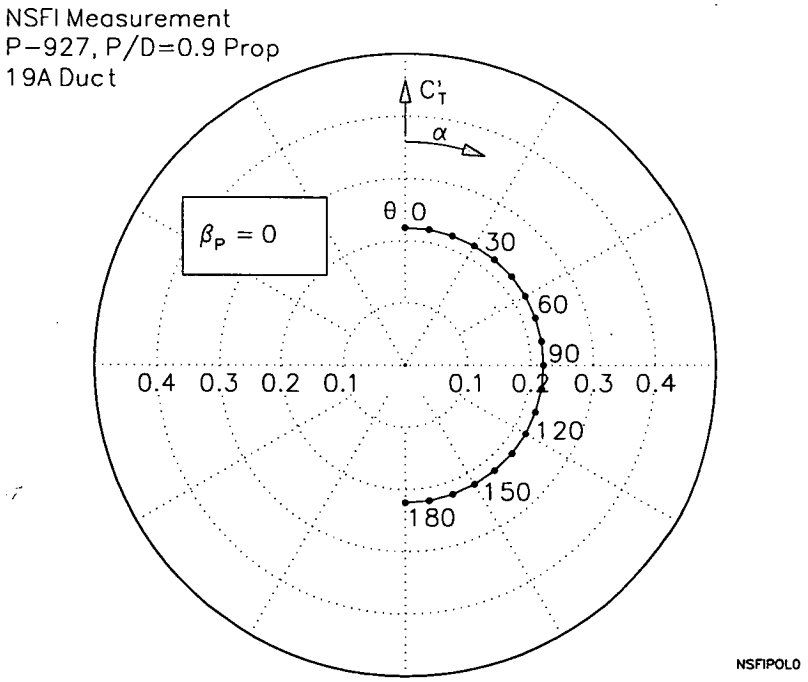

Figure 4.17 NSFI Experiments, Polar Thrust Characteristic, $\beta_P = 0°$, Adapted from Minsaas and Lehn, 1978

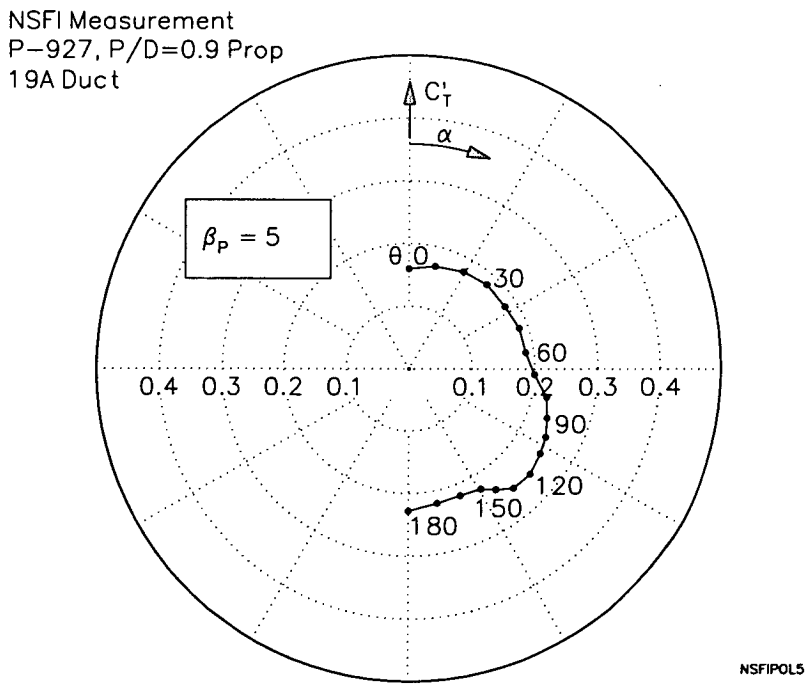

Figure 4.18 NSFI Experiments, Polar Thrust Characteristic, $\beta_P = 5°$, Adapted from Minsaas and Lehn, 1978

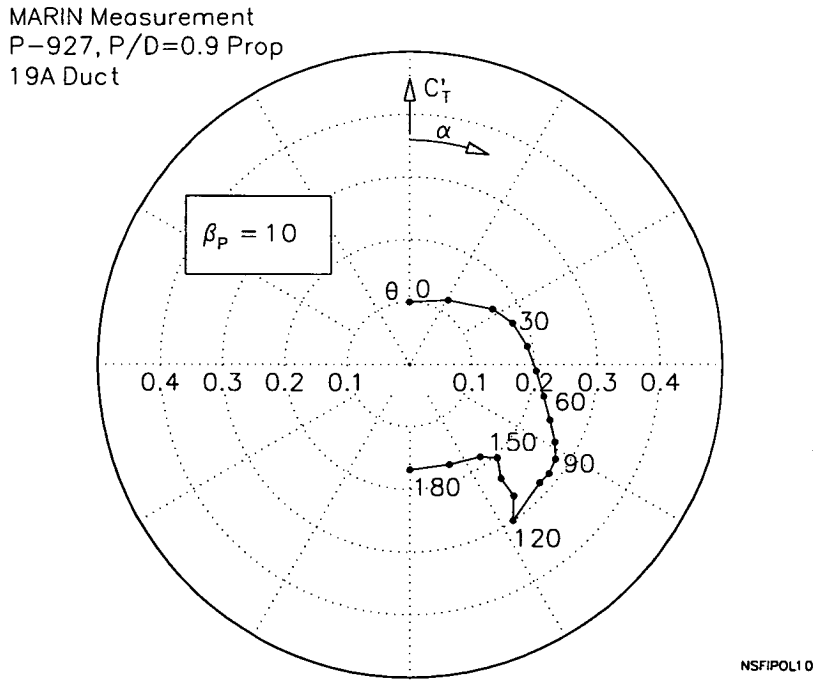

Figure 4.19 NSFI Experiments, Polar Thrust Characteristic, $\beta_P = 10°$, Adapted from Minsaas and Lehn, 1978

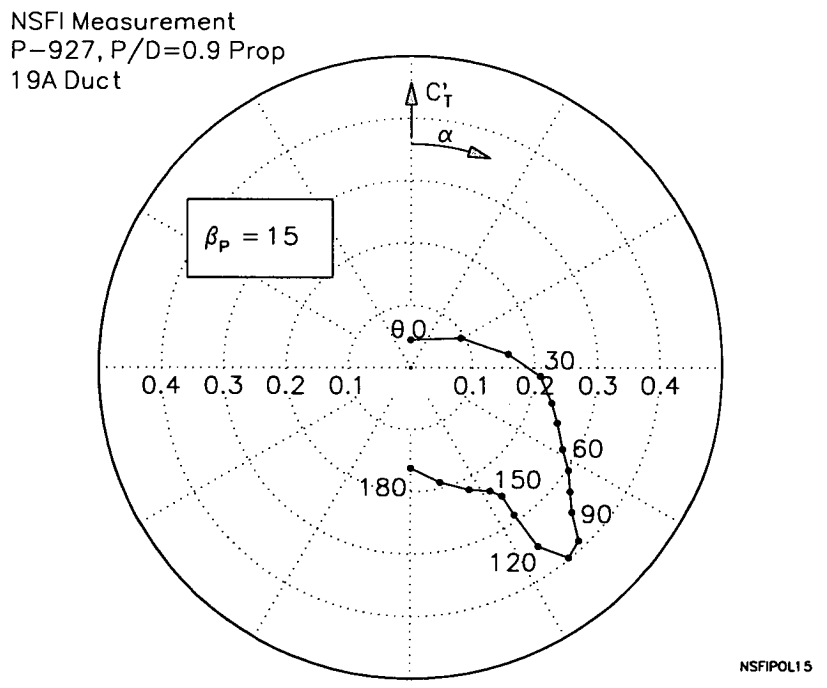

Figure 4.20 NSFI Experiments, Polar Thrust Characteristic, $\beta_P = 15°$, Adapted from Minsaas and Lehn, 1978

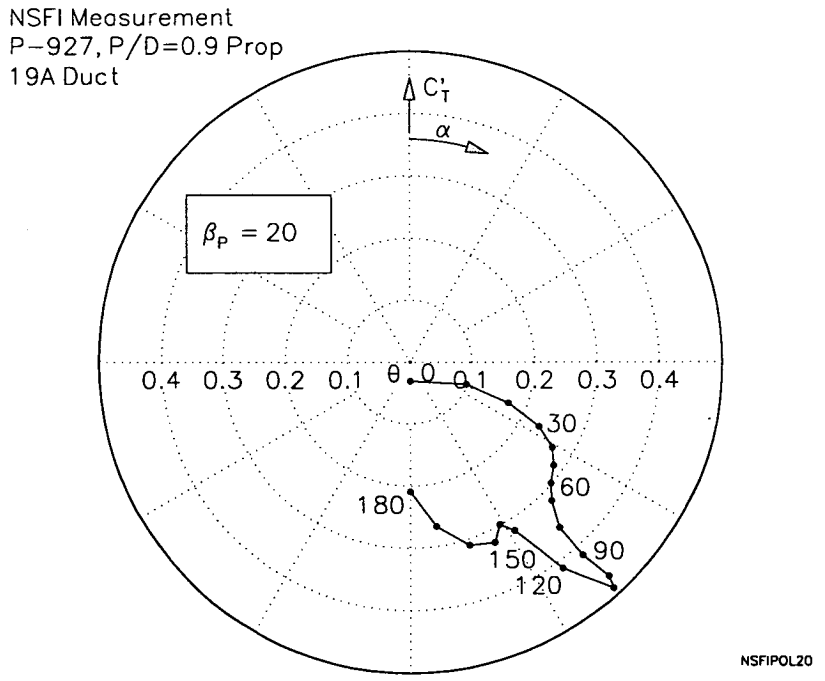

Figure 4.21 NSFI Experiments, Polar Thrust Characteristic, $\beta_P = 20°$, Adapted from Minsaas and Lehn, 1978

4.4 AMC Open Water Experiments

As part of a program to measure hydrodynamic interactions between thrusters and between the thrusters and tug hull, a series of open water experiments were performed at the AMC. A further objective of these experiments was to examine in detail the characteristics of a thruster with appendages, based on practical thrusters in the range of advance angles $0° \leq \beta_P \leq 25°$ where thruster forces most influence tug performance. The model was tested below a large shallow draft ground board. General details of experimental facilities and apparatus used at the AMC are given in Appendix B and details of the thrusters are given in Appendix C.

As the thrusters were also tested fitted to the tug model, limits on the scale of the thruster models were constrained by the size of tug model that could be practically tested in the towing tank at the AMC. This also meant that for meaningful comparison of open water and behind condition thruster characteristics, open water experiments were constrained to Froude scaling. Based on full scale dimensions of typical Australian tugs, a scale of 1:25 was determined appropriate. Details of the full scale vessels upon which this study has been based are given in Appendix A. This gives a propeller diameter of 0.088m and, from Froude scaling, revolutions of 19.6 rps and a range of velocities between $0 \leq V_A \leq 1.76$m/s, hence the propeller Reynolds Number will be in the range, $R_{nP} = 1.2$ to 1.4×10^5. The diameter of propeller and Reynolds Number at which the experiments were carried out indicate the influence of scale effects is of concern. There are numerous recommendations in the literature on threshold values of propeller diameter and Reynolds Number to avoid scale effects and corrections that may be applied when such values are not met.

For complex propulsors such as azimuthing thrusters, scale effects become more complex due to the number of interactions occurring between individual elements of the thruster. Bussemaker, 1987, discusses the influence of scale effects upon the various elements of an azimuthing thruster and suggests methods for their correction. In general, these methods are more applicable to thruster operation at zero angle of attack and where very precise prediction is required. A series of tests performed at MARIN, 1989, to compare performance of thrusters with propeller diameters of 0.10, 0.14 and 0.21m, concluded that scale effects where not significant.

In light of the above, no attempt has been made to correct the present measurements for scale effects. As mentioned, turning moments acting on the thruster are small and have not been measured and for the purposes of these experiments, propeller torque was not considered necessary and was also not measured. The thruster was tested at positive angles of attack only, at intervals of 10° and advance angle intervals of 5°. The results are presented in Figures 4.22 and 4.23, using the same two quadrant representation as used with the MARIN and NSFI results. Polar thrust diagrams are presented in Figures 4.24 to 4.29, using the same coordinate system as that shown in Figure 4.2.

From the results it can seen that larger forces are generated, both in the longitudinal and transverse directions, compared with those of the MARIN and NSFI results. Larger forces in the longitudinal direction can most likely be attributed to the differences in propeller pitch and those in the transverse direction, due to the more substantial strut, gear-case and duct supporting fins used. In general, the results are quite well behaved, except for the discontinuity's apparent in the two quadrant representation for $50°<\theta<90°$ (or $90°<\theta<130°$ in polar coordinates) and $\beta_P \approx 15°$. These are possibly the result of flow separation effects since the thruster is operating in negative flow conditions, although there are no significant fluctuations present in the polar plots as was the case with the MARIN and NSFI results.

The three thrusters considered all have the same duct and similar propellers but somewhat different strut, gear-case and duct supporting fin geometry's. From this it may be concluded that such alterations in geometry have only marginal effects on the thrust characteristics in positive flow conditions (small angles of attack), but significant effects in negative flow conditions (large angles of attack). In negative flow conditions it could be expected that the appendage geometry will have a greater impact on inflow conditions to the propeller. The thrusters tested at MARIN and NSFI were larger in size than that tested at the AMC. This raises the question of whether the relatively smooth variation of thrust direction and magnitude with angle of attack for the AMC results is due to differing appendage geometry or possible scale effects. Clearly, more experiments with larger scale thrusters of similar geometry would provide valuable information.

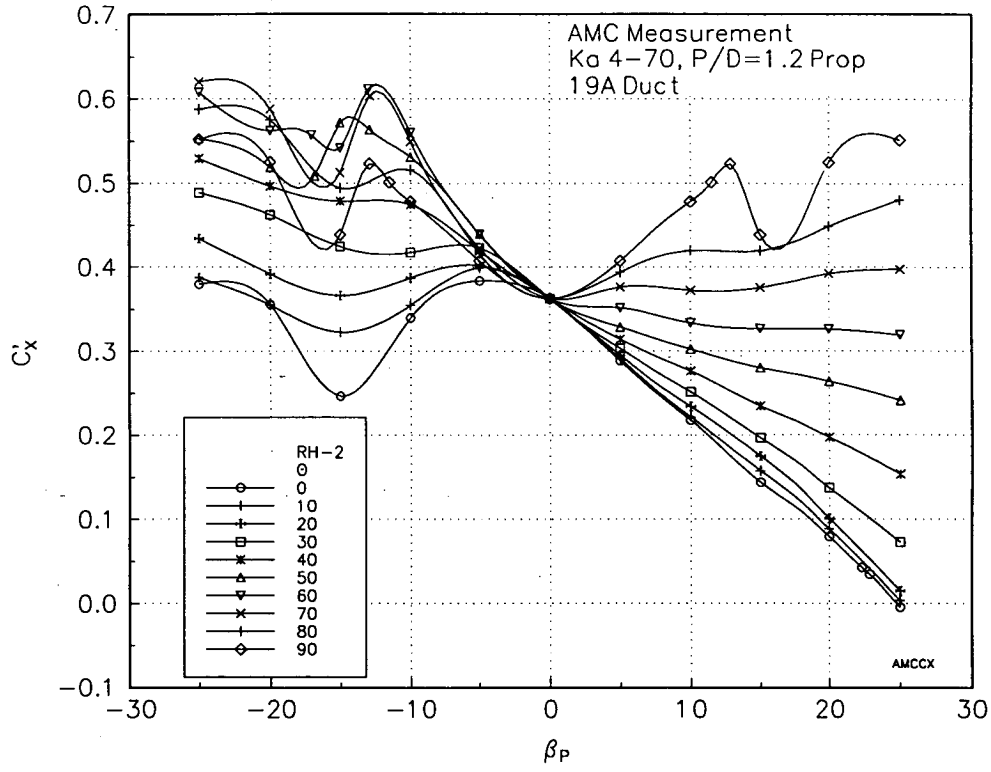

Figure 4.22 AMC Experiments, Longitudinal Force

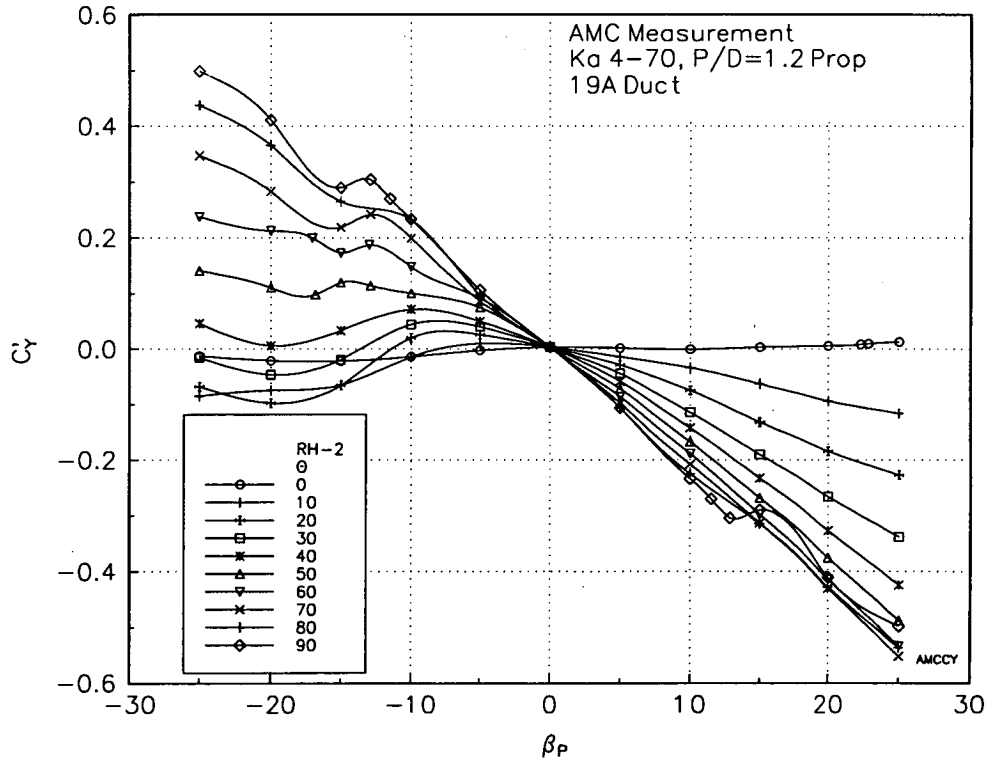

Figure 4.23 AMC Experiments, Transverse Force

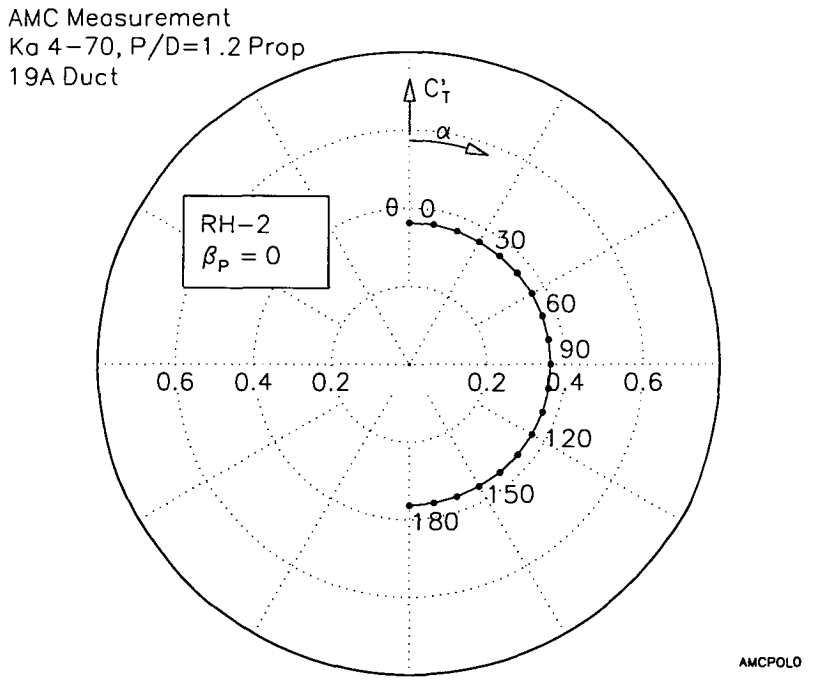

Figure 4.24 AMC Experiments, Polar Thrust Characteristic, $\beta_P = 0°$

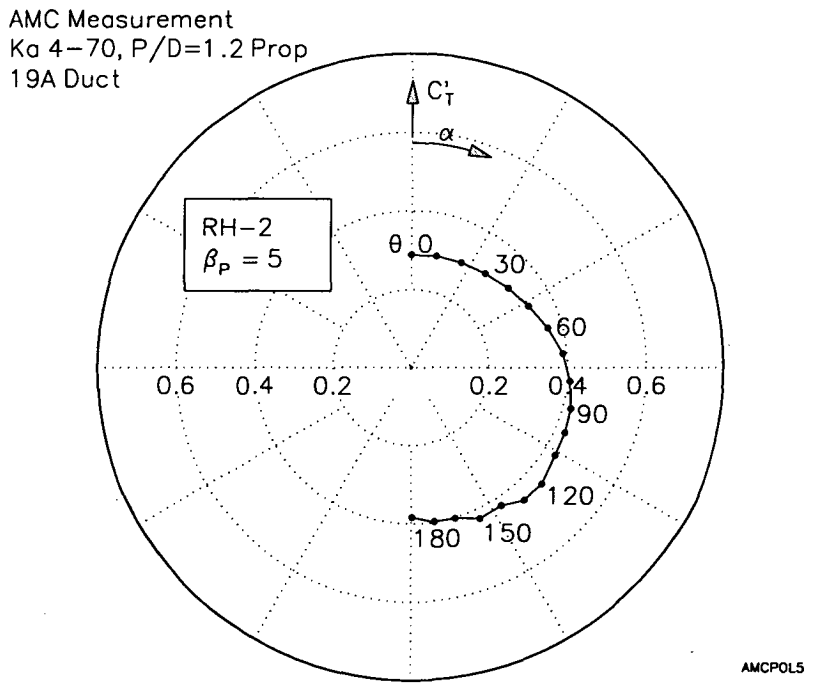

Figure 4.25 AMC Experiments, Polar Thrust Characteristic, $\beta_P = 5°$

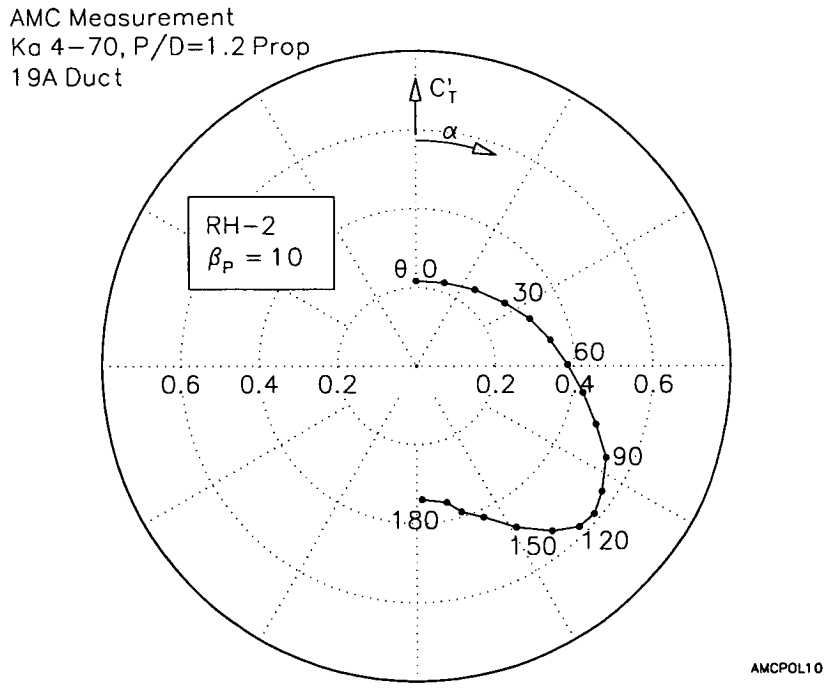

Figure 4.26 AMC Experiments, Polar Thrust Characteristic, $\beta_P = 10°$

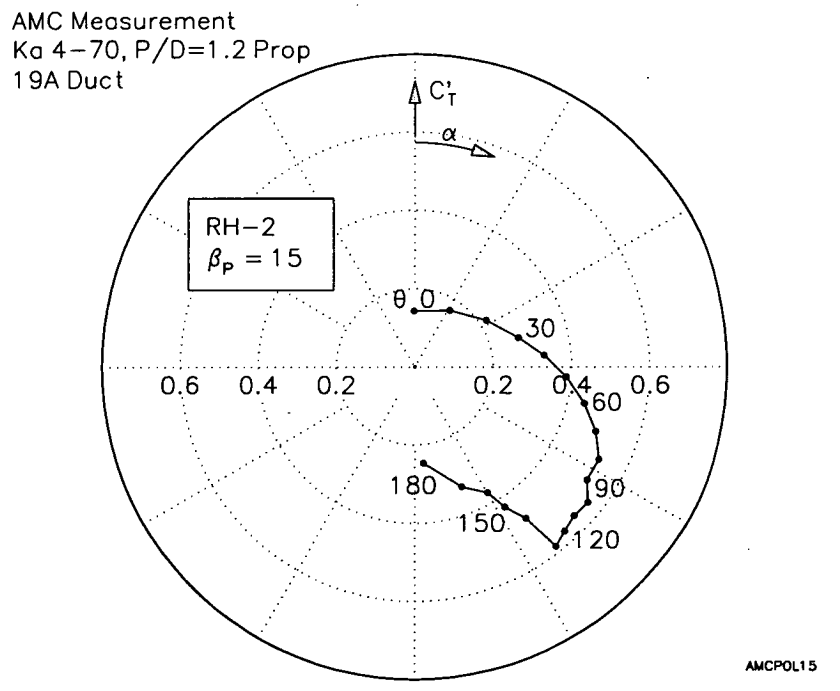

Figure 4.27 AMC Experiments, Polar Thrust Characteristic, $\beta_P = 15°$

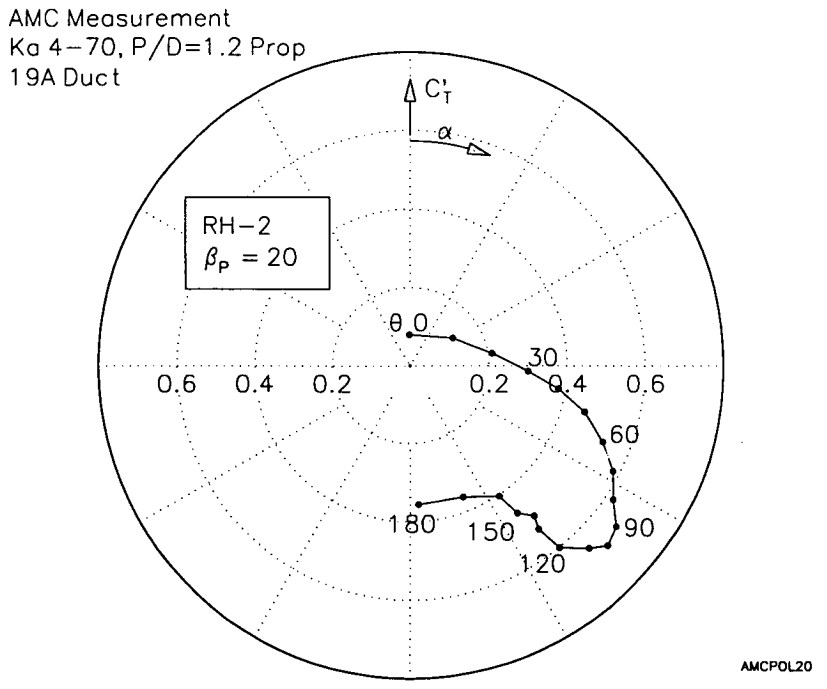

Figure 4.28 AMC Experiments, Polar Thrust Characteristic, $\beta_P = 20°$

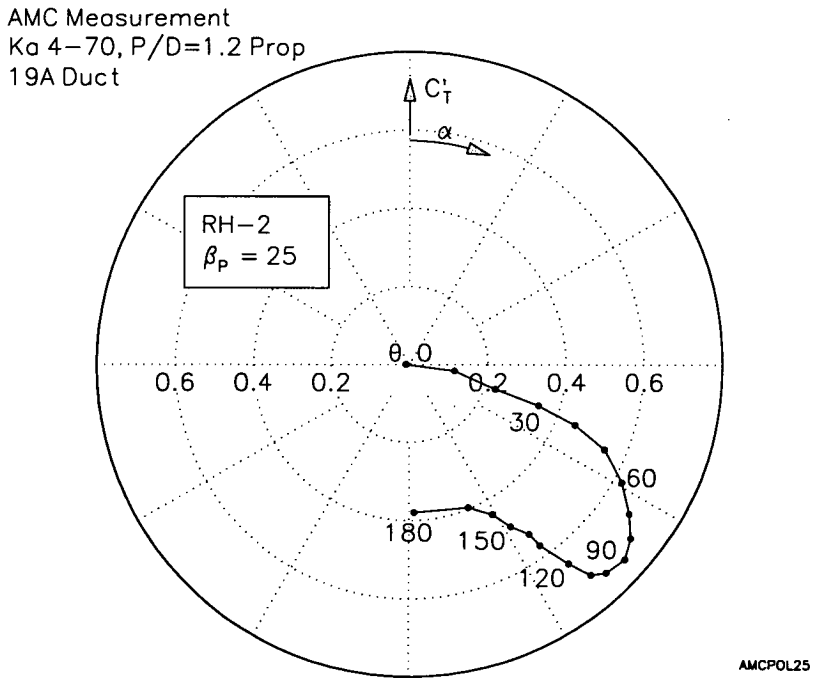

Figure 4.29 AMC Experiments, Polar Thrust Characteristic, $\beta_P = 25°$

5 INTERACTION BETWEEN THRUSTERS

5.1 Introduction

Previous studies investigating interaction between thrusters have been limited to dynamic positioning applications where thrusters are generally separated by large distances and speeds are low. The most recent of these studies by Nienhuis, 1992, correlates extensive theoretical and experimental work. However, in the case of tugs, the thrusters employed are proportionately large compared with the vessel size, limiting the thruster spacing to around 2 diameters. Also, the enhanced performance of omni-directional drive tugs has led to shiphandling operations being performed at comparatively high speeds. Hence, the above mentioned work is of only limited assistance in describing the nature of interaction between thrusters fitted to tugs.

A series of model tests have been performed at the AMC to investigate in detail the interaction between two thrusters which are closely spaced for a range of speeds and orientations. To isolate the effects of pure thruster-thruster interaction, a series of open water experiments have been performed where the two thrusters were tested below a shallow draft ground board. The extent of interaction has then been determined from comparison of these results with open water experiments where a single thruster was tested below the ground board, as detailed in Chapter 4. Interaction between thrusters in the behind condition has also been determined from measurement of thruster forces during a series of free running model tests performed at the AMC. The influence of the tug hull on interaction between the thrusters has been determined from comparison of the results from the open water and behind condition experiments, covered in Chapter 6. General details of experimental facilities and apparatus used at the AMC are given in Appendix B and details of the thrusters are given in Appendix C. Using results from the experiments, a semi-empirical mathematical model for interaction between thrusters is also developed which is suitable for use in simulation procedures.

For a thruster i, interacting with another j, forces and moments in the horizontal plane and propeller torque may be considered a function of the following parameters:

$$(X,Y,N,Q)_i = f\left[s,\beta_H,(\beta_{PV},\theta,P)_i,(\beta_{PV},\theta,P)_j\right] \qquad (5.1)$$

where, β_{PV} is the apparent propeller advance angle based on the free stream velocity, i.e.:

$$\beta_{PV} = \arctan\left(\frac{V}{0.7\pi n D_o}\right) \qquad (5.2)$$

For practical reasons, only cases of equal propeller revolutions n and angle of attack θ are considered. However, the effective advance angle β_P and angle of attack θ for each thruster may be different due to thruster-thruster interaction. As mentioned in Chapter 4, the turning moments N and propeller pitch P may be conveniently ignored. For the purposes of these experiments, the propeller torque Q was not considered necessary and was not measured. Generally, for omni-directional stern drive tugs the constraint of the beam permits little variation of the thruster spacing s and consequently was fixed at a typical value of 2.1 diameters for these experiments. The orientation of the thrusters with respect to the free stream is defined by the drift

angle β_H as described in Chapter 2, for both open water and behind condition tests. In Chapter 4, thrust characteristics for a single thruster were conveniently represented in polar coordinates and the same system is used for these results. For the present experiments, Equation 5.1 may be rewritten for port and starboard thrusters,

$$(T,\alpha)_{p,s} = f(\beta_H, \beta_{PV}, \theta) \tag{5.3}$$

The coordinate system used for representing the results is shown in Figure 5.1.

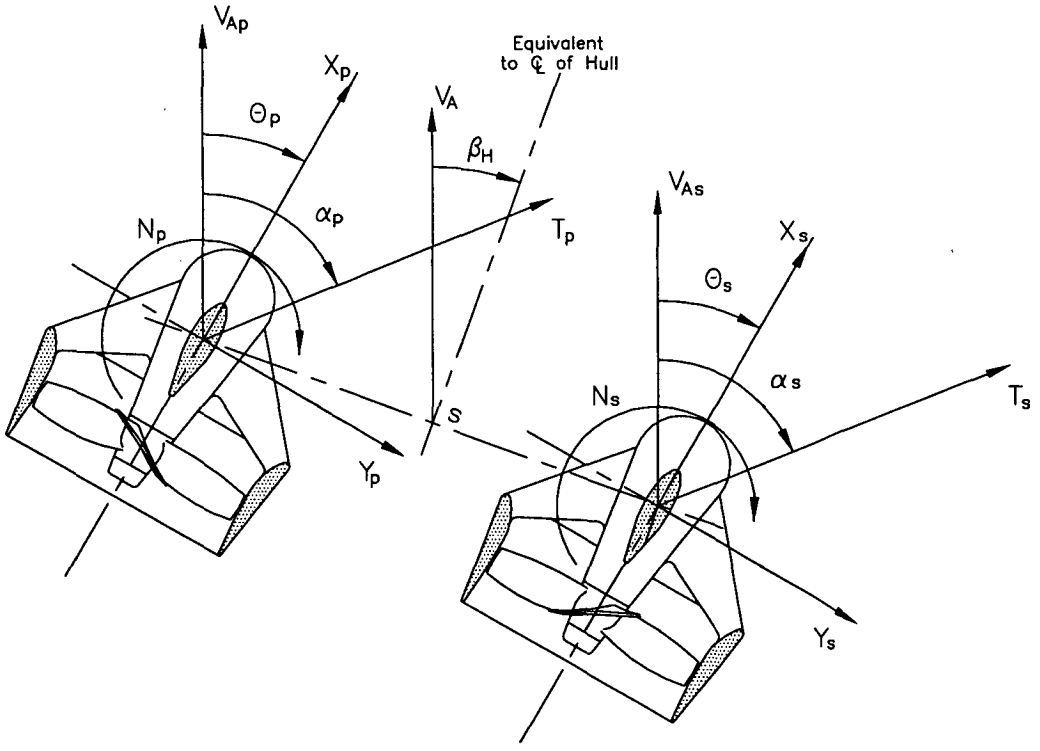

Figure 5.1 Coordinate System for Interaction Between Thrusters

5.2 Interaction Experiments

5.2.1 Experimental Matrix

From Equation 5.3, interaction between thrusters has been assumed to be dependent on three parameters; the drift angle β_H, the advance angle β_P and the angle of attack θ. An appropriate matrix of these parameters for testing has been determined from consideration of practical modes of tug operation. For shiphandling operations, thruster advance angles β_P would not exceed around 12° at maximum revolutions; in situations of partial power this may be increased. However, it will be shown in Chapter 6 that thruster forces dominate tug capability at low advance angles and hull forces dominate at high advance angles. For operation at advance angles exceeding 12°, thruster forces become small compared with hull forces, making the influence of thruster-thruster interaction on the overall forces negligible. Thus, apparent advance angles up to 15° were tested at intervals of 5°, allowing direct comparison with the open water results for a single thruster. Combinations of drift angle, β_H, and angle of attack, θ, can be found from consideration of the geometry and forces acting for varoius modes of practical tug operation. Four modes of operation are possible, as shown in Figure 5.2:

- pushing (Fig 5.2(a));
- pulling with forward tow point-direct (Fig 5.2(b));
- pulling with forward tow point-indirect (Fig 5.2(c)); and
- pulling with aft tow point (Fig 5.2(d)).

Angle of attack may be plotted against drift angle and regions mapped for each mode of operation. Clearly, from symmetry, only either positive or negative drift angles need be considered. Operation in each mode where the drift angle is negative has been examined, as shown in Figure 5.2. The most convenient parameter in constructing envelopes of tug operation in various modes is the thruster angle, δ, relative to the tug's fore-aft axis, as defined in Figure 2.1. In Chapter 6 the thruster angle is used for constructing analagous $\delta - \beta_H$ envelopes for experiments to investigate interaction between thrusters and hull. However, to investigate thruster-thruster interaction the thruster angle is irrelevant and the angle of attack is the appropriate parameter allowing direct comparison of thruster characteristics for both a single thruster and two thrusters interacting.

Operation in the pushing mode is shown in Figure 5.2(a). In this mode the tug drift angle may vary between 0 and –90°. The objective of pushing is generally to apply a pure sway force to the ship and this is achieved, as shown Chapter 6, for drift angles between 0 and –90°. From Figures 3.1(b) to 3.3(b) it can be seen that the centre of pressure of the hull force will always lie between the point of contact on the fenders and the location of the thrusters and the results presented in Chapter 6 show that hull forces due to thruster-hull interaction are negligible. Therefore, to push, the thrusters must be ahead and the angle of attack may vary between the extremes of 0° and linearly from 0° at 0° drift angle to –90° at –90° drift angle, as shown in Figure 5.2(a).

Pulling with the forward tow point in the direct mode is shown in Figure 5.2(b). In this mode the tug drift angle may vary from 0° when pulling astern, to –180° when pulling ahead but running astern. From Figures 3.1(b) to 3.3(b) it can be seen that the centre of pressure of the hull force will always lie between the tow point and the location of the thrusters and from the results presented in Chapter 6 this can also be shown to be the case including hull forces due to thruster-hull interaction. Therefore, to pull, the thrusters must be astern so that angles of attack may vary between the extremes of, linearly between 180° pulling astern to 0° pulling ahead and linearly between 90° pulling astern to –90 pulling ahead, as shown in Figure 5.2(b).

Pulling with the forward tow point in the indirect mode is shown in Figure 5.2(c). The objective here is to create force in the line using sway forces generated by the hull. The drift angle may vary between 0 and –90° and as described above the results of Chapters 3 and 6 can once again be used to show that the centre of pressure of the hull force including forces due to thruster-hull interaction always lies between the tow point and the thruster locations. Therefore, from the similarities this mode has with both pushing and pulling, possible combinations of angle of attack and drift angle include those for pushing and pulling as shown in Figure 5.2(c).

Pulling with the aft tow point is shown in Figure 5.2(d). In this traditional mode of tug operation drift angles may vary between 0 and –90°. From Figures 3.1(b) to

3.3(b) it can be seen that the tow point will always lie between the centre of pressure of the hull force and the location of the thrusters. As described in Chapter 6, from the similarity with pushing, hull forces due to thruster-hull interaction in this mode may also be considered negligible. Therefore, to pull, the thrusters must be ahead and the angle of attack may vary between the extremes of –90° and linearly from 0° at 0° drift angle to –90° at –90° drift angle, as shown in Figure 5.2(d).

Using the areas mapped for each mode of operation, a total envelope may then be defined as shown in Figure 5.2(e). It can be shown that there is anti-symmetry in combinations of the drift angle and angle of attack about the lines $\beta_H = -90°$ and $\theta = 0°$. Therefore, only drift angles between 0 and –90° need to be considered and the total envelope may be reduced to the area marked, as shown in Figure 5.2(e). In the case of tractor tugs, variations in angle of attack and drift angle are a subset of the above matrix, since the line can only be made fast to one end of the tug (refer Chapter 1). To maximise detail and coverage of the measurements a fine and coarse grid system was used. Measurements were made at intervals of 20 and 30° for the angle of attack and drift angle respectively and, in areas requiring more detailed measurement, these intervals were reduced to 10 and 15° respectively.

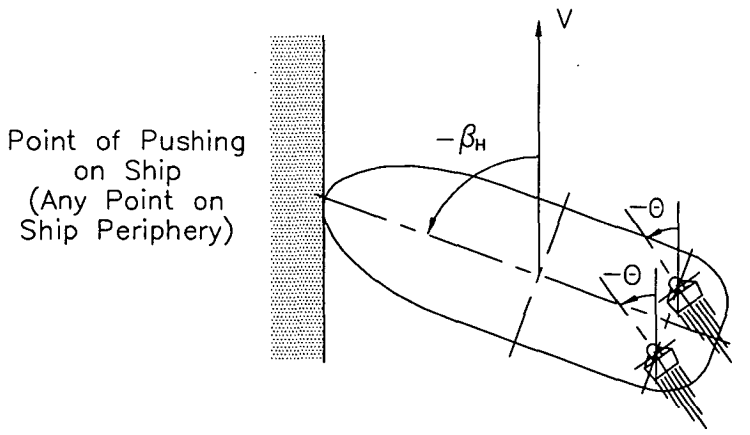

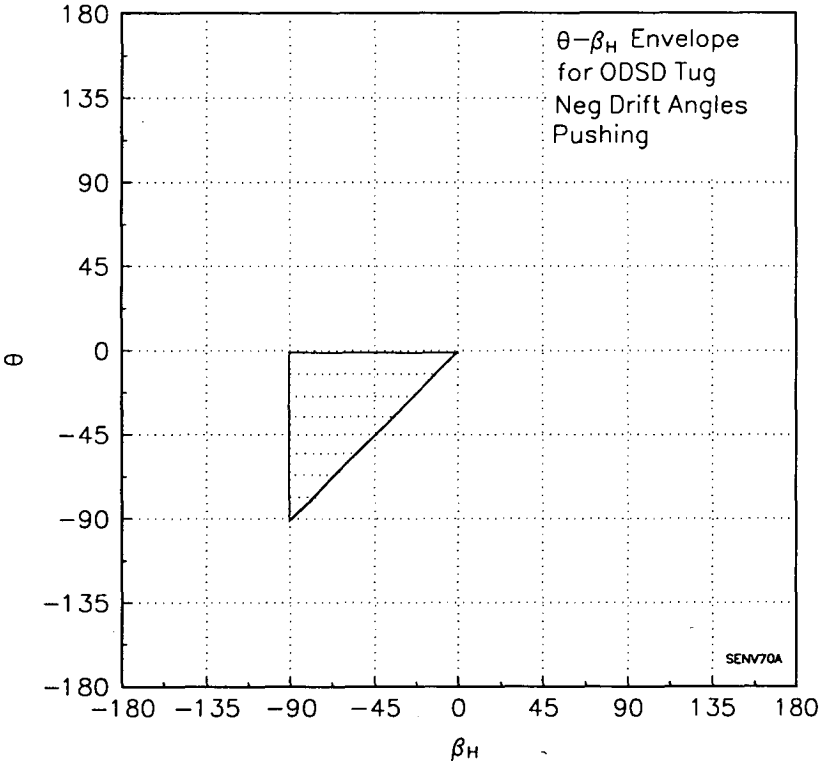

(a) Pushing

Figure 5.2 Angle of Attack and Drift Angle Combinations for Omni-directional Stern Drive Tugs Operating at Negative Drift Angles

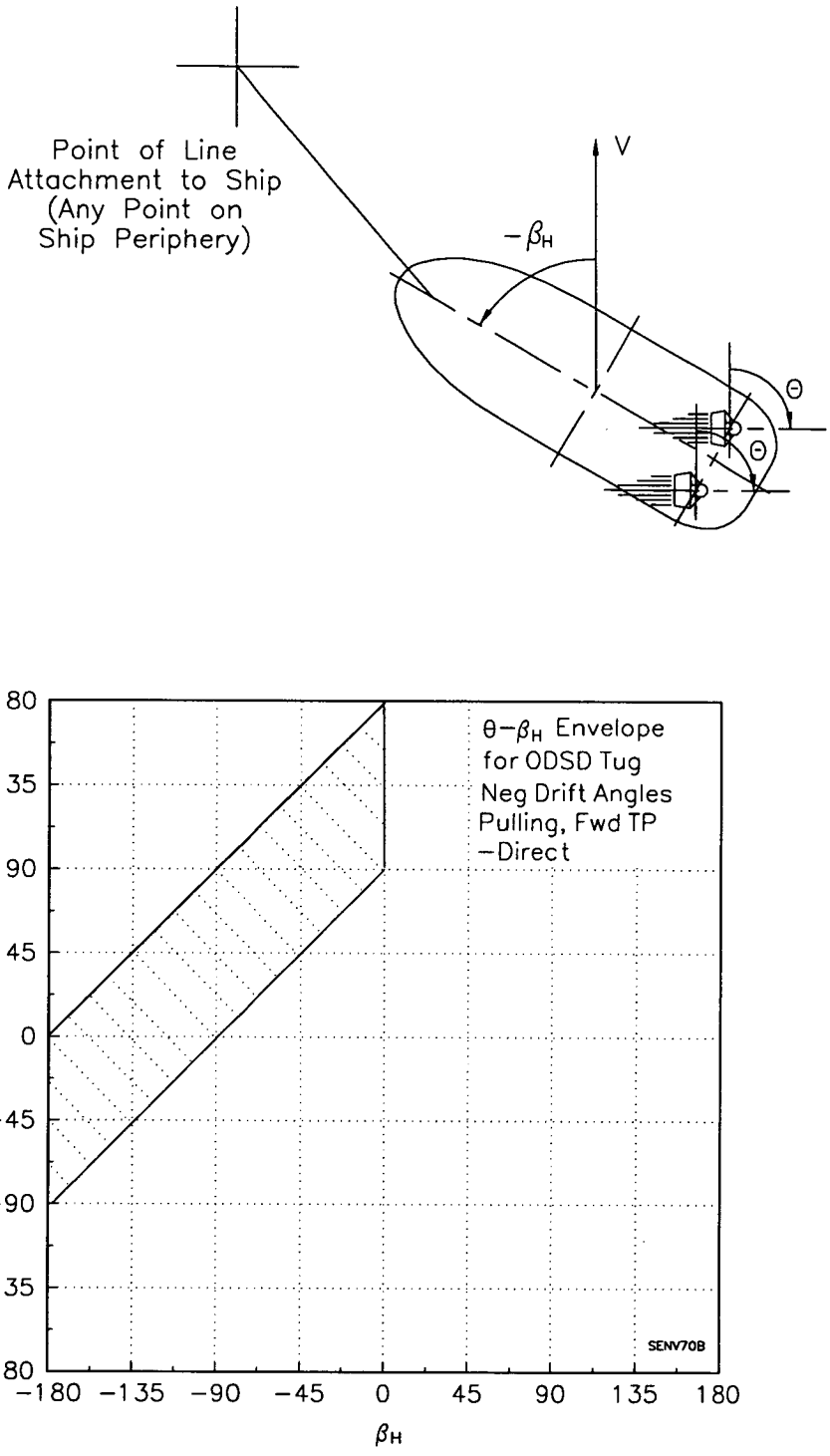

(b) Pulling with Forward Tow Point-Direct Mode

Figure 5.2 Angle of Attack and Drift Angle Combinations for Omni-directional Stern Drive Tugs Operating at Negative Drift Angles

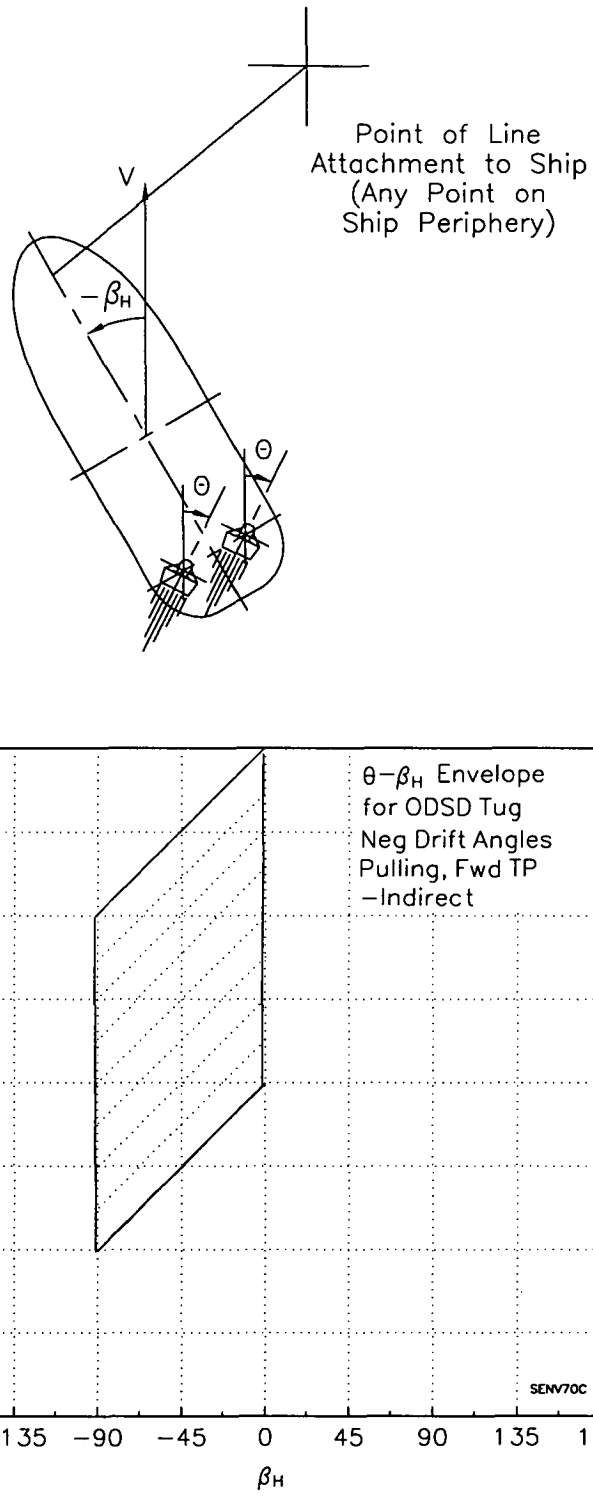

(c) Pulling with Forward Tow Point-Indirect Mode

Figure 5.2 Angle of Attack and Drift Angle Combinations for Omni-directional Stern Drive Tugs Operating at Negative Drift Angles

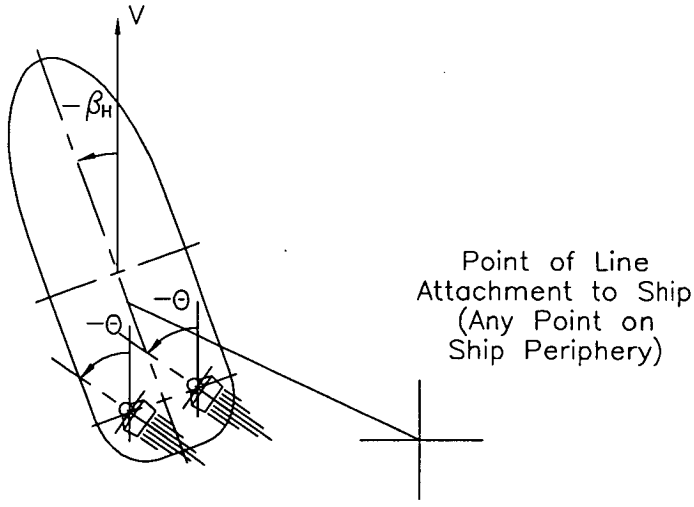

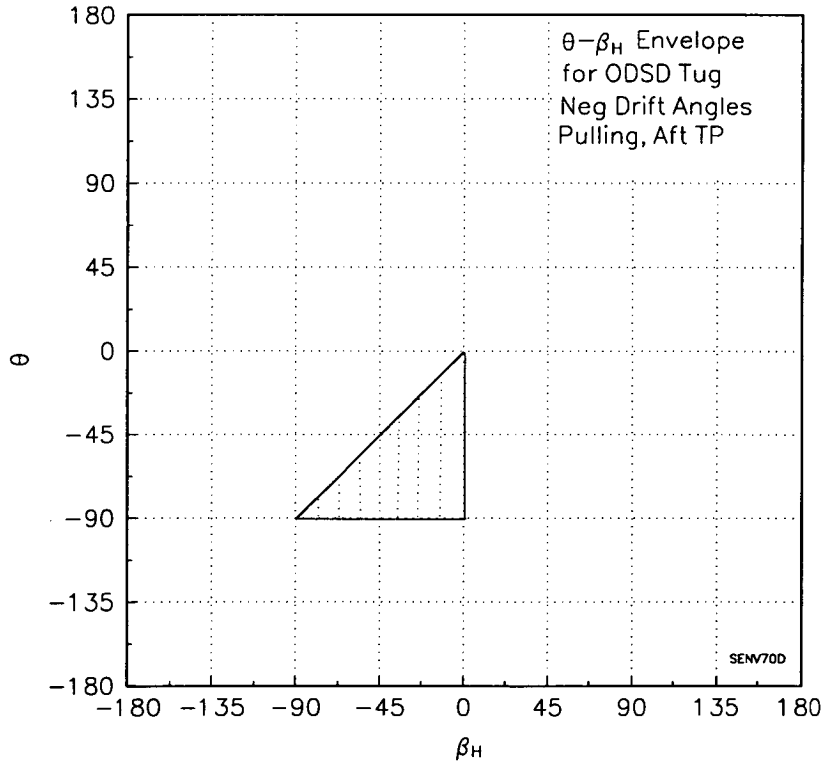

(d) Pulling with Aft Tow Point

Figure 5.2 Angle of Attack and Drift Angle Combinations for Omni-directional Stern Drive Tugs Operating at Negative Drift Angles

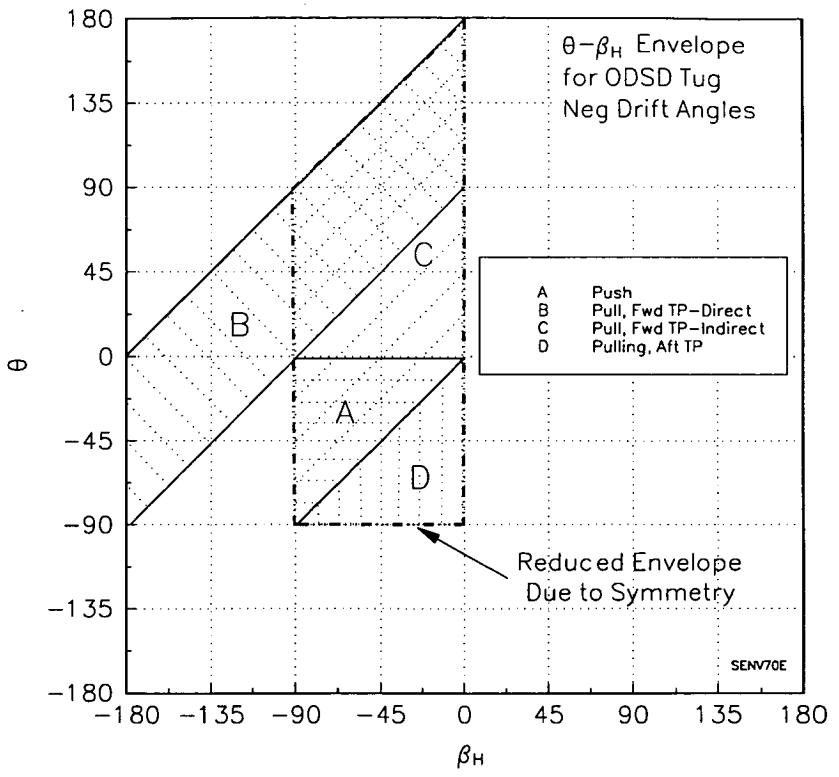

(e) Operational Envelope

Figure 5.2 Angle of Attack and Drift Angle Combinations for Omni-directional Stern Drive Tugs Operating at Negative Drift Angles

5.2.2 Experimental Results

For practical reasons left and right hand propellers were used for the free running experiments (refer Chapter 6) and, hence, the same configuration was also used for the thruster interaction experiments. The propellers were fitted as outward turning, that is port side-left hand and starboard side-right hand. Propeller revolutions for each thruster were set at equal values, being the same as that used for the open water tests on a single thruster, that is 19.6 rps. Measured forces have been non-dimensionalised with the same coefficients used for the open water tests on a single thruster, as described in Chapter 4. The results for port and starboard thrusters are presented in Figures 5.3, 5.4, 5.5 and 5.6 for advance angles of 0, 5, 10, and 15° respectively. To clearly show the influence of interaction, the open water characteristic for a single thruster (right hand propeller) is also plotted.

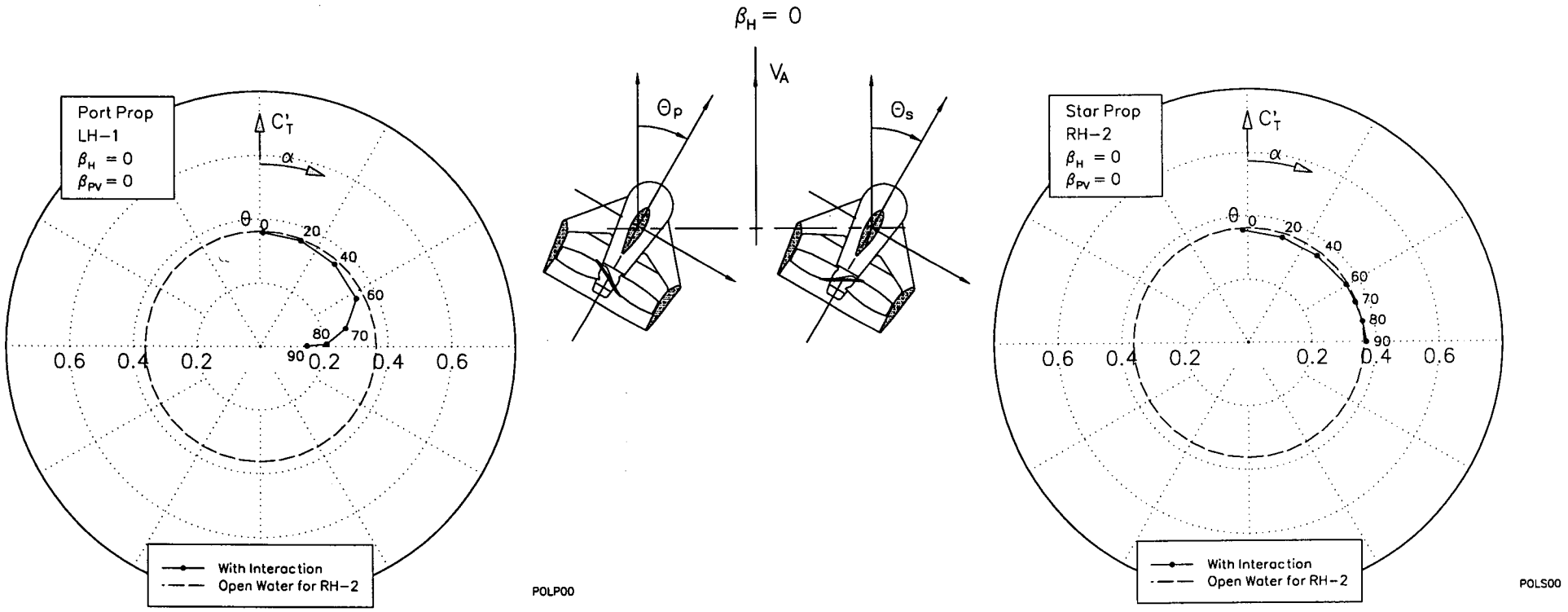

Figure 5.3 Interaction Between Thrusters - Port and Starboard Polar Thrust Characteristic, $\beta_H = 0°$ and $\beta_{PV} = 0°$

From the plots, it can be seen that the starboard thruster is essentially unaffected by the presence of the port thruster, whereas the port thruster, as expected, is dramatically affected by the presence of the starboard thruster. A cusp in the port thruster characteristic indicating a maximum in the influence of the race from the starboard thruster can be clearly seen. For 0° apparent advance angle, only *angles of attack* up to 90° where tested due to symmetry, ignoring the influence of direction of propeller rotation.

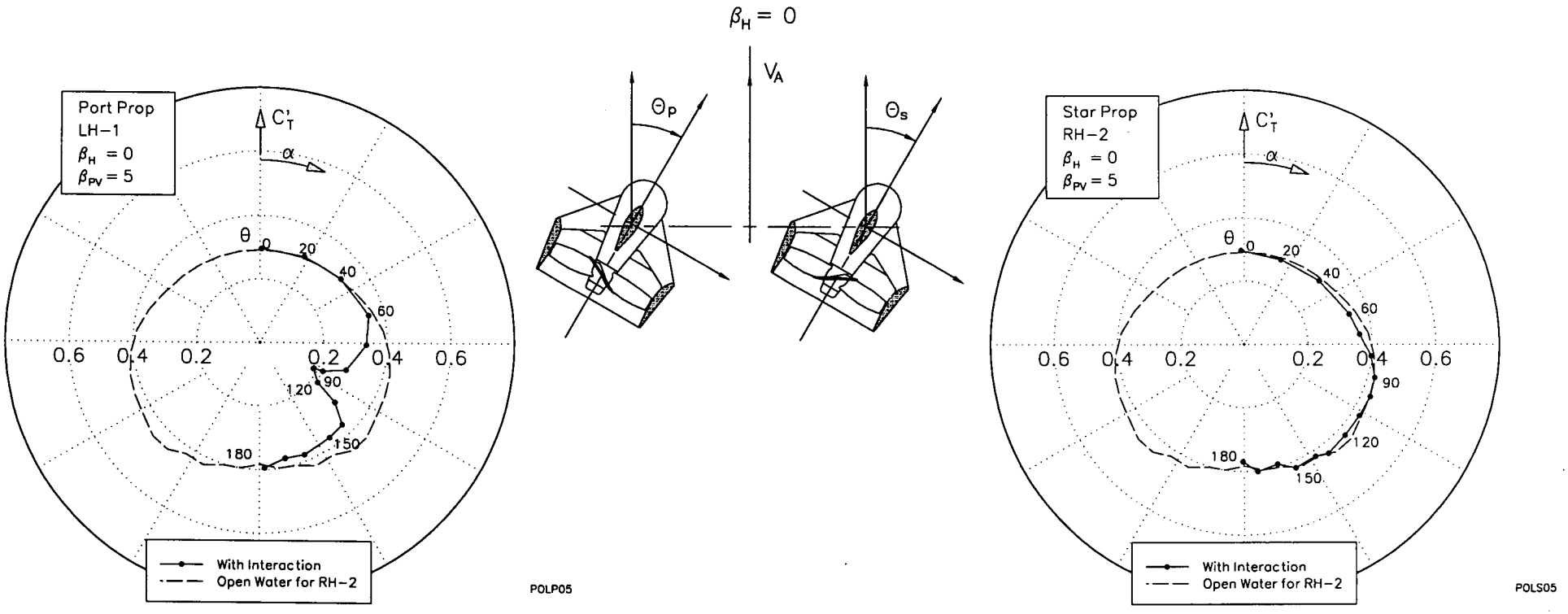

(a) $\beta_H = 0°$

Figure 5.4 Interaction Between Thrusters - Port and Starboard Polar Thrust Characteristic, $\beta_{PV} = 5°$

From the plots, it can be seen that the starboard thruster is essentially unaffected by the presence of the port thruster, whereas the port thruster, as expected, is dramatically affected by the presence of the starboard thruster. A cusp in the port thruster characteristic indicating a maximum in the influence of the race from the starboard thruster can be clearly seen. The cusp occurs at an angle of attack between 100 and 110° due to the race being deflected by the free stream. Forces at angles of attack greater than that at the cusp do not return to the corresponding open water values for a single thruster, but tend to values close to bollard pull indicating stagnant flow in the lee of the race.

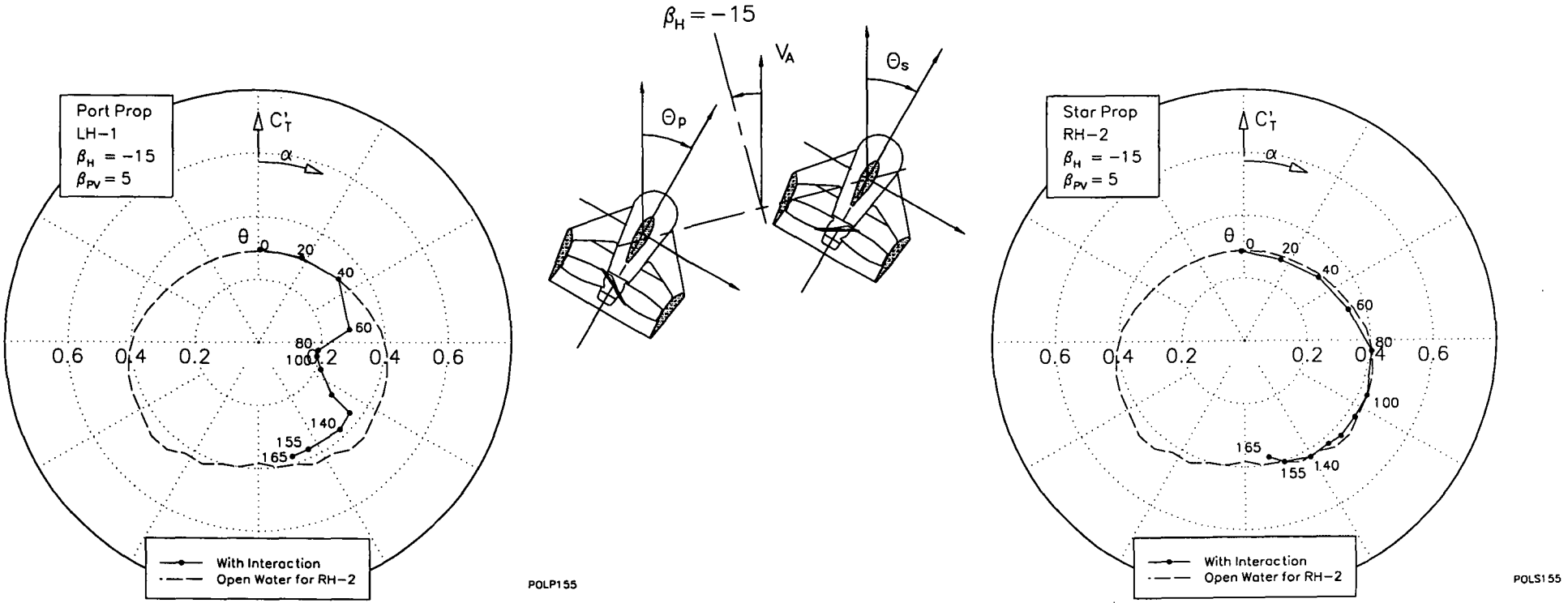

(b) $\beta_H = -15°$

Figure 5.4 Interaction Between Thrusters - Port and Starboard Polar Thrust Characteristic, $\beta_{PV} = 5°$

From the plots, it can be seen that the starboard thruster is essentially unaffected by the presence of the port thruster, whereas the port thruster, as expected, is dramatically affected by the presence of the starboard thruster. A cusp in the port thruster characteristic indicating a maximum in the influence of the race from the starboard thruster can be clearly seen. The cusp occurs at an angle of attack between 80 and 100° due to the race being deflected by the free stream. Forces at angles of attack greater than that at the cusp do not return to the corresponding open water values for a single thruster, but tend to values close to bollard pull indicating stagnant flow in the lee of the race.

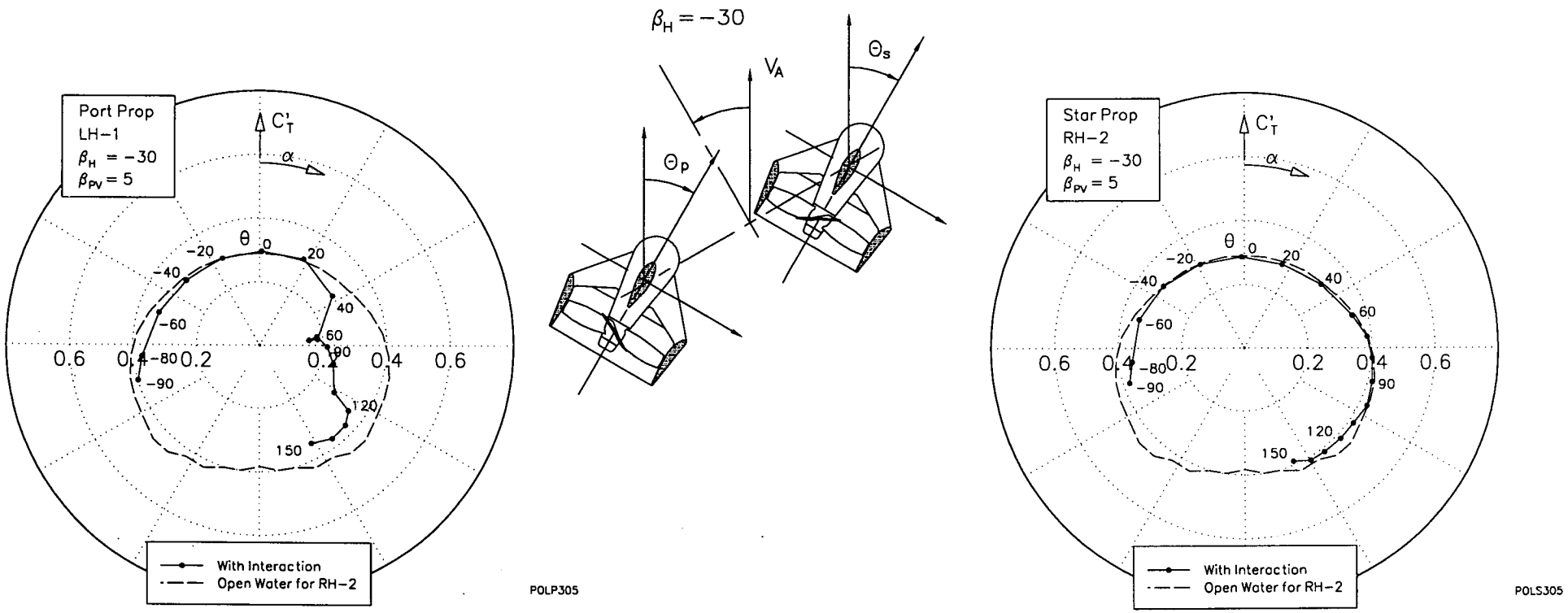

(c) $\beta_H = -30°$

Figure 5.4 Interaction Between Thrusters - Port and Starboard Polar Thrust Characteristic, $\beta_{PV} = 5°$

From the plots, it can be seen that the starboard thruster is essentially unaffected by the presence of the port thruster, whereas the port thruster, as expected, is dramatically affected by the presence of the starboard thruster. A cusp in the port thruster characteristic indicating a maximum in the influence of the race from the starboard thruster can be clearly seen. The cusp occurs at an angle of attack of approximately 70° due to the race being deflected by the free stream. Forces at angles of attack greater than that at the cusp do not return to the corresponding open water values for a single thruster, but tend to values close to bollard pull indicating stagnant flow in the lee of the race.

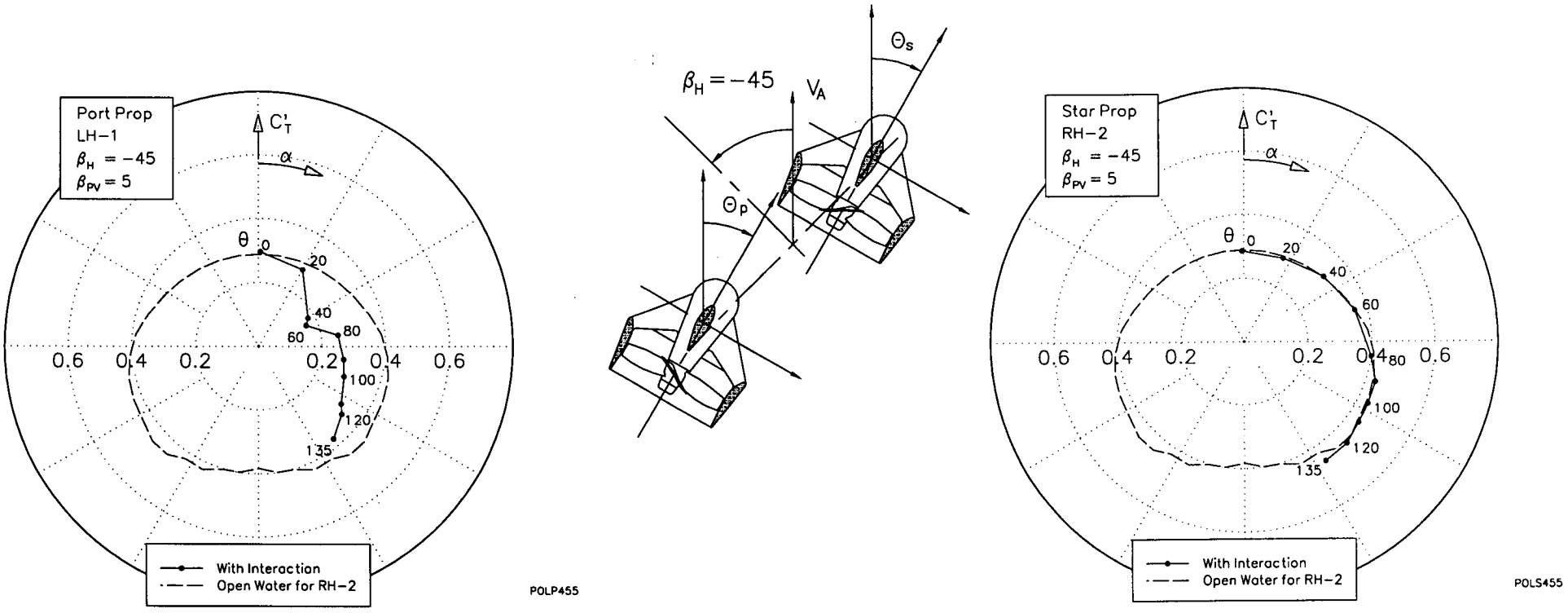

(d) $\beta_H = -45°$

Figure 5.4 Interaction Between Thrusters - Port and Starboard Polar Thrust Characteristic, $\beta_{PV} = 5°$

From the plots, it can be seen that the starboard thruster is essentially unaffected by the presence of the port thruster, whereas the port thruster, as expected, is dramatically affected by the presence of the starboard thruster. A cusp in the port thruster characteristic indicating a maximum in the influence of the race from the starboard thruster can be clearly seen. The cusp occurs at an angle of attack of approximately 60° due to the race being deflected by the free stream. Forces at angles of attack greater than that at the cusp do not return to the corresponding open water values for a single thruster despite, most likely, being free from direct impingement of the race. Assuming the thruster is free from race impingement at higher angles of attack, these differences could be attributed to distortion of the flow field by the starboard thruster i.e. flow straightening or flow rectification effects.

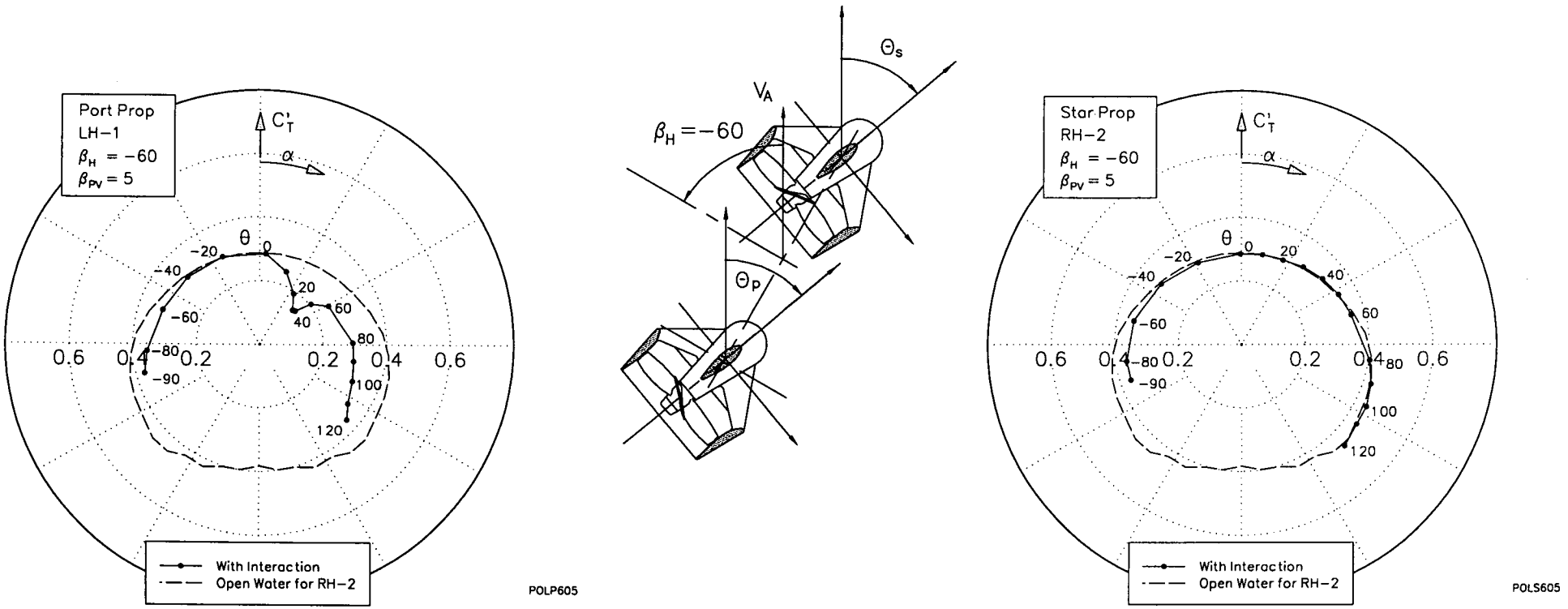

(e) $\beta_H = -60°$

Figure 5.4 Interaction Between Thrusters - Port and Starboard Polar Thrust Characteristic, $\beta_{PV} = 5°$

From the plots, it can be seen that the starboard thruster is essentially unaffected by the presence of the port thruster, whereas the port thruster, as expected, is dramatically affected by the presence of the starboard thruster. A cusp in the port thruster characteristic indicating a maximum in the influence of the race from the starboard thruster can be clearly seen. The cusp occurs at an angle of attack between 30 and 40° due to the race being deflected by the free stream. Forces at angles of attack greater than that at the cusp do not return to the corresponding open water values for a single thruster despite, most likely, being free from direct impingement of the race. Assuming the thruster is free from race impingement at higher angles of attack, these differences could be attributed to distortion of the flow field by the starboard thruster i.e. flow straightening or flow rectification effects.

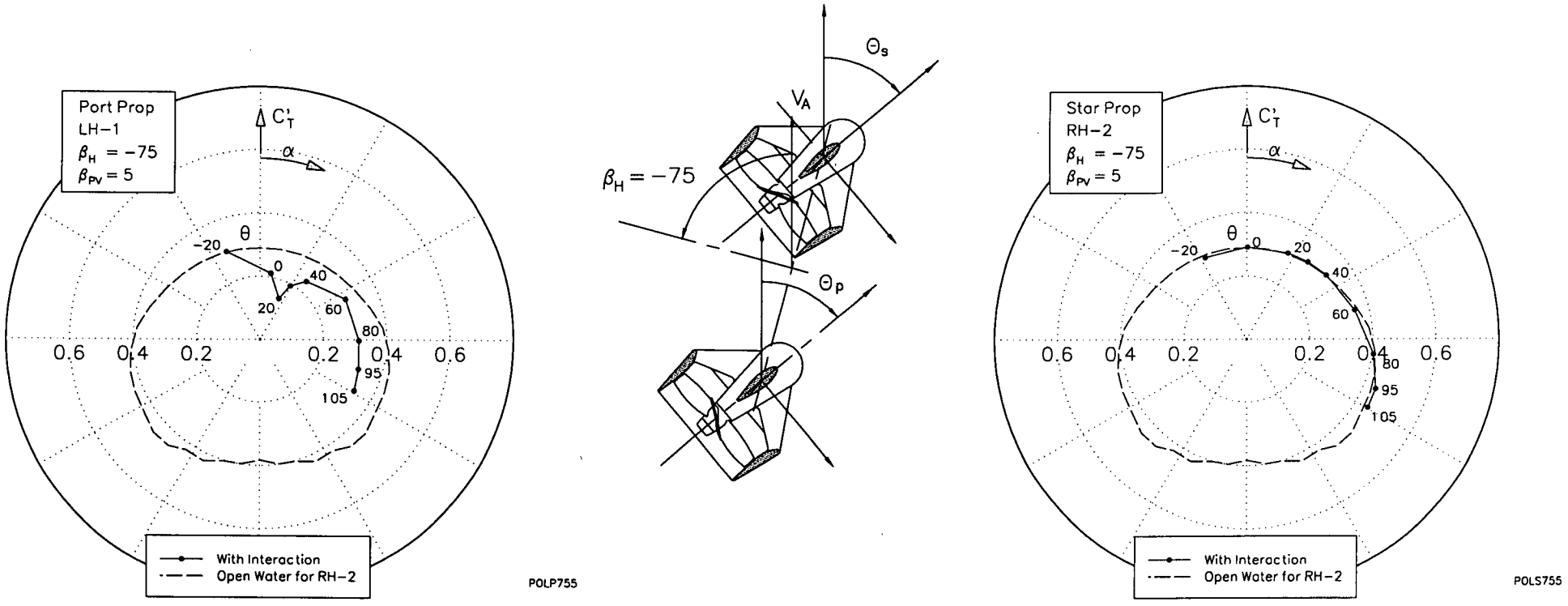

(f) $\beta_H = -75°$

Figure 5.4 Interaction Between Thrusters - Port and Starboard Polar Thrust Characteristic, $\beta_{PV} = 5°$

From the plots, it can be seen that the starboard thruster is essentially unaffected by the presence of the port thruster, whereas the port thruster, as expected, is dramatically affected by the presence of the starboard thruster. A cusp in the port thruster characteristic indicating a maximum in the influence of the race from the starboard thruster can be clearly seen. The cusp occurs at an angle of attack of approximately 20° due to the race being deflected by the free stream. Forces at angles of attack greater than that at the cusp do not return to the corresponding open water values for a single thruster despite, most likely, being free from direct impingement of the race. Assuming the thruster is free from race impingement at higher angles of attack, these differences could be attributed to distortion of the flow field by the starboard thruster i.e. flow straightening or flow rectification effects.

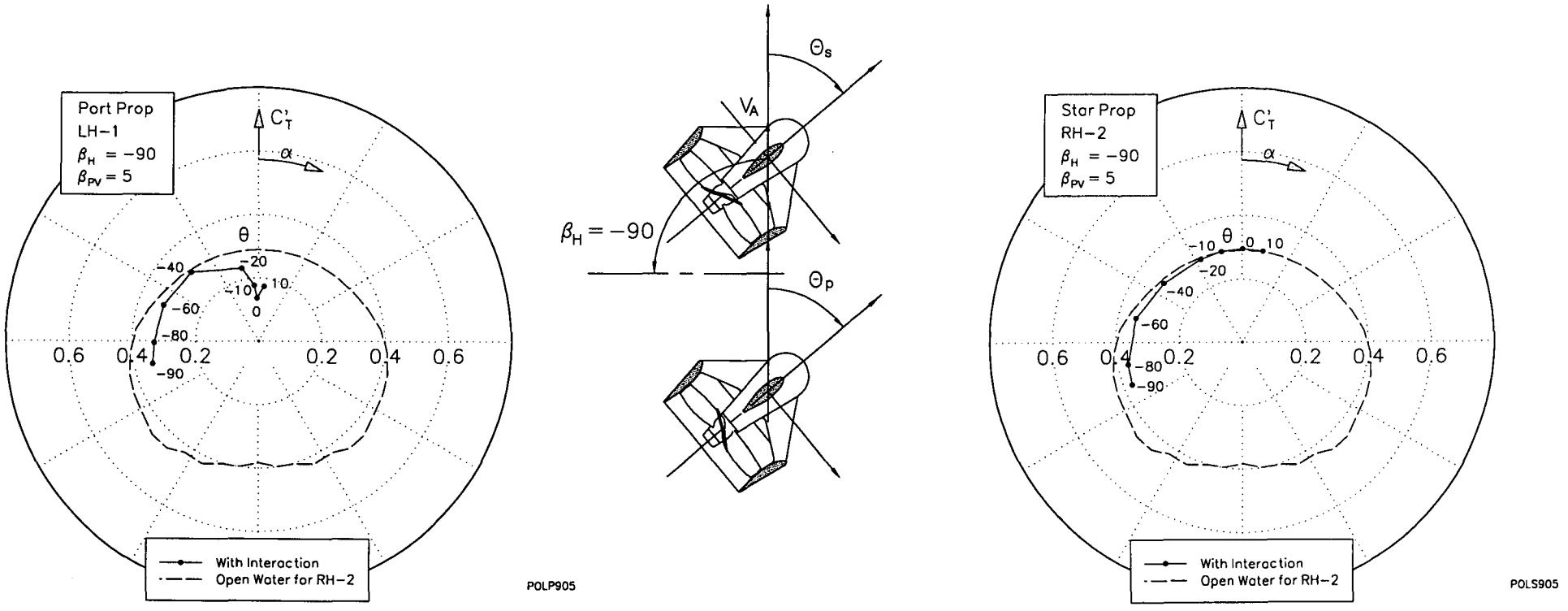

(g) $\beta_H = -90°$

Figure 5.4 Interaction Between Thrusters - Port and Starboard Polar Thrust Characteristic, $\beta_{PV} = 5°$

From the plots, it can be seen that the starboard thruster is essentially unaffected by the presence of the port thruster, whereas the port thruster, as expected, is dramatically affected by the presence of the starboard thruster. A cusp in the port thruster characteristic indicating a maximum in the influence of the race from the starboard thruster can be clearly seen. The cusp occurs at 0° angle of attack since, at 90° drift angle, the race is not deflected by the free stream when the thrusters are in line. Forces at angles of attack remote from the cusp do not return to the corresponding open water values for a single thruster despite, most likely, being free from direct impingement of the race. Assuming the thruster is free from race impingement at higher angles of attack, these differences could be attributed to distortion of the flow field by the starboard thruster i.e. flow straightening or flow rectification effects.

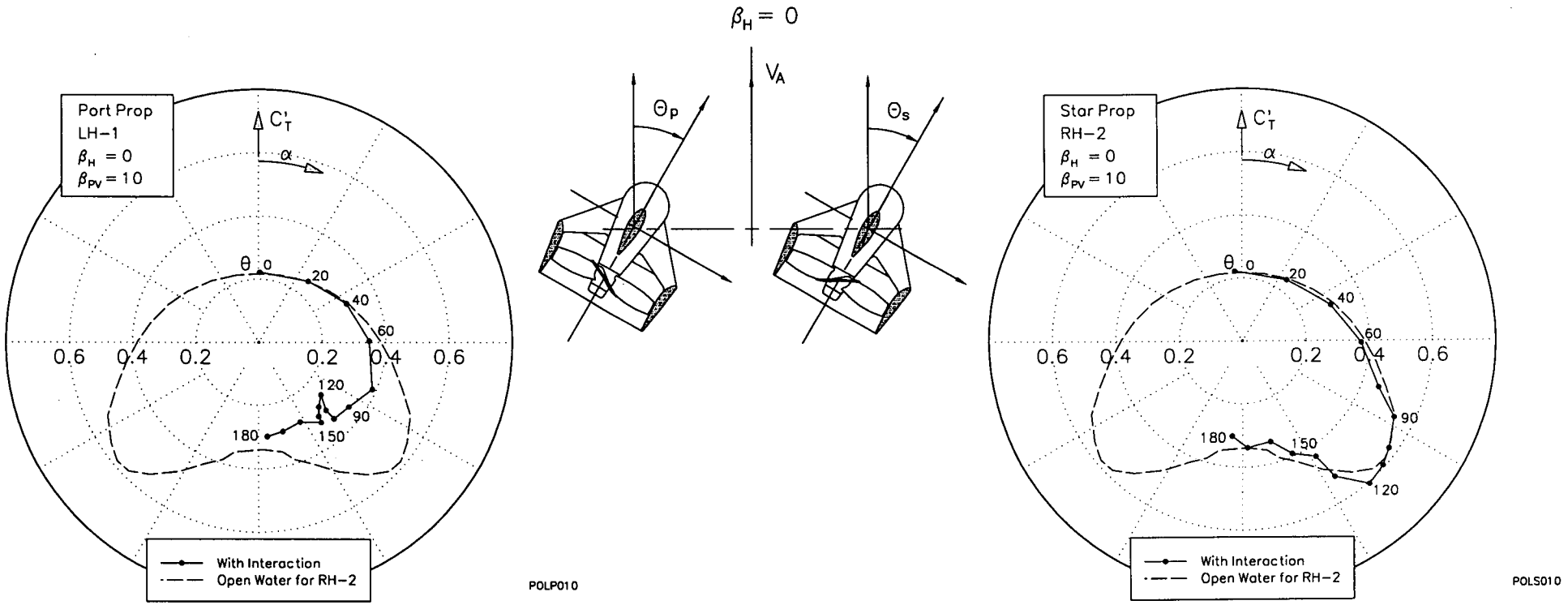

(a) $\beta_H = 0°$

Figure 5.5 Interaction Between Thrusters - Port and Starboard Polar Thrust Characteristic, $\beta_{PV} = 10°$

From the plots, it can be seen that the starboard thruster is essentially unaffected by the presence of the port thruster, whereas the port thruster, as expected, is dramatically affected by the presence of the starboard thruster. A cusp in the port thruster characteristic indicating a maximum in the influence of the race from the starboard thruster can be clearly seen. The cusp occurs at an angle of attack of approximately 120° due to the race being deflected by the free stream. Forces at angles of attack greater than that at the cusp do not return to the corresponding open water values for a single thruster, but tend to values close to bollard pull indicating stagnant flow in the lee of the race.

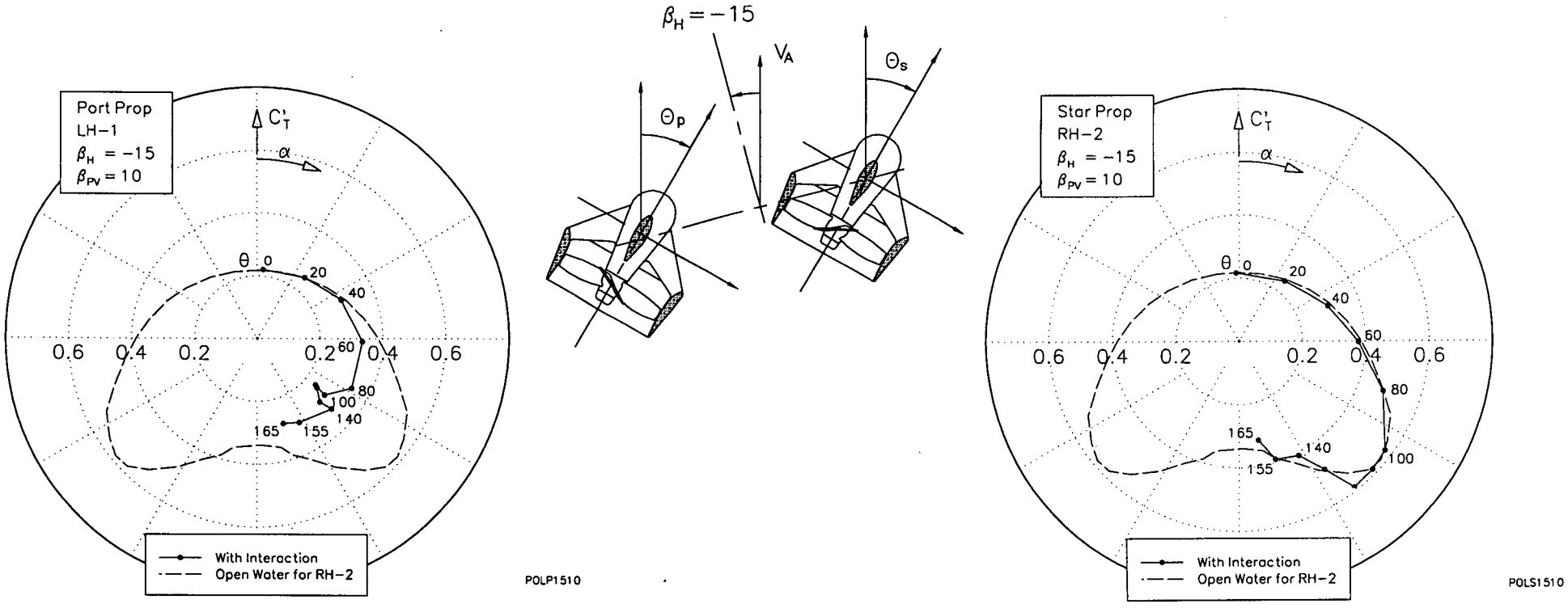

(b) $\beta_H = -15°$

Figure 5.5 Interaction Between Thrusters - Port and Starboard Polar Thrust Characteristic, $\beta_{PV} = 10°$

From the plots, it can be seen that the starboard thruster is essentially unaffected by the presence of the port thruster, whereas the port thruster, as expected, is dramatically affected by the presence of the starboard thruster. A cusp in the port thruster characteristic indicating a maximum in the influence of the race from the starboard thruster can be clearly seen. The cusp occurs at an angle of attack between 110 and 120° due to the race being deflected by the free stream. Forces at angles of attack greater than that at the cusp do not return to the corresponding open water values for a single thruster, but tend to values close to bollard pull indicating stagnant flow in the lee of the race.

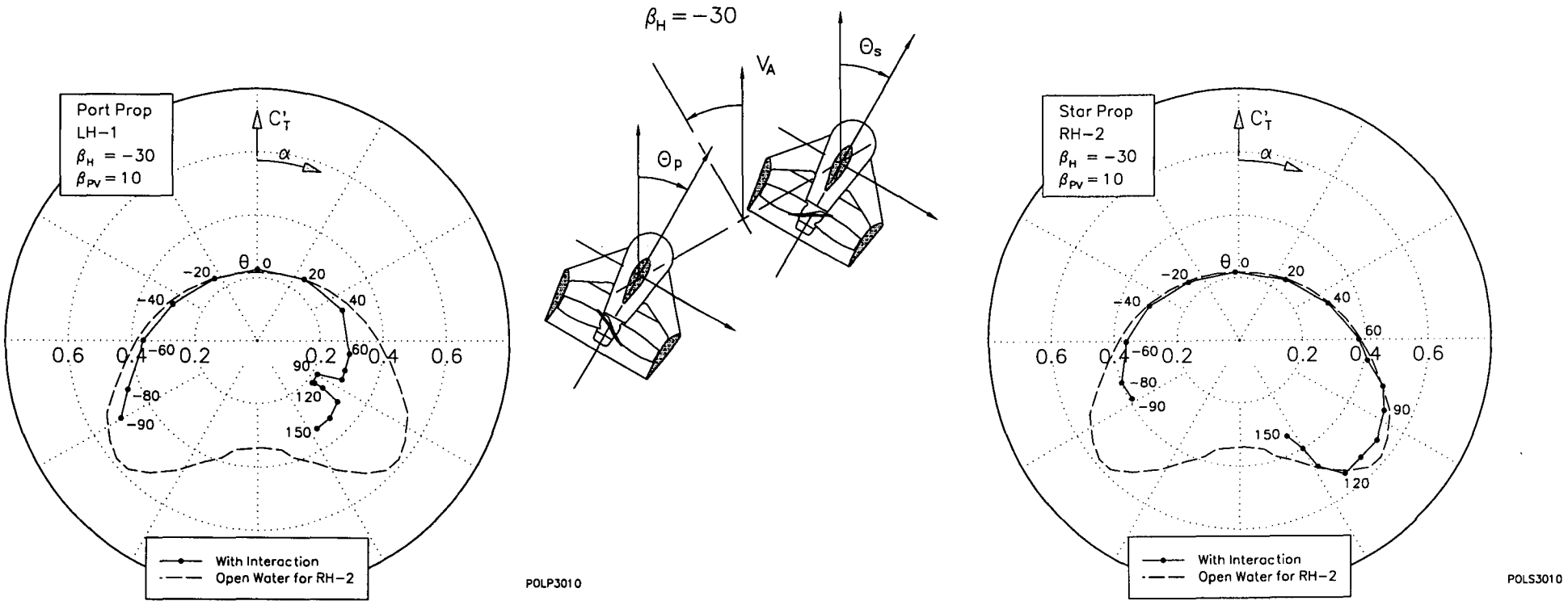

(c) $\beta_H = -30°$

Figure 5.5 Interaction Between Thrusters - Port and Starboard Polar Thrust Characteristic, $\beta_{PV} = 10°$

From the plots, it can be seen that the starboard thruster is essentially unaffected by the presence of the port thruster, whereas the port thruster, as expected, is dramatically affected by the presence of the starboard thruster. A cusp in the port thruster characteristic indicating a maximum in the influence of the race from the starboard thruster can be clearly seen. The cusp occurs at an angle of attack between 90 and 100° due to the race being deflected by the free stream. Forces at angles of attack greater than that at the cusp do not return to the corresponding open water values for a single thruster, but tend to values close to bollard pull indicating stagnant flow in the lee of the race.

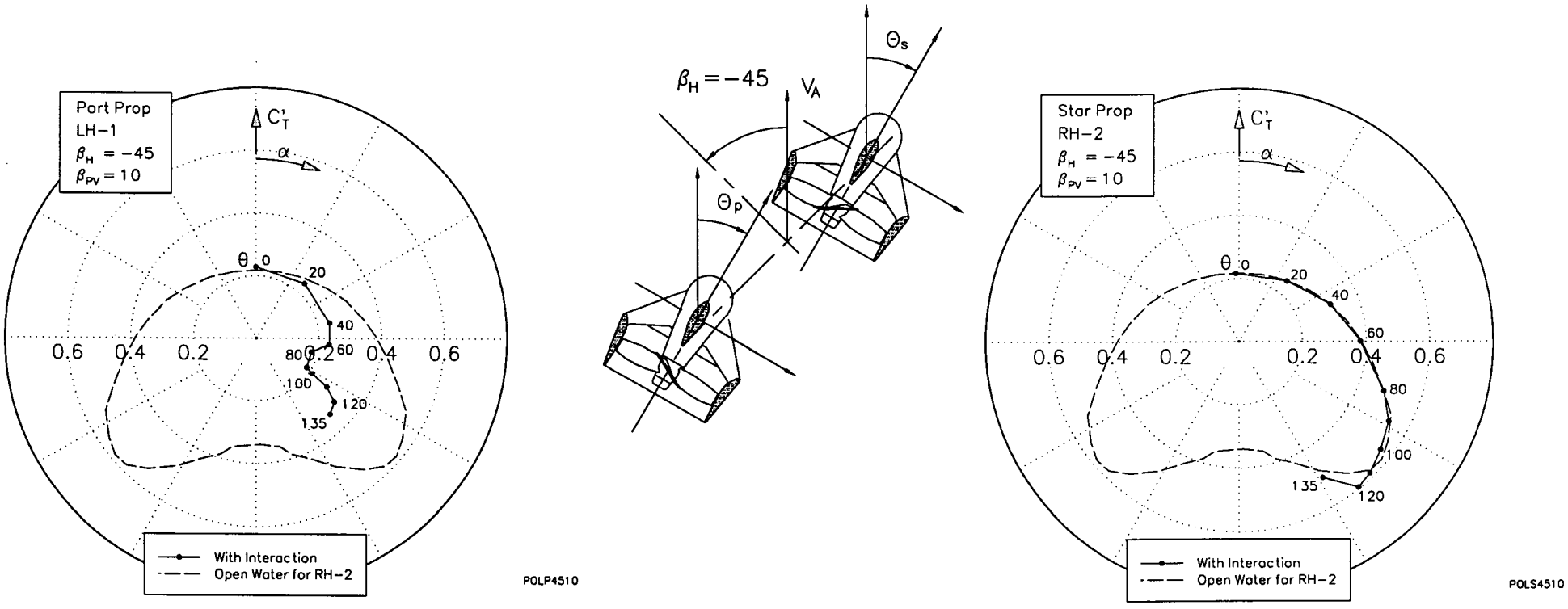

(d) $\beta_H = -45°$

Figure 5.5 Interaction Between Thrusters - Port and Starboard Polar Thrust Characteristic, $\beta_{PV} = 10°$

From the plots, it can be seen that the starboard thruster is essentially unaffected by the presence of the port thruster, whereas the port thruster, as expected, is dramatically affected by the presence of the starboard thruster. A cusp in the port thruster characteristic indicating a maximum in the influence of the race from the starboard thruster can be clearly seen. The cusp occurs at an angle of attack between 80 and 90° due to the race being deflected by the free stream. Forces at angles of attack greater than that at the cusp do not return to the corresponding open water values for a single thruster despite, most likely, being free from direct impingement of the race. Assuming the thruster is free from race impingement at higher angles of attack, these differences could be attributed to distortion of the flow field by the starboard thruster i.e. flow straightening or flow rectification effects.

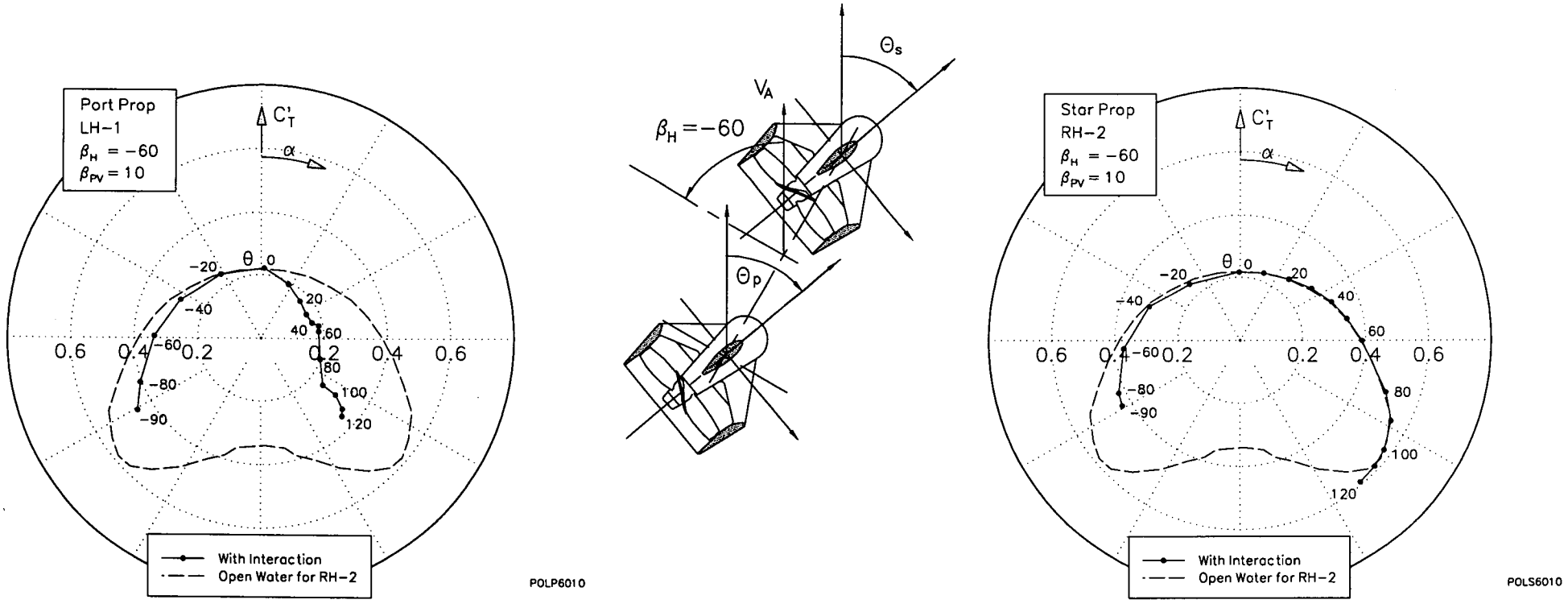

(e) $\beta_H = -60°$

Figure 5.5 Interaction Between Thrusters - Port and Starboard Polar Thrust Characteristic, $\beta_{PV} = 10°$

From the plots, it can be seen that the starboard thruster is essentially unaffected by the presence of the port thruster, whereas the port thruster, as expected, is dramatically affected by the presence of the starboard thruster. In this case, a cusp in the port thruster characteristic indicating a maximum in the influence of the race from the starboard thruster is not apparent (e.g. refer plots for 5° apparent advance angle). Forces at higher angles of attack do not return to the corresponding open water values for a single thruster despite, possibly, being free from direct impingement of the race. Assuming the thruster is free from race impingement at higher angles of attack, these differences could be attributed to distortion of the flow field by the starboard thruster ie flow straightening or flow rectification effects.

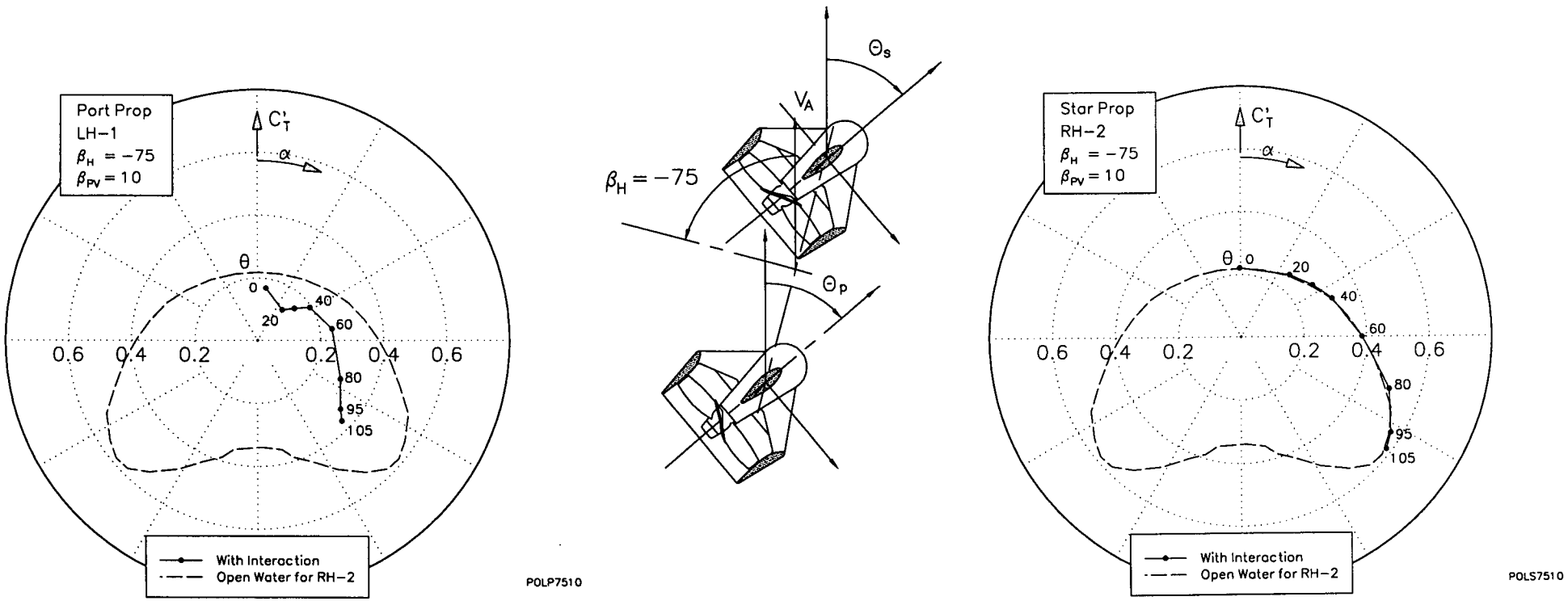

(f) $\beta_H = -75°$

Figure 5.5 Interaction Between Thrusters - Port and Starboard Polar Thrust Characteristic, $\beta_{PV} = 10°$

From the plots, it can be seen that the starboard thruster is essentially unaffected by the presence of the port thruster, whereas the port thruster, as expected, is dramatically affected by the presence of the starboard thruster. A cusp in the port thruster characteristic indicating a maximum in the influence of the race from the starboard thruster can be seen. The cusp occurs at an angle of attack of approximately 20° due to the race being deflected by the free stream. Forces at angles of attack greater than that at the cusp do not return to the corresponding open water values for a single thruster despite, most likely, being free from direct impingement of the race. Assuming the thruster is free from race impingement at higher angles of attack, these differences could be attributed to distortion of the flow field by the starboard thruster ie flow straightening or flow rectification effects.

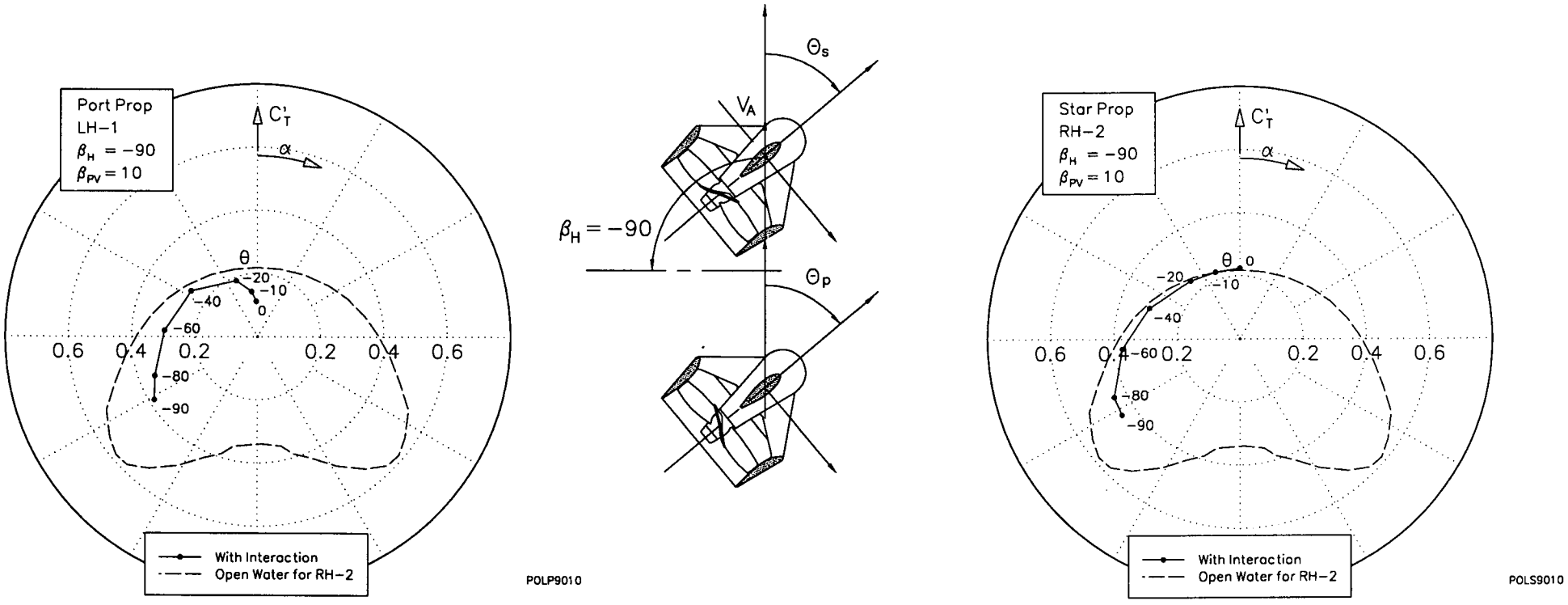

(g) $\beta_H = -90°$

Figure 5.5 Interaction Between Thrusters - Port and Starboard Polar Thrust Characteristic, $\beta_{PV} = 10°$

From the plots, it can be seen that the starboard thruster is essentially unaffected by the presence of the port thruster, whereas the port thruster, as expected, is dramatically affected by the presence of the starboard thruster. A cusp in the port thruster characteristic indicating a maximum in the influence of the race from the starboard thruster can be clearly seen. The cusp occurs at 0° angle of attack since, at 90° drift angle, the race is not deflected by the free stream when the thrusters are in line. Forces at angles of attack remote from the cusp do not return to the corresponding open water values for a single thruster despite, most likely, being free from direct impingement of the race. Assuming the thruster is free from race impingement at higher angles of attack, these differences could be attributed to distortion of the flow field by the starboard thruster i.e. flow straightening or flow rectification effects.

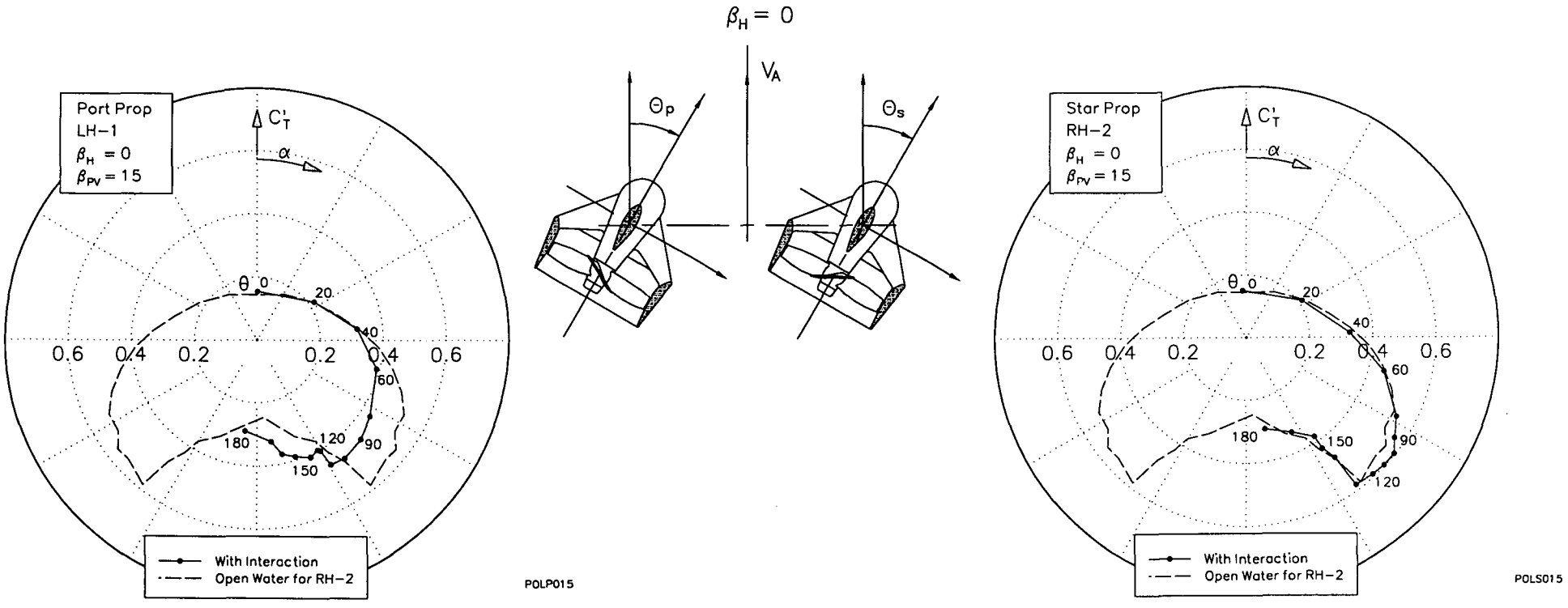

(a) $\beta_H = 0°$

Figure 5.6 Interaction Between Thrusters - Port and Starboard Polar Thrust Characteristic, $\beta_{PV} = 15°$

From the plots, it can be seen that the starboard thruster is essentially unaffected by the presence of the port thruster, whereas the port thruster, as expected, is significantly affected by the presence of the starboard thruster. In this case, a cusp in the port thruster characteristic indicating a maximum in the influence of the race from the starboard thruster is not apparent (e.g. refer plots for 5° apparent advance angle). This is most likely due to the port thruster never becoming fully immersed in the race from the starboard thruster, due to rapid deflection of the race by the free stream at this advance angle. As can be seen from the plot, presumably the port thruster is partially affected by the race for almost all angles of attack tested.

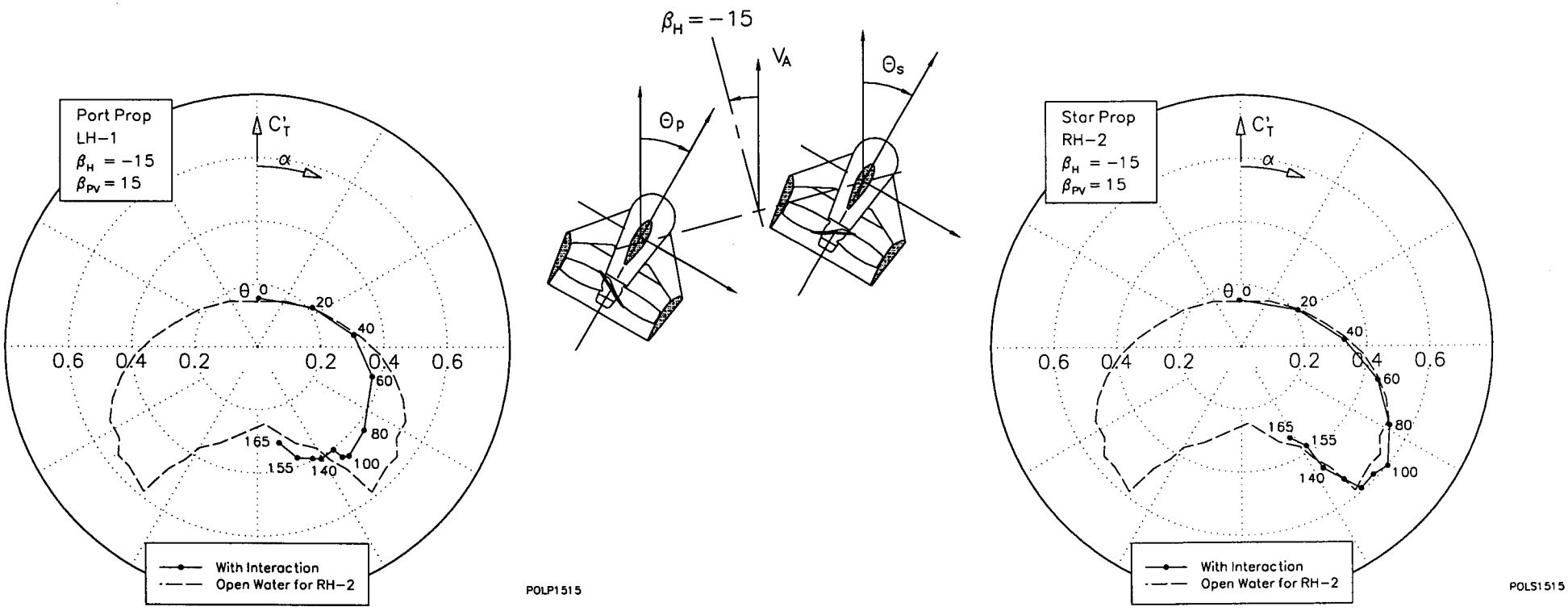

(b) $\beta_H = -15°$

Figure 5.6 Interaction Between Thrusters - Port and Starboard Polar Thrust Characteristic, $\beta_{PV} = 15°$

From the plots, it can be seen that the starboard thruster is essentially unaffected by the presence of the port thruster, whereas the port thruster, as expected, is significantly affected by the presence of the starboard thruster. In this case, a cusp in the port thruster characteristic indicating a maximum in the direct influence of the race from the starboard thruster is not apparent (e.g. refer plots for 5° apparent advance angle). This is most likely due to the port thruster never becoming fully immersed in the race from the starboard thruster, due to rapid deflection of the race by the free stream at this advance angle. As can be seen from the plot, presumably the port thruster is partially affected by the race for almost all angles of attack tested.

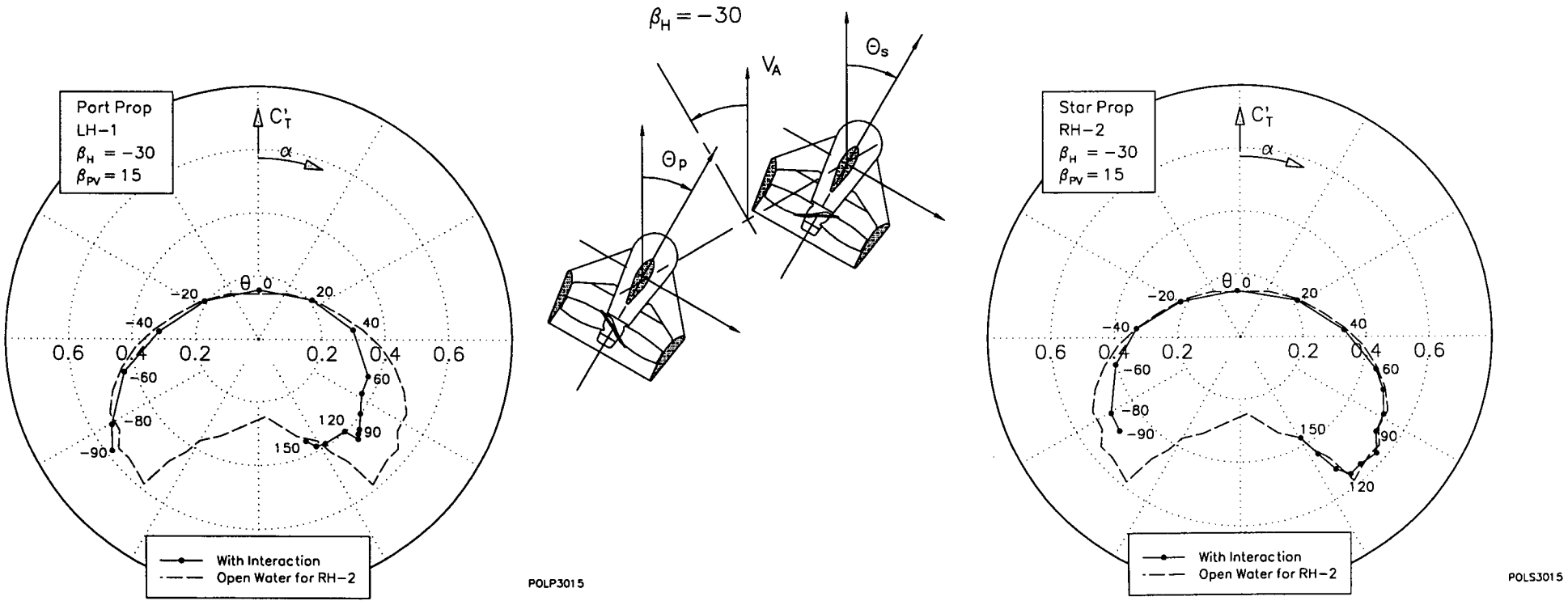

(c) $\beta_H = -30°$

Figure 5.6 Interaction Between Thrusters - Port and Starboard Polar Thrust Characteristic, $\beta_{PV} = 15°$

From the plots, it can be seen that the starboard thruster is essentially unaffected by the presence of the port thruster, whereas the port thruster, as expected, is significantly affected by the presence of the starboard thruster. In this case, a cusp in the port thruster characteristic indicating a maximum in the influence of the race from the starboard thruster is not apparent (e.g. refer plots for 5° apparent advance angle). This is most likely due to the port thruster never becoming fully immersed in the race from the starboard thruster, due to rapid deflection of the race by the free stream at this advance angle. As can be seen from the plot, presumably the port thruster is partially affected by the race for almost all angles of attack tested.

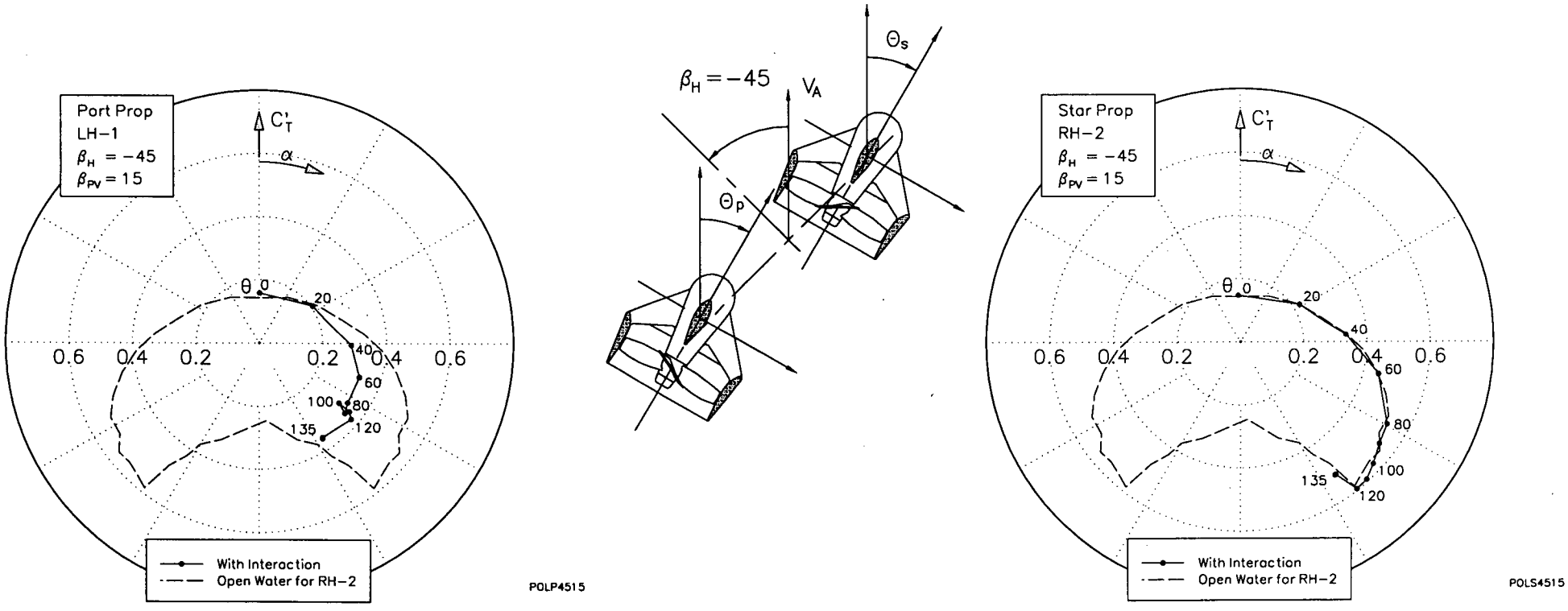

(d) $\beta_H = -45°$

Figure 5.6 Interaction Between Thrusters - Port and Starboard Polar Thrust Characteristic, $\beta_{PV} = 15°$

From the plots, it can be seen that the starboard thruster is essentially unaffected by the presence of the port thruster, whereas the port thruster, as expected, is dramatically affected by the presence of the starboard thruster. A cusp in the port thruster characteristic indicating a maximum in the influence of the race from the starboard thruster can be seen. The cusp occurs at an angle of attack of approximately 100° due to the race being deflected by the free stream. Forces at angles of attack greater than that at the cusp do not return to the corresponding open water values for a single thruster despite, most likely, being free from direct impingement of the race. Assuming the thruster is free from race impingement at higher angles of attack, these differences could be attributed to distortion of the flow field by the starboard thruster i.e. flow straightening or flow rectification effects.

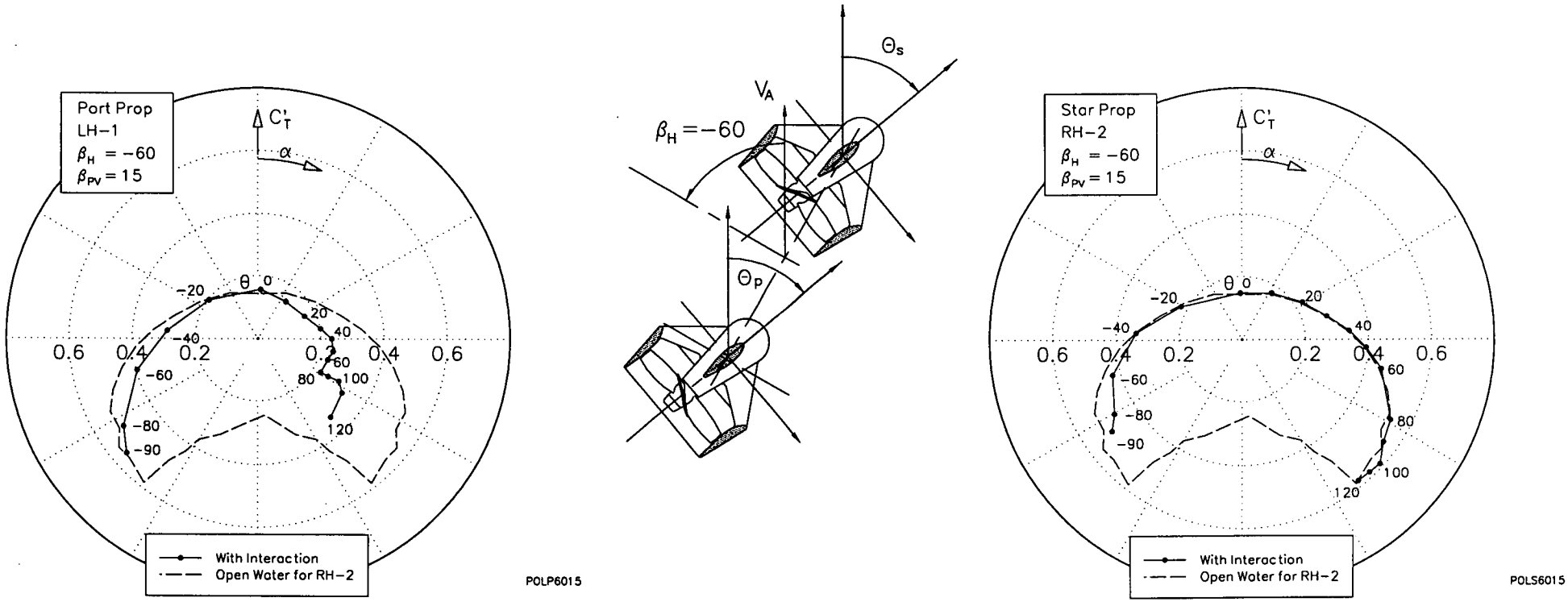

(e) $\beta_H = -60°$

Figure 5.6 Interaction Between Thrusters - Port and Starboard Polar Thrust Characteristic, $\beta_{PV} = 15°$

From the plots, it can be seen that the starboard thruster is essentially unaffected by the presence of the port thruster, whereas the port thruster, as expected, is dramatically affected by the presence of the starboard thruster. A cusp in the port thruster characteristic indicating a maximum in the influence of the race from the starboard thruster can be seen. The cusp occurs at an angle of attack of approximately 80° due to the race being deflected by the free stream. Forces at angles of attack greater than that at the cusp do not return to the corresponding open water values for a single thruster despite, most likely, being free from direct impingement of the race. Assuming the thruster is free from race impingement at higher angles of attack, these differences could be attributed to distortion of the flow field by the starboard thruster i.e. flow straightening or flow rectification effects.

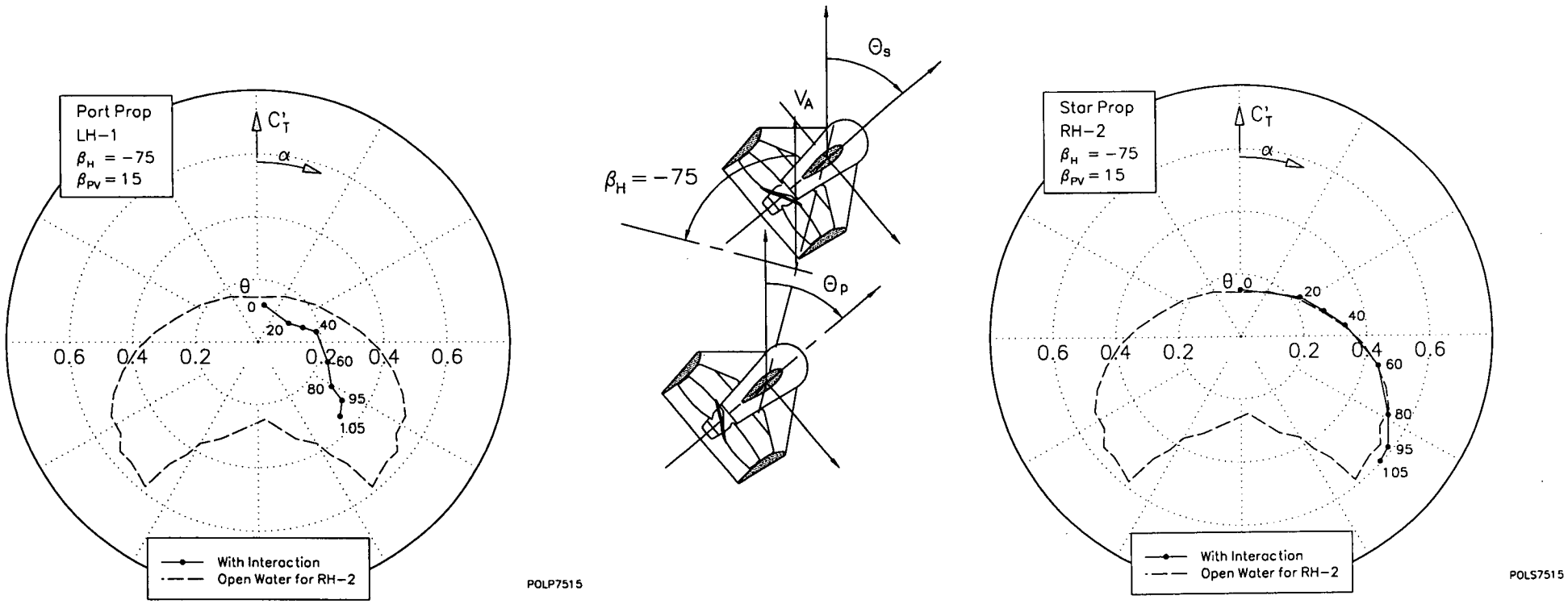

(f) $\beta_H = -75°$

Figure 5.6 Interaction Between Thrusters - Port and Starboard Polar Thrust Characteristic, $\beta_{PV} = 15°$

From the plots, it can be seen that the starboard thruster is essentially unaffected by the presence of the port thruster, whereas the port thruster, as expected, is dramatically affected by the presence of the starboard thruster. In this case, a cusp in the port thruster characteristic indicating a maximum in the influence of the race from the starboard thruster is not apparent (e.g. refer plots for 5° apparent advance angle). Forces at higher angles of attack do not return to the corresponding open water values for a single thruster despite, possibly, being free from direct impingement of the race. Assuming the thruster is free from race impingement at higher angles of attack, these differences could be attributed to distortion of the flow field by the starboard thruster i.e. flow straightening or flow rectification effects.

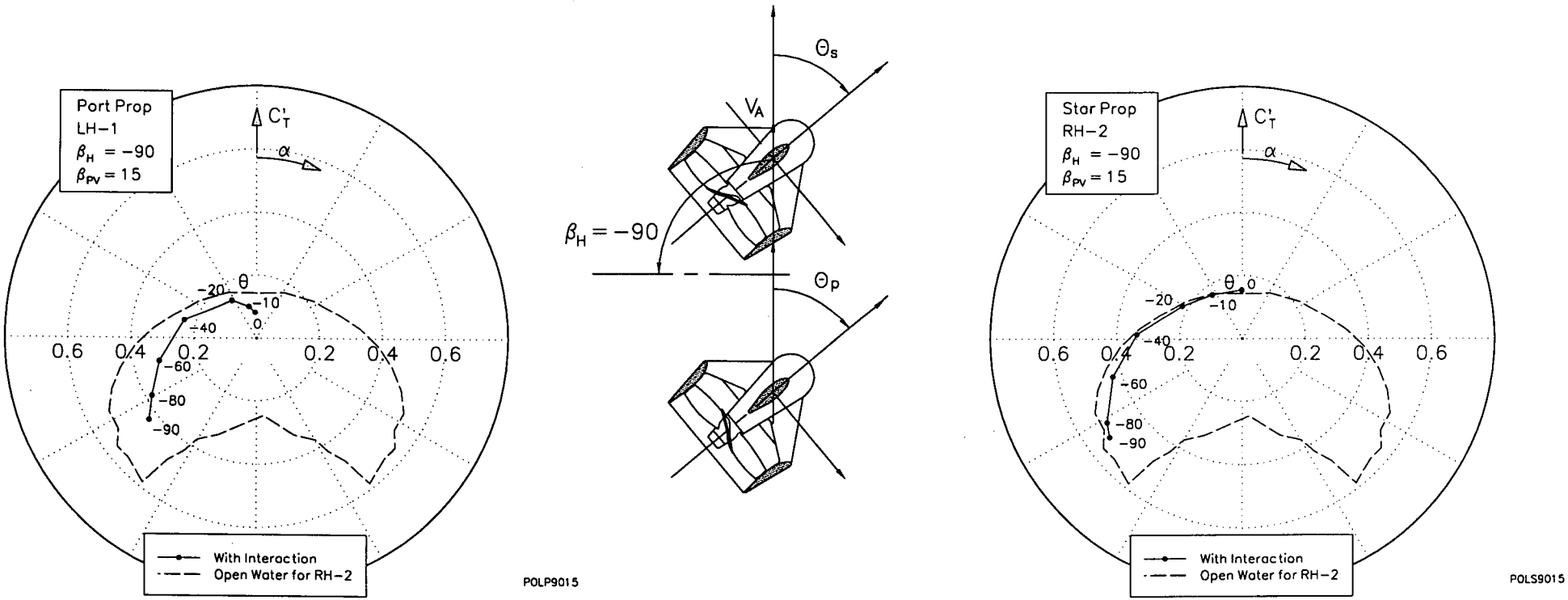

(g) $\beta_H = -90°$

Figure 5.6 Interaction Between Thrusters - Port and Starboard Polar Thrust Characteristic, $\beta_{PV} = 15°$

From the plots, it can be seen that the starboard thruster is essentially unaffected by the presence of the port thruster, whereas the port thruster, as expected, is dramatically affected by the presence of the starboard thruster. A cusp in the port thruster characteristic indicating a maximum in the influence of the race from the starboard thruster can be seen. The cusp occurs at 0° angle of attack since, at 90° drift angle, the race is not deflected by the free stream when the thrusters are in line. Forces at angles of attack remote from the cusp do not return to the corresponding open water values for a single thruster despite, most likely, being free from direct impingement of the race. Assuming the thruster is free from race impingement at higher angles of attack, these differences could be attributed to distortion of the flow field by the starboard thruster i.e. flow straightening or flow rectification effects.

5.2.3 Discussion of Results

The combinations of angle of attack and drift angle tested result in the starboard thruster operating ahead of the port thruster and, in general, the propeller race from the starboard thruster is directed toward the port thruster, as can be seen from Figures 5.2(b) and (c). Hence, the port thruster will be affected by the high energy or exhaust part of the induced flow field from the starboard thruster. Conversely, the starboard thruster can only be affected by the low energy or inlet part of the induced flow field of the port thruster. This would imply that the port thruster will have little or no influence on the starboard thruster. Lehn, 1980, measured interaction between two thrusters, one located behind the other at zero speed and concluded that only for spacings less than two diameters will the rear thruster have any significant effect on the front thruster. The influence of the free stream is to localise the induced velocity field with increasing advance angle, further reducing the likelihood of the trailing thruster effecting the leading thruster. It can be seen from the results that this is indeed the case. There is excellent comparison between the open water measurements for a single thruster and the measurements for the starboard thruster. The only significant discrepancies are at large negative angles of attack where the high energy part of the induced flow field from the port thruster may have some effect on the starboard thruster, although this could, in part, be attributed to propeller induced asymmetry. In any case, these effects may be realistically ignored since they are comparatively small and occur at negative angles of attack at the extreme of the operating envelope, as can be seen in Figure 5.2(b).

In the case of the port thruster, dramatic interaction effects are expected and the results clearly show this. A cusp is apparent in most of the plots where there is maximum interaction due to impingement of the race from the starboard thruster. At the cusp, loss of thrust may be up to 60%. The dependence of the angle of attack where the cusp occurs on the drift angle and advance angle can be easily seen. At 0° drift angle and low advance angle the cusp occurs at just over 90°, as can be seen in Figure 5.4(a). With increasing drift angle the cusp will occur at increasingly smaller angles of attack until the drift angle is 90° where it will occur at 0° angle of attack, as can be seen in Figure 5.4(g). For increasing advance angle, the race is deflected by the free stream and the cusp occurs at increasingly larger angles of attack, as can be seen from comparison of Figures 5.4(a) and 5.5(a). This effect is reduced with increasing drift angle, since the angles of attack where the cusp occurs are reduced. At 90° drift angle the cusp will occur at 0° angle of attack, irrespective of the advance angle, as can be seen from Figures 5.4(g), 5.5(g) and 5.6(g).

Interaction effects are not confined to impingement of the race, but also involve the extended flow field created by the starboard thruster. When the thruster is operating ahead of the race there is clear water and interaction effects are negligible. However, behind the race there is a complex wake field which has a significant effect. This effect is dominant at low drift angles and can be easily seen from the results where forces do not return to the corresponding single thruster values for angles of attack greater than those at the cusp, e.g. Figures 5.4(a) and (b). When the port thruster is more remote from the race and free from its effects, there still exists the possibility of interaction from the general distortion of the free stream created by the starboard thruster. The thruster tends to bend the free stream flow in line with its longitudinal axis. In ship manoeuvring studies this flow straightening effect created by hull and propellers is often termed *flow rectification*. This effect is dominant at high drift angles and can easily be seen from the results where forces do not return to the

corresponding single thruster values at high angles of attack, e.g. Figures 5.4(g) and 5.5(g). Further discussion of the specific nature of thruster interaction is presented in Section 5.3 where a simple mathematical model is formulated.

Correlation of the results with the angle of attack/drift angle envelope shown in Figure 5.2(e), enable observations to be made with regard to the influence interaction will have on each mode of tug operation. As mentioned above, maximum interaction generally occurs where there is direct impingement of the race and these points may be plotted on the angle of attack/drift angle envelope shown in Figure 5.2(e). Curves of maximum interaction for each advance angle tested have been plotted on the envelope, as shown in Figure 5.7. It can immediately be seen that for pulling using the forward tow point in both the direct and indirect modes, there is the possibility of interaction between the thrusters from race impingement. For pulling using the aft tow point and pushing, interaction from race impingement is avoided. However, there is still the possibility of interaction due to distortion of the extended flow field.

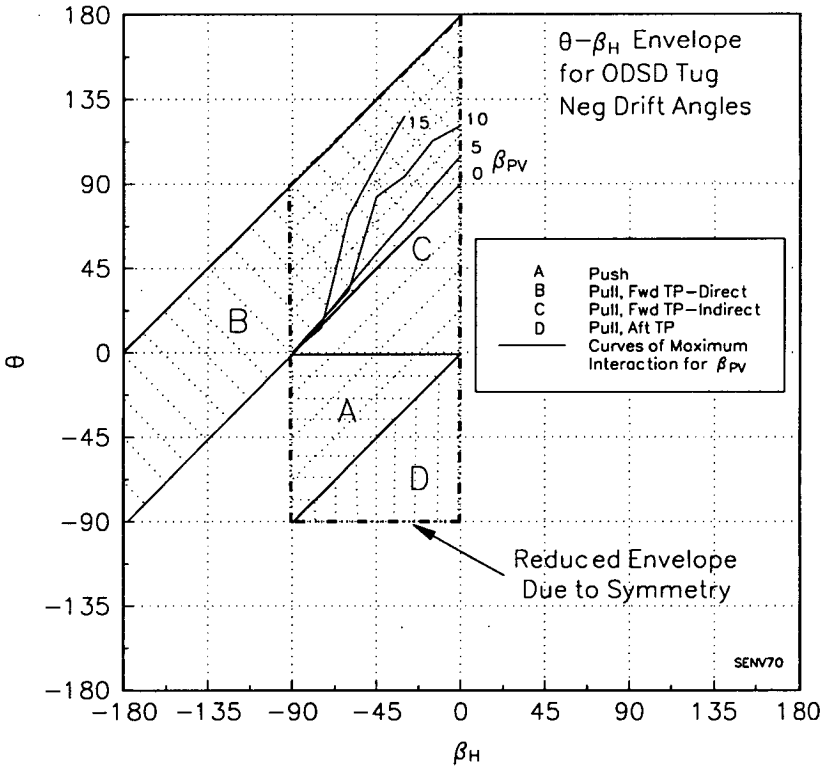

Figure 5.7 Envelope of Angle of Attack and Drift Angle Combinations for Omni-directional Stern Drive Tugs with Curves of Maximum Interaction

5.3 Mathematical Model

In the previous section, from consideration of realistic combinations of angle of attack and drift angle and the experimental results, it was possible to show that interaction effects are essentially confined to the trailing thruster only. Hence, in formulating a mathematical model it is assumed that the characteristics of the leading thruster are the same as that of a single thruster. Further, it is also assumed that the flow field induced by the leading thruster is the same as that of a single thruster.

From the experimental results, as described in the previous section, it would appear that the influence of interaction can be separated into specific flow effects, depending

on the relative positions of each thruster. Three effects have been identified as follows:

- race impingement;
- race wake, and;
- flow rectification.

Each effect is discussed in detail below and simple relations are presented for their modelling.

5.3.1 Race Impingement

The race, being the highest energy part of the induced flow, causes the most significant interaction effects and, hence, requires the most consideration of the above listed effects. Properties of the race required to be determined include the velocity, diameter and trajectory. The following approach has been used in estimating the characteristics of the race for thruster i and its effect on thruster j upon which it is impinging:

- calculate the mean velocity of the race at duct exit from thruster i using momentum considerations;
- calculate properties and trajectory of race from momentum considerations; and
- calculate forces produced from the affected thruster j using both free stream and race velocities from open water measurements for a single thruster.

To calculate the initial velocity of the race, the linear momentum equation is applied along the longitudinal axis of the thruster and the influence of swirl in the propeller race is ignored. An appropriate control volume may be defined enclosing the thruster and upstream part of the induced streamtube, as shown in Figure 5.8. The streamtube entrance is located sufficiently upstream to assume free stream conditions and the exit is coincident with the duct exit.

The linear momentum equation for applications of steady flow and where the control volume is fixed and rigid may be written as follows:

$$\oint_{A_{cv}} \rho \vec{V}\left(\vec{V}_{rel} \cdot \hat{n}\right) dA = \sum \vec{F} \tag{5.4}$$

The momentum flux term is evaluated from the velocities at the entrance and exit of the streamtube as follows:

$$\oint_{A_{cv}} \rho \vec{V}\left(\vec{V}_{rel} \cdot \hat{n}\right) dA = \rho A_O V_O \left(V_R - V_A \cos\theta\right) \tag{5.5}$$

The force term comprises the two external forces acting on the control volume, the thrust in the longitudinal direction X and the net force inducing the curvature in the streamtube resolved along the longitudinal axis of the thruster as follows:

$$\sum \vec{F} = X - \rho V_O A_O V_A (1 - \cos\theta) \tag{5.6}$$

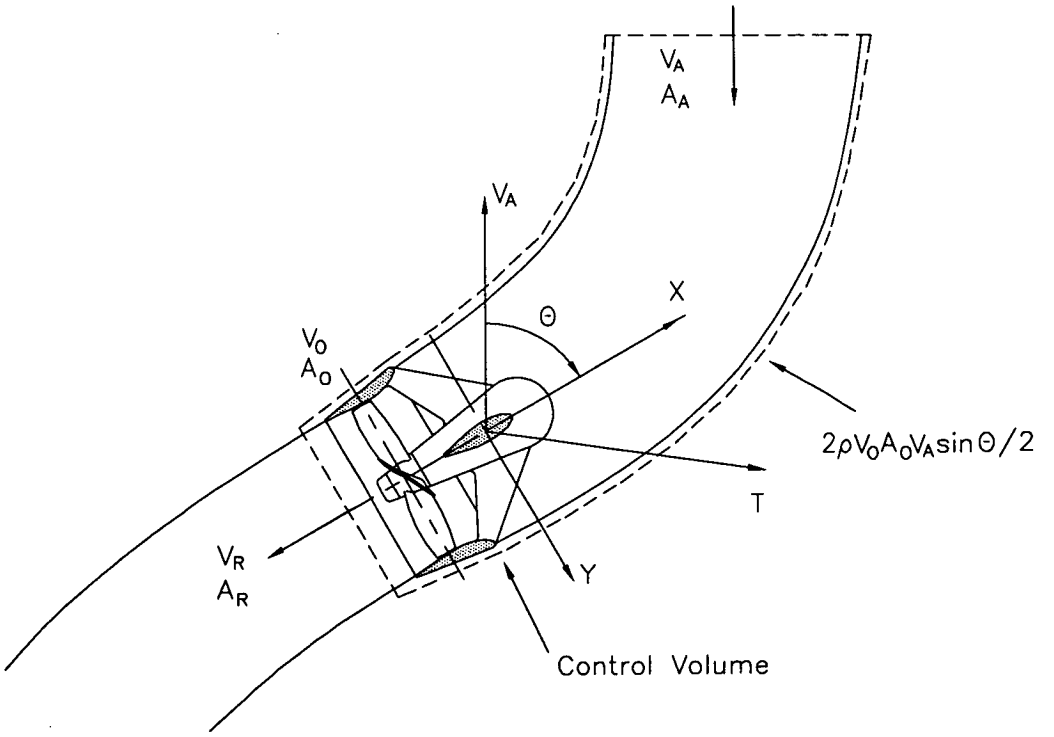

Figure 5.8 Assumed Geometry of Thruster Streamtube and Control Volume for Calculation of Initial Race Velocity.

The force inducing curvature in the streamtube is assumed to be simply that required to deflect a streamline with velocity V_A through the angle of attack θ. From continuity, and ignoring contraction of the race at exit, the velocity at the disc V_O may be replaced by that at exit V_R. In applying momentum theory to propeller race calculation, it is generally accepted that an empirical coefficient, the so called *race coefficient k*, is required. This is commonly applied to the thrust term. Combining equations 5.5 and 5.6 and introducing the above mentioned changes results in an expression which may be solved for V_R, hence:

$$V_R = \frac{1}{2}\left[V_A(2\cos\theta - 1) + \sqrt{V_A^2(2\cos\theta - 1)^2 + \frac{4kX}{\rho A_O}}\right] \qquad (5.7)$$

In analysing the interaction between thrusters it is more convenient to consider the velocity of the race in terms of an advance angle, hence, equation 5.7 may be non-dimensionalised in terms of the free stream and race advance angles as follows:

$$\tan\beta_{PR} = \frac{1}{2}\left[\tan\beta_{PV}(2\cos\theta - 1) + \sqrt{\tan^2\beta_{PV}(2\cos\theta - 1)^2 + \frac{2kC'_X}{\cos^2\beta_{PV}}}\right] \qquad (5.8)$$

Another useful parameter is the velocity ratio R_V, which may be defined as follows:

$$R_V = \frac{V_A}{V_R} = \frac{\tan\beta_{PV}}{\tan\beta_{PR}} \qquad (5.9)$$

The race coefficient k may be determined from the experimental results using the so called *thrust identity* technique. This involves comparison of measured forces from

the thruster effected by interaction with those from a single thruster in open water, enabling the effective angle of attack and advance angle to be determined. Details of this method are given in Appendix D. The simplest case of interaction between thrusters is where the drift angle is 90° and the angle of attack is 0°. A straight forward assumption for this configuration is that the race velocity and diameter do not change from that at exit, particularly since the distance from the duct exit to the centre of rotation of the rear thruster is only 1.3 diameters. From the experimental data, effective advance angles have been calculated using thrust identity. A value of $k = 0.43$ has been found from comparison of the experimental results with equation 5.8, as shown in Figure 5.9. It can be seen from Figure 5.9 that with adjustment of this coefficient there is favourable comparison between equation 5.8 and the experimental results.

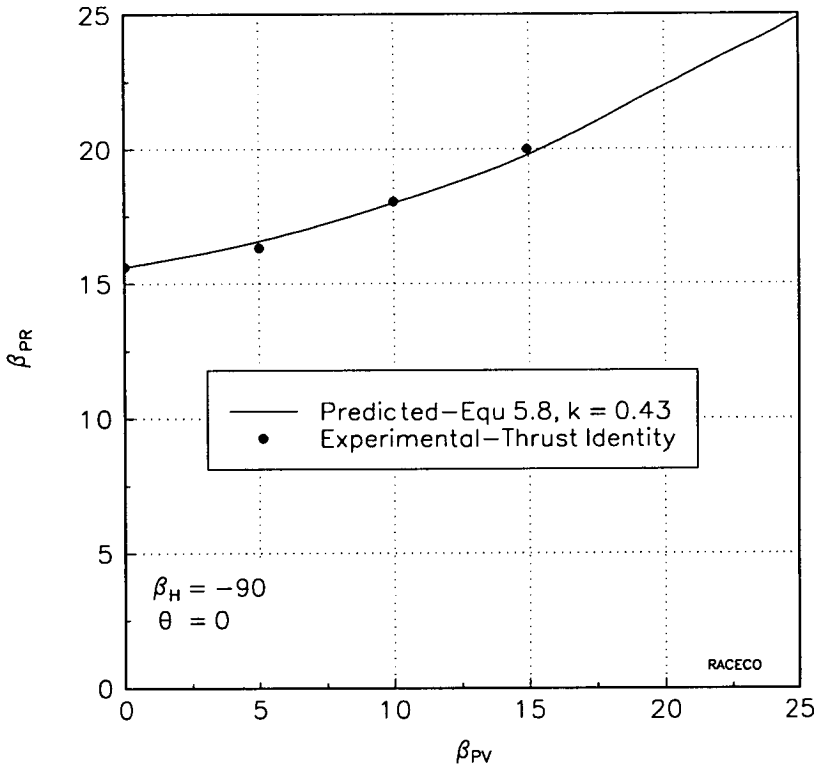

Figure 5.9 Determination of Race Coefficient from Experimental Data

An indication of how well the race velocity can be predicted using equation 5.8 for a range of drift angles, advance angles and angles of attack can, once again, be obtained using the experimental results. In the previous section, points of maximum interaction were found for every advance angle and drift angle tested, as shown in Figure 5.7. Assuming the race velocity is constant and for maximum interaction the affected thruster is completely immersed in the race, approximate values of the race velocity can be obtained using the thrust identity method described above. These results are compared with equation 5.8 as shown in Figure 5.10. It can be seen from Figure 5.10 there is favourable agreement, particularly at low advance angles. However, at higher advance angles the race velocity is somewhat over predicted by equation 5.8.

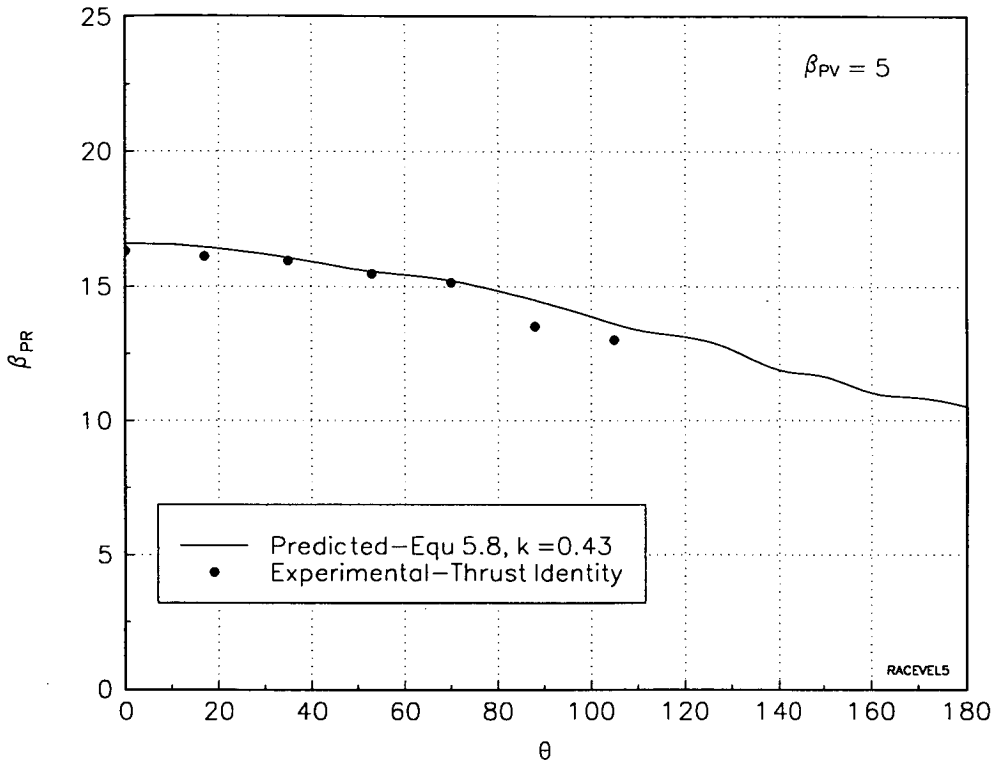

(a) $\beta_P = 5°$

Figure 5.10 Comparison of Theoretical and Experimental Determination of Race Velocity

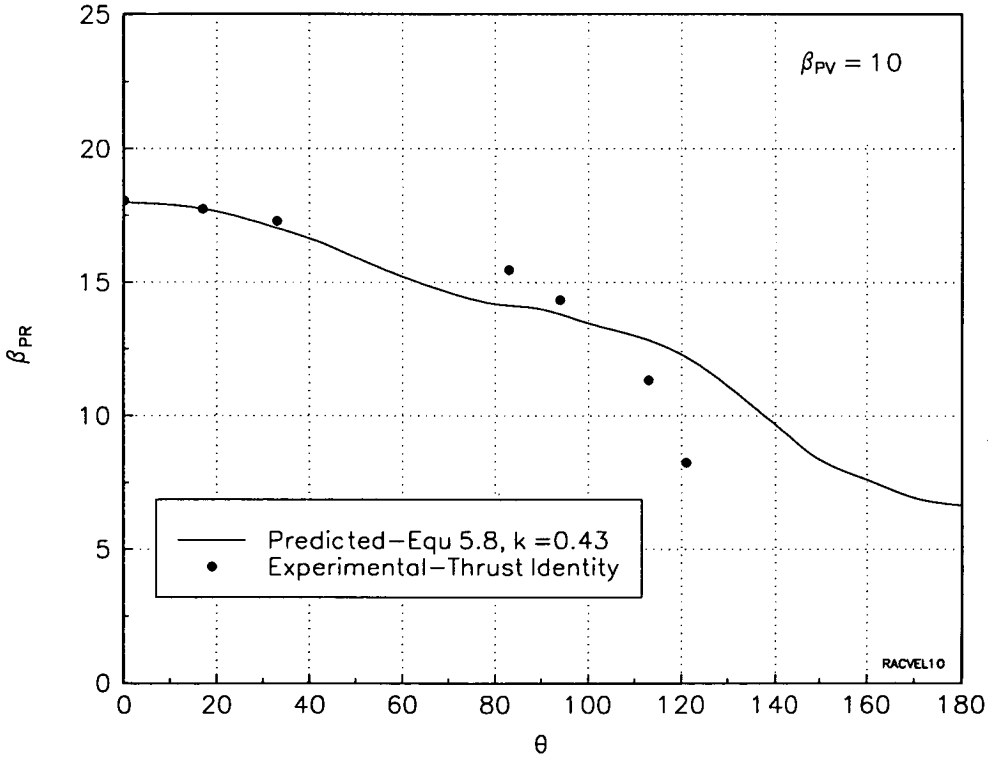

(b) $\beta_P = 10°$

Figure 5.10 Comparison of Theoretical and Experimental Determination of Race Velocity

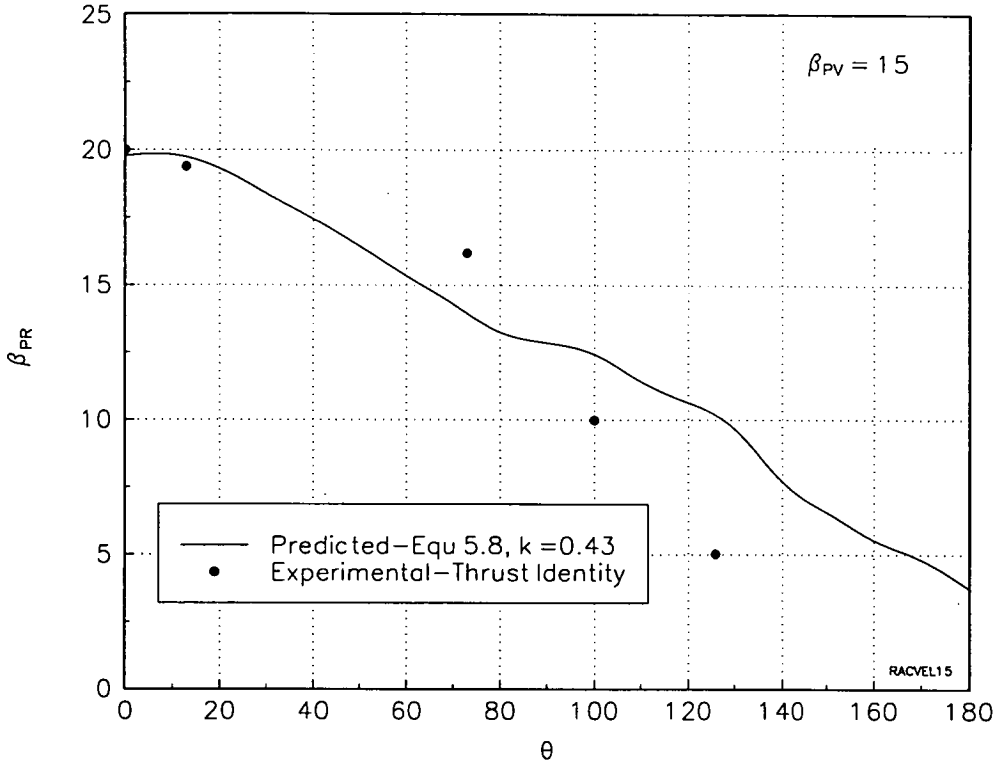

(c) $\beta_P = 15°$

Figure 5.10 Comparison of Theoretical and Experimental Determination of Race Velocity

Having derived an expression for the initial race velocity, it is possible to consider the trajectory of the race. This problem is closely related to that of a turbulent jet in a cross flow for which numerous experimental and theoretical studies have been carried out. Despite the very complex nature of such flows, significant success has been achieved in describing their characteristics for cases of both perpendicular and arbitrary angle of jet injection. A number of empirical expressions have been developed from experimental data. Margason, 1968, performed a series of experiments using flow visualisation to determine the jet trajectory and derived an empirical expression to match the data. Margason also provides a review of empirical expressions and measured data from other sources. Various analytical methods have also been developed and a number of these methods consider the processes affecting an element of the jet, integrating to find the jet trajectory and variation of jet properties. Rajaratnam, 1976 and Schetz, 1980 provide a comprehensive review of the literature dealing with this approach. Methods of CFD have also been applied to the problem e.g. Nienhuis, 1992, used a computational approach in relation to the performance of tunnel thrusters.

There are some significant differences between the present problem and the above mentioned work. Only limited ranges of the freestream/jet velocity ratio have been investigated, i.e. R_V as defined by equation 5.9. The present problem involves a very large range of the velocity ratio. In general, these analyses are more concerned with jet behaviour for extended distances downstream, whereas the present problem is concerned with only the first two diameters. As with jets in a stagnant environment, jets in a cross flow may be described in terms of a series of zones. The present study is confined to the initial zone where there are considerable differences in the velocity

profiles for a standard initially uniform jet and the propeller race. Nienhuis, 1992, made LDV measurements in the propeller race of a thruster at low advance angles and showed that the velocity profile in the initial region is extremely annular, with the velocity at the centre being negative due to the influence of the gear case and hub. Neinhuis also showed that downstream the profile became essentially that of a turbulent jet, however, the annular profile persists for approximately eight diameters. Chassaing et al., 1974, performed experiments for the case of perpendicular injection with cylindrical and coaxial jets and found that the jet with the annular profile was significantly less deflected by the free stream, i.e. the outer jet delays the shearing of the central jet. Other factors that no doubt have some influence include swirl in the race and the presence of the ground board. Finally, in general, the above mentioned analyses involve numerical solution of extensive algorithms and it should be noted that the present problem is considered only a relatively small part of the larger numerical algorithm to predict tug behaviour. With this in mind, the objective here is not to attempt to carry out a detailed study into the fluid mechanics of the propeller race in a cross flow, but to develop a simple model, preferably in closed form, that suitably predicts the relevant trends. An appropriate approach would then be similar to that mentioned above, where an element of the race is considered, introducing simplifying assumptions so that a closed form solution can be found.

A global coordinate system aligned with the free stream for representing the race trajectory is shown in Figure 5.11 and a fixed control volume enclosing an element of the race is defined. A coordinate system fixed to the element is also shown defining the local normal and tangential directions.

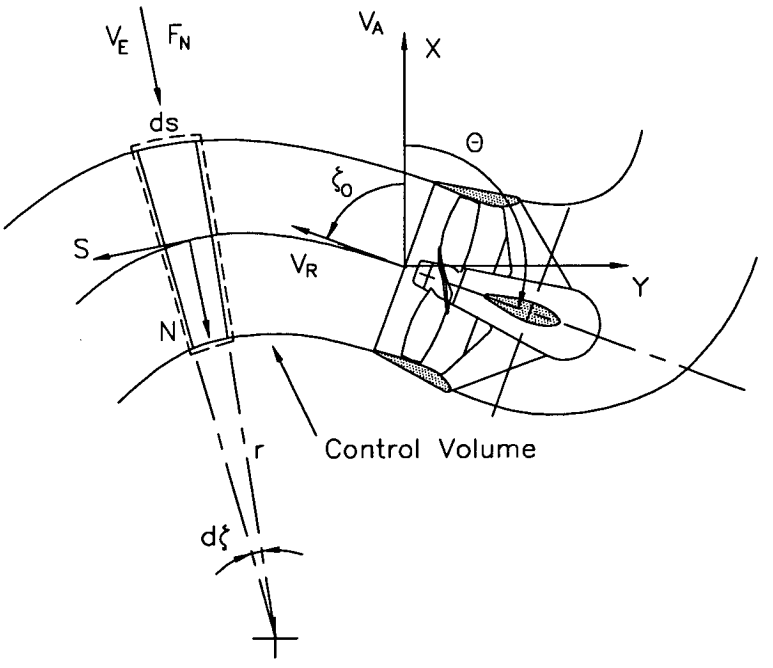

Figure 5.11 Global and Local Coordinate System for Representing Race Trajectory

The linear momentum equation, as expressed by equation 5.4, may be applied along the normal and tangential axes of the element to simplify the analysis and since only the first two diameters of the race are of interest, momentum in the normal direction only is considered. The dominant fluid processes affecting the element are forces due to blockage of the free stream and entrainment of the free stream. Normal forces due

to the freestream may be calculated, assuming that the element of the race acts as an element of an infinite cylinder aligned at the local angle of attack, as first proposed by Volinskiy and described by Abramovich, 1963. To determine the area of the jet exposed to the free stream, it is assumed that the mean velocity is constant, i.e. only the diameter increases due to entrainment, hence the force term in equation 5.4 may be evaluated:

$$\sum \bar{F} = F_N = \tfrac{1}{2}\rho\left(V_A \sin\zeta\right)^2 C_N\left(D_R + \frac{dD_R}{2}\right)ds \tag{5.10}$$

Entrainment of fluid into the control volume is represented by the usual expression:

$$\frac{d\dot{m}}{ds} = \frac{d\left(\rho A_R V_R\right)}{ds} = \rho l V_E \tag{5.11}$$

where l, the perimeter of the turbulent region, is assumed to be equal to the circumference of the race. Kamotani and Greber, 1974, performed experiments for the case of perpendicular injection with cylindrical jets and found that the components of the free stream in the normal and tangential directions independently control the entrainment rate, hence, equation 5.11 may be rewritten as follows:

$$\frac{d\left(\rho A_R V_R\right)}{ds} = \rho\pi D_R E_N V_A \sin\zeta \tag{5.12}$$

where E_N is the entrainment coefficient for the normal direction. The momentum flux term in equation 5.4 is evaluated as the sum of the terms due to entrainment and acceleration of the fluid in the element as follows:

$$\oint_{A_{cv}} \rho\vec{V}\left(\vec{V}_{rel}\cdot\hat{n}\right)dA = \rho\left(A_R + dA_R\right)V_R^2 d\zeta - d\left(\rho A_R V_R\right)V_A \sin\zeta \tag{5.13}$$

Equating equations 5.10 and 5.13 and substituting equation 5.12 gives:

$$\tfrac{1}{2}\rho\left(V_A \sin\zeta\right)^2 C_N D_R ds + \rho\left(V_A \sin\zeta\right)^3 C_N \frac{E_N}{V_R} ds^2$$

$$= \frac{\rho A_R V_R^2 ds}{r} + \frac{\rho\pi D_R V_R E_N V_A \sin\zeta ds^2}{r} - \rho\pi D_R E_N\left(V_A \sin\zeta\right)^2 ds \tag{5.14}$$

Higher order terms may be ignored, which is equivalent to neglecting the growth of the diameter for calculation of forces from the free stream and the influence of the entrainment on the curvature of the element. Hence, the following differential equation for the race trajectory is obtained:

$$\frac{d^2 y_R}{dx_R^2} + K\left(\frac{dy_R}{dx_R}\right)^2 \sqrt{1+\left(\frac{dy_R}{dx_R}\right)^2} = 0, \text{ where } K = \frac{2R_V}{\pi D_O}\left(C_N + 2\pi E_N\right) \tag{5.15}$$

Integrating equation 5.15 and rearranging to make x_R the dependent variable gives the equation for the race trajectory:

$$\bar{x}_R = \frac{e^{\bar{y}_R}\left|\tan\frac{\zeta_O}{2}\right|}{2} + \frac{1}{2e^{\bar{y}_R}\left|\tan\frac{\zeta_O}{2}\right|} - \frac{1}{\sin\zeta_O} \tag{5.16}$$

where,

$$\bar{x}_R = -R_V^2 \frac{2}{\pi}\frac{x_R}{D_O}\left(C_N + 2\pi E_N\right) \tag{5.17}$$

and

$$\bar{y}_R = -R_V^2 \frac{2}{\pi}\frac{y_R}{D_O}\left(C_N + 2\pi E_N\right) \tag{5.18}$$

Equation 5.16 is of the same form as that presented by Shandorov and described by Margason, 1968, except Shandorov only considered the influence of forces from the free stream on the jet and not entrainment. (As noted by Margason, Shandorov's solution is very similar to that presented by Volinskiy which is described by Abramovich, 1963). Typical values for the coefficients in equation 5.16 have been assumed, that is for the drag coefficient 1.2 and the entrainment coefficient 0.3, although Kamotani and Greber, 1974, showed that the entrainment coefficient is a function of the velocity ratio. Results from equation 5.16 have been compared with the experimental results of Margason, 1968 and there is favourable comparison. An indication of how well equation 5.16 compares with results from the present experiments can be determined using the relative thruster locations at points of maximum interaction, as found in the previous section (refer Figure 5.7). This comparison shows that, in general, equation 5.16 over predicts the deflection of the race. This could be attributed to the effects noted by Chassaing et al., 1974, for coaxial jets, as described above and, possibly, to distortion of the free stream from the induced flow of the affected thruster. To attempt to rectify this discrepancy it would seem reasonable, in light of the above, to ignore the influence of entrainment particularly since only the first two diameters of the trajectory are of interest. This results in the equation by Shandorov, as mentioned above, although the coefficients used by Shandorov correspond to a drag coefficient of 4.7. Introducing this modification, equations 5.17 and 5.18 may be rewritten:

$$\bar{x}_R = -R_V^2 \frac{2C_N}{\pi}\frac{x_R}{D_O} \tag{5.19}$$

and

$$\bar{y}_R = -R_V^2 \frac{2C_N}{\pi}\frac{y_R}{D_O} \tag{5.20}$$

This modification significantly improves the comparison between equation 5.16 and the experimental results. The relative position of thrusters for maximum interaction and the corresponding predicted race trajectory are shown in Figure 5.12. From which, it can be seen that comparison is favourable at 5° becoming progressively worse with increasing advance angle such that at 15° the comparison is poor. This partly could be attributed to changes in the race structure and cross section that occur with changes in the velocity ratio or advance angle. However, this is satisfactory since thruster forces become less important with increasing advance angle such that differences due to interaction are negligible above about 12°, as mentioned in section 5.2.1. The location of the affected thruster shown in Figure 5.12 is the centre of the leading edge of the duct relative to the centre of the trailing edge of the other, which is considered more representative of the thruster's location, as shown in Figure 5.11. Hence, for the purposes of interaction the relative location of each thruster can be calculated using the following transformation in the free stream aligned coordinate system defined in Figure 5.11:

$$\begin{aligned} x_{ps} &= +s\sin\beta_H - L_{CLD}\cos\theta_p + L_{CTD}\cos\theta_s \\ y_{ps} &= -s\cos\beta_H - L_{CLD}\sin\theta_p + L_{CTD}\sin\theta_s \end{aligned} \tag{5.21}$$

where, s, L_{CLD} and L_{CTD} are the thruster spacing, distance between centre of rotation and leading edge of duct and distance between centre of rotation and trailing edge of duct respectively. For the case of the location of the starboard thruster relative to the port, the sign of the first term in each equation would need to be reversed.

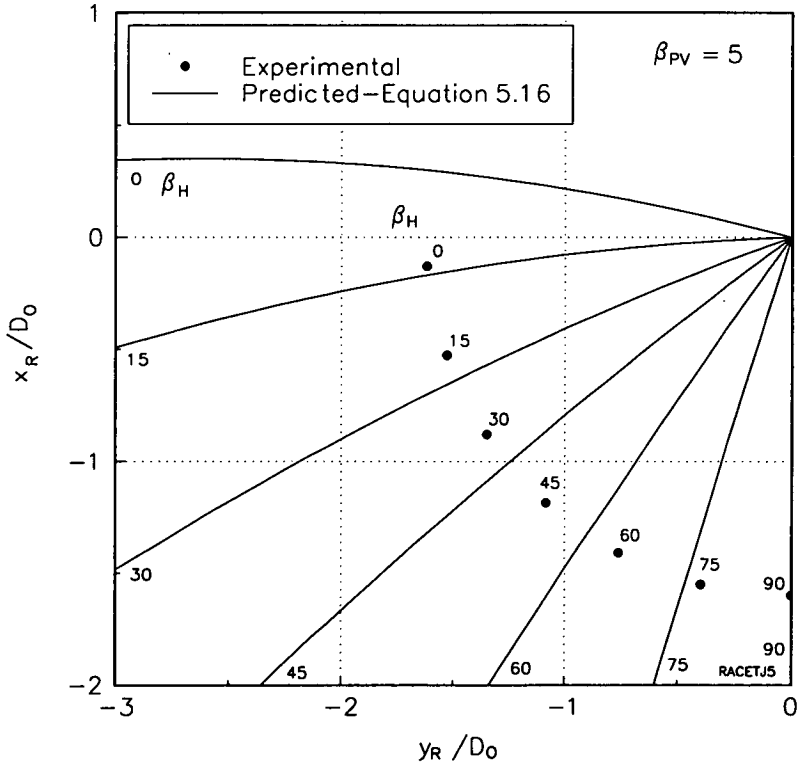

(a) $\beta_P = 5°$

Figure 5.12 Comparison of Predicted Race Trajectory and Measured Location of Thruster for Maximum Interaction

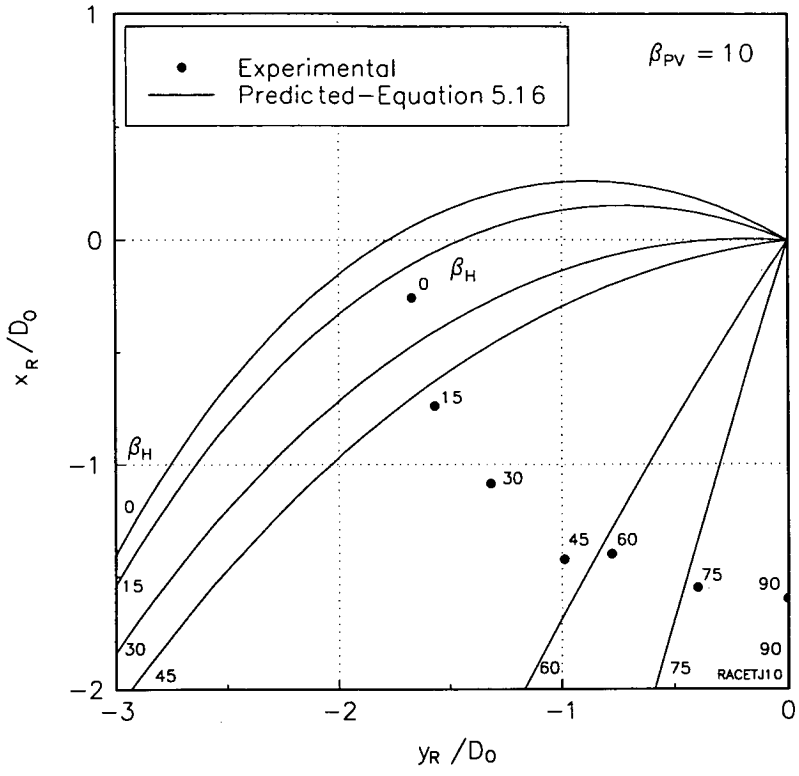

(b) $\beta_P = 10°$

Figure 5.12 Comparison of Predicted Race Trajectory and Measured Location of Thruster for Maximum Interaction

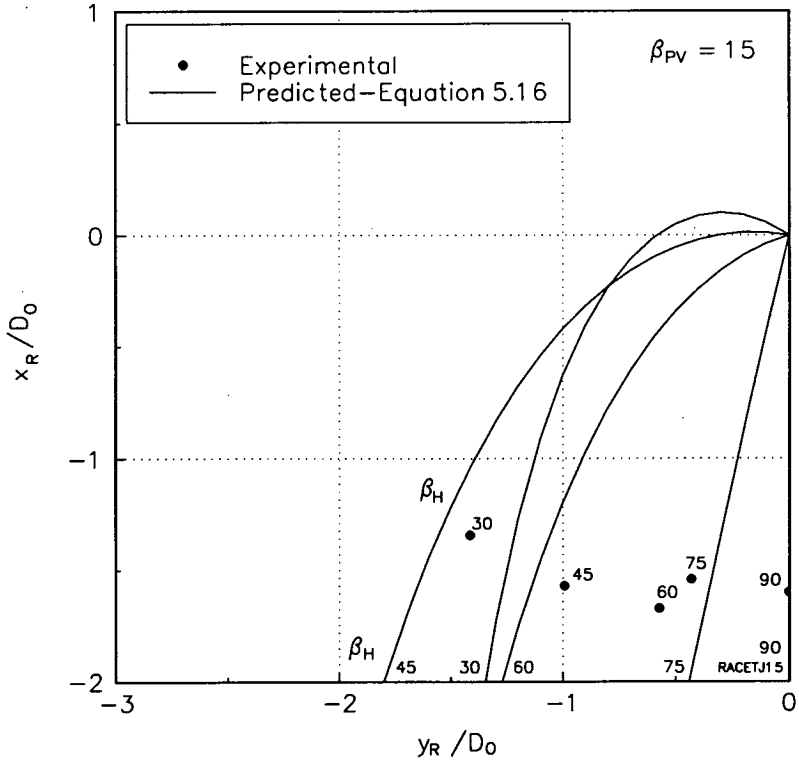

(c) $\beta_P = 15°$

Figure 5.12 Comparison of Predicted Race Trajectory and Measured Location of Thruster for Maximum Interaction

With the location of the race known, it is possible to estimate the degree of interaction as a function of the drift angle, angle of attack and advance angle. The point along the race where the distance between the race trajectory and the location of the thruster is a minimum, has been determined from numerical solution of the following equation:

$$\left(x_{ps}-x_R\right)\cot\zeta+\left(y_{ps}-y_R\right)=0 \tag{5.22}$$

where the slope of the trajectory is calculated from:

$$\cot\zeta=\frac{d\bar{x}_R}{d\bar{y}_R}=\frac{e^{\bar{y}_R}\left|\tan\frac{\zeta_o}{2}\right|}{2}-\frac{1}{2e^{\bar{y}_R}\left|\tan\frac{\zeta_o}{2}\right|} \tag{5.23}$$

Given the distance between the thruster and race, the proportion of the thruster effected by the race can be calculated on the basis of the overlap of the thruster and race cross sections, as shown in Figure 5.13. It would seem reasonable to assume that the profile of the thruster in the plane perpendicular to the race trajectory is a circle equal in diameter to that of the outside of the duct. Clearly, very little is known of the race cross section. In the case of cylindrical jets the cross section undergoes rapid change and is extremely complex, as discussed eg by Kamotani and Greber, 1974. In the absence of other data, the cross section is assumed to be circular. In order to achieve 100% interaction the diameter assumed for the race must be greater than, or equal to, that assumed for the thruster profile. For the present it is assumed that the race and thruster cross sections are of equal diameter, although the experimental results indicate that larger cross sections could be assumed. Using this approach the proportion of the thruster affected by the race can be calculated using the following expressions:

$$\xi=\frac{1}{2\pi}\left[\left(\lambda_D-\sin\lambda_D\right)+\left(\frac{D_R}{D_D}\right)^2\left(\lambda_R-\sin\lambda_R\right)\right]$$

$$\cos\frac{\lambda_D}{2}=\frac{4e^2+D_D^2-D_R^2}{4eD_D}$$

$$\cos\frac{\lambda_R}{2}=\frac{4e^2+D_R^2-D_D^2}{4eD_R} \tag{5.24}$$

where ξ is the proportion of the thruster affected by the race and e is the minimum distance between the race and thruster, as shown in Figure 5.13. As with the race cross section, little is known regarding the velocity distribution; in the absence of other data it has been assumed that the velocity is constant across the cross section. The angle of attack the race makes with the affected thruster is simply determined from the change in slope between the point of minimum distance and the duct exit. Hence, the thruster forces can be calculated from proportioning the forces that would be produced if the thruster were fully immersed in the race and free stream, as follows, in thruster fixed coordinates:

$$X = \xi\left(X(\beta_P,\theta)_R - X(\beta_P,\theta)_A\right) + X(\beta_P,\theta)_A$$
$$Y = \xi\left(Y(\beta_P,\theta)_R - Y(\beta_P,\theta)_A\right) + Y(\beta_P,\theta)_A \qquad (5.25)$$

The propeller torque can also be calculated from an analogous expression.

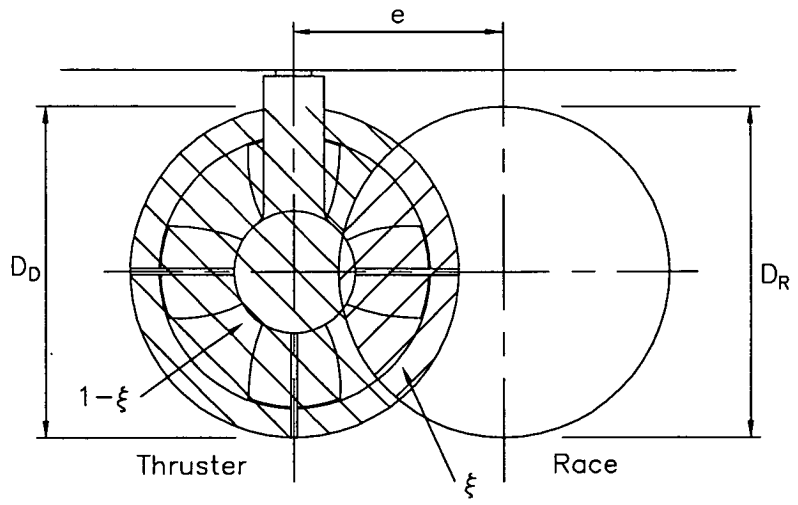

Figure 5.13 Overlap of Thruster and Race Cross Sections

5.3.2 Race Wake Effects

As described in section 5.2, it can be seen from the experimental results that when the race is projected ahead of the affected thruster, although free of direct impingement, forces do not return to open water values. These effects can be attributed to the wake region formed in the lee of the race. Using thrust identity, it is possible to show that inflow velocities approach zero at low drift angles where the affected thruster is fully immersed in the wake and at high drift angles, where the thruster is more exposed, inflow velocities approach free stream values. Hence, it can be assumed that wake effects are a function of the relative position of the thrusters, that is a maximum at 0° drift angle and a minimum at 90° drift angle.

Very little information describing the relevant aspects of the wake field have been found. In the absence of such information it has been assumed that the wake is similar to that in the lee of a cylinder, aligned perpendicular to the free stream. Forces acting on a cylinder immersed in the wake of an identical cylinder, have been measured by Cooper, 1972, as described by Zdravkovich, 1977. These have been converted to an equivalent velocity as shown in Figure 5.14. A simple expression that follows the general trend of the data is also shown in Figure 5.14, ie for thruster i effected by the wake of the race from thruster j:

$$\frac{V_{Ai}}{V_A} = 1 - e^{-0.015\left(\frac{x_R - x_{ij}}{D_O}\right)^{1.4}} \qquad (5.26)$$

The variation in the influence of the wake, as described above, can be included assuming that the wake effect varies linearly with the drift angle, hence equation 5.26 may be modified as follows:

$$\frac{V_{Ai}}{V_A} = 1 - \left(1 - \frac{2\beta_H}{\pi}\right) e^{-0.015\left(\frac{x_R - x_{ij}}{D_O}\right)^{1.4}} \qquad (5.27)$$

Although this approach is crude, it will be shown that results achieved compare well with the experimental data and are relatively insensitive to the variation of velocity with position.

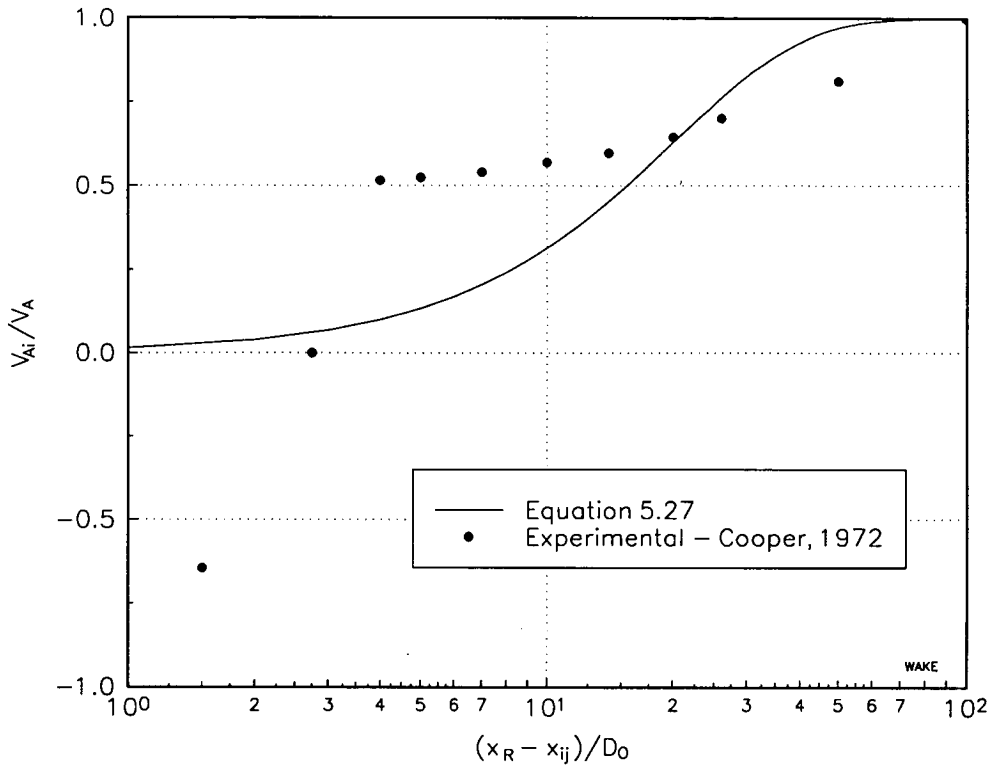

Figure 5.14 Velocity in the Wake of a Cylinder Derived from Force Measurements of an Identical Cylinder Immersed in the Wake, Cooper, 1972

5.3.3 Flow Rectification Effects

As described in Section 5.2, at high drift angles and high angles of attack the trailing thruster is relatively remote from the race and its wake; however, there are still interaction effects. As described above, using thrust identity, it is possible to show that inflow velocities approach free stream values in these situations and that the angle of attack is considerably different to that based on the free stream. This can be attributed to the tendency of the leading thruster to bend the free stream in line with its longitudinal axis, as shown in Figure 5.8. Plots of actual against apparent angle of attack from thrust identity are presented in Figure 5.15. It can be seen that, in general, the points fall on a straight line with slope of approximately 0.5 at 75 and 90° drift angle. As with the race effects above, it has been assumed that the flow rectification varies linearly with the drift angle, hence the following equation:

$$\frac{\theta_i}{\theta_j} = 1 - 0.5\frac{2\beta_H}{\pi} \qquad (5.28)$$

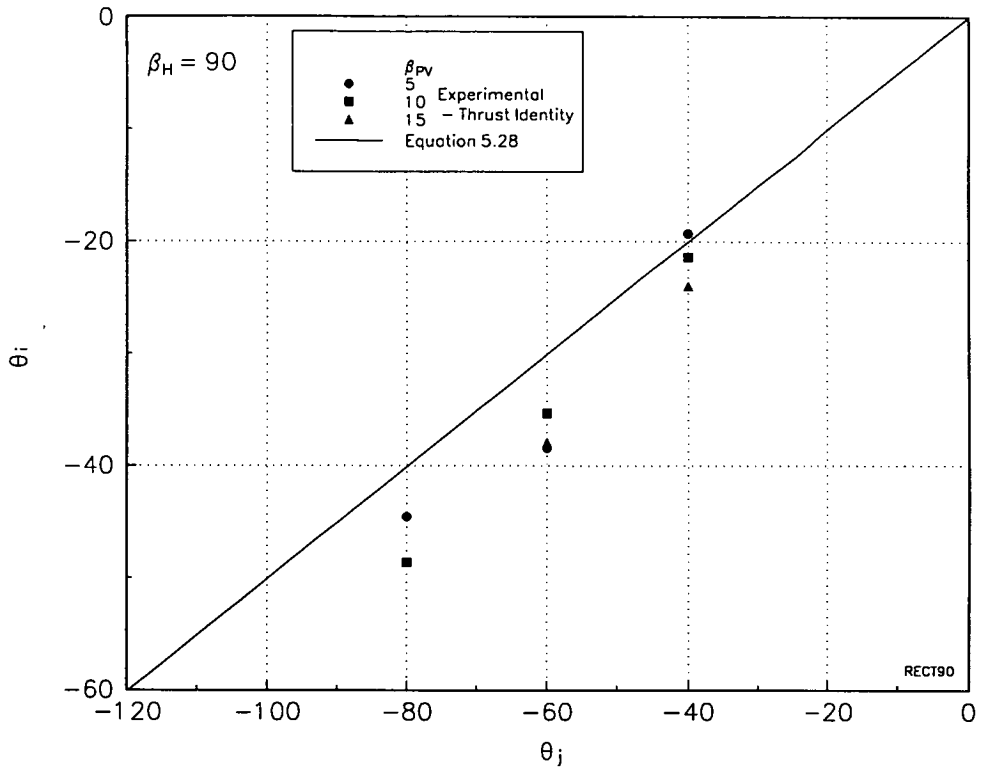

(a) $\beta_H = 90°$

Figure 5.15 Comparison of Actual and Apparent Thruster Angle of Attack from Thrust Identity

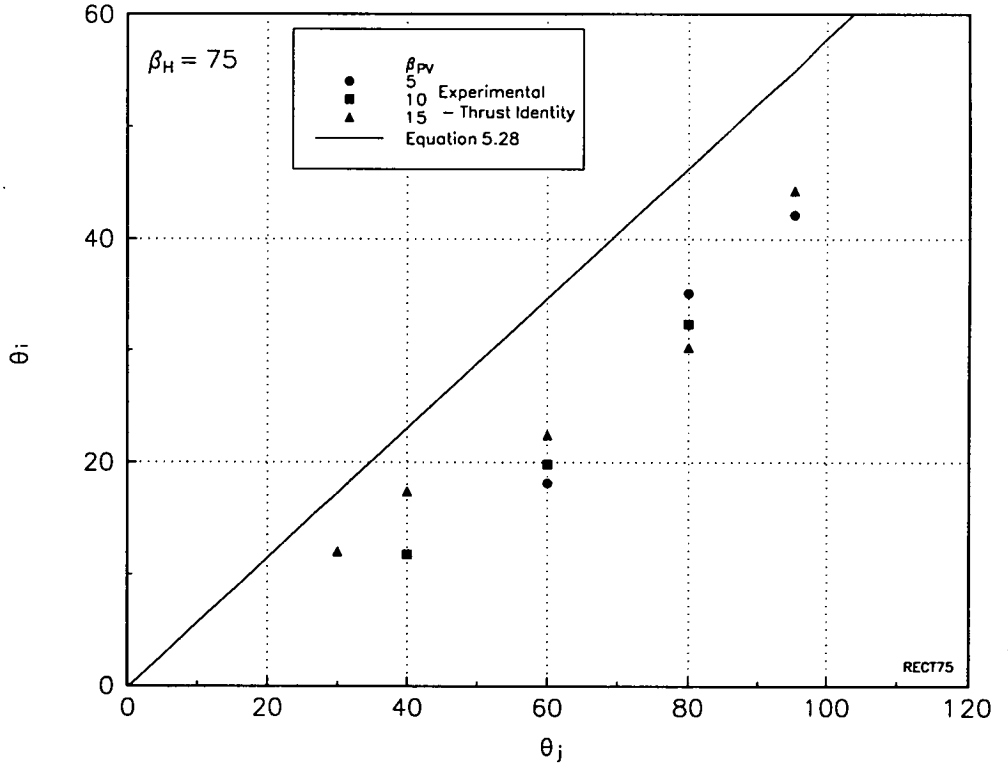

(b) $\beta_H = 75°$

Figure 5.15 Comparison of Actual and Apparent Thruster Angle of Attack from Thrust Identity

5.4 Comparison of Predicted and Experimental Results

The mathematical model described in the previous section is compared with the experimental results for the port thruster, as shown in Figures 5.16, 5.17, 5.18, and 5.19 for apparent advance angles β_{PV} of 0, 5, 10 and 15° respectively. It can be seen from the results that, the method predicts the overall trends and generally, there is reasonable agreement. Significant discrepancies can be attributed to prediction of the race trajectory, structure and cross section. As shown in Figure 5.12 prediction of the race trajectory is more precise at lower advance angles and this is reflected in Figure 5.17(a), where it can be seen that there is favourable prediction of the cusp corresponding to maximum interaction due to race impingement. At 15° advance angle the trajectory is poorly predicted, however this is not so important in that the port thruster at low drift angles does not become fully immersed in the race since it is washed downstream almost immediately. This can be clearly seen in Figures 5.19(a), (b) and (c). The cusp does not become clearly defined until the port thruster is more behind the starboard thruster as can be seen in Figure 5.19(e) for –60° drift angle. It should also be kept in mind that as mentioned in Section 5.2.1, thruster forces are small compared with hull forces at 15° advance angle making the influence of interaction on the overall forces negligible.

The force produced by the port thruster is determined from proportioning the forces that would be produced if the thruster were completely immersed in the free stream and the race, assuming each is of circular cross section. This approach appears to work well in some cases e.g., Figures 5.16 and 5.17(a), and not so well in others, e.g., Figures 5.17(b) and 5.17(c) where the race has an effect over a greater range of angles of attack. This demonstrates that the race cross section varies considerably as a function of both the angle of attack and advance angle. It can be seen that in most cases comparison is favourable for angles of attack less than that at the cusp and poor for angles of attack that are greater, particularly at low drift angles. For angles of attack greater than that at the cusp, the thruster is being affected by the flow in the downstream side of the race which is more complex than that in the upstream side. At high angles of attack the race is deflected through greater angles, which facilitates greater breakup of the race and more complex flow in its wake. At high drift angles the race is deflected very little before impinging on the port thruster explaining the relatively favourable agreement between the experimental and predicted results e.g., Figures 5.17(f) and (g). For low drift angles, angles of attack are greater before the race impinges on the port thruster. Consequently, the race is deflected through much greater angles and more complex flow occurs around the downstream side of the race and in its wake. This explains the poor comparison for angles of attack greater than the cusp, e.g. Figures 5.17(b) and (c).

A significant limitation of this approach has been ignoring the induced flow from the affected thruster since, although it does not effect the upstream thruster, it may influence the trajectory and other properties of its race. Inspection of the experimental results show that for points in the neighbourhood of the cusp, transverse forces are small, indicating that the effective angle of attack is small. This is contrary to that implied from deflection of the race trajectory, which shows that the race is straightened by the induced flow at the duct inlet.

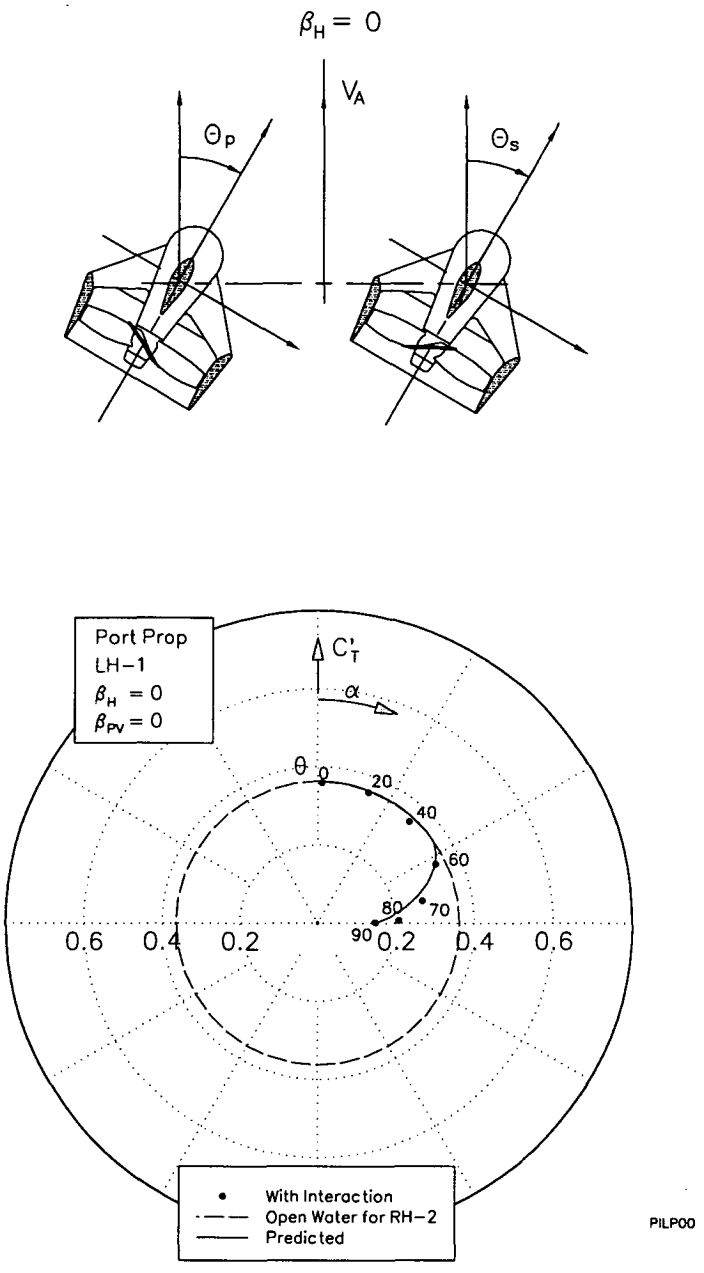

Figure 5.16 Interaction Between Thrusters-Comparison of Experimental and Predicted Results for Port Thruster, $\beta_H = 0°$ and $\beta_P = 0°$

From the plot, it can be seen that the predicted characteristic compares favourably with the experimental results. It is assumed that the race from the starboard thruster has a constant velocity profile and is equal in diameter to that of the outside of the duct.

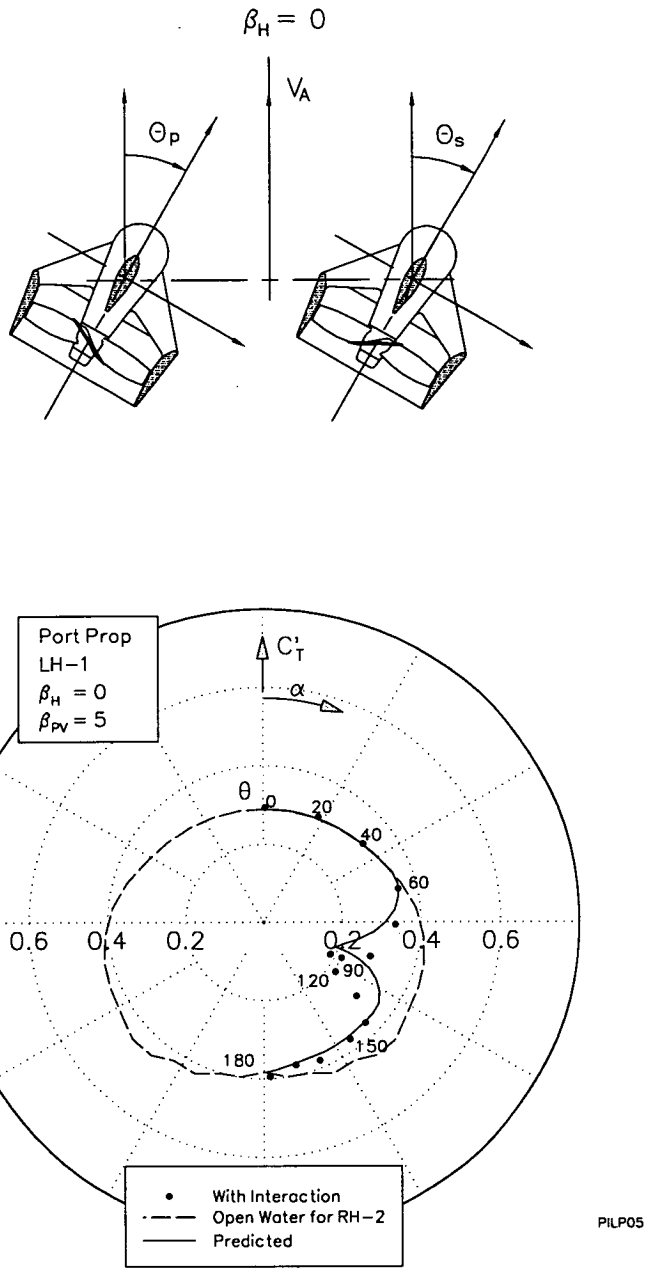

(a) $\beta_H = 0°$

Figure 5.17 Interaction Between Thrusters-Comparison of Experimental and Predicted Results for Port Thruster, $\beta_P = 5°$

From the plot, it can be seen that the predicted characteristic compares favourably with the experimental results. A slight difference in phase is evident which indicates differences in the predicted and actual trajectory of the starboard thruster race. For angles of attack less than that at the cusp, the thruster is assumed to be affected by the race and flow straightening effects, whereas for angles of attack greater, it is assumed the thruster is affected by the race, its wake and flow straightening effects from the starboard thruster. The flow in the wake of the race and flow straightening effects are assumed to be a function of the drift angle, angle of attack and location of the thruster behind the race, see equations 5.27 and 5.28.

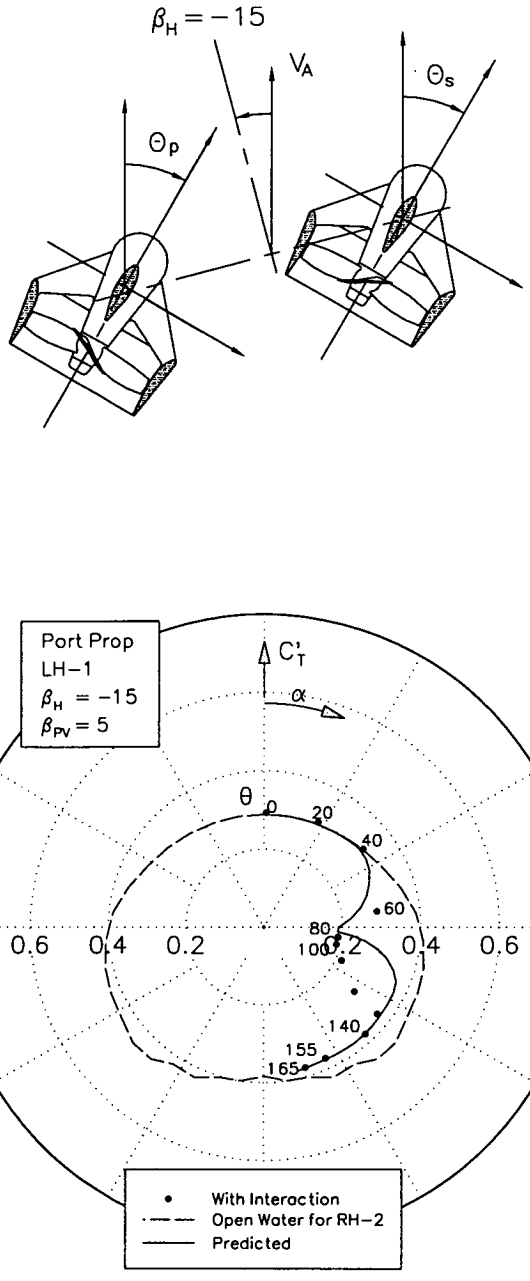

(b) $\beta_H = -15°$

Figure 5.17 Interaction Between Thrusters-Comparison of Experimental and Predicted Results for Port Thruster, $\beta_P = 5°$

From the plot, it can be seen that the predicted characteristic follows the overall trends, however, a noticeable difference in predicted and experimental results for angles of attack greater than that at the cusp is evident. This is possibly due to differences in the assumed and actual race cross-section and velocity profile. At lower drift angles, angles of attack corresponding to maximum interaction due to race impingement are greater and the race is therefore deflected through greater angles facilitating greater breakup of the race and more complex flow in its wake. This reduces the validity of the assumption that the race cross section is round and of constant velocity profile.

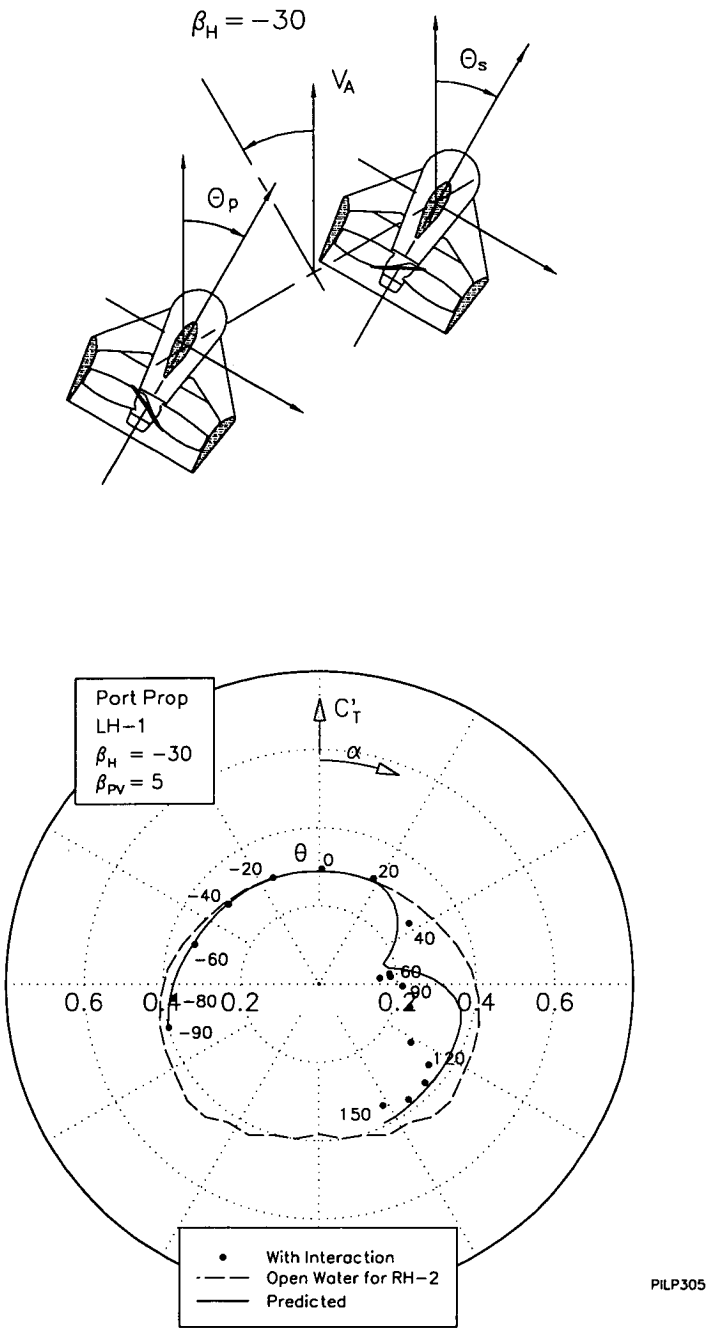

(c) $\beta_H = -30°$

Figure 5.17 Interaction Between Thrusters-Comparison of Experimental and Predicted Results for Port Thruster, $\beta_P = 5°$

From the plot, it can be seen that the predicted characteristic follows the overall trends, however, a noticeable difference in predicted and experimental results for angles of attack greater than that at the cusp is evident. This is possibly due to differences in the assumed and actual race cross-section and velocity profile. At lower drift angles, angles of attack corresponding to maximum interaction due to race impingement are greater and the race is therefore deflected through greater angles facilitating greater breakup of the race and more complex flow in its wake. This reduces the validity of the assumption that the race cross section is round and of constant velocity profile.

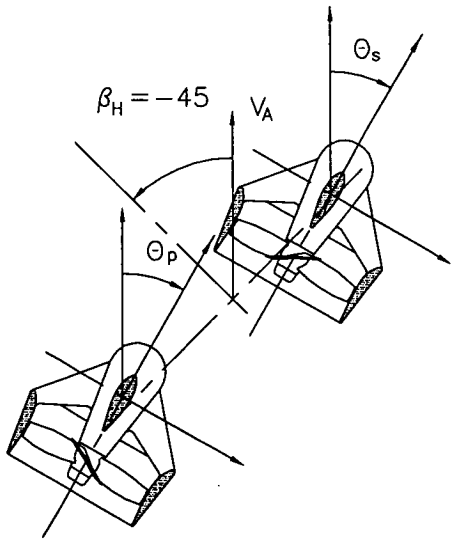

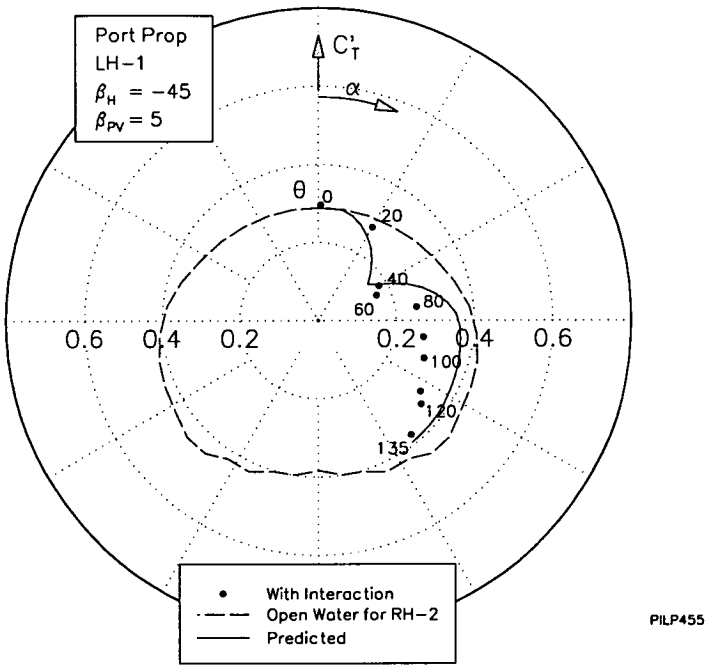

(d) $\beta_H = -45°$

Figure 5.17 Interaction Between Thrusters-Comparison of Experimental and Predicted Results for Port Thruster, $\beta_P = 5°$

From the plot, it can be seen that the predicted characteristic follows the overall trends, however, a noticeable difference in predicted and experimental results for angles of attack greater than that at the cusp is evident. This is possibly due to differences in the assumed and actual flow in the wake of the race. For angles of attack less than that at the cusp, the thruster is assumed to be affected by the race and flow straightening effects, whereas for angles of attack greater, it is assumed the thruster is affected by the race, its wake and flow straightening effects from the starboard thruster. The flow in the wake of the race and flow straightening effects are assumed to be a function of the drift angle, angle of attack and location of the thruster behind the race, see equations 5.27 and 5.28.

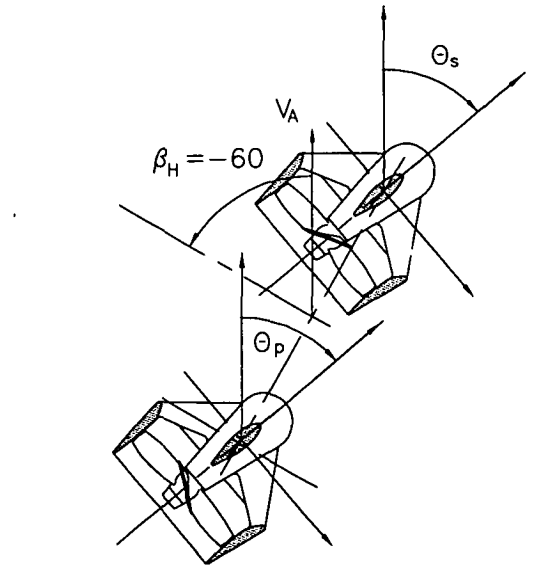

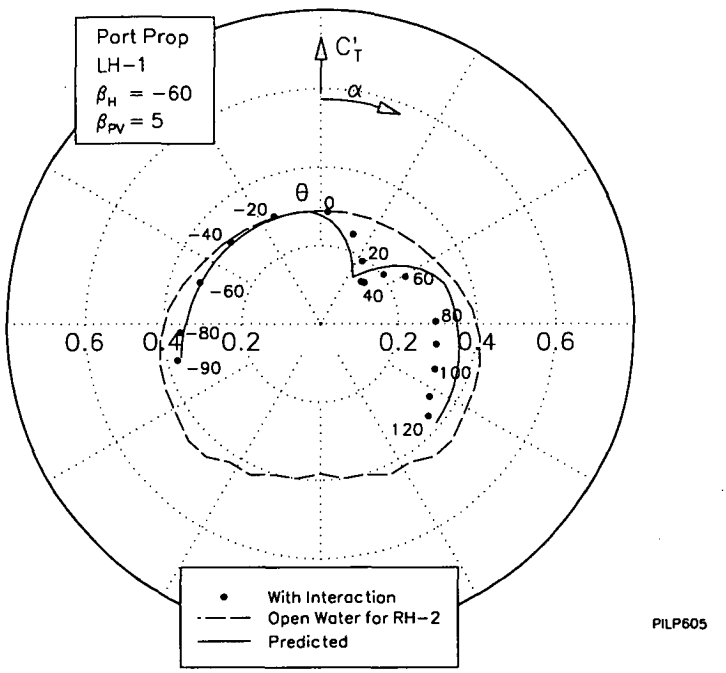

(e) $\beta_H = -60°$

Figure 5.17 Interaction Between Thrusters-Comparison of Experimental and Predicted Results for Port Thruster, $\beta_P = 5°$

From the plot, it can be seen that the predicted characteristic compares favourably with the experimental results. A slight difference in phase is evident which indicates differences in the predicted and actual trajectory of the starboard thruster race. Differences are also noticeable for angles of attack greater than that at the cusp, which are due to differences in the assumed and actual flow in the wake of race. For angles of attack less than that at the cusp, the thruster is assumed to be affected by the race and flow straightening effects, whereas for angles of attack greater, it is assumed the thruster is affected by the race, its wake and flow straightening effects from the starboard thruster. The flow in the wake of the race and flow straightening effects are assumed to be a function of the drift angle, angle of attack and location of the thruster behind the race, see equations 5.27 and 5.28.

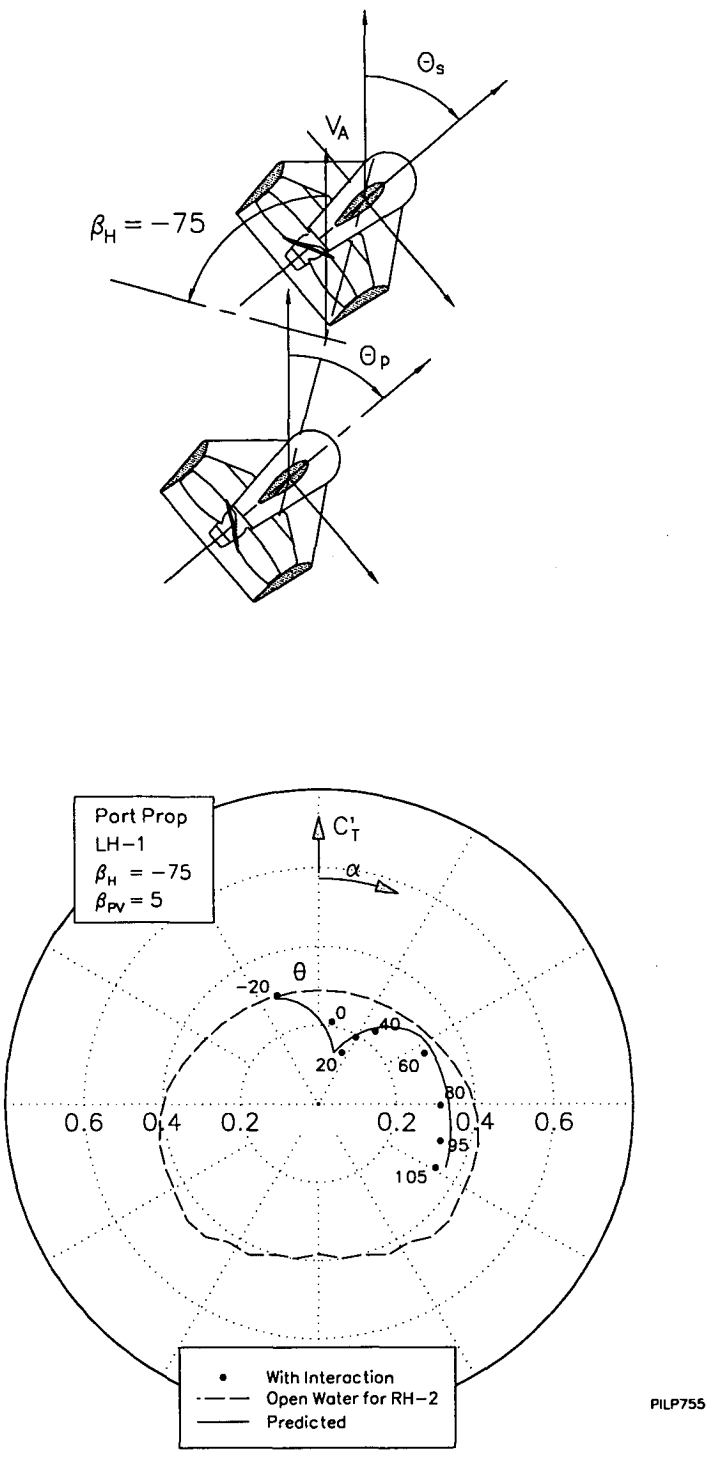

(f) $\beta_H = -75°$

Figure 5.17 Interaction Between Thrusters-Comparison of Experimental and Predicted Results for Port Thruster, $\beta_P = 5°$

From the plot, it can be seen that the predicted characteristic compares favourably with the experimental results. At high drift angles, the race is deflected very little by the free stream, therefore minimising distortion of the velocity profile and errors in the trajectory prediction.

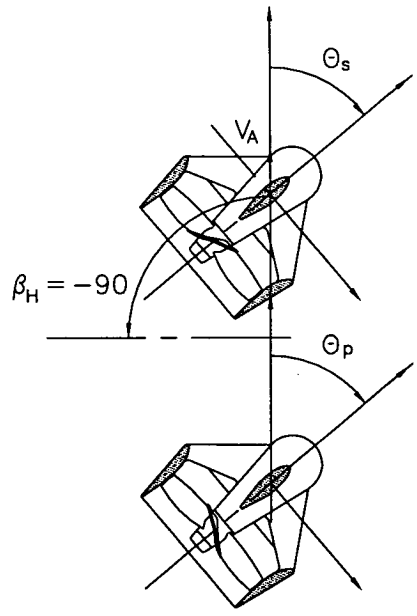

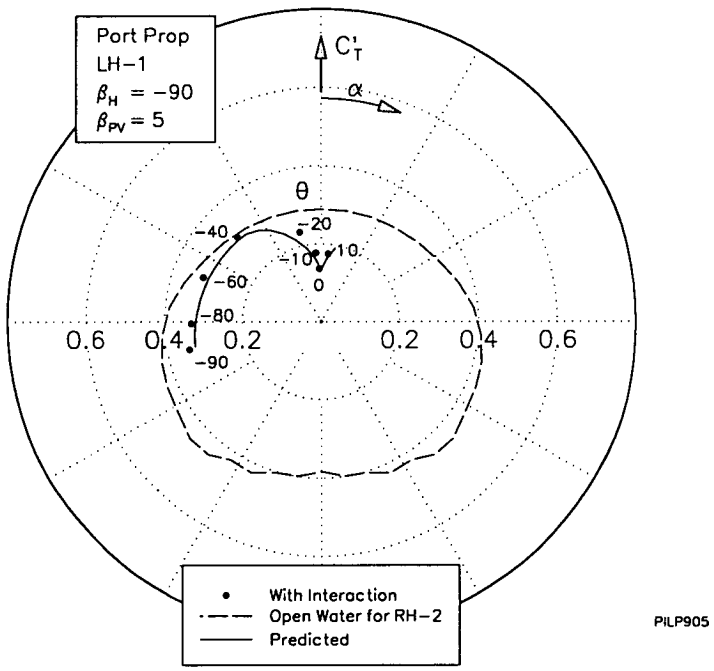

(g) $\beta_H = -90°$

Figure 5.17 Interaction Between Thrusters-Comparison of Experimental and Predicted Results for Port Thruster, $\beta_P = 5°$

From the plot, it can be seen that the predicted characteristic compares favourably with the experimental results. At high drift angles, the race is deflected very little by the free stream, therefore minimising distortion of the velocity profile and errors in the trajectory prediction.

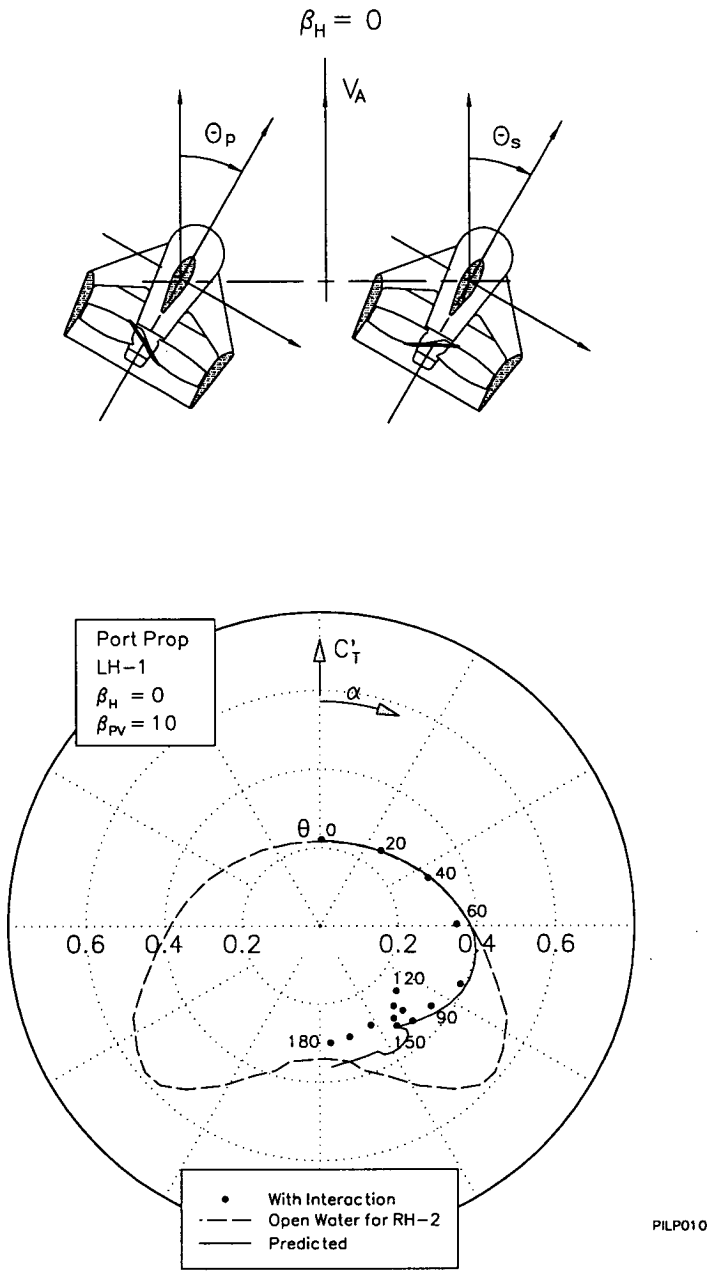

(a) $\beta_H = 0°$

Figure 5.18 Interaction Between Thrusters-Comparison of Experimental and Predicted Results for Port Thruster, $\beta_P = 10°$

From the plot, it can be seen that the predicted characteristic follows the overall trends, however, a noticeable difference in predicted and experimental results for angles of attack greater than that at the cusp is evident. This is possibly due to differences in the assumed and actual flow in the wake of the race. For angles of attack less than that at the cusp, the thruster is assumed to be affected by the race and flow straightening effects, whereas for angles of attack greater, it is assumed the thruster is affected by the race, its wake and flow straightening effects from the starboard thruster. The flow in the wake of the race and flow straightening effects are assumed to be a function of the drift angle, angle of attack and location of the thruster behind the race, see equations 5.27 and 5.28.

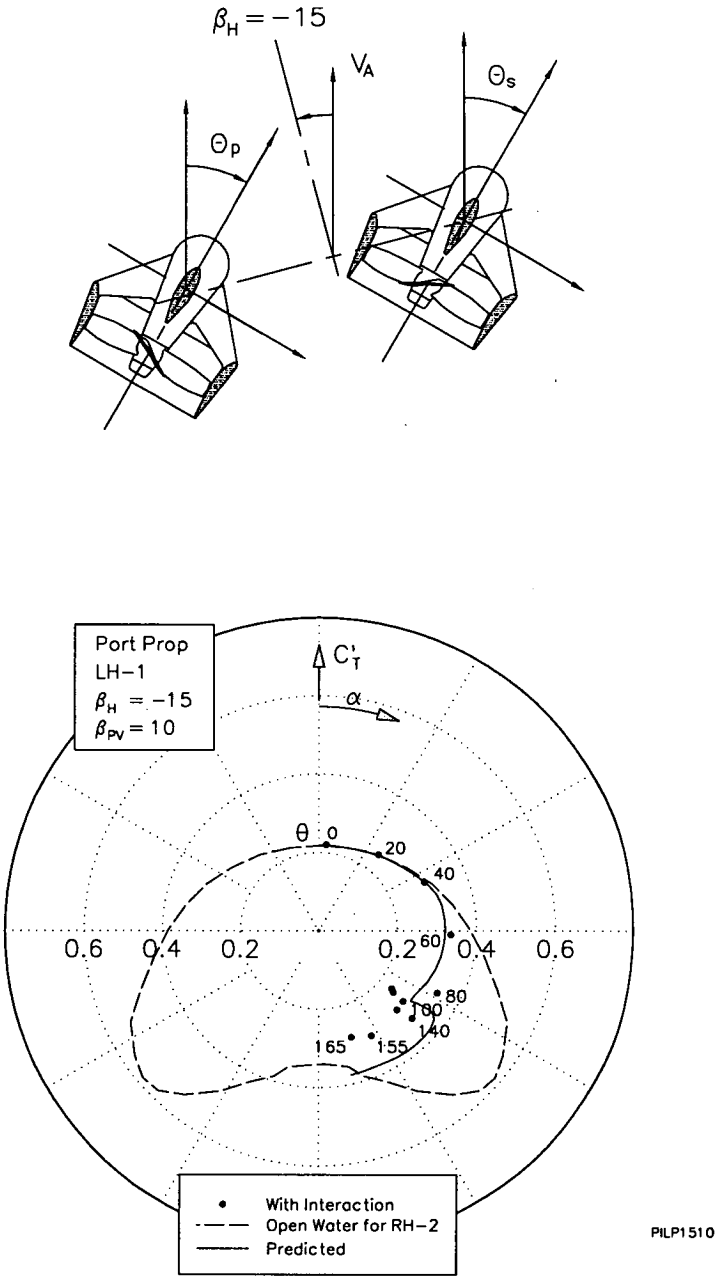

(b) $\beta_H = -15°$

Figure 5.18 Interaction Between Thrusters-Comparison of Experimental and Predicted Results for Port Thruster, $\beta_P = 10°$

From the plot, it can be seen that the predicted characteristic follows the overall trends, however, a noticeable difference in predicted and experimental results for angles of attack greater than that at the cusp is evident. This is possibly due to differences in the assumed and actual flow in the wake of the race. For angles of attack less than that at the cusp, the thruster is assumed to be affected by the race and flow straightening effects, whereas for angles of attack greater, it is assumed the thruster is affected by the race, its wake and flow straightening effects from the starboard thruster. The flow in the wake of the race and flow straightening effects are assumed to be a function of the drift angle, angle of attack and location of the thruster behind the race, see equations 5.27 and 5.28.

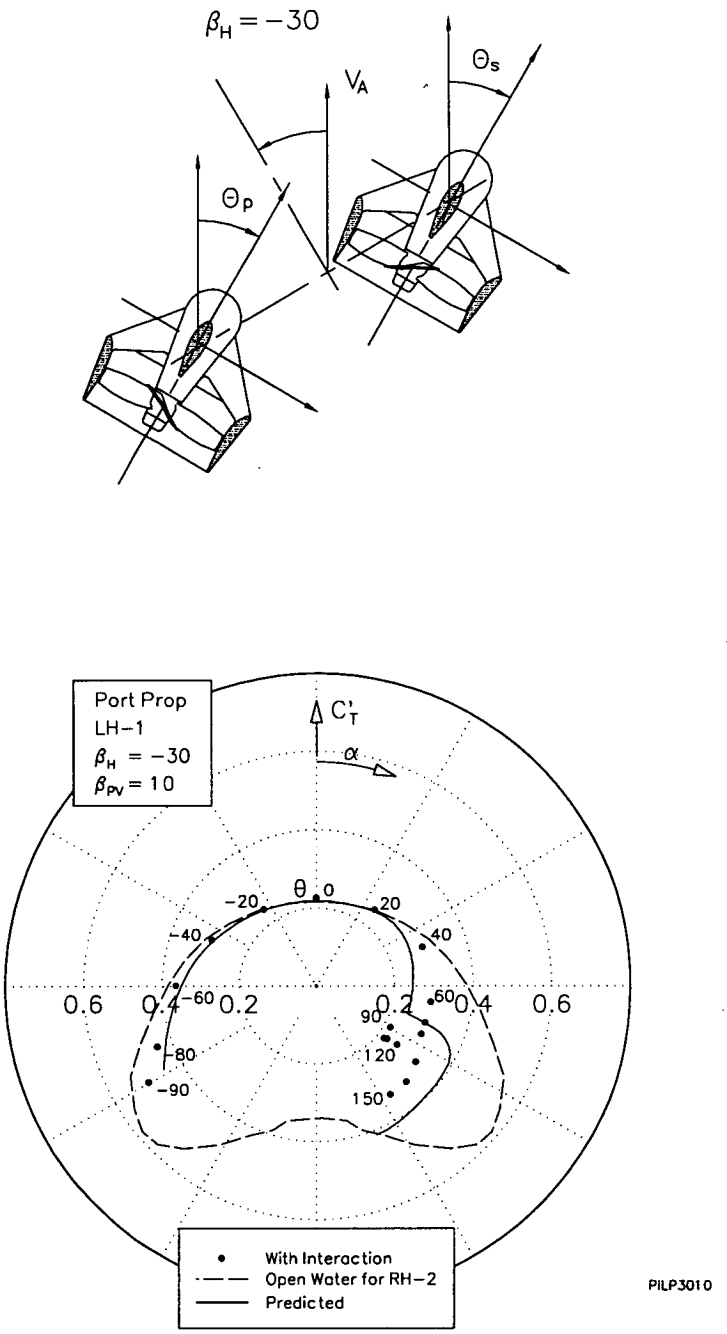

(c) $\beta_H = -30°$

Figure 5.18 Interaction Between Thrusters-Comparison of Experimental and Predicted Results for Port Thruster, $\beta_P = 10°$

From the plot, it can be seen that the predicted characteristic compares favourably with the experimental results. A difference in phase is evident which indicates differences in the predicted and actual trajectory of the starboard thruster race. Differences are also noticeable for angles of attack greater than that at the cusp, which are due to differences in the assumed and actual flow in the wake of race. For angles of attack less than that at the cusp, the thruster is assumed to be affected by the race and flow straightening effects, whereas for angles of attack greater, it is assumed the thruster is affected by the race, its wake and flow straightening effects from the starboard thruster. The flow in the wake of the race and flow straightening effects are assumed to be a function of the drift angle, angle of attack and location of the thruster behind the race, see equations 5.27 and 5.28.

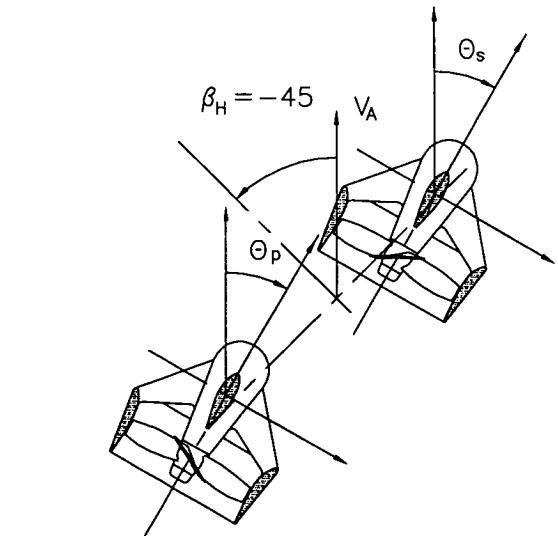

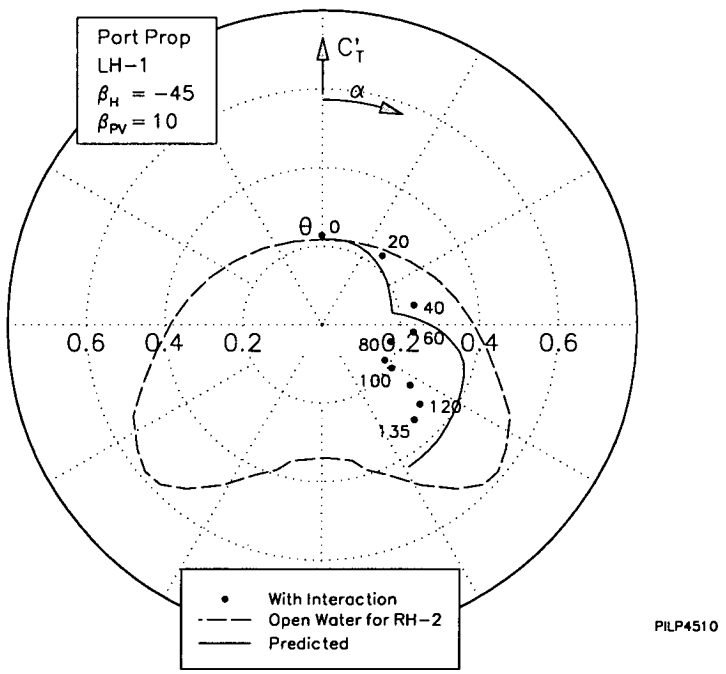

(d) $\beta_H = -45°$

Figure 5.18 Interaction Between Thrusters-Comparison of Experimental and Predicted Results for Port Thruster, $\beta_P = 10°$

From the plot, it can be seen that the predicted characteristic compares favourably with the experimental results. A significant difference in phase is evident which indicates differences in the predicted and actual trajectory of the starboard thruster race. Differences are also noticeable for angles of attack greater than that at the cusp, which are due to differences in the assumed and actual flow in the wake of race. For angles of attack less than that at the cusp, the thruster is assumed to be affected by the race and flow straightening effects, whereas for angles of attack greater, it is assumed the thruster is affected by the race, its wake and flow straightening effects from the starboard thruster. The flow in the wake of the race and flow straightening effects are assumed to be a function of the drift angle, angle of attack and location of the thruster behind the race, see equations 5.27 and 5.28.

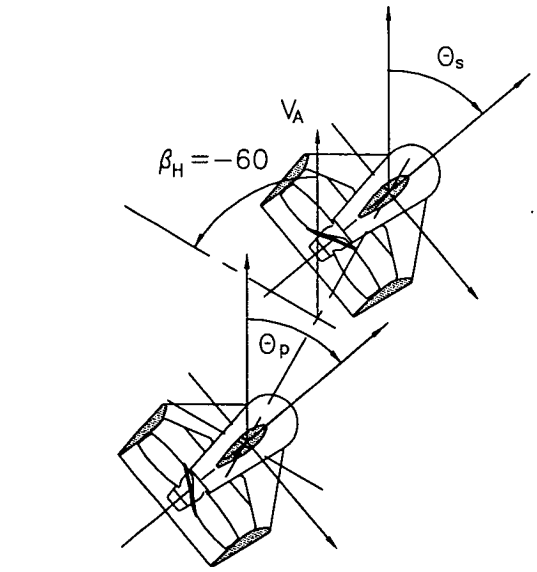

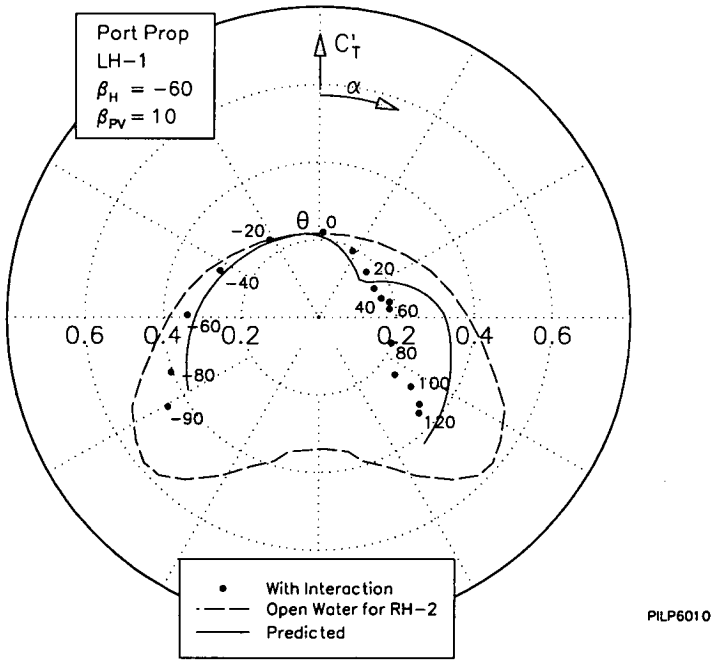

(e) $\beta_H = -60°$

Figure 5.18 Interaction Between Thrusters-Comparison of Experimental and Predicted Results for Port Thruster, $\beta_P = 10°$

From the plot, it can be seen that the predicted characteristic follows the overall trends, however, a significant difference in predicted and experimental results for angles of attack greater than that at the cusp is evident. This is possibly due to differences in the assumed and actual flow in the wake of the race. For angles of attack less than that at the cusp, the thruster is assumed to be affected by the race and flow straightening effects, whereas for angles of attack greater, it is assumed the thruster is affected by the race, its wake and flow straightening effects from the starboard thruster. The flow in the wake of the race and flow straightening effects are assumed to be a function of the drift angle, angle of attack and location of the thruster behind the race, see equations 5.27 and 5.28.

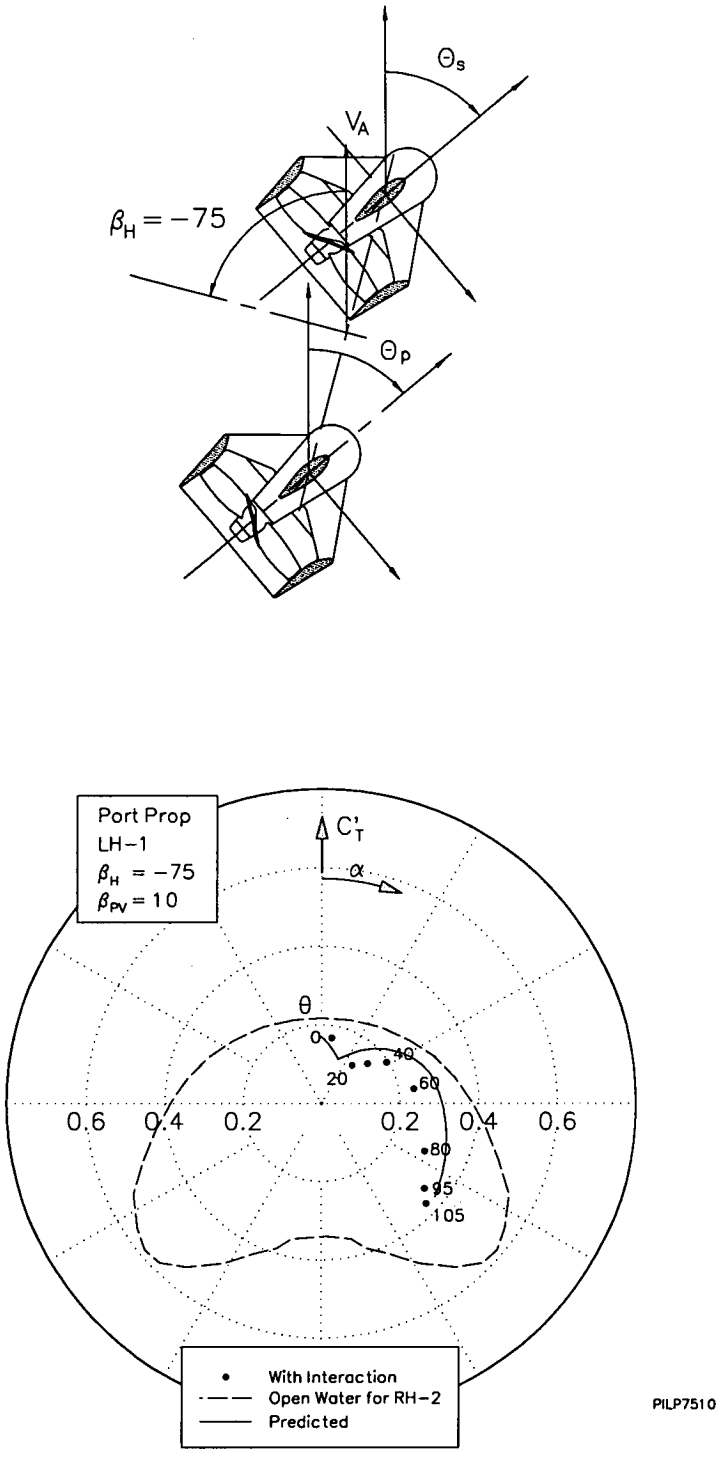

(f) $\beta_H = -75°$

Figure 5.18 Interaction Between Thrusters-Comparison of Experimental and Predicted Results for Port Thruster, $\beta_P = 10°$

From the plot, it can be seen that the predicted characteristic compares favourably with the experimental results. At high drift angles, the race is deflected very little by the free stream, therefore minimising distortion of the velocity profile and errors in the trajectory prediction.

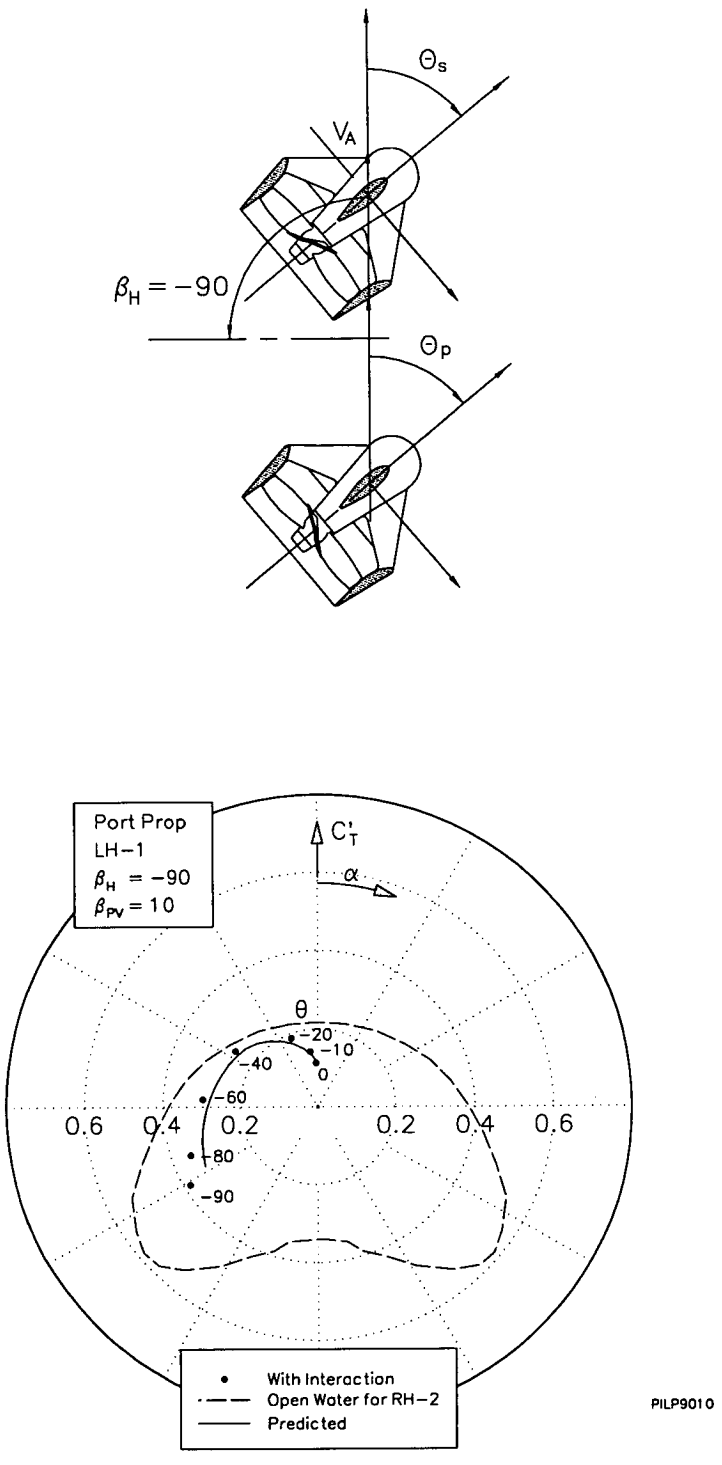

(g) $\beta_H = -90°$

Figure 5.18 Interaction Between Thrusters-Comparison of Experimental and Predicted Results for Port Thruster, $\beta_P = 10°$

From the plot, it can be seen that the predicted characteristic compares favourably with the experimental results. At high drift angles, the race is deflected very little by the free stream, therefore minimising distortion of the velocity profile and errors in the trajectory prediction.

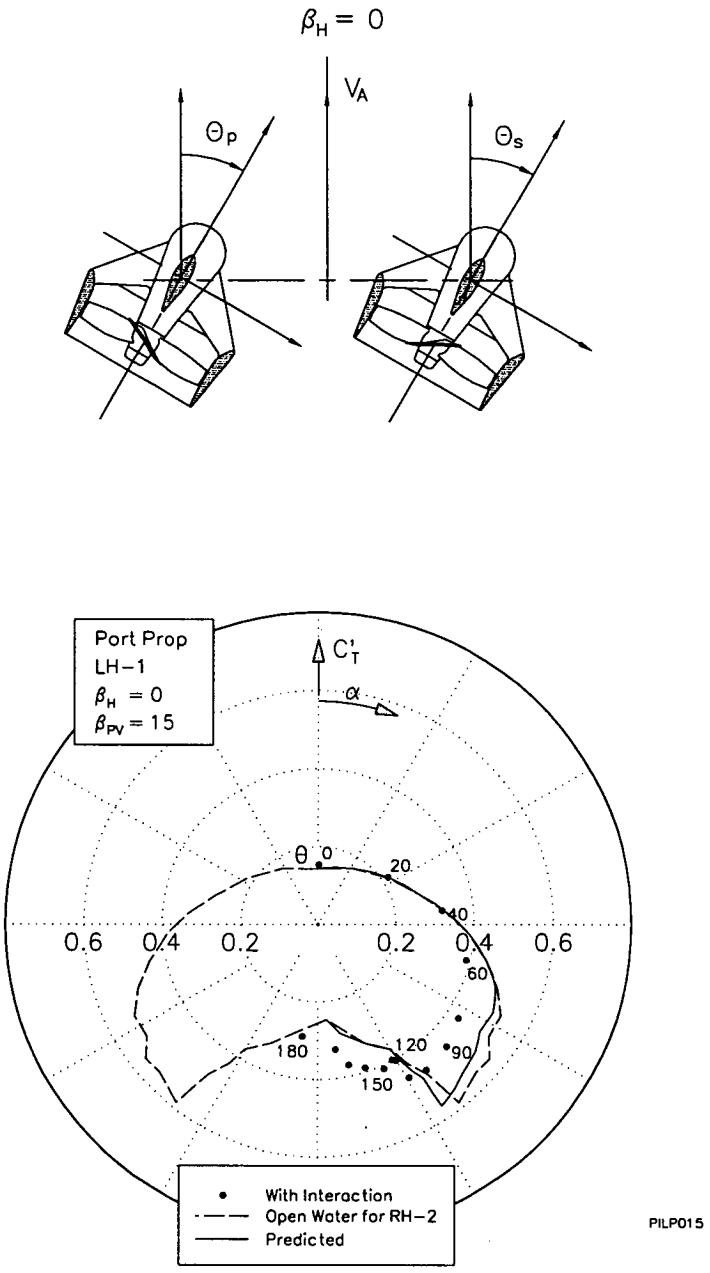

(a) $\beta_H = 0°$

Figure 5.19 Interaction Between Thrusters-Comparison of Experimental and Predicted Results for Port Thruster, $\beta_P = 15°$

From the plot, it can be seen that there are some significant differences between the predicted characteristic and the experimental results. This is due to differences in the predicted and actual race trajectory. At this advance angle and drift angle, the port thruster is never fully immersed in the race from the starboard thruster, due to rapid deflection of the race by the free stream. Therefore, it is assumed that the port thruster is affected only by the race and flow straightening effects from the starboard thruster.

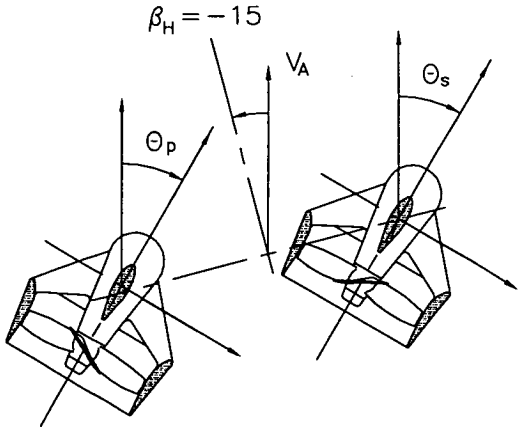

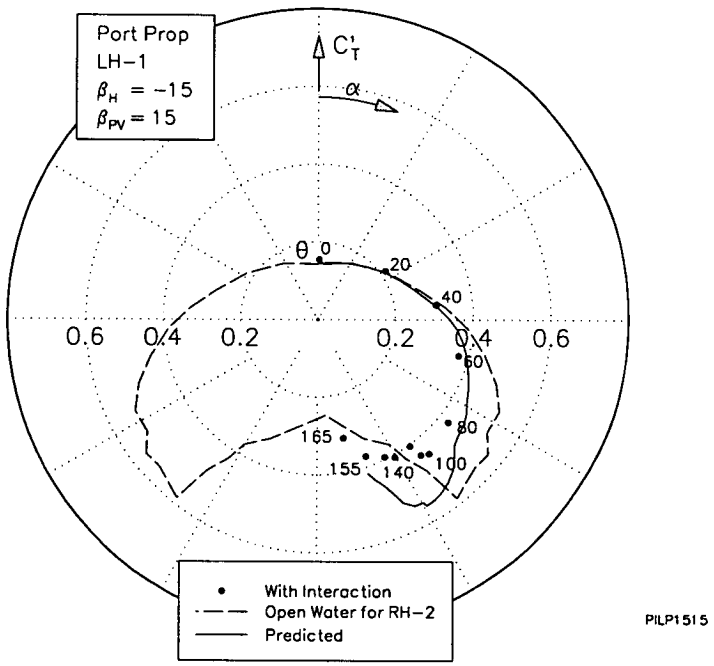

(b) $\beta_H = -15°$

Figure 5.19 Interaction Between Thrusters-Comparison of Experimental and Predicted Results for Port Thruster, $\beta_P = 15°$

From the plot, it can be seen that there are some significant differences between the predicted characteristic and the experimental results. This is due to differences in the predicted and actual race trajectory. At this advance angle and drift angle, the port thruster is never fully immersed in the race from the starboard thruster, due to rapid deflection of the race by the free stream. Therefore, it is assumed that the port thruster is affected only by the race and flow straightening effects from the starboard thruster.

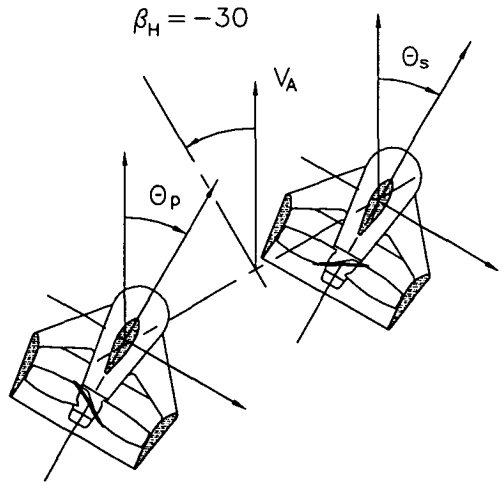

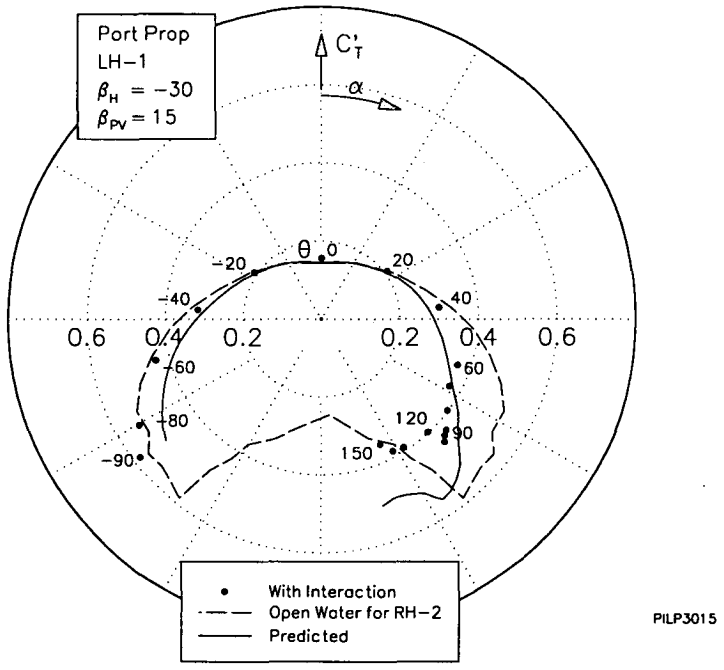

(c) $\beta_H = -30°$

Figure 5.19 Interaction Between Thrusters-Comparison of Experimental and Predicted Results for Port Thruster, $\beta_P = 15°$

From the plot, it can be seen that there are some significant differences between the predicted characteristic and the experimental results. This is due to differences in the predicted and actual race trajectory. At this advance angle and drift angle, the port thruster is never fully immersed in the race from the starboard thruster, due to rapid deflection of the race by the free stream. Therefore, it is assumed that the port thruster is affected only by the race and flow straightening effects from the starboard thruster.

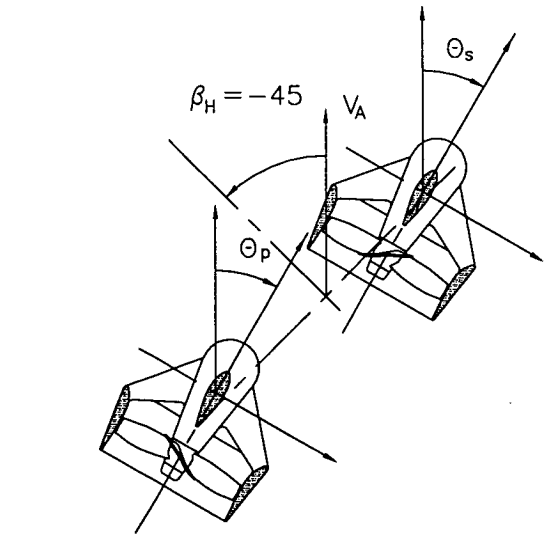

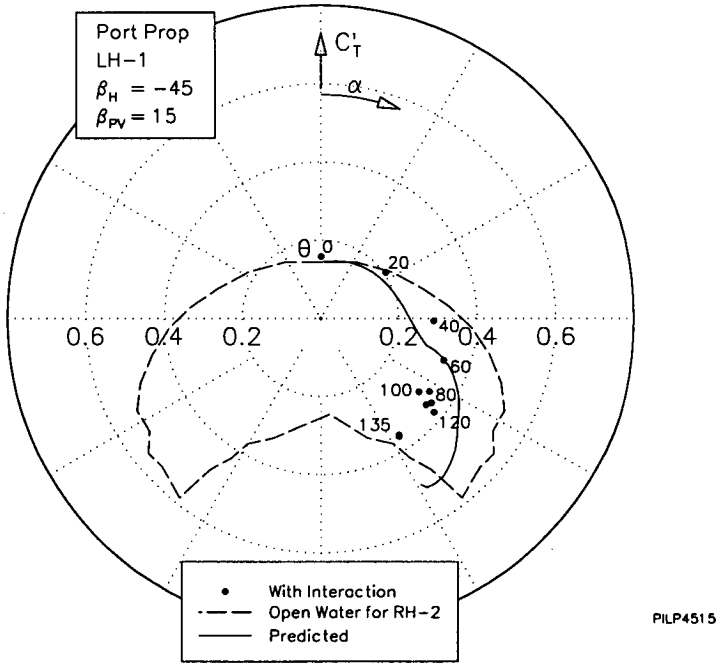

(d) $\beta_H = -45°$

Figure 5.19 Interaction Between Thrusters-Comparison of Experimental and Predicted Results for Port Thruster, $\beta_P = 15°$

From the plot, it can be seen that there are some significant differences between the predicted characteristic and the experimental results. This is due to differences in the predicted and actual race trajectory. There is a cusp present in the experimental results indicating a maximum in the interaction due to race impingement, which is not shown in predicted results. At this advance angle and drift angle, the predicted results indicate the port thruster is never fully immersed in the race from the starboard thruster, due to rapid deflection of the race by the free stream. Therefore, it is assumed that the port thruster is affected only by the race and flow straightening effects from the starboard thruster.

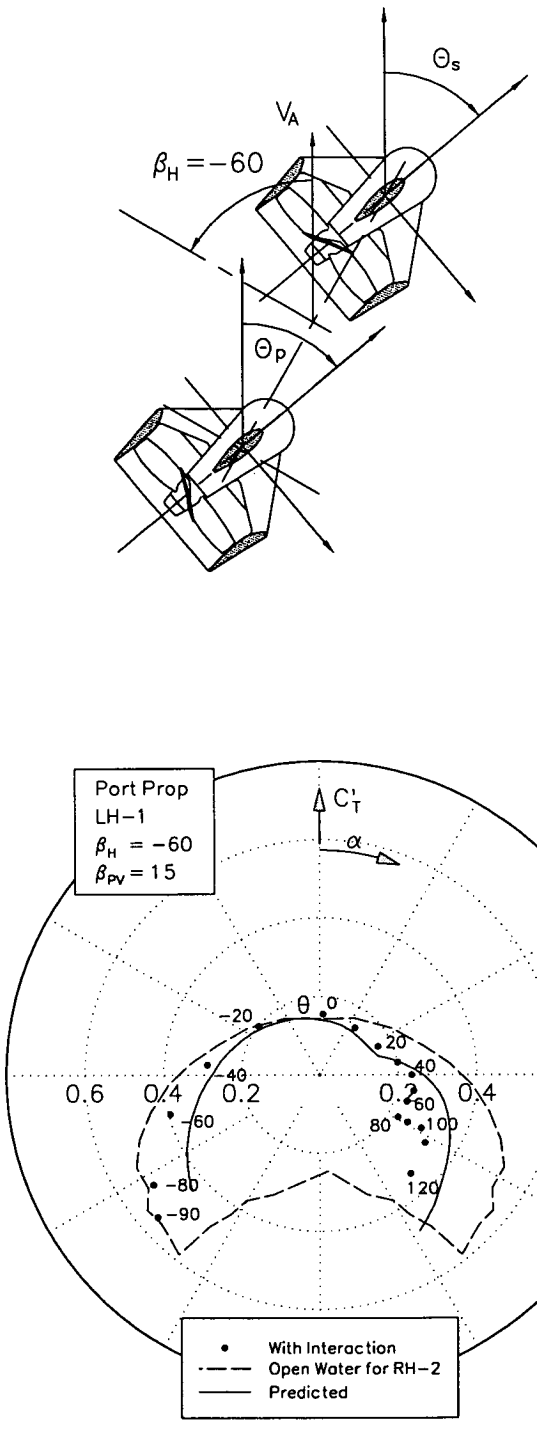

(e) $\beta_H = -60°$

Figure 5.19 Interaction Between Thrusters-Comparison of Experimental and Predicted Results for Port Thruster, $\beta_P = 15°$

From the plot, it can be seen that there are some significant differences between the predicted characteristic and the experimental results. This is due to differences in the predicted and actual race trajectory. There is a cusp present in the experimental results indicating a maximum in the interaction due to race impingement, which is not shown in predicted results. At this advance angle and drift angle, the predicted results indicate the port thruster is never fully immersed in the race from the starboard thruster, due to rapid deflection of the race by the free stream. Therefore, it is assumed that the port thruster is affected only by the race and flow straightening effects from the starboard thruster.

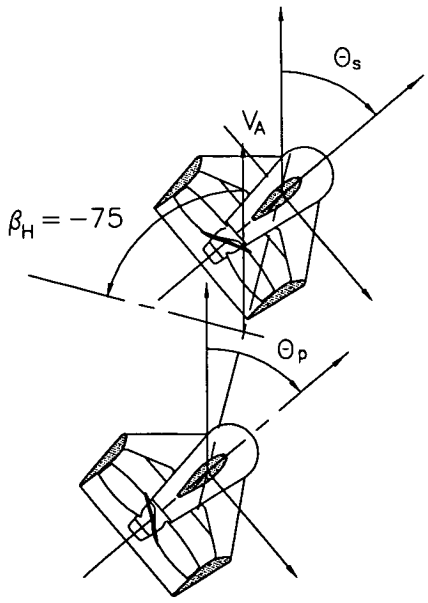

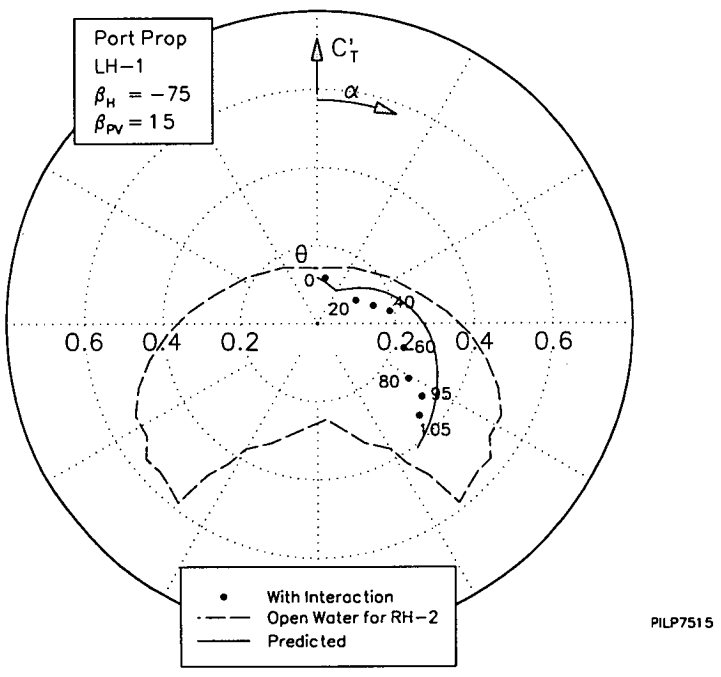

(f) $\beta_H = -75°$

Figure 5.19 Interaction Between Thrusters-Comparison of Experimental and Predicted Results for Port Thruster, $\beta_P = 15°$

From the plot, it can be seen that the predicted characteristic compares reasonably well with the experimental results. At high drift angles, the race is deflected very little by the free stream, therefore minimising distortion of the velocity profile and errors in the trajectory prediction.

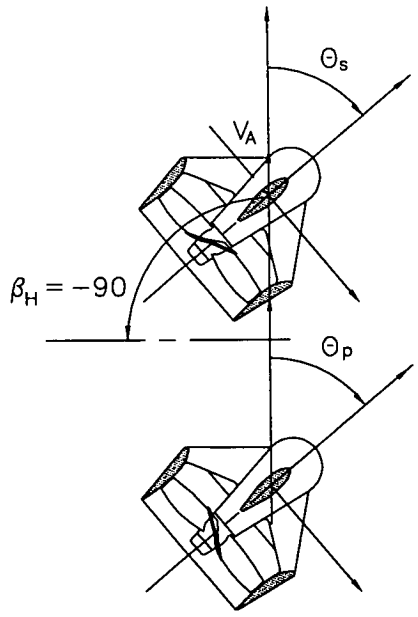

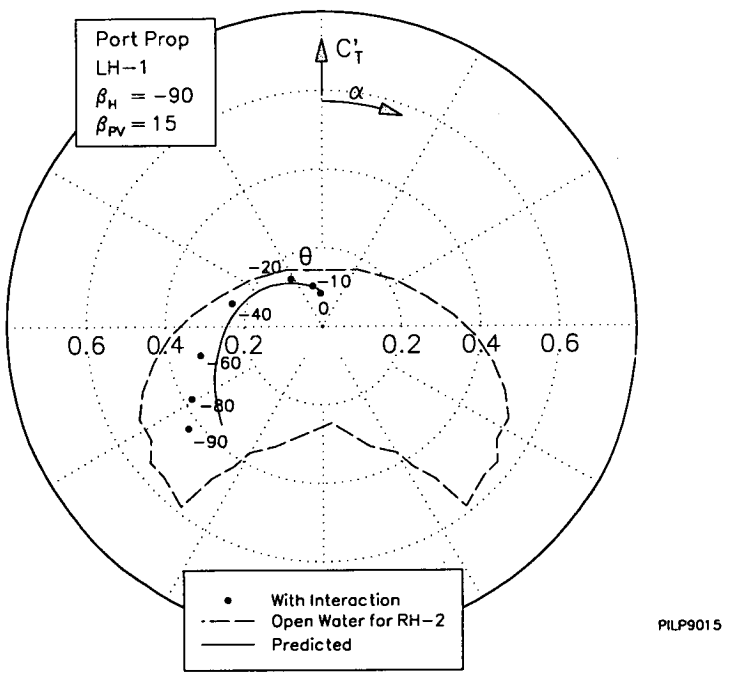

(g) $\beta_H = -90°$

Figure 5.19 Interaction Between Thrusters-Comparison of Experimental and Predicted Results for Port Thruster, $\beta_P = 15°$

From the plot, it can be seen that the predicted characteristic compares reasonably well with the experimental results. At high drift angles, the race is deflected very little by the free stream, therefore minimising distortion of the velocity profile and errors in the trajectory prediction.

6 INTERACTION BETWEEN THRUSTERS AND HULL

6.1 Introduction

As with thruster-thruster interaction, the majority of studies investigating thruster-hull interactions are limited to applications involving offshore exploration vessels with dynamic positioning systems. The most recent of these studies by Nienhuis, 1992, correlates extensive theoretical and experimental work. For the problem of thruster-hull interaction relating to tugs, this previous work is of limited assistance due to significant differences in speeds of operation and thruster and hull configurations. With recent interest in escort tugs, a number of investigations into tug capability at high speed have been carried out. Some of these studies have involved experiments with propelled models and limited details on thruster-hull interaction have been presented. Hutchison et al., 1993, describe a series of experiments with a self propelled constrained model of a Voith Water Tractor. Measurements were made for braking, towing, running ahead and pulling in the indirect mode. From their results Hutchison et al. concluded that for the tractor hull form with Voith Schneider propellers beneath the forebody, thruster-hull interaction is small and may be ignored. Gale et al., 1994, performed a series of experiments with self propelled free running models of both stern drive and tractor omni-directional tugs. In each case the propulsion units were azimuthing thrusters. These results show that for braking, thruster-hull interaction is significant for both stern drive and tractor configurations. However, limited results and details of the experiments were actually presented, as was the case with Hutchison et al., 1993.

A series of experiments with a self propelled free running model of an omni-directional stern drive tug have also been carried out at the AMC. A free running experiment was chosen since equilibrium is automatically found, avoiding the necessity for a number of runs, as would be the case with constrained experiments. The objective of these experiments was to determine thruster-hull interaction, thruster-thruster interaction in the behind condition and to obtain overall tug force measurements for a range of operating modes. Measurements were made of overall tug forces and thruster forces and, from equilibrium hull forces could be calculated. In Chapter 3 results from bare hull experiments were presented and in Chapters 4 and 5 results from open water experiments on first one and then two thrusters were presented. By comparing these results with those from the free running experiments, interaction effects between thrusters were separated from those due to the hull. Thus, it was possible to identify which interactions are significant and which are not. Details of the hull are given in Appendix A, general details of experimental facilities and apparatus used at the AMC are given in Appendix B and details of the thrusters are given in Appendix C. Using the results from the experiments, empirical relations have been developed for thruster-hull interaction which are suitable for use in simulation procedures.

Tugs can apply forces to a ship either by pushing or pulling, and in each case, the force applied will be a function of the following parameters.

$$F_{TUG_{PUSH/PULL}} = f\left(\beta_{PV}, \delta_p, \delta_s\right) \tag{6.1}$$

For practical reasons only cases of equal propeller apparent advance angle β_{PV} (i.e. equal revolutions n) are considered. However, the presence of the hull and interaction between thrusters may cause the actual thruster advance angle β_P to be different for each thruster. Specifically, cases of equal thruster angles δ_p and δ_s are considered, although some limited tests have also been performed with unequal thruster angles. The coordinate system used for representing the results is shown in Figure 6.1.

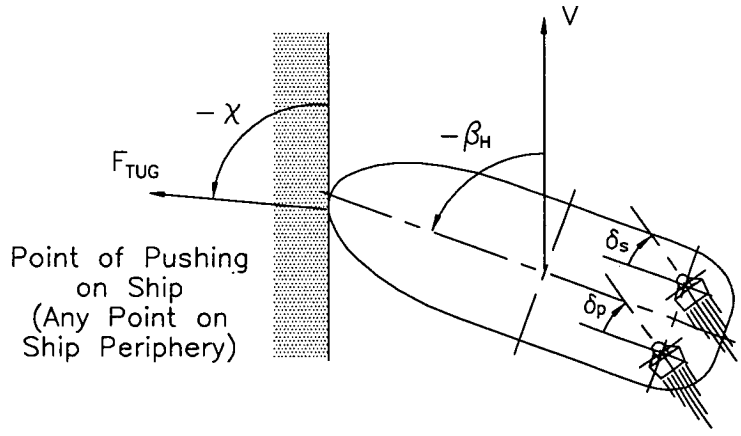

(a) Pushing

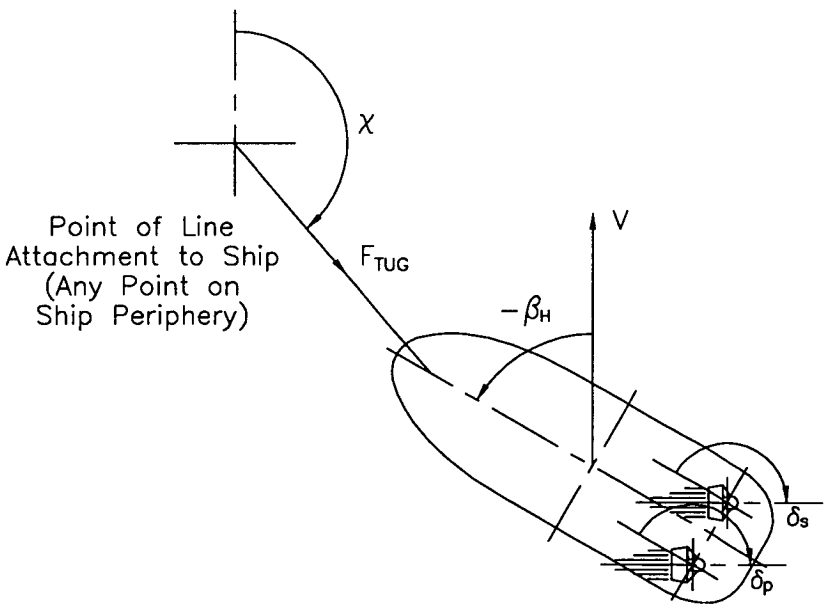

(b) Pulling

Figure 6.1 Coordinate System for Free Running Experiments

6.2 Free Running Model Experiments

6.2.1 Experimental Matrix

From Equation 6.1, tug forces depend on the thruster angles δ and the apparent thruster advance angle β_{PV}. In addition to these parameters, interaction involving the hull will also depend on the hull drift angle β_H. An appropriate matrix of these parameters which fully defines tug capability and interaction involving the hull, has been determined from consideration of practical modes of tug operation. The four practical modes of operation, as shown in Figure 6.2, were introduced in Chapter 5 namely:

- pushing (Figure 6.2(a));
- pulling with forward tow point-direct (Figure 6.2(b));
- pulling with forward tow point-indirect (Figure 6.2(c)); and
- pulling with aft tow point (Figure 6.2(d)).

In Chapter 5, combinations of hull drift angle and thruster angle of attack were considered for each mode to determine an appropriate experimental matrix for the measurement of thruster-thruster interaction. For measurement of interaction with the hull it would appear more appropriate to consider combinations of hull drift angle and thruster angles δ (tug fixed coordinates), rather than angle of attack. The thruster angle and thruster angle of attack are related simply by:

$$\delta = \theta - \beta_H \tag{6.2}$$

Diagrams of hull drift angle and thruster angle analogous to those presented in Chapter 5 are shown in Figure 6.2. Once again only negative drift angles have been considered due to symmetry.

Operation in the pushing mode is shown in Figure 6.2(a). In this mode, the tug drift angle may vary between 0 and −90°. The objective of pushing is generally to apply a pure sway force to the ship and this is achieved, as shown in the results presented later, for drift angles between 0 and −90°. From Figures 3.1(b) to 3.3(b) it can be seen that the centre of pressure of the hull force will always lie between the point of contact on the fenders and the location of the thrusters, and the results presented later show that hull forces due to thruster-hull interaction are negligible. Therefore, to push, the thrusters must be ahead and the thruster angle may vary between the extremes of 0° and linearly from 0° at 0° drift angle to 90° at −90° drift angle, as shown in Figure 6.2(a).

Pulling with the forward tow point in the direct mode is shown in Figure 6.2(b). In this mode the tug drift angle may vary from 0° when pulling astern, to −180° when pulling ahead but running astern. From Figures 3.1(b) to 3.3(b) it can be seen that the centre of pressure of the hull force will always lie between the tow point and the location of the thrusters and from the results presented later this can also be shown to be the case including hull forces due to thruster-hull interaction. Therefore, to pull, the thrusters must be astern so that the thruster angle may vary between the extremes of 180° and 90° for any drift angle between 0 and −180°, as shown in Figure 6.2(b).

Pulling with the forward tow point in the indirect mode is shown in Figure 6.2(c). The objective here is to create force in the line using sway forces generated by the hull. The drift angle may vary between 0 and −90° and as described above, the results of Chapter 3 and the present Chapter can once again be used to show that the centre of pressure of the hull force including forces due to thruster-hull interaction always lies between the tow point and the thruster locations. Therefore, from the similarities this mode has with both pushing and pulling, possible combinations of thruster angle and drift angle include those for pushing and pulling as shown in Figure 6.2(c).

Pulling with the aft tow point is shown in Figure 6.2(d). In this traditional mode of tug operation drift angles may vary between 0 and −90°. From Figures 3.1(b) to 3.3(b) it can be seen that the tow point will always lie between the centre of pressure of the hull force and the location of the thrusters. As described later, from the similarity with pushing, hull forces due to thruster-hull interaction in this mode may also be considered negligible. Therefore, to pull, the thrusters must be ahead and the thruster angle may vary between the extremes of 0° and linearly from −90° at 0° drift angle to 0° at −90° drift angle, as shown in Figure 6.2(d).

A total envelope may be defined using the areas mapped for each mode of operation, similar to that performed in Chapter 5, as shown in Figure 6.2(e). With the exception of the area for pulling with the aft tow point, all the areas marked fall in the range $0° \geq \beta_H \geq -180°$ and $0° \leq \delta \leq 180°$. Within this region four quadrants may be defined, as follows:

- 1st quadrant — running ahead, thrust ahead
  $0° \geq \beta_H \geq -90°, 0° \leq \delta \leq 90°$;
- 2nd quadrant — running ahead, thrust astern
  $0° \geq \beta_H \geq -90°, 90° \leq \delta \leq 180°$;
- 3rd quadrant — running astern, thrust astern
  $-90° \geq \beta_H \geq -180°, 90° \leq \delta \leq 180°$; and
- 4th quadrant — running astern, thrust ahead
  $-90° \geq \beta_H \geq -180°, 0° \leq \delta \leq 90°$.

The first quadrant covers pushing and half the area applicable to pulling with the forward tow point in the indirect mode. In this quadrant, as the hull is ahead of the thrusters they will be operating in the hull wake and with the thrusters directed ahead, the propeller race is directed astern so as not to effect the hull. Hence, it would be expected that in this quadrant the influence of the hull on the thrusters will dominate the influence of the thrusters on the hull.

The second quadrant covers half each of the areas applicable to pulling with the forward tow point in the direct and indirect modes. In this quadrant, the hull is ahead of the thrusters and they are directed astern, so that water is drawn from the free stream about the hull and the propeller race is directed at the hull. Hence, it would be expected that in this quadrant the influence of the thrusters on the hull will be greater than the influence of the hull on the thrusters.

The third quadrant covers the remaining half of the area applicable to pulling with the forward tow point in the direct mode. In this quadrant, the thrusters are operating

ahead of the hull and are directed astern so that the propeller race is directed toward the hull. Hence, the influence of the thrusters on the hull will be greater than the influence of the hull on the thrusters.

Finally, in the fourth quadrant, no practical mode of operation is possible and therefore this quadrant may be ignored here. It is possible for operation in the fourth quadrant to occur in the pushing mode, if the drift angle becomes greater than 90°, although impractical this situation is considered in Chapter 7.

It is shown in Chapter 7, from predictions of the mathematical model and observations of the free running model experiments, that of the four modes of operation or regions therein, not all result in the tug being in stable equilibrium. Modes or regions therein, where the tug is not in stable equilibrium, include pulling with the aft tow point and pulling with the forward tow point when the drift angle is greater than 90°, that is in the third quadrant. For this reason, operation in these positions is not favoured at high speed, making prediction of interaction less important compared with the other modes. Interactions in these unstable modes may be reliably extrapolated from measurements in the other modes. Interactions for pulling with the aft tow point are similar to those for pushing, the difference being that thruster angles are negative rather than positive as with pushing. It is shown in section 6.3 that the influence of the hull on the thrusters in the pushing mode is only weakly dependent on the thruster angles themselves and may be ignored. This implies that interactions for pulling with the aft tow point may be determined from those measured for pushing. Interactions for pulling with the forward tow point in the third quadrant can be satisfactorily predicted from those measured for the astern bollard pull (i.e. $\beta_P = 0$).

In light of the above, only modes of operation or regions therein that result in the tug being in stable equilibrium have been tested. These include; pushing; pulling with the forward tow point in the indirect mode; and pulling with the forward tow point in the direct mode in the second quadrant. As mentioned in Chapter 5, for shiphandling operations, apparent thruster advance angles generally would not exceed around 12° at maximum revolutions. Thus, experiments were performed with apparent advance angles up to 12° in intervals of 3°, with some limited measurements also being made at 15°. Thruster angles were varied in intervals of 2.5, 5 or 10° depending on the detail required.

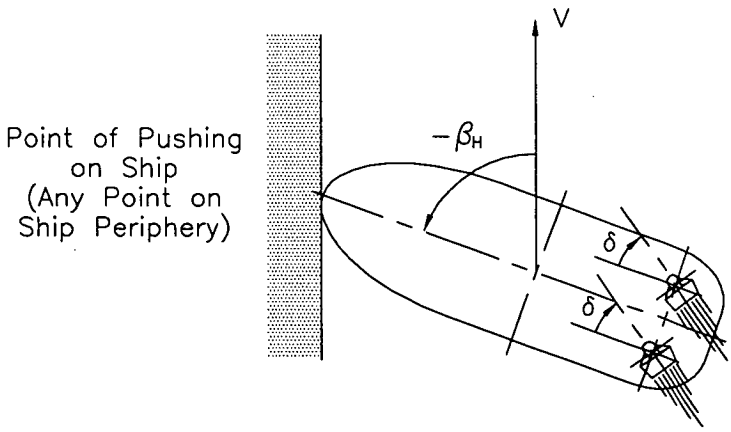

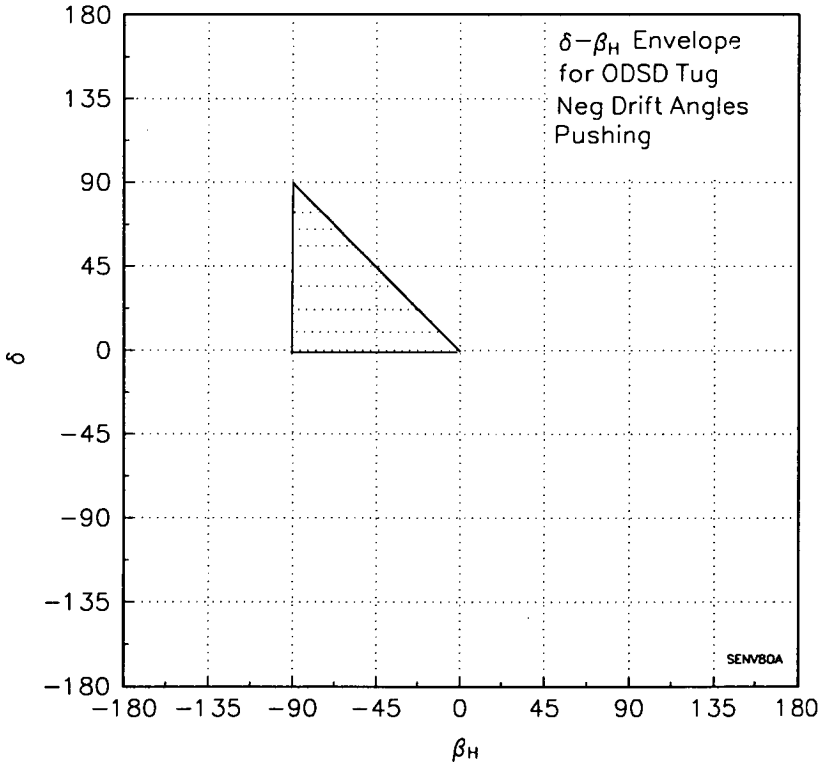

(a) Pushing

Figure 6.2 Thruster Angle and Drift Angle Combinations for Omni-directional Stern Drive Tugs Operating at Negative Drift Angles

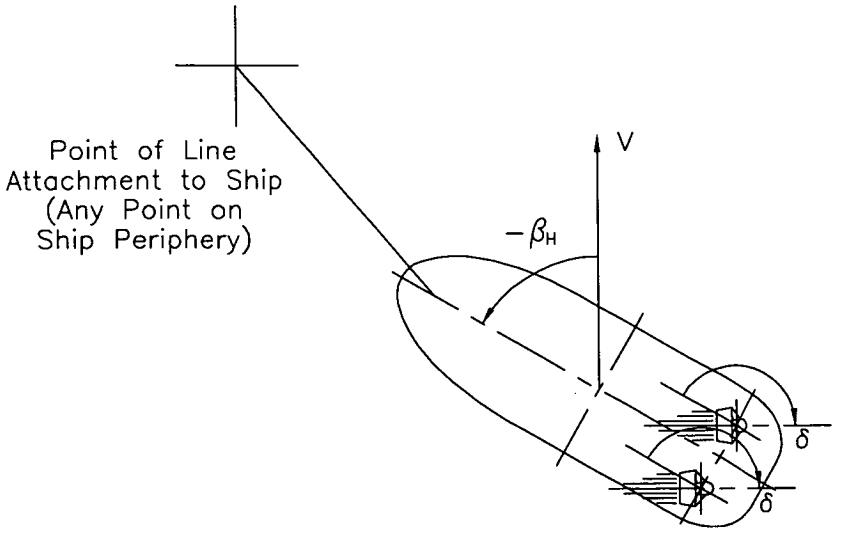

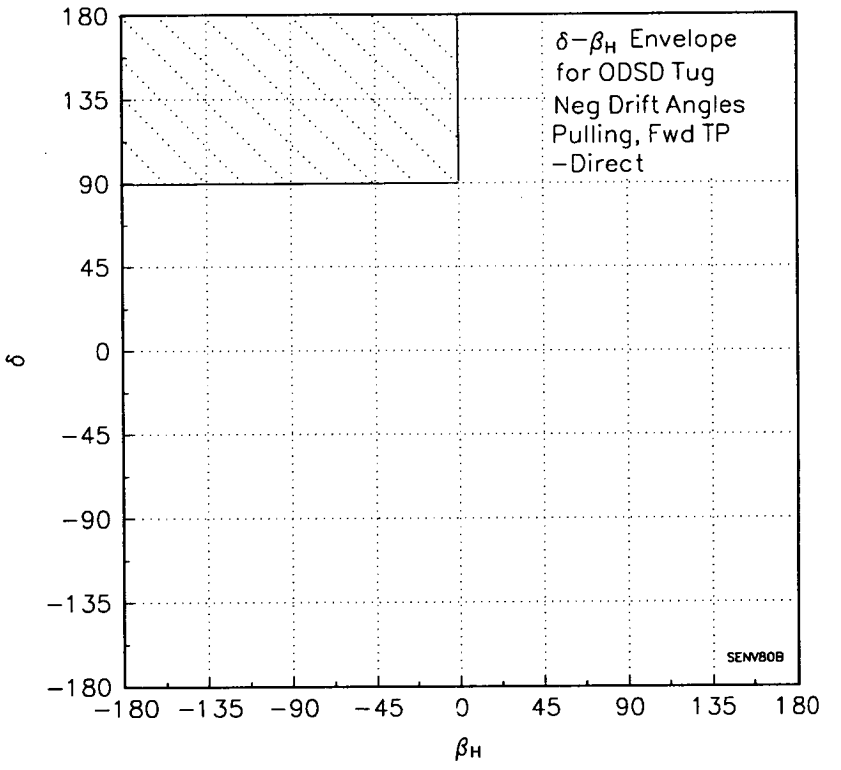

(b) Pulling with Forward Tow Point-Direct Mode

Figure 6.2 Thruster Angle and Drift Angle Combinations for Omni-directional Stern Drive Tugs Operating at Negative Drift Angles

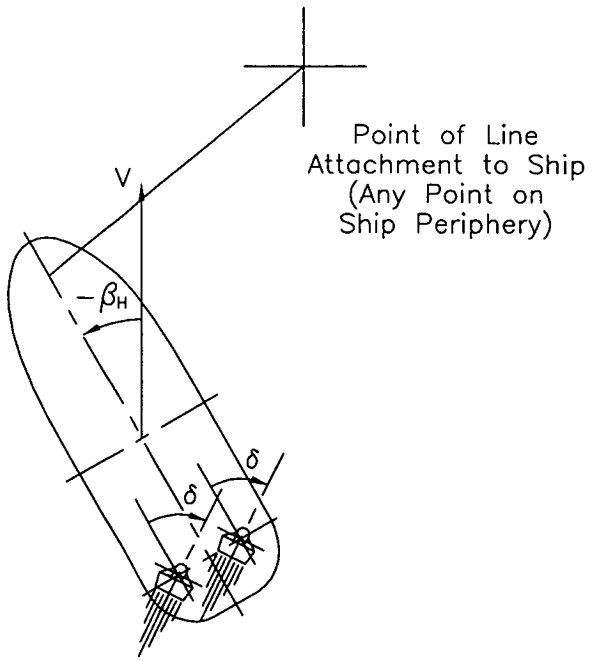

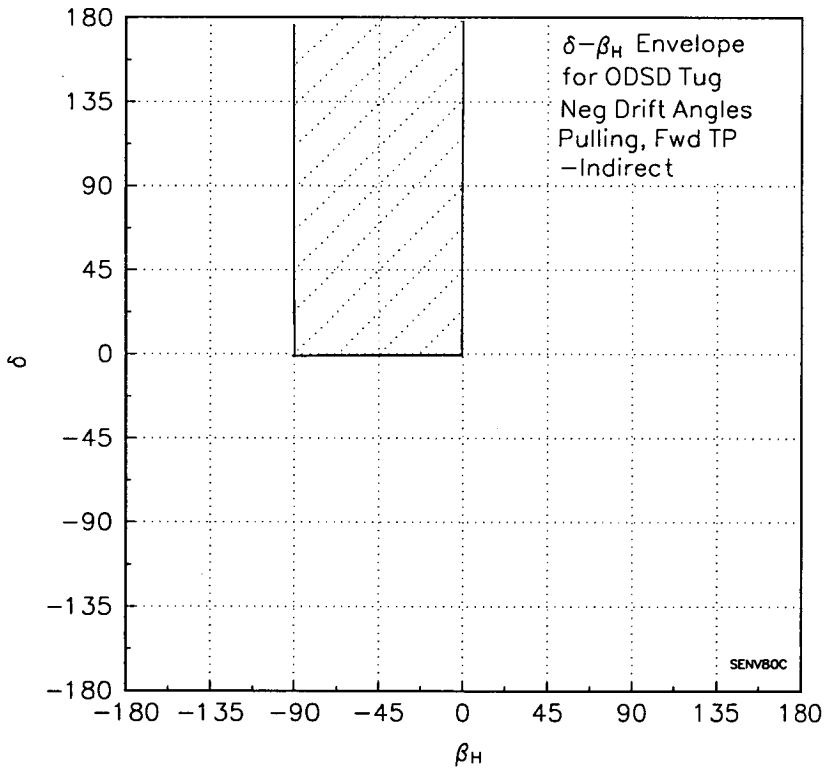

(c) Pulling with Forward Tow Point-Indirect Mode

Figure 6.2 Thruster Angle and Drift Angle Combinations for Omni-directional Stern Drive Tugs Operating at Negative Drift Angles

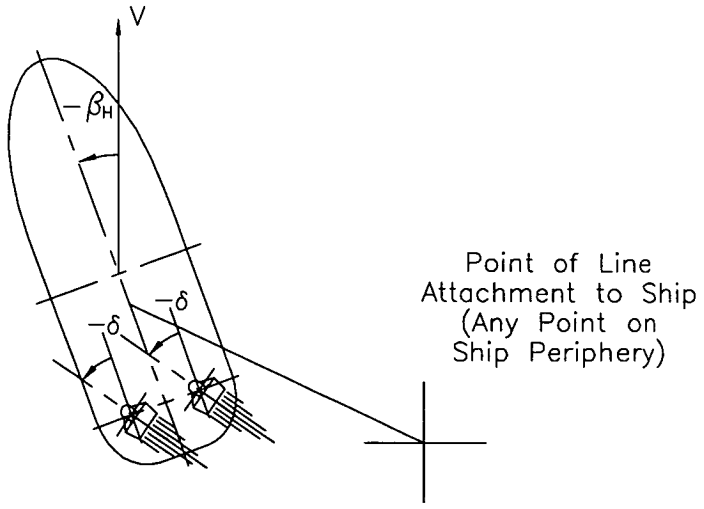

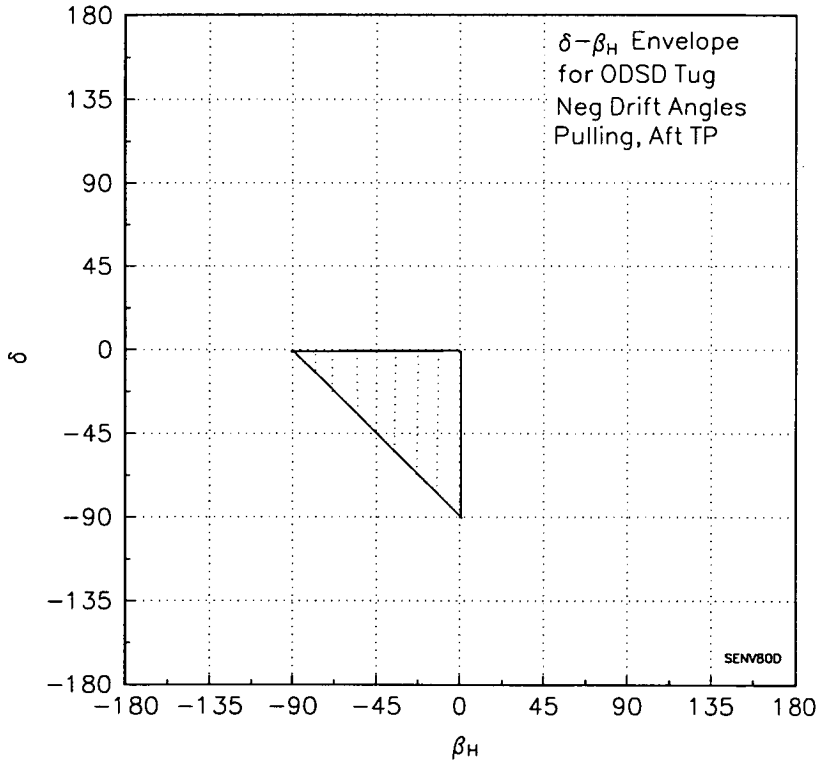

(d) Pulling with Aft Tow Point

Figure 6.2 Thruster Angle and Drift Angle Combinations for Omni-directional Stern Drive Tugs Operating at Negative Drift Angles

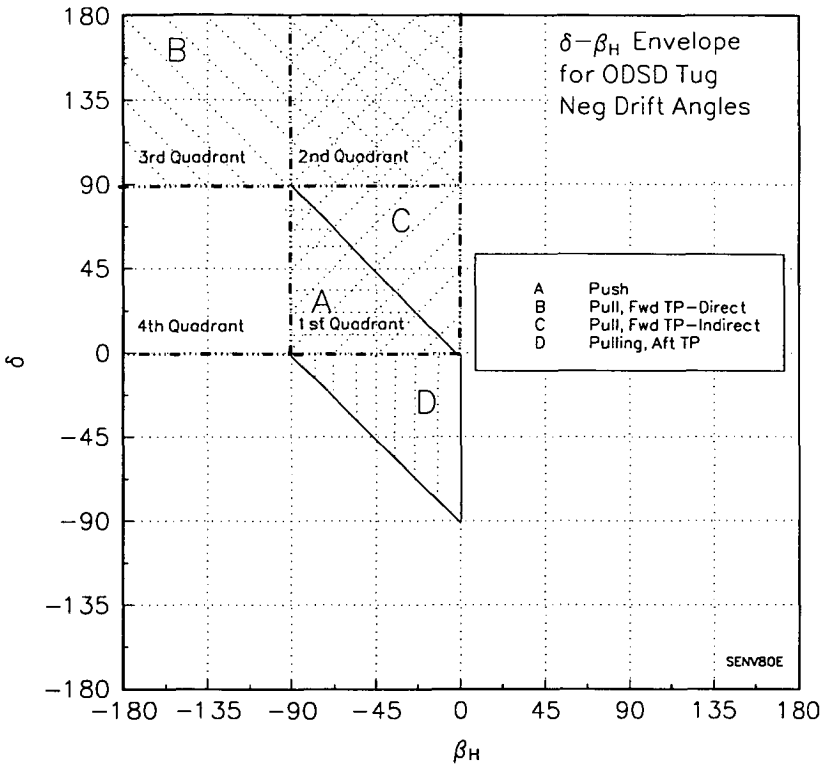

(e) Operational Envelope

Figure 6.2 Thruster Angle and Drift Angle Combinations for Omni-directional Stern Drive Tugs Operating at Negative Drift Angles

6.2.2 Tug Force Measurements

Left and right handed propellers were used to avoid the asymmetry that would occur with two propellers of the same hand. The propellers were fitted as outward turning, that is port side-left hand and starboard side-right hand. Propeller revolutions for each thruster were set at equal nominal values, being the same as that used for the open water tests for a single thruster and two thrusters, that is 19.6 rps. Measured tug forces have been non-dimensionalised by twice the bollard pull of a single thruster in open water. The measured revolutions were never different from the nominal value by more than 2%. To account for small changes, the bollard pull corresponding to the actual measured revolutions is used, i.e.:

$$F^*_{TUG} = \frac{F_{TUG}}{\tfrac{1}{2}\rho A_O (0.7\pi D_O)^2 \left(n_p^2 + n_s^2\right) C'_{X,\beta_P=0}}$$

where,

$$C'_{X,\beta_P=0} = 0.363 \qquad (6.3)$$

This system of non-dimensionalising allows tug performance at bollard pull to be compared directly with performance at each advance angle.

For revolutions set at 19.6 rps the velocity, V, was varied in steps of 0.2 m/s to obtain the desired apparent advance angles of 0, 3, 6, 9, 12 and 15°. Thruster angles tested at each advance angle are presented in Tables 6.1 and 6.2 for pulling and pushing respectively. The variation of drift angle with thruster angle at each advance angle is shown in Figures 6.3 and 6.9 for pulling and pushing respectively. Tug force

measurements for each advance angle are presented in Figures 6.4 to 6.8 for pulling and Figures 6.10 to 6.15 for pushing, using the coordinate system shown in Figure 6.1. For advance angles greater than zero, two plots are shown in each figure. One is a polar plot of (F^*_{TUG}, χ) from which forces in the directions parallel and perpendicular to the flow direction can be easily seen. These forces may be directly related to longitudinal and transverse forces applied to a ship for the case of zero yaw and sway. The other plot is a rectangular plot of (F^*_{TUG}, χ) and the contribution to F^*_{TUG} from hull forces F^*_H, which has been calculated using the measured thruster forces from equilibrium. The results presented in Figures 6.3 to 6.15 are for the case where port and starboard thruster angles are equal.

The polar diagrams shown in Figures 6.3 to 6.15 also show results derived from equilibrium using the procedure described in Chapter 2, assuming no interactions. Measured bare hull forces and open water thruster characteristics for the same hull and thrusters, as presented in Chapters 3 and 4 respectively, were used as input data to the model. Comparison of the experimental and predicted results demonstrates the overall effects of interactions between the thrusters and the thrusters and hull.

In addition to experiments where the thrusters were rotated to equal angles, a limited series of experiments were also carried out with unequal thruster angles. Although rotation of the thrusters to equal angles is the most common and, arguably, the most efficient configuration, methods are in use where this is not the case. A prevalent application of this method is in the pushing mode, where the leading thruster is fixed at 0° rotation to apply force in the tug's axial direction and the trailing thruster is used to control the drift angle. Clearly, as discussed by Brandner, 1992, the greatest combined force is created from two thrust vectors that are parallel which, in the absence of interactions, means that thruster angles should be equal. However, interactions are present and may possibly make this approach more efficient. To investigate this, a series of experiments were performed at apparent advance angles of 3, 6 and 9°. Thruster angles tested at each advance angle are presented in Table 6.3. Tug force measurements for each advance angle are presented in Figures 6.16 to 6.18 as polar diagrams of (F^*_{TUG}, χ) only. Plotted also in the figures are the results for equal thruster angles allowing comparison of the forces applied.

Thruster forces measured in the free running experiments and derived hull forces are presented in sections 6.3 and 6.4.

β_{PV}			
3°	6°	9°	12°
180	180	180	180
175	175	175	175
170	170	170	170
165	165	165	165
160	162.5	160	160
155	160	155	155
150	155	150	150
148.5	150	145	145
147.5	145	140	140
	140	135	130
	137.5	130	120
	135	125	110
			100
			90
			80
			70
			60
			50
			45
			40
			35
			30

Table 6.1 Thruster Angles Tested for Self Propelled Free Running Model Experiments for Pulling

β_{PV}				
3°	6°	9°	12°	15°
5	10	10	15	15
10	15	15	20	20
15	20	20	25	25
17.5	25	25	30	30
		30	35	

Table 6.2 Thruster Angles Tested for Self Propelled Free Running Model Experiments for Pushing

β_{PV}					
3°		6°		9°	
Port	Star	Port	Star	Port	Star
10	0	20	0	40	0
20	0	30	0	60	0
30	0	40	0	80	0
		50	0		
		60	0		
		90	0		

Table 6.3 Thruster Angles Tested for Self Propelled Free Running Model Experiments for Pushing with Unequal Thruster Angles

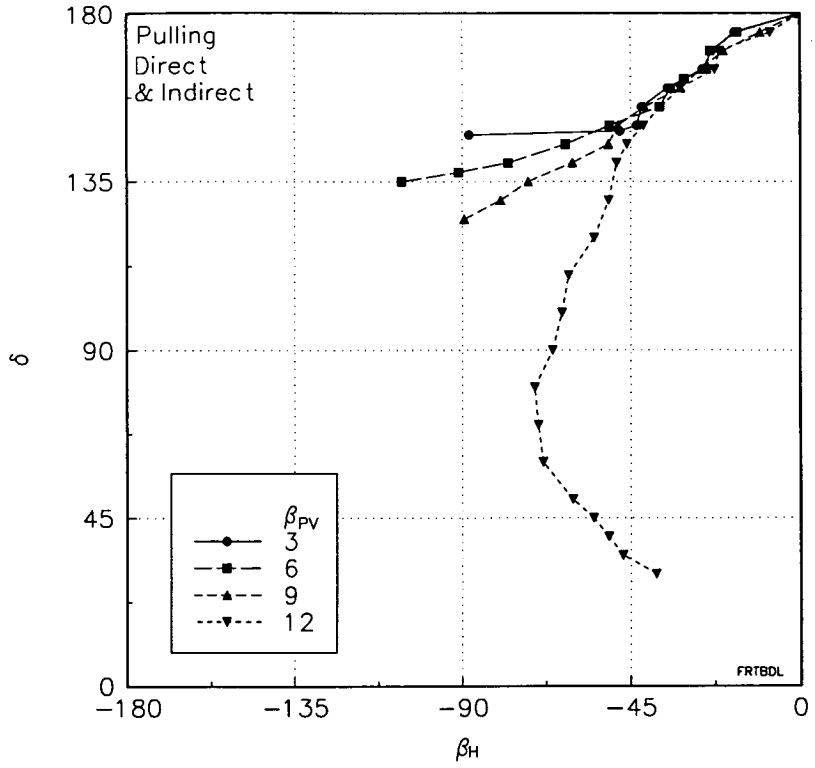

Figure 6.3 Variation of Drift Angle with Thruster Angle from Self Propelled Free Running Model Experiments for Pulling

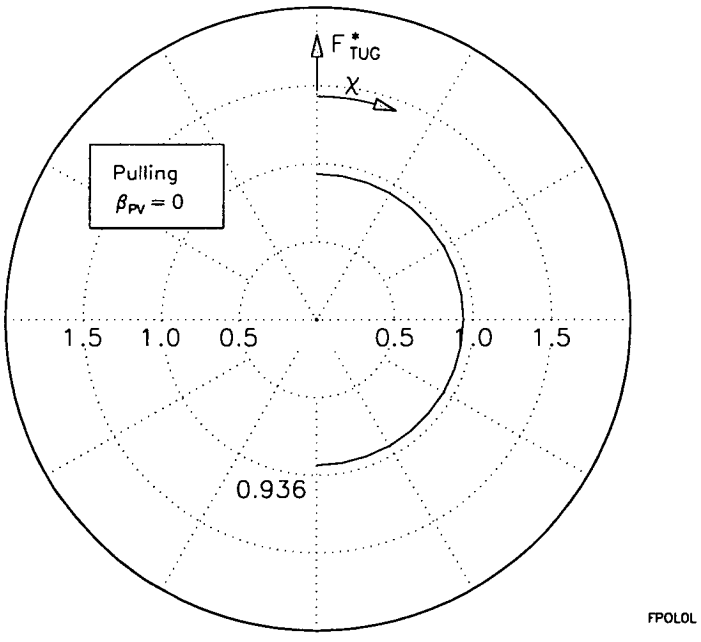

Figure 6.4 Tug Force Measurements from Self Propelled Free Running Model Experiments for Pulling, $\beta_{PV} = 0°$

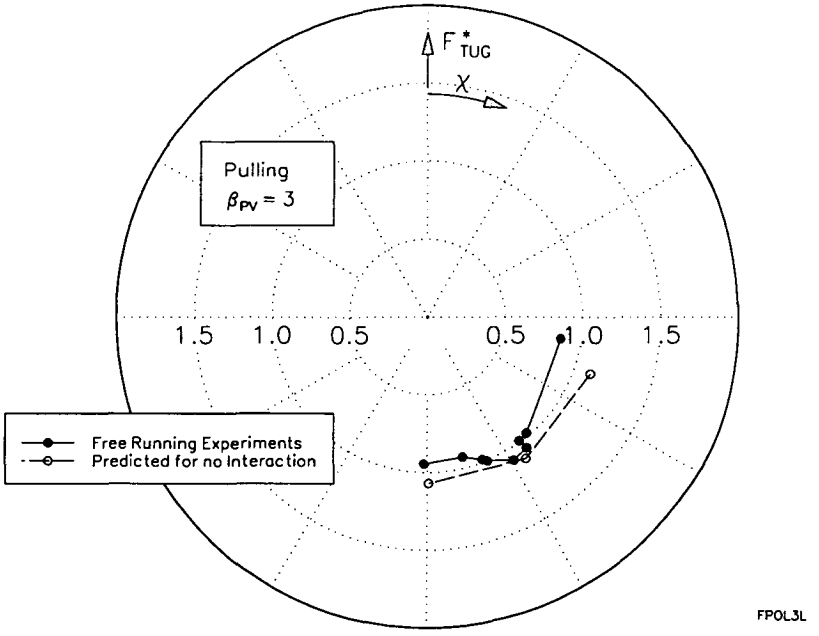

(a) Polar Plot of Tug Force,

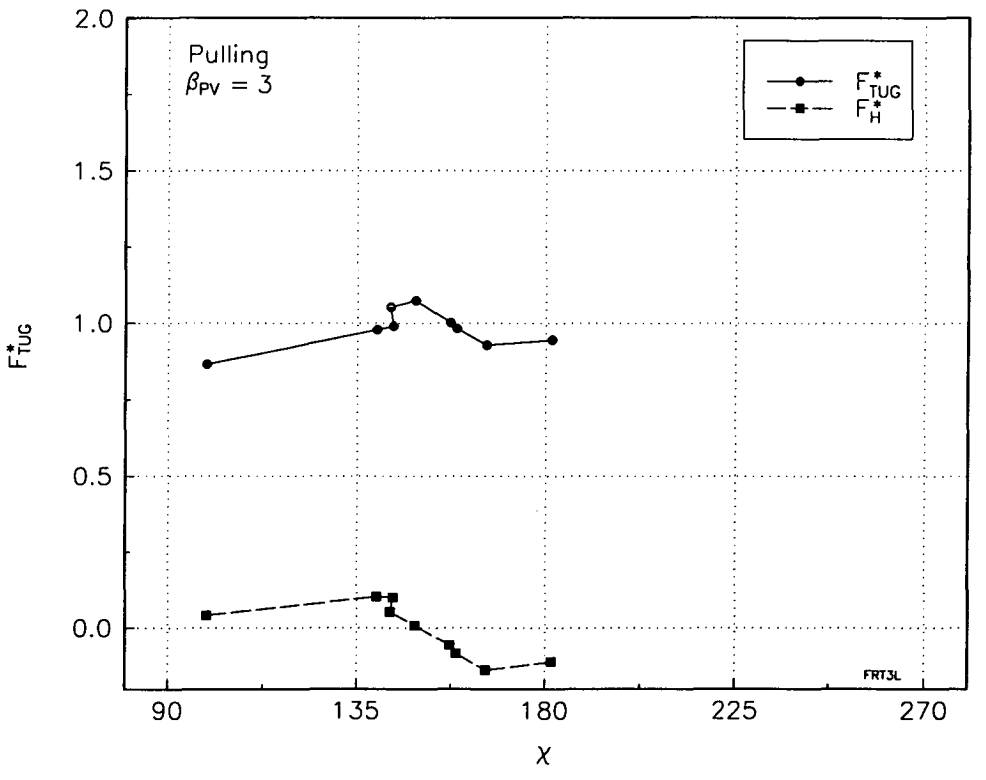

(b)Rectangular Plot of Tug Force with Contribution from Hull Force

Figure 6.5 Tug Force Measurements from Self Propelled Free Running Model Experiments for Pulling, $\beta_{PV} = 3°$

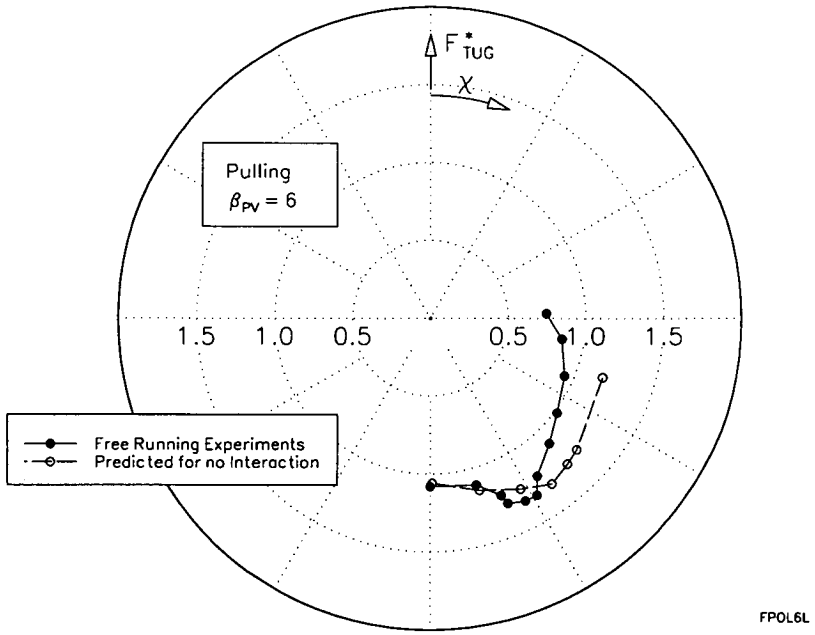

(a) Polar Plot of Tug Force

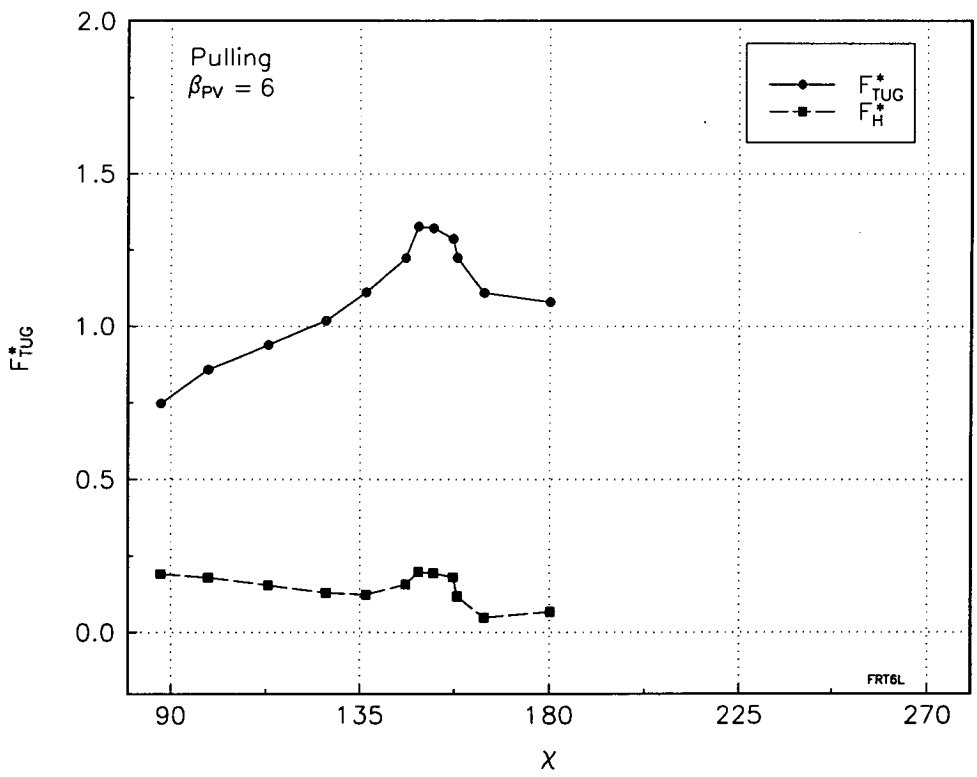

(b) Rectangular Plot of Tug Force with Contribution from Hull Force

Figure 6.6 Tug Force Measurements from Self Propelled Free Running Model Experiments for Pulling, $\beta_{PV} = 6°$

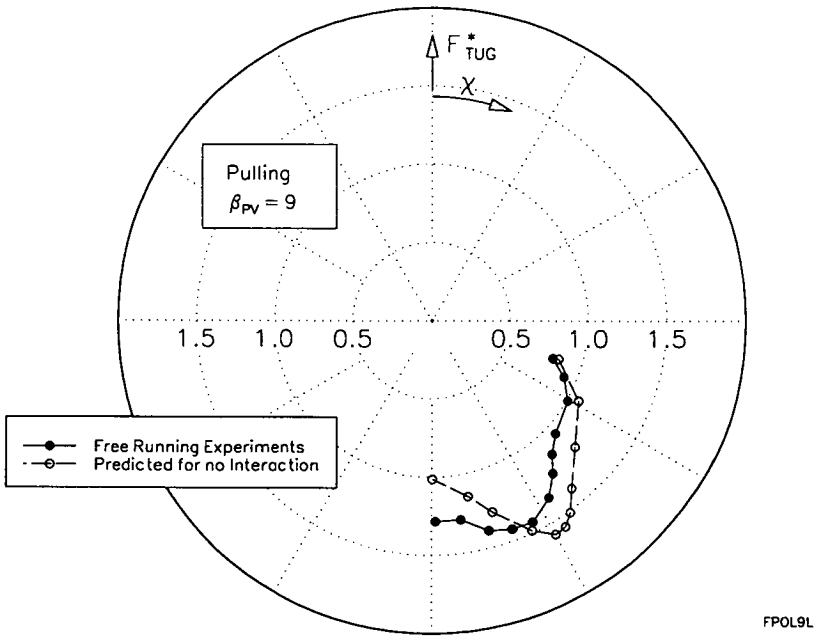

(a) Polar Plot of Tug Force

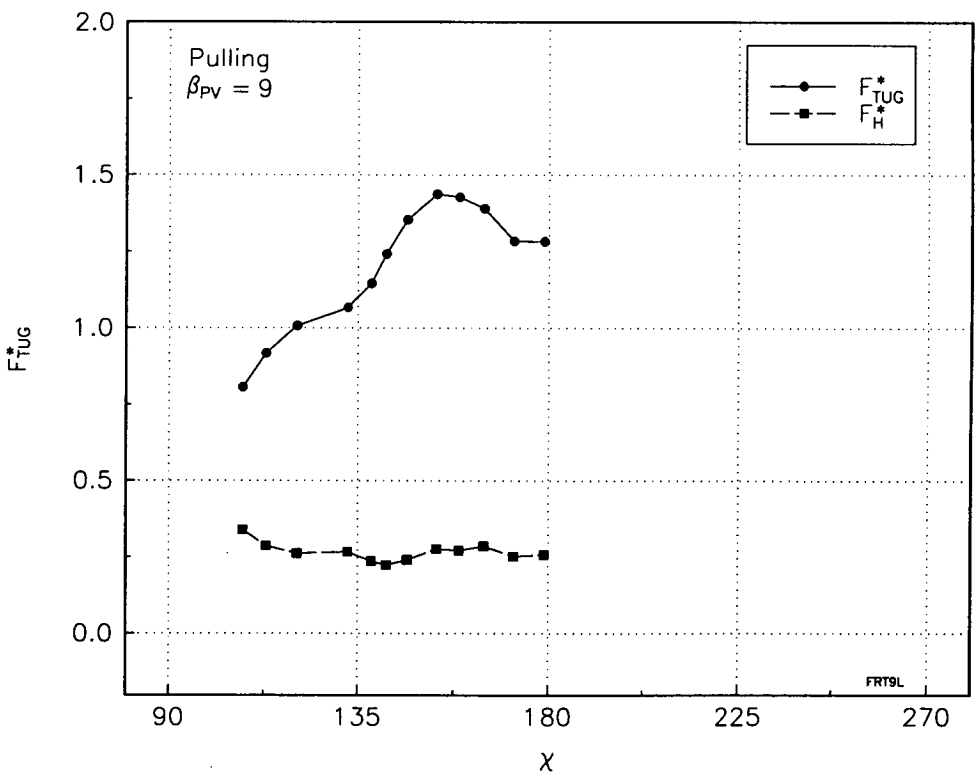

(b) Rectangular Plot of Tug Force with Contribution from Hull Force

Figure 6.7 Tug Force Measurements from Self Propelled Free Running Model Experiments for Pulling, $\beta_{PV} = 9°$

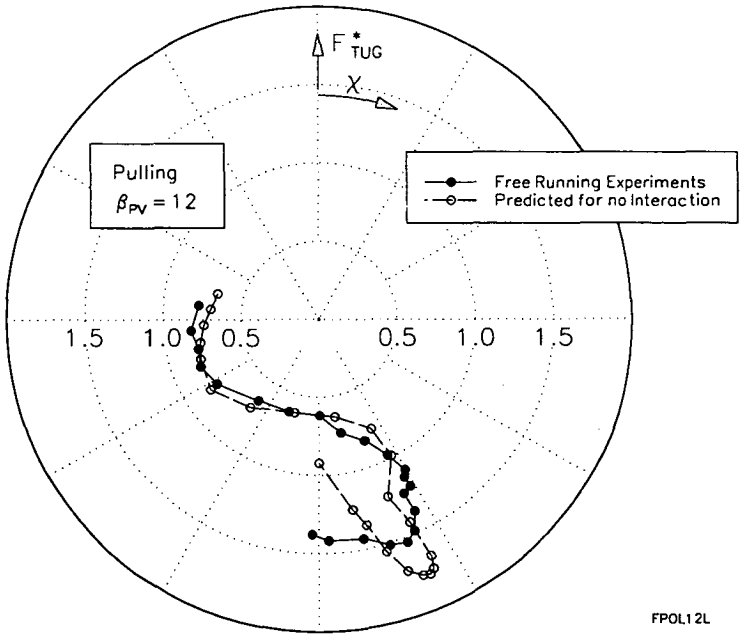

(a) Polar Plot of Tug Force

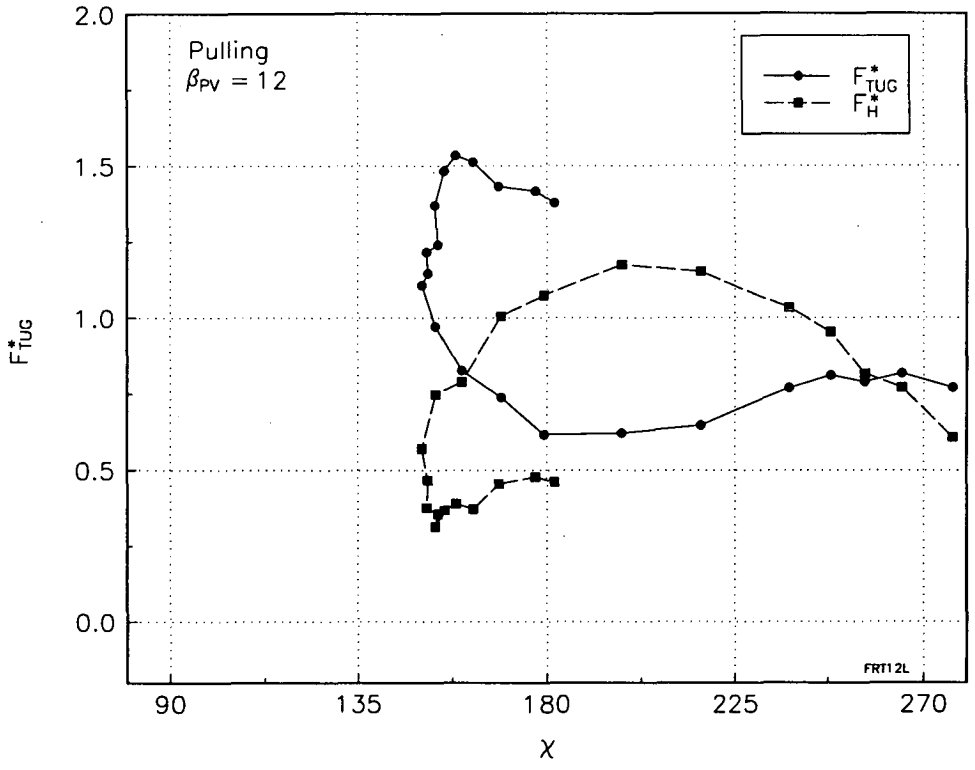

(b) Rectangular Plot of Tug Force with Contribution from Hull Force

Figure 6.8 Tug Force Measurements from Self Propelled Free Running Model Experiments for Pulling, β_{PV} = 12°

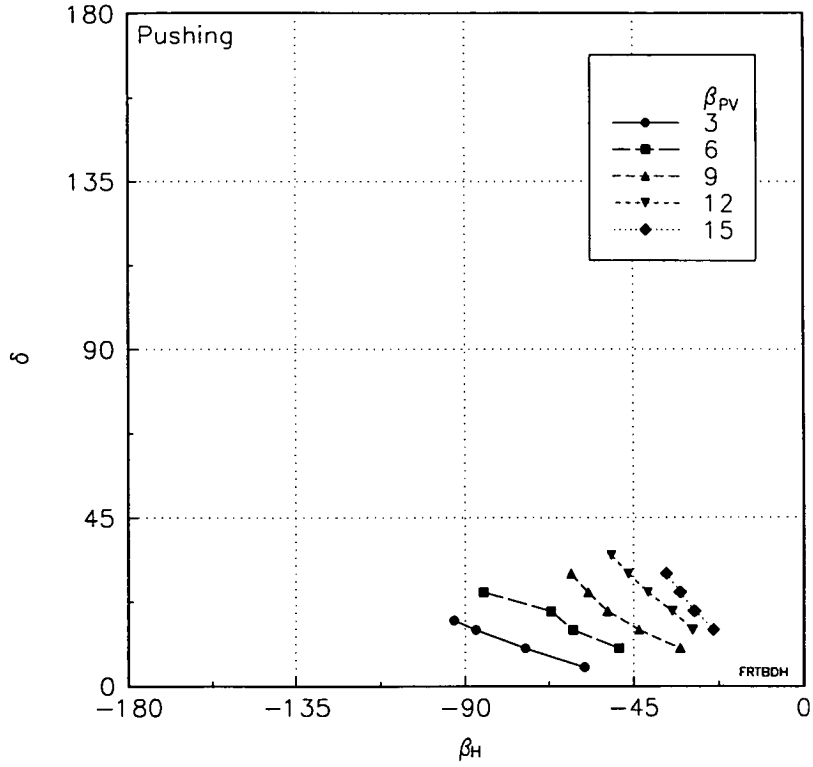

Figure 6.9 Variation of Drift Angle with Thruster Angle from Self Propelled Free Running Model Experiments for Pushing

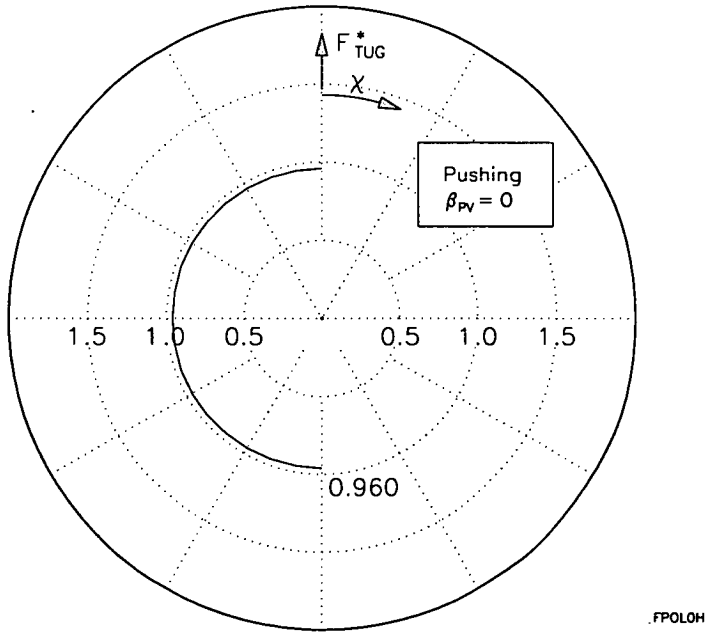

Figure 6.10 Tug Force Measurements from Self Propelled Free Running Model Experiments for Pushing, $\beta_{PV} = 0°$

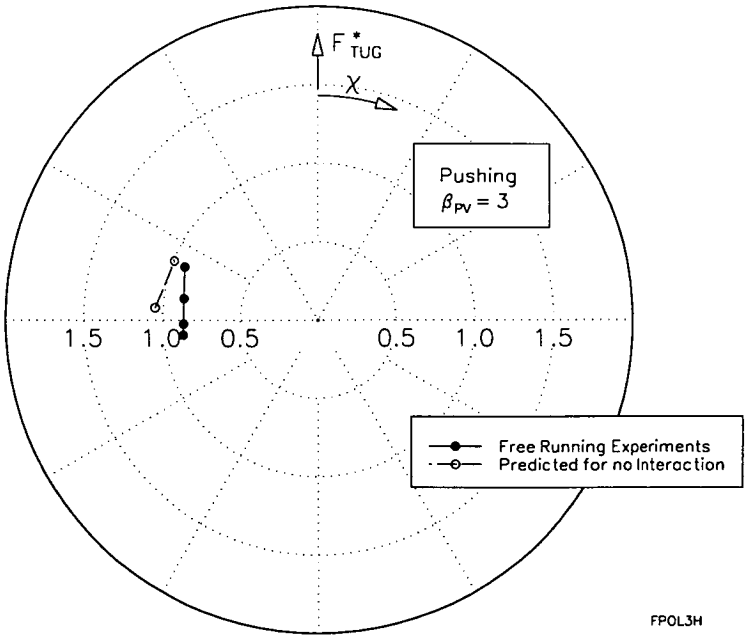

(a) Polar Plot of Tug Force

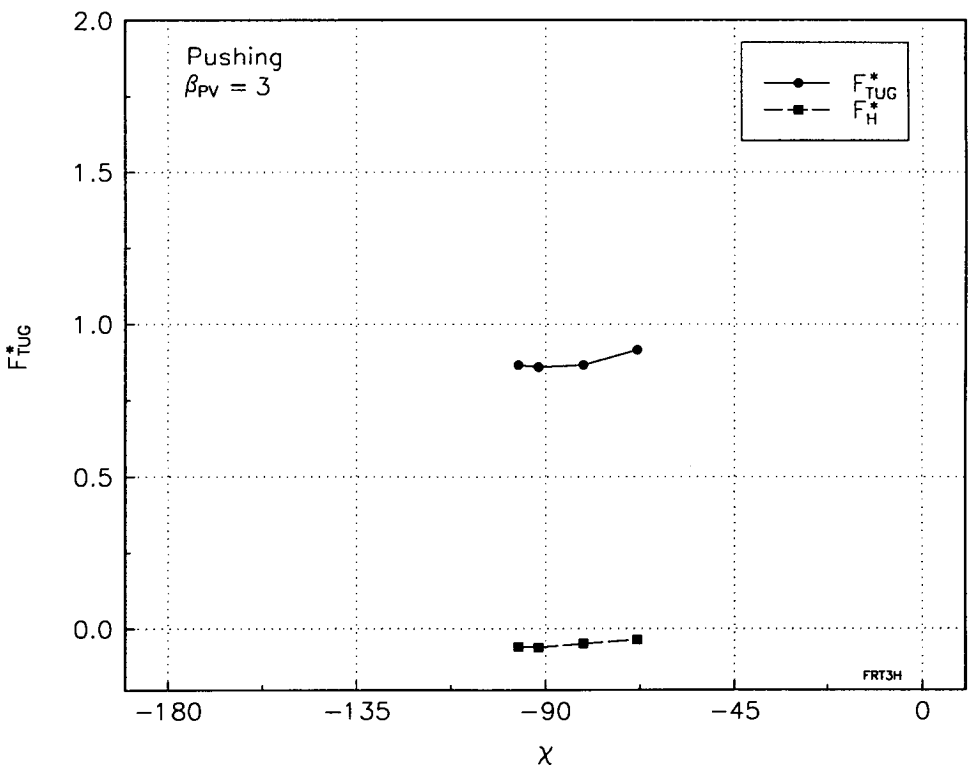

(b) Rectangular Plot of Tug Force with Contribution from Hull Force

Figure 6.11 Tug Force Measurements from Self Propelled Free Running Model Experiments for Pushing, $\beta_{PV} = 3°$

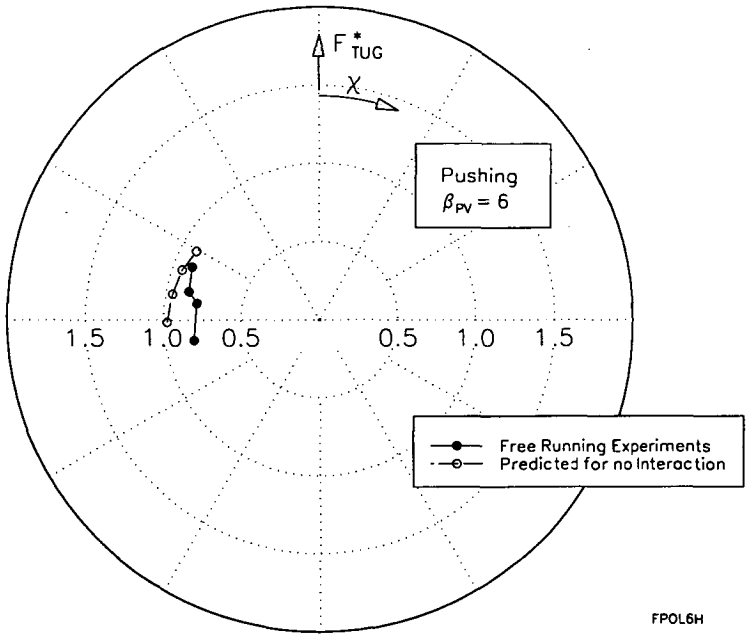

(a) Polar Plot of Tug Force

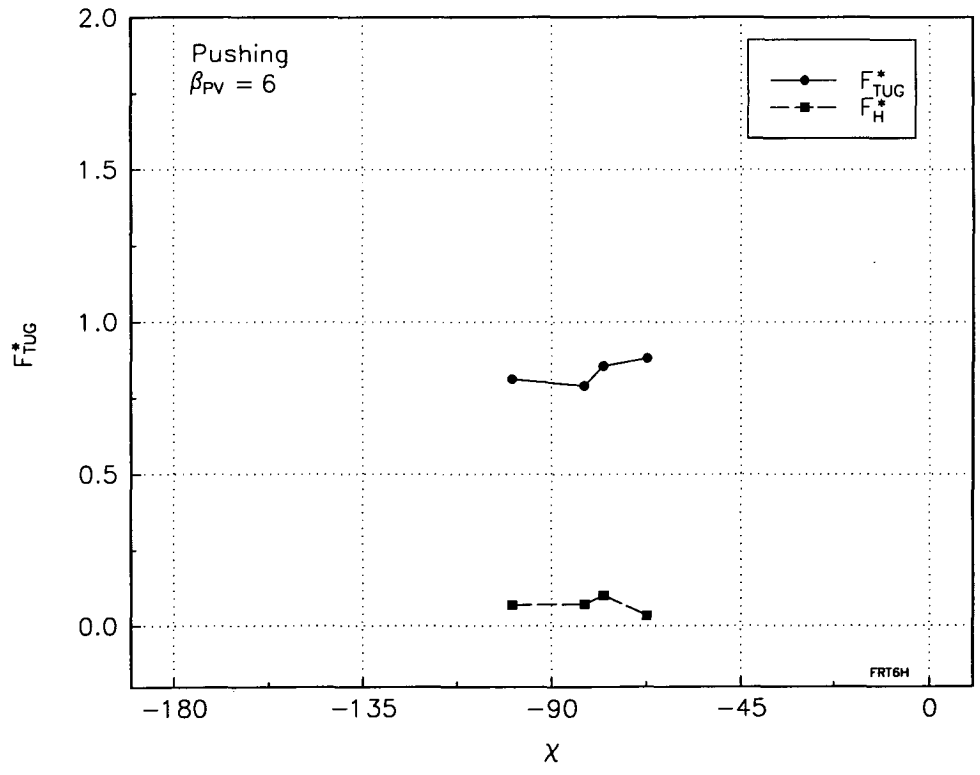

(b) Rectangular Plot of Tug Force with Contribution from Hull Force

Figure 6.12 Tug Force Measurements from Self Propelled Free Running Model Experiments for Pushing, $\beta_{PV} = 6°$

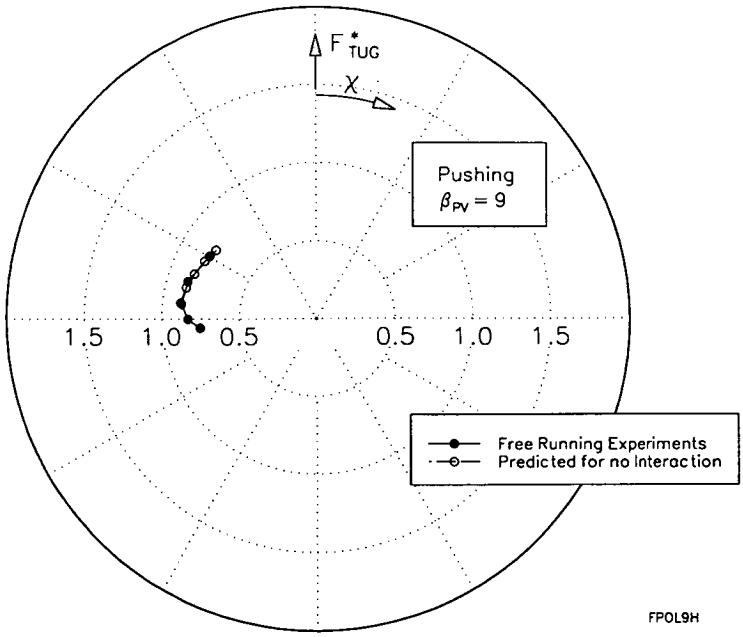

(a) Polar Plot of Tug Force

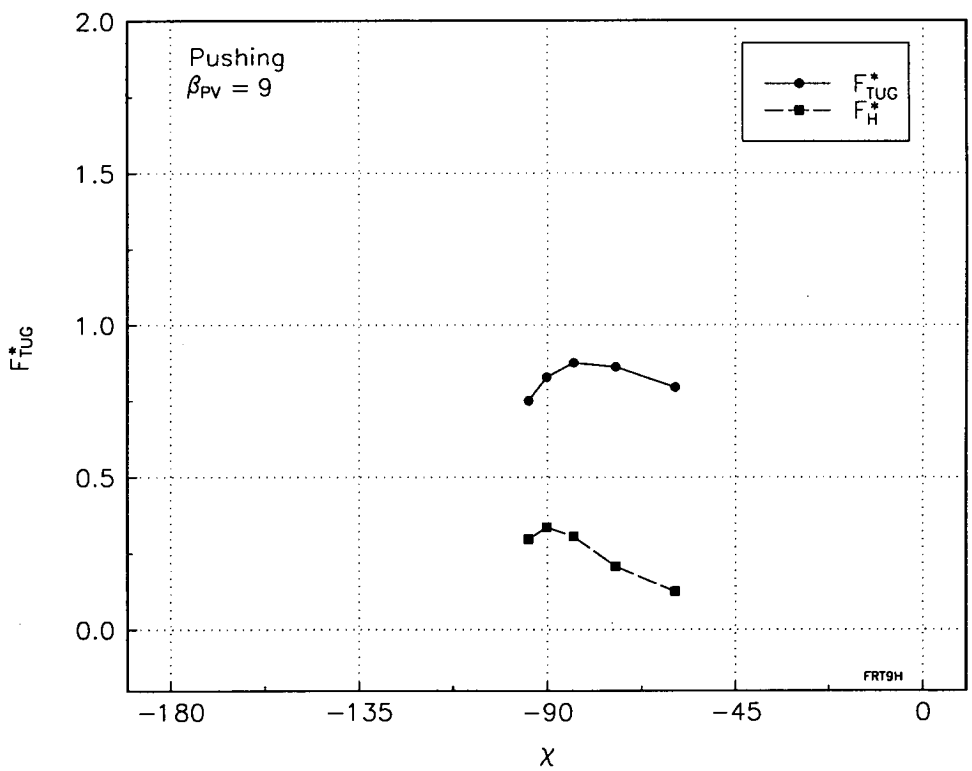

(b) Rectangular Plot of Tug Force with Contribution from Hull Force

Figure 6.13 Tug Force Measurements from Self Propelled Free Running Model Experiments for Pushing, $\beta_{PV} = 9°$

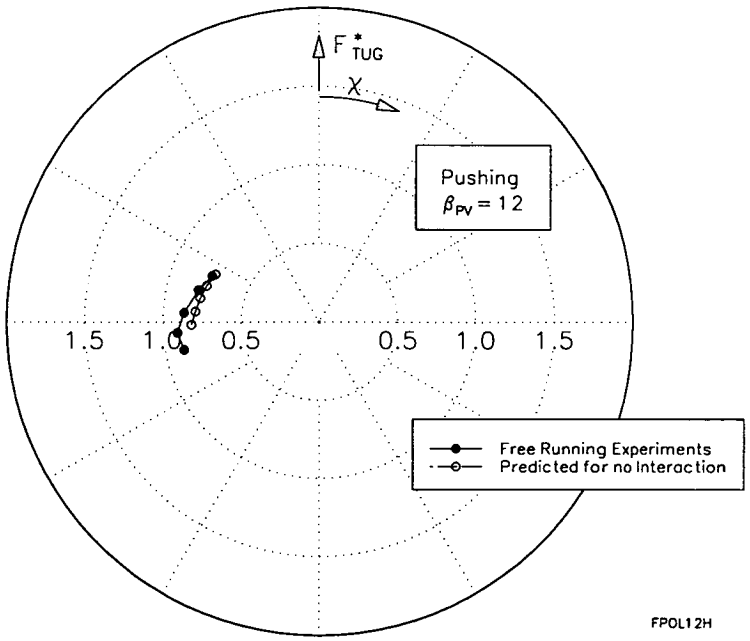

(a) Polar Plot of Tug Force

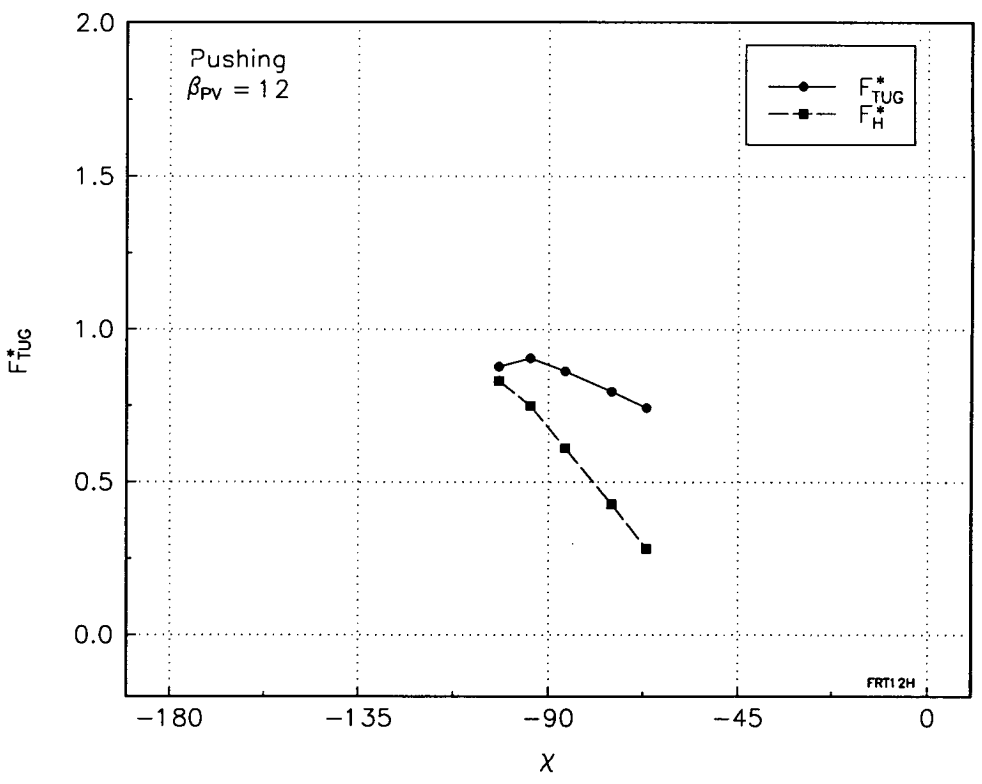

(b) Rectangular Plot of Tug Force with Contribution from Hull Force

Figure 6.14 Tug Force Measurements from Self Propelled Free Running Model Experiments for Pushing, β_{PV} = 12°

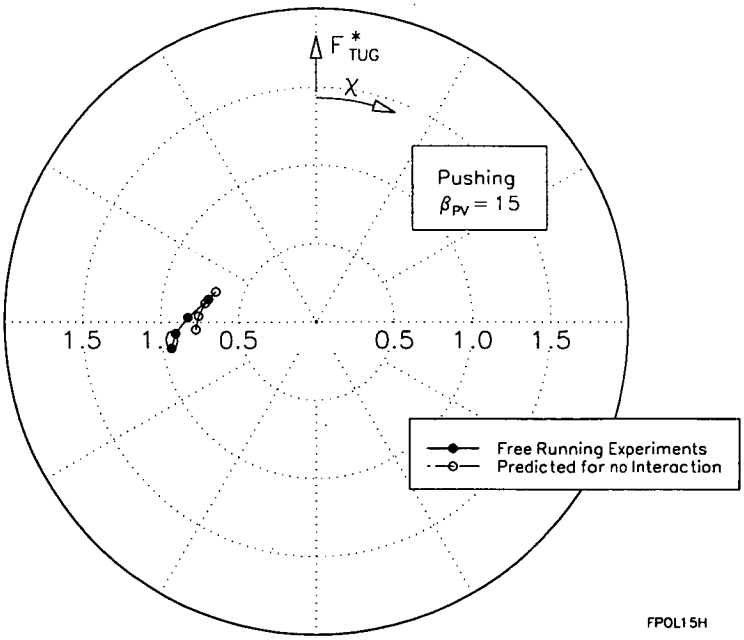

(a) Polar Plot of Tug Force

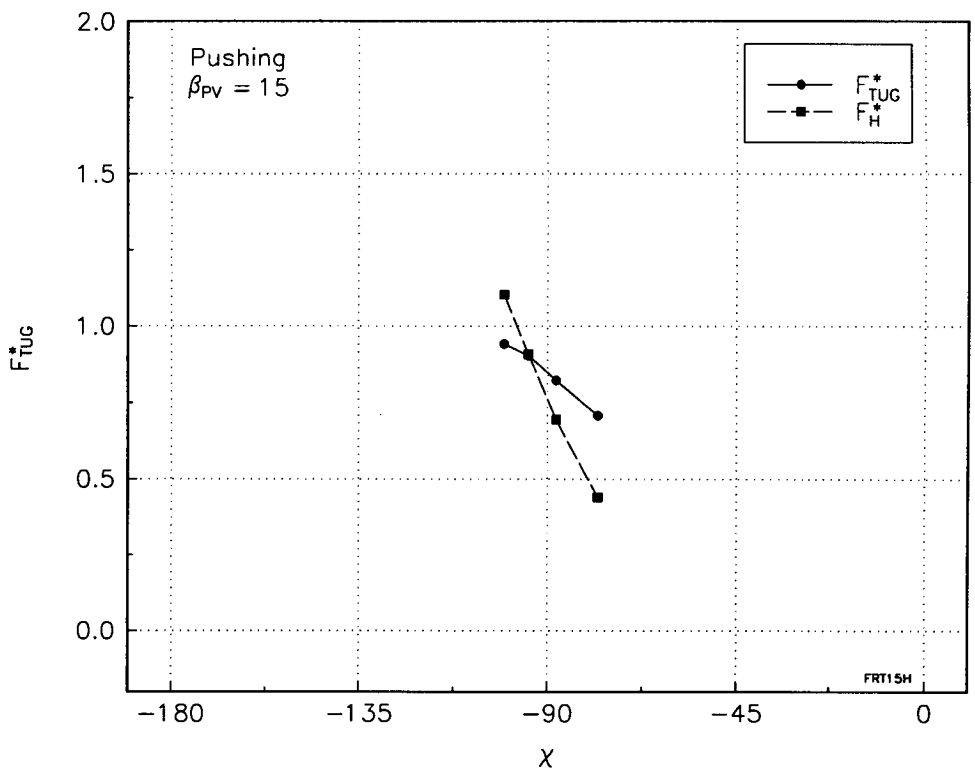

(b) Rectangular Plot of Tug Force with Contribution from Hull Force

Figure 6.15 Tug Force Measurements from Self Propelled Free Running Model Experiments for Pushing, $\beta_{PV} = 15°$

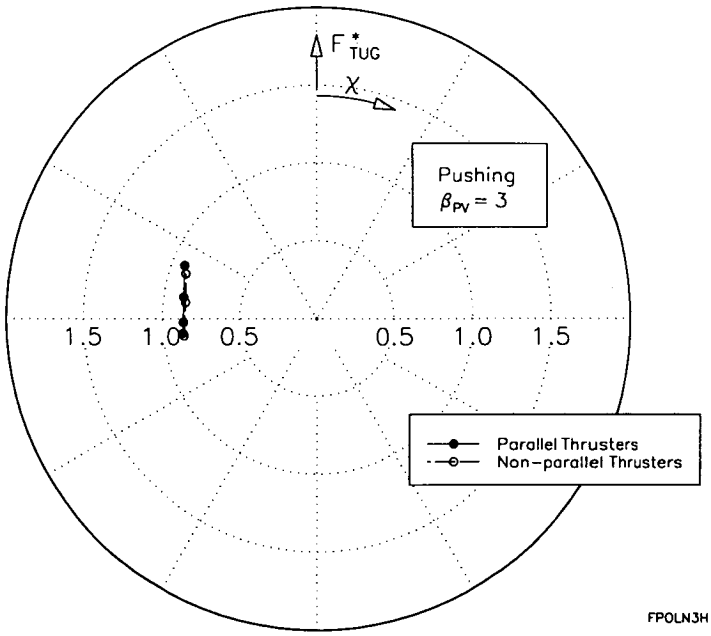

Figure 6.16 Tug Force Measurements from Self Propelled Free Running Model Experiments for Pushing with Unequal Thruster Angles, $\beta_{PV} = 3°$

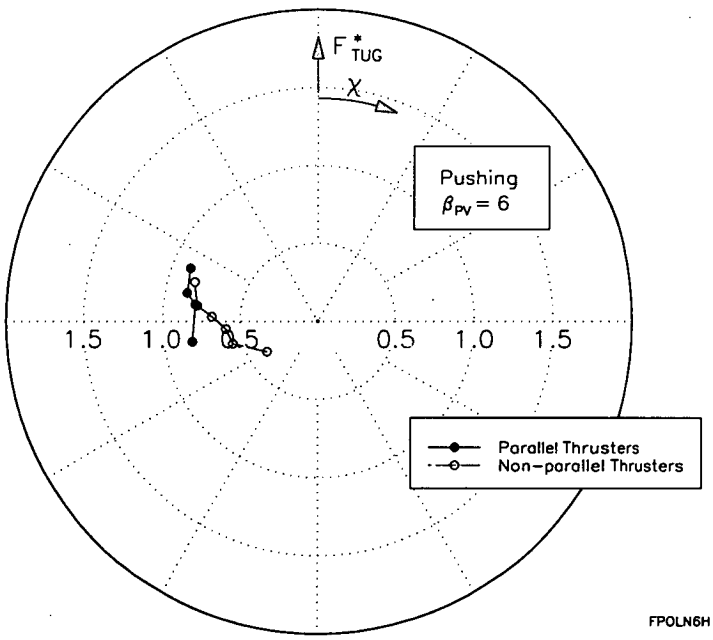

Figure 6.17 Tug Force Measurements from Self Propelled Free Running Model Experiments for Pushing with Unequal Thruster Angles, $\beta_{PV} = 6°$

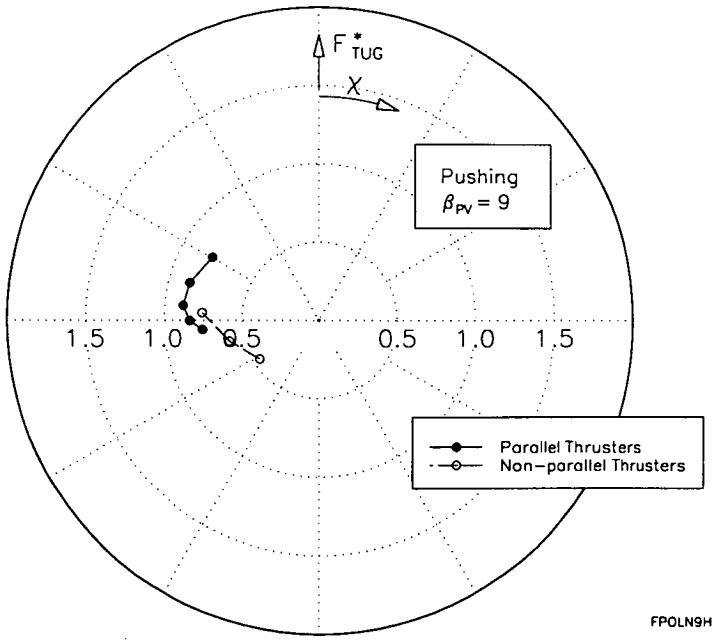

Figure 6.18 Tug Force Measurements from Self Propelled Free Running Model Experiments for Pushing with Unequal Thruster Angles, $\beta_{PV} = 9°$

6.2.3 Discussion of Tug Force Results for Pulling

The measured force for pulling at 0° apparent advance angle (the astern bollard pull) is shown in Figure 6.4. From Figure 5.3, it can be seen that interaction between two thrusters side-by-side in open water is negligible therefore, ideally, this value would be unity, corresponding to no loss due to interaction with the hull. The measured value of 0.936 indicates a loss of 6.4% due to the hull being immersed in the high energy part of the propeller induced flow field. Clearly, the greatest part of this interaction is due to the direct impingement of the propeller race on the afterbody of the tug.

From Figure 6.5(a) it can be seen that at 3° apparent advance angle, the polar diagram is already significantly altered from that at 0°. It can be easily shown that at this advance angle, hull forces due to the free stream, are small and therefore the differences can be attributed to the influence of the thrusters on the hull. From Figures 6.5(a) and (b) it can be seen that as the thruster angles are reduced from 180°, there is a steady decrease in the line angle and drift angle until 160°, where only small changes result. At 148.5° thruster angle, however, a reduction of only 1° causes a large reduction in the line angle and drift angle. These effects can possibly be explained in terms of the effect of the propeller race on the hull. At the higher thruster angles the race is directed along the hull, but, as the angles are reduced, the race from the starboard thruster is directed toward the hull and skeg. The flow velocity at this advance angle is not sufficient to deflect the propeller race from the starboard thruster and prevent it from impinging on the hull and skeg. Thus, the race impinging on the hull or skeg tends to cancel the transverse thruster forces holding the tug at a reduced drift angle until, at 147.5° thruster angle, this effect appears to reduce suddenly and the line angle and drift angle decrease significantly. Comparison of the experimental and predicted results for no interaction show that, as with the bollard pull, there is reduction of line force due to race impingement on the hull. However, in this situation, due to the small hull forces from the free stream, thruster-hull interaction has a far more dramatic effect on the direction of the tug force than on its magnitude.

Similar trends to those for 3° apparent advance angle are also present at 6°, as can be seen from Figure 6.6. As described above, the propeller race from the starboard thruster impinges on the skeg and tends to cancel the transverse forces from the thrusters, which reduces the rate of change of line angle with thruster angle. This can be seen for thruster angles in the neighbourhood of 160° although the effect is not as dramatic as it was for 3° apparent advance angle. From Figure 6.6 it can be seen that as the line angle decreases, the force initially increases and then decreases. This can be explained in terms of the forces acting on the thrusters and hull and their interactions. In Chapter 4 it was shown that thruster forces significantly increase when operating obliquely in negative flow, i.e. for angles of attack between 90 and 180°. The localised increase in force around χ = 150° can, in part, be attributed to this effect, as is shown in the measured forces presented in Section 6.3. The remainder of the increase can be attributed to an increase in hull resistance due to thruster-hull interaction which is discussed in Section 6.4. As the line angle approaches 90° the drift angle does also and transverse hull forces become larger, therefore more transverse force is required from the thrusters. The combined decrease of thruster angle and angle of attack mean that less force is applied in the direction of the line and consequently, the line force decreases with decreasing line angle.

For 9° apparent advance angle there is little evidence of the propeller race from the starboard thruster affecting the rate of change of line angle with thruster angle, as can be seen from Figure 6.7. At this advance angle the free stream velocity, presumably, is such that the race is always deflected before impinging on the afterbody or skeg. It can be seen from Figure 6.3, that for drift angles up to 45° the rate of change of drift angle with thruster angle is similar for all advance angles although, as described above this is not for the same reasons. At the lower advance angles where the thruster race is not significantly deflected, impingment of the race on the afterbody and skeg tends to cancel the transverse thruster forces. On the other hand, at higher advance angles, the race is deflected and tends not to impinge on the afterbody or skeg however, transverse thruster forces must overcome significantly increased hull forces. Comparison of Figure 6.7 with Figures 6.5 and 6.6 shows the overall trend of increasing line force with increasing advance angle, due to thruster forces and hull forces increasing. The latter is due to the increase in hull resistance from thruster-hull interaction, which is particularly apparent comparing measured and predicted line forces for pure braking (χ = 180°). The variation of line force with line angle is similar to that for 6° and may be explained as above.

At 12° apparent advance angle, hull forces become large and play a much greater part in the tug's behaviour, as can be seen from Figure 6.8. The magnitude of the transverse hull forces is such that they can only be overcome by the thrusters for a limited range of drift angles. As can be seen from Figure 6.8(a), the minimum line angle achievable is approximately 150° for thruster angles of 120°. Further decrease in thruster angle initially results in the tug being dragged along at a high drift angle and then moving into the indirect mode, as can be seen from Figure 6.3. Comparison of the measured and predicted braking forces (χ = 180°) for each advance angle demonstrates the effect of advance angle on thruster-hull interaction. With decreasing thruster angle and angle of attack, thruster-hull and thruster-thruster interaction are reduced, as can be seen from the improved comparison between measured and predicted results.

6.2.4 Discussion of Tug Force Results for Pushing

The measured force for pushing at 0° apparent advance angle (the ahead bollard pull) is shown in Figure 6.10. Ideally, this value would be unity corresponding to no loss due to interaction with the hull. The measured value of 0.960 indicates a loss of 4.0% due to the hull being immersed in the low energy part of the propeller induced flow field. Clearly, the greatest part of this interaction is due to the low pressure region created over the afterbody of the tug.

With reference to Figures 6.10 to 6.15 it can be seen that the most notable feature of the pushing results is that the tug force does not significantly vary as a function of the advance angle. The magnitude of the force is always within the range 0.75 to 1 and the direction within the range −60 to −90°. This consistency of the imparted force can be explained in terms of the forces acting on the hull and thrusters. At low advance angles transverse forces acting on the tug hull are small, therefore, a large drift angle is easily maintained and the force imparted is essentially due entirely to thruster forces. At higher advance angles transverse hull forces become large, decreasing the drift angle and hence the component of the thruster forces imparted. However, the centre of pressure of the hull force moves forward with decreasing drift angle toward the point of contact on the fendering. In this way the loss of thruster force is compensated for by lift forces acting on the tug hull, as can be clearly seen

from Figures 6.14 and 6.15. For pushing, the tug is operating in the first quadrant (as defined in Section 6.1) where it is expected that thruster-hull interaction will be dominated by the influence of the hull on the thrusters. The overall favourable comparison between measured and predicted results imply that interactions for pushing are smaller than those for pulling.

Figures 6.16 to 6.18 show that for pushing with the range of unequal thruster angles tested, there are no favourable interactions and less force results compared with equal angles.

6.3 Influence of Hull on Thrusters

Thruster forces measured during the free running experiments can be compared with those measured during open water experiments and the extent of interactions affected by the hull determined. Results from the open water experiments on one and two thrusters are presented in Chapters 4 and 5 respectively. Using these results it is possible to determine the influence of the hull on each individual thruster and whether the influence of the hull must be considered when calculating thruster-thruster interaction.

The behind hull and open water thruster forces are compared separately for operation in the pulling and pushing modes. The behind hull thruster forces have been non-dimensionalised using the free stream velocity and presented as polar thrust diagrams similar to the results presented in Chapters 4 and 5. Open water characteristics were measured at apparent advances angles every 5° and the behind hull characteristics at apparent advance angles of 3°. Hence, to allow comparison, the open water characteristics have been interpolated to match the behind hull apparent advance angles as well as the apparent angles of attack.

6.3.1 Influence of the Hull on Thrusters for Operation in the Pulling Mode

The open water characteristics for one and two thrusters and the behind hull characteristics are presented in Figure 6.19 for the apparent advance angles of 3, 6, 9 and 12°. The results shown in Figures 6.19(a), (b) and (c) are for pulling in the direct mode only, whereas those in Figure 6.19(d) are for pulling in both the direct and indirect modes. The thruster forces for the astern bollard pull have not been presented as they are essentially equal to those measured in open water conditions. Hence, it can be concluded that the hull has negligible influence on the thrusters in the astern bollard condition.

As described in Section 6.1, combinations of drift angle and thruster angle may be separated into quadrants compatible with the nature of interaction expected. Pulling in the direct mode corresponds to the second quadrant where thruster-hull interaction is expected to be dominated by the influence of the thrusters on the hull. Also, it was shown in Chapter 5 that interaction between thrusters is greatest in the second quadrant and that for negative drift angles only the port thruster is affected. It can be seen from Figure 6.19 that the behind hull results for the starboard thruster compare favourably with the open water results for one and two thrusters. For the port thruster the behind hull results compare favourably with the open water results for two thrusters. This demonstrates that as expected, in the second quadrant the hull has little influence on either thruster or on the interaction between thrusters.

Pulling in the indirect mode corresponds to the first and second quadrants where thruster-hull interaction may be dominated by the influence of either hull or thrusters respectively. However, it can be easily shown that the measurements made here for indirect towing are limited to only the first quadrant. Hence interactions are expected to be dominated by the influence of the hull. Also, it was shown in Chapter 5 that interaction between thrusters is small in the first quadrant, therefore significant differences in open water and behind hull characteristics may be attributed to the influence of the hull. The results for indirect towing are shown in Figure 6.19(d) corresponding to the measurements at small angles of attack. It can be seen from the results that the open water curves for two thrusters in this area compare favourably, showing that thruster-thruster interaction is small. There are significant differences between the behind hull curve for the port thruster and the open water curve indicating the influence of the hull. This demonstrates that as expected, in the first quadrant the hull has a significant effect on the thrusters.

6.3.2 Influence of the Hull on Thrusters for Operation in the Pushing Mode

The open water characteristics for one and two thrusters and the behind hull characteristics are presented in Figure 6.20 for the apparent advance angles of 3, 6, 9, 12 and 15°. The results shown are for pushing with the thrusters rotated to equal angles only. As with the astern bollard pull, thruster forces for the ahead bollard pull have not been presented, as they are essentially equal to those measured in open water conditions. Hence, it can be concluded that the hull has negligible influence on the thrusters in the ahead bollard condition.

From the results for operation in the pulling mode it was shown that the influence of the hull on the thrusters is significant in the first quadrant and negligible in the second. Operation in the pushing mode corresponds to the first quadrant and, as mentioned above, thruster-thruster interaction is small, therefore significant differences in behind hull and open water results can be attributed to the influence of the hull. From Figure 6.20 significant differences can be seen indicating the influence of the hull. As with the pulling indirect results, the port thruster being the trailing thruster is most dramatically affected.

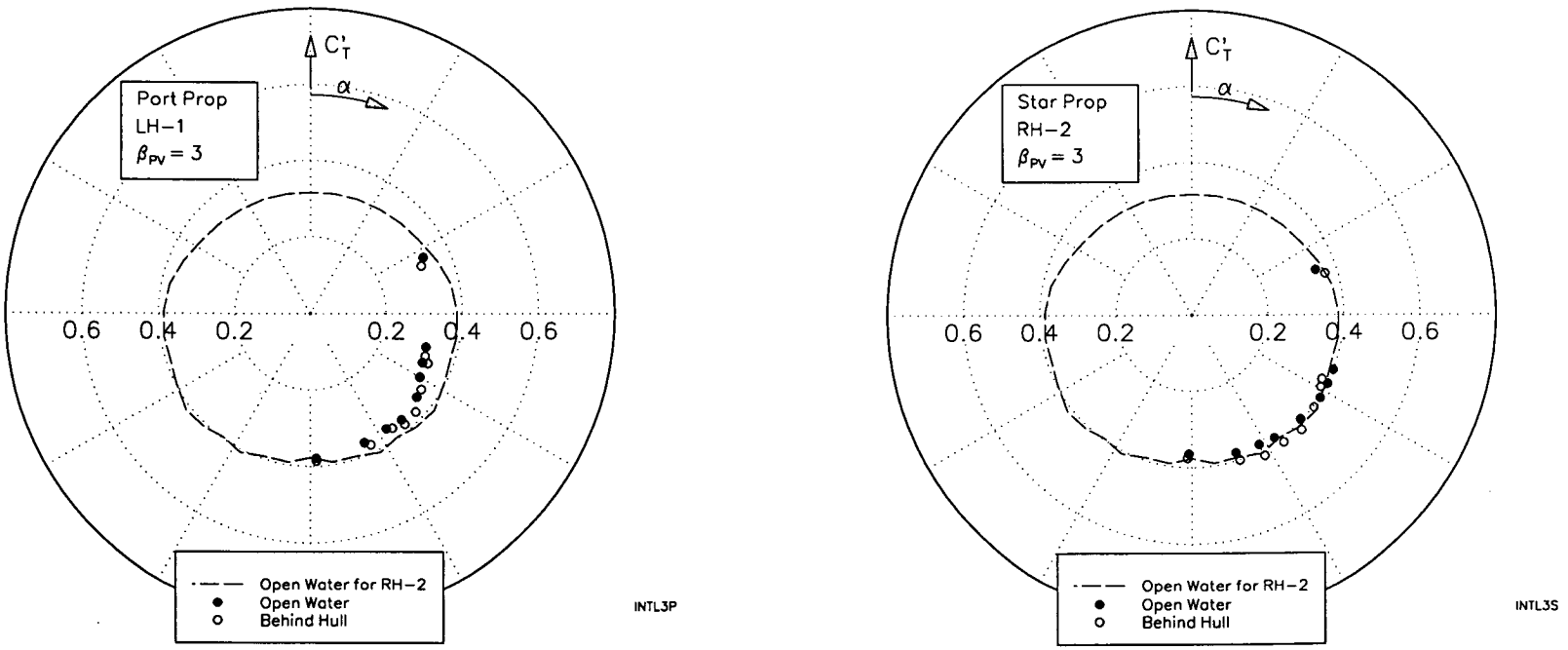

(a) $\beta_{PV} = 3°$

Figure 6.19 Comparison of Open Water Characteristics for One and Two Thrusters with Behind Hull Characteristics for Two Thrusters, for Operation in the Pulling Mode

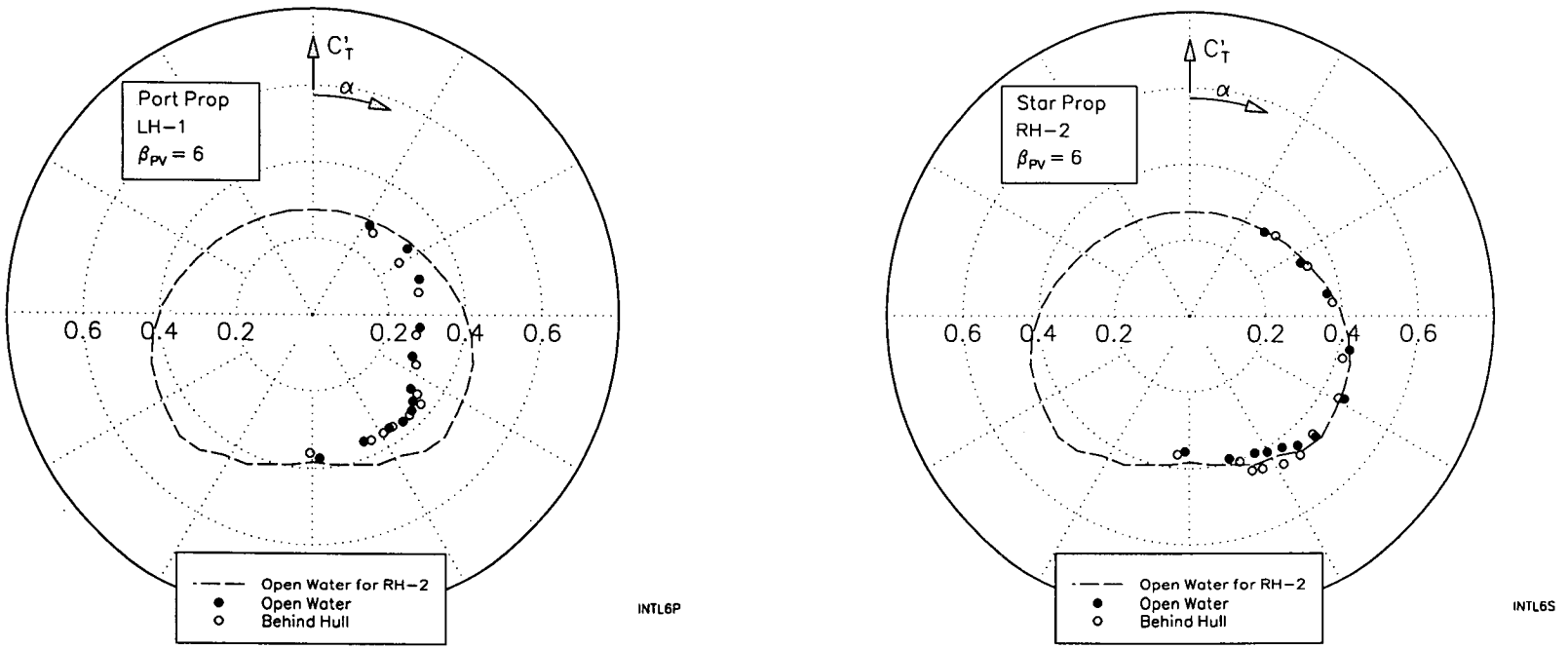

(b) $\beta_{PV} = 6°$

Figure 6.19 Comparison of Open Water Characteristics for One and Two Thrusters with Behind Hull Characteristics for Two Thrusters, for Operation in the Pulling Mode

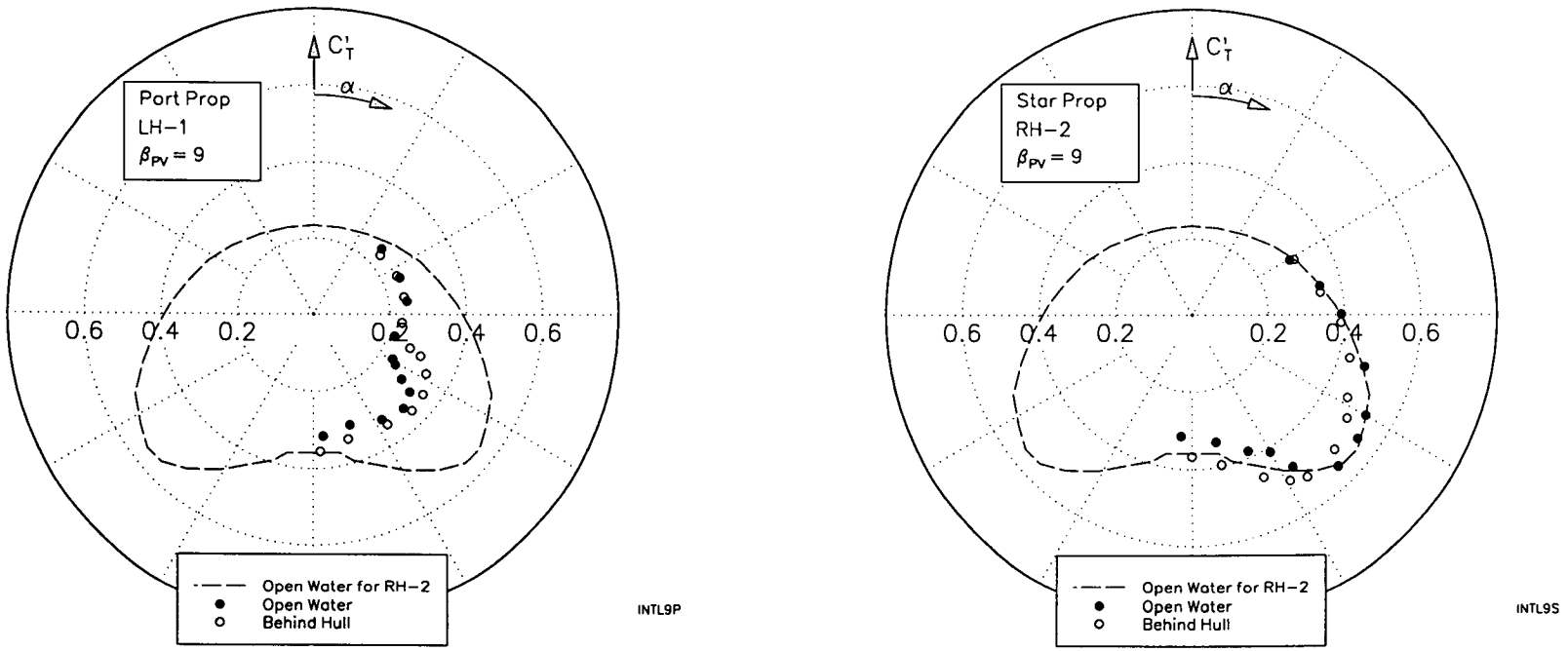

(c) $\beta_{PV} = 9°$

Figure 6.19 Comparison of Open Water Characteristics for One and Two Thrusters with Behind Hull Characteristics for Two Thrusters, for Operation in the Pulling Mode

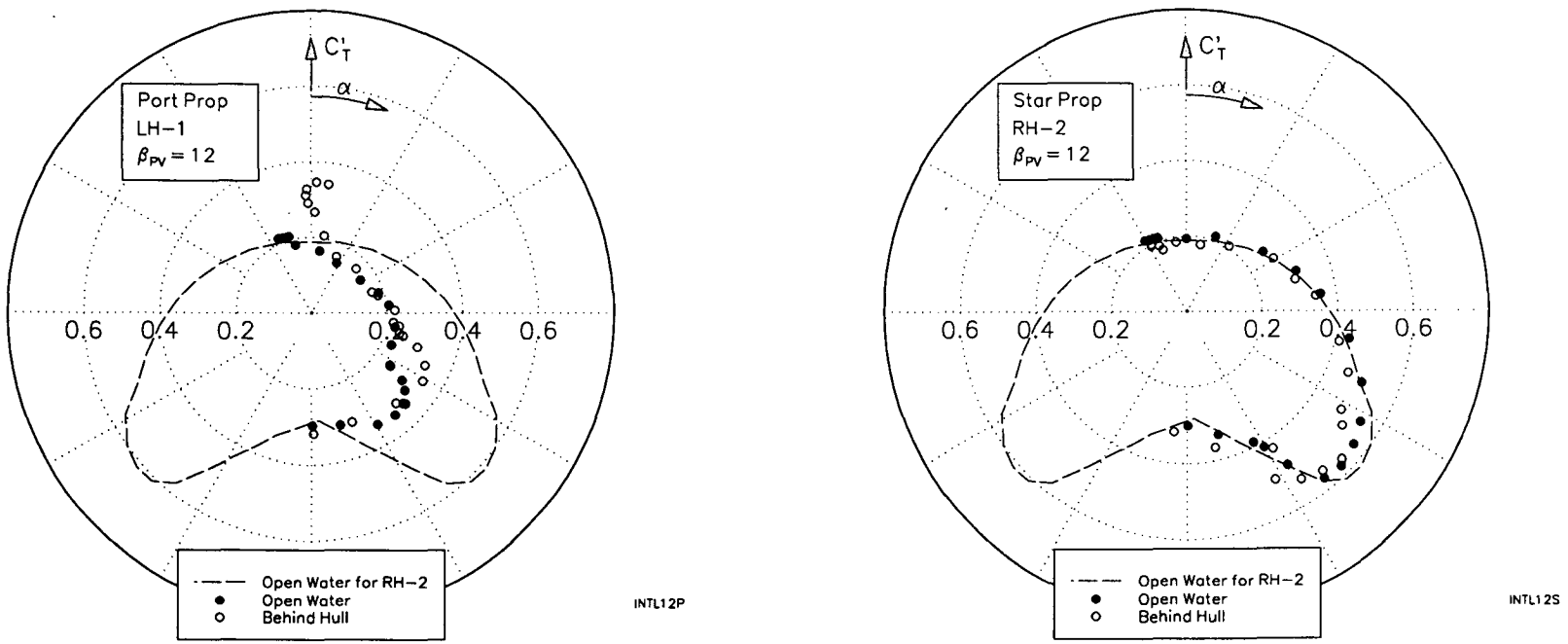

(d) $\beta_{PV} = 12°$

Figure 6.19 Comparison of Open Water Characteristics for One and Two Thrusters with Behind Hull Characteristics for Two Thrusters, for Operation in the Pulling Mode

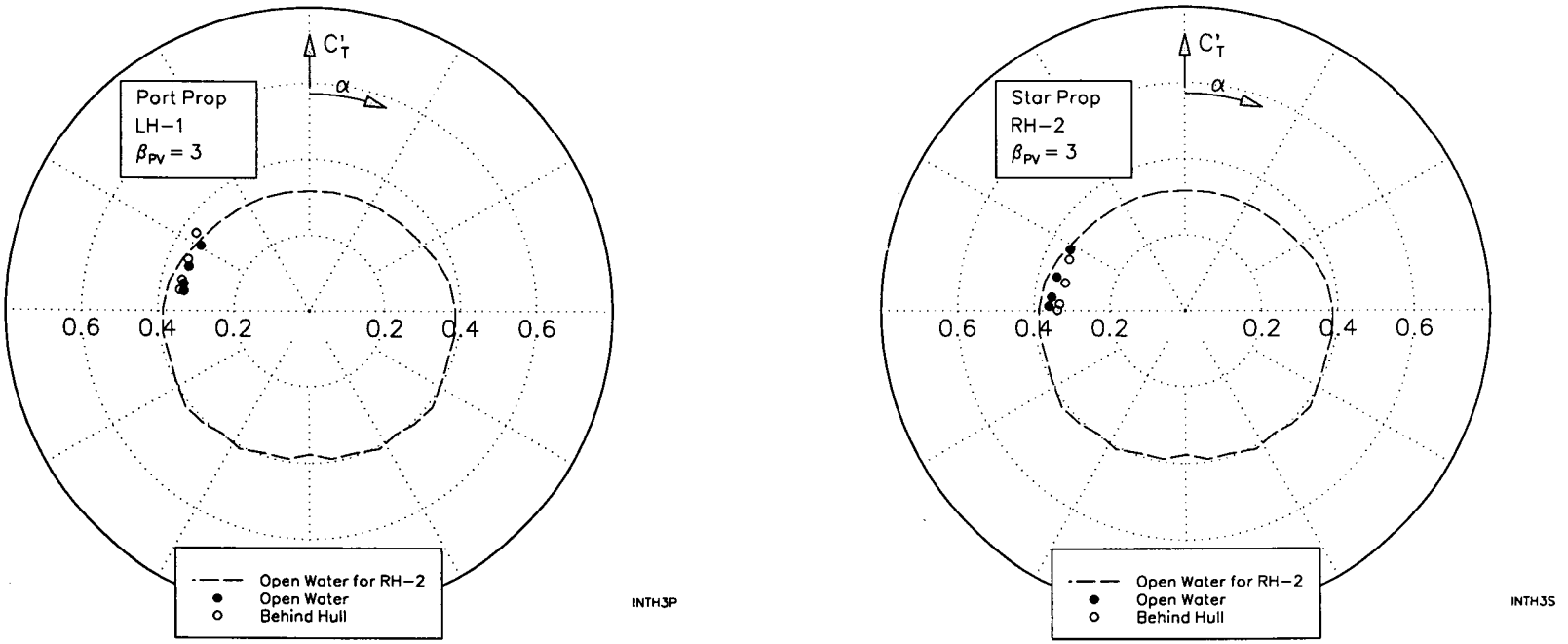

(a) $\beta_{PV} = 3°$

Figure 6.20 Comparison of Open Water Characteristics for One and Two Thrusters with Behind Hull Characteristics for Two Thrusters, for Operation in the Pushing Mode

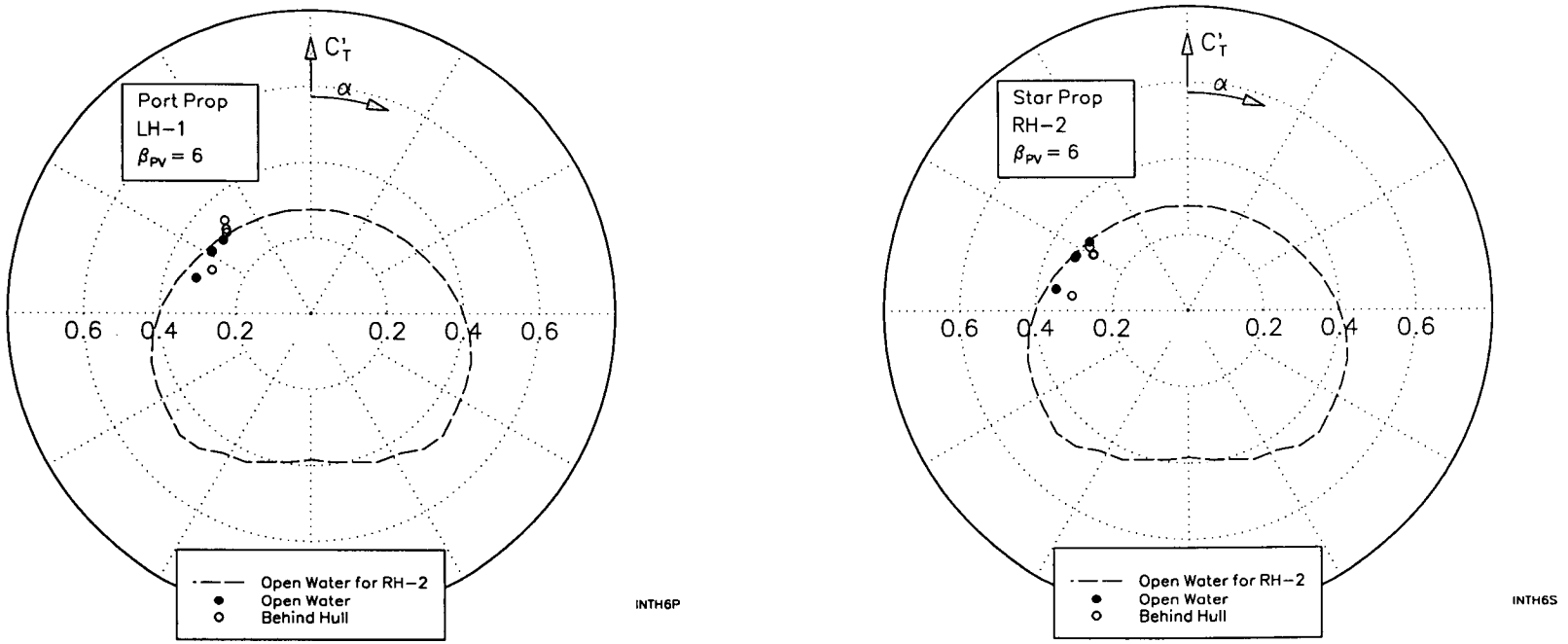

(b) $\beta_{PV} = 6°$

Figure 6.20 Comparison of Open Water Characteristics for One and Two Thrusters with Behind Hull Characteristics for Two Thrusters, for Operation in the Pushing Mode

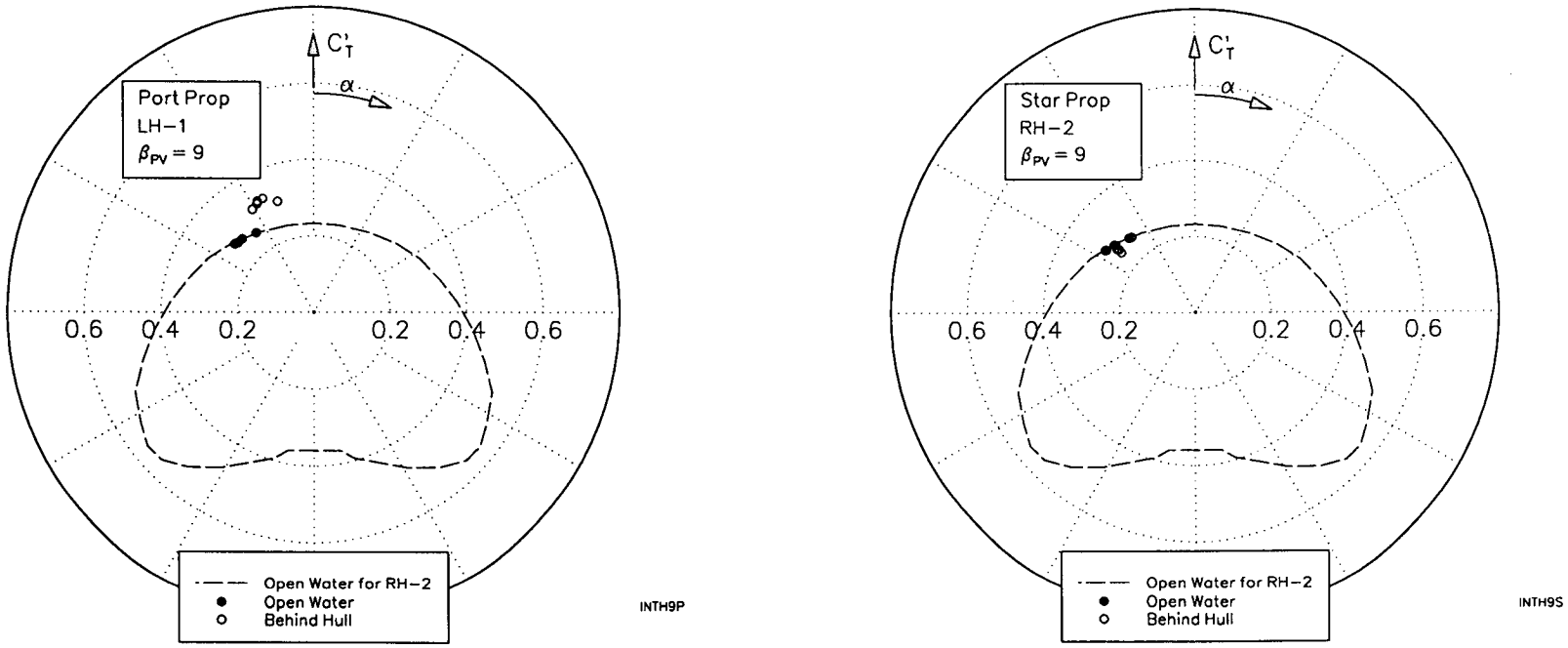

(c) $\beta_{PV} = 9°$

Figure 6.20 Comparison of Open Water Characteristics for One and Two Thrusters with Behind Hull Characteristics for Two Thrusters, for Operation in the Pushing Mode

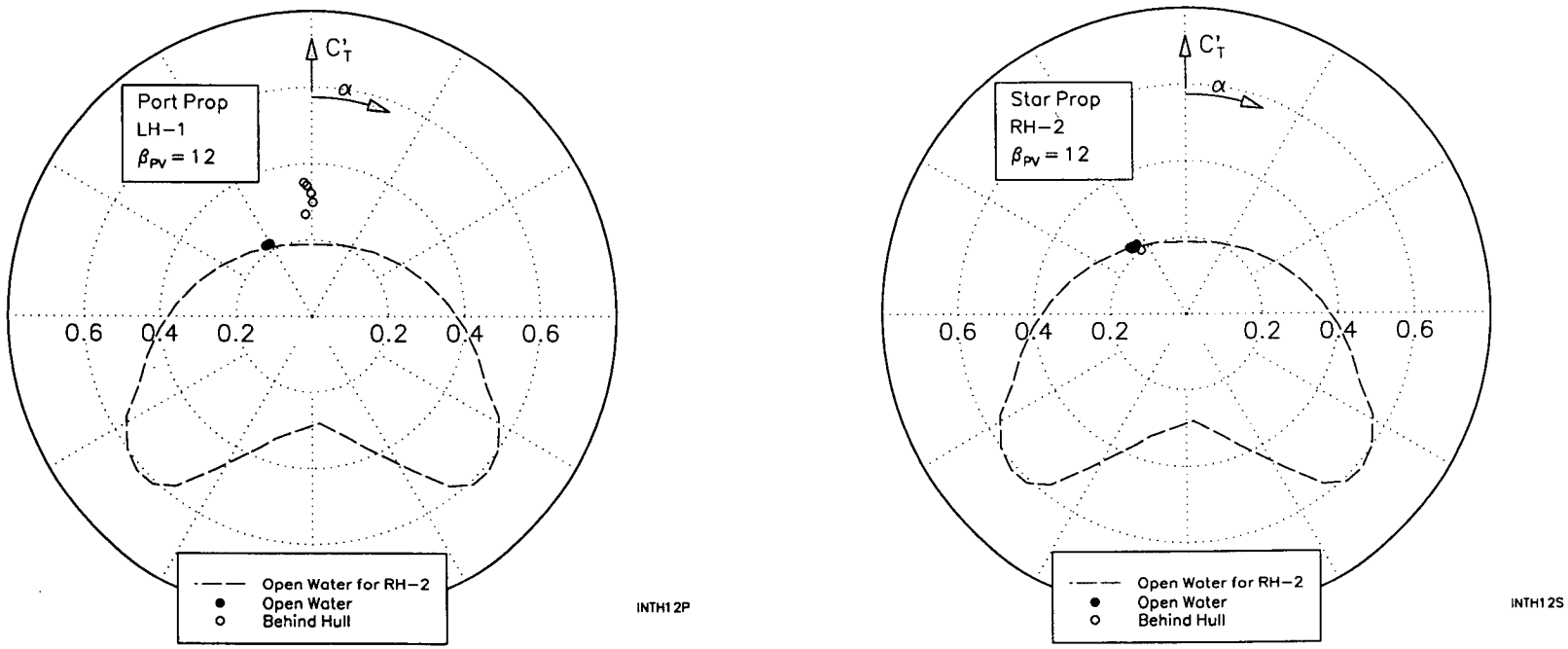

(d) $\beta_{PV} = 12°$

Figure 6.20 Comparison of Open Water Characteristics for One and Two Thrusters with Behind Hull Characteristics for Two Thrusters, for Operation in the Pushing Mode

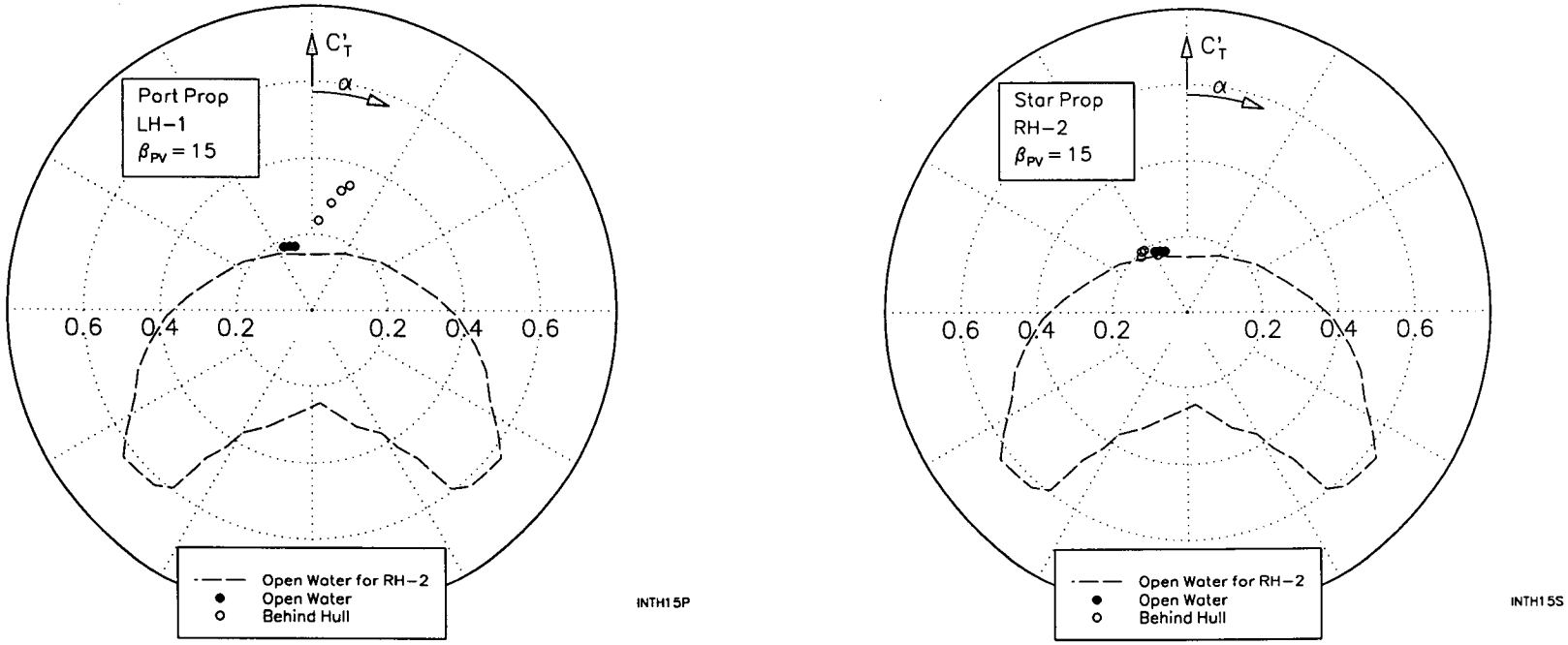

(e) $\beta_{PV} = 15°$

Figure 6.20 Comparison of Open Water Characteristics for One and Two Thrusters with Behind Hull Characteristics for Two Thrusters, for Operation in the Pushing Mode

6.3.3 Evaluation of Hull Wake and Flow Rectification

As explained above, the results for operation in both pulling and pushing modes show that the influence of the hull on the thrusters is confined to the first quadrant where thruster-thruster interaction is small. From the measured thruster forces in the behind hull condition, the effective flow for each thruster can be determined using the thrust identity technique introduced in Chapter 5. This involves comparison of behind hull forces with those from a single thruster in open water, enabling the effective angle of attack and advance angle to be determined. Details of this method are given in Appendix D.

Ship manoeuvring models generally use empirical factors to determine the influence of surge, sway and yaw motions on the effective longitudinal and transverse velocities at the rudder and propeller. In the case of the longitudinal velocity, this is calculated using a wake factor (as used in ship resistance and propulsion studies) which may be defined in the usual way:

$$u_A = (1-w)u \tag{6.4}$$

Applying this equation to the tug at each thruster location then u_A is the effective advance velocity in the longitudinal direction, w the wake fraction and u the surge velocity. For transverse velocities, flow straightening or flow rectification factors are used which are applied to the transverse velocities due to sway and yaw motions. Numerous methods of applying such factors have been presented, depending on the application and desired precision. A single flow rectification factor may be applied to the transverse velocity at the desired location, as suggested by e.g. Oltman and Sharma, 1984:

$$v_A = (v + x_T r)k_{HR} \tag{6.5}$$

Applying this equation to the tug at each thruster location then v_A is the effective advance velocity in the transverse direction, v is the sway velocity, r the rate of turn, x_T the distance to thrusters from midships and k_{HR} the flow rectification factor. Other methods have been suggested where a factor is applied to each of the sway and yaw terms, e.g. by Norrbin, 1971 and Ankudinov et al., 1993. Various modifications to equations 6.4 and 6.5 have also been suggested to account for changes in the factors with extended variation of the drift or yaw rate angle, e.g. by Ogawa and Kasai, 1978 and Kose, 1982. For the present investigation, the variation of interaction factors with the drift angle is of particular interest, due to the tug's frequent operation at large drift angles. Furthermore, equilibirium only is considered, as discussed in Chapter 2 therefore, no experiments involving a yaw rate have been performed. Tugs may operate at high yaw rate angles; however, during ship assist operations, such motions are small and for the purposes of time domain solution it may be assumed that the influence of yaw rate can be included with sway as per equation 6.5.

Effective angles of attack and advance angles have been calculated using the thrust identity technique mentioned above. These are presented in Figures 6.21 and 6.22 as effective longitudinal and transverse velocities for each thruster as a function of the drift angle. The longitudinal and transverse velocities have been non-dimensionalised using the free stream velocity as follows, for the port thruster:

$$u'_{Ap} = \frac{u_{Ap}}{V} = \frac{u_{Ap}}{\sqrt{u^2 + v^2}}$$
$$v'_{Ap} = \frac{v_{Ap}}{V} = \frac{v_{Ap}}{\sqrt{u^2 + v^2}} \qquad (6.6)$$

and an analagous equations may also be defined for the starboard thruster.

The data points plotted correspond to all measurements made in the first quadrant, including pulling in the indirect mode, pushing with parallel thrusters and pushing with non-parallel thrusters.

It can be seen from the results that there is considerable scatter of the data points, particularly toward the higher drift angles. At the higher drift angles, advance angles are low and thruster forces vary very little with angle of attack, making the thrust identity method less precise. It can also be shown that the thrust identity method may be imprecise at higher angles of attack, as mentioned in Appendix D. However, by similar reasoning it can be shown that thruster forces for angles of attack less than 90° are relatively insensitive to changes in the advance angle and angle of attack. For operation in the first quadrant, thruster angles of attack are less than 90°.

Despite the scatter in the results, overall trends can be seen and it has been assumed that the variation of the velocities with drift angle can be approximated with linear functions. Comparison of the results for pushing with parallel and non-parallel thrusters shows that the interaction effect is relatively insensitive to the thruster angles. Hence, it may be assumed that interactions are a function of the drift angle only. Linear functions have been chosen as follows for port and starboard longitudinal and transverse velocities:

$$u'_{Ap} = \eta'_{up}\beta_H + (1-w) \qquad (6.7)$$
$$v'_{Ap} = \eta'_{vp}\beta_H \qquad (6.8)$$
$$u'_{As} = \eta'_{us}\beta_H + (1-w) \qquad (6.9)$$
$$v'_{As} = \eta'_{vs}\beta_H \qquad (6.10)$$

In the case of longitudinal velocities, equations 6.7 and 6.9 return the wake factor at zero drift angle, as defined by equation 6.4. Bussemaker, 1987, quoted a value of w = 0.3 for vessels with pram sterns similar to those used for stern drive tugs. In the case of transverse velocities it is assumed that these are zero for zero drift angle. Using these constants, least square fits have been made and the derived coefficients corresponding to equations 6.7 to 6.10 are given in Table 6.4.

η_{up}	η_{vp}	η_{us}	η_{vs}
0.302	–0.085	–0.137	–0.945

Table 6.4 Coefficients for the influence of the Hull on Thrusters from Thrust Identity

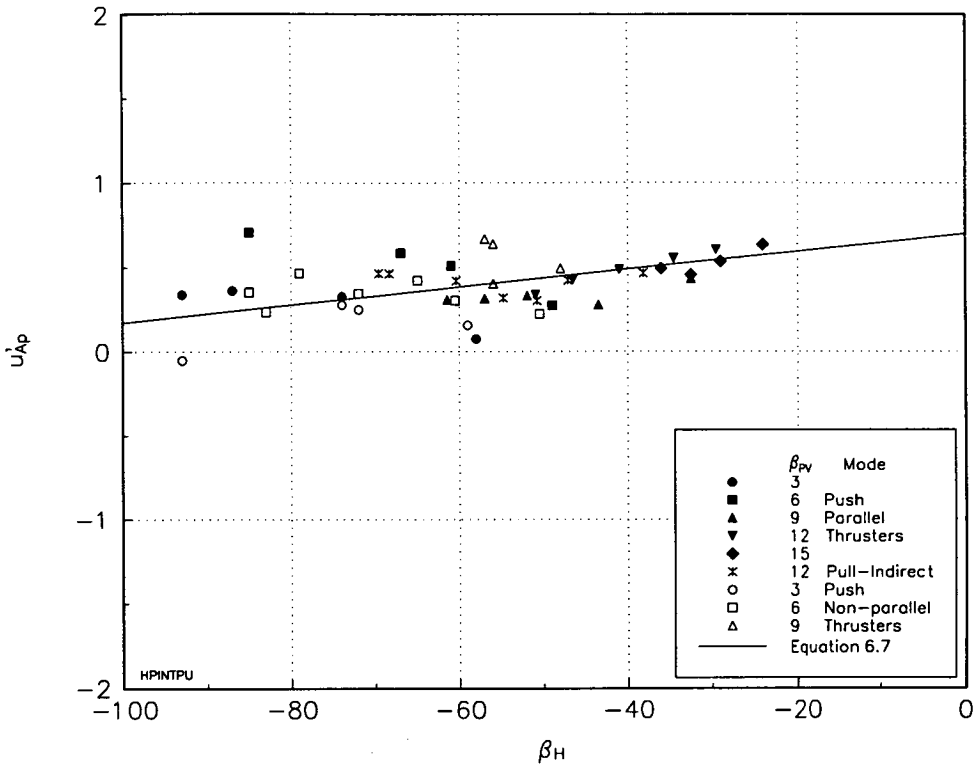

(a) Longitudinal Velocity

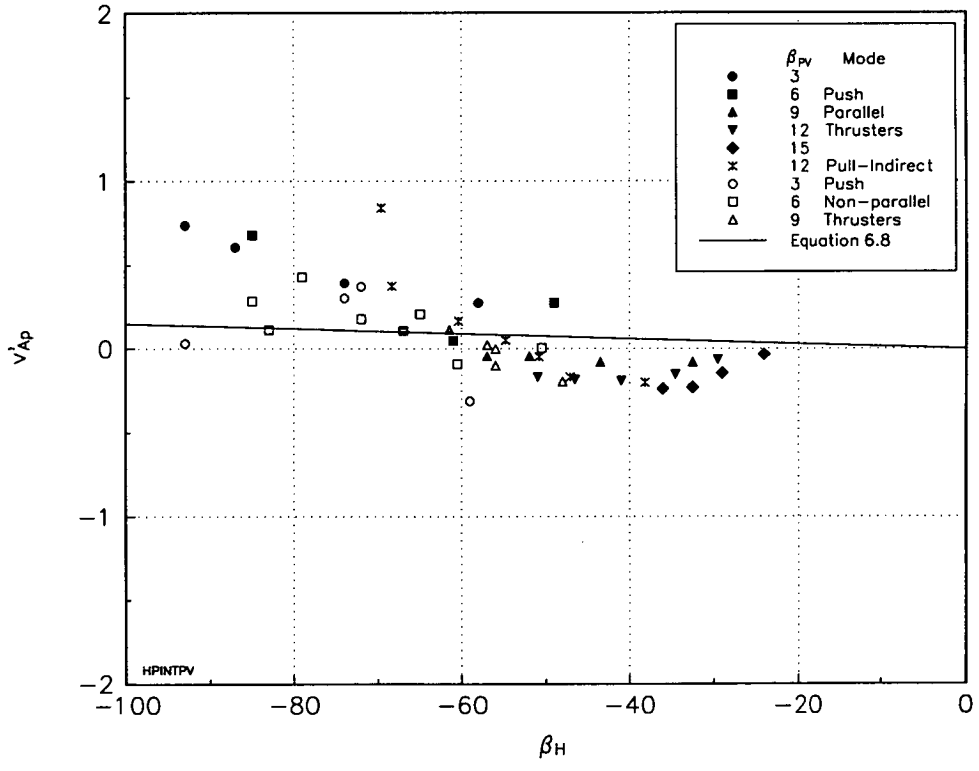

(b) Transverse Velocity

Figure 6.21 Effective Longitudinal and Transverse Velocities for Port Thruster from Thrust Identity

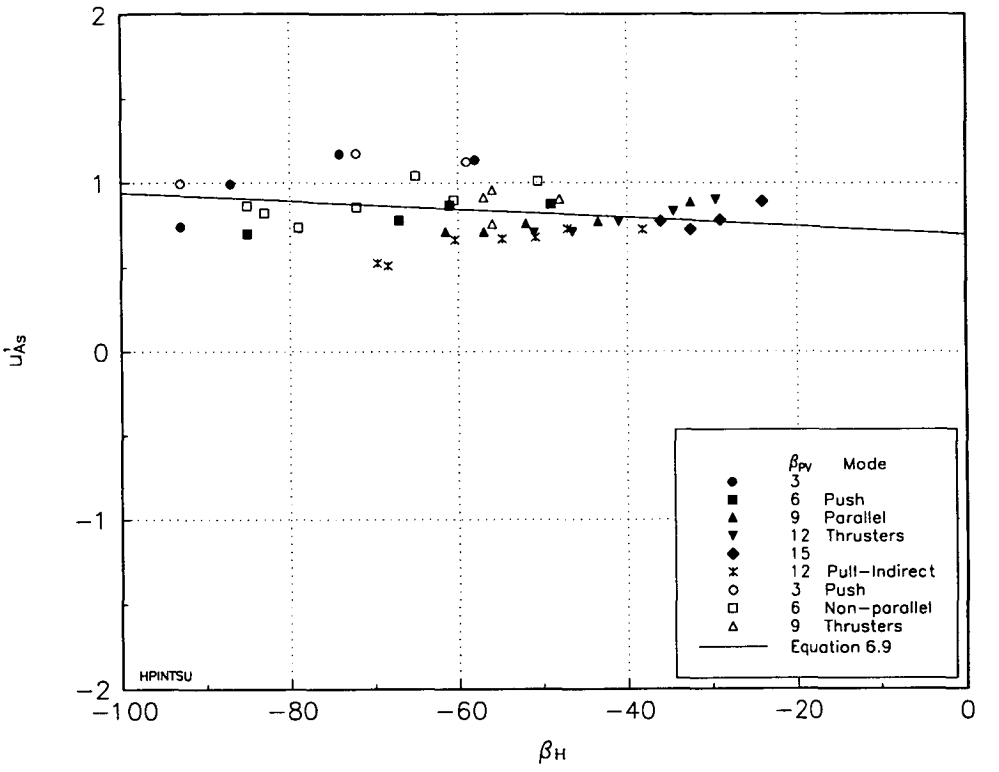

(a) Longitudinal Velocity

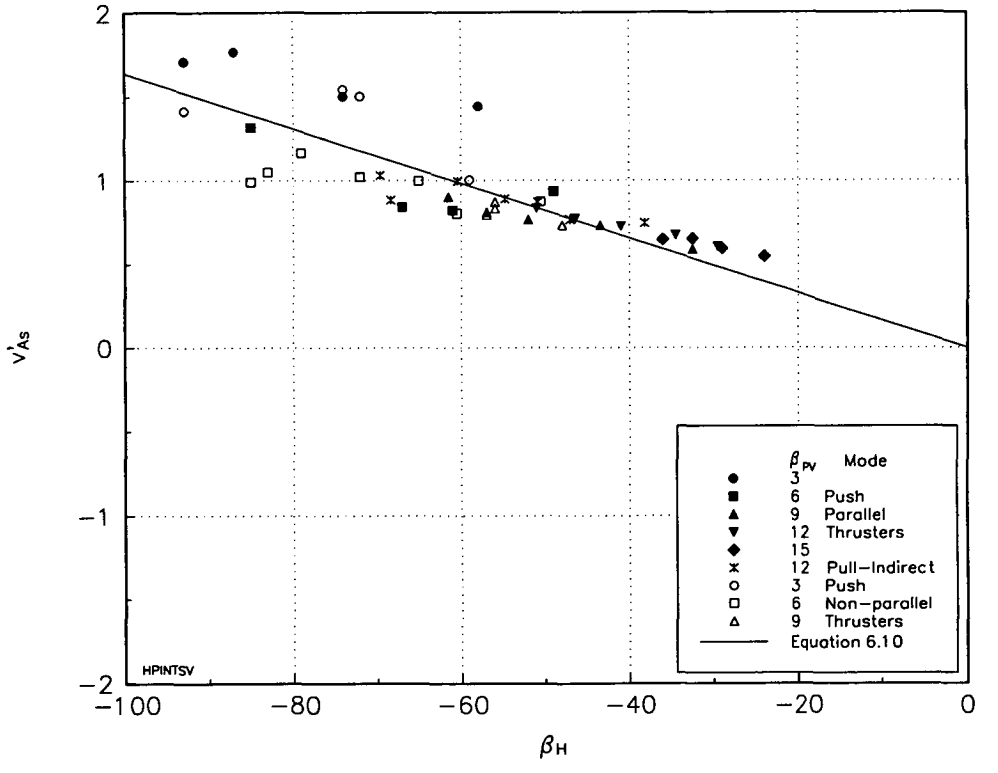

(b) Transverse Velocity

Figure 6.22 Effective Longitudinal and Transverse Velocities for Starboard Thruster from Thrust Identity

For the starboard thruster which is exposed to the free stream, the assumption of a linear approximation appears reasonable. The port thruster, which operates in the lee of the hull and the starboard thruster, is subject to more complicated interaction effects. This can be seen from Figure 6.21(b), where the transverse flow reverses direction at small drift angles. It is difficult to interpret the results for the port thruster as it is probable that they are influenced by scale effects due to low hull Reynolds Numbers. In Chapter 3 it was mentioned that hull force measurements are unstable, due to scale effects for hull Froude Numbers below 0.11 which corresponds to an apparent advance angle of 6°. The linear approximation, as shown in Figure 6.21(b), appears unfavourable, particularly as it does not account for the reversal of flow direction. However, this approximation may be justified on the basis of the insensitivity to operating conditions mentioned above and that thruster forces are not as critical at high advance angles, as discussed in Section 6.2.

6.4 Influence of Thrusters on Hull

Forces acting on the hull of the tug during the free running experiments can be calculated from the measured thruster and resultant tug forces using equilibrium. These forces can be compared with those measured during constrained bare hull experiments and the influence of the thrusters on the hull determined. Results from the constrained bare hull experiments are presented in Chapter 3.

The bare and appended hull forces are compared separately for operation in the pulling and pushing modes. The forces have been non-dimensionalised using the same system as that used to present the tug force results in Section 6.2. Applying this to the measured surge force, sway force and yaw moment respectively, Equation 6.3 may be extended as follows:

$$X_H^* = \frac{X_H}{\tfrac{1}{2}\rho A_O (0.7\pi D_O)^2 \left(n_p^2 + n_s^2\right) C'_{X,\beta_P=0}} \tag{6.11}$$

$$Y_H^* = \frac{Y_H}{\tfrac{1}{2}\rho A_O (0.7\pi D_O)^2 \left(n_p^2 + n_s^2\right) C'_{X,\beta_P=0}} \tag{6.12}$$

$$N_H^* = \frac{N_H}{\tfrac{1}{2}\rho A_O L (0.7\pi D_O)^2 \left(n_p^2 + n_s^2\right) C'_{X,\beta_P=0}} \tag{6.13}$$

where,

$$C'_{X,\beta_P=0} = 0.363$$

The * superscript has been used for these hull force and moment coefficients to denote that they are non-dimensionalised differently to those used to represent bare hull forces presented in Chapter 3.

In Chapter 3 it was shown that bare hull force coefficients are essentially independent of the Froude Number hence, forces may be calculated from non-dimensionalised results corresponding to a typical Froude Number. A value of $F_n = 0.18$ was chosen as typical. From this result, bare hull forces have been calculated for each velocity corresponding to the apparent advance angles tested in the free running experiments.

6.4.1 Influence of the Thrusters on Hull in the Pulling Mode

Forces acting on the bare and appended hull are presented in Figures 6.23, 6.24, 6.25 and 6.26 for apparent advance angles of 3, 6, 9 and 12°. The results shown in Figures

6.23, 6.24 and 6.25 are for pulling in the direct mode only, whereas those in Figure 6.26 are for pulling in both the direct and indirect modes. In the case of the astern bollard pull bare hull forces are obviously zero, whereas surge forces acting on the appended hull are non-zero, due to propeller race impingement. As explained in Section 6.2.3 for the astern bollard pull the surge force acting on the appended hull, $X_H^* = 0.064$.

As described in Section 6.1, combinations of drift angle and thruster angle may be separated into quadrants compatible with the nature of interaction expected. Pulling in the direct mode corresponds to the second quadrant where thruster-hull interaction is expected to be dominated by the influence of the thrusters on the hull. It can be seen from the results that there are significant differences between the forces acting on the bare and appended hull, due to the influence of the thrusters. Of particular interest is the variation of differences in surge forces with advance angle, particularly at small drift angles. From Figure 6.23, for 3° apparent advance angle it can be seen that the difference in surge forces at small drift angles is positive, as at bollard pull. However, as can be seen from Figures 6.24 to 6.26, with increasing advance angle the difference in forces becomes increasingly negative. At 12° advance angle and zero drift angle the surge force has increased by almost an order of magnitude compared with the bare hull result, as shown in Figure 6.26. This effect can be explained from consideration of what occurs to the propeller race when the thrusters are operating in negative flow conditions, particularly when the angle of attack is close to 180° where also the drift angle is close to 0°. When operating astern the propeller race is projected ahead into the free stream and, depending on the advance angle may, or may not, extend beyond the tug's length. At low advance angles the race extends beyond the tug and a positive surge force acts on the hull, as if moving astern. With increasing advance angle the race is reversed in increasingly shorter distances and presents an obstruction to the free stream adjacent to the tug hull. The proximity of such an obstruction is presumably responsible for the increase in surge force acting on the hull due to so called *interference drag*, as described, eg by Hoerner, 1965. At non-zero drift angles, thruster angles of attack are less than 180° and the propeller race is projected obliquely into the free stream reducing the interference effect, as can be seen from Figures 6.25 and 6.26.

Sway forces and yaw moments acting on the appended hull are essentially zero at zero drift angle due to symmetry for thruster angles at 180°. With decreasing thruster angle and hence, increasing drift angle, the race from the starboard thruster impinges obliquely on the tug's afterbody and skeg, creating negative sway forces and hence, positive yaw moments. For the port thruster the race is directed away from the hull, however, negative pressures may be created on the port side of the tug's afterbody that enhance the forces and moments produced from the starboard thruster. These effects are particularly dramatic at low advance angles where the race velocity is large, as can be seen from Figures 6.23 and 6.24. The discontinuity that can be seen in both the sway force and yaw moment plots are possibly due to the variation of forces from the race impinging on the afterbody or skeg. The interaction reduces at higher advance angles, particularly for the sway force, as can be seen from Figures 6.23 and 6.26. This can be attributed to a number of factors. With increasing advance angle the race velocity becomes smaller, reducing the interaction effect. This combined with smaller thruster angles allows the race to be more easily deflected away from the hull by the free stream. Further, thruster-thruster interaction reduces the effectiveness of the port thruster which, in turn, may reduce the influence

of this thruster on the hull. It can also be seen from Figures 6.25 and 6.26 that the sway force is not only reduced, but may be less than the bare hull value indicating favourable interaction. This may be due to the so called *coanda effect* where the race is deflected by the tug's bilge, particularly since it occurs at small drift angles where thruster angles are close to 180°. The yaw moments being less than the bare hull values also support this suggestion, since the centre of pressure of a coanda effect in this situation would be forward.

From Figure 6.26 it can be seen that as the thruster angles are reduced, the drift angle increases up to approximately 70° and then reduces, where the tug begins to pull in the indirect mode. The section of the graph where drift angles increase from 0 to approximately 70°, thruster angles are greater than 90°, therefore the tug is operating in the second quadrant. From the data point at the maximum drift angle onwards, thruster angles are less than 90°, so that the tug is operating in the first quadrant, as can be seen from Figure 6.3. In the first quadrant, thruster-hull interaction is expected to be dominated by the influence of the hull on the thrusters. It can be seen from Figure 6.26 that in the section of the plot corresponding to the first quadrant, surge and sway forces are closer to the bare hull values compared with the section corresponding to the second quadrant. However, there is only marginal variation of yaw moments toward the bare hull values in this section. The differences in sway force may be regarded as negligible and although the differences in surge force represent a large change proportionately, they may be regarded as small compared with other forces.

It can be concluded from the results that for pulling in the direct mode which corresponds to the second quadrant, the influence of the thrusters on the hull is significant, particularly at low advance angles. For pulling in the indirect mode which, in this case, corresponds to the first quadrant, the influence of the thrusters on the hull is not significant in surge and sway forces, but appears to be significant in yaw moments.

6.4.2 Influence of the Thrusters on Hull in the Pushing Mode

The bare and appended hull forces are presented in Figures 6.27, 6.28, 6.29, 6.30 and 6.31 for apparent advance angles of 3, 6, 9, 12 and 15°. As with the astern bollard pull, bare hull forces for the ahead bollard pull are obviously zero. Surge forces acting on the appended hull are non-zero, due in this case, to the propeller induced flow creating a low pressure field on the tug's afterbody. As explained in Section 6.2.4, for the ahead bollard pull the surge force acting on the appended hull, $X_H^* = -0.040$.

Operation in the pushing mode corresponds to the first quadrant, where it is expected that thruster-hull interaction is dominated by the influence of the hull on the thrusters. It can be seen from the results that, in general, the bare and appended sway forces and yaw moments compare favourably. The differences in surge force represent a large change proportionately however, they may be regarded as small compared with other forces. A similar observation was also made for pulling in the indirect mode, apart from apparent differences in the yaw moments acting on the bare and appended hull. Therefore, in general, it would appear reasonable to assume that in the first quadrant the influence of the thrusters on the hull may be ignored.

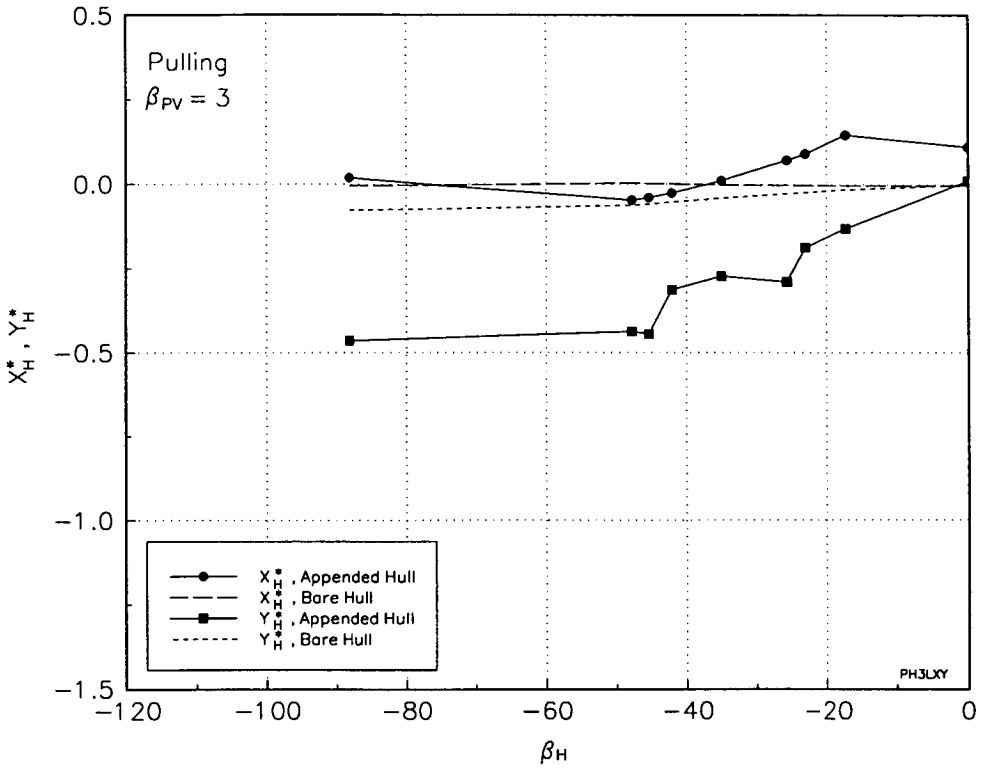

(a) Longitudinal and Transverse Forces

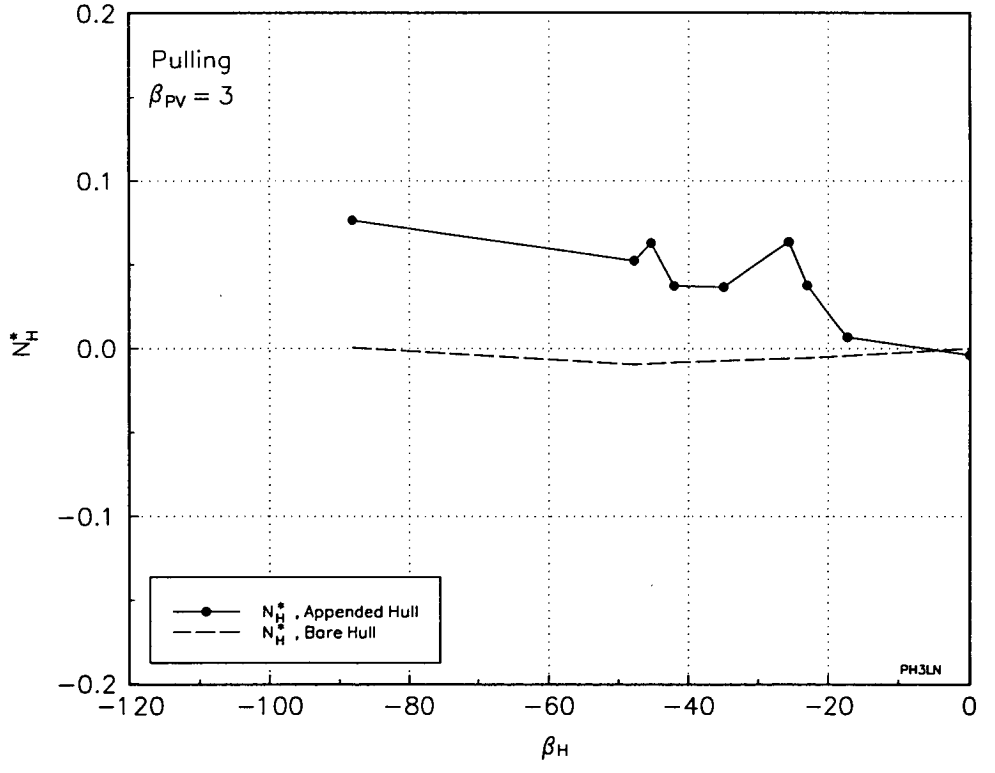

(b) Yaw Moments

Figure 6.23 Comparison of Bare and Appended Hull Forces for Pulling, $\beta_{PV} = 3°$

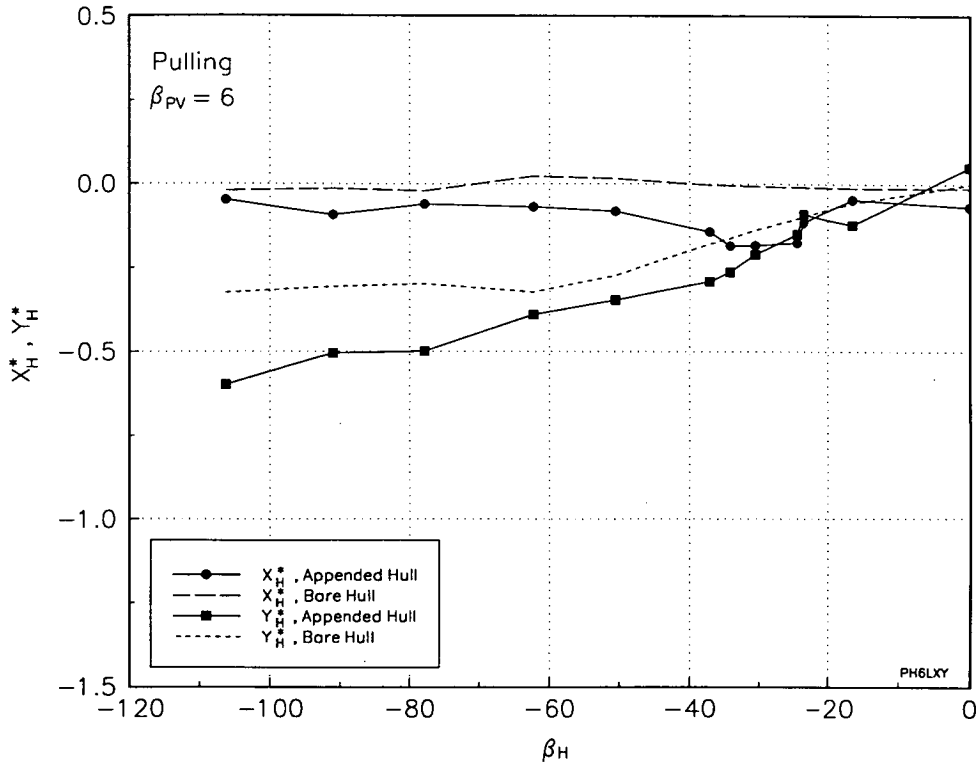

(a) Longitudinal and Transverse Forces

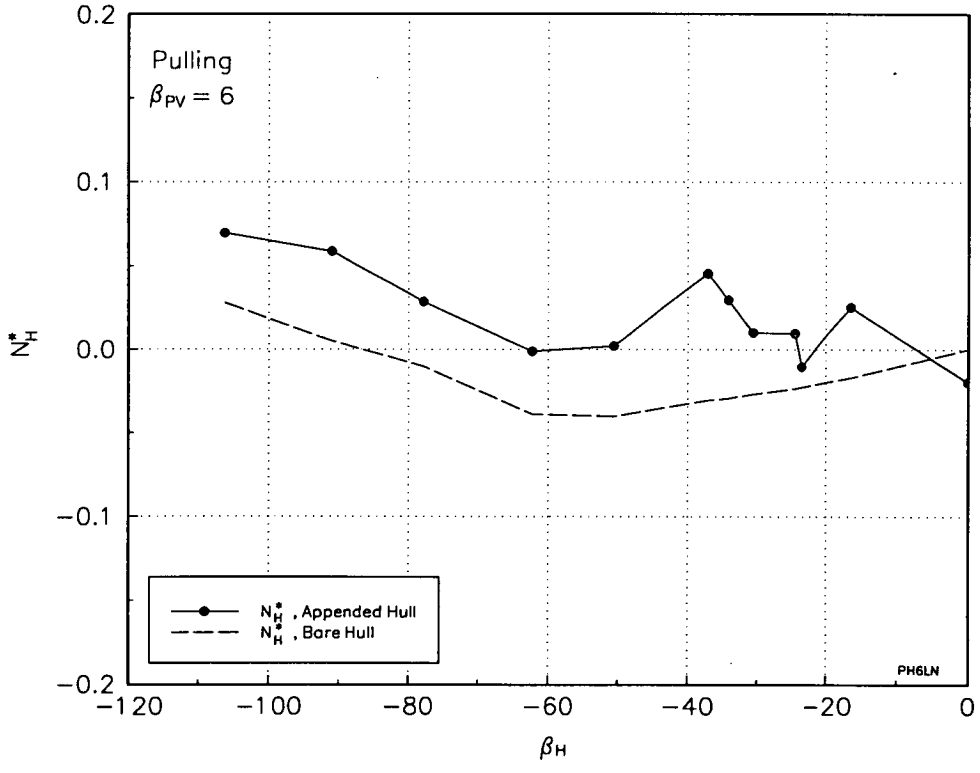

(b) Yaw Moments

Figure 6.24 Comparison of Bare and Appended Hull Forces for Pulling, $\beta_{PV} = 6°$

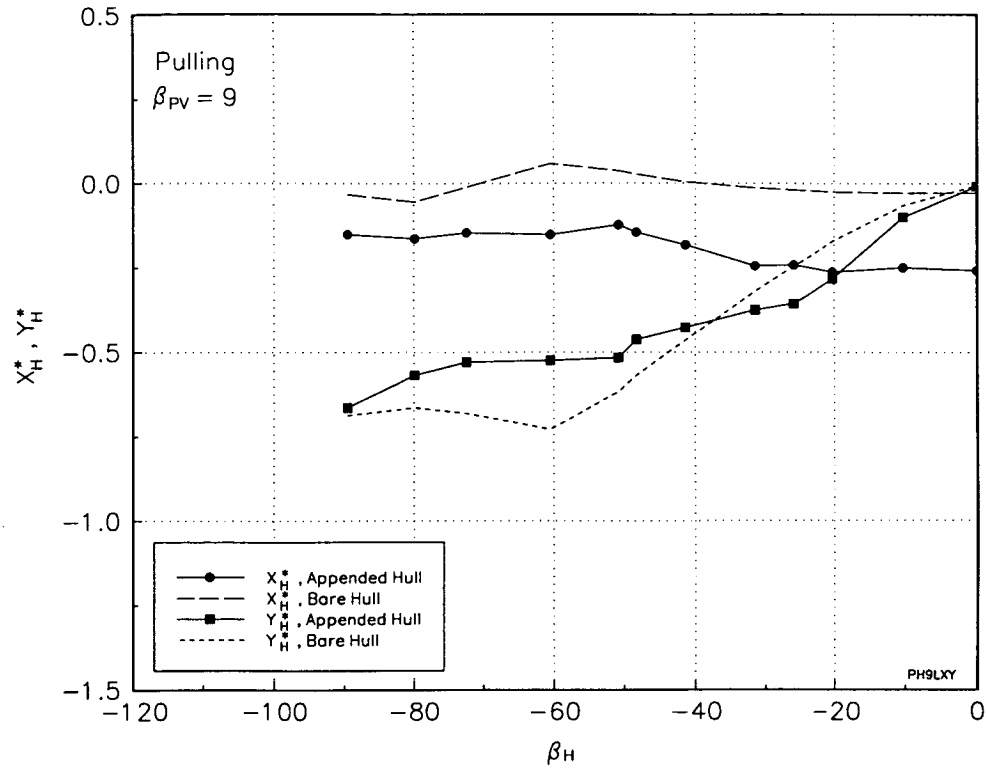

(a) Longitudinal and Transverse Forces

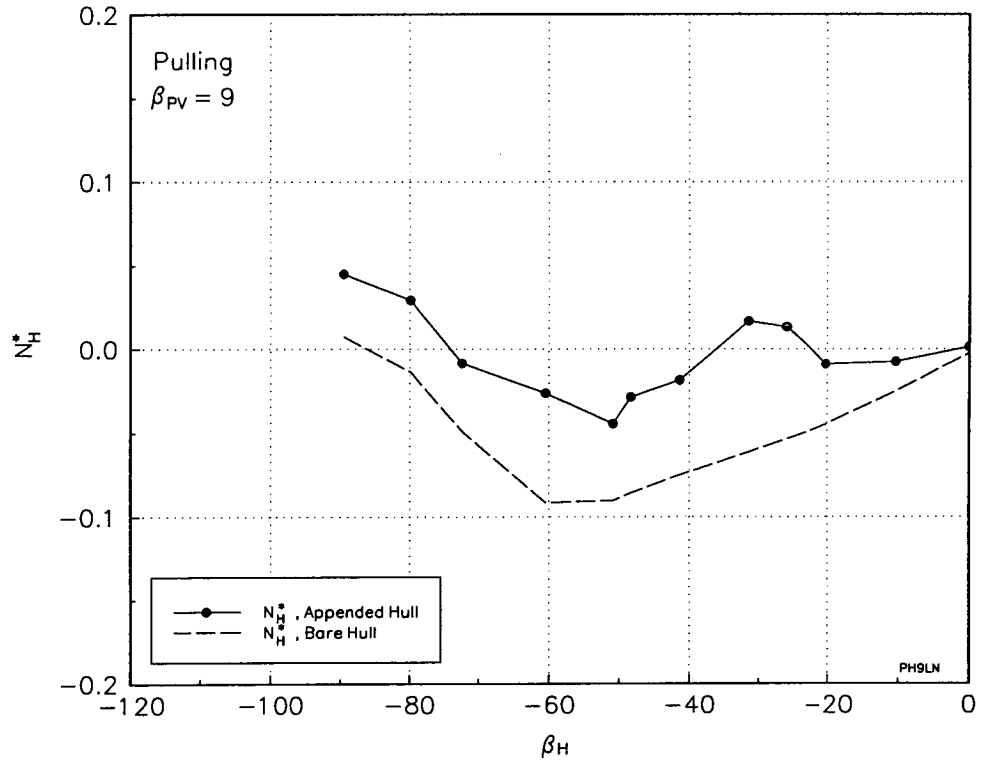

(b) Yaw Moments

Figure 6.25 Comparison of Bare and Appended Hull Forces for Pulling, $\beta_{PV} = 9°$

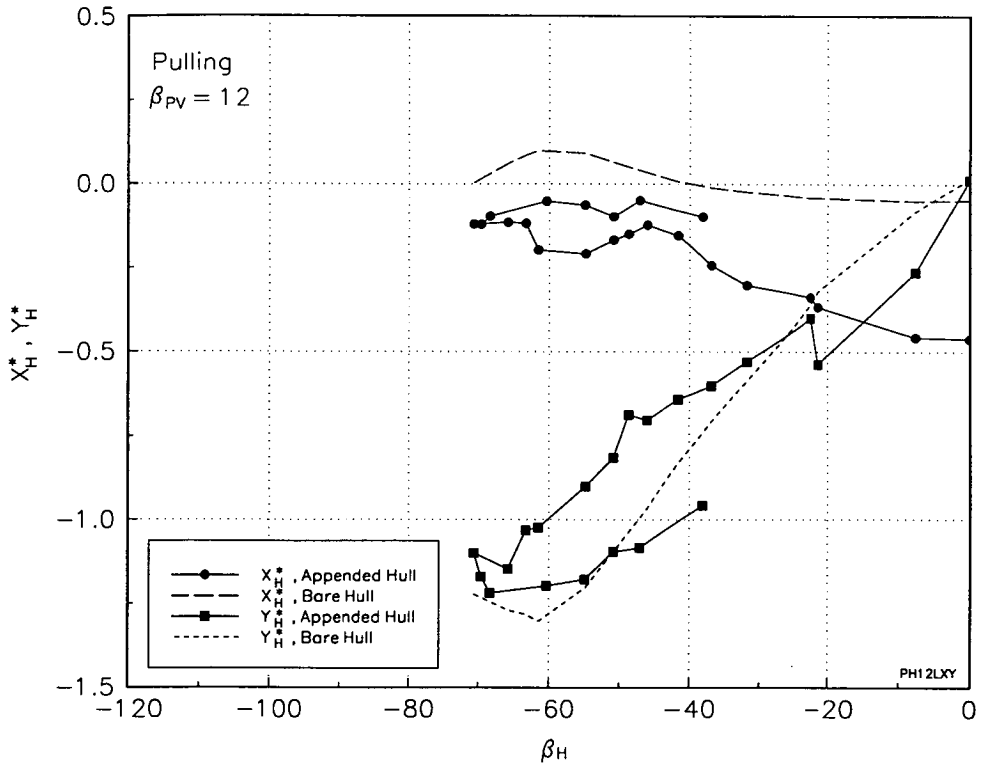

(a) Longitudinal and Transverse Forces

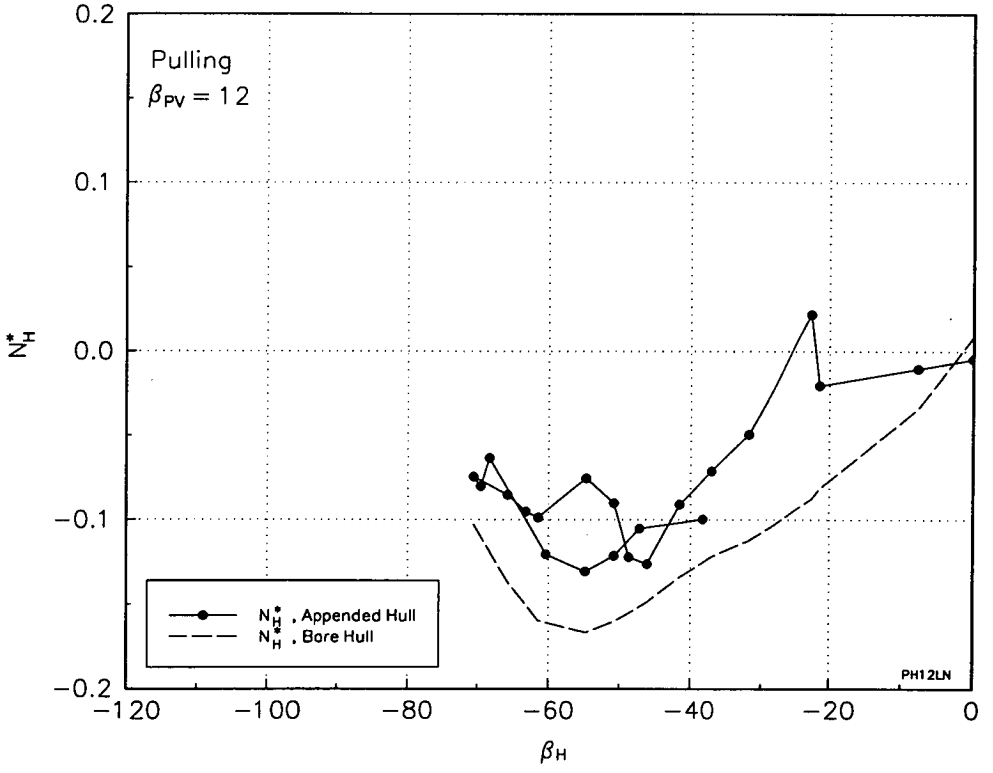

(b) Yaw Moments

Figure 6.26 Comparison of Bare and Appended Hull Forces for Pulling, $\beta_{PV} = 12°$

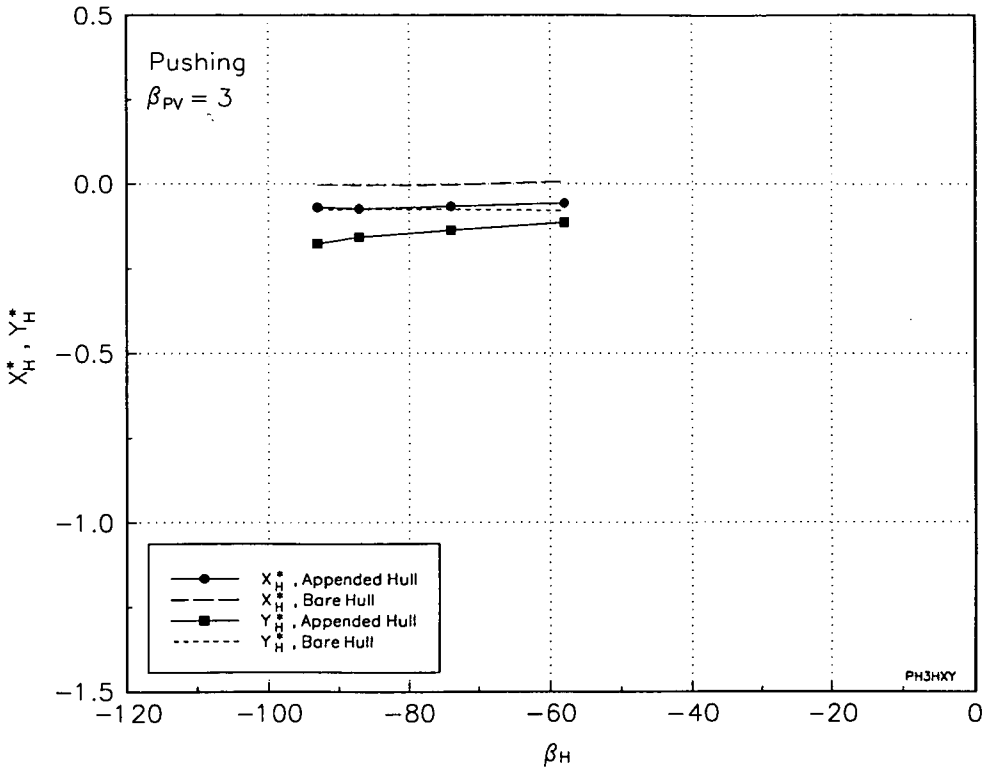

(a) Longitudinal and Transverse Forces

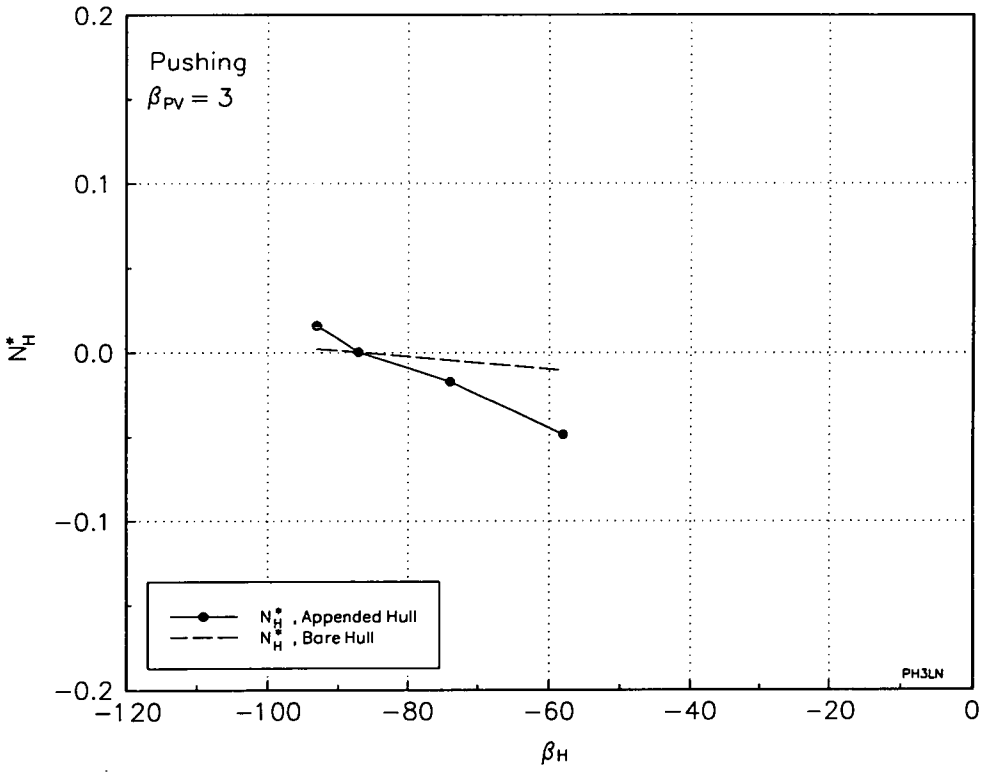

(b) Yaw Moments

Figure 6.27 Comparison of Bare and Appended Hull Forces for Pushing, $\beta_{PV} = 3°$

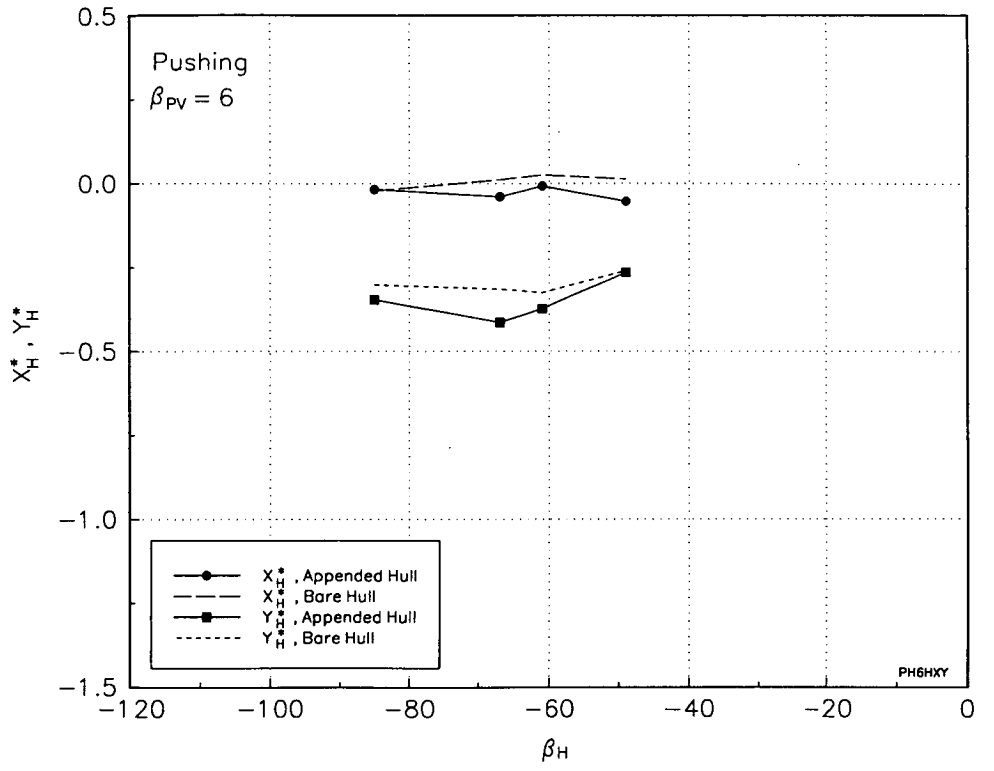

(a) Longitudinal and Transverse Forces

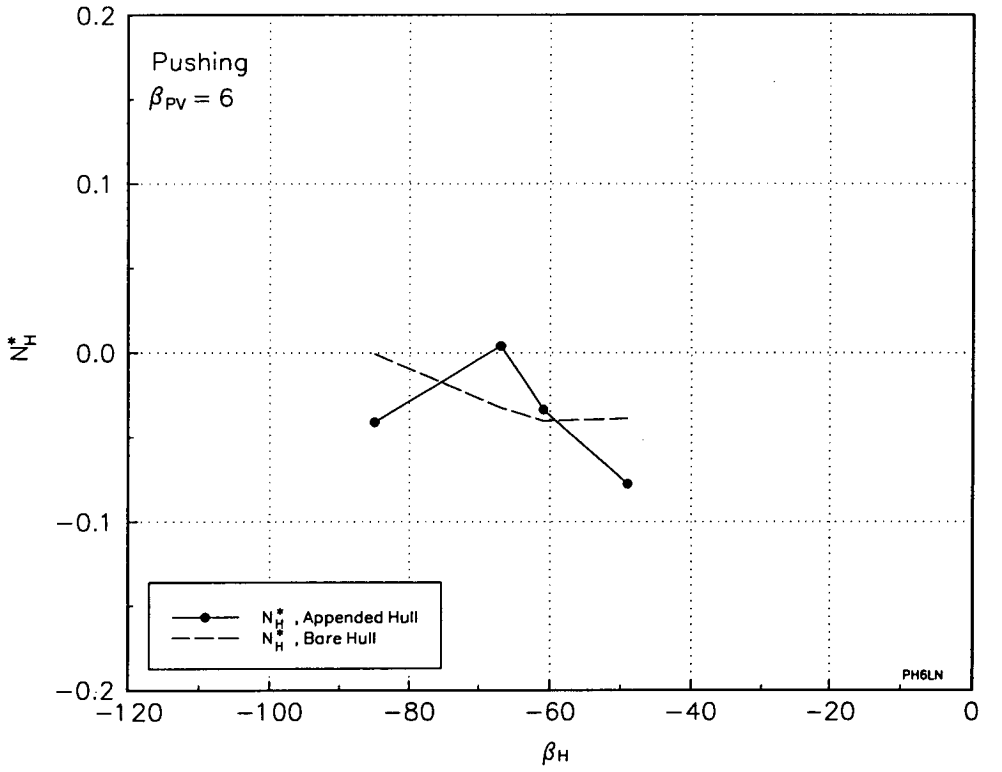

(b) Yaw Moments

Figure 6.28 Comparison of Bare and Appended Hull Forces for Pushing, $\beta_{PV} = 6°$

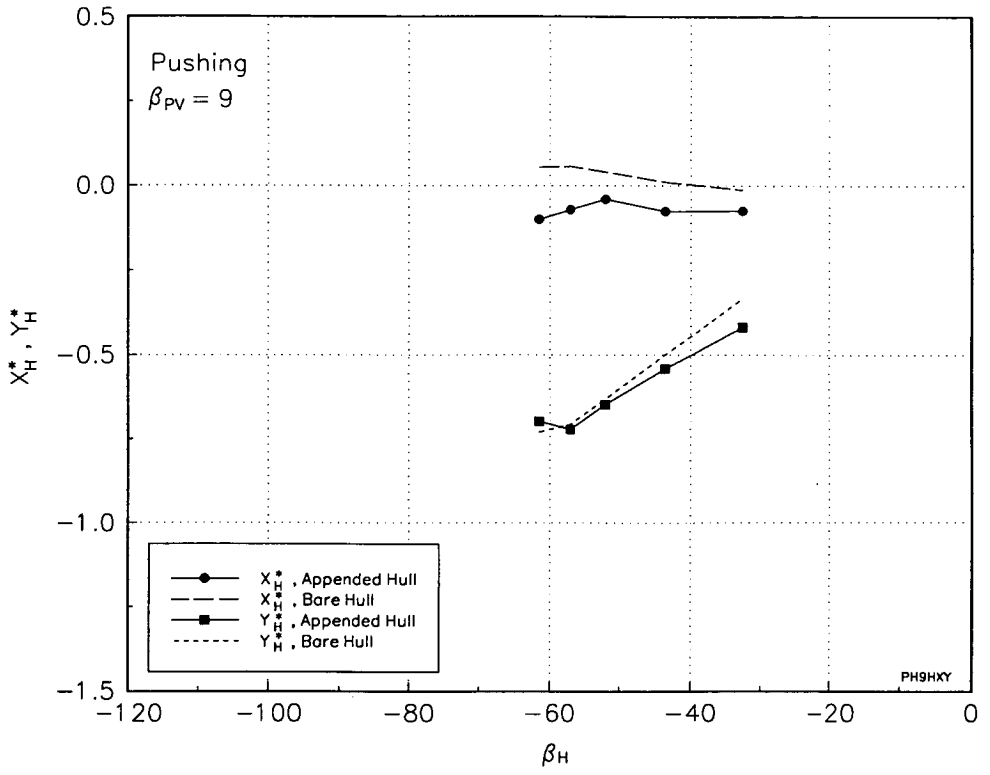

(a) Longitudinal and Transverse Forces

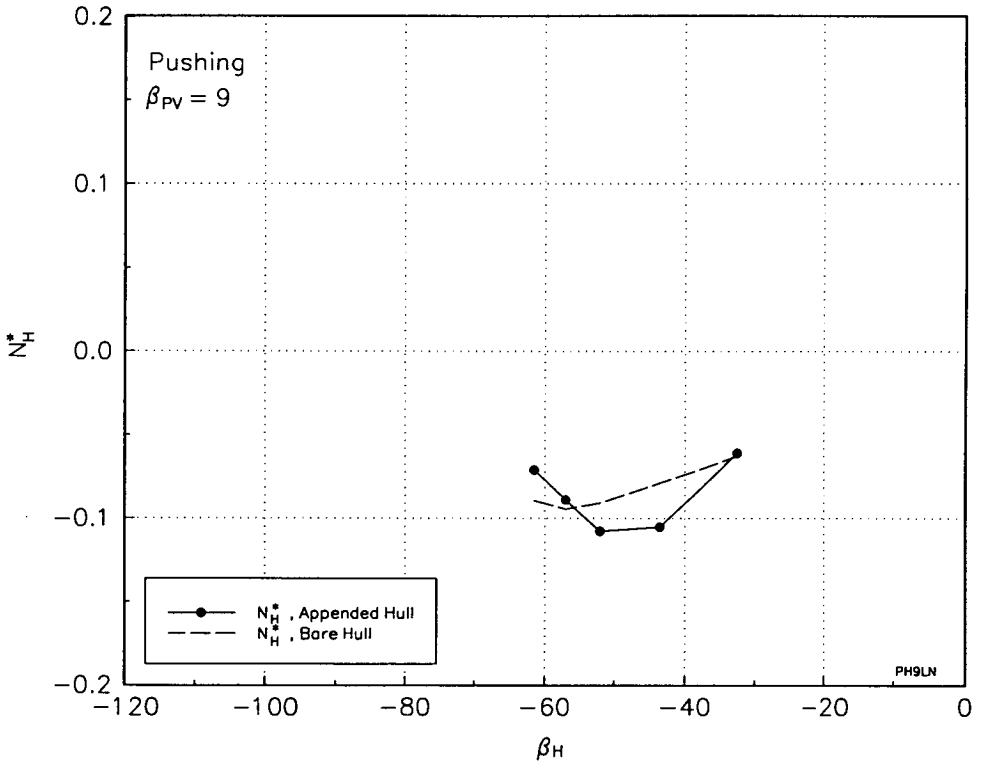

(b) Yaw Moments

Figure 6.29 Comparison of Bare and Appended Hull Forces for Pushing, $\beta_{PV} = 9°$

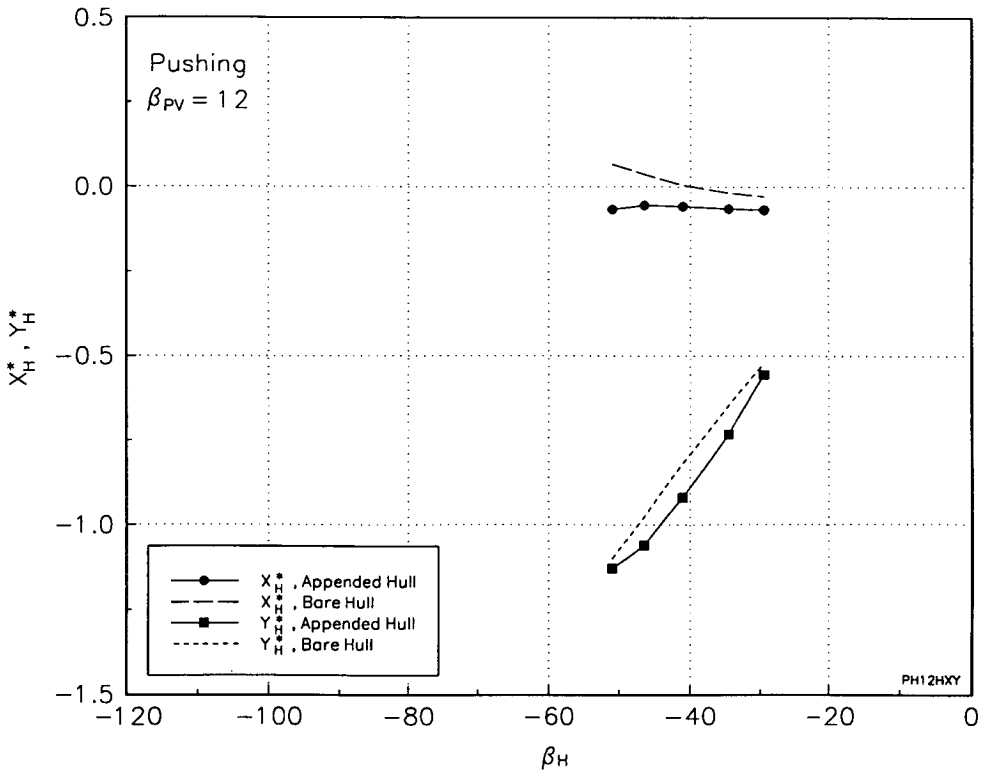

(a) Longitudinal and Transverse Forces

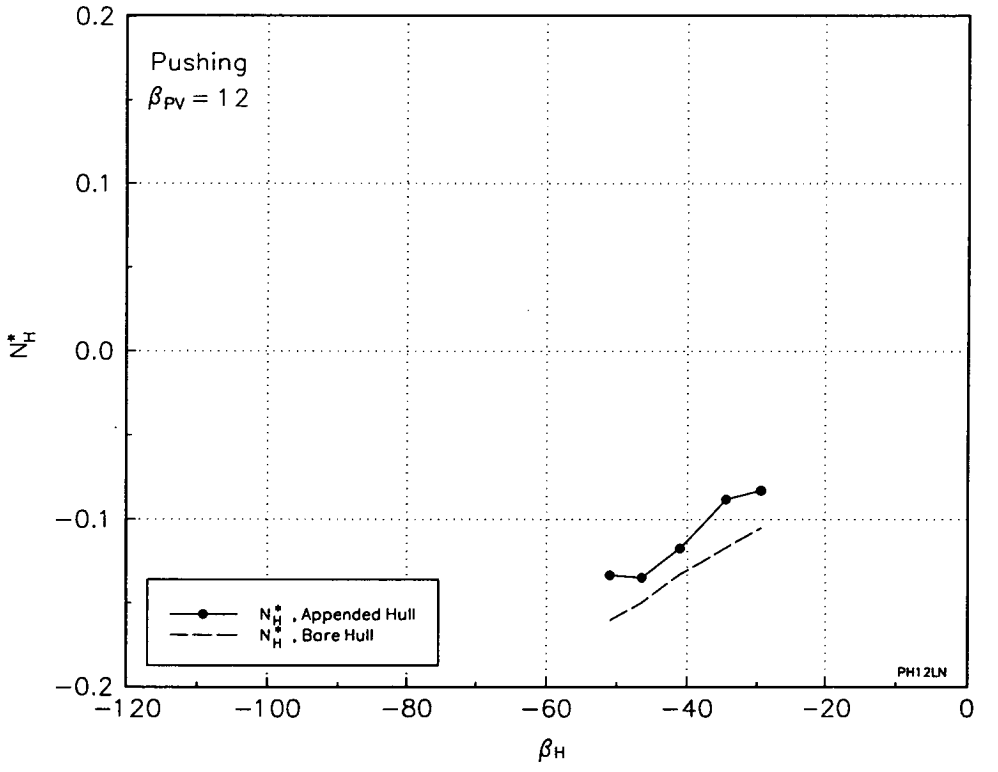

(b) Yaw Moments

Figure 6.30 Comparison of Bare and Appended Hull Forces for Pushing, β_{PV} = 12°

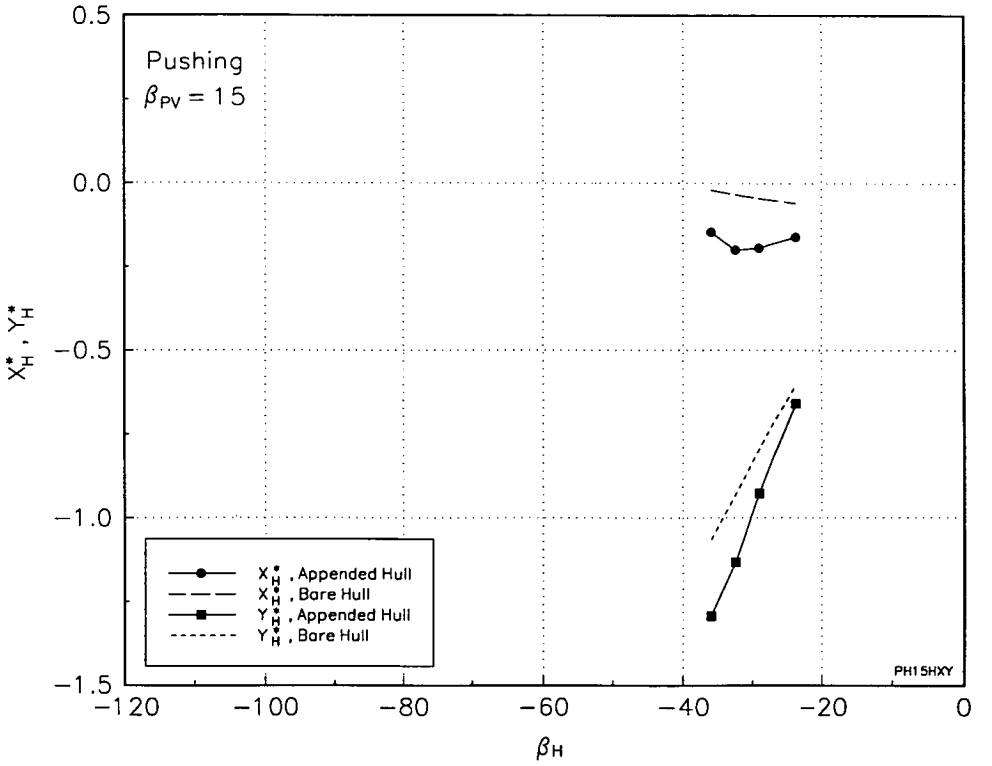

(a) Longitudinal and Transverse Forces

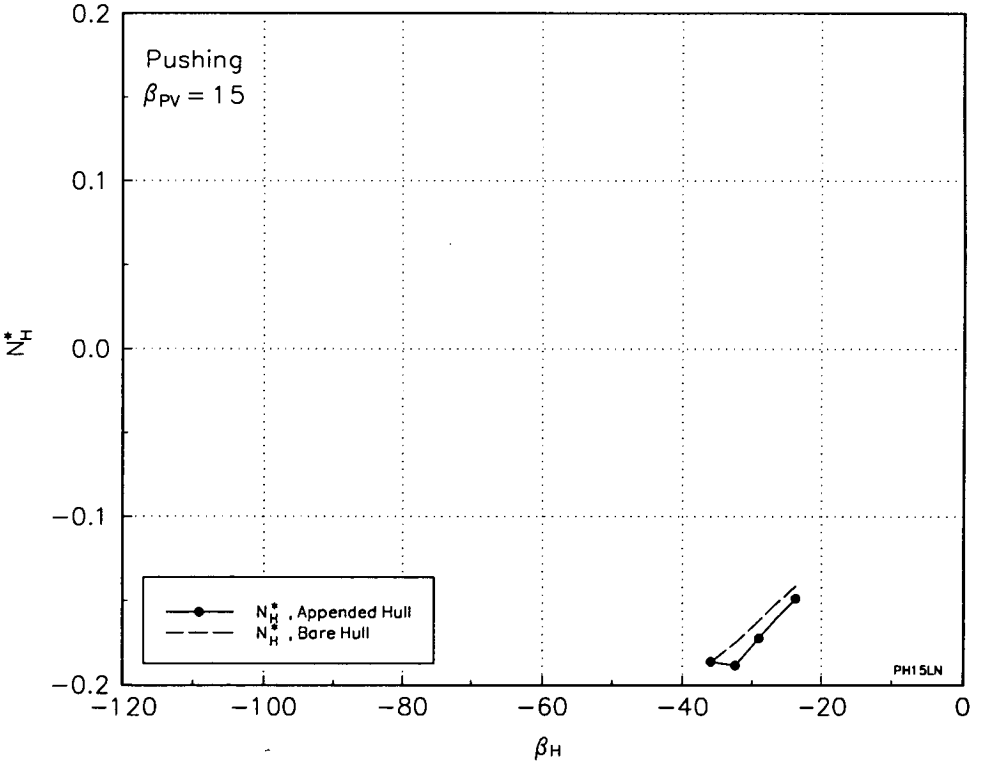

(b) Yaw Moments

Figure 6.31 Comparison of Bare and Appended Hull Forces for Pushing, β_{PV} = 15°

6.4.3 Evaluation of Thrust Deduction

The results for operation in both pulling and pushing modes show that the influence of the thrusters on the hull is confined essentially to the second quadrant. To examine this in more detail, the differences between the appended and bare hull forces are considered, from which a method for the representation of the influence of thrusters on the hull is derived.

In ship resistance and propulsion studies, the influence of the propeller on the hull is generally considered as a variation of the propeller thrust, rather than a variation of resistance. The empirical factor applied to the propeller thrust to account for this interaction is known as the thrust deduction factor which may be defined in the usual way:

$$T_D = (1-t)T \tag{6.14}$$

where, T is the propeller thrust, t the thrust deduction fraction and T_D the modified thrust to account for resistance augmentation. Conventional ship manoeuvring models generally use this approach and assume that t is independent of sway and yaw motions, Kose, 1982. The thrust deduction factor is known to vary considerably with propeller loading and quadrant of operation, Harvald, 1967 and Oltman and Sharma, 1984. Investigations into the variation of thrust deduction with propeller loading have also been carried out by Adachi and Sugai, 1978. Numerous methods are suggested to account for these effects, e.g. Oltman and Sharma simply used discrete values of t for ahead and astern motion. To account for the dependence of t on propeller loading for manoeuvring studies, Ishiguro et al., 1988, applied results from the investigations by Adachi and Sugai, 1978.

The influence of manoeuvring devices such as azimuthing or tunnel thrusters on the hull is considerably more complex than that for conventional propulsion. Simulations for vessels fitted with such devices often require model experiments to determine interactions affecting the hull. Experimental data is then used directly in the simulation or empirical relations derived, as described, eg by Nienhuis, 1986(1) for dynamically positioned offshore structures. In these situations it is often more convenient to consider the influence of the thrusters on the hull as indeed a force acting on the hull, rather than a pseudo variation in propulsor thrust.

In the previous sections forces acting on both the appended and bare hull were presented. The difference of these is the forces acting on the hull due to interaction, ie:

$$\begin{aligned} X^*_{HT} &= X^*_{H,appended} - X^*_{H,bare} \\ Y^*_{HT} &= Y^*_{H,appended} - Y^*_{H,bare} \\ N^*_{HT} &= N^*_{H,appended} - N^*_{H,bare} \end{aligned} \tag{6.15}$$

where, X^*_{HT}, Y^*_{HT} and N^*_{HT} are the surge force, sway force and yaw moment respectively, acting on the hull due to the influence of the thrusters. These forces and moments are a function of the thruster angle and apparent advance angle. The forces and moments for operation in both pushing and pulling modes are presented in Figures 6.32, 6.33 and 6.34, as a function of the thruster angle, with the advance angle as a parameter. From these results, the differences in interaction forces

between the first and second quadrants can be seen, showing that, in general, significant interactions are limited to the second quadrant. There is considerable variation in the data, some of which may be attributable to scatter. This may, in part, be a result of the data being derived from two separate experiments, one in which the forces were measured directly and another where they were not. However, trends are discernible, particularly in the surge and sway plots and it has been assumed that the variation of forces can be approximated with linear functions in the thruster angle and advance angle. For the sway force and yaw moment only the second quadrant is considered, however, for completeness, surge forces in both first and second quadrants are considered, accounting for the differences in ahead and astern bollard pulls. Therefore, linear functions have been chosen as follows for surge forces, sway forces and yaw moments:

$$X^*_{HT} = X^*_{\beta\delta}\beta_{PV}\delta + X^*_{\delta}\delta + t \tag{6.16}$$

$$Y^*_{HT} = Y^*_{\beta\delta}\beta_{PV}(\pi - \delta) + Y^*_{\delta}(\pi - \delta) \tag{6.17}$$

$$N^*_{HT} = N^*_{\beta\delta}\beta_{PV}(\pi - \delta) + N^*_{\delta}(\pi - \delta) \tag{6.18}$$

In Equation 6.16, t is the thrust deduction as defined by Equation 6.14 for the ahead bollard pull, since the interaction forces are non-dimensionalised using twice the bollard pull of a single thruster in open water. Similarly, X^*_{δ} can be derived from the ahead and astern bollard pull thrust deductions. The remaining coefficients have been determined from least square fits and are given along with the above in Table 6.5.

$X^*_{\beta\delta}$	-0.565	$Y^*_{\beta\delta}$	5.022	$N^*_{\beta\delta}$	-0.366
X^*_{δ}	0.033	Y^*_{δ}	-0.804	N^*_{δ}	0.152
t	-0.040				

Table 6.5 Coefficients for the Influence of the Thrusters on the Hull

With reference to Figures 6.32 to 6.34, locally there are some significant discrepancies between the data and the chosen functions, however, they do conform favourably with the overall trends. By its nature, the influence of the thrusters on the hull is considerably more complex than the influence of the hull on the thrusters. For the latter, it is possible to consider interaction effects as a variation in operating conditions affecting the thrusters as a whole. The influence of the thrusters on the hull, may be the result of localised thruster induced effects, such as direct impingement/deflection of the propeller race on concave aspects of the tug hull and/or curvature of the race from the coanda effect on convex surfaces. There are also less localised effects such as the interference drag discussed above where, the influence of the free stream on the propeller race substantially increases forces acting on the hull. Independent paramenters that describe this problem include the apparent advance angle, the thruster angle, thruster characteristics and the hull geometry. The apparent advance angle and the thruster angle have a significant effect on thruster-hull interaction as can be seen from Figures 6.32 to 6.34 and have therefore been chosen for empirical representation as per equations 6.16 to 6.18. By this method thruster characteristics are indirectly accounted for, be it somewhat approximately, by using the thruster bollard pull thrust coefficient in non-dimensionalising the interaction forces. Given the nature and quantity of the measured data it is

impractical to attempt to isolate the influence of the hull geometry. However, given the similarity of thruster and afterbody configurations for particularly Australian omni-directional stern drive tugs, equations 6.16 to 6.18 should provide useful generic predictions of thruster-hull interaction for this class of vessel.

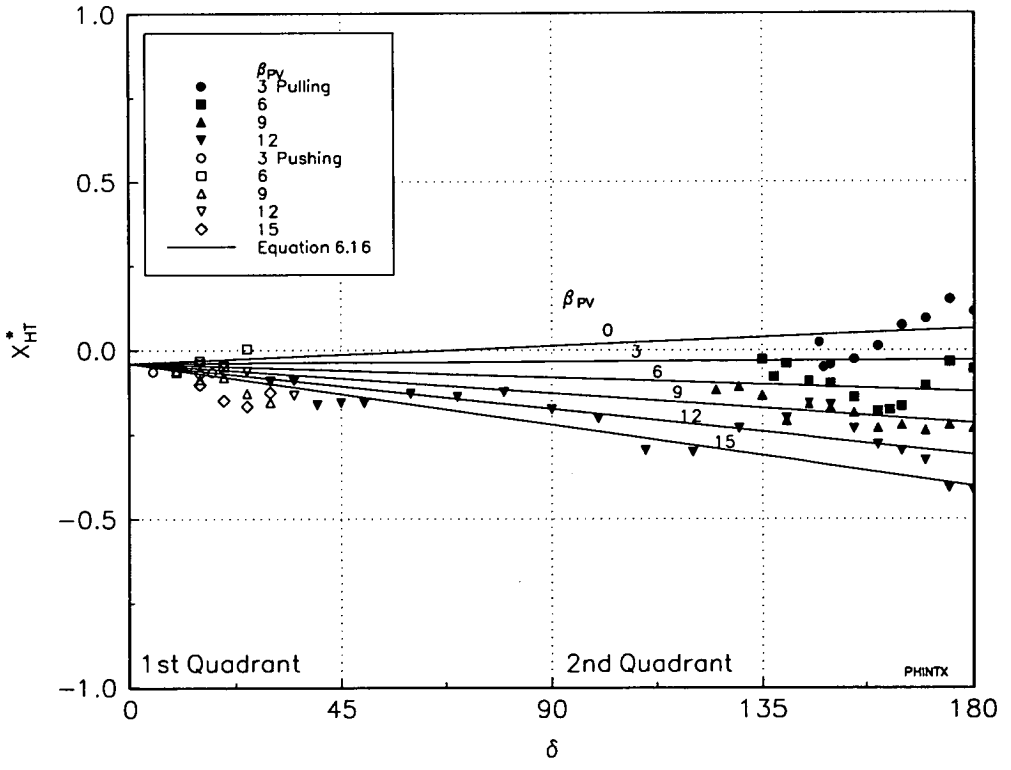

Figure 6.32 Surge Forces Acting on the Hull due to the Influence of the Thrusters

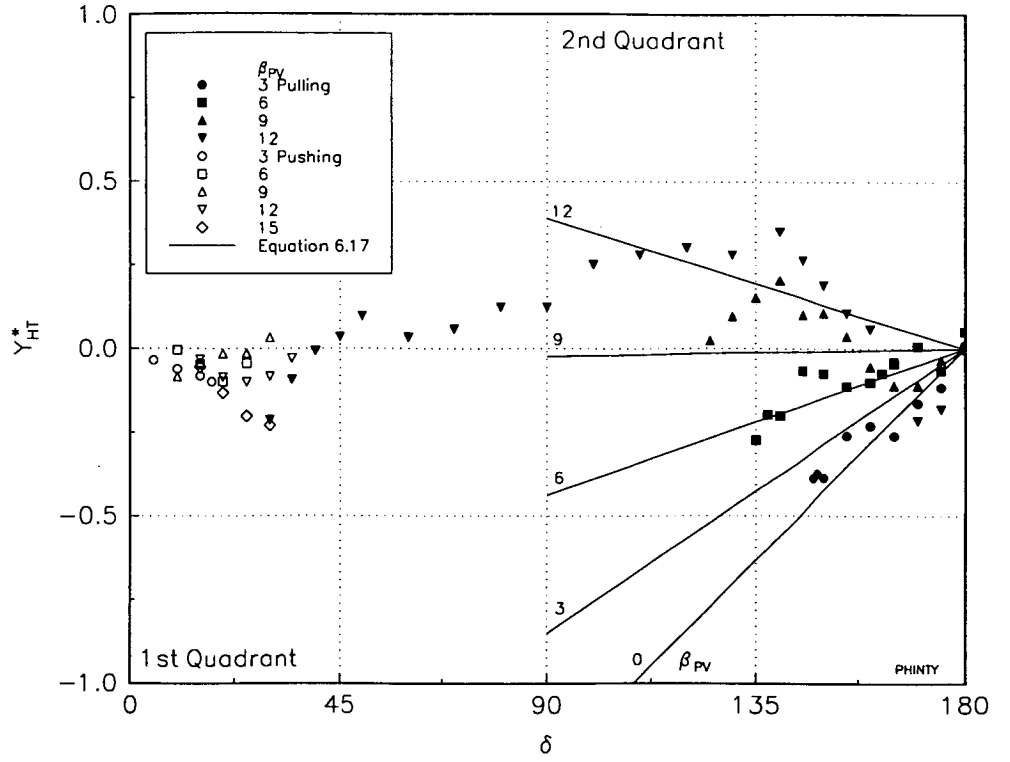

Figure 6.33 Sway Forces Acting on the Hull due to the Influence of the Thrusters

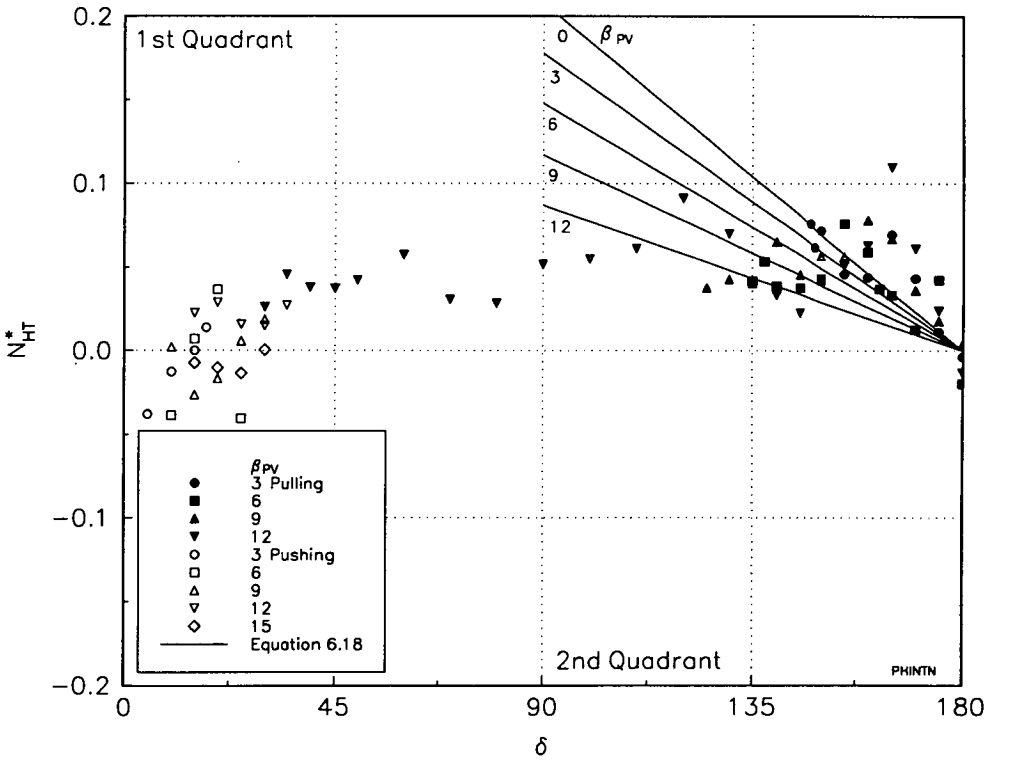

Figure 6.34 Yaw Moments Acting on the Hull due to the Influence of the Thrusters

7 MATHEMATICAL MODEL AND PREDICTIONS

Formulation of the mathematical model is discussed in Chapter 2. A schematic of the model and a summary of the formulae developed in the previous chapters is presented below. The mathematical model is then used to examine the capabilities of a typical Australian omni-directional stern drive tug in various modes of operation. This includes prediction of full scale envelopes of tug forces and stability of equilibrium.

7.1 Summary of Mathematical Model

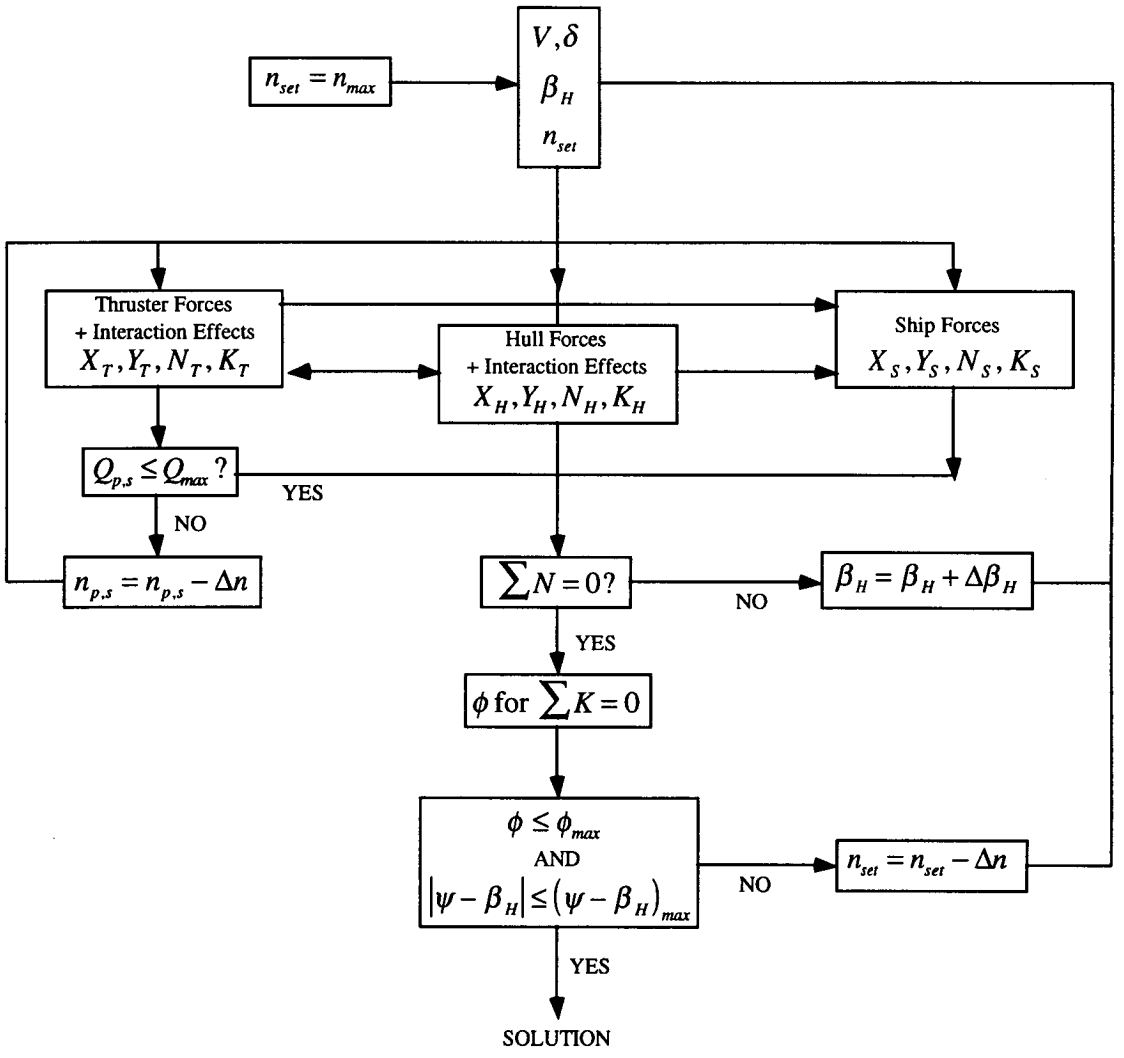

Figure 7.1 Schematic of Mathematical Model

7.1.1 Thruster Forces

Thruster forces for the leading and trailing thrusters are calculated from open water experimental results depending on the $\beta_H - \delta$ quadrant, as follows:

- 1st quadrant running ahead, thrust ahead
  $0° \geq \beta_H \geq -90°, 0° \leq \delta \leq 90°$;
- 2nd quadrant running ahead, thrust astern
  $0° \geq \beta_H \geq -90°, 90° \leq \delta \leq 180°$;
- 3rd quadrant running astern, thrust astern
  $-90° \geq \beta_H \geq -180°, 90° \leq \delta \leq 180°$; and
- 4th quadrant running astern, thrust ahead
  $-90° \geq \beta_H \geq -180°, 0° \leq \delta \leq 90°$.

Thruster forces in thruster fixed coordinates (refer Chapter 4) and the propeller torque are calculated as follows:

$$X = \tfrac{1}{2}\rho A_O\left[V_A^2 + (0.7\pi n D_O)^2\right]C'_X \tag{4.3}$$

$$Y = \tfrac{1}{2}\rho A_O\left[V_A^2 + (0.7\pi n D_O)^2\right]C'_Y \tag{4.4}$$

$$Q = \tfrac{1}{2}\rho A_O D_O\left[V_A^2 + (0.7\pi n D_O)^2\right]C'_Q \tag{4.7}$$

The coefficients $C'_X(\beta_P,\theta), C'_Y(\beta_P,\theta)$ and $C'_Q(\beta_P,\theta)$ which are functions of the advance angle and thruster angle of attack are derived from experimental results presented in Chapter 4.

1st quadrant

In this quadrant, thrusters are only affected by hull-thruster interaction. β_P and θ are calculated for each thruster from effective surge and sway velocities for each thruster location as follows:

$$\beta_P = \arctan\left(\frac{V_A}{0.7\pi n D_O}\right) \tag{4.2}$$

$$\theta = \delta + \arctan\left(\frac{v_A}{u_A}\right) \tag{6.2}$$

where,

$$V_A = \sqrt{u_A^2 + v_A^2} \tag{7.1}$$

and

$$u_A = u'_A V$$
$$v_A = v'_A V \tag{6.6}$$

where u'_A and v'_A are calculated for each thruster as follows:

leading thruster

$$u'_{Al} = \eta_{ul}|\beta_H| + (1-w) \tag{6.7}$$
$$v'_{Al} = \eta_{vl}\beta_H \tag{6.8}$$

and

trailing thruster

$$u'_{At} = \eta_{ut}|\beta_H| + (1-w) \tag{6.9}$$
$$v'_{At} = \eta_{vt}\beta_H \tag{6.10}$$

The coefficients in equations 6.7 to 6.10 are given in Table 6.4 where the starboard thruster is the leading thruster and the port thruster is the trailing thruster.

2nd quadrant

In this quadrant, thrusters are only affected by thruster-thruster interaction.

The leading thruster is assumed to be operating in open water conditions, i.e.:

$$\beta_P = \beta_{PV} = \arctan\left(\frac{V}{0.7\pi n D_O}\right) \tag{5.2}$$

$$\theta = \delta + \beta_H \tag{6.2}$$

where,

$$\beta_H = -\arctan\left(\frac{v}{u}\right) \tag{3.1}$$

The trailing thruster is affected by the leading thruster due to race impingement, flow rectification and race wake effects:

β_P and θ due to race effects are calculated as follows:

The race velocity expressed as an advance angle is calculated from:

$$\tan\beta_{PR} = \frac{1}{2}\left[\tan\beta_{PV}(2\cos\theta - 1) + \sqrt{\tan^2\beta_{PV}(2\cos\theta - 1)^2 + \frac{2kC'_{Xl}}{\cos^2\beta_{PV}}}\right] \tag{5.8}$$

The equation for the minimum distance between the trailing thruster and the race from leading thruster:

$$(x_{tl} - x_R)\cot\zeta + (y_{tl} - y_R) = 0 \tag{5.22}$$

where,

$$x_{tl} = +s\sin\beta_H - L_{CLD}\cos\theta_t + L_{CTD}\cos\theta_l$$
$$y_{tl} = -s\cos\beta_H - L_{CLD}\sin\theta_t + L_{CTD}\sin\theta_l \tag{5.21}$$

where, the coefficients s, L_{CLD} and L_{CTD} in equations 5.21 are derived from thruster geometry, as described in Chapter 5, and

$$x_R = -\frac{\pi D_O \bar{x}_R}{2C_N R_V^2} \tag{5.19}$$

$$y_R = -\frac{\pi D_O \bar{y}_R}{2C_N R_V^2} \tag{5.20}$$

where,

$$\bar{x}_R = \frac{e^{\bar{y}_R}\left|\tan\frac{\zeta_O}{2}\right|}{2} + \frac{1}{2e^{\bar{y}_R}\left|\tan\frac{\zeta_O}{2}\right|} - \frac{1}{\sin\zeta_O} \tag{5.16}$$

and

$$R_V = \frac{V_A}{V_R} = \frac{\tan\beta_{PV}}{\tan\beta_{PR}} \tag{5.9}$$

and
$$\cot\zeta = \frac{d\bar{x}_R}{d\bar{y}_R} = \frac{e^{\bar{y}_R}\left|\tan\frac{\zeta_O}{2}\right|}{2} - \frac{1}{2e^{\bar{y}_R}\left|\tan\frac{\zeta_O}{2}\right|} \tag{5.23}$$

From the solution to equations 5.22 and 5.23 the angle of attack due to the race:

$$\theta_R = \theta - \zeta \pm 2\pi \tag{7.2}$$

and from equation 5.22 the minimum distance between thruster and race:

$$e = \sqrt{(x_{tl} - x_R)^2_{\min} + (y_{tl} - y_R)^2_{\min}} \tag{7.3}$$

therefore, the proportion of the trailing thruster affected by the race, ξ is calculated as follows:

$$\xi = \frac{1}{2\pi}\left[(\lambda_D - \sin\lambda_D) + \left(\frac{D_R}{D_D}\right)^2(\lambda_R - \sin\lambda_R)\right]$$
$$\cos\frac{\lambda_D}{2} = \frac{4e^2 + D_D^2 - D_R^2}{4eD_D}$$
$$\cos\frac{\lambda_R}{2} = \frac{4e^2 + D_R^2 - D_D^2}{4eD_R} \tag{5.24}$$

θ due to flow rectification effects is calculated as follows:

$$\frac{\theta_t}{\theta_l} = 1 - 0.5\frac{2\beta_H}{\pi} \tag{5.28}$$

β_P due to race wake effects is calculated as follows:

if $x_R(y_{tl}) > x_{tl}$ then:
$$\frac{V_{At}}{V} = 1 - \left(1 - \frac{2\beta_H}{\pi}\right)e^{-0.015\left(\frac{x_R - x_{tl}}{D_O}\right)^{1.4}} \tag{5.27}$$

otherwise:
$$V_{At} = V$$

Finally, thruster forces and propeller torque calculated on the basis of race effects and those due to flow rectification/race wake effects are combined to give the trailing thruster forces, i.e.:

$$X = \xi\left(X(\beta_P,\theta)_R - X(\beta_P,\theta)_A\right) + X(\beta_P,\theta)_A$$
$$Y = \xi\left(Y(\beta_P,\theta)_R - Y(\beta_P,\theta)_A\right) + Y(\beta_P,\theta)_A$$
$$Q = \xi\left(Q(\beta_P,\theta)_R - Q(\beta_P,\theta)_A\right) + Q(\beta_P,\theta)_A \tag{5.25}$$

3rd quadrant

In the third quadrant it is assumed that the thrusters are only affected by thruster-thruster interaction. The leading thruster is assumed to be operating in open water conditions as described above. The trailing thruster is affected by flow rectification effects only and hence, θ is calculated as follows:

$$\frac{\theta_t}{\theta_l} = 1 - 0.5\frac{2(\pi - |\beta_H|)}{\pi} \tag{5.28}$$

4th quadrant

Operation in this quadrant is impractical however, there are situations, although rare, where this may occur e.g., operation in the pushing mode where the drift angle is greater than 90°. In this situation, given that the drift angle would not be much greater than 90° and that the thrusters would still be operating in the *wake* of the hull, hull-thruster interaction can be reliably estimated as per the 1st quadrant. From similar reasoning it is possible to show that hull-thruster interactions may also be estimated as per the 1st quadrant for operation in the pulling mode in the 4th quadrant.

7.1.2 Hull Forces

Bare hull forces expressed as surge, sway and yaw actions in the coordinate system defined in Chapter 1 are calculated as follows:

$$X_H = \tfrac{1}{2}\rho V^2 BTX'_H(\beta_H) \tag{3.4}$$
$$Y_H = \tfrac{1}{2}\rho V^2 LTY'_H(\beta_H) \tag{3.5}$$
$$N_H = \tfrac{1}{2}\rho V^2 L^2 TN'_H(\beta_H) \tag{3.6}$$
$$K_H = z_H Y_H \tag{7.4}$$

The coefficients $X'_H(\beta_H), Y'_H(\beta_H), N'_H(\beta_H)$ which are a function of the drift angle are derived from experimental results presented in Chapter 3, for a mean Froude Number of 0.18. The vertical centre of pressure z_H is assumed to be at the centroid of the underwater lateral profile area.

Forces acting on the hull due to thruster-hull interaction are determined depending on the $\beta_H - \delta$ quadrant as follows:

- 1st quadrant running ahead, thrust ahead
  $0° \geq \beta_H \geq -90°, 0° \leq \delta \leq 90°$;
- 2nd quadrant running ahead, thrust astern
  $0° \geq \beta_H \geq -90°, 90° \leq \delta \leq 180°$;
- 3rd quadrant running astern, thrust astern
  $-90° \geq \beta_H \geq -180°, 90° \leq \delta \leq 180°$; and
- 4th quadrant running astern, thrust ahead
  $-90° \geq \beta_H \geq -180°, 0° \leq \delta \leq 90°$.

1st quadrant

$$X_{HT} = \tfrac{1}{2}\rho A_O (0.7\pi D_O)^2 \left(n_p^2 + n_s^2\right) C'_{X,\beta_P=0} X^*_{HT}(\beta_{PV}, \delta) \tag{6.15}$$

2nd quadrant

$$X_{HT} = \tfrac{1}{2}\rho A_O (0.7\pi D_O)^2 (n_p^2 + n_s^2) C'_{X,\beta_P=0} X^*_{HT}(\beta_{PV},\delta)$$
$$Y_{HT} = \tfrac{1}{2}\rho A_O (0.7\pi D_O)^2 (n_p^2 + n_s^2) C'_{X,\beta_P=0} Y^*_{HT}(\beta_{PV},\delta) \quad (6.15)$$
$$N_{HT} = \tfrac{1}{2}\rho A_O L(0.7\pi D_O)^2 (n_p^2 + n_s^2) C'_{X,\beta_P=0} N^*_{HT}(\beta_{PV},\delta)$$
$$K_{HT} = z_T Y_{HT} \quad (7.5)$$

3rd quadrant

$$X_{HT} = t, \text{ for astern bollard pull}$$
$$Y_{HT} = \tfrac{1}{2}\rho A_O (0.7\pi D_O)^2 (n_p^2 + n_s^2) C'_{X,\beta_P=0} Y^*_{HT}(\beta_{PV},\delta)$$
$$N_{HT} = \tfrac{1}{2}\rho A_O L(0.7\pi D_O)^2 (n_p^2 + n_s^2) C'_{X,\beta_P=0} N^*_{HT}(\beta_{PV},\delta) \quad (6.15)$$
$$K_{HT} = z_T Y_{HT} \quad (7.5)$$

4th quadrant

Operation in this quadrant is impractical however, there are situations, although rare, where this may occur e.g., operation in the pushing mode where the drift angle is greater than 90°. In this situation, given that the drift angle would not be much greater than 90° and that the thrusters would still be operating in the *wake* of the hull, thruster-hull interaction can be reliably estimated as per the 1st quadrant. From similar reasoning it is possible to show that thruster-hull interactions may also be estimated as per the 1st quadrant for operation in the pulling mode in the 4th quadrant.

The coefficients $X^*_{HT}(\beta_{PV},\delta), Y^*_{HT}(\beta_{PV},\delta)$ and $N^*_{HT}(\beta_{PV},\delta)$ which are functions of the apparent advance angle and the thruster angle are calculated as follows:

$$X^*_{HT} = X^*_{\beta\delta}\beta_{PV}\delta + X^*_{\delta}\delta + t \quad (6.16)$$
$$Y^*_{HT} = Y^*_{\beta\delta}\beta_{PV}(\pi - \delta) + Y^*_{\delta}(\pi - \delta) \quad (6.17)$$
$$N^*_{HT} = N^*_{\beta\delta}\beta_{PV}(\pi - \delta) + N^*_{\delta}(\pi - \delta) \quad (6.18)$$

The coefficients in equations 6.16 to 6.18 are derived from experimental results and are given in Table 6.5 and β_{PV} is calculated as follows:

$$\beta_{PV} = \arctan\left(\frac{V}{0.7\pi n D_O}\right) \quad (5.2)$$

In situations where different torque loadings cause the propeller revolutions to be different for each thruster, the mean revolutions, $n = (n_p + n_s)/2$, may be used to calculate β_{PV} in equation 5.2.

7.1.3 Force Transformations

To solve the equations of equilibrium, as follows:

$$X_H + X_S + X_T = 0 \quad (2.1)$$
$$Y_H + Y_S + Y_T = 0 \quad (2.2)$$
$$N_H + N_S + N_T = 0 \quad (2.3)$$
$$K_H + K_S + K_T = -\Delta g GM \sin\phi \quad (2.4)$$

all forces and moments need to be expressed in the coordinate system with its origin at amidships as defined in Figure 2.1. Hull forces are expressed in this coordinate system, however, thruster forces and reactions of the tug force or ship forces are not and are transformed as follows:

Thruster Forces and Moments

$$X_T = \left(X_p + X_s\right)\cos\delta - \left(Y_p + Y_s\right)\sin\delta \quad (7.6)$$
$$Y_T = \left(X_p + X_s\right)\sin\delta + \left(Y_p + Y_s\right)\cos\delta \quad (7.7)$$
$$N_T = y_T\left[\left(X_p - X_s\right)\cos\delta - \left(Y_p - Y_s\right)\sin\delta\right] - x_T Y_T \quad (7.8)$$
$$K_T = z_T Y_T \quad (7.9)$$

Reaction Forces and Moments

$$X_S = -\left(X_H + X_{HT} + X_T\right) \quad (7.10)$$
$$Y_S = -\left(Y_H + Y_{HT} + Y_T\right) \quad (7.11)$$
$$N_S = x_S X_S - y_S Y_S \quad (7.12)$$
$$K_S = z_S Y_S \quad (7.13)$$

where, for pushing, assuming an elliptical bow fender profile:

$$x_S = \frac{1}{\sqrt{\left(\frac{y_e}{x_e}\tan\beta_H\right)^2 + 1}} - x_e + x_f \quad (7.14)$$

$$y_S = \frac{\beta_H}{|\beta_H|} y_e \sqrt{1 - \left(\frac{x_S + x_e - x_f}{x_e}\right)^2} \quad (7.15)$$

z_s = fender height

or, for pulling:

x_S = distance to tow point

$y_S = 0$

z_s = tow point height

where x_e and y_e are the semi-major and minor axes of the assumed ellipse and x_f is the distance along the tug x-axis to the bow fender.

7.2 Full Scale Prediction of Tug Forces

The mathematical model outlined in the previous section has been used to predict full scale performance of a typical omni-directional stern drive tug, for a range of speeds and modes of operation. The predictions are based on the 30m tug introduced in Chapter 3, details of which are given in Appendix A. All practical modes of tug operation have been investigated, as introduced in Chapter 5 and discussed further in Chapter 6. Each mode of operation has been investigated at corresponding practical speeds, as discussed in Chapter 6 and by Hensen, 1990. The results have been calculated assuming the attended ship is neither swaying nor yawing and the angles of rotation and set propeller revolutions for each thruster are equal. Despite the set propeller revolutions being equal, the actual revolutions for each thruster may be different due to different torque loadings, resulting from interactions among the thrusters and hull and prime mover limitations. The coordinate system used to represent the results is presented in Figure 2.1.

On the basis of the investigations described in the previous chapters, fundamental factors which determine a tug's capability may be listed as follows:

(a) hull force characteristics;
(b) thruster force characteristics and locations;
(c) interactions among the thrusters and hull;
(d) prime mover power and torque-revolutions characteristic;
(e) tug transverse stability;
(f) tug line-superstructure interference and towpoint/fender geometry; and
(g) stability of equilibrium or position keeping ability.

Factors (a), (b) and (c) in the list are investigated in Chapters 3, 4 and 5 respectively. In Chapter 3 it was shown that hull forces made non-dimensional using the major dimensions of the hull vary relatively little for two hulls that are significantly different, for this type of vessel. Therefore, the measured non-dimensional hull characteristics can be used for general predictions. However, in Chapter 4 it was shown from experimental data for three different thrusters, that forces vary significantly given changes in the thruster geometry and configuration. The thrusters considered had the same ducts, similar propellers (although different pitch) but somewhat different struts, gear-cases and duct supporting fins. To investigate the influence of thruster characteristics on tug forces, including interactions among the thrusters and hull, two sets of predictions have been made using data for two different thrusters. The open water data used for the predictions is that measured at AMC as part of the present investigation and that measured at MARIN by Oosterveld and van Oortmerssen, 1972, as presented in Chapter 4. Details of the thrusters are given in Appendix C. The location of the thrusters determine a tugs general performance characteristics and influence heavily the hull design, e.g., differences in stern drive and tractor configurations, as discussed in Chapter 1. However, for each configuration practical considerations mean that longitudinal thruster positions vary very little and the constraint of the beam permits little variation in the transverse thruster spacing, as mentioned in Chapter 4. Therefore, no variation in thruster locations have been considered. For these predictions the mathematical model was used with constant propeller revolutions corresponding to rated maximum for the prime mover, that is, the remaining factors in the list above are not considered.

Clearly, for realistic assessment of a tug's capability the remaining factors in the list above must be considered. To compensate for constraints due to factors (d), (e) and (f), the set propeller revolutions must be reduced below the rated maximum for the prime mover until previously determined limits relating to all these factors are met, as discussed in Chapter 2 and shown schematically in Figure 7.1. Constraints due to factor (d) are maximum engine torque in addition to maximum engine revolutions which requires not only thruster open water force characteristics but also open water torque characteristics. As no torque characteristics were measured for the thruster used as part of the present investigation predictions have been made using the thruster data presented by Oosterveld and van Oortmerssen, 1972. Limiting propeller revolutions are calculated assuming a diesel prime mover with constant maximum torque and governing based on revolutions, as described in Chapter 2.

To account for factor (e), a maximum angle of tug heel may be defined. There are a number of criteria that may be used to determine this limit including angle of deck edge immersion and reserve stability before down-flooding, as discussed by Hendy and Freathy, 1993. For the present investigation, a maximum angle of heel of 8° has been assumed which is 60% of that for deck edge immersion at rest.

For practical operation in the pulling mode the tug's line should not interfere with structures located on it's deck. This may be accounted for by checking that the angle between the tug's x-axis and the line, $\psi - \beta_H$, is within a range of angles excluding interference for both forward and aft tow points. For the forward tow point a suitable range is ±150° and for the aft tow point ±110°. The location of the tow points and the fender profile influence both the forces imparted and the tug's safety of operation in various modes. Their geometry is determined by practical considerations. The influence of tow point and fender geometry in relation to that of other forces acting, for each mode of operation, is discussed below.

Insight into operational constraints due to factor (g) in the list above, can be gained from consideration of whether the forces acting on the tug are in stable equilibrium. Results from the mathematical model for various speeds and modes of operation can be graded in terms of the stability of the obtained positions of equilibrium. The stability of equilibrium is evaluated from the slope of the $N - \beta_H$ curve at equilibrium, as described in Chapter 2. The extent to which this effects the tug's ability to operate in various modes depends on the relative magnitude of thruster and hull forces which in turn depends on the speed and mode of operation. No limits on operation relating to stability of equilibrium have been defined, although results from the mathematical model are in agreement with accepted practices on the use of omni-directional stern drive tugs, as detailed by Hensen, 1980.

7.2.1 Tug Force Predictions at Constant Propeller Revolutions

The tug force predictions for constant propeller revolutions using AMC and MARIN thruster characteristics are presented in Figures 7.2(a), (b), (c), (d) and (e) for 2, 4, 6, 8 and 10 knots ship speed respectively. The pitch of the propellers fitted to each thruster is different, therefore, revolutions have been set to give the same nominal thruster force at zero speed of advance, i.e., 500 kN corresponding to that of the full scale vessel. Hence, the propeller revolutions for predictions with the MARIN and AMC thrusters were set at 265 and 235 rpm respectively.

No results have been presented for zero speed since the bollard pull of the tug in the ahead and astern directions is independent of the thrusters fitted. These will be reduced below the 500kN nominal thruster force at zero speed of advance in accordance with the measured thrust deduction factors given in Chapter 6.

From Figure 7.2 it can be seen that apart from pulling with the forward tow point abaft the ships beam ($90° \leq \chi \leq 180°$), predictions using the AMC and MARIN thruster data compare closely. In Chapter 4 polar thrust characteristics for the thrusters tested at MARIN and at AMC were presented and it was shown that there are significant differences between the two. These differences are essentially confined to negative flow conditions (angles of attack greater than 90°) where differences in appendage geometry have more influence on flow conditions due to separation effects, etc. In all modes, apart from pulling with the forward tow point abaft the ships beam, the thrusters operate at relatively small angles of attack where there are smaller differences in the characteristics of the thrusters tested at AMC and at MARIN. This explains the close agreement between the predictions for these modes of operation. For pulling with the forward tow point abaft the ships beam, the thrusters are operating in negative flow conditions explaining the differences between the predictions for this mode of operation. These differences increase with increasing speed since the influence of the different thruster appendages on flow conditions increases with increasing speed.

At 8 and 10 knots it can be seen that for pushing and pulling with the forward tow point-indirect the two predictions are essentially identical, since thruster forces contribute very little in these modes and at this speed, as shown in Chapter 6.

From the results it can be concluded that different thrusters (with the same nominal force at zero speed) significantly effect tug forces only for pulling with the forward tow point abaft the ship's beam. However, this is a frequently used tug deployment and, as shown in Chapter 8, one of the most effective in ship turning. This does limit the generality of the predictions that can be achieved using only characteristics for a single thruster. Differences between the two sets of predictions are however, smaller than those due to different modes of operation, therefore, predictions made using characteristics for a particular thruster provide valuable generic information.

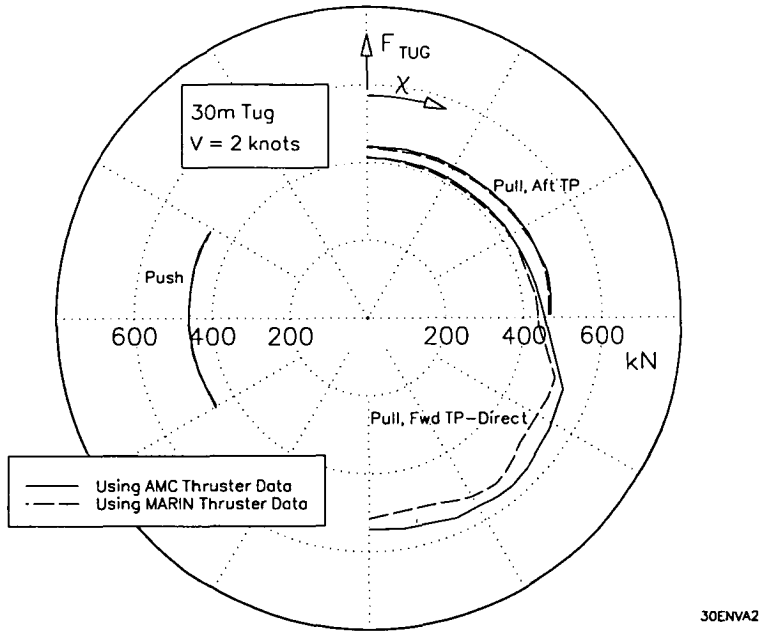

(a) 2 knots Ship Speed

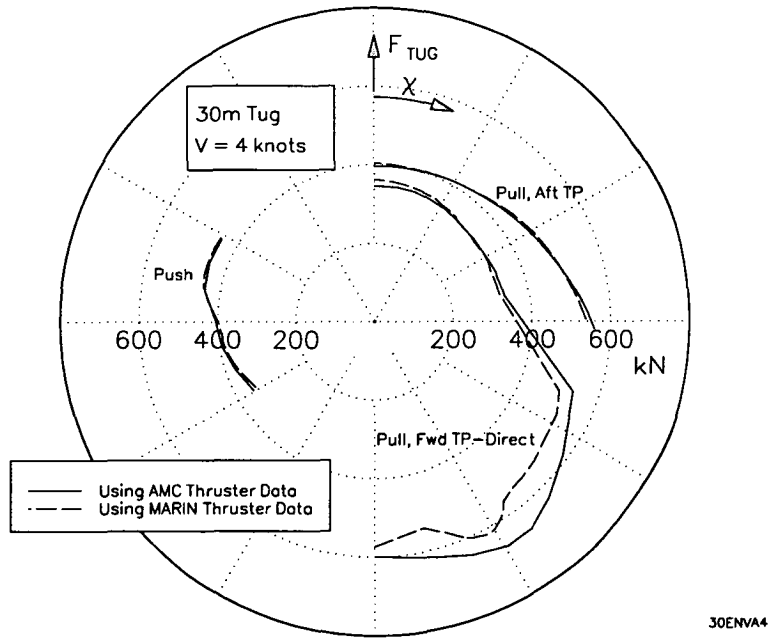

(b) 4 knots Ship Speed

Figure 7.2 Comparison of Tug Force Predictions at Constant Propeller Revolutions Using MARIN and AMC Thruster Data

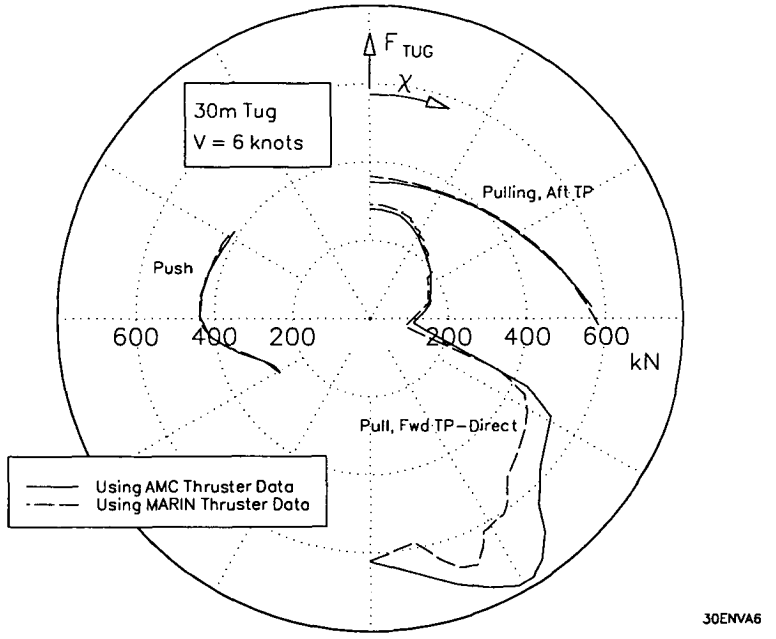

(c) 6 knots Ship Speed

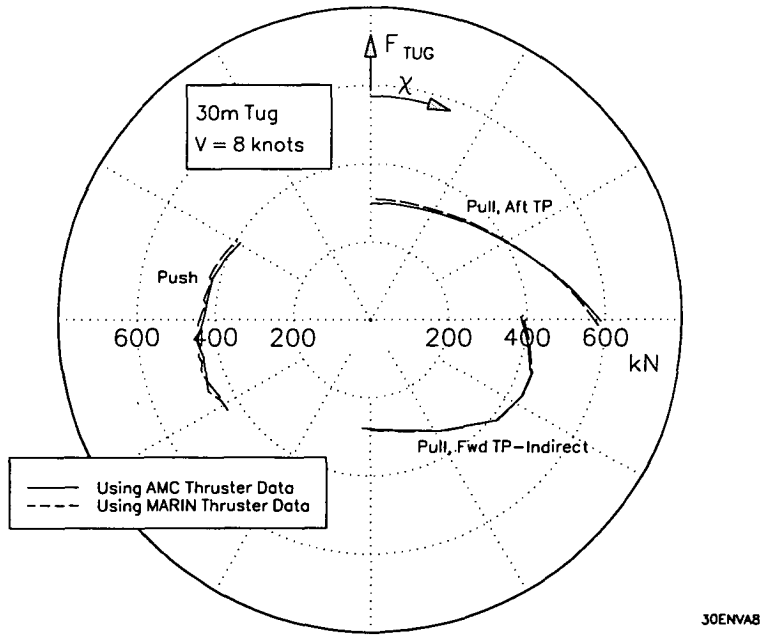

(d) 8 knots Ship Speed

Figure 7.2 Comparison of Tug Force Predictions at Constant Propeller Revolutions Using MARIN and AMC Thruster Data

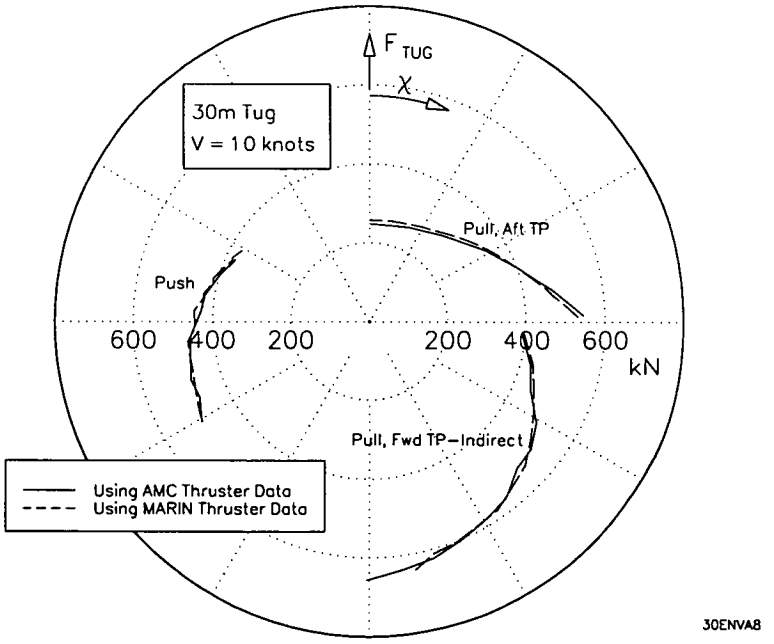

(e) 10 knots Ship Speed

Figure 7.2 Comparison of Tug Force Predictions at Constant Propeller Revolutions Using MARIN and AMC Thruster Data

7.2.2 Tug Force Predictions with Constraints on Propeller Revolutions

The tug force predictions with constraints on propeller revolutions using the MARIN thruster characteristics are presented in Figures 7.3(a), (b), (c), (d) and (e) for 2, 4, 6, 8 and 10 knots ship speed respectively. Constraints which limit the propeller revolutions do not affect the tug at zero speed, therefore, no bollard pull results are given for reasons explained in the previous section.

At 2 knots ship speed, the forces are essentially the same as those presented in the previous section since torque loads or excessive heel are not yet great enough to limit the propeller's revolutions. It can be seen that the forces produced are similar to the nominal bollard pull irrespective of the mode of operation. At this speed hull forces due to thruster-hull interaction are greater than those due to the free stream, as shown in Chapter 6. The difference in forces produced when pulling with the aft tow point and pulling with the forward tow point forward of the ship's beam are due to differences in thruster-hull interaction. For the former, the hull is affected only by the low energy or inlet part of the thruster induced flow field, whereas for the latter, it is affected by the high energy or exhaust part of the induced flow field. Forces produced when pushing are similar in magnitude to those produced by pulling with the aft tow point due to similar thruster-hull interaction effects. Forces produced when pulling with the forward tow point abaft the ship's beam are slightly greater than those produced in the other deployments due to increased thruster forces from operation in negative flow conditions, as described in Chapter 4.

At 4 knots ship speed, hull forces due to the free stream begin to modify performance slightly. For the case of pulling with the forward tow point forward of the ship's beam, combined increase in hull resistance and loss of thruster force due to higher advance speed reduces the available pull. For pulling with the aft tow point, lift forces acting on the hull increase the pull as the line tends toward the ships beam. The greatest forces available are from pulling with the forward tow point abaft the ship's beam resulting from increased thruster forces due to negative flow conditions, increased hull forces due to the free stream and favourable thruster-hull interaction. Thruster-hull interaction produces favourable forces in the surge direction but unfavourable forces in the sway direction, reducing the ability of the tug to be moved sideways. The effects of the former increase with increasing speed, whereas those of the latter decrease with increasing speed, as shown in Chapter 6. The variations in this part of the envelope are due to localised fluctuations in both thrust and torque characteristics of the thrusters when operating in negative flow conditions, as described in Chapter 4. The fluctuations present in the open water thruster characteristics are actually smoothed due to the effects of thruster-thruster and hull-thruster interactions. If interactions are not included then fluctuations present in the open water curves are directly reflected in the tug force predictions, as shown in those presented by Brandner and Renilson, 1993.

At 6 knots ship speed, the situation is similar to that at 4 knots except that hull forces are greatly increased. This further reduces the pull available for operation forward of the ship's beam and increases the pull for operation abaft the ship's beam. For pulling with the forward tow point forward of the ship's beam, heel is small and since the thrusters are operating in positive flow conditions, the limiting constraint is maximum engine revolutions. For pulling with the aft tow point forward of the ship's beam, thrusters are also operating in positive flow conditions hence, the limiting constraint is maximum engine revolutions. However, as the direction of the line approaches the ship's beam, increasing sway forces acting on the hull make heel the limiting constraint.

There are fundamental differences between the geometry of the forces acting when pulling with the aft tow point and pulling with the forward tow point which have implications on both the forces produced and the safety of the tug. For pulling with the aft tow point, the tow point lies between the hull force and the thruster location, as shown in Figure 7.4(a). For pulling with the forward tow point, similarly for pushing, the location of the hull force lies between the tow point (or point of contact on the fenders) and the thruster location, as shown in Figure 7.5(a). The consequences of this are that, for the former case, transverse thruster and hull forces must act in the same direction for equilibrium whereas, for the latter they act in opposition, as can be seen from Figures 7.4(b) and 7.5(b) respectively. This means that, for pulling with the aft tow point, greater forces are applied to the line but both thruster and hull forces act to overturn the tug whereas, for pulling with the forward tow point, smaller forces are applied to the line but the thruster forces act to right the tug. The difference in forces applied for these two modes with increasing speed can be clearly seen from Figures 7.3(b) and (c). Pulling with the aft tow point is most critical at high speeds as the direction of the line approaches the ship's beam, as it also approaches the tug's beam, creating large overturning moments as reflected in the truncated force predictions presented in Figures 7.3(c), (d) and (e). In this situation the tug risks being girted, as introduced in Chapter 1, capsize of the tug being prevented only by the righting moment produced from the tug's hull stability.

At 6 knots it can be seen that large forces are generated for pulling with the forward tow point abaft the ship's beam for line angles greater than 135°. However, at this speed various factors act to limit the tug's performance. Propeller revolutions for the leading thruster, which is operating in negative flow conditions and exposed to the free stream, are limited due to torque overload. The propeller revolutions of the trailing thruster are also limited due to torque overload at line angles close to 180° where it is exposed to the free stream. At smaller line angles, although not effected by torque overload, the trailing thruster is heavily affected by thruster-thruster interaction, as shown in Chapters 5 and 6. Furthermore, given the large hull forces acting at this speed and the reduced reserve thrust, it may be difficult for the tug to be accelerated into position against the free stream. Indeed, there is a limiting speed after which the tug cannot generate significant steering force components in this mode, as shown in Chapter 6. For this particular tug, this speed is approximately 6 knots. Therefore, to generate larger steering forces at and above 6 knots, methods which rely less on thruster forces and more on hull forces must be used. That is, in addition to pushing and pulling with the aft tow point, there is pulling indirect with the forward tow point. At 6 knots, pulls of some magnitude can be realised in the indirect mode and although there is a limited range of equilibrium positions, these are most likely easier to achieve and maintain compared with pulling direct.

At 8 and 10 knots it can be seen that, due to increased hull forces, a larger range of line angles are possible when pulling indirect. The tug's drift angle controls the position and magnitude of the sway force acting on the hull, and therefore, the magnitude of the force applied. As the line angle approaches 180°, the drift angle increases and therefore the sway force increases but less is transferred to the line since the centre of pressure is more remote from the tow point. The largest forces are generated at line angles approaching 90° where although the sway force is smaller, it's position is not so remote from the tow point. For pulling indirect, the thrusters are operating in positive flow conditions, therefore limitations on the propeller revolutions are due to either maximum engine revolutions or excessive heel. At 8 knots, heel has not exceeded the maximum, hence the limiting constraint is simply maximum engine revolutions. At 10 knots, sway forces have increased such that heel becomes excessive at higher line angles as shown by the truncated curve in Figure 7.3(e). The magnitude of the overturning moment is dependent on the relative magnitudes and heights of the sway force, thruster forces and line force, as shown in Figure 7.6. The relative magnitude of these forces in addition to hull and thruster characteristics, depends on equilibrium in the horizontal plane. For fixed height of the hull sway force, to reduce the overturning moment it is desirable to move the vertical position of the tow point as close as possible to the vertical position of the sway force, thereby reducing overturning moment. Likewise, it is desirable to move the thrusters away from the vertical position of the sway force, thereby increasing the countering moment. The restoring moment produced by the tug is a function of the tug's GM and displacement. Obviously the greater the GM and displacement, the greater the restoring moment.

With reference to Figures 7.3(a), (b), (c), (d) and (e) it can be seen that for operation in the pushing mode, there is not significant reduction in the force available with increasing speed. Operation in the pushing mode is very similar to pulling in the indirect mode and can be explained in a similar manner. At low speed, hull forces are small and the tug can maintain a high drift angle allowing direct transfer of force from the thrusters. With increasing speed, the tug cannot maintain a high drift angle, decreasing the direct transfer of thruster force. However, the hull force is much greater and the location of the sway force moves forward to the neighbourhood of the point of contact between fender and ship, enabling a large portion of the hull force to be transferred to the ship. For pushing, the thrusters are operating in positive flow conditions and therefore constraints on tug performance are limited to maximum engine revolutions since tug heel never exceeds the maximum. It can be seen that the forces shown are never more than ±30° either side of $\chi = 270°$. To achieve this, particularly at low speeds, the tug is required to be either over square or laid back alongside the ship in what might be considered impractical operating positions. This demonstrates that the force produced from pushing is at approximately ±90° to the ship's heading.

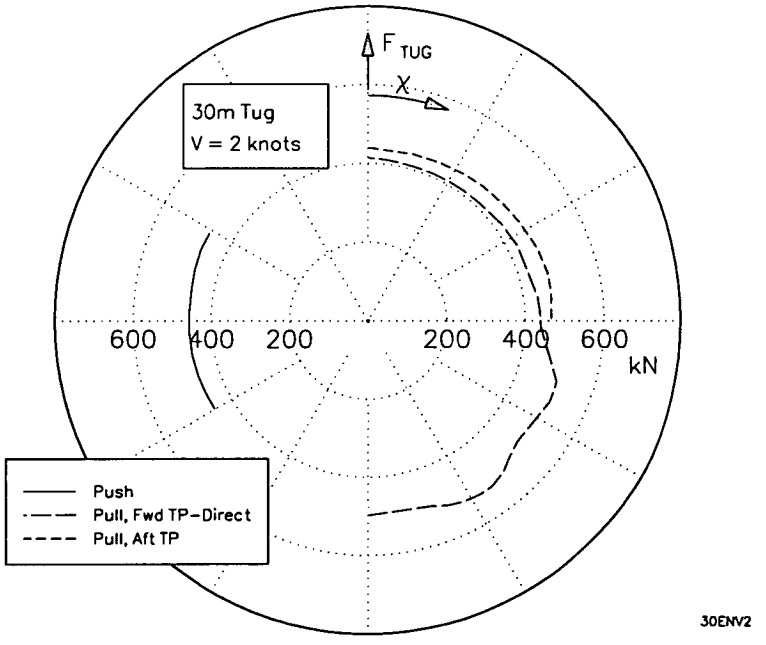

(a) 2 knots Ship Speed

Figure 7.3 Tug Force Predictions with Constraints on Propeller Revolutions Using MARIN Thruster Data

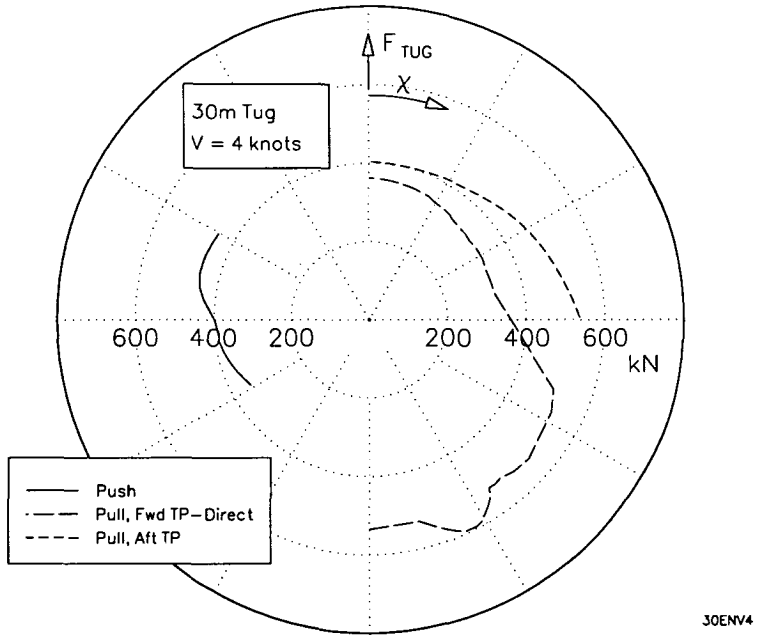

(b) 4 knots Ship Speed

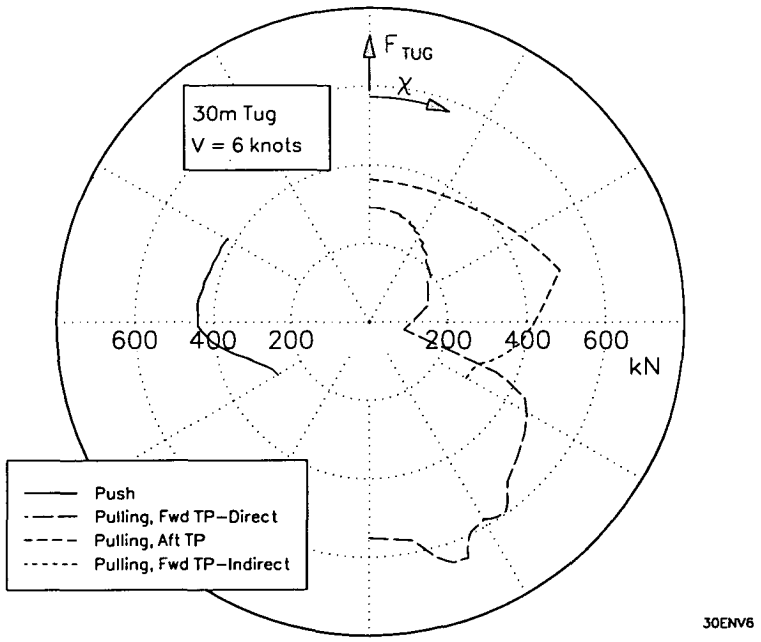

(c) 6 knots Ship Speed

Figure 7.3 Tug Force Predictions with Constraints on Propeller Revolutions Using MARIN Thruster Data

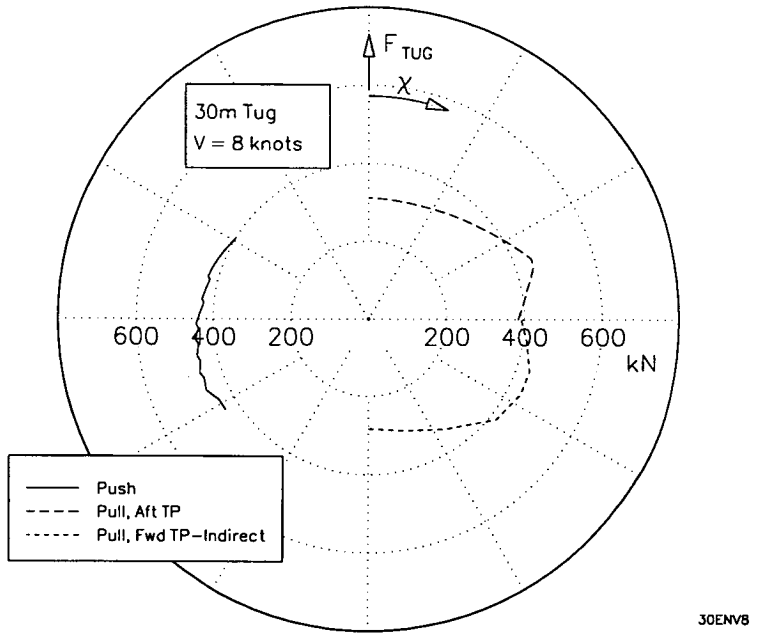

(d) 8 knots Ship Speed

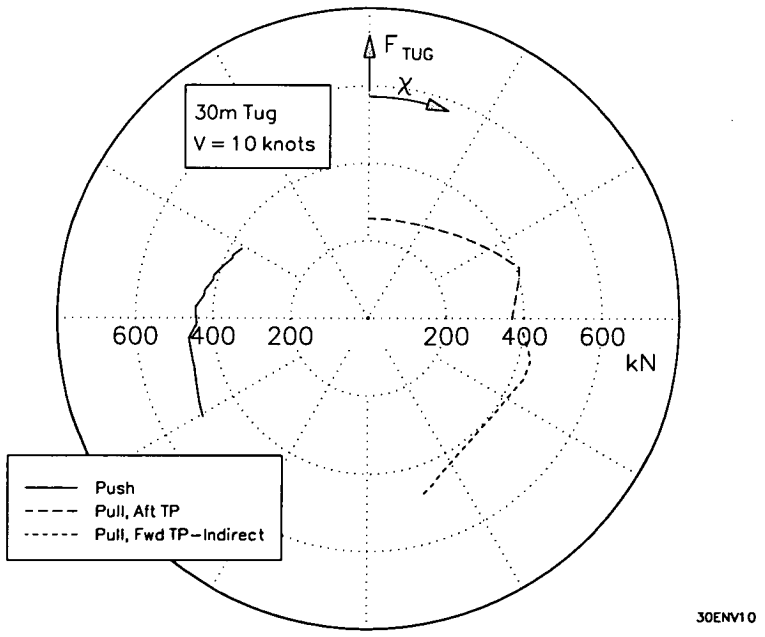

(e) 10 knots Ship Speed

Figure 7.3 Tug Force Predictions with Constraints on Propeller Revolutions Using MARIN Thruster Data

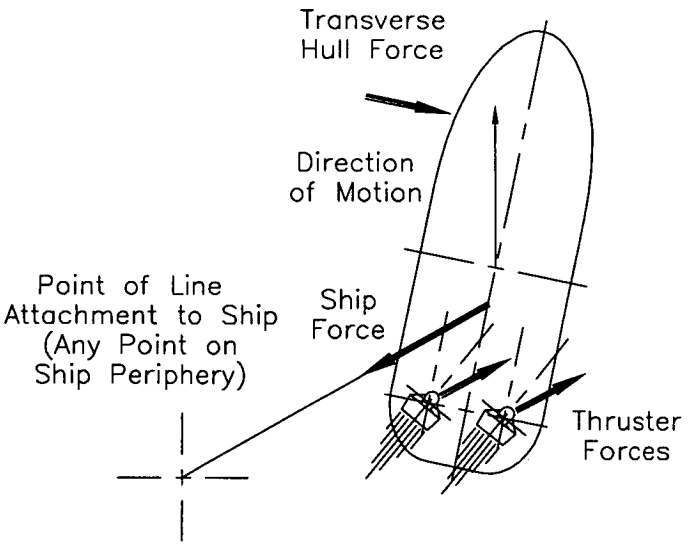

(a) Forces in the Horizontal Plane

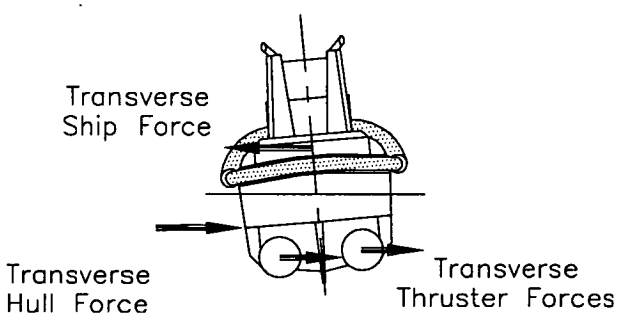

(b) Forces Affecting Transverse Stability

Figure 7.4 General Geometry of Forces Acting on the Tug When Pulling with the Aft Tow Point Forward of the Ship's Beam

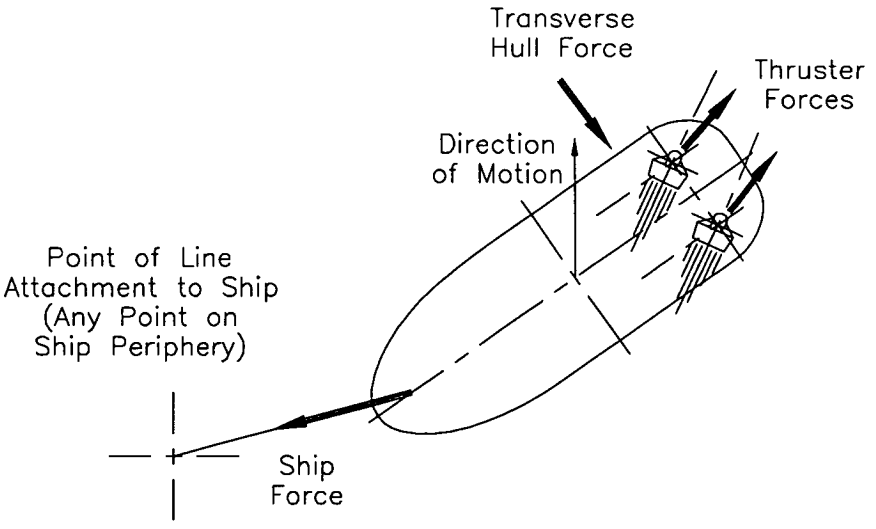

(a) Forces in the Horizontal Plane

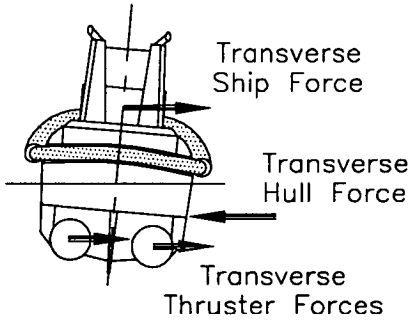

(b) Forces Affecting Transverse Stability

Figure 7.5 General Geometry of Forces Acting on the Tug When Pulling with the Forward Tow Point Forward of the Ship's Beam

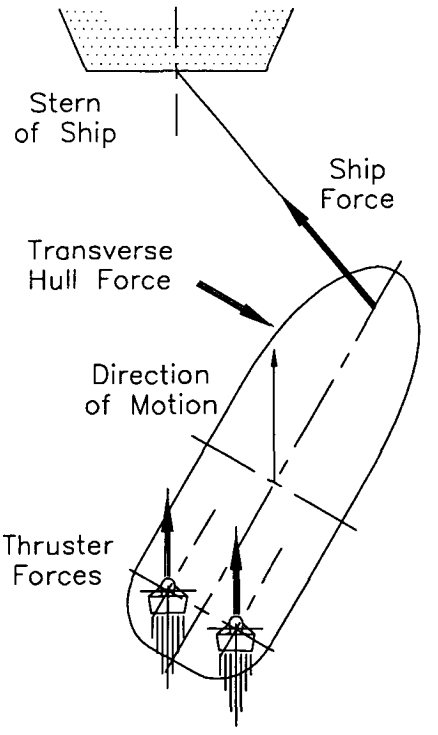

(a) Forces in the Horizontal Plane

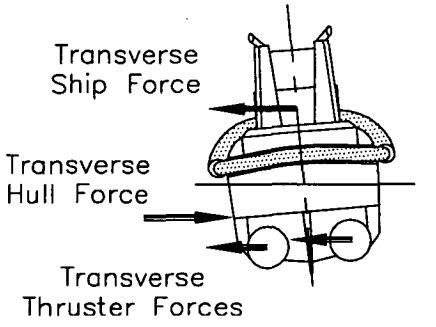

(b) Forces Affecting Transverse Stability

Figure 7.6 General Geometry of Forces Acting on the Tug When Pulling Indirect

The predictions presented above give forces available for various speeds and modes of operation, however they provide no information as to whether the positions of equilibrium found are maintainable. The ability of a tug to maintain position can be assessed from its stability of equilibrium, as mentioned above and discussed in Chapter 2. At each position of equilibrium found using the mathematical model, the slope of the $N-\beta_H$ curve has been evaluated in addition to the forces presented above. Figure 7.7 shows non-dimensional values of the derivative, $\partial N/\partial\beta_H$, plotted against angle of the force for each mode of operation. The derivative has been non-dimensionalised as follows:

$$\frac{\partial N'}{\partial \beta'_H} = \frac{\partial N / \partial \beta_H}{\frac{1}{2}\rho V^2 T L^2} \tag{7.18}$$

It was found that the variation of $\partial N'/\partial\beta'_H$ with angle of the force for each mode of operation varies relatively little with increasing speed therefore, for clarity, curves are given for each mode at one speed only.

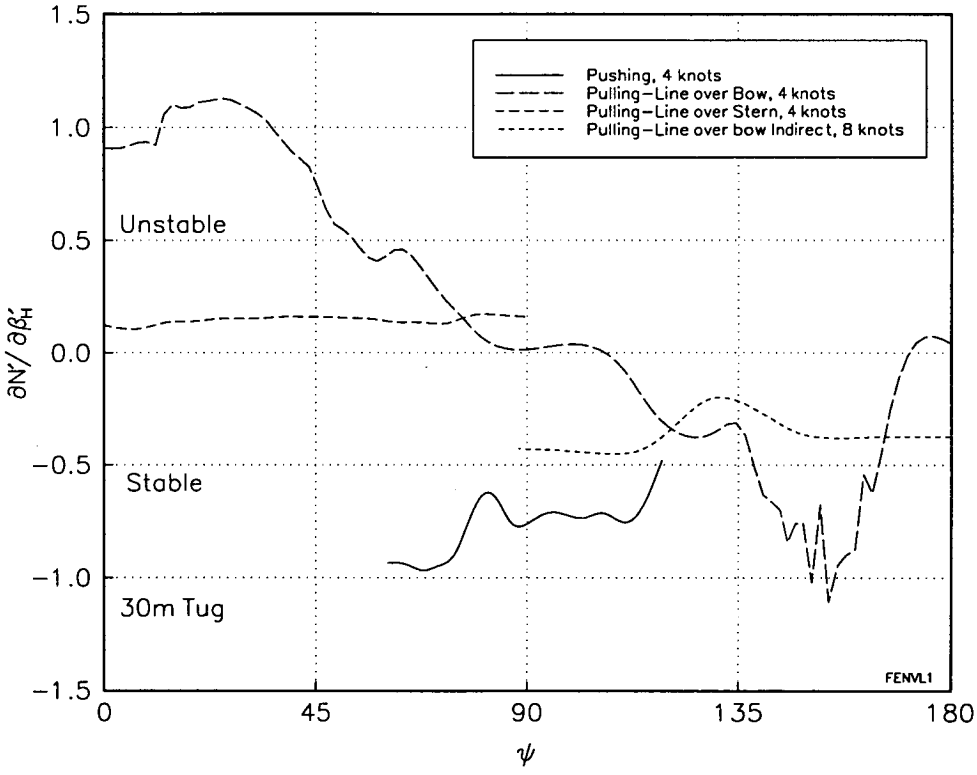

Figure 7.7 Tug Stabilising/Destabilising Moments at Equilibrium for Various Modes of Operation

For pulling with the aft tow point, it can be seen that equilibrium in this mode is marginally unstable for all line angles. This implies the tug could maintain position relatively easily in this mode, although control input from the tug master would be required at all times. This result is somewhat expected given that this is the mode of operation used with the conventional tug which is still in popular use with omni-directional stern drive tugs. For pulling with the forward tow point, equilibrium is unstable when the line angle is less than 90° (tug running astern) and stable when the line angle is greater than 90° (tug running ahead). What can be concluded from this

is that once the stern becomes the leading edge, equilibrium becomes unstable. This explains the popularity of this mode when operating abaft the beam, in addition to other factors, including the relatively larger forces that are produced. The relatively large instability when operating forward of the beam explains why this deployment is rarely used other than at low speeds, in addition to other factors, including the relatively small forces that are produced.

For pushing, equilibrium is stable for all practical directions of the force produced which explains, among other reasons, the universal acceptance of this mode of operation when the ship is underway with stern driven tugs.

At higher speeds where hull forces become larger and thruster forces are reduced it is important that there is stability of equilibrium. It can be seen that for pulling indirect, equilibrium is stable for all line angles. Clearly, tugs of the type considered here have sufficient power and response from thruster units to counter destabilising moments while engaged in towing, particularly at low speeds. However, at higher speeds, this capability may be reduced requiring greater concentration and skill from the tug operator. Accepted practices detailed by Hensen, 1980, show that tugs are rarely used at higher speeds in modes where positions of equilibrium are unstable.

8 INFLUENCE OF TUG FORCES ON SHIP MOTIONS & OPTIMISATION

8.1 Introduction

The ability of omni-directional stern drive tugs to render assistance at relatively higher speeds than their predecessors not only raises the question of what forces the tugs can generate, but also what affect they have on ship motions at these higher speeds. Using the developed mathematical model, performance envelopes for a typical omni-directional stern drive tug have been derived and are presented in Chapter 7. Of equal importance to the tug master and marine pilot and in simulation studies is the extent to which tug forces influence ship motions and its optimisation. Generally, the manoeuvre of most interest in harbour situations is that of turning, as shown in Figure 8.1. The ship turning circle may be considered in two phases, the initial transient phase where forces acting on the ship vary until a steady state is achieved, followed by the final steady phase of turning. The initial transient phase is of most interest for harbour manoeuvring and corresponds essentially to the part of the turn where the ship's heading is altered by 90°. This part of the turning circle is characterised by the advance and transfer, as shown in Figure 8.1. To investigate the influence of tug forces on the advance and transfer, a series of simulations have been performed on the AMC shiphandling simulator, using the predictions from Chapter 7 as input.

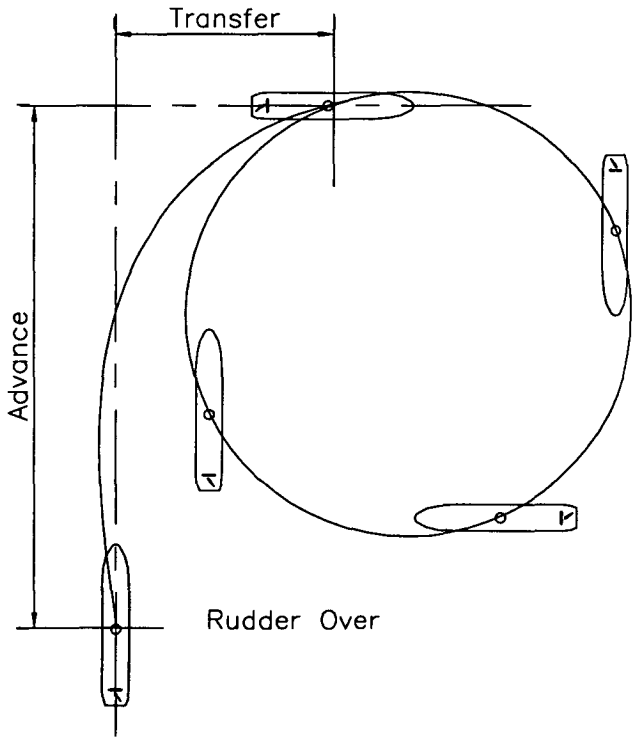

Figure 8.1 The Turning Circle

Forces acting on the ship in a turn that are of interest to the present investigation include the following:

- inertia forces;
- rudder forces;
- hull forces;
- propeller forces; and
- tug forces.

Inertia forces depend on the loading condition and trim of the ship, i.e. ballast, fully loaded or partly loaded. Hull forces depend on a number of parameters including the ship's motions, loading condition, trim and the depth to draft ratio. Rudder forces essentially depend on the ships motions and propeller revolutions, i.e., whether increased revolutions are used to improve the rudder's effectiveness. For the present investigation only ships where the rudder(s) is immersed in the race of the propeller(s) are considered. The influence of tug forces also depend on a number of parameters including the ship's motions, tug location and percentage of power used to apply the force. To investigate tug-ship interaction, all of the above mentioned parameters need to be considered, although there are some obvious simplifications that can be made.

The loading conditions of full load and ballast are the most critical as they represent the extremes in ship manoeuvring behaviour. In the full load condition, ships are generally required to manoeuvre in extremely shallow water (of the order of 1.1 depth to draft ratio) and are therefore affected by large hydrodynamic hull forces in addition to large inertia forces. In the ballast condition, the relatively low displacement and consequent high windage areas mean that ships may be affected by large aerodynamic forces. For reasons of control, and propeller and rudder immersion, ships in the ballast condition are generally trimmed by the stern which considerably alters the hull forces acting on the ship and therefore, the handling characteristics. It is rare that a ship entering a port in the ballast condition is significantly affected by shallow water phenomena. On the basis of the above discussion, the present investigation is limited to the more critical manoeuvring cases of full load in shallow water and ballast in deep water. From these cases it is possible, to extrapolate the influence of tug forces for intermediate cases, such as part load trimmed and untrimmed in deep water.

The ship used for the turning simulations is a 220,000 dwt very large bulk carrier; 315m length and 52m beam. Details of the ship for the loading conditions considered are given in Table 8.1. The speed of the ship at the beginning of each simulation is 4 knots which is typical of harbour manoeuvring in the full load condition. Simulations in the ballast load condition are also started with 4 knots initial speed to allow comparison with those for the full load cases, although ships in ballast are usually handled at higher speeds due to the lower inertia. This speed corresponds approximately to an engine telegraph setting of dead slow ahead. For simulations where the rudder is used, then full 35° deflection is set for the duration of the simulation. In cases where propeller boost is also used through the turn, the engine telegraph setting is moved to half ahead at the beginning of simulation. In deep water, half ahead telegraph setting corresponds to ship speed of 8 knots at equilibrium. The ship manoeuvring mathematical model used in the shiphandling simulator at the AMC is based on that by Norrbin, 1971.

Condition	Displacement (tonnes)	Draft, Fwd/Aft (m)	Trim (°)	Depth/Draft
Full Load	258,000	18.3/18.3	0	1.2
Ballast	112,300	7.0/10.3	0.6	∞

Table 8.1 Details of Loading Conditions used for Turning Simulations of Very Large Bulk Carrier

Tug forces used for the turning simulations are those derived in Chapter 7 for a 30m tug which is typical of an Australian omni-directional stern drive tug. Details of the 30m tug are given in Appendix A. The location and direction of tug forces are limited by the location of ship's bitts and by modes of operation compatible with the tug placement and practical usage. Cases of typical tug deployment (for a turn to starboard) are considered, as shown in Figure 8.2 and listed in Table 8.2. For each deployment it is assumed that the tug is operating at full power. For the present investigation where relative effects are sought, it is assumed that the tug forces remain constant at those corresponding to the initial speed of 4 knots. The magnitude of the force applied and its direction with respect to the ship's heading is given in Table 8.2 for each case.

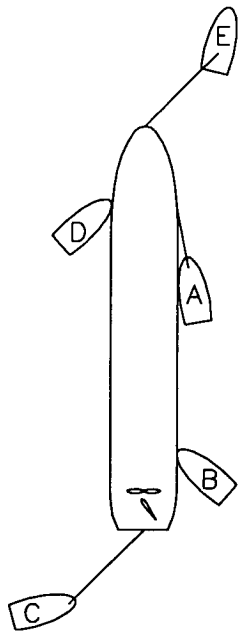

Figure 8.2 Typical Cases of Tug Deployment for a Turn to Starboard

Tug	Deployment	Force Magnitude (kN)	Force Direction wrt Ships Head(°)
A	Starboard shoulder -pulling aft	530	170
B	Starboard quarter -pushing	400	90
C	Centre lead aft -pulling off port quarter	530	135
D	Port shoulder -pushing	400	90
E	Headline -pulling off starboard shoulder	430	45

Table 8.2 Tug Forces for each Deployment used in Ship Turning Simulation

To investigate the interactions between hull, rudder, propeller and tug forces, simulations have been performed using various methods of turning the ship, as listed in Table 8.3. Each simulation listed in Table 8.3 is performed for each ship loading

condition: fully loaded and ballast, as listed in Table 8.1. The first simulation is simply a starboard turn through 90° using the rudder only with no propeller boost, which provides a basis for comparison with other turns and the effectiveness of the rudder compared with that of the tugs at this speed. Simulations 2 and 3 use only tugs B and D respectively to turn the ship, examining the influence of pure sway forces and their location in the absence of rudder forces. However, in realistic manoeuvring situations where minimum advance and transfer are required, the rudder is almost always used with propeller boost, as well as a number of tugs. Of equal importance in a turning manoeuvre is not only the trajectory, but also the speed which is a trade off between control and minimising the advance and transfer. Therefore, simulations 5 to 9 consider individually the influence of each of the tug deployments shown in Figure 8.2 and listed in Table 8.2, using the rudder and propeller boost in each case. Simulation 4 is a starboard turn through 90° using only the rudder and propeller boost which provides a basis for comparison of the improvements in turning performance for each tug deployment. The tug deployments described above not only impart steering forces to the ship but also accelerating and decelerating forces which are used to control the ship's speed in addition to the turn. Finally, in simulation 10 a number of combined tug deployments with rudder and propeller boost are used to turn the ship to investigate the combined effects of the tugs. Simulations 1 to 3 and 4 to 10 are presented and discussed below under separate sections for the influence of sway forces and combined surge and sway forces respectively.

Simulation	Tug(s)	Rudder Angle, (°)	Engine Telegraph
1	-	35	Dead Slow Ahead
2	B	0	Dead Slow Ahead
3	D	0	Dead Slow Ahead
4	-	35	Half Ahead
5	A	35	Half Ahead
6	B	35	Half Ahead
7	C	35	Half Ahead
8	D	35	Half Ahead
9	E	35	Half Ahead
10	A, B and C	35	Half Ahead

Table 8.3 Turning Simulations Performed For Loading Conditions of Full load and Ballast

8.2 Influence of Sway Forces

The results from simulations 1, 2 and 3 for the loading conditions of full load and ballast are presented in Figures 8.3 and 8.4 respectively. Relevant parameters from each of the simulations are presented in Table 8.4.

Simulation	Time (mins)	Final Speed (knots)	Advance (ship lengths)	Transfer (ship lengths)
Full Load, Depth/Draft = 1.2				
1	13.7	2.8	3.4	2.3
2	16.2	3.1	4.1	2.8
3	10.5	3.7	-	-
Ballast, Deep Water				
1	7.8	3	2.3	1.1
2	11.8	4.8	3.8	2.6
3	13.0	5.5	3.9	3.8

Table 8.4 Parameters from Turning Simulations to Compare the Influence of the Rudder with Sway Forces from Tugs Pushing on the Shoulder and Quarter

The trajectory for the full load case using the rudder only, as shown in Figure 8.3, is typical of a shallow water turn. The low under-keel clearance limits sway and yaw motions resulting in a relatively large radius turn compared with that expected in deep water. The minimal sway and yaw motions also mean that there is little induced resistance and the ship loses less speed through the turn, as can be seen from Table 8.4, compared with a deep water turn where speed is typically reduced to 40% of the initial speed. The tug pushing on the starboard quarter results in a turn with slightly greater advance and transfer compared with those when the rudder alone is used. In this case, tug B is not as effective as the rudder in turning the ship, given the size of the ship used in the simulations and hence, the size of the rudder fitted. For smaller ships, tug B may be more effective than the rudder in the same turning situation, as shown by Brandner and Renilson, 1993, for a Panamax size bulk carrier. This reflects the influence of tug size or force applied, in comparison to ship size, on turning effectiveness for this particular tug deployment. It can be seen that the tug pushing on the shoulder has little effect in turning the ship and may result in turning the ship in the opposite direction. An analogous result was also shown by Brandner and Renilson, 1993, for a Panamax size bulk carrier. This demonstrates that, unlike tug B, where the size of the tug relative to that of the ship influences its' effectiveness, the effect of tug D or force applied on the turn is essentially independent of its' size relative to that of the ship. In the absence of significant sway and yaw motions, induced resistance is small and there is very little reduction in speed compared with the previous cases, as can be seen from Table 8.4.

The results for the ballast load condition demonstrate different responses to various turning methods compared to those for the loaded condition, as shown in Figure 8.4. The trajectory for the case of using the rudder only is typical of a deep water turning circle, be it either in ballast or fully loaded. In deep water, resistance to lateral motions is significantly reduced compared with shallow water and hence the advance and transfer are correspondingly reduced. Despite increased sway and yaw motions compared with the shallow water case there is not a greater reduction in ship speed, as can be seen from Table 8.4, since propeller forces are greater in comparison to hull

forces. Unlike the loaded case, it can be seen from Figure 8.4 that in the ballast condition, a tug pushing on the shoulder is almost as effective as one pushing on the quarter, although neither is as effective as using the rudder alone. The differences in turning performance between using the tugs and the rudder alone depend on the relative sizes of tug forces and rudder/ship hull forces, as explained above. Therefore, it is possible that tug deployments B and D may be more effective than the rudder, depending on tug size relative to ship size. Furthermore, the ship's hydrodynamic hull characteristics may vary the differences between the effectiveness of these deployments, as explained further below. The tug pushing on the quarter tends to increase the outward drifting motion, natural in ship turning which implies this tug would slow the ship due to increased resistance, as mentioned above. However, the ship's velocity has actually increased. This could be attributed to the propeller accelerating the ship, since there is less resistance compared with the full load case, and there is less drag on the rudder when fixed amidships. The tug pushing on the shoulder opposes the outward drifting motion natural in ship turning and actually causes the ship to drift toward the inside of the trajectory, as can be seen from Figure 8.4. In minimising the drifting motion, this tug reduces the ship's resistance and since there is a small drifting motion toward the inside of the trajectory, there is a component of the tug force that acts in the direction of motion, thus increasing the ship's velocity, as can be seen from Table 4.8. Obviously, there is a greater component of the tug force acting in the direction of motion when the tug is pushing on the quarter, due to the greater drift angle, but there is little or no acceleration due to the much greater resistance. From these results, it can be concluded that the choice of shoulder or quarter tug is dictated by what change in velocity is desired at the end of the turning manoeuvre.

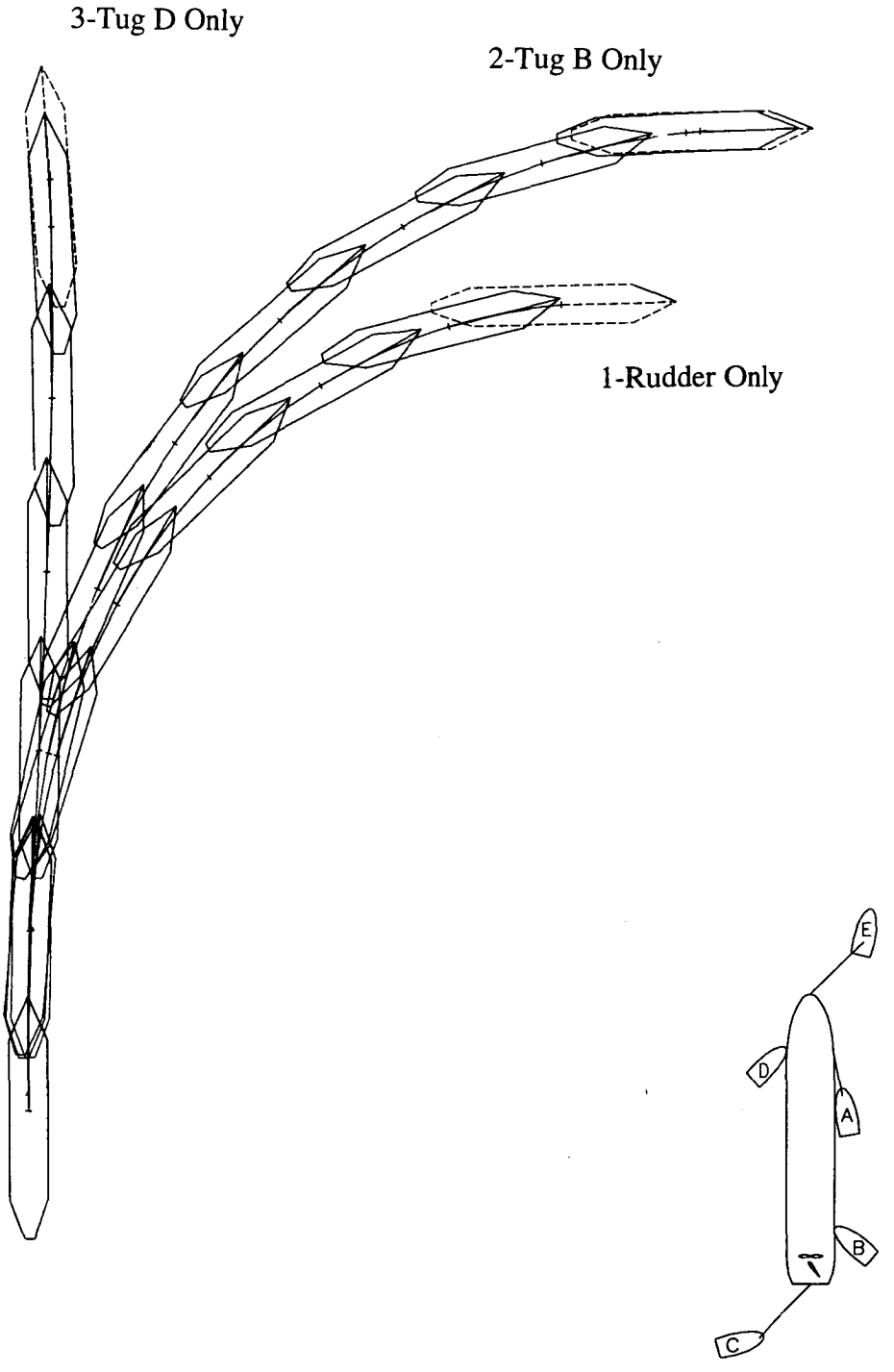

Figure 8.3 Turning Simulations to Compare the Influence of the Rudder with Sway Forces from Tugs Pushing on the Shoulder and Quarter for Full Load in Shallow Water

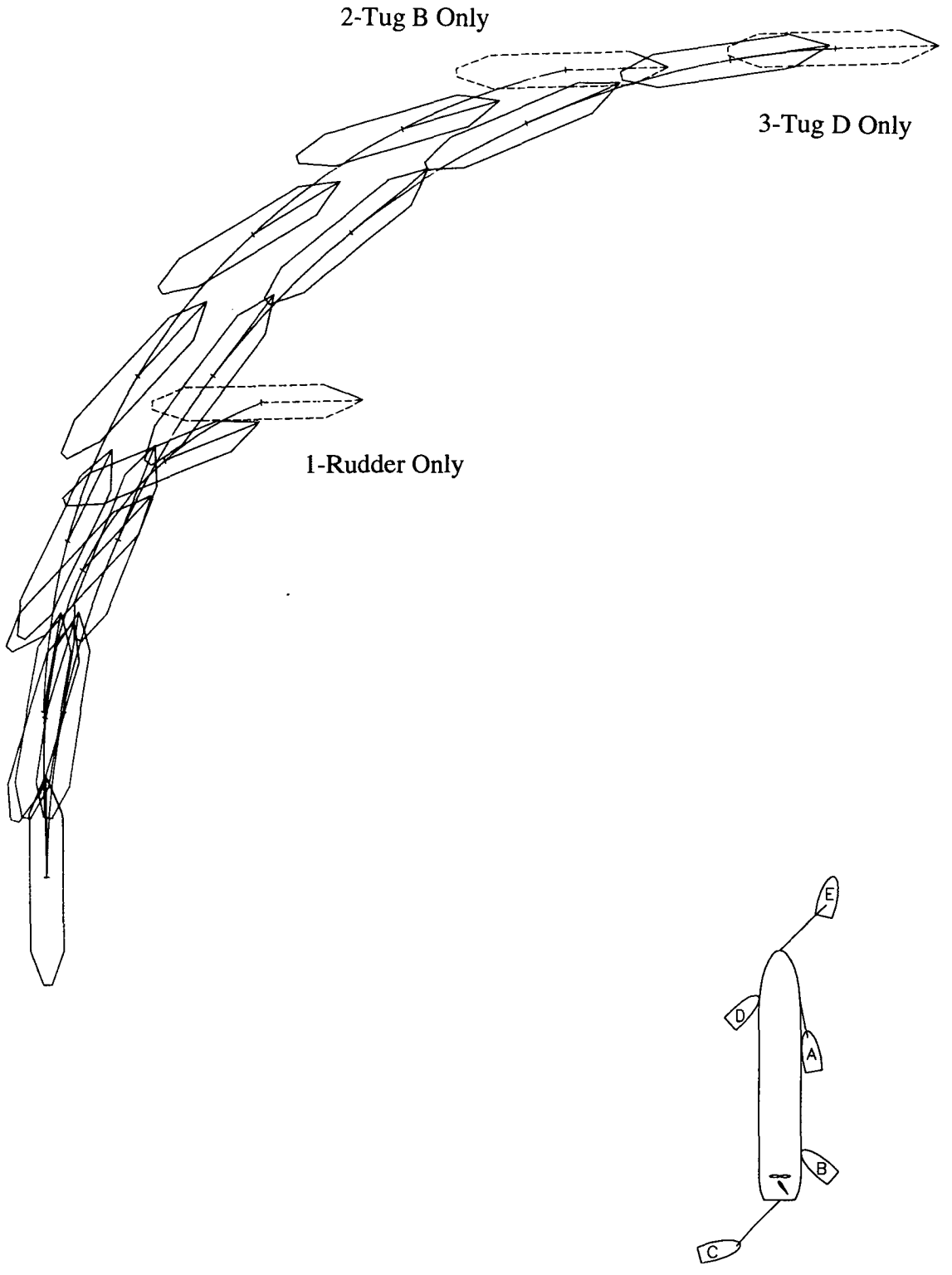

Figure 8.4 Turning Simulations to Compare the Influence of the Rudder with Sway Forces from Tugs Pushing on the Shoulder and Quarter for Ballast in Deep Water

The quite significant differences in turning behaviour for the loading conditions of full load and ballast can be explained in terms of the forces acting on the hull in each case. Insight into the effect of tug forces or manoeuvring forces on ship turning can be gained from application of the linear equations of motion for sway and yaw, Lewis, 1988, to steady turning as follows:

$$\begin{aligned} -Y'_v v' - \left(Y'_r - \Delta'\right) r' &= Y'_{TUG} \\ -N'_v v' - N'_r r' &= N'_{TUG} \end{aligned} \tag{8.1}$$

where the equations are non-dimensionalised in the typical format used in ship manoeuvring, as follows:

$$Y' = \frac{Y}{\frac{1}{2}\rho V^2 L^2} \tag{8.2}$$

$$N' = \frac{N}{\frac{1}{2}\rho V^2 L^3} \tag{8.3}$$

$$\Delta' = \frac{\Delta}{\frac{1}{2}\rho L^3} \tag{8.4}$$

$$v' = \frac{v}{V} \tag{8.5}$$

$$r' = \frac{rL}{V} \tag{8.6}$$

The left hand side of equations 8.1 contain the sway and yaw velocities and the respective stability derivatives, and the right hand side is the applied tug sway force and yaw moment. The moment derivatives can be replaced by the so called *stability levers* and sway derivatives and the *tug* moment may likewise be replaced by a lever and the sway force:

$$\begin{aligned} &\text{hull sway} && l'_v = \frac{N'_v}{Y'_v} \\ &\text{hull yaw} && l'_r = \frac{N'_r}{Y'_r - \Delta'} \\ &\text{tug sway} && l'_{TUG} = \frac{N'_{TUG}}{Y'_{TUG}} \end{aligned} \tag{8.7}$$

Substituting equations 8.7 into equations 8.1 and solving the latter for the rate of turn results in the following:

$$r' = \frac{L}{R} = -\frac{\left(l'_{TUG} - l'_v\right) Y'_{TUG}}{\left(l'_r - l'_v\right)\left(Y'_r - \Delta'\right)} \tag{8.8}$$

where R is the radius of turn and L the ship length. From equation 8.8 it can be seen that the rate of turn or curvature of trajectory is proportional to the tug force and the distance between the location of tug force and the centre of pressure of the sway force and inversely proportional to the terms in the denominator. The first term in the denominator is the dynamic stability criterion which must be positive for a dynamically stable ship. Equation 8.8 relates strictly only to the slope of the $r' - Y'_{TUG}$

curve at the origin and therefore, is only applicable to dynamically stable ships however, the phenomena illustrated is applicable to all ships. The second term in the denominator is the sway force due to yaw including inertia. From equation 8.8 it can be seen that to maximise the influence of the tug force, Y_{TUG}, it should be applied as remote from the location of the sway force, $Y_v v$, as possible.

For conventional ship forms, on even keel in deep or shallow water, Y_v and N_v are both negative that is, $Y_v v$ is centred forward and therefore, for maximum effect, the tug force should be located as far aft as possible. An analogous result to this relating to rudder forces was shown by Crane, 1973 and Lewis, 1988. This explains why the tug pushing on the quarter is more effective than the tug pushing on the shoulder for the simulations performed in the full load condition, as shown in Figure 8.3. This can be explained in simple terms from consideration of the general geometry of the hull and tug forces, as shown in Figure 8.5. The tug pushing on the shoulder causes the ship to sway to starboard creating an opposing hull sway force, $Y_v v$, also centred forward, hence the forces tend to cancel, resulting in little or no net turning moment. Further, if the tug force is aft of the hull sway force, then the ship may actually turn in the direction opposite to that required. The tug pushing on the quarter causes the ship to sway to port creating an opposing hull sway force, $Y_v v$, centred forward which creates a moment that supplements that due to the tug. Indeed, the tug pushing on the ship's quarter acts very much like the ship's rudder, that is, acting as a trigger causing the ship to sway - generating the large $Y_v v$ force, which actually turns the ship. Therefore, it can be concluded that a tug pushing on the quarter of a ship on even keel acts to enhance the ships natural turning mechanism, whereas a tug pushing on the shoulder acts to retard this response.

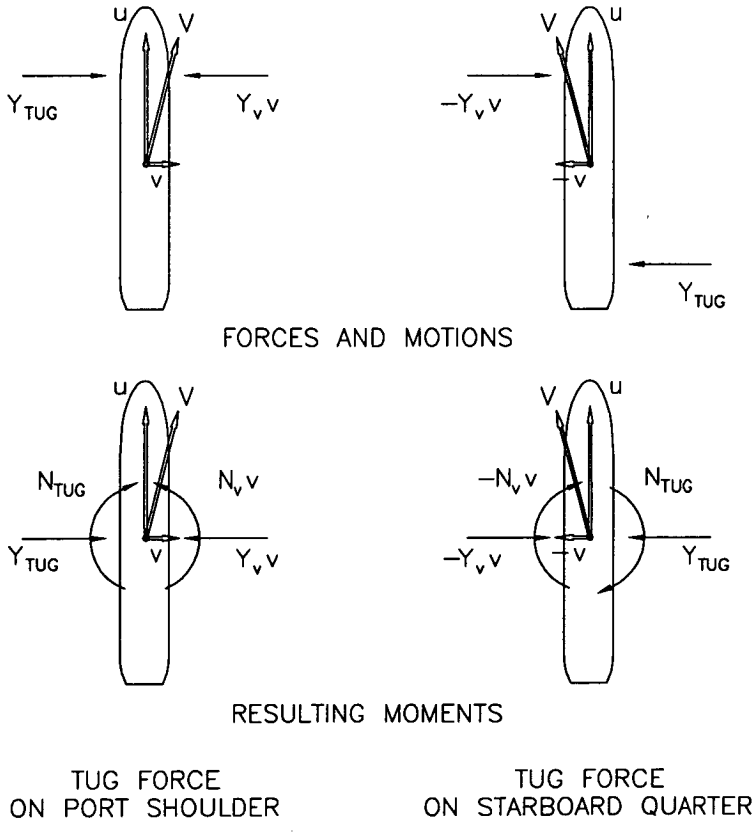

Figure 8.5 General Geometry of Hull and Tug Forces for Turning with the Ship Fully Loaded (Even Keel Condition)

In the case of a ship trimmed by the stern, as in the ballasted load condition, Y_v will be negative but N_v may approach zero and possibly become negative, that is $Y_v v$ may be centred close to midships, as shown by Inoue et al., 1981 and Kijima et al., 1990. According to equation 8.8 this implies that for maximum effectiveness the tug force may be applied as far aft or as far forward as possible. This explains why the tugs pushing on the shoulder and quarter are of similar effectiveness for the simulations with the ship loaded in the ballast condition, that is trimmed by the stern. An analogous diagram to that shown in Figure 8.5 may be drawn to show the general geometry of the forces acting in the ballast condition, as shown in Figure 8.6. The tug pushing on the shoulder causes the ship to sway to starboard creating an opposing hull sway force, $Y_v v$, located in the neighbourhood of midships, therefore the net moment acting is essentially that due to the tug. The tug pushing on the quarter causes the ship to sway to port creating an opposing hull sway force, $Y_v v$, also located in the neighbourhood of midships, therefore, once again, the net moment acting is essentially that due to the tug. Hence, each tug creates similar turning moments but they are enhanced very little by hull forces acting on the ship, that is, the turning moment is only approximately half that produced when the ship is in an even keel condition. Despite the reduced interactive effects, the tugs, and the rudder and propeller are more effective due to reduced inertia and hydrodynamic hull forces in the ballast condition compared with the full load. However, the reduction of turning moment is a fact of some importance, considering it is usually aerodynamic forces that are critical in the handling of ballasted ships.

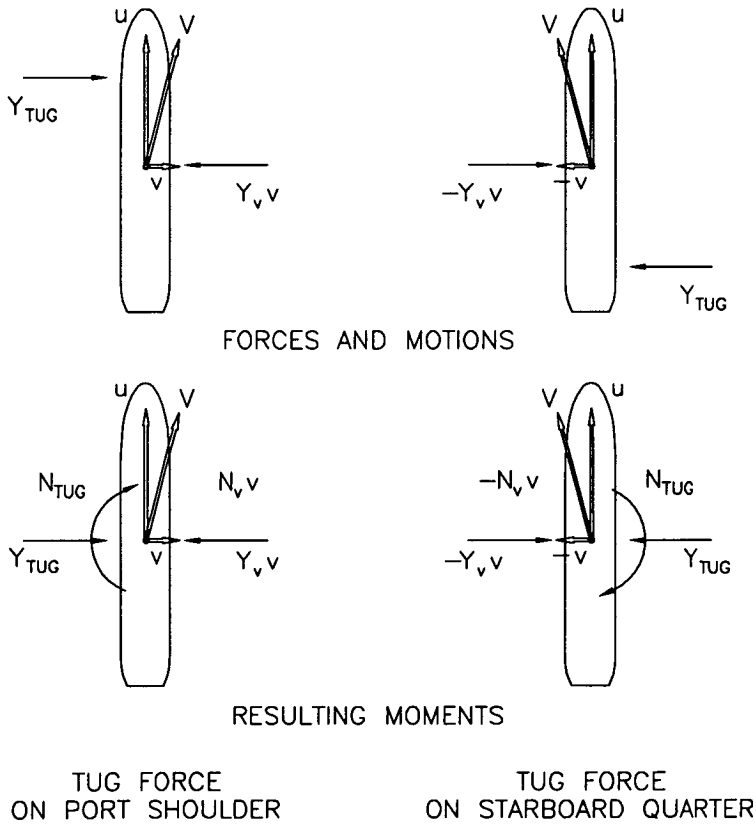

Figure 8.6 General Geometry of Hull and Tug Forces for Turning with the Ship Ballasted (Trimmed Condition)

8.3 Influence of Surge and Sway Forces

The results from simulations 5, 6, 7, 8, 9 and 10 for the loading conditions of full load and ballast are presented in Figures 8.7 and 8.8 respectively. Simulation 4, for each load case, is superimposed on each of the above simulations to allow comparison of the effectiveness of each of the tug deployments with that of the rudder combined with propeller boost. Relevant parameters from each of the simulations are presented in Table 8.5.

Simulation	Time (mins)	Final Speed (knots)	Advance (ship lengths)	Transfer (ship lengths)
Full Load, Depth/Draft = 1.2				
4	8.2	3.9	2.3	1.6
5	8.0	2.7	2.0	1.2
6	7.0	3.6	2.0	1.3
7	7.1	2.8	1.8	1.1
8	7.9	4.1	2.3	1.6
9	7.5	4.5	2.3	1.6
10	6.1	1.7	1.4	0.7
Ballast, Deep Water				
4	4.9	4.2	1.7	0.7
5	4.5	2.5	1.3	0.4
6	4.2	3.9	1.5	0.6
7	4.0	2.8	1.3	0.4
8	4.0	4.2	1.4	0.7
9	4.0	5.0	1.5	0.7
10	3.3	1.6	0.9	0.1

Table 8.5 Parameters from Turning Simulations to Compare the Influence of Surge and Sway Forces from Various Tug Deployments through a Turn Using Combined Rudder and Propeller Boost

Considering initially the simulations with the ship in the full load condition. From Figure 8.7 and Table 8.5, it can be seen that the tug deployments used in simulations 5, 6, and 7 significantly reduce the advance and transfer compared with using the rudder and propeller alone. In contrast, those used in simulations 8 and 9 do little to reduce the advance and transfer compared with using the rudder and propeller alone. Differences in the trajectories can be explained in terms of whether the tugs act to enhance or retard the ship's inherent turning mechanisms. As discussed above, for a ship on even keel, hull forces play a greater role in turning the ship compared with one trimmed by the stern, as in the ballast load condition. Therefore, to minimise the advance and transfer, tugs must be deployed such that they supplement the development of hull forces. This involves the use of tugs to not only create a turning moment but also to increase the ship's drift angle thus increasing sway damping forces and moments. The drift angle may be increased by increasing the ship's sway velocity in comparison to its surge velocity. Once again, use of propeller boost to improve rudder performance is only effective if the tugs are deployed such that they supplement this mechanism. Clearly, if the ship is accelerated by a particular tug deployment then the propeller race velocity will be reduced thus decreasing the rudder's effectiveness. Considering these factors it is possible to explain relative differences in tug effectiveness for each of the deployments used in the simulations.

Comparison of the advance and transfer values from Tables 8.4 and 8.5 for simulations 1 and 4 show the significant improvement in turning performance achieved from using propeller boost. This demonstrates the effectiveness of this mechanism and why it is universally used by the marine pilot in situations where the advance and transfer are to be minimised. Therefore, it is in this situation that the effects of various tug deployments are of most interest.

Figure 8.7(a), comparing simulations 4 and 5, shows the improvement in advance and transfer using a tug made fast on the starboard shoulder pulling aft. This tug deployment, although creating only a small turning moment, is particularly effective due to the braking force applied. This reduces the ship velocity which increases the propeller race velocity thus increasing rudder lift and drag forces. The application of a braking force may also be looked upon as reducing the surge velocity in comparison to the sway velocity thus increasing the drift angle and the resulting sway damping moment. This deployment therefore makes indirect use of the tug force to improve the net turning moment.

Figure 8.7(b), comparing simulations 4 and 6, shows the improvement in advance and transfer using a tug pushing on the starboard quarter. A pure sway force is applied using this tug deployment, hence no improvement in propeller race effect on the rudder is achieved. However, a turning moment is directly applied and since its application is such that it causes the ship to sway to port, it increases the drift angle and therefore, the sway damping moment, as detailed in the previous section.

Figure 8.7(c), comparing simulations 4 and 7, shows the improvement in advance and transfer using a tug pulling off the port quarter. With this tug deployment, a combined braking and sway force is applied to the ship which takes advantage of both the mechanisms used by each of the deployments described above. From the results, it can be seen that this is the most effective of all the deployments considered in reducing the advance and transfer. It is also the most effective in reducing speed through the turn (although this may not always be desired) due to the braking force applied and the increase in resistance resulting from the increased drift angle.

Figure 8.7(d), comparing simulations 4 and 8, shows that a tug pushing on the port shoulder has essentially no effect in reducing the advance and transfer through a boosted turn. The same moment is applied to the ship in this deployment as is applied with a tug pushing on the quarter. However, since the applied force acts to reduce the drift angle or acts close to the ship's sway force centre of pressure, it tends to oppose the ship's inherent turning mechanism and thus, contribute little to actually turning the ship, as detailed in the previous section.

Finally, Figure 8.7(e), comparing simulations 4 and 9, shows that a tug made fast forward and pulling off the starboard bow has essentially no effect in reducing the advance and transfer through a boosted turn. This deployment in applying an accelerating force and a force tending to cause the ship to sway to starboard tends to oppose the influence of both the hull damping moment and the propeller race effect. That is, the accelerating force increases ship velocity thus reducing the propeller race velocity and reducing the drift angle, and the sway force reduces the drift angle similar to the tug pushing on the port shoulder.

In summary, from the results it can be seen that tug deployments A, B and C, as shown in Figure 8.2, are the most effective in reducing the advance and transfer through a boosted turn. There is little difference in the improvements in advance and transfer between each deployment but there is some differences in the final velocities. From Table 8.5, it can be seen that deployments A and C reduce the velocity significantly since a braking force is applied, whereas, deployment B in applying a pure sway force results in less reduction in speed. From this, a deployment may be chosen compatible with the desired velocity loss through the turn. Given the most effective tug deployments, it is of interest as to what effect these combined have on the boosted turn as performed in simulation 10. The trajectories of simulations 4 and 10 are compared as shown in Figure 8.7(f). For a ship turning in shallow water where drift angles and rates of turn are relatively small it might be expected that hull forces and moments do not extend significantly into the non-linear range. From the results given in Table 8.5 it can be seen that the ship's response is close to linear. This indicates that there is no apparent limit to the improvement in turning performance that can be gained from increasing the number or power of tugs deployed.

A particularly interesting outcome of these results is that the traditional and ubiquitous tug deployments D and E, as shown in Figure 8.2 are essentially redundant in reducing the advance and transfer through a boosted turn. Furthermore, they also notably increase the velocity at the completion of the turn. Both of these outcomes are of significant importance in the development of ship handling techniques.

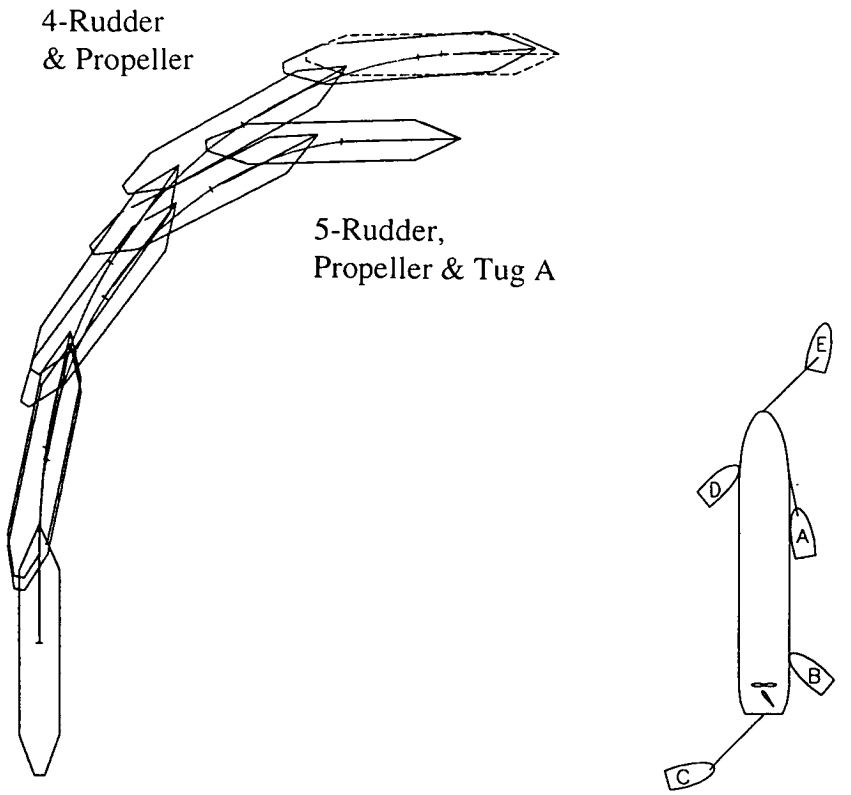

(a) Comparison of Simulations 4 and 5

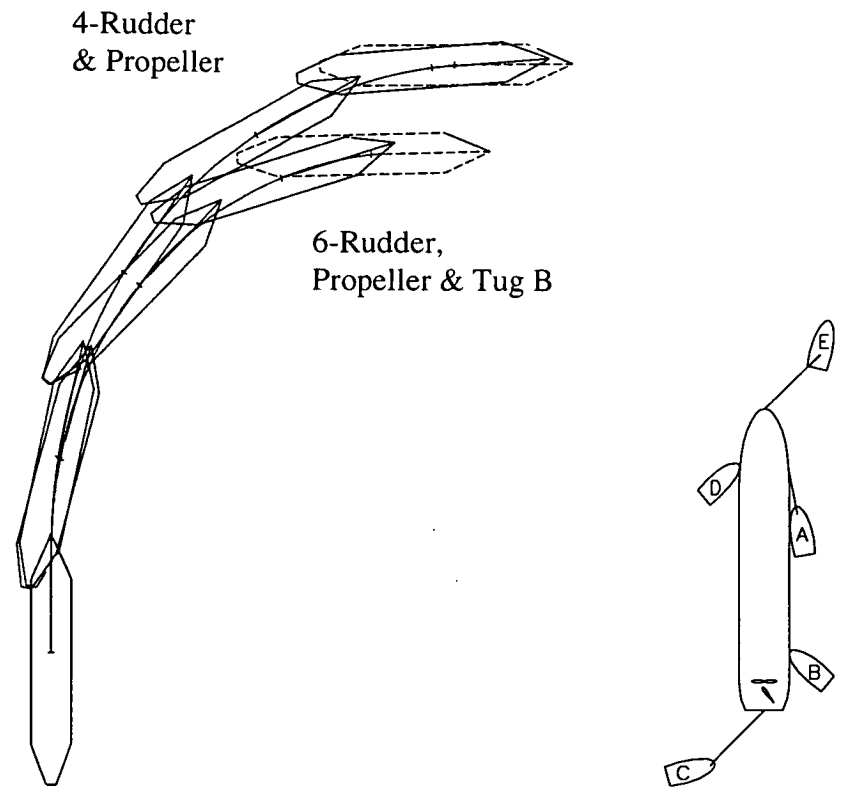

(b) Comparison of Simulations 4 and 6

Figure 8.7 Turning Simulations to Compare the Influence of Surge and Sway Forces from Various Tug Deployments through a Turn Using Combined Rudder and Propeller Boost for Full Load in Shallow Water

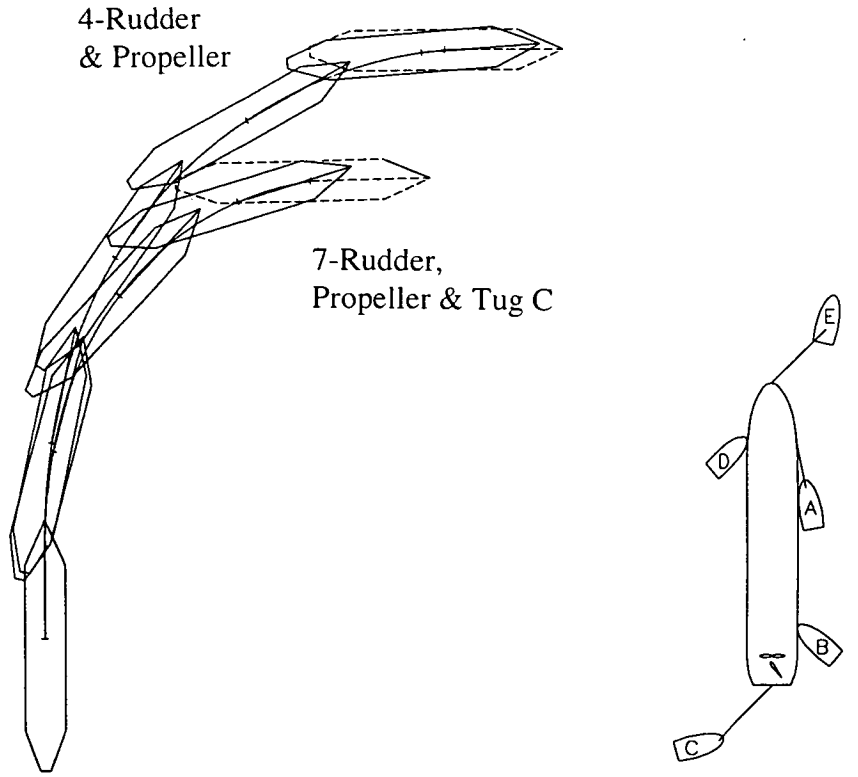

(c) Comparison of Simulations 4 and 7

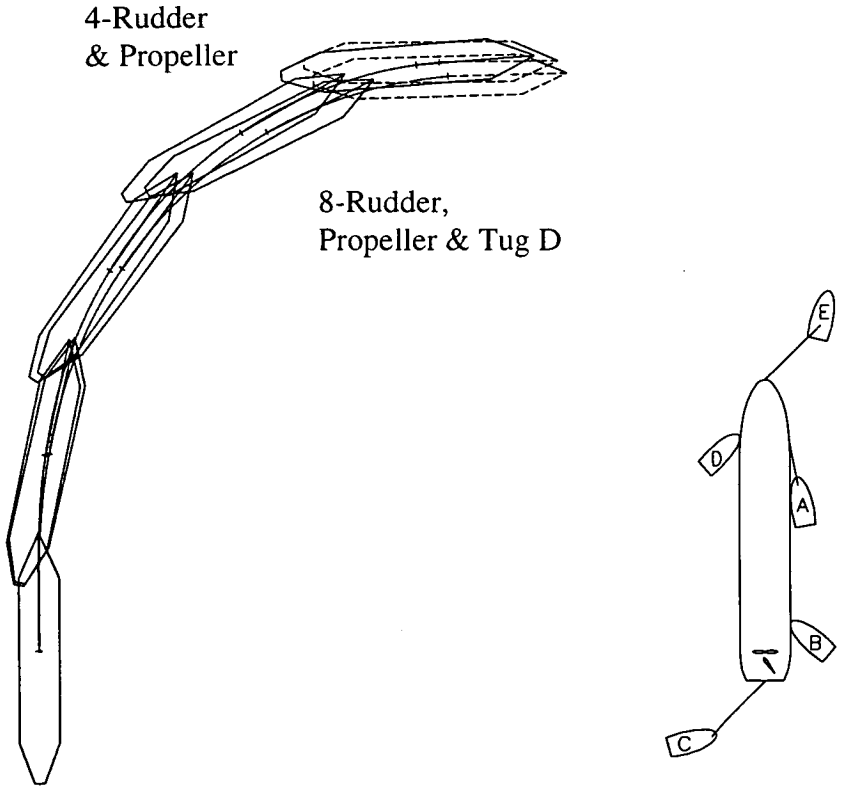

(d) Comparison of Simulations 4 and 8

Figure 8.7 Turning Simulations to Compare the Influence of Surge and Sway Forces from Various Tug Deployments through a Turn Using Combined Rudder and Propeller Boost for Full Load in Shallow Water

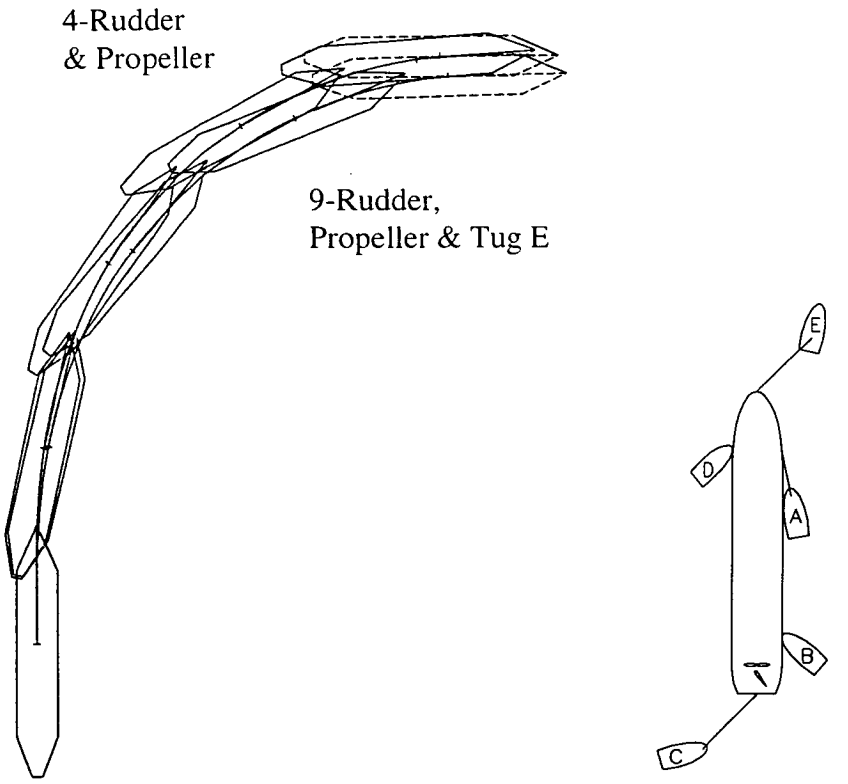

(e) Comparison of Simulations 4 and 9

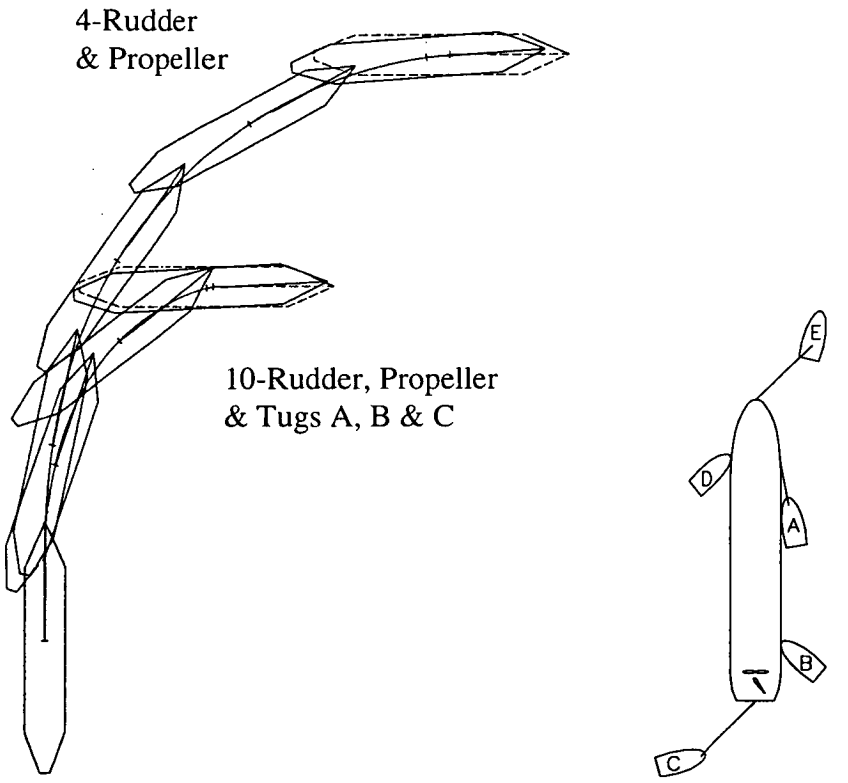

(f) Comparison of Simulations 4 and 10

Figure 8.7 Turning Simulations to Compare the Influence of Surge and Sway Forces from Various Tug Deployments through a Turn Using Combined Rudder and Propeller Boost for Full Load in Shallow Water

Considering now the simulations with the ship in the ballast condition. From Figure 8.8 and Table 8.5, it can be seen that unlike the loaded case, each of the tug deployments considered has a noticeable effect on reducing the advance and transfer, compared with using the rudder and propeller alone. As discussed in the previous section, hull forces do not play as greater role in turning the ship in the ballast condition which is trimmed by the stern as they do in the loaded condition, where the ship is on an even keel. Not only do hull forces play a reduced role due to their geometry, but also, due to their significant reduction, along with the ship's inertia. Therefore, tug forces have a greater effect, and the constraints on their use relating to compatibility with hull forces in the loaded condition are relaxed. Comparison of the results for the loaded and ballast conditions, shows clearly the considerable reduction in advance and transfer in the ballast condition, due to increased propeller, rudder and tug effectiveness due to reduced hull forces and inertia. From Figure 8.8 and Table 8.5, it can be seen that the various tug deployments can be effectively used to control variations in the advance and transfer, as well as the final velocity.

From the results it can be seen that the most effective deployments are those where a braking force is applied, that is deployments A and C, as shown in Figure 8.2. The ship trajectories using each of these deployments are shown in Figures 8.8(a) and (c) respectively. The application of a braking force reduces the ship's velocity increasing the propeller race velocity, thus increasing rudder lift and drag, similarly with the full loaded case. Deployments A and C, in applying a braking force, also cause the greatest reduction in the final velocity, as shown in Table 8.5.

The two deployments where the tugs are pushing give very similar results, as can be seen from Figures 8.8(b) and (d) and Table 8.5. In applying pure sway forces these deployments provide no direct enhancement of propeller race effects and only slightly effect the ship's final velocity. Each deployment provides the same turning moment and since there are only small interactive effects with ship hull forces, as described in the previous section, the resulting ship trajectories are similar. The slight difference in final velocity is a result of the tug pushing on the quarter, increasing the ship's drift angle and hence the induced resistance, whereas the tug pushing on the shoulder decreases the ship's drift angle and hence the induced resistance. With these deployments, the advance is significantly reduced compared with using the rudder and propeller alone, but since there is no braking force applied there is little reduction in the transfer.

Finally, the last deployment considered where a tug is made fast forward pulling off the starboard bow is least effective in reducing the advance and transfer compared with using the rudder and propeller alone, as can be seen from Table 8.5 and Figure 8.8(e). The application of an accelerating force reduces the propeller race effect and hence the rudder effectiveness. As with the pushing deployments discussed above, the absence of a braking force results in little improvement in the transfer compared with using the rudder and propeller alone. The combination of a force to starboard reducing the drift angle and an accelerating force significantly increases the final velocity. This may be a desired outcome for ship manoeuvring in the ballast condition since, as mentioned above, generally large aerodynamic forces affect the ship in this condition, hence high velocity is sought for favourable controllability.

In summary, as with the loaded case, the deployments where a braking force is applied are most effective in reducing the advance and transfer and the final velocity. Furthermore, deployments A, B and C are the most effective, as with the full load case, however, there is much less difference between these and the other deployments in this case. In situations where minimal variation in velocity and reduced advance in particular is sought, then deployments B and D are appropriate. In situations where an increase in velocity is sought and a reduction in advance only is tolerable, then deployment E is appropriate. Similarly with the loaded case, the ship's response to combined tug deployments A, B and C is of interest, as per simulation 10 shown in Figure 8.8(f). From Figure 8.8(f) and Table 8.5 it can be seen that despite the larger drift angles and rates of turn for a deep water manoeuvre, the ship's response to combined deployments is approximately linear.

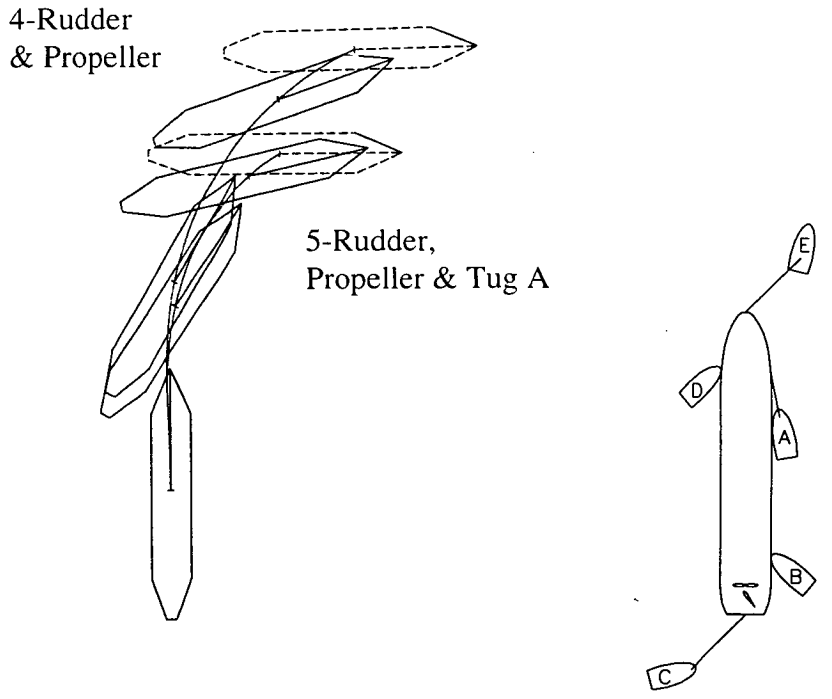

(a) Comparison of Simulations 4 and 5

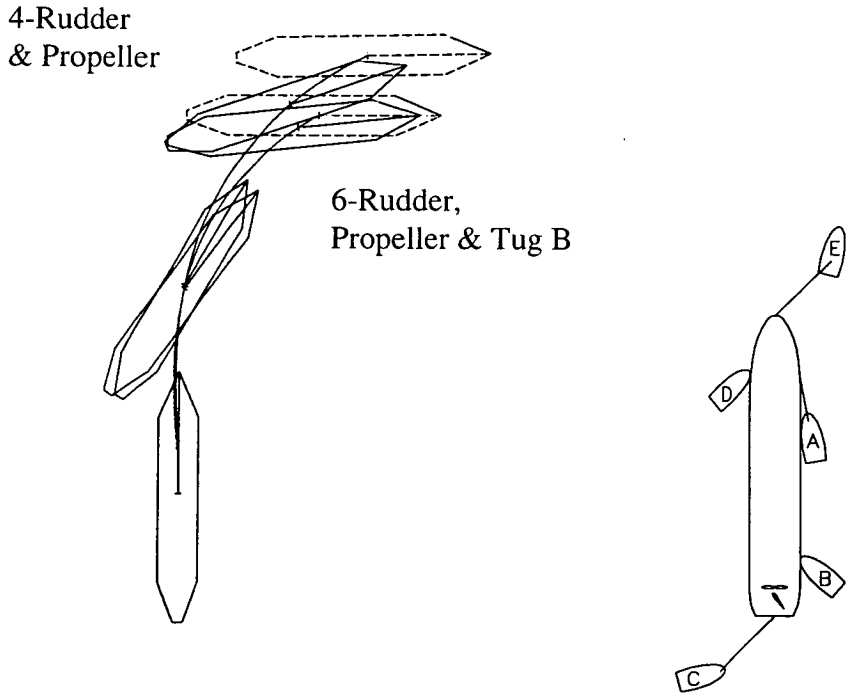

(b) Comparison of Simulations 4 and 6

Figure 8.8 Turning Simulations to Compare the Influence of Surge and Sway Forces from Various Tug Deployments through a Turn Using Combined Rudder and Propeller Boost for Ballast in Deep Water

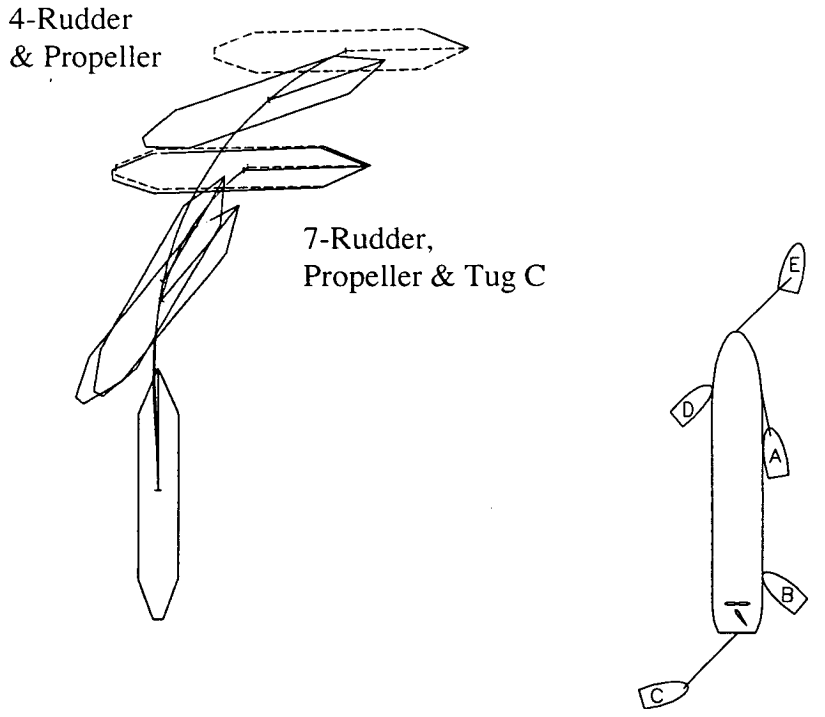

(c) Comparison of Simulations 4 and 7

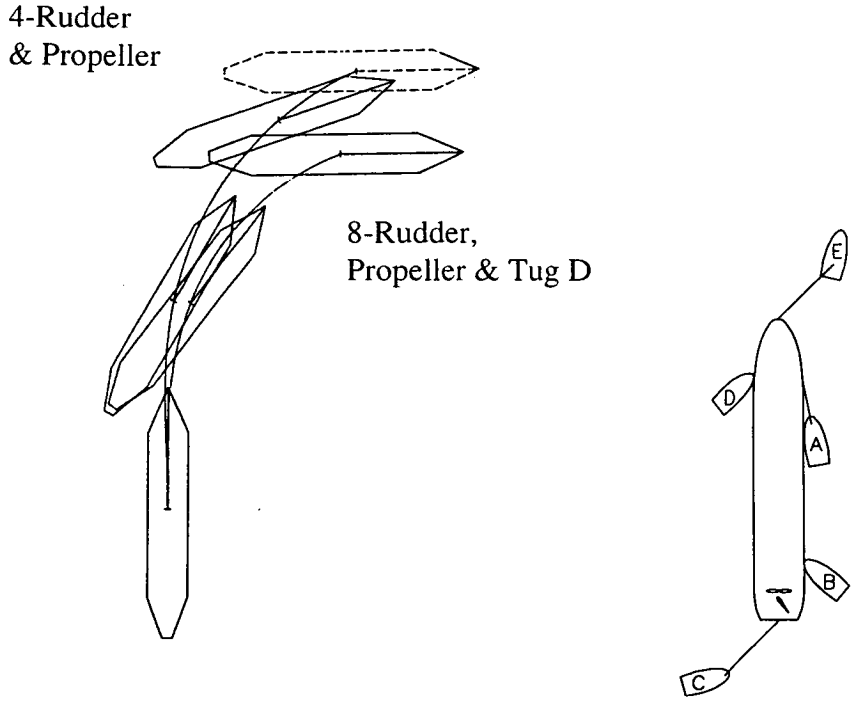

(d) Comparison of Simulations 4 and 8

Figure 8.8 Turning Simulations to Compare the Influence of Surge and Sway Forces from Various Tug Deployments through a Turn Using Combined Rudder and Propeller Boost for Ballast in Deep Water

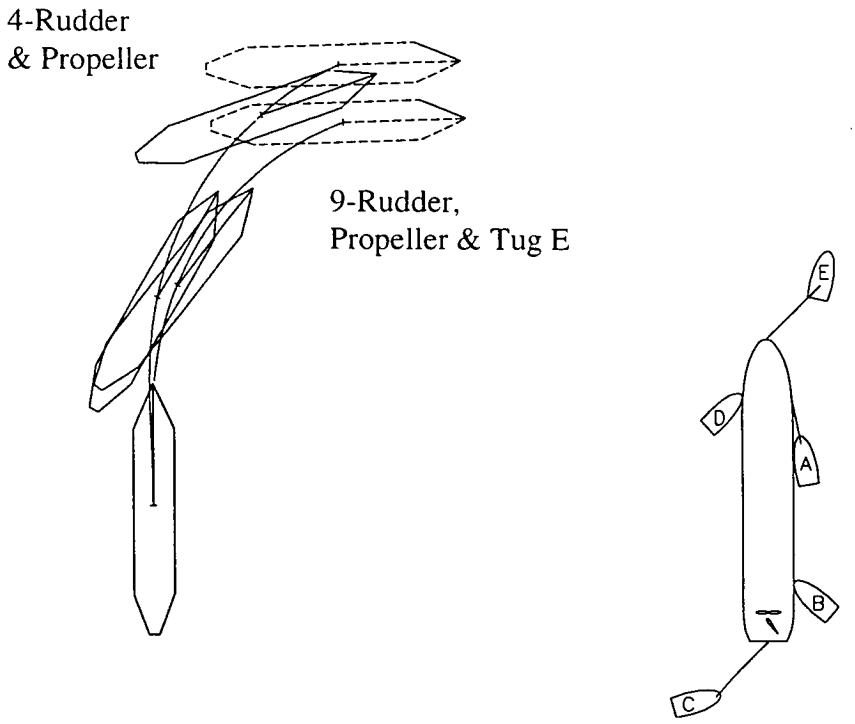

(e) Comparison of Simulations 4 and 9

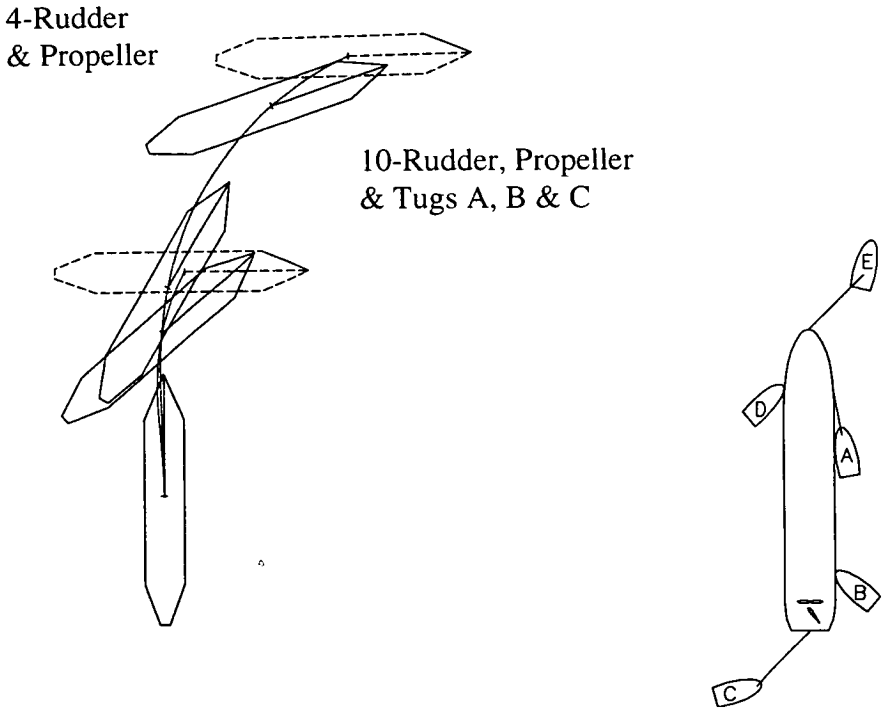

(f) Comparison of Simulations 4 and 10

Figure 8.8 Turning Simulations to Compare the Influence of Surge and Sway Forces from Various Tug Deployments through a Turn Using Combined Rudder and Propeller Boost for Ballast in Deep Water

9 CONCLUSIONS

The present work has involved the development of a largely empirical manoeuvring model for omni-directional stern drive tugs. Quasi-steady predictions of available tug forces have been derived from the model, however it is also suitable for extension to solution in the time domain, as may be desired for real time simulation. The model is modular and physically motivated, hence investigations have involved a systematic study of hydrodynamic characteristics affecting tug performance, namely:

- hull forces;
- thruster forces;
- interaction between thrusters; and
- interaction between thrusters and hull.

A series of model experiments were designed to isolate each of the above characteristics. Experiments were carried out with bare tug hulls to measure forces acting in the absence of appendages. A range of parameters were involved, including tests with two significantly different hull models for this type of vessel to assess the effect of hull geometry. Open water characteristics of a single thruster were measured and to obtain the effects of thruster-thruster interaction, open water tests with two thrusters together were carried out. Thruster-thruster interactions were quantified by comparison of the open water characteristics from tests with a single thruster with those for two thrusters. A semi-empirical method was developed to represent thruster-thruster interactions. To determine interactions between the thrusters and the hull, thrusters were fitted to the hull and free running model experiments where performed. Total tug forces, as well as thruster forces were measured for when the tug model was both pushing and pulling. Using equilibrium it was possible to determine forces acting on the tug hull. The influence of the thrusters on the hull was quantified by comparison of the derived forces acting on the appended hull with those acting on the bare hull determined from earlier experiments. The influence of the hull on the thrusters and on interaction between thrusters was quantified by comparison of the measured behind hull characteristics with those measured on one and two thrusters in open water. Conclusions drawn from each of the model experiments designed to investigate the characteristics listed above are detailed below.

Two areas of critical interest to tug operators, marine pilots and simulation analysts in the development of ship handling techniques were then investigated, namely;

- predictions of quasi-steady tug forces; and
- the influence of tug forces on ship motions.

Results derived from the model experiments were used in the mathematical model mentioned above to assess the quasi-steady capabilities of omni-directional stern drive tugs in various modes of operation. Given predictions for tug forces, a number of simulations were performed to assess the effects of commonly used tug deployments on the turning performance of a very large bulk carrier in both ballast and full load conditions in deep and shallow water respectively. Conclusions drawn from each of these investigations are given below.

Finally, some recommendations for future investigations are given.

9.1 Hull Forces

1. Non-dimensional hull forces measured as part of the present investigation are independent of the Froude Number in the speed range applicable to normal harbour shiphandling.

2. Hull forces non-dimensionalised using parameters appropriate to the relevant profile areas as the reference areas are essentially independent of expected variations in the ratios of length, beam and draft. This allows generic predictions to be made for hulls similar to the ones tested as part of the present investigation.

3. Surge forces exhibit much more variation with drift angle and hull form and are much smaller compared with sway forces.

4. Unlike the smooth lifting characteristics of slender ship forms, two discontinuities are present in the variation of sway force with drift angle indicating stall for when the stem is the leading edge and for when the stern is the leading edge.

9.2 Thruster Forces

1. In positive flow conditions (small angles of attack), thrusters generate relatively small forces and torques due to small propeller blade angles of attack. In negative flow conditions (large angles of attack), thrusters generate relatively large forces and torques due to increased propeller blade angles of attack and increased drag of the strut, gear-case and duct supporting fins.

2. The geometry of the strut, gear-case and duct supporting fins has only a marginal effect on thrust characteristics in positive flow conditions (small angles of attack) but a large effect on thrust characteristics in negative flow conditions (large angles of attack). These differences are presumably due to flow separation effects and the resulting variations in inflow conditions to the propeller.

9.3 Interaction Between Thrusters

1. The effects of interaction between thrusters is essentially confined to the downstream thruster which is affected by the high energy part of the upstream thruster's induced flow field.

2. At the thruster spacing tested, loss of thrust due interaction may be up to 60% of that achieved with an isolated thruster for the same conditions of operation.

3. In general, the effects of interaction are smaller when the horizontal axes of the thrusters are close to being perpendicular to the line connecting the thruster axes of rotation and large when they are close to being aligned with the line connecting the thruster axes of rotation.

4. At the thruster spacing tested, interaction between thrusters may be looked upon as the result of three distinct effects, namely: race impingement, race wake effects and flow rectification or flow straightening effects.

5. The modes of tug operation where interaction between thrusters has a significant effect include pulling with the forward tow point in the direct and indirect modes.

6. The developed semi-empirical mathematical model for interaction between thrusters satisfactorily predicts trends in the range of advance angles appropriate to tug operation.

9.4 Interaction Between Thrusters and Hull

1. The interaction between thrusters and hull may be considered in four quadrants of thruster angle and drift angle, i.e.:

   - 1st quadrant — running ahead, thrust ahead
     $0° \geq \beta_H \geq -90°, 0° \leq \delta \leq 90°$;
   - 2nd quadrant — running ahead, thrust astern
     $0° \geq \beta_H \geq -90°, 90° \leq \delta \leq 180°$;
   - 3rd quadrant — running astern, thrust astern
     $-90° \geq \beta_H \geq -180°, 90° \leq \delta \leq 180°$; and
   - 4th quadrant — running astern, thrust ahead
     $-90° \geq \beta_H \geq -180°, 0° \leq \delta \leq 90°$.

   The first three quadrants contain practical combinations of these angles although combinations in the third are uncommon.

2. In the first quadrant, the effect of the thrusters on the hull is small since the hull is influenced only by the low energy part of the flow field induced by the thrusters. In contrast the thrusters are significantly effected by the hull since they are operating in the wake of the hull or the thruster inflow is drawn locally from about the hull. Interactions between thrusters in this quadrant are negligible compared to the influence of the hull on the thrusters.

3. The influence of the hull on the effective surge and sway velocities at each thruster location, in the first quadrant, may be satisfactorily represented as linear functions of the drift angle.

4. In the second quadrant, the effect of the thrusters on the hull is significant since the hull is affected by the high energy part of the induced flow field. This is due to direct impingement of the propeller race on the hull, as well as interference drag from the obstruction to the free stream created by the counter-flowing propeller race. Interference drag effects are essentially confined to influencing hull surge forces. The thruster inflow in this quadrant is drawn from the free stream remotely about the hull and therefore the effect of the hull on the thrusters is small. Interaction between thrusters is large in this quadrant and the influence of the hull on this is small.

5. Forces acting on the hull due to the influence of the thrusters in the second quadrant may be satisfactorily represented as linear functions of the thruster angle and advance angle.

9.5 Predictions of Tug Forces

1. Four practical modes of operation can be identified for omni-directional stern drive tugs, namely:

   - pushing;
   - pulling with forward tow point-direct;
   - pulling with forward tow point-indirect; and
   - pulling with aft tow point.

   Different thrusters (with the same nominal force at zero speed) significantly effect net tug forces only for pulling with the forward tow point abaft the ship's beam. For the remaining modes of operation, different thrusters have very little effect on net tug forces. In these modes, thrusters operate in positive flow conditions, where there are only small differences in characteristics between thrusters with differing geometries. Pulling direct with the forward tow point is the only situation where the thrusters are operating in negative flow conditions-where there are significant differences in characteristics between thrusters with differing geometries.

2. A tug operating in the pushing mode should be able to impart a force of the order of its bollard pull over the full range of shiphandling speeds and this force is always at approximately 90° to the ship's heading. The ability of the tug to operate effectively in this mode is due to the hull acting as a crude lifting surface at higher speeds supplementing loss of thruster forces.

3. A tug pulling direct with the forward tow point should be able to impart forces of the order of its bollard pull, up to speeds such that hull forces become similar in magnitude to thruster forces. In this mode, thruster and hull forces oppose each other such that at higher speeds they tend to cancel.

4. A tug pulling indirect with the forward tow point should be able to impart forces of the order of its bollard pull at speeds above those where hull forces become greater than thruster forces, however, this ability may be limited by the tug's heel.

5. A tug pulling with the aft tow point should be able to impart forces of the order of its bollard pull over the full range of shiphandling speeds, however, this ability may be limited by the tug's heel and position keeping ability.

6. A tug pulling with the aft tow point will be acted upon by greater overturning moments than other modes of operation due to the geometry of the forces acting at the tow point, hull lateral centre of pressure and thrusters. For pulling with the aft tow point, the tow point lies between the hull force and the thruster location whereas, for the other modes of operation, the location of the hull force lies between the tow point (or point of contact on the fenders) and the thruster location.

7. The stability of equilibrium or position keeping ability of omni-directional stern drive tugs may be summarised for each mode of operation as follows:

• pushing	stable;
• pulling with forward tow point-direct	unstable for operation forward of the ships beam;
• pulling with forward tow point-direct	stable for operation abaft the ships beam;
• pulling with forward tow point-indirect	stable; and
• pulling with aft tow point	marginally unstable.

This indicates that, for pulling with the forward tow point once the stern becomes the leading edge, the tug's equilibrium becomes unstable hence explaining the lack of use of this mode.

9.6 The Influence of Tug Forces on Ship Motions

1. For tugs to minimise the advance and transfer in turning manoeuvres when the ship is loaded on even keel in deep or shallow water, forces should be applied such that:

   • they increase sway toward the outside of the turn increasing the drift angle and therefore enhancing the ship's natural turning mechanism; and

   • they slow the ship which indirectly enhances the ship's natural turning mechanism by improving rudder effectiveness and increasing the drift angle.

2. The five common tug deployments considered in this work may be rated in terms of their effectiveness in reducing the advance and transfer in a turning manoeuvre, for a ship loaded on even keel in deep or shallow water, as follows, for a turn to starboard:

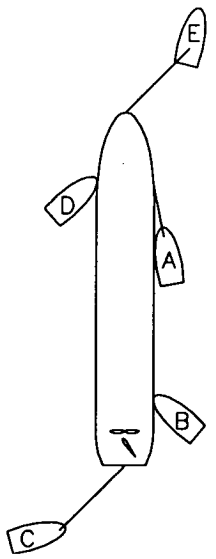

1 C-Centre lead aft-pulling off port quarter
2 A-Starboard shoulder-pulling aft
3 B-Starboard quarter-pushing
4 E-Headline-pulling off starboard shoulder
5 D-Port shoulder-pushing

The first three deployments are particularly effective whereas the last two are essentially redundant.

3. For a ballasted ship, i.e. trimmed by the stern, tug forces may be applied such that they cause the ship to sway toward the inside or outside of the turn and still reduce the advance and transfer. This is due to the lesser role played by ship hull forces for turning in this condition compared with the even keel case. Tug forces may also be applied such that they accelerate or decelerate the ship through the turn depending on the desired final velocity, with relatively little influence on the trajectory.

4. The five common tug deployments considered in this work rate in the same order in their effectiveness in reducing the advance and transfer through a turning manoeuvre in the ballast loading condition, as they do for the fully loaded condition. However, in the case of the ballast condition, there is considerably less difference between the effectiveness of each deployment, that is, all tug deployments are effective in reducing the advance and transfer.

9.7 Future Work

The present work has demonstrated the complexity of the phenomena involved in developing a hydrodynamic model for omni-directional stern drive tug performance. The approach used has been largely experimental, however in the future, numerical methods will no doubt provide greater opportunities for more detailed investigations. Areas of particular interest include-development of thruster characteristics in oblique flow with changing appendage geometries, interaction between thrusters at close spacing and interaction between thrusters and hull.

An area of particular interest in ship manoeuvring simulation is ship-waterway interactions, and the presence of assisting tugs possibly play a part in this, as they may also be significantly affected by it. Mariners are well aware of confinement affects due to e.g. blockage and fluid memory effects and what effect they have on the ship and assisting tugs, However, often these effects are either not simulated or they are only partially accounted for. As more is learnt of these effects it will be of interest to consider how the ship assist tug may be involved.

Finally, with the acceptance and still growing interest in escort tugs to safe guard tankers against environmentally damaging accidents, time domain simulation of omni-directional drive tugs may be increasingly required. The ability to simulate the operation of these vessels alongside a tanker underway is a powerful tool in assessing both their capabilities and the development of operational procedures. The mathematical model developed as part of the present investigation may be relatively easily extended for such purposes.

BIBLIOGRAPHY

Abramovich, G.N., *The Theory of Turbulent Jets*, (English Edition), MIT Press, Cambridge, Mass., 1960.

Adachi, H. and Sugai, N., *On the Thrust Deduction Coefficient-Consideration on the Thrust Augmentation as a Function of Propeller Load*, Journal of the Kansai Society of Naval Architects, Japan, No. 171, Nov. 1978.

Ankudinov, V., Kaplan, P. and Jacobsen, B.K., *Assesment and Principal Structure of the Modular Mathematical Model for Ship Manoeuvrability Prediction and Real-Time Manoeuvring Simulations*, Proceedings of MARSIM'93 International Conference on Marine Simulation and Ship Manoeuvrability, St. John's, Canada, Sept. 26-Oct. 2, 1993.

Armstrong, T., *On the Actual Performance of Tugs*, Proceedings of the 10th International Tug Convention, Sydney, Aust., 1988, pp. 57-74.

Ashburner, R.H.le F. and Norrbin, N.H., *Tug Assisted Stopping of Large Ships in the Suez Canal - A Study of Safe Handling Techniques*, Proceedings of the International Symposium on Ocean Engineering Ship Handling, Gothenburg, Sweden, 1980, Paper No. 14.

Baer, W., *Der Voith-Wassertrecker*, Hansa 90, 1953, pp 114-117.

Baer, W., *Influence of the Location of the Towing Hook in the Voith Water Tractor on Safety and Performance*, Proceedings of the 2nd International Tug Convention, London, U.K., 1971.

Baer, W., *Safety in Towing*, Proceedings of the 1st North American Tug Convention, Vancouver, Canada, 1973. (or International Tug Conference Papers by Baer, W., Voith Brochure ts 2176 e).

Bogaerts, M.P., de Vries, W.A., Boer, J.P.A. and Perdok, J., *Simulation of Lock Entry Manoeuvres*, Proceedings of the 4th International Conference on Marine Simulation, Trondheim, Norway, 1987, pp. 216-225.

van den Boom, H.J.J. and Nienhuis, U., *Hydrodynamic Analysis of Dynamically Positioned Vessels*, Proceedings of International Workshop on Ship and Platform Motions, Berkeley, U.S.A., 1983.

Brandner, P.A., *Hydrodynamics of Shiphandling Tugs*, Proceedings of the 11th Australasian Fluid Mechanics Conference, Hobart, Aust., Dec. 14-18, 1992, pp. 651-654.

Brandner, P.A. and Renilson, M.R., *Simulation of Shiphandling Using Omni-directional Stern Drive Tugs*, Proceedings of MARSIM'93 International Conference on Marine Simulation and Ship Manoeuvrability, St. John's, Canada, Sept. 26-Oct. 2, 1993, pp. 49-58.

Brandner, P.A. and Renilson, M.R., *Hydrodynamic Aspects of Shiphandling Tugs*, Proceedings of the 3rd International Conference on Manoeuvring and Control of Marine Craft, Southampton, U.K., Jul. 7-9, 1994, pp. 335-348.

Brandner, P.A. and Tasker, R.L., *Performance and Effectiveness of Omni-directional Stern Drive Tugs*, Proceedings of International Towage and Salvage Convention ITS'94, Southampton, U.K., 1994, pp. 103-119.

Bussemaker, O. and Corlett E.C.B., *Tractor Tug Family Fitted with Rudder Propeller*, Proceedings of the 2nd International Tug Convention, London, U.K., 1971.

van Leest, H. and Bussemaker, O., *The Performance and Characteristics of Thrusters*, Proceedings of Offshore South East Asia Conference, Singapore, 1976.

Bussemaker, O. and van der Made A., *Thrusters for Dynamic Positioning*, Proceedings of Offshore Craft Conference, London U.K., 1976.

Bussemaker, O., *Thruster Performance*, Schottel-Nederland B.V. Publication, 1987, (Ref. AMC Library Q623 862/7).

Chassaing P., George, J., Claria, A. and Sananes, F., *Physical Characteristics of Subsonic Jets in a Cross-stream*, Journal of Fluid Mechanics, Vol. 62, Pt. 1, 1974, pp. 41-64.

Crane, Jr., C.L., *Manoeuvring Safety of Large Tankers: Turning and Speed Selection*, S.N.A.M.E. Transactions, Vol. 81, 1973.

Dand, I.W., *Some Aspects of Tug-Ship Interaction*, Proceedings of the 4th International Tug Convention, New Orleans, U.S.A, 1975, pp. 61-80.

Dand, I.W., *Physical Causes of Interaction and its Effects*, Proceedings of Nautical Institute Conference on Shiphandling, Plymouth, U.K., Nov. 24-25, 1977, pp. 34-73.

Dand, I.W., *Tug Wash Effects in Confined Waters*, Proceedings of the 7th International Tug Convention, London, U.K., 1982, pp. 163-173.

Dand, I.W., *Disabled Ship Handling with Tugs*, Proceedings of the 8th International Tug Convention, Singapore, 1984, pp. 171-188.

Dand, I.W., *On Modular Manoeuvring Models*, Proceedings of the R.I.N.A International Conference on Ship Manoeuvrability-Prediction and Achievement, London, U.K., Apr. 29-30 and May 1, 1987, Paper No.8.

Davison, N.J., Thomas, N.T., Nienhuis, U. and Pinkster, J.A., *Application of an Alternative Concept in Dynamic Positioning to a Tanker Floating Production System*, Proceedings of the 19th Offshore Technology Conference, Houston, Texas, U.S.A., Apr. 27-30, 1987, Paper No. 5444.

Dewhurst, P.K., *Propulsive Forces Generated by Steerable Right Angle Drive Units Fitted with Nozzles*, Proceedings of 3rd Ship Control Symposium, Bath, U.K., Sept., 1972.

Elzinga, Ir Th. and Stuurman, Ir P.M., *The Use of Simulators in Towing Disabled Vessels into Port*, Proceedings of the 9th International Tug Convention, London, U.K., 1986, pp. 87-99.

English, J.W., *Propeller/Hull Interaction*, 14th International Towing Tank Conference, 1975.

English, J.W. and Wise, D.A., *Hydrodynamic Aspects of Dynamic Positioning*, Transactions of the North East Coast Institution of Engineers and Shipbuilders, 1975.

Gale, C., Skogman, A., Eronen, H. and Hellevaara, M., *Perceived Advantages of Z-Drive Escort Tugs*, Proceedings of International Towage and Salvage Convention ITS'94, Southampton, U.K., 1994, pp. 163-176.

Hendy, N. and Freathy, R., *Quasi-static and Dynamic Behaviour of Escort Tugs-A Designers Viewpoint*, Proceedings of the R.I.N.A International Conference on Escort Tugs-Defining the Technology, London, U.K., Oct. 18-29, 1993, Paper No. 6.

Hensen, H., *Harbour Tugs-Types and Assisting Methods*, All Marine, Rotterdam, The Netherlands, 1990.

Hirano, M. and Takashina, J., *A Calculation of Ship Turning Motion Taking Coupling Effect due to Heel into Consideration*, Transactions of the West Japan Society of Naval Architects, No. 59, March, 1980, pp. 71-81.

Hoerner, S.F. *Fluid Dynamic Drag*, Hoerner Fluid Dynamics, Bricktown, New Jersey, U.S.A., 1965, Chapter VIII.

Hutchison, B.L., Gray, D.L. and Sridhar, J., *New Insights into Voith Schneider Tractor Tug Capability*, Marine Technology Vol. 3, No. 4, SNAME, 1993, pp. 233-242.

Inoue, S., Hirano, M., and Kijima, K., *Hydrodynamic Derivatives on Ship Manoeuvring*, International Shipbuilding Progress, Vol. 28, No. 321, 1981.

Ishiguro, T., Tanaka, M., Shouji, K. and Mizoguchi, S., *Simulation Program for Manoeuvrability of Ship in Harbour and its Application*, IHI Engineering Review, Vol. 21, No.3, July, 1988, pp. 104-109.

Kamotani, RY. and Greber, I., *Experiments on a Turbulent Jet in a Cross Flow*, AIAA Journal, Vol.10, 1972, pp. 1425-1429.

Khattab, O., *Ship Handling in Harbours Using Real Time Simulation*, Proceedings of the R.I.N.A International Conference on Ship Manoeuvrability-Prediction and Achievement, London ,U.K., Apr. 29-30 and May 1, 1987, Paper No.11.

Khattab, O., *A Mathematical Model for Simulation of Tug Handling*, Proceedings of the 4th International Symposium, Practical Design of Ships and Mobile Units, Oct. 23-28, 1989, pp. 19-1-19-8.

Kijima, K., Katsuno, T., Nakiri, Y. and Furukawa, Y., *On the Manoeuvring Performance of a Ship with the Parameter of Loading Condition*, Journal of the Society of Naval Architects of Japan, Vol. 168, 1990, pp. 141-148.

Kose, K., *A New Mathematical Model of Manoeuvring Motions of a Ship and its Applications*, International Shipbuilding Progress, Vol. 29, No. 330, 1982, pp. 205-220.

Kose, K., Hirao, S., Yoshikawa, K. and Nagagawa, Y., *Study of Abilities of Harbour Tugboats*, Papers of the Autumn Lectures of the Japanese Shipbuilding Institute, 1987, No. 162.

Lehn, E., *Thruster Interaction Effects*, NSFI Report R-102.80, 1980.

Lehn, E., *Thruster-Hull Interaction Effects*, NSFI Report R-119.81, 1981.

Lewis, E.V.(Ed), *Principles of Naval Architecture*, Vol II & III, Second Revision, S.N.A.M.E., Jersey City, N.J., U.S.A., 1988.

Margason, R.J., *The Path of a Jet Directed at Large Angles to a Subsonic Stream*, NASA, TN.D.-4919, Langley Research Center, Hampton, Virginia, 1968.

MARIN, *MARIN Report*, No.38, 1989.

McIlroy, W., Grossman, H., Eda, H. and Shizume, P., *Validation Procedures for Ship Motion and Human Perception*, Proceedings of MARSIM'81 International Conference on Marine Simulation, New York, U.S.A., 1981.

Minsaas, K.J. and Lehn, E., *Hydrodynamical Characteristics of Rotatable Thrusters*, NSFI Report R-69.78, 1978.

Moberg, S. and Hellström S.A., *Dynamic Positioning of a Four Column Semi-submersible. Model Tests of Interaction Forces and a Philosophy about Optimum Strategy when Operating the Thrusters*, Proceedings of the 2nd International Symposium on Ocean Engineering and Ship Handling, Gothenburg, Sweden, 1983.

Müller, E., *Results of Open Water Tests with Ducted and Non-ducted Propellers with Angle of Attack from 0 to 360°*, Proceedings of the Symposium on Advances in Propeller Research and Design, Gdansk, Poland, 1981, Paper No. 12.

Nienhuis, U.(1), *Simulation of Low Frequency Motions of Dynamically Positioned Offshore Structures*, R.I.N.A. Transactions Vol. 129, 1986, pp. 127-142.

Nienhuis, U.(2), *Propulsive Aspects of Dynamically Positioned Vessels*. Proceedings of the International Conference on Stationing and Stability of Semi-submersibles, Glasgow, U.K., 1986, Paper No. 13.

Nienhuis, U., *Analysis of Thruster Effectivity for Dynamic Positioning and Low Speed Manoeuvring*, PhD Thesis, Delft University of Technology, Delft, The Netherlands, 1992.

Norrbin, N., *Theory and Observations on the Use of a Mathematical Model for Ship Manoeuvring in Deep and Confined Waters*, SSPA Publication No. 68, 1971.

Norrby, R.A. and Ridley, D.E., *Notes on Thrusters for Ship Manoeuvring and Dynamic Positioning*, S.N.A.M.E. Transactions, Vol. 88, 1980, pp. 377-402.

Ogawa, A. and Kasai, H., *On the Mathematical Model of Manoeuvring Motion of Ships*, International Shipbuilding Progress, Vol. 25, No. 292, 1978, pp. 306-319.

Oosterveld, M.W.C., *Wake Adapted Ducted Propellers*, PhD Thesis, Delft University of Technology, Delft, The Netherlands, 1970.

Oosterveld, M.W.C. and van Oortmerssen, G., *Thruster Systems for Improving the Manoeuvrability and Position Keeping Ability of Floating Objects*, Proceedings of the 4th Offshore Technology Conference, Dallas, USA, 1972, Paper No. 1625.

Oosterveld, M.W.C., *Ducted Propeller Systems Suitable for Tugs and Pushboats*, International Shipbuilding Progress, Vol. 19, No. 219, 1972, pp.351-371.

Oosterveld, M.W.C., *Ducted Propeller Characteristics*, Proceedings of the R.I.N.A Symposium on Ducted Propellers, London, U.K., 1973, Paper No. 4.

Ottoson, P., *Mathematical Models in PORTSIM*, Proceedings of the 3rd International Conference on Manoeuvring and Control of Marine Craft, Southampton, U.K., Jul. 7-9, 1994, pp. 177-196.

Rajaratnam, M., *Turbulent Jets*, Vol. 5, *Developments in Water Science*, Elsevier Science Publishing Co., Amsterdam, 1976.

Renilson, M.R., Brandner, P.A. and Tasker, R.L., *Realistic Simulation of Tug Forces on a Manoeuvring Vessel*, Proceedings of the 2nd International Conference on Manoeuvring and Control of Marine Craft, Southampton, U.K., Jul. 14-17, 1992, pp. 87-100.

Ross, K. H., *Inaugural Paper* Proceedings of the 10th International Tug Convention, Sydney, Aust., 1988, pp. xiv-xvi.

Ross, K. H., *Harbour Towage in the 90's*, Proceedings of the 11th International Tug Convention, Genoa, Italy, 1992, pp. 107-113.

Sas, F.M., Timmers, R.A. and Gallin, C., *Simulation of the Effective Pull Forces Produced by Tugs*, Proceedings of the R.I.N.A International Conference on Escort Tugs-Defining the Technology, London, U.K., Oct. 18-29, 1993, Paper No. 7.

Schetz, J.A., *Injection and Mixing in Turbulent Flow*, AIAA (Progress in Astronautics and Aeronautics, Vol. 68). New York, 1980.

Spaulding, P. F., *Shiphandling at Ras Tanura Sea Island*, Proceedings of the 7th International Tug Convention, London, U.K., 1982.

Tasker, R.L., *The Implementation of an Improved Tug Model for the Port of Newcastle, N.S.W.*, Proceedings of the 10th International Tug Convention, Sydney, Aust., 1988, pp. 31-44.

Tregardh, P., *Simulation of Tugs at the SSPA Manoeuvring Simulator*, Proceedings of the 4th International Tug Convention, New Orleans, U.S.A, 1975, pp. 125-137.

Van Manen, J.D., *Open Water Test Series with Propellers in Nozzles*, International Shipbuilding Progress, Vol. 1, No.3, 1954.

Van Manen, J.D., *Recent Research on Propellers in Nozzles*, International Shipbuilding Progress, Vol. 4, No.36, 1957.

Van Manen, J.D. and Superina, A., *The Design of Screw Propellers in Nozzles*, International Shipbuilding Progress, Vol. 6, No.55, 1959.

Van Manen, J.D. and Oosterveld, M.W.C., *Analysis of Ducted Propeller Design*, S.N.A.M.E. Transactions, Vol. 74, 1966.

van Maanen, W.Ph., de Boer, W. and Froese, J., *Caland Bridge Windscreen - A Simulation Study of the Effects of a Windscreen on Ship Manoeuvring*, Proceedings 4th International Conference on Marine Simulation, Trondheim, Norway, 1987, pp. 193-202.

Webb, D., *Modern Trends in Harbour Towage*, Proceedings of the Queensland Harbour Master's Conference, Cairns, Aust., 1985, Paper No. 4.

Wise, D.A. and English, J.W., *Tank and Wind Tunnel for a Drill-ship with Dynamic Positioning Control*, Proceedings of the 7th Offshore Technology Conference, Houston, Texas, U.S.A., May 5-8, 1975, Paper No. 2345.

Yumuro, A., *A Model Experiment on Incoming Flow Direction to the Rudder of a Ship Sailing Obliquely*, 14th International Towing Tank Conference, 1975.

Zdravkovich, M.M., *Review of Flow Interference Between Two Circular Cylinders in Various Arrangements*, Journal of Fluids Engineering, Trans. ASME, Vol. 99, 1977, pp. 618-633.

Zhu, D.M., *A Computational Method for Cycloidal Propellers*, International Shipbuilding Progress, Vol. 28, 1981, pp. 102-111.

APPENDIX-A FULL SCALE AND MODEL TUG DETAILS

Two tug hull models where used to investigate the variation of hull forces with a range of parameters. Details of the hulls as well as general details of the full scale vessels are presented below.

A.1 Details of 30m Tug

Figure A.1 Photograph of 30m Tug

designers	Barnes and Fleck, Newcastle
design purpose	dedicated harbour tug
length overall	31.3m
length between perpendiculars	28.04m
beam molded	10.7m
beam overall	11.75m
nominal draft to baseline	4.4m
nominal displacement	565t
nominal initial metacentric height	2.12m
nominal power x 2	2650kW
maximum revolutions	720
maximum torque	17.5kNm
gear reduction ratio	2.718
propeller diameter	2.2m
nominal bollard pull	45t

Table A.1 Details of 30m Tug

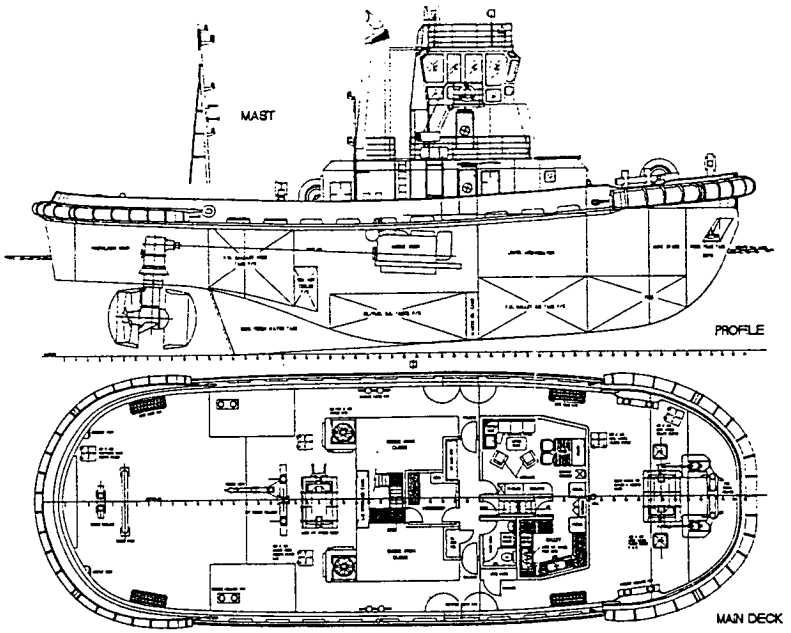

Figure A.2 General Arrangement of 30m Tug

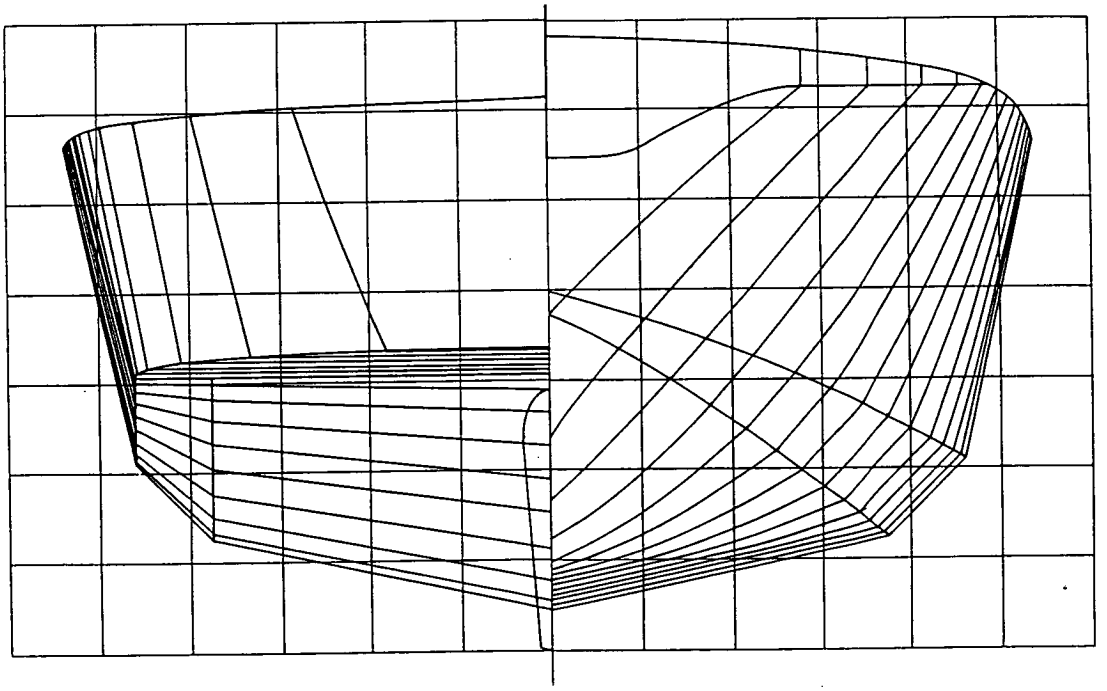

Figure A.3 Body Plan of 30m Tug

A.2 Details of 32m Tug

Figure A.4 Photograph of 32m Tug

designers	Barnes and Fleck, Newcastle
design purpose	combined harbour and salvage tug
length overall	33m
length between perpendiculars	29.4m
beam molded	10.6m
beam overall	11.6m
nominal draft to baseline	4.8m
nominal displacement	800t
nominal initial metacentric height	2m
nominal power x 2	2650kW
maximum revolutions	720
maximum torque	17.5kNm
gear reduction ratio	2.718
propeller diameter	2.2m
nominal bollard pull	45t

Table A.2 Details of 32m Tug

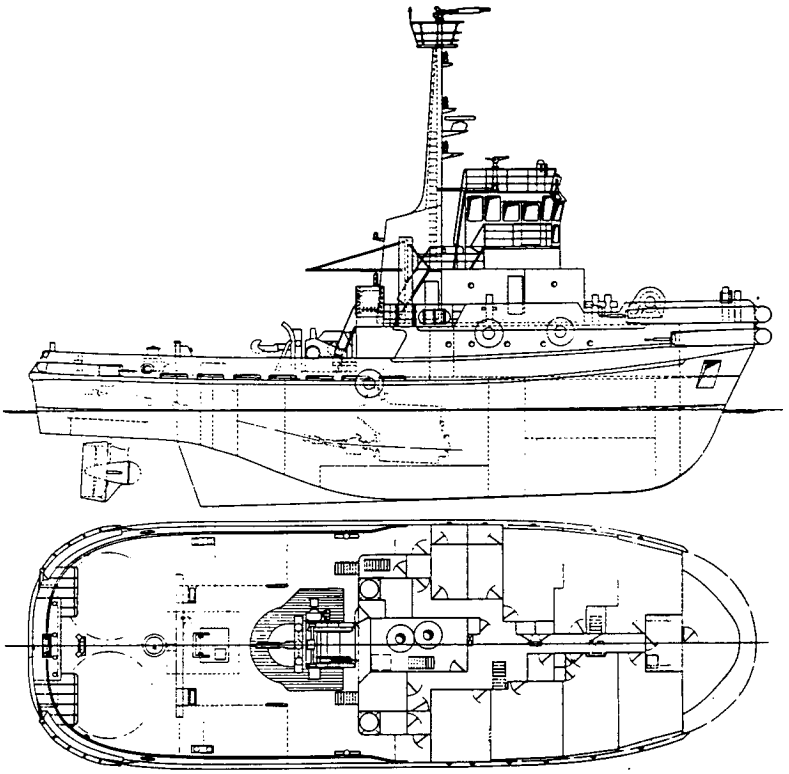

Figure A.5 General Arrangement of 32m Tug

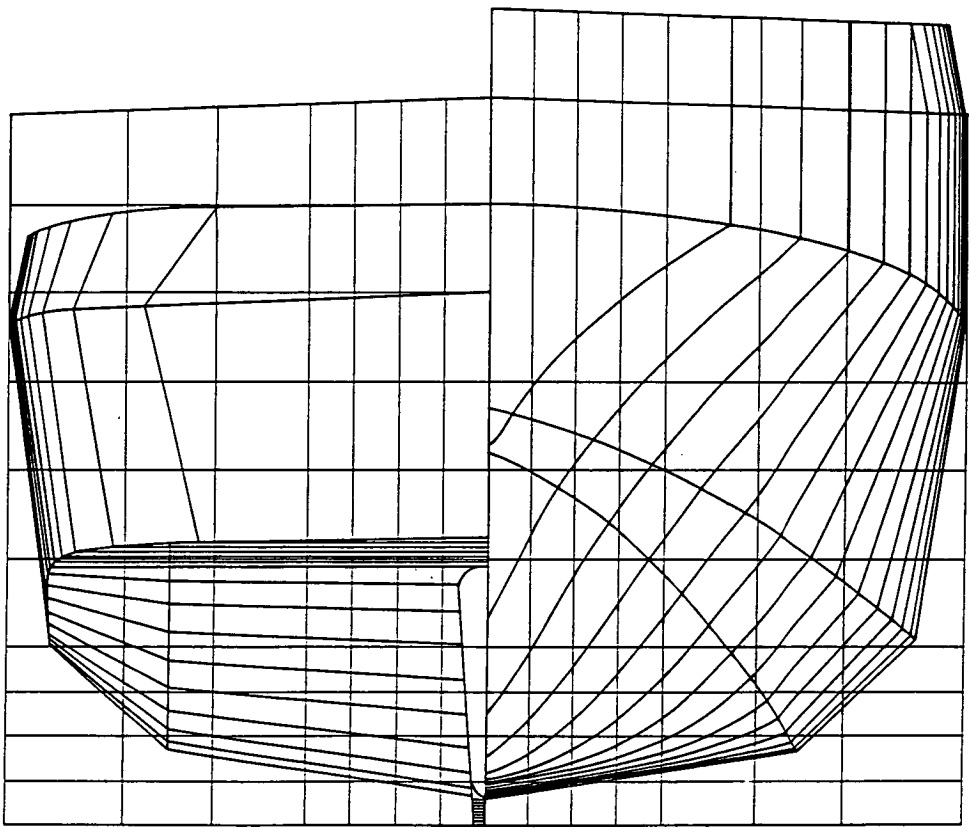

Figure A.6 Body Plan of 32m Tug

APPENDIX-B EXPERIMENTAL DETAILS

B.1 Experimental Facilities

Two experimental facilities at the AMC were used to carry out physical model experiments for the present work, namely the towing tank and the circulating water channel. The towing tank was used to carry out bare hull experiments and open water thruster experiments, and the circulating water channel was used for free running experiments. The towing tank is 60m long, 3.5m wide and 1.6m deep with maximum carriage velocity of 4.5m/s, and the circulating water channel has a working section of 20m long, 5m wide and 2.5m deep with maximum flow velocity of 1.5m/s.

The shiphandling simulator at the AMC was used to perform numerical ship manoeuvring experiments. The ship manoeuvring mathematical model used in the simulator is based on that by Norrbin, 1971. The model comprises three degrees of freedom namely: surge, sway and yaw. The ship's equations of motion are numerically integrated using the Euler-Cauchy method with 1 second time step on a Gould 32/27 super mini-computer.

B.2 Apparatus

Forces acting on the bare hull models during towing tank experiments were measured using a rotatable two post model dynamometer, as shown in Figures B.3 and B.4. The dynamometer allowed the model to be fixed at drift angle intervals of 10° and be free to move in heave, roll and pitch. Surge and sway forces and yaw moments were derived from force measurements using three MARIN 421/801 uni-directional shear load cells. Two of which where located on the forward post measuring surge and sway forces and one which was mounted on the aft post measuring sway force, as shown in Figures B.3 and B.4.

Open water experiments with one and two thrusters were carried out in the towing tank using a shallow draft ground board, as shown in Figures B.7 and B.8. Detailed drawings of the ground board are shown in Figure B.9. Forces acting on the thrusters were measured using a dynamometer designed as part of the present investigation. The dynamometer and thrusters were mounted on a turntable within the ground board that could be rotated to adjust the drift angle of the pair of thrusters. The base of the turntable, in contact with the water, was made of perspex enabling the thrusters to be viewed during a run. Each thruster unit can be rotated independent of its dynamometer and protractors were fitted allowing the thruster angles to be set. Close-up photographs of the dynamometers are shown in Figures B.10 and B.11 and detailed drawings are shown in Figures B.12, B.13 and B.14. The force measuring component of the dynamometer consists of two orthogonal pairs of flexures which are flexible along one horizontal axis and stiff along the other enabling the net thruster force to be measured as rectangular components. The influence of moments about the horizontal axes is minimised, since the flexure pairs are of sufficient width that axial forces in the columns are small in comparison to transverse forces thus introducing only small non-linearities and cross-talk. The influence of moments about the vertical axis is minimised by measurement of the flexure displacements at the location of the centroid of the volume enclosed by each flexure pair. The propellers are driven with tooth belts and their rpm is derived from the electric motor rpm using an optical sensor and chopper disk with sixty holes.

The dynamometers were also designed to be re-configured for fitting in the model tug hull to measure thruster forces in the behind condition. These were measured during free running model experiments carried out in the circulating water channel, as shown in Figures B.15, B.16, B.17, B.18, B.19 and B.20. Total tug forces, for both pushing and pulling were measured with two MARIN 421/801 uni-directional shear load cells, as can be seen in the above mentioned figures. One load cell was aligned with the flow direction and the other perpendicular to the flow direction, enabling the direction of the tug force relative to the free stream to be determined. For operation in the pushing mode, the tug's drift angle was measured manually with a hand protractor using the carriage as a reference. For operation in the pulling mode, the tug's drift angle was measured manually with a protractor mounted on the tow point. Given the tug's drift angle, thruster forces and the total force, forces acting on the hull can be calculated from equilibrium.

Signals from load cells and transducer elements within the dynamometers where digitally logged at 100 Hz using a PC486 with a standard analog to digital conversion card and custom software. Before recording, signals were appropriately amplified to give maximum precision and filtered with a 1Hz low pass filter.

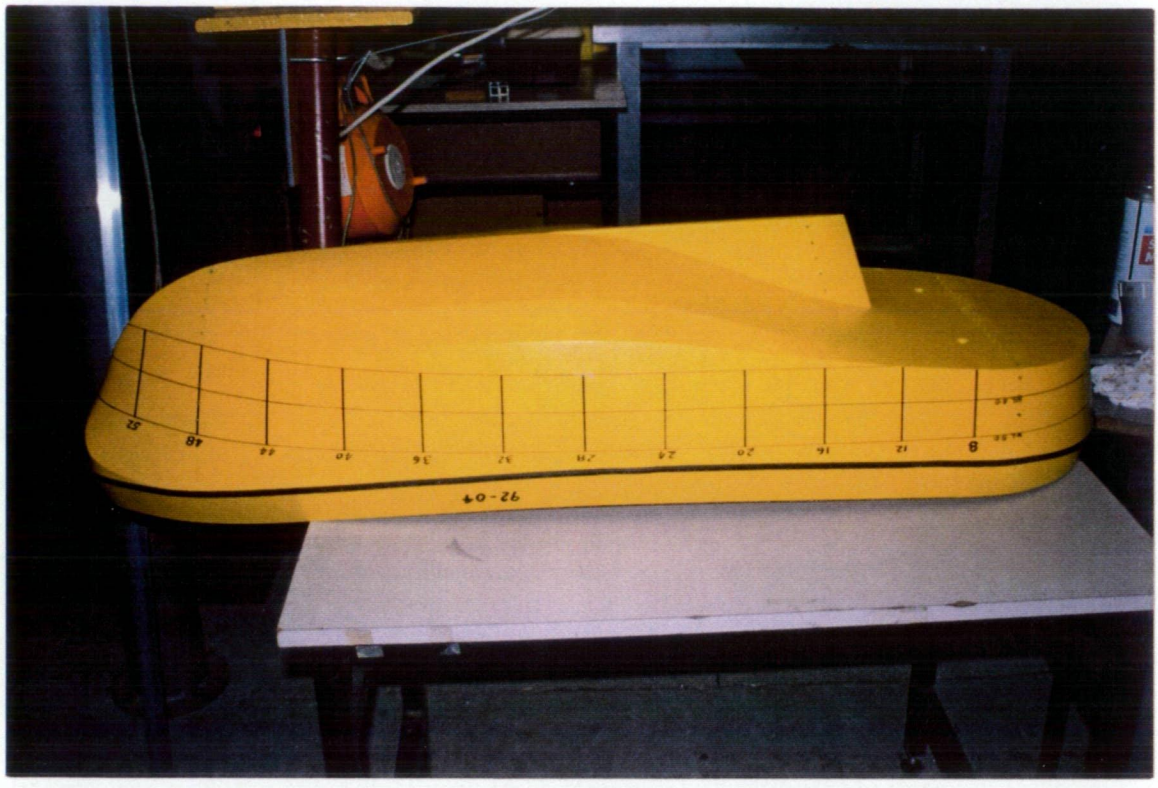

Figure B.1 Photograph of 30m Tug Model

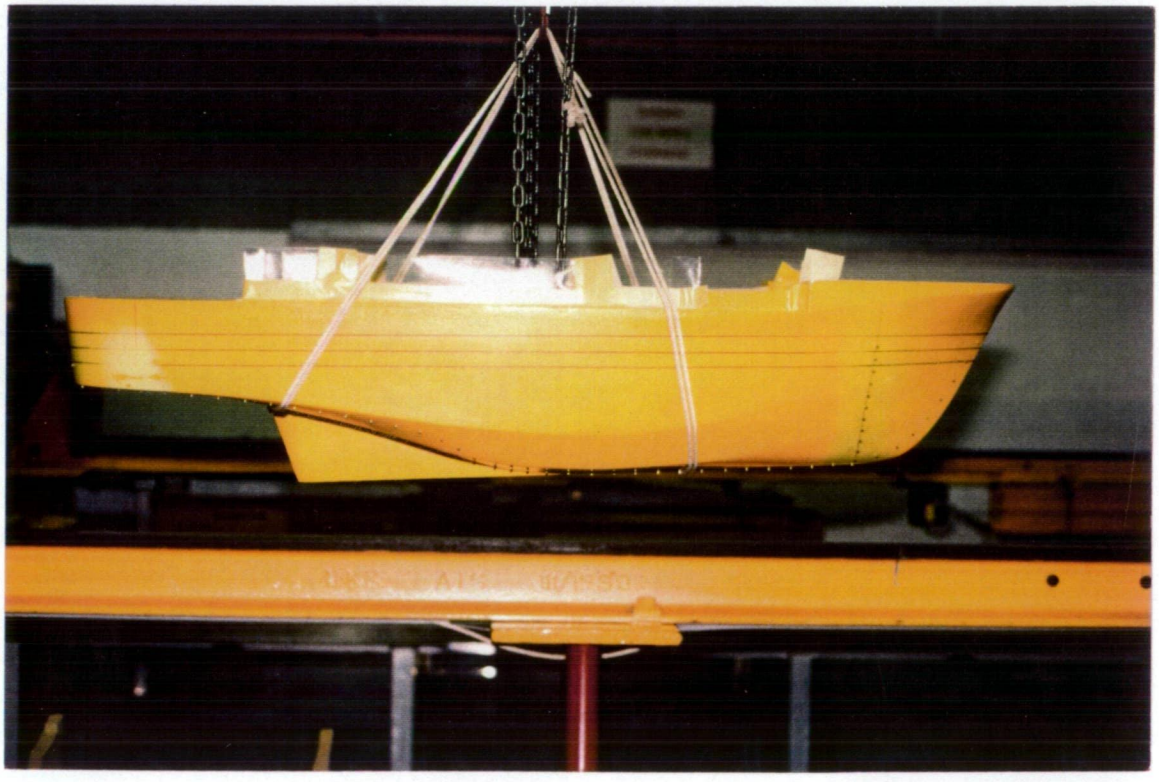

Figure B.2 Photograph of 32m Tug Model

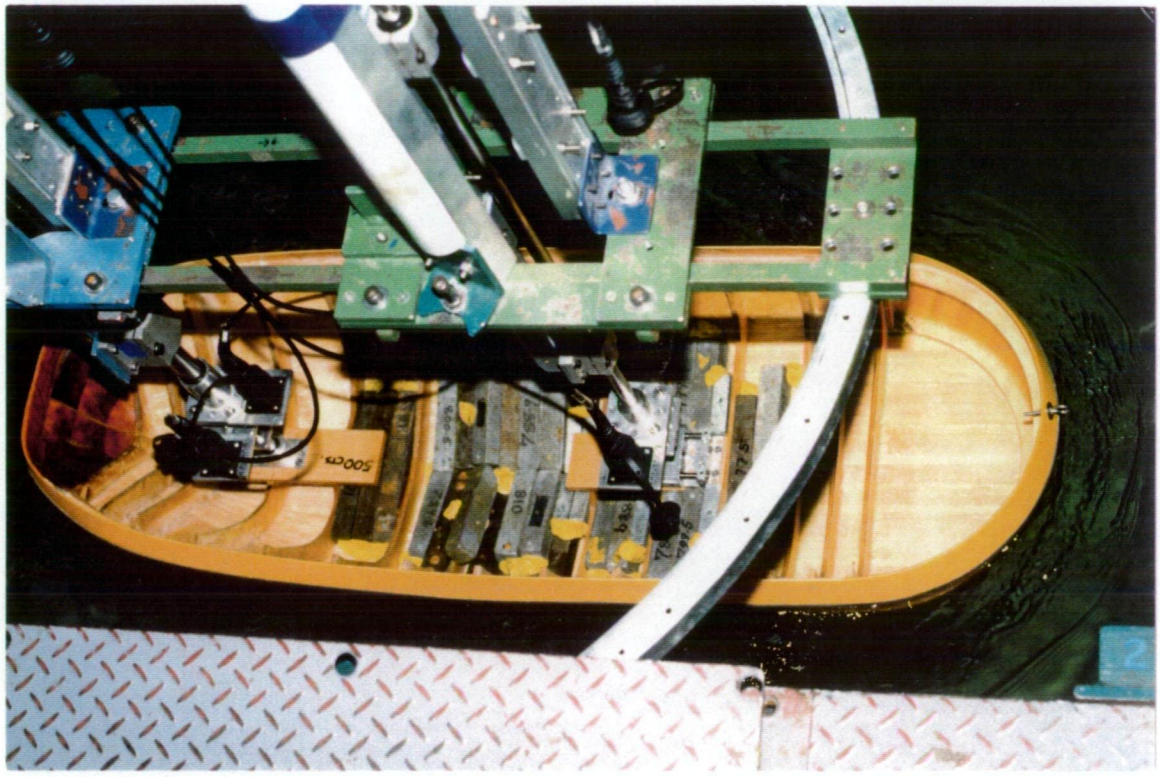

Figure B.3 Photograph of 30m Tug Model Connected to Rotatable Model Dynamometer on Towing Tank Carriage

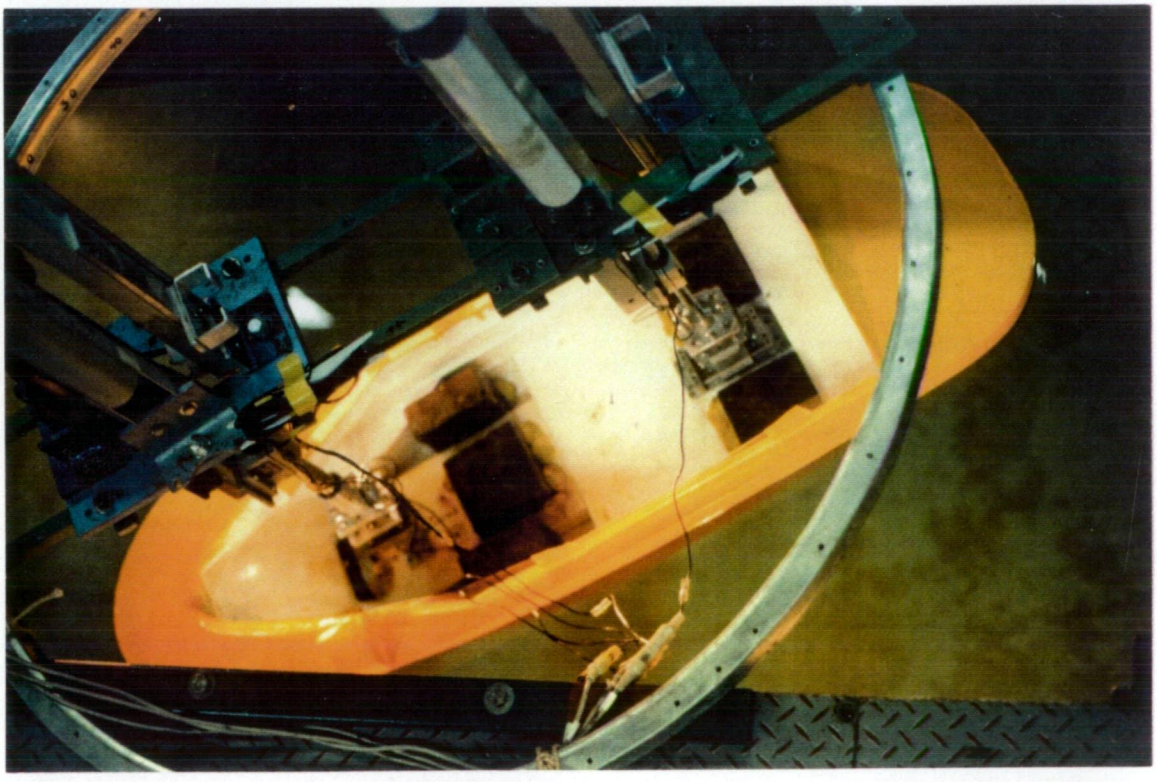

Figure B.4 Photograph of 32m Tug Model Connected to Rotatable Model Dynamometer on Towing Tank Carriage

Figure B.5 Photograph of Towing Tank Carriage and 30m Tug Model

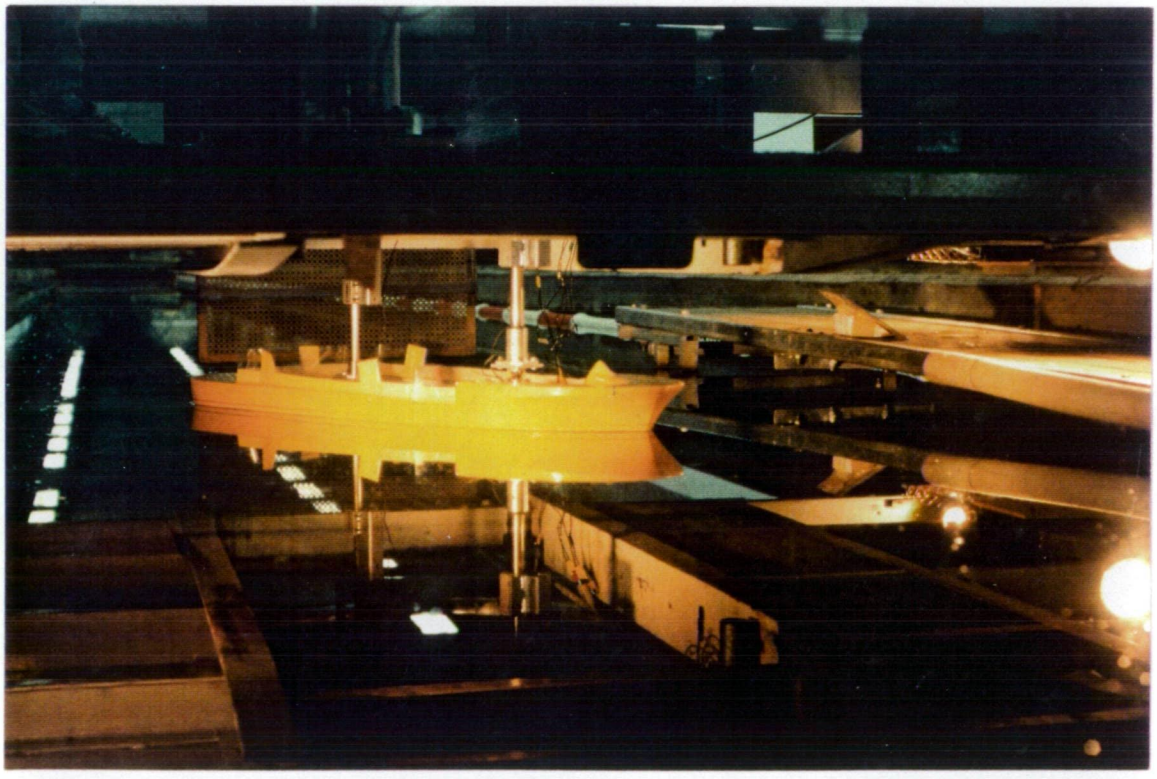

Figure B.6 Photograph of Towing Tank Carriage and 32m Tug Model

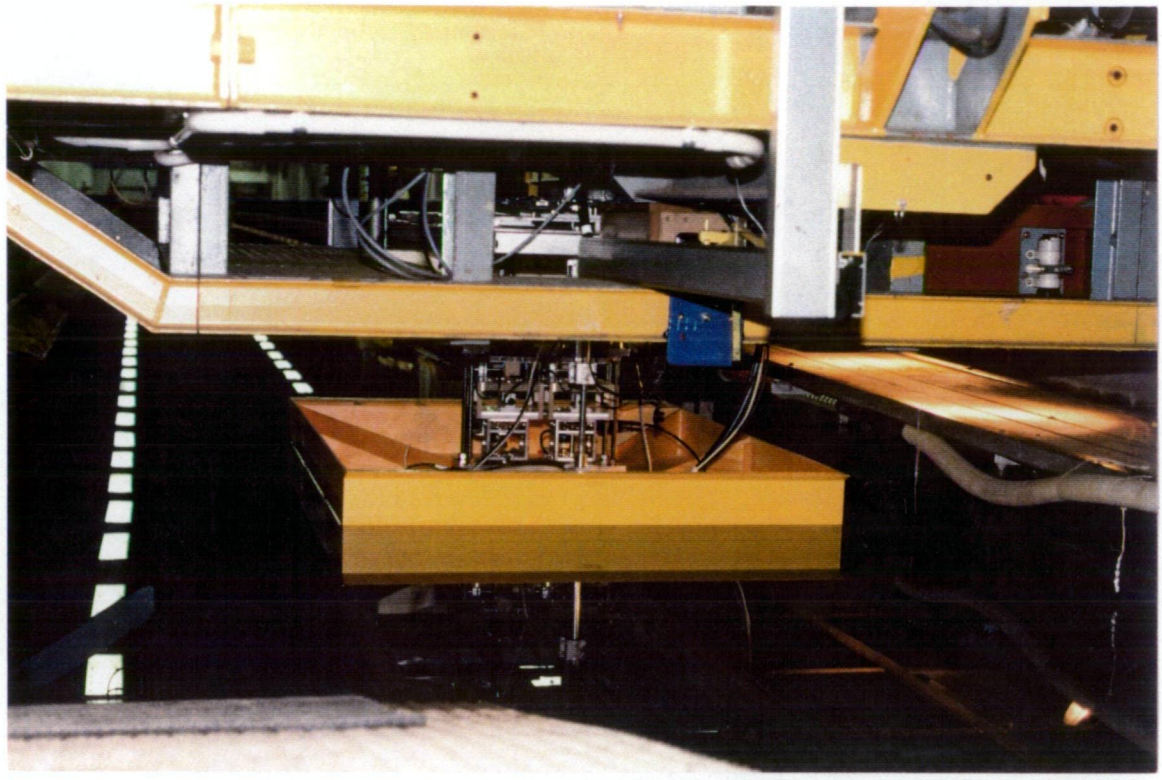

Figure B.7 Photograph, Looking Forward, of Ground Board and Thruster Dynamometer for Open Water Experiments with One and Two Thrusters in Towing Tank

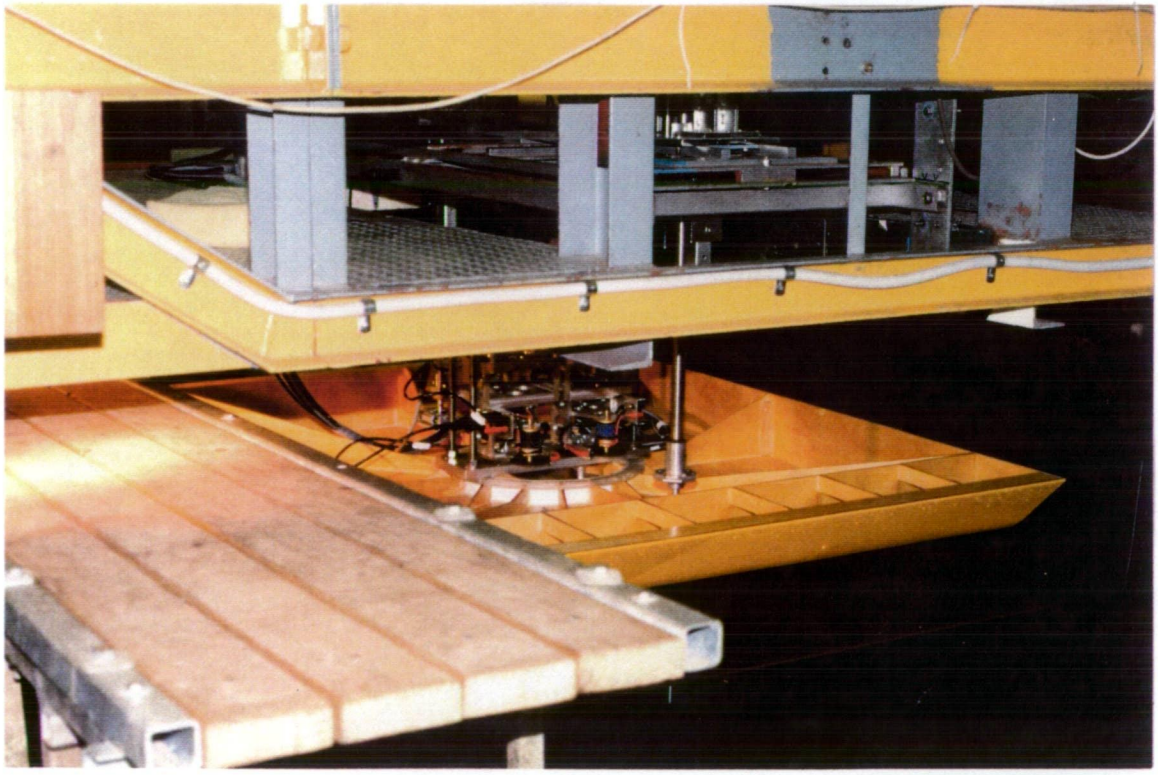

Figure B.8 Photograph, Looking Aft, of Ground Board and Thruster Dynamometer for Open Water Experiments with One and Two Thrusters in Towing Tank

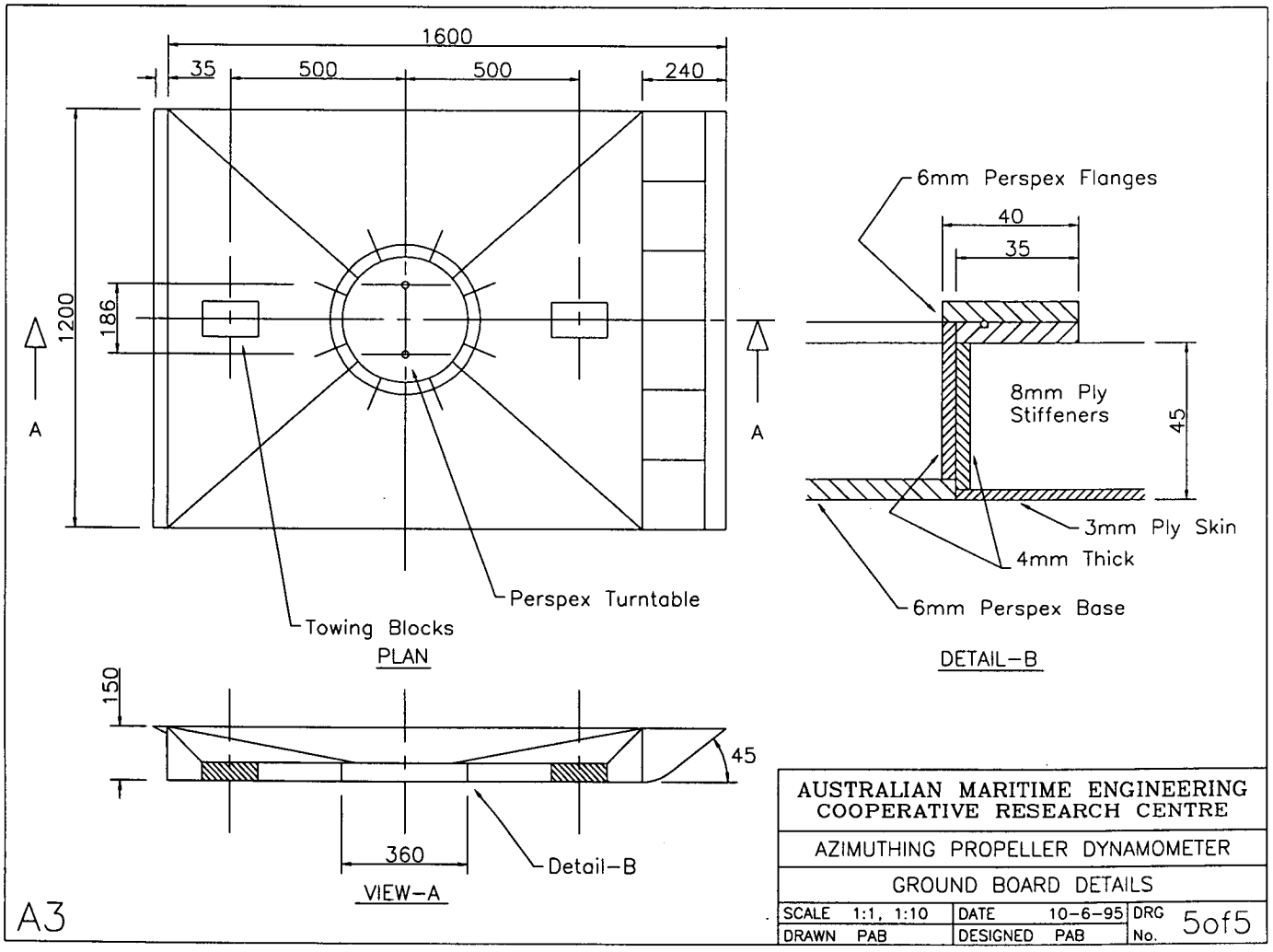
1600
35
500
500
240
1200
186
A
A
Towing Blocks
Perspex Turntable
PLAN
6mm Perspex Flanges
40
35
8mm Ply
Stiffeners
45
3mm Ply Skin
4mm Thick
6mm Perspex Base
DETAIL–B
150
45
360
Detail–B
VIEW–A
A3
AUSTRALIAN MARITIME ENGINEERING
COOPERATIVE RESEARCH CENTRE
AZIMUTHING PROPELLER DYNAMOMETER
GROUND BOARD DETAILS
SCALE 1:1, 1:10
DATE 10–6–95
DRG No. 5of5
DRAWN PAB
DESIGNED PAB

Figure B.9

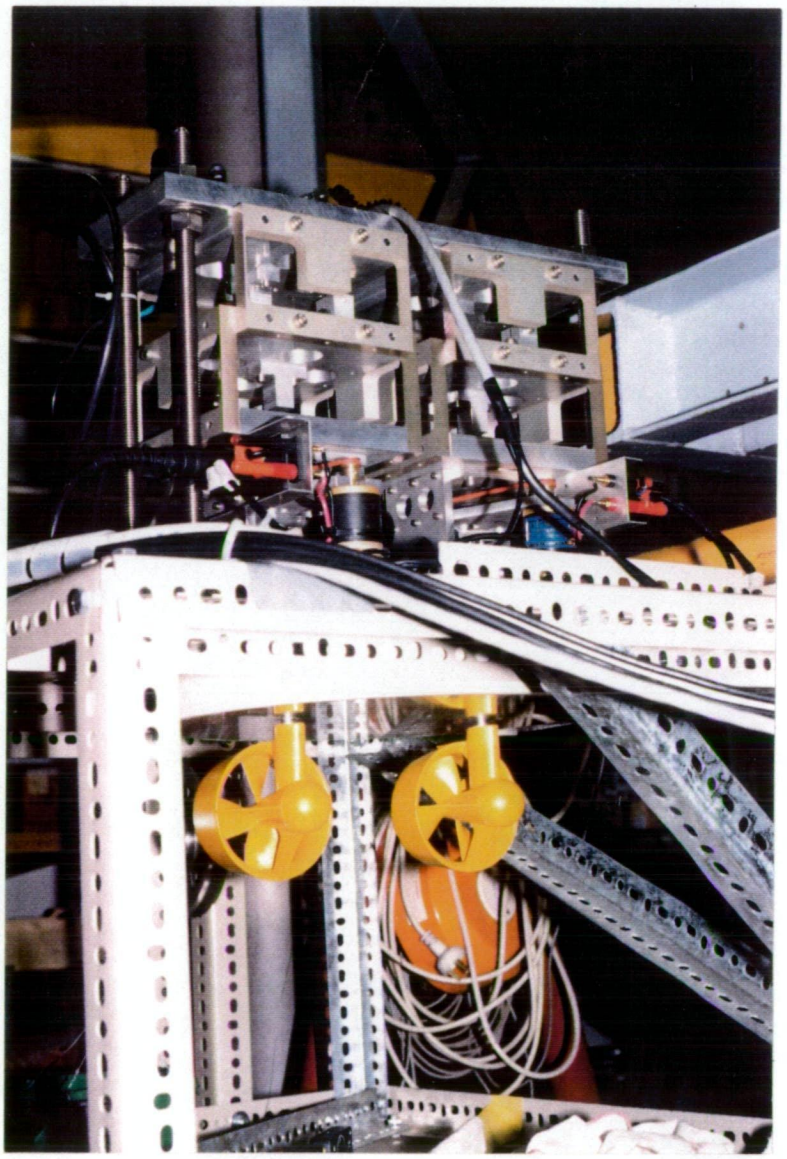

Figure B.10 Photograph, Looking Up, of Thruster Dynamometer in Calibration Frame for Open Water Experiments with One and Two Thrusters

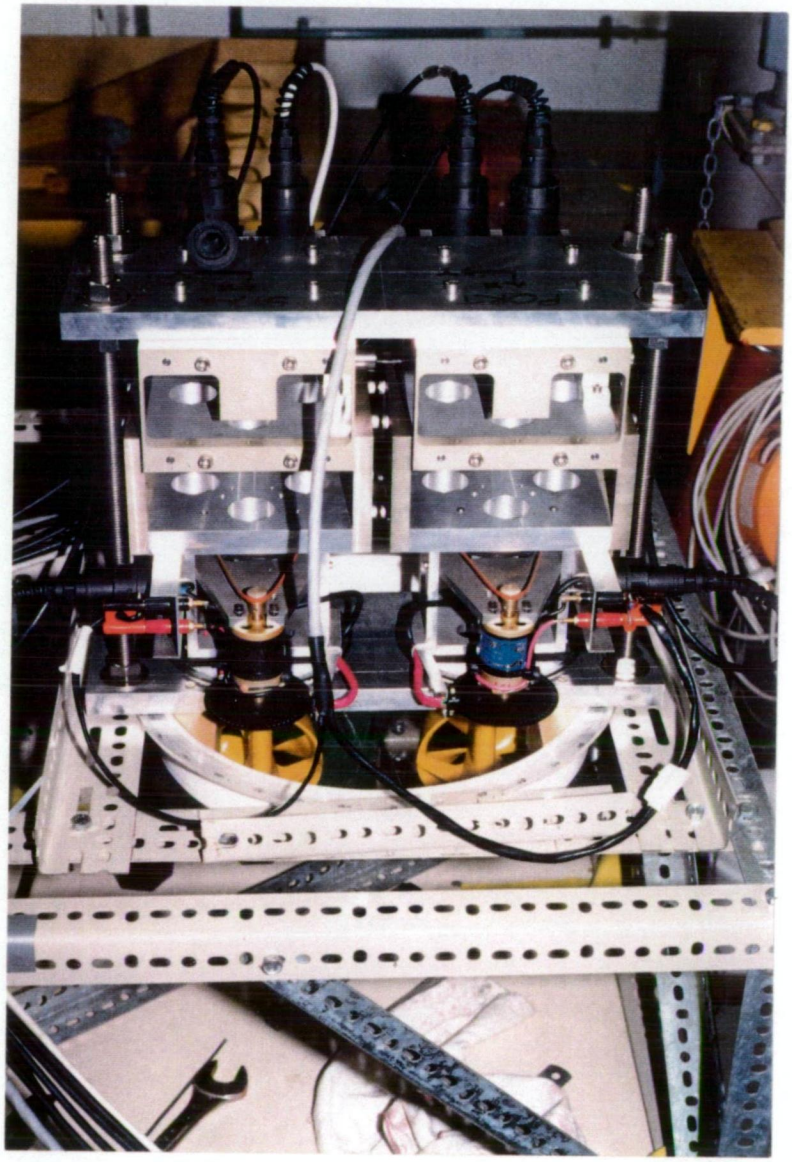

Figure B.11 Photograph, Looking Down, of Thruster Dynamometer in Calibration Frame for Open Water Experiments with One and Two Thrusters

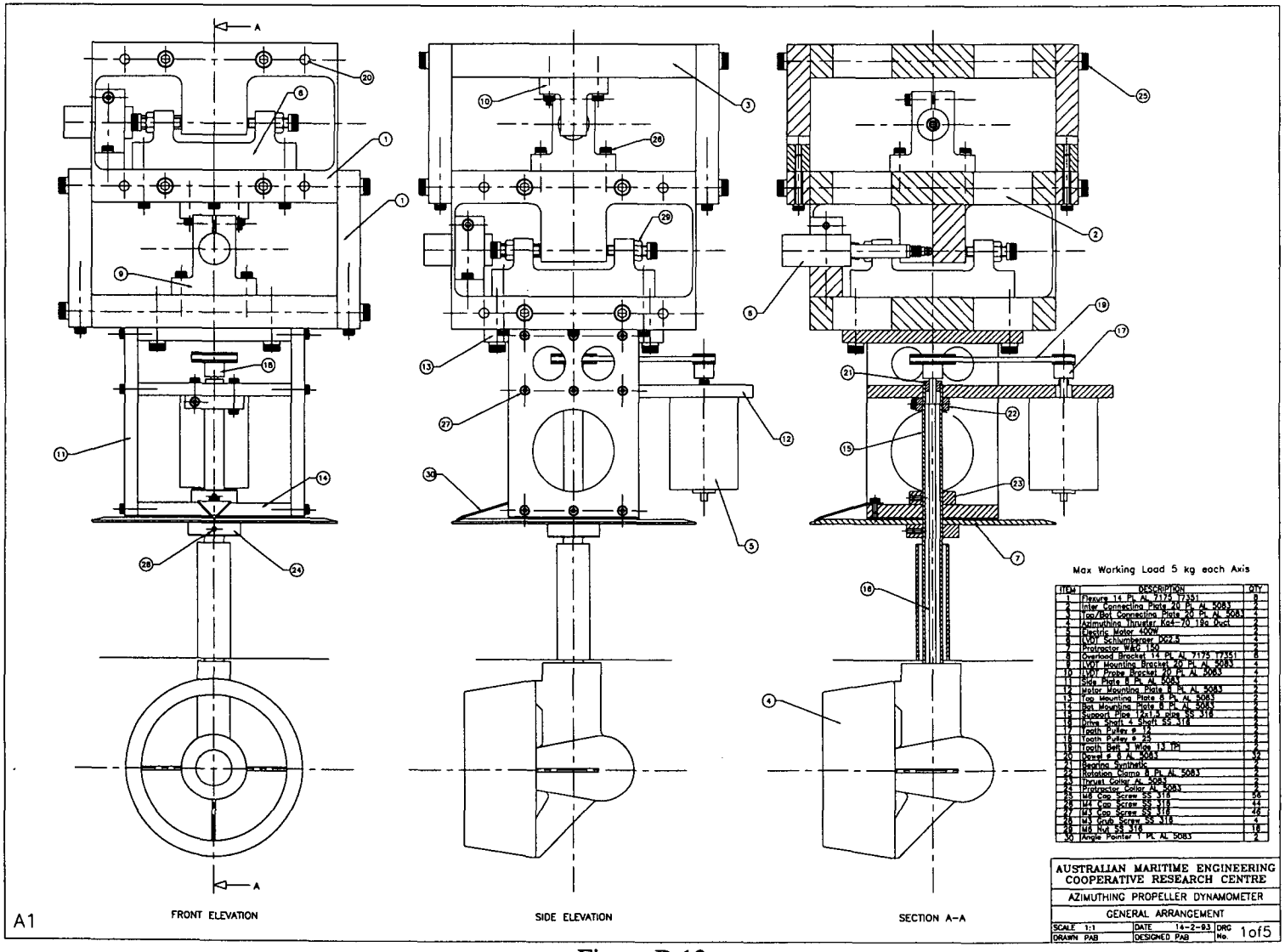
A1
FRONT ELEVATION
SIDE ELEVATION
SECTION A-A
Max Working Load 5 kg each Axis
AUSTRALIAN MARITIME ENGINEERING COOPERATIVE RESEARCH CENTRE
AZIMUTHING PROPELLER DYNAMOMETER
GENERAL ARRANGEMENT
SCALE 1:1
DATE 14-2-93
DRG No. 1of5
DRAWN PAB
DESIGNED PAB

Figure B.12

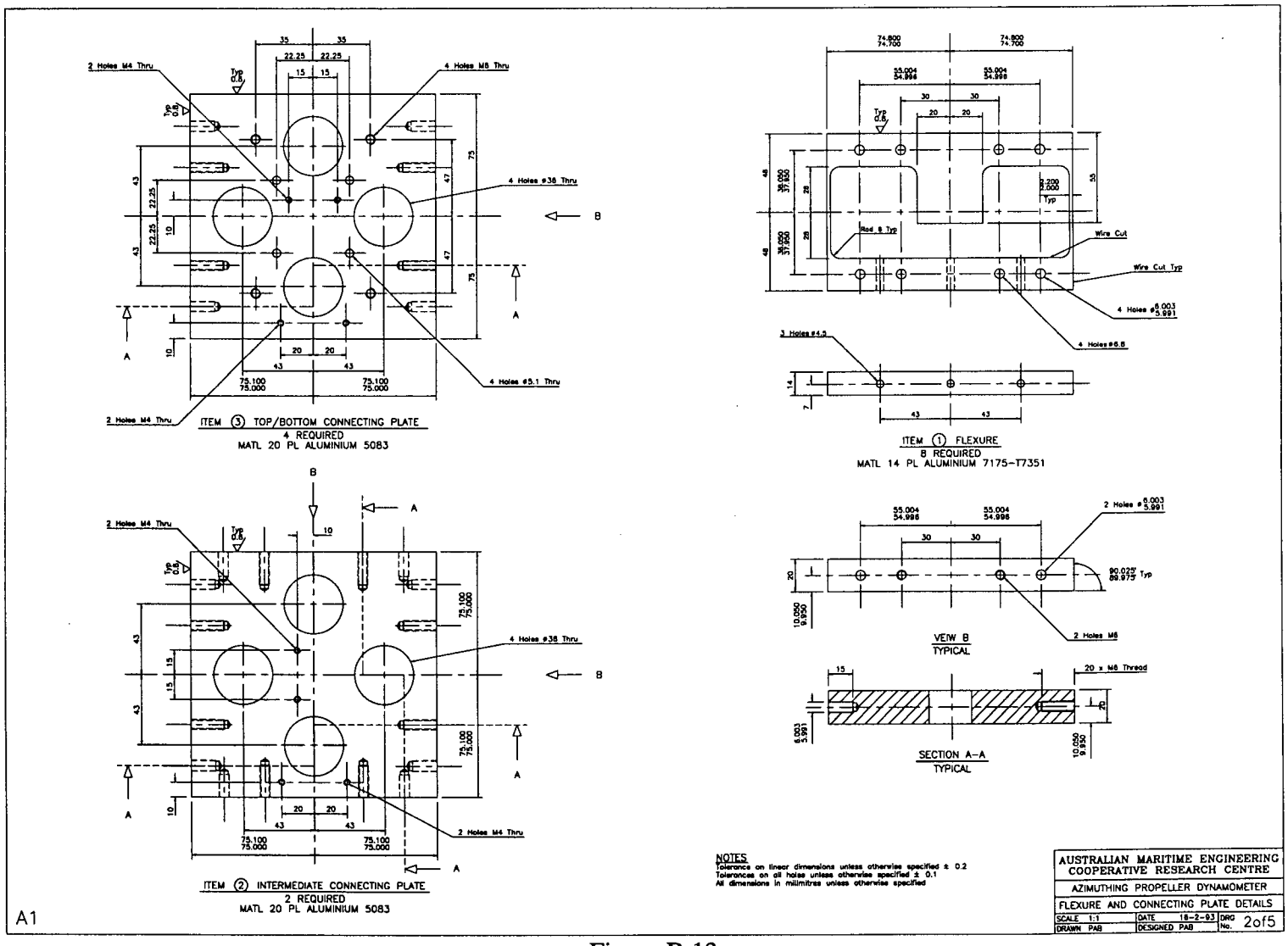
2 Holes M4 Thru
4 Holes M8 Thru
4 Holes ø36 Thru
4 Holes ø5.1 Thru
2 Holes M4 Thru
ITEM (3) TOP/BOTTOM CONNECTING PLATE
4 REQUIRED
MATL 20 PL ALUMINIUM 5083
4 Holes ø36 Thru
2 Holes M4 Thru
ITEM (2) INTERMEDIATE CONNECTING PLATE
2 REQUIRED
MATL 20 PL ALUMINIUM 5083
Wire Cut
Wire Cut Typ
4 Holes ø6.6
3 Holes ø4.5
ITEM (1) FLEXURE
8 REQUIRED
MATL 14 PL ALUMINIUM 7175-T7351
2 Holes ø6.003 5.991
2 Holes M8
VIEW B
TYPICAL
20 x M8 Thread
SECTION A-A
TYPICAL
NOTES
Tolerance on linear dimensions unless otherwise specified ± 0.2
Tolerances on all holes unless otherwise specified ± 0.1
All dimensions in millimitres unless otherwise specified
AUSTRALIAN MARITIME ENGINEERING COOPERATIVE RESEARCH CENTRE
AZIMUTHING PROPELLER DYNAMOMETER
FLEXURE AND CONNECTING PLATE DETAILS
SCALE 1:1
DATE 18-2-93
DRG No. 2of5
DRAWN PAB
DESIGNED PAB
A1

Figure B.13

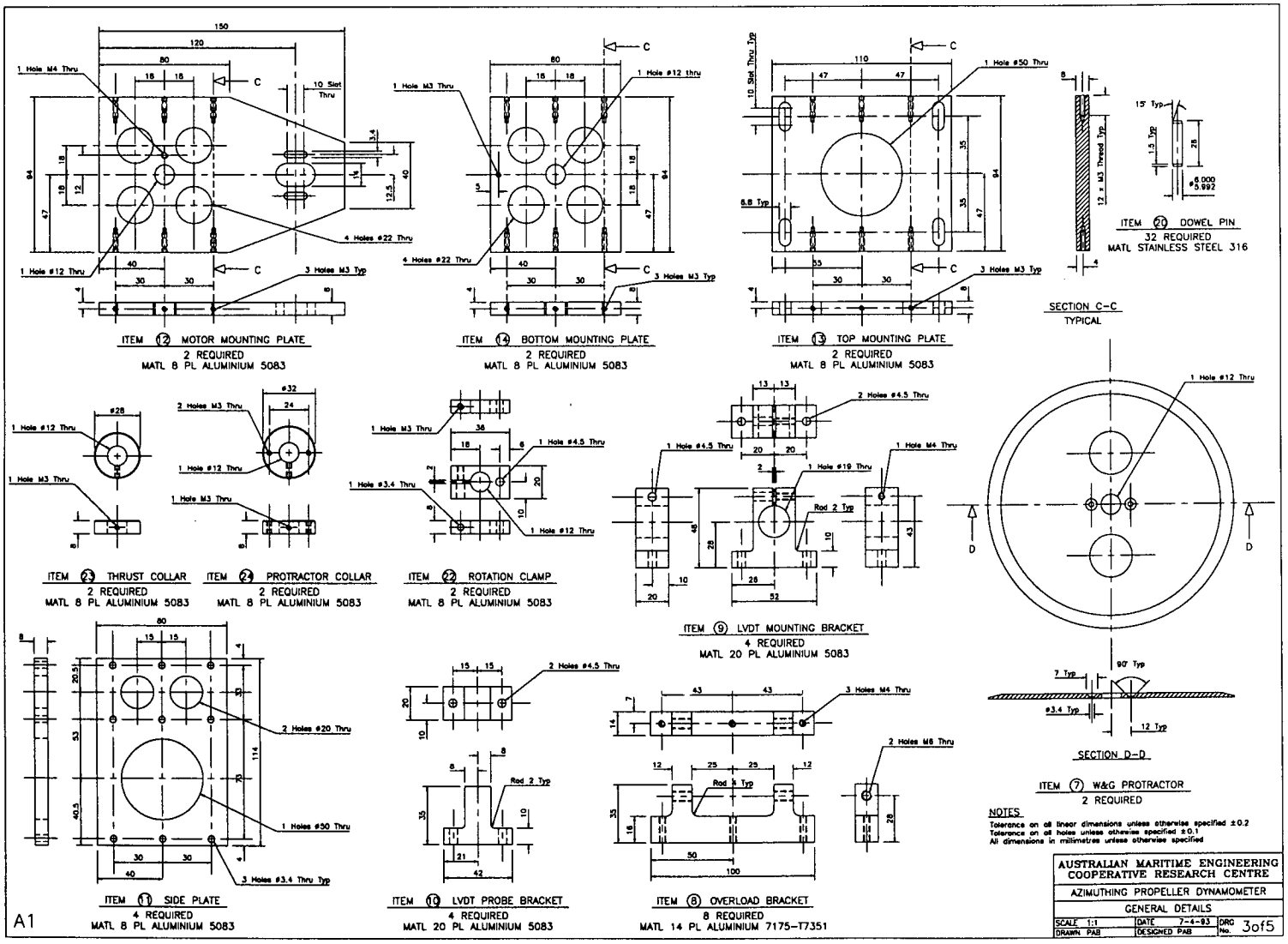
ITEM (12) MOTOR MOUNTING PLATE
2 REQUIRED
MATL 8 PL ALUMINIUM 5083
ITEM (14) BOTTOM MOUNTING PLATE
2 REQUIRED
MATL 8 PL ALUMINIUM 5083
ITEM (13) TOP MOUNTING PLATE
2 REQUIRED
MATL 8 PL ALUMINIUM 5083
ITEM (20) DOWEL PIN
32 REQUIRED
MATL STAINLESS STEEL 316
SECTION C-C
TYPICAL
ITEM (23) THRUST COLLAR
2 REQUIRED
MATL 8 PL ALUMINIUM 5083
ITEM (24) PROTRACTOR COLLAR
2 REQUIRED
MATL 8 PL ALUMINIUM 5083
ITEM (22) ROTATION CLAMP
2 REQUIRED
MATL 8 PL ALUMINIUM 5083
ITEM (9) LVDT MOUNTING BRACKET
4 REQUIRED
MATL 20 PL ALUMINIUM 5083
ITEM (11) SIDE PLATE
4 REQUIRED
MATL 8 PL ALUMINIUM 5083
ITEM (10) LVDT PROBE BRACKET
4 REQUIRED
MATL 20 PL ALUMINIUM 5083
ITEM (8) OVERLOAD BRACKET
8 REQUIRED
MATL 14 PL ALUMINIUM 7175-T7351
SECTION D-D
ITEM (7) W&G PROTRACTOR
2 REQUIRED
NOTES
Tolerance on all linear dimensions unless otherwise specified ±0.2
Tolerance on all holes unless otherwise specified ±0.1
All dimensions in millimetres unless otherwise specified
AUSTRALIAN MARITIME ENGINEERING COOPERATIVE RESEARCH CENTRE
AZIMUTHING PROPELLER DYNAMOMETER
GENERAL DETAILS
SCALE 1:1
DATE 7-4-93
DRG No. 3of5
DRAWN PAB
DESIGNED PAB
A1

Figure B.14

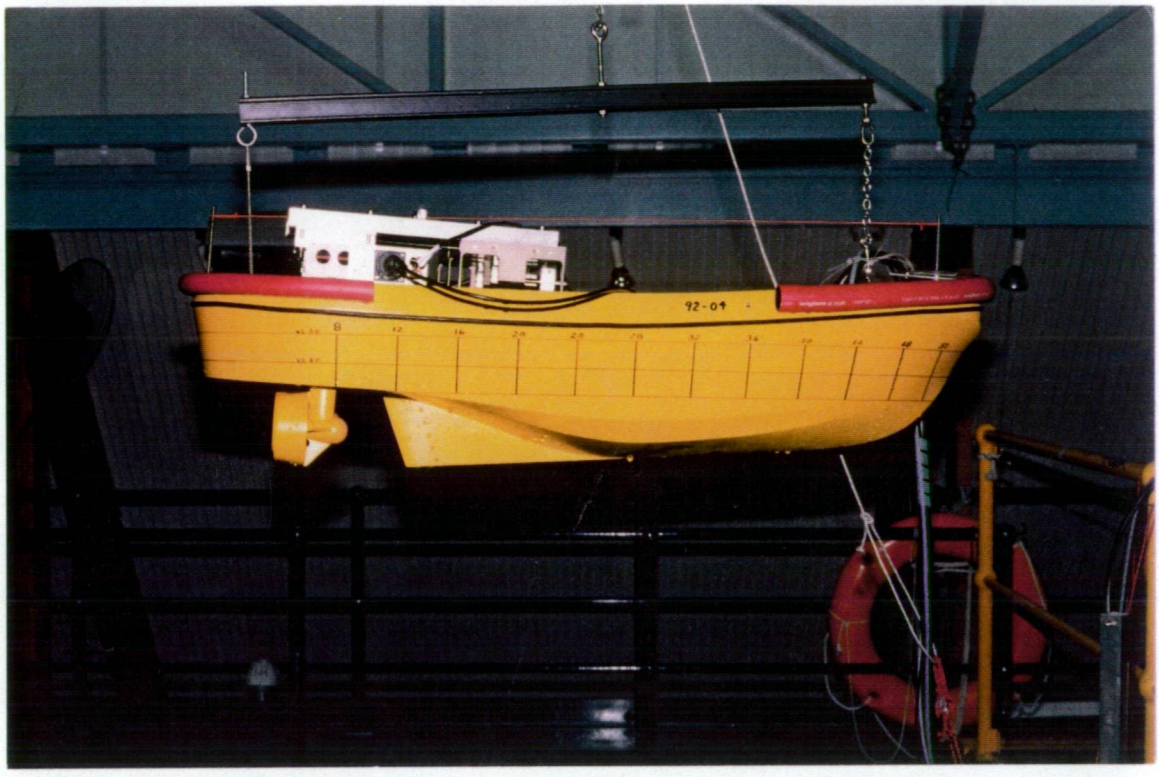

Figure B.15 Photograph of Tug Model Fitted with Thrusters for Free Running Model Experiments in Circulating Water Channel

Figure B.16 Photograph of Free Running Model Experiments in Circulating Water Channel-Ahead Bollard Pull

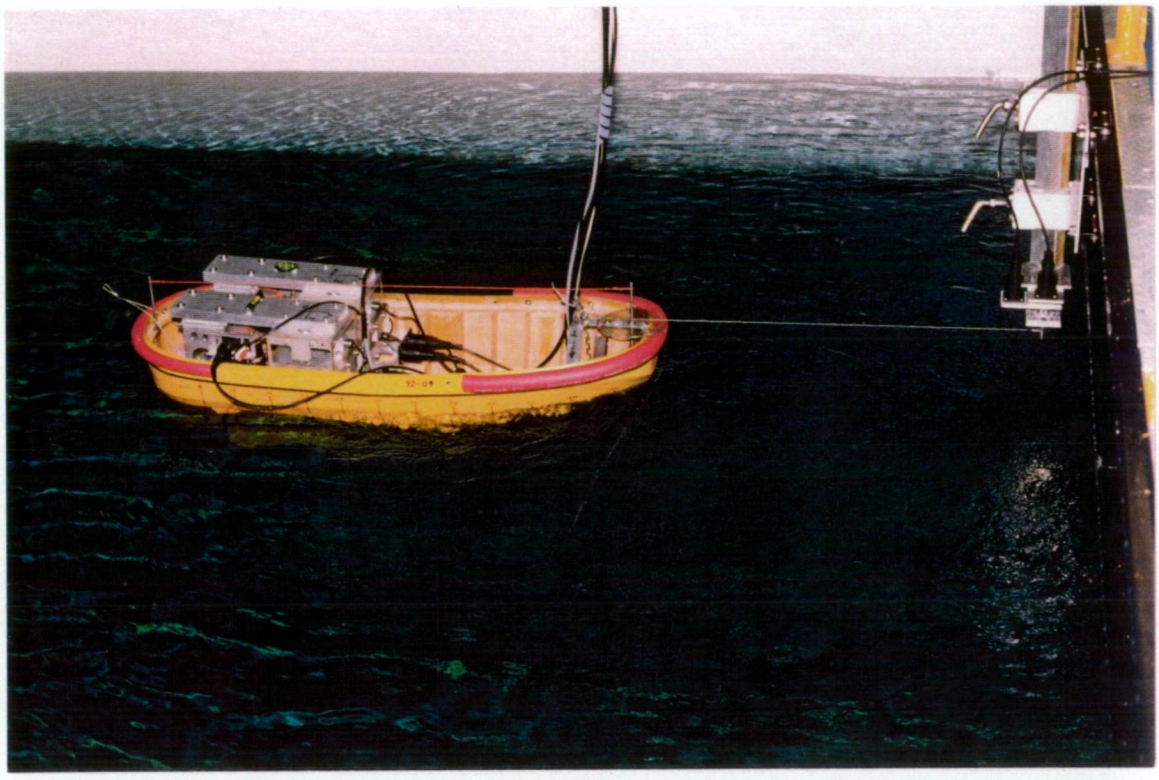

Figure B.17 Photograph of Free Running Model Experiments in Circulating Water Channel-Astern Bollard Pull

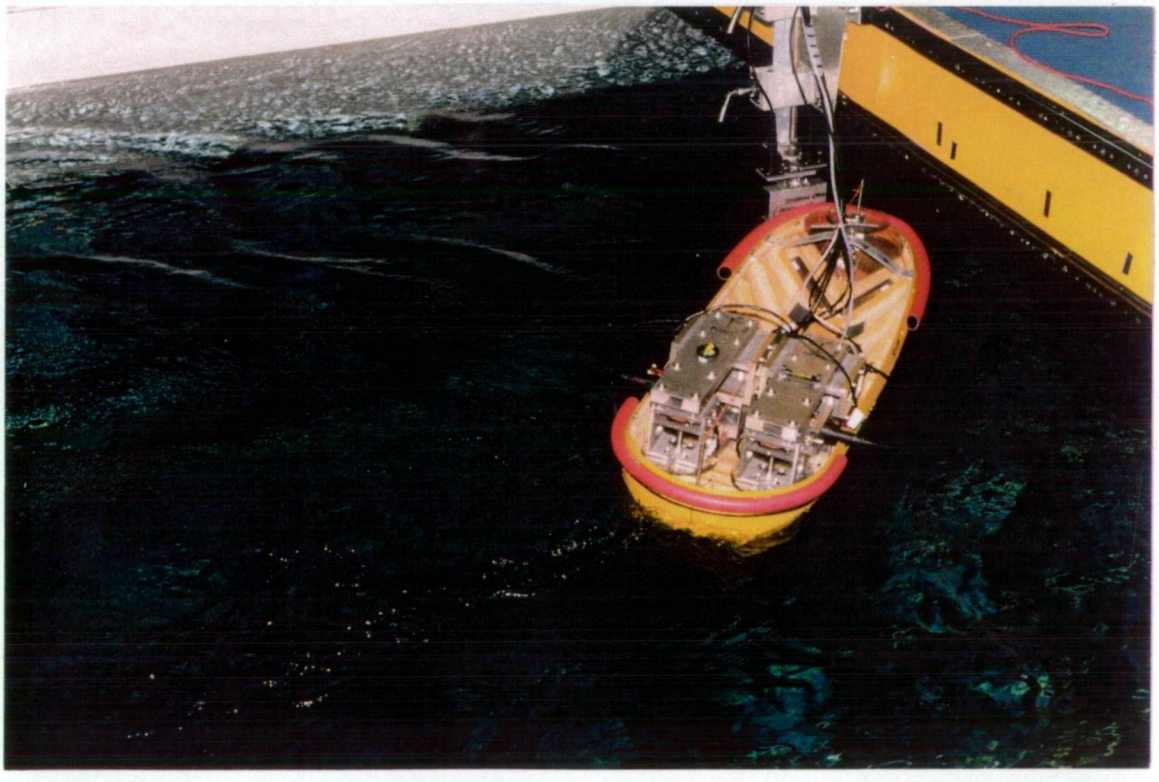

Figure B.18 Photograph of Free Running Model Experiments in Circulating Water Channel-Pushing

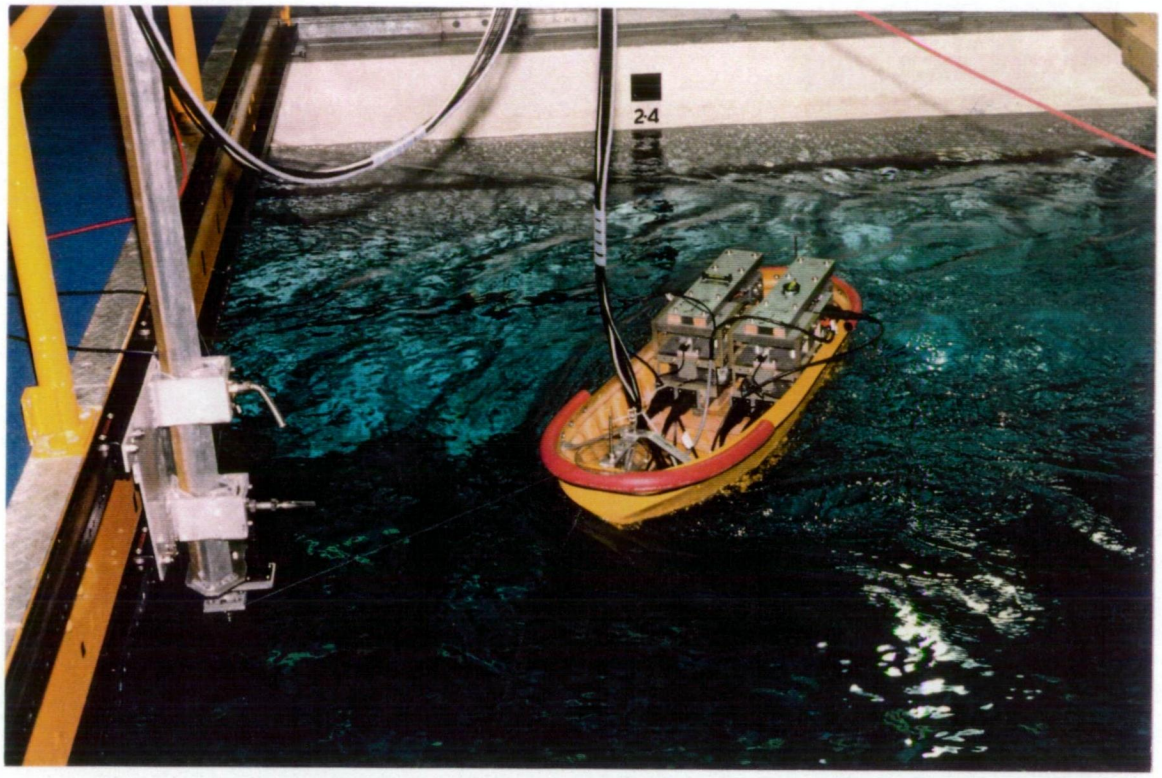

Figure B.19 Photograph of Free Running Model Experiments in Circulating Water Channel-Pulling Direct Using the Forward Tow Point

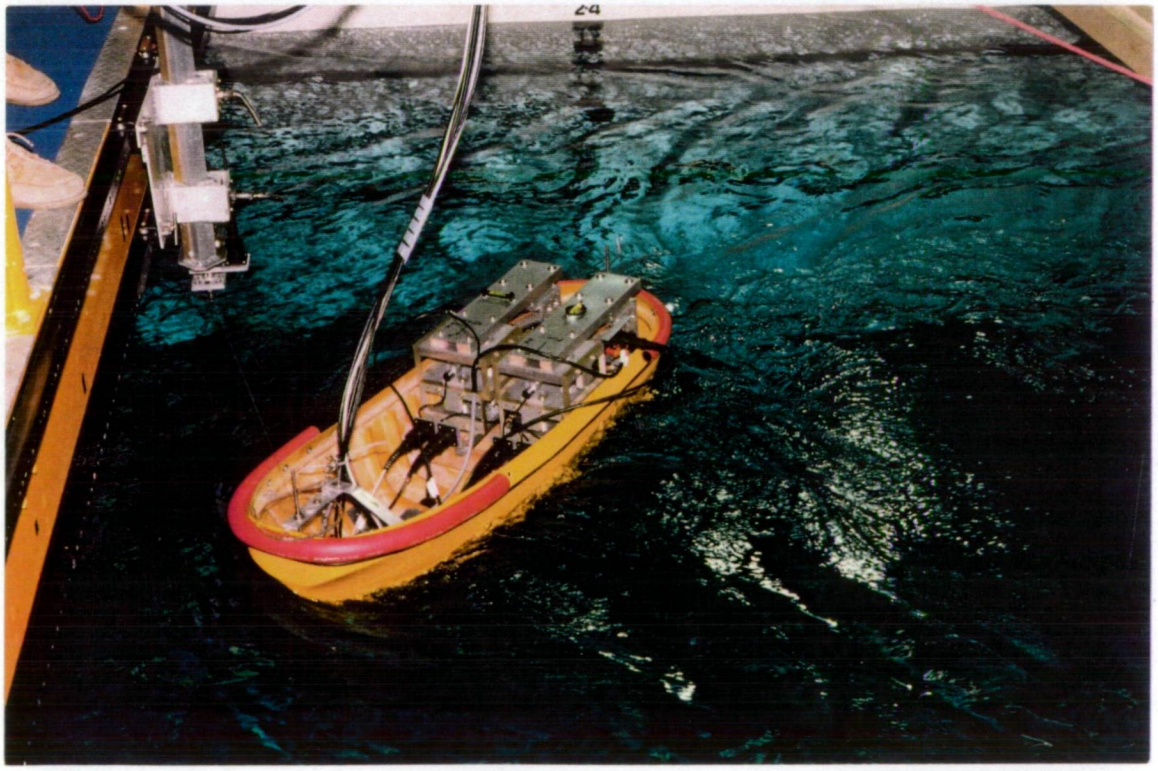

Figure B.20 Photograph of Free Running Model Experiments in Circulating Water Channel-Pulling Indirect Using the Forward Tow Point

APPENDIX-C THRUSTER DETAILS

C.1 MARIN Open Water Thruster Experiments

Details of the MARIN 19A duct and Ka series screws and the thruster tested at MARIN by Oosterveld and van Oortmerssen, 1972, are given in Figures C.1, C.2 and C.3.

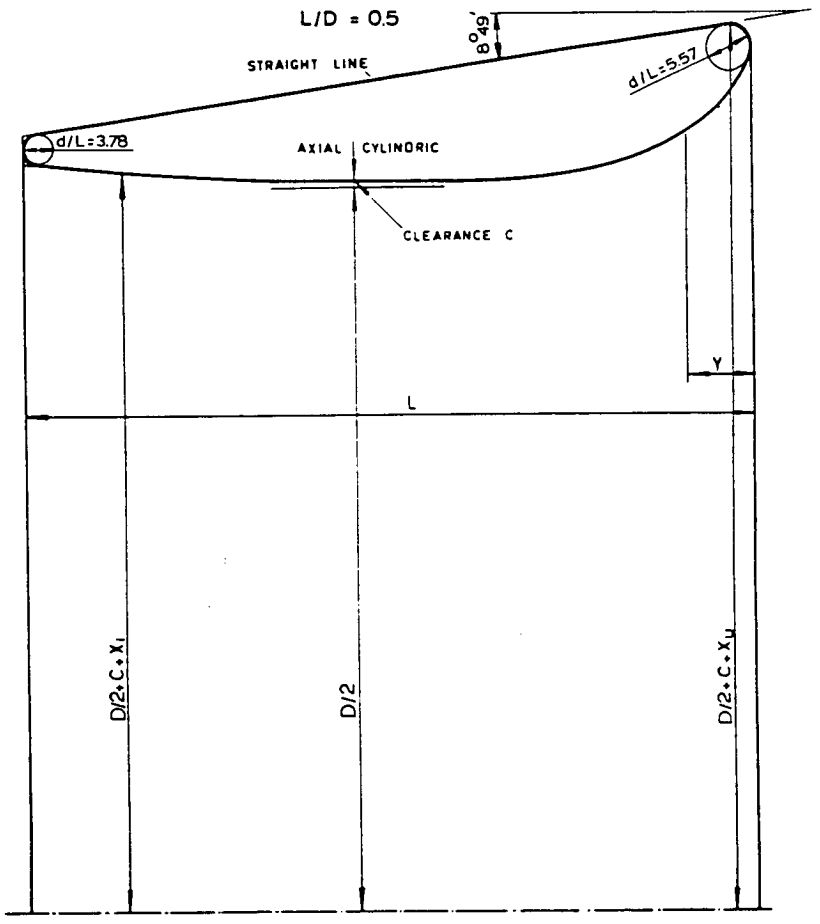

ORDINATES FOR NOZZLE PROFILE 19[a]

Y/L	0	1.25	2.50	5.0	7.5	10	15	20	25	30	40	50	60	70	80	90	95	100
X_I/L	18.25	14.66	12.80	10.87	8.00	6.34	3.87	2.17	1.10	0.48	CIRCULAR CYLINDRIC			0.29	0.82	1.45	1.86	2.36
X_U/L	—	20.72	21.07	20.80	STRAIGHT LINE													±6.36

Figure C.1 Details of MARIN 19A Duct, from Lewis, 1988

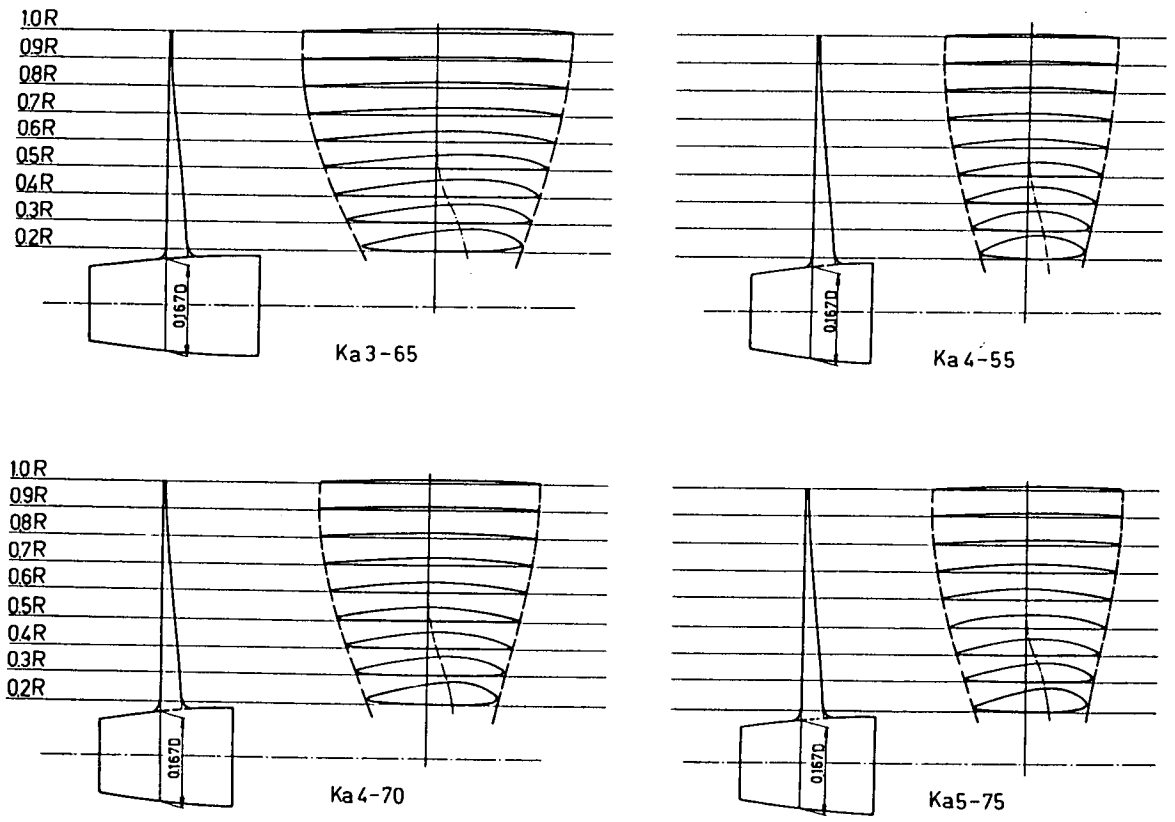

(a)

Figure C.2 Details of MARIN Ka Series Screws, from Lewis, 1988

Dimensions	r/R	0.2	0.3	0.4	0.5	0.6	0.7	0.8	0.9	1.0	
Length of the blade sections in percentages of the maximum length of the blade section at 0.6 R	from center lane to trailing edge	30.21	36.17	41.45	45.99	49.87	52.93	55.04	56.33	56.44	Length of blade section at 0.6 R
	from center line to leading edge	36.94	40.42	43.74	47.02	50.13	52.93	55.04	56.33	56.44	$1.969 \frac{1}{Z} \cdot \frac{A_E}{A_O}$
	total length	67.15	76.59	85.19	93.01	100.00	105.86	110.08	112.66	122.88	
Max. blade thickness in percentage of the diam.		4.00	3.52	3.00	2.45	1.90	1.38	0.92	0.61	0.50	Maximum thickness at center of shaft = 0.049 D
Distance of maximum thickness from leading edge in percentages of the length of the sections		34.98	39.76	46.02	49.13	49.98	—	—	—	—	

Ordinates

	Distance of the ordinates from the maximum thickness										
	Trailing edge					Leading edge					
r/R, percent	100	30	60	40	20	20	40	60	80	90	95	100
	Ordinates for the back											
0.2	—	38.23	63.65	82.40	95.00	97.92	90.83	77.19	55.00	38.75	27.40	—
0.3	—	39.05	66.63	84.14	95.86	97.63	90.06	75.62	53.02	37.87	27.57	—
0.4	—	40.56	66.94	85.69	96.25	97.22	88.89	73.61	50.00	34.72	25.83	—
0.5	—	41.77	68.59	86.42	96.60	96.77	87.10	70.46	45.84	30.22	22.24	—
0.6	—	43.58	68.26	85.89	96.47	96.47	85.89	68.26	43.58	28.59	20.44	—
0.7	—	45.31	69.24	86.33	96.58	96.58	86.33	69.24	45.31	30.79	22.88	—
0.8	—	48.16	70.84	87.04	96.76	96.76	87.04	70.84	48.16	34.39	26.90	—
0.9	—	51.75	72.94	88.09	97.17	97.17	88.09	72.94	51.75	38.87	31.87	—
1.0	—	52.00	73.00	88.00	97.00	97.00	88.00	73.00	52.00	39.25	32.31	—
	Ordinates for the face											
0.2	20.21	7.29	1.77	0.1	—	0.21	1.46	4.37	10.52	16.04	20.62	33.33
0.3	13.85	4.62	1.07	—	—	0.12	0.83	2.72	6.15	8.28	10.30	21.18
0.4	9.17	2.36	0.56	—	—	—	0.42	1.39	2.92	3.89	4.44	13.47
0.5	6.62	0.68	0.17	—	—	—	0.17	0.51	1.02	1.36	1.53	7.81

(b)

Figure C.2 Details of MARIN Ka Series Screws, from Lewis, 1988

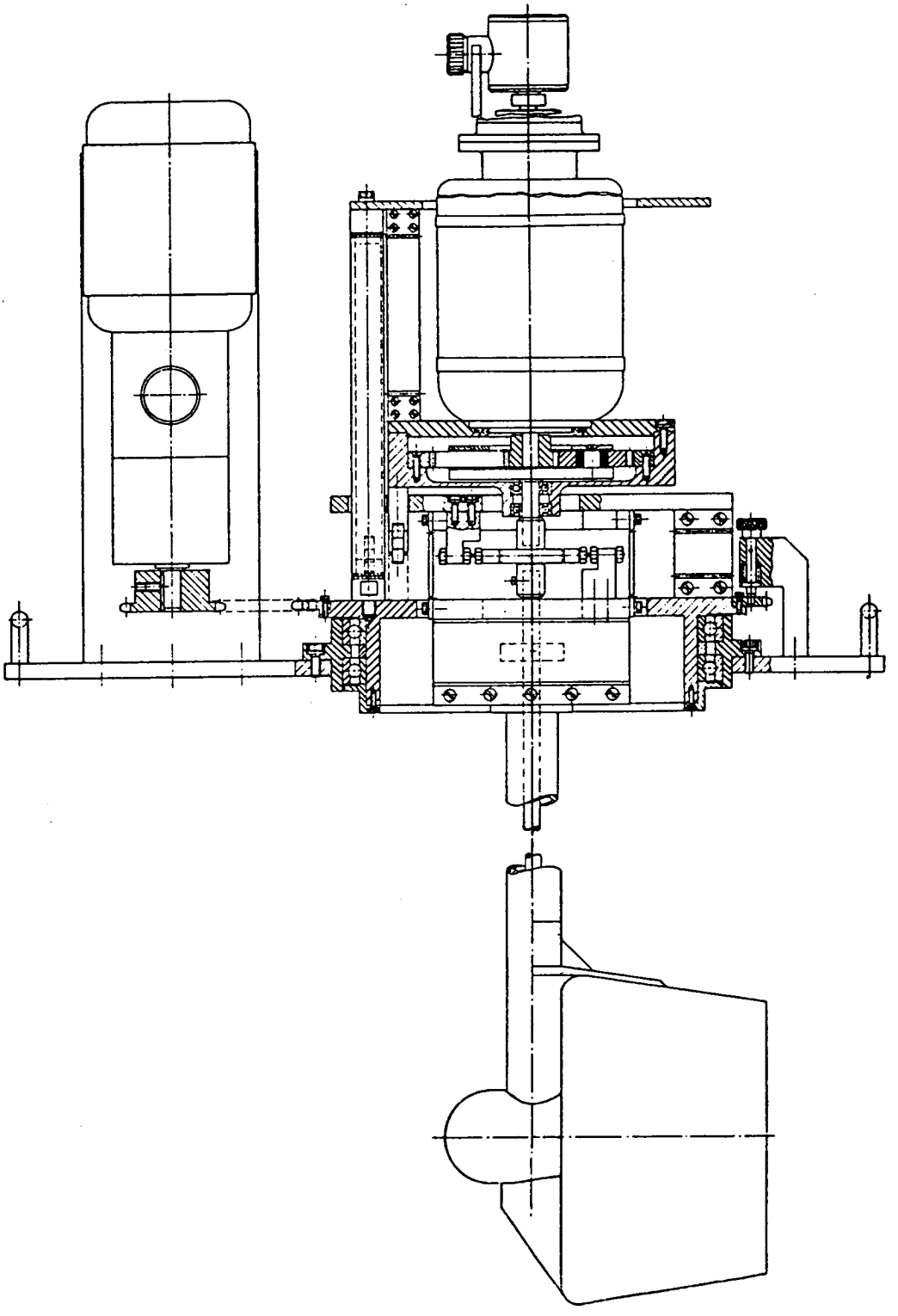

Figure C.3 Details of Thruster Tested by Oosterveld and van Oortmerssen, 1972

C.2 NSFI Open Water Thruster Experiments

Details of the NSFI P-927 screw and the thruster tested at NSFI by Minsaas and Lehn, 1978, are given in Figures C.4 and C.5.

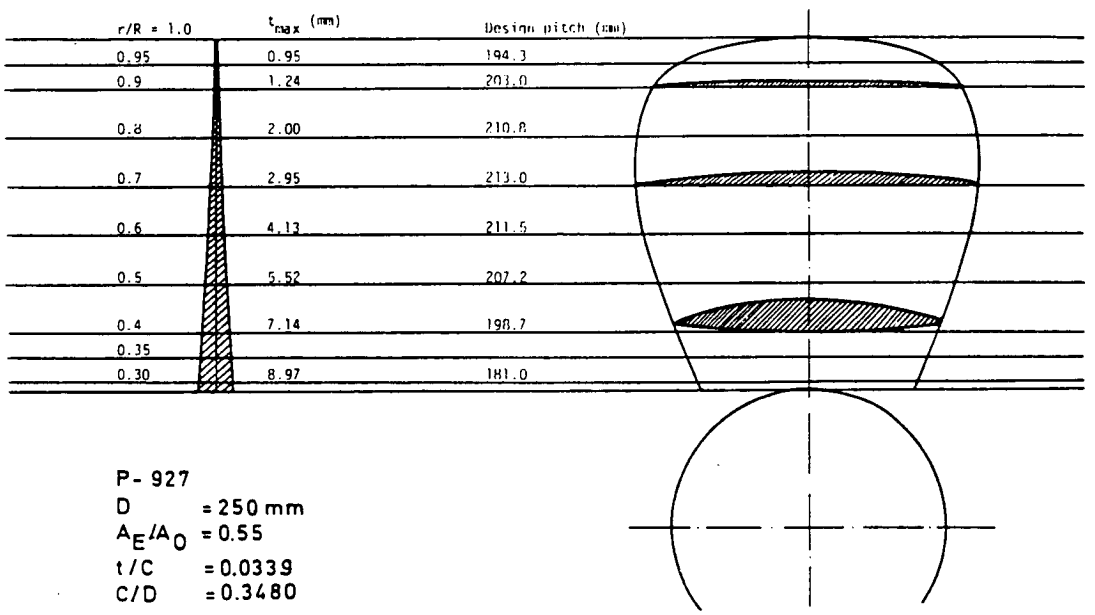

Figure C.4 Details of the NSFI P-927 Screw from Minsaas and Lehn, 1978

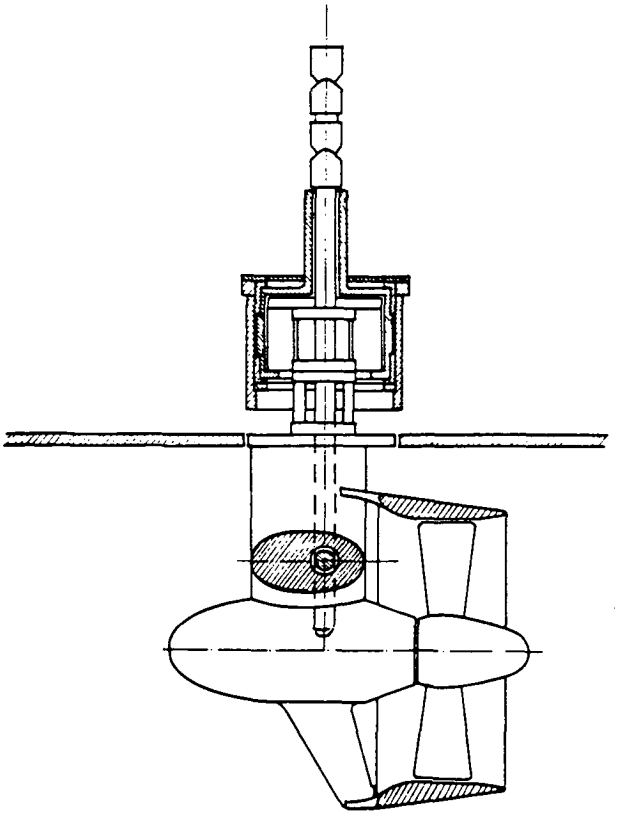

Figure C.5 Details of Thruster Tested by Minsaas and Lehn, 1978
(fitted with MARIN 19A duct)

C.3 AMC Open Water Thruster Experiments

Details of the thruster tested at AMC as part of the present investigation are given in Figure C.6.

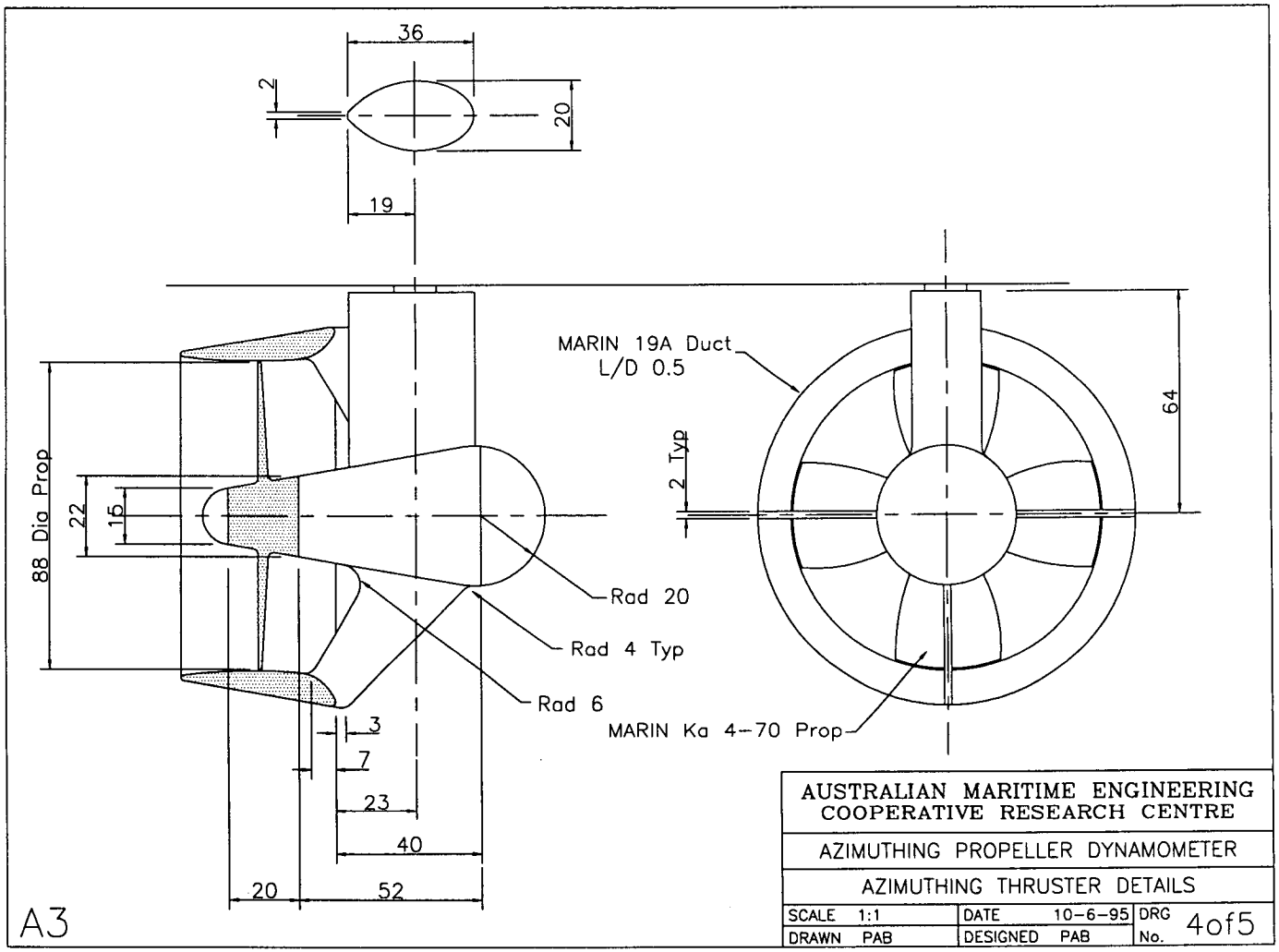
36
2
20
19
MARIN 19A Duct
L/D 0.5
64
2 Typ
88 Dia Prop
22
16
Rad 20
Rad 4 Typ
Rad 6
MARIN Ka 4-70 Prop
3
7
23
40
20
52
A3
AUSTRALIAN MARITIME ENGINEERING
COOPERATIVE RESEARCH CENTRE
AZIMUTHING PROPELLER DYNAMOMETER
AZIMUTHING THRUSTER DETAILS
SCALE 1:1
DATE 10-6-95
DRG No. 4of5
DRAWN PAB
DESIGNED PAB

Figure C.6

APPENDIX-D THRUST IDENTITY TECHNIQUE

In resistance and propulsion investigations, thrust identity and sometimes torque identity methods are used to determine the interaction between ship hull and propeller. This involves comparison of the open water propeller characteristics with those measured in the behind condition, i.e. a self propulsion experiment. From this comparison it is possible to determine, for a particular ship speed and propeller rpm, the mean open water speed of advance that results in the same measured thrust in the behind condition, i.e. the mean effective wake.

This method can also be applied in two dimensions to determine effective thruster advance velocities in perpendicular directions or, advance velocity and angle of attack. The effects of interactions between thrusters and between hull and thrusters have been determined using this method. Longitudinal and transverse thruster forces, X and Y, measured in the behind condition or in the presence of a nearby thruster are compared with those measured in the open water condition. Rearrangement of equations 4.3 and 4.4:

$$C'_X = \frac{X}{\frac{1}{2}\rho A_O\left[V_A^2 + (0.7\pi n D_O)^2\right]} \tag{4.3}$$

$$C'_Y = \frac{Y}{\frac{1}{2}\rho A_O\left[V_A^2 + (0.7\pi n D_O)^2\right]} \tag{4.4}$$

give,

$$C'_X(\beta_P,\theta)(0.7\pi n D_O)^2 - \frac{X}{\frac{1}{2}\rho A_O}\cos^2\beta_P = 0 \tag{A.1}$$

$$C'_Y(\beta_P,\theta)(0.7\pi n D_O)^2 - \frac{Y}{\frac{1}{2}\rho A_O}\cos^2\beta_P = 0 \tag{A.2}$$

where, X and Y are now the measured forces for which the unknown operating conditions are desired and $C'_X(\beta_P,\theta)$ and $C'_Y(\beta_P,\theta)$ are taken from the open water characteristics, as presented in Figures 4.22 and 4.23. For a particular angle of attack, equations A.1 and A.2 may be solved for advance angles that result in the desired longitudinal and transverse forces. The advance angle and angle of attack that result in the desired forces can be found from solution at successive angles of attack until the resulting advance angles are equal, i.e.:

$$\beta_P(X) - \beta_P(Y) = 0 \tag{A.3}$$

A particular short coming of this approach is that solutions may not be unique since thruster characteristics are such that at higher angles of attack, similar forces may be produced at different advance angles.